

Middle Atmosphere Program

HANDBOOK FOR MAP VOLUME 25

Edited by
R. G. Roper

N88-14502
--THRU--
N88-14560
Unclas
0113628

G3/46

(NASA-CR-181571) MIDDLE ATMOSPHERE PROGRAM.
HANDBOOK FOR MAP, VOLUME 25 (International
Council of Scientific Unions) 435 pCSCI 04A

ICSU

International Council of Scientific Unions

SCOSTEP

Scientific Committee on Solar-Terrestrial Physics

J. G. Roederer, President
W. I. Axford, Vice President
C. H. Liu, Scientific Secretary

MAP ORGANIZATION

MIDDLE ATMOSPHERE PROGRAM STEERING COMMITTEE

S. A. Bowhill, SCOSTEP, Chairman
K. Labitzke, COSPAR, Vice Chairman
C. H. Liu, SCOSTEP, Secretary

H. S. Ahluwalia, IUPAP
R. D. Bojkov, WMO
A. D. Danilov, COSPAR
J. C. Gille, COSPAR
I. Hirota, IUGG/IAMAP
A. H. Manson, SCOSTEP

T. Nagata, SCAR
R. G. Roper, IUGG/IAMAP
P. C. Simon, IAU
J. Taubenheim, IUGG/IAGA
T. E. VanZandt, URSI
R. A. Vincent, URSI

MAP STANDING COMMITTEES

Data Management -- G. Hartmann and I. Hirota, Co-Chairmen
Publications -- Belva Edwards, Chairman

MAP STUDY GROUPS

MSG-5 Ions and Aerosols, F. Arnold and M. P. McCormick, Co-Chairmen
MSG-8 Atmospheric Chemistry, G. Witt, Chairman
MSG-9 Measurement of Middle Atmosphere Parameters by Long Duration
Balloon Flights, J. E. Blamont, Chairman

MAP PROJECTS

	Coordinator
AMA:	T. Hirasawa
ATMAP:	J. M. Forbes
DYNAMICS:	K. Labitzke
GLOBMET:	R. G. Roper
GLOBUS:	J. P. Pommereau
GOSSA:	M. P. McCormick
GRATMAP:	D. C. Fritts
MAC-EPSILON:	E. V. Thrane

	Coordinator
MAC-SINE:	E. V. Thrane
MAE:	R. A. Goldberg
MASH:	A. O'Neill
NIEO:	S. Kato
OZMAP:	D. F. Heath
SSIM:	P. C. Simon
SUPER CAMP:	E. Kopp
WINE	U. von Zahn

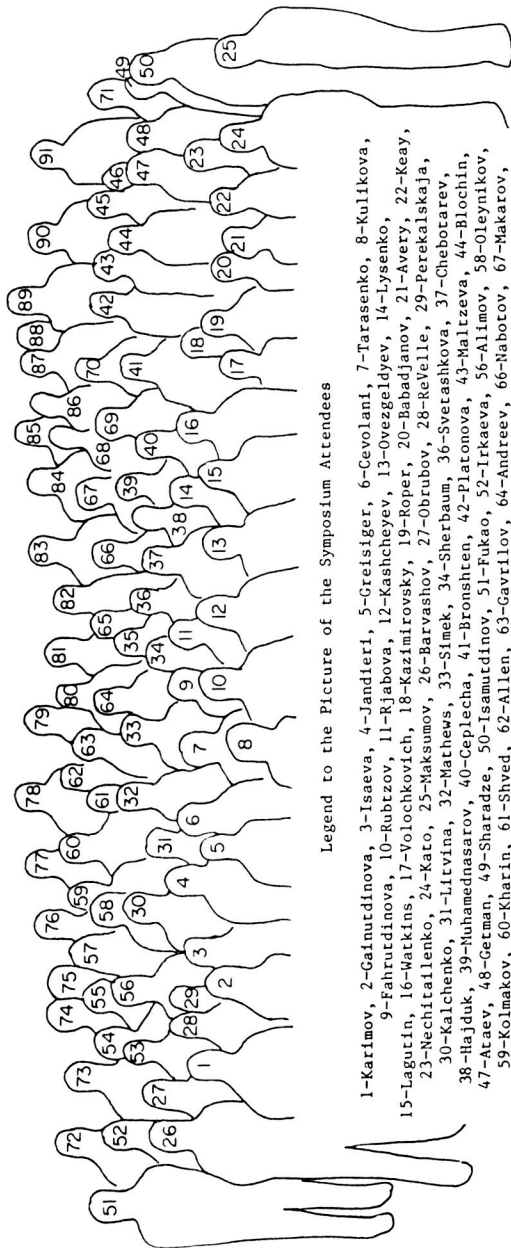
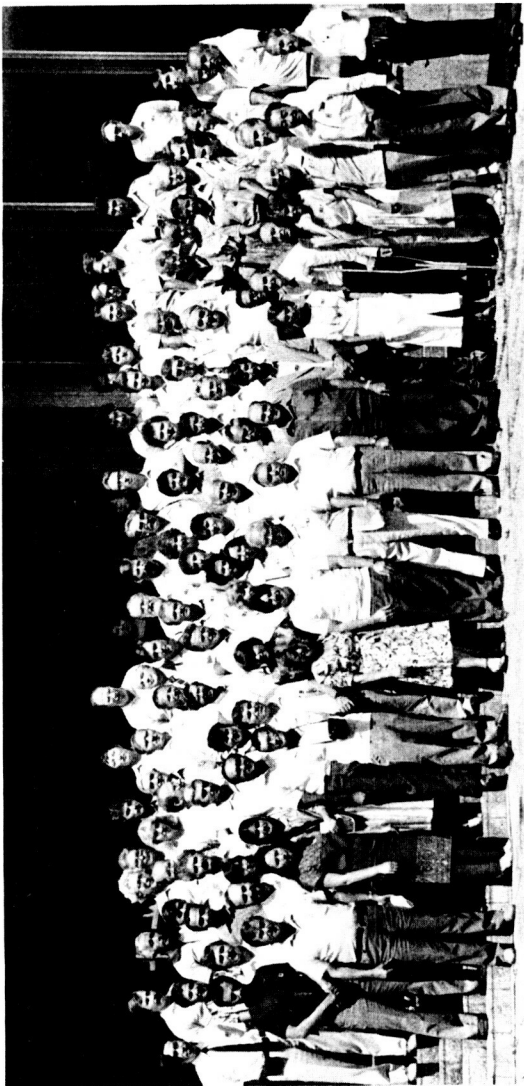
MAP REGIONAL CONSULTATIVE GROUP

Europe: M. L. Chanin, Chairman

First GLOBMET Symposium

Dushanbe, Tajicistan, USSR

August 19-24, 1985



Legend to the Picture of the Symposium Attendees

- 1-Karl'mov, 2-Gainutdinova, 3-Isaeva, 4-Jandieri, 5-Greisiger, 6-Cevolani, 7-Tarasenko, 8-Kul'kova, 9-Fahrtudinova, 10-Rubtsov, 11-Rjabova, 12-Kashcheyev, 13-Ovezgeldyev, 14-Lysenko, 15-Lagutin, 16-Watkins, 17-Volochkovich, 18-Kazimirovsky, 19-Roper, 20-Babadjanov, 21-Avery, 22-Keay, 23-Nechitailenko, 24-Kato, 25-Maksumov, 26-Barvashov, 27-Obrubov, 28-ReVelle, 29-Perekal'skaja, 30-Kalchenko, 31-Litvina, 32-Mathews, 33-Simek, 34-Sherbaum, 36-Svetashkova, 37-Cheborarev, 38-Hajduk, 39-Muhamednasarov, 40-Ceplecha, 41-Bronshten, 42-Platonova, 43-Maltzeva, 44-Blochkin, 47-Ataev, 48-Getman, 49-Sharadze, 50-Isamutdinov, 51-Fukao, 52-Irkaeva, 56-Allimov, 58-Oleynikov, 59-Kolmakov, 60-Kharin, 61-Shved, 62-Allen, 63-Gavrilov, 64-Andreev, 66-Nabotov, 67-Makarov, 68-Kostyl'jov, 69-Spasov, 70-Sidorov, 72-Lukin, 74-Belkovich, 75-Bibarsov, 77-Bekbasarov, 78-Meisel, 80-McIntosh, 81-Zlotnikov, 82-Shestaka, 83-Tokhtasiev, 86-Shafiev, 87-Sallimov, 91-Moskalenko

M I D D L E
A T M O S P H E R E
P R O G R A M

HANDBOOK FOR MAP

Volume 25

Edited by

R. G. Roper

August 1987

Published for the ICSU Scientific Committee on Solar-Terrestrial Physics (SCOSTEP) with financial assistance from the National Aeronautics and Space Administration under the 1986 Middle Atmosphere Program Management contract and Unesco Subvention 1986-1987.

Copies available from SCOSTEP Secretariat, University of Illinois, 1406 W. Green Street, Urbana, Illinois 61801

PREFACE

The First GLOBMET Symposium was held in Dushanbe, Tajicistan, USSR, August 19-24, 1985, under the sponsorship of SCOSTEP (the Scientific Committee on Solar-Terrestrial Physics), IAGA (the International Association of Geomagnetism and Aeronomy), ICMUA (the International Commission on the Meteorology of the Upper Atmosphere), the Soviet Geophysical Committee of the Academy of Sciences of the USSR and the Institute for Astrophysics, Tajic Academy of Sciences.

GLOBMET (the Global Meteor Observation System) was first proposed by the Soviet Geophysical Committee (by B. L. KASCHFYEV and V.A. NECHJTAILENKO), and was accepted by the Middle Atmosphere Program Steering Committee as a MAP Project in 1982. While the atmospheric dynamics data from the system are of primary interest to MAP, GLOBMET also encompasses the astronomical radio and optical observations of meteoroids, and the physics of their interaction with the earth's atmosphere.

In addition to more than one hundred Soviet participants, the conference was attended by scientists from nine other nations, including eight from the USA.

During the opening ceremony, the attendees were greeted by Mr. USMANOV, the Deputy Prime Minister of the Republic of Tajicistan; Professor ASIMOV, President of the Tajic Academy of Sciences; Professor OVEZGELDYEV, Chairman of the Soviet National Committee for GLOBMET; and Professor BABADZHANOV, Proctor of the Lenin Tajic State University and prior director of the Astrophysical Observatory. This ceremony firmly established the atmosphere of conviviality which was continued throughout the meeting.

With some 46 oral and 30 poster presentations, the review which follows emphasizes invited papers, with an overview of the other contributions.

The first scientific session of the symposium consisted of four invited papers presented by members of the GLOBMET Panel. ROPER opened with a review of currently operating radio meteor systems, with emphasis on meteor wind radars, but also including the proposed three station Georgia Tech Radio Meteor Facility, which is designed to measure meteoroid orbits as well as both large and small scale parameters of the mesopause level wind field. He discussed the relative merits of beam antennas versus all sky (dipole) systems, with the latter producing not only a somewhat greater height coverage but also a greater radiant distribution for orbit measurement. ROPER also referenced the Soviet Hydrometeorological Service "Cyclone" radar (LYSENKO), the ST/MST radar as a meteor radar (AVERY), the MU radar as a meteor radar (FUKAO) and the Newcastle radar (KEAY) scheduled to be discussed later in the meeting.

BABADZHANOV then discussed what is currently known about the dynamics of meteor streams, emphasizing both evolutionary theories and observational evidence. The role of gravitational and non-gravitational perturbations were discussed in the context of the concrete examples provided by the Gemenid, Quadrantid and Perseid streams. Estimated lifetimes for these

streams were presented, as determined from a mathematical model of the structure and shape of meteor streams versus time.

OVEZGELDYEV followed with a presentation on the spectra and aeronomy of meteor trails, using the meteor-atmosphere interaction as a unique phenomenon for the study of elementary gaseous processes, such as atomic and molecular oscillations, excitation and ionization, dissociation, recombination, ion-molecular reactions, and so on. The collision processes involved cannot be simulated in the laboratory (the average meteoroid has a velocity of a few tens of kilometers per second). The lines and bands of observed meteor spectra are a combination of radiation from both incoming meteor atoms and molecules, and those of the ambient atmosphere. Many species and reaction schemes have already been identified, and efforts are being made to improve both the observational instrumentation, and the reduction, analysis and interpretation schemes. Special emphasis was placed on the importance of metallic and other meteor ions to the aeronomy of the middle atmosphere.

The collection of data and exchange of information was addressed next by NECHITAIENKO, who emphasized the need for validation and editing of data during the reduction and interpretation process, and that the algorithm for achieving this should be standardized, if possible, and, if not, should be readily available to users of the data. He suggested the development of a meteor data indexing system, to establish criteria of compatibility, homogeneity and representativeness of any given data set, and the requirement for standardized formats for international data exchange, as have already been proposed for wind reporting by the GLOBMET Panel.

The opening paper of the session on "Dynamics of Atmospheric Processes in the Meteor Zone," which was to have been presented by PORTNYAGIN, was unfortunately withdrawn due to the absence of the author. This was especially unfortunate in that PORTNYAGIN has been in the forefront of the measurement and interpretation of mesopause level winds for almost two decades.

The results from the meteor wind radar at Shigaraki, near Kyoto, Japan, which has been operating almost continually since 1979, were presented by Kato. Prevailing winds, tides, gravity waves with periods of a few hours, and some long term means for the lunar tide were discussed - the thermal tides in the context of global observations, as exemplified by the ATMAP (Atmospheric Tides in the Middle Atmosphere Program) project. This was followed by a paper by KASHCHEYEV on the dynamics of the equatorial meteor region. While this is "old" data (from the period August, 1968 to July, 1970) taken on a Soviet expedition to Mogadishu, Somalia (2°N, 45°E), it is very important because it is the only long term data set from the equatorial regions. The equatorial lower thermosphere is characterized by predominant easterlies, a diurnal tide greater in amplitude than the semidiurnal, a two day component, and, on occasion very large wind speeds (greater than 150 m/sec).

These papers were followed by contributions related to the solar cycle dependence of long term variations in mesopause level circulation, extensive observations of lower thermospheric winds over Europe and Asia,

the relationship of such circulations to the occurrence of midwinter stratospheric warmings, and the possible forcing of these motions by tropospheric meteorology.

Presenters on Wednesday morning continued the discussion of the previous afternoon's topics, with additional material on tidal winds. In the afternoon, GAVRILOV presented an overview of the current state of the art in gravity wave theory, prior to presentations on lower thermospheric turbulence, the role of fragmentation in the interaction of meteoroids with the atmosphere, and an invited paper by MATHEWS which considered some aspects of metallic ion chemistry and dynamics in the meteor region. These were followed by presentations on meteor trail spectra, fireball end heights, and a film on the dynamics of magnetic storms.

Thursday's papers concentrated on the astronomical aspects of meteor science. BELKOVICH discussed the importance of global observations of the meteor flux, and was followed by CEPLECHA's review of many years involvement with photographic fireball networks. VOLOSCHCHUK presented data from about two decades of observations from KHARKOV of the temporal and three-dimensional structure of the meteor complex in the vicinity of the Earth's orbit, and SIMEK a method for improving the statistics of meteor shower data analysis from long term observations. Further papers on observations of the Eta-Aquarid and Orionid meteor showers, the density of the incident meteoroid flux, and the modeling of sporadic and shower meteoroid distribution followed. Predictions relative to the "Valec" Fiberball fall and the relationship of the Eta-Aquarids and Orionids to the orbit of Halley's comet completed this session.

Friday morning's session was entitled "Methodological Problems; Techniques and Facilities for Studying Meteors and the Middle Atmosphere." AVERY and FUKAO, in separate papers, presented some results of meteor wind determinations from MST radar facilities. The concept of MENTOR (Meteor Echoes - No Transmitters, Only Receivers) which proposes to use the Colorado Wind Profiler Network of ST radars was presented by ROPER, and KEAY discussed the new Newcastle (Australia) meteor patrol radar. A paper on lidar sounding of the meteor zone was followed by MEISEL's discussion of the reception of various beacon transmitters by amateur radio operators as a data source for meteor rate studies and a paper by McINTOSH on the archiving of a data base as part of the International Halley Watch. Papers on the treatment of data from radar observations of meteor showers and the technical problems of spaced image intensifier observations completed the formal presentations.

Friday afternoon was highlighted by a panel discussion which included summary presentations by session chairmen. In addition to contributions to GLOBMET, involvement of the radio meteor community in the international programs such as the Halley Watch, ATMAP (the Atmospheric Tides in the Middle Atmosphere Project) and GTMS - the Global Thermospheric Mapping Study, of which the URSI/IAGA CTOP (Coordinated Tidal Observations Program) is an important facet, was discussed. The proliferation of such programs has greatly increased the need for standardized formats for data exchange. Further emphasis was put on the need for continuous observations, both of winds and meteoroid fluxes and associated astronomical parameters. This is now relatively easily achieved, because of the rapid advances in the

techniques of automatic recording. There is still much work to be done on the number densities and mass distributions associated with both daytime and nighttime showers and sporadics. While meteor radiant measurements are not as accurate as optical, the ability to measure during the daytime, and continuously independent of cloud cover or moonlight more than offsets this limitation.

The formal program ended with a closing ceremony in which the participants thanked the sponsors and organizers and, in particular, the translators, who provided excellent simultaneous translations in English or Russian for the whole program.

The formal presentation program was greatly enhanced by the poster sessions, for which time out from the oral presentations was arranged on Wednesday and Thursday afternoons. One must compliment the Soviet scientists for the amount of time it must have taken to present all their poster texts and figure captions in English. It was here that the "nitty gritty" of the session topics could be discussed in more detail than could be accommodated in the formal sessions, and the significance of the Soviet contributions to an area receiving little attention in the West could be fully appreciated.

Extended abstracts of nearly all of the presentations and posters appear in this forthcoming issue of the MAP Handbook.

In addition to the scientific program, the local organizing committee provided a social program, a visit to the Astrophysical Observatory, and a day trip to Samarkand which provided all participants the opportunity to not only participate in scientific exchange, but also to learn more of the history and people of Central Asia. A great time was had by all.

R. G. Roper

THE FIRST GLOBMET SYMPOSIUM
Dushanbe, Tajicistan, USSR
August 19-24, 1985

Frontispiece.	
Preface	iii
Table of Contents	vii
OPENING PLENARY	
State-of-the-art meteor radars, R. G. Roper	1
Dynamics of meteor streams, P. B. Babadjanov, and Yu. V. Obrubov. .	2
Elementary processes and meteor train spectra, O. G. Ovezgeldyev. .	11
The archiving of meteor research inforamtion, V. A. Nechitailenko .	22
I. THE DYNAMICS OF ATMOSPHERIC PROCESSES IN THE METEOR ZONE	
The climatic wind regime in the lower thermosphere from radar observations, Yu. I. Portnyagin.	31
Meteor observations by the Kyoto meteor radar, Susumu Kato, and Toshitaka Tsuda.	45
Atmosphere dynamics in the equatorial meteor zone, B. L. Kascheyev.	50
Long-period variations of wind parameters in the mesopause region and the solar cycle dependence, K. M. Greisiger, R. Schminder, and D. Kurschner.	58
The lower thermosphere wind regime from simultaneous observations over Euroasia (Collm, Dushanbe, Frunze), R. Schminder, D. Kurschner, K. A. Karimov, R. B. Bekbasarov, L. A. Riazanova, R. P. Chebotarev, and Kh. Nabotov	62
Wind regime peculiarities in the lower thermosphere in the winter of 1983-84, I. A. Lysenko, N. A. Makarov, Yu. I. Portnyagin, B. I. Petrov, K. M. Greisiger, R. Schminder, and D. Kurschner	66
On the interconnection of dynamic processes in the lower thermosphere with meteorological phenomena in the tropo-stratosphere, A. N. Fakhrutdinova, A. M. Stepanov, and I. P. Perevedentsev.	70
Mean pressure distribution and geostrophic circulation in the meteor zone, Yu. P. Koshelkov.	76
Circulation in the mesosphere and lower thermosphere during the MAP/WINE period, D. A. Tarasenko	101

Characteristics of atmospheric disturbances with a quasi two day period, B. V. Kalchenko.	112
Variations of the semidiurnal tidal wind in the meteor region with periods of about 27 and 13.5 days, K. M. Greisiger. . .	119
Tidal activity in the meteor zone over Budrio, Italy, G. Cevolani.	121
Main results of atmospheric fine structure parameter observation in the lower thermosphere, V. V. Sidorov, A. N. Fakhrutdinova, and V. A. Ganin	138
On connection between evolution of troposphere fronts and changes of circulation regime in meteor zone, K. A. Karimov.	143
A study of the mechanism of internal gravity wave genera- tion by quasigeostrophic meteorological motions, A. S. Medvedev	146
Study of internal gravity waves in the meteor zone N. M. Gavrilov	153
Numerical modeling of troposphere-induced gravity wave propagation, N. M. Gavrilov, and V. A. Yudin	167
A statistical study of variations of internal gravity wave energy characteristics in meteor zone, N. M. Gavrilov, and E. D. Kalov.	173
On the dependence of the lower thermospheric wind regime on the solar cycle, V. A. Djachenko, I. A. Lysenko, and Yu. I. Portnyagin.	180
Longitudinal peculiarities of meridional circulation in lower thermosphere and mesosphere, R. B. Bekbasarov, K. A. Karimov, and M. A. Takyrbashev	186
Lower thermosphere wind regime according to radiometer measurements in Kazan, V. V. Sidorov, A. N. Fakhrutdinova, and V. A. Makarov.	189
Atmosphere dynamic processes structure at 80-105 km altitude, B. V. Kalchenko, and A. N. Oleinikov	194
Internal gravity waves in the meteor zone in the Tbilisi Region, Z. S. Sharadze, G. B. Kikhvilashili, Z. L. Liadze, and N. V. Mosashvili	200
Mesoscale density variability in the mesosphere and thermo- sphere: effects of vertical flow accelerations, D. O. ReVelle.	204

II. THE PHYSICS OF THE INTERACTION OF METEORS WITH THE EARTH'S ATMOSPHERE

On the wave excitation in the turbulent meteor trace, G. V. Jandieri, G. Sh. Kevanishvili, and V. I. Lenin	207
Methods and first results of plasma non-isothermal parameters measurements in meteor trails, K. K. Kostylev, and V. S. Tokhtashev	211
The role of fragmentation in interaction of meteoroids with the earth's atmosphere, P. B. Babadjanov, G. G. Novikov, V. N. Lebedinets, and A. V. Blokhin.	218
On the meteor trail spectra, O. G. Ovezgeldyev, S. Mukhamednazarov, R. I. Shafiev, and N. V. Maltsev.	222
Some aspects of metallic ion chemistry and dynamics in the mesosphere and lower thermosphere, J. D. Mathews	228
The end height of fireballs as a function of their residual kinetic energy, D. O. ReVelle	255
Ozone formation due to interaction of meteoroids with the earth's atmosphere, R. Sh. Bibarsov.	258
Meteor matter interaction with the earth's atmosphere and the ionospheric E region structure, O. Alimov.	261
The nonlinear thermodynamics of meteors, noctilucent clouds, enhanced airglow and global atmospheric circulation, J. Rajchl.	266

III. METEOR FLUX AND STRUCTURE OF THE METEOR COMPLEX

A processing method and results of meteor shower radar observations, O. I. Belkovich, N. I. Suleimanov, and V. S. Tokhtashev	272
Photographic fireball networks, Z. Cepulecha.	280
A method of long term radar shower data analysis, M. Simek	288
Incident meteoroid flux density, P. B. Babadjanov, R. Sh. Bibarsov, V. S. Getman, and V. M. Kolmakov	294
Models of sporadic meteor body distribution, V. V. Andreev, and O. I. Belkovich.	298
On meteor stream spatial structure theory, G. V. Andreev	305
Density variations of meteor flux along the earth's orbit, N. V. Svetashkova.	311

	Meteor velocity distribution and an optimum monitoring mathematical model, N. G. Volkov, and O. N. Salimov.	316
IV.	STRUCTURE AND EVOLUTION OF METEOR SHOWERS	
	"VALEC" fireball and predicted meteorite fall, Z. Cep-lecha, and P. Spurny.	321
	Results of observations of the Eta Aquarid and Orionid meteor showers in 1980-1984, A. Hajduk	329
	Monte Carlo modeling and meteor showers, N. V. Kulikova. . .	336
	On the spatial structure of the Perseids meteor stream, G. V. Andreev, L. N. Rubtsov, and I. I. Tarasova	339
	Some models of the Geminids meteor stream formation, O. I. Belkovich, and G. O. Ryabova	344
	Structural peculiarities of the Quadrantid meteor shower, Sh. O. Isamutdinov, and R. P. Chebotarev	351
	On the possible origin of meteoroid generating asteroid orbits, A. M. Kazantsev, and L. M. Sherbaum.	356
V.	METHODOLOGICAL PROBLEMS, TECHNIQUES AND FACILITIES FOR STUDYING METEORS AND THE MIDDLE ATMOSPHERE	
	Meteor detection on ST (MST) radar, S. K. Avery.	361
	The "CYCLONE" meteor radar system for routine wind measurements in the lower thermosphere, I. A. Lysenko, P. P. Mikhailiek, and B. I. Petrov	376
	The Newcastle meteor radar, Colin Keay	381
	New approaches to some methodological problems of meteor science, David D. Meisel	389
	Lidar investigations of M-zone, O. G. Ovezgeldyev, K. Kurbanmuradov, M. F. Lagutin, A. A. Zarudny, Yu. E. Meghel, A. A. Torba, and V. E. Melnikov.	405
	Optical electronics for meteor observations, R. I. Shafiev, S. Mukhamednazarov, and I. A. Atamas	410
	Hard- and software problems of spaced meteor observations by optical electronics, R. I. Shafiev, S. Mukhamednazarov, and A. Sh. Ataev	416
	AUTHOR INDEX.	421

STATE-OF-THE-ART METEOR RADARS

R. G. Roper

School of Geophysical Sciences
Georgia Institute of Technology
Atlanta, GA 30332

ABSTRACT

The requirements of a "state-of-the-art" meteor wind radar, and acceptable compromises in the interests of economy, are detailed. Design consideration of some existing and proposed radars are discussed. The need for international cooperation in mesopause level wind measurement, such as that being fostered by the MAP GLOBMET (Global Meteor Observations System) project, is emphasized.

[This paper has already been published in the "Handbook for MAP", 13, 124-134, November, 1984.]

DYNAMICS OF METEOR STREAMS

P. B. Babadjanov and Yu. U. Obrubov

Institute of Astrophysics
Dushanbe, USSR

At present, the overwhelming majority of meteor streams are generally assumed to be formed due to the decay of comets. The most effective process of the release of solid particles from a cometary nucleus is their ejection by sublimating gases when the comet approaches the Sun.

It seems that some asteroids may also be progenitors of meteor streams if we assume these asteroids to be crumbly, porous, fragile bodies disintegrating into numerous small fragments upon collision. The possible formation of meteor streams from asteroids, for example, of groups of Apollos, Amors and Atens is often based on the assumption that some fraction of these asteroids are defunct comets.

In any case, no matter what source of meteor streams we assume the particles must of necessity have small relative ejection velocity ($1-10^3$ ms). This assumption is based on our notion of a meteor stream as an ensemble of particles moving in close orbits as well as on observations of cometary phenomena and theoretical calculations.

The well known 1951 formula (WHIPPLE), for the particle ejection velocity C at a distance r_{AU} from the Sun may be written down as:

$$C_1 = 3.28 \sqrt{\left(\frac{4}{\rho \delta r^{3/4}} - 0.052 R_c\right) R_c} \text{ m/s} \quad (1)$$

where R_c is the radius of the cometary nucleus in km, ρ = particle density and δ = particle radius both in CGS units. Then the maximum difference between the semimajor axis $\Delta_1 a$ and the eccentricity $\Delta_1 e$ of ejected particles' orbits from those of the comet's orbit will be:

$$\Delta_1 a = \pm 6.72 \cdot 10^{-5} a_{oc}^2 \sqrt{\frac{2}{r} - \frac{1}{a_o}} \text{ AU},$$

$$\Delta_1 e = \pm 6.72 \cdot 10^{-5} r_{oc} \sqrt{\frac{2}{r} - \frac{1}{a_o}}, \quad (2)$$

where r is the heliocentric distance, a_o is the semimajor axis of the comet's orbit in AU and e_o is its eccentricity.

According to RADZIEVSKIY (1951), variations in the semimajor axis and eccentricity of the released particle's orbit under the radiation pressure are:

$$\Delta_2 a = \pm 5.76 \cdot 10^{-5} (\rho \delta)^{-1} a_o \left(\frac{2a_o}{r} - 1 \right) \text{ AU},$$

$$\Delta_2 e = \pm 5.76 \cdot 10^{-5} (\rho \delta)^{-1} \rho_o e_o^{-1} \left(\frac{1}{r} - \frac{1}{a_o} \right). \quad (3)$$

In the formula (3) $\rho_o = a_o(1 - e_o^2)$ is the parameter of the comet's orbit in AU.

The ejection velocity and radiation pressure define the initial dispersion of the orbital semimajor axes and eccentricity of particles released from the comet. This dispersion is of great importance for the subsequent evolution of meteor streams. The rest of orbital elements of the ejected particles differ only slightly from those of the cometary ones and these differences are of minor importance.

The rate of particle dissipation along the progenitor's orbit is considered a significant characteristic of meteor stream dynamics. The loop formation time T is estimated by the formula (FOX et al., 1983):

$$T = \frac{P_{\max}^2}{P_{\max} - P_{\min}} \quad (4)$$

where P_{\max} and P_{\min} are maximum and minimum orbital periods of particles. Table 1 gives values of T for particles with different $\rho \delta$ (for the Geminids and Quadrantids).

Table 1

Loop formation time by stream particles of different mass.

Geminids ($a_o = 1.32 \text{ AU}$)						Quadrantids ($a_o = 3.08 \text{ AU}$)			
m		a_{AU}		T		a_{AU}		T	
g/cm^2	g	max.	min.	yr	per.	max.	min.	yr	per
10^{-2}	$4 \cdot 10^{-6}$	2.03	0.85	4	2.6	3.31	3.05	53	10
10^{-1}	$4 \cdot 10^{-3}$	1.53	1.14	5	3.3	3.13	3.05	150	28
10^0	$4 \cdot 10^0$	1.39	1.26	12	7.9	3.09	3.07	460	85
10^1	$4 \cdot 10^3$	1.34	1.30	36	23.6	3.083	3.077	2300	425

In calculating the values of Table 1, we have taken into account the joint influence of the ejection velocity and radiation pressure. Masses of particles were calculated for a density of 1 g/cm^3 . Radii of the parent comets were considered to be 5 km.

An interesting study of the Geminids was done by FOX et al., (1983). According to their model, the stream has a flat shape at a distance of 1 a.u. The ratio between the stream width and its thickness is about 7:1 which is the theoretical meteor stream cross-section in the ecliptic plane needed to obtain the observed meteor rate profiles with respect to the mass of particles and points where the Earth intersects the stream. The meteor rate profiles obtained explain the asymmetry observed in the Geminids shower. However, FOX et al., taking into account planetary perturbations, ignored the dependence on the value of the orbital semimajor axes. Furthermore, the meteor stream evolution over only a short period of time was considered, so that maxima of the rate of meteors produced by particles of different masses fell at the same solar longitude.

The discovery of the asteroid 1983 TB was an important event in the study of the Geminids origin and evolution. It should be noted that COOK (1973) assumed asteroids to exist in the Geminids stream. The asteroid 1983 TB moves in the orbit which is very similar to the mean orbit of the Geminids so it is natural to assume the asteroid to be a remnant of the Geminid parent body and obviously a "defunct" comet.

The Geminid meteor stream evolution has been dealt with in a number of our papers (BABADJANOV, OBRUBOV, 1971a, 1983, 1984). In the present paper we give new results of investigation of Geminid evolution. We assume that during the formation of the stream the semimajor axes of individual particles of 10^{-3} g might differ from the orbital semimajor axis of the asteroid 1983 TB by $\pm 0.3 \text{ AU}$, and their eccentricities - by 0.022, these differences being caused by an ejection velocity of 650 ms and by the comet's radius of 6-8 km. These sizes of a cometary nucleus correspond to the present observational data.

According to our calculations the age of the Geminids does not exceed 20 thousand years (BABADJANOV, OBRUBOV, 1979a). So our results are given for a 20,000-year period.

Calculations of secular perturbations of the asteroid 1983 TB were performed by the Halphen-Goryachev method taking into account 5-planet perturbations (Venus-Saturn) and included the secular variations in orbits of the planets themselves. For the Geminid particles with the orbital semimajor axes of 1 AU and 1.65 AU. Secular variations were allowed in the arguments of perihelion, inclination, eccentricities and $\Delta\pi$ (the difference between longitudes of perihelions of particles' orbits and the orbit of the asteroid).

It can be seen that secular variations in the orbital elements of the asteroid and the Geminids are described accurately enough by the following motion integrals:

$$(1 - e^2) \cos^2 i = C_1 = \text{const} \quad , \quad (4)$$

$$e^2 \left(\frac{2}{5} - \sin^2 i \cdot \sin^2 \omega \right) = C_2 = \text{const} \quad . \quad (5)$$

The relation (4) comes from Jacoby's integral when only secular perturbations are taken into account ($a = \text{const.}$) and the relation (5) was obtained by Lidov (1961).

The difference in longitude of perihelion of the orbits of particles ejected from the parent comet nucleus at the velocities of 650 m/s averages 5° - 10° over the period under review. Hence, we may assume that the stream precesses around the Sun as a single whole. In order to estimate the stream shape under the influence of planetary perturbations we shall assume the first approximation:

$$\pi = \Omega + \omega = C_3 = \text{const.} \quad (6)$$

The orbital evolution rate is estimated by the semimajor axis, so as time passes the particles will fill out the total volume in space defined by both the relations (4-6) and differences in a . Plenty of orbits filling out the volume may be obtained in the following way. The values of $C_1 = 0.13$ and $C_2 = 0.29$ correspond to the orbital semimajor axis of 1.65 AU. Giving the argument of perihelion values from 0° to 360° and using (4-6) we are able to derive e , i , and Ω . Plenty of calculated orbits with $a = 1.65$ AU would define the outer (with respect to the Sun) surface bounding the meteor stream. Using the analogous method for the orbit with $a = 1$ AU and $C_1 = 0.20$, $C_2 = 0.27$ we obtain the surface restricting the stream on the inside surface. In order to estimate the shape of the volume in space restricted by the derived surfaces, we have constructed cross-sections of these surfaces in a plane perpendicular to the velocity vector at different points of the present orbit of the asteroid 1983 TB. For simplicity, when constructing the cross-sections, the inclination of the asteroid orbit was assumed to be zero. Fig. 1 illustrates some of the calculated cross-sections. Fig. 2 shows the Geminids spatial shape constructed using these cross-sections. This shape differs very much from traditional notions of meteor streams. Eventually, due to planetary perturbations, the Geminid stream takes on a shape most characterized by stream thickness perpendicular to the ecliptic plane. At the distance of 1 AU from the Sun the ratio between the stream's width and its thickness is 1:10.

Let us estimate the time during which the Geminids can take the form caused by long-period planetary perturbations. It may be assumed that the particles will fill out the total volume when the nodal lines of orbits with maximum and minimum semimajor axes differ by 180° - 270° . According to data presented in Table 1, the nodal lines of orbits with $a = 1.00$ AU and $a = 1.65$ AU will differ by 270° in another 20 thousand years. Hence, the volume in space estimated by the relations (4-6) and by the differences in a is considered to be filled out.

The investigation of secular variations in the radii-vectors of the ascending and descending nodes of the Geminids orbit with semimajor axes from 1 to 1.65 AU shows that at present (i.e., over 20 thousand years after the stream's formation) only four groups of particles could intersect the Earth's orbit. These groups produce meteor showers: the Geminids, Daytime Sextantids, Canisids (a radiant in the Canis Minor constellation) and Daytime δ -Leonides. The orbital semimajor axes of particles responsible for these showers are close to the values of 1.36 AU, 1.15 AU, 1.65 AU and 1.55 AU respectively.

Observation data show that among these four meteor showers at least three are active, namely the Geminids, Canisids [the shower "B" found by

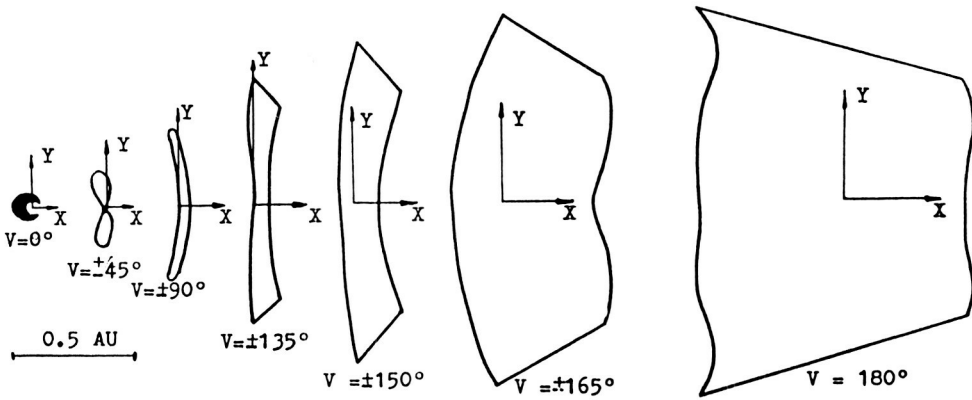


Fig. 1 The model Geminid stream cross-sections in the planes perpendicular to the velocity vector of the asteroid 1983 TB orbit (at $i = 0^\circ$) at different values of true anomaly V .

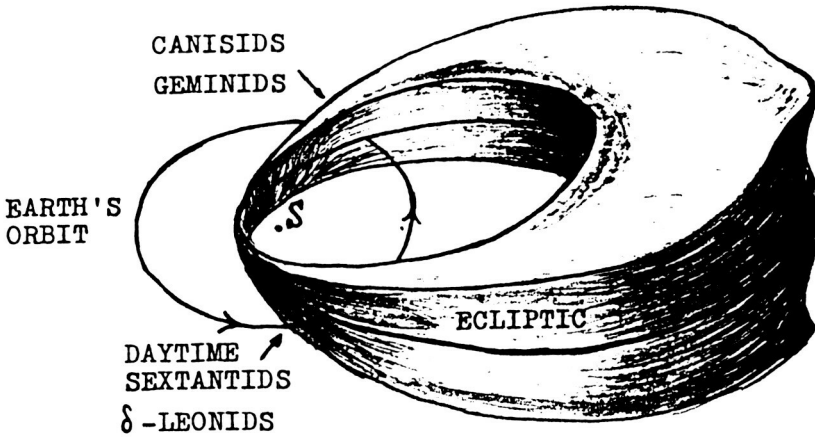


Fig. 2 The Geminid stream shape.

KRESAKOVA (1974)] and Sextantids. The shower "B" was discovered by KRESAKOVA from photographic and visual observations. She also suspected the Canisids and Sextantids to be associated with the Geminids.

At the distance of 1 AU from the Sun, in the region of intersection of the Sextantids orbit with that of the Earth, the stream thickness defined by the observed mean orbits of the Geminids and Canisids is 0.7 AU. This agrees well with the above Geminid stream model.

By the way, it should be mentioned the MCINTOSH and HAJDUK (1984) also came to the conclusion that the stream associated with Halley's comet had a considerable thickness. According to their investigations the stream thickness is 0.44 AU and its width - 0.044 at a distance of 1 AU from the Sun.

As is known in the case of the Geminids, the Earth first encounters small particles and then later the large ones. In the case of the Sextantids the Earth crosses the stream from the outside, so that we should expect the reverse picture, i.e., meteors having more prolonged radioechoes must occur preferentially at the beginning of the shower activity. In connection with this, a careful study of the Sextantids meteor shower and searches for a northern branch the δ -Leonids are of interest.

Now we shall consider the question of the Quadrantids stream shape assuming from observation that the orbital semimajor axes of particles are in the range of 2.8-3.1 AU. First, it should be noted that for the orbits of this stream the equations (4-5) are satisfied only qualitatively. Calculations of secular perturbations of the orbital elements carried out by the Halphen-Goryachev method as well as by the method of Runge-Kutta (WILLIAMS et al., 1979) give a wider range of variations in inclination (from 12° to 74°) (BABADJANOV, OBRUBOV, 1979b, 1980) as compared to the range obtained from equations (4-5): $28^\circ \leq i \leq 73^\circ$. Longitudes of perihelion of the Quadrantids orbits liberate in small ranges. So, using the equations (4-6) we may derive a lower limit of the volume in space which may be filled out by the Quadrantid particles in time. The result of investigation of the Quadrantid meteor stream evolution by the numerical method of Runge-Kutta show that the particles have differences only in initial positions on the orbit and then under the influence of Jovian perturbations the orbital elements of these particles may differ strongly. Here, in contrast to the Geminids, the evolution rate is estimated not only by the orbital semimajor axis, but the positions of particles on their orbits. This leads to quicker filling out of the stream volume estimate by the long-period perturbations, i.e., to a quicker formation of the stream branches. The cross-section of the Quadrantids on the ecliptic plane is presented in Fig. 3. The distinctive feature of the Quadrantids (in comparison with the Geminids) is a narrow "jet" near perihelion caused by the orbits of the highest inclinations and of the largest perihelion distances. The Quadrantids shower is observed at the intersection of this jet. One other interesting feature of the Quadrantids shape lies in the fact that the Earth crosses the stream three times, i.e., in principle, this stream can produce three pairs of meteor showers. We have calculated theoretical geocentric radiants and velocities for the Earth-crossing orbits at points different from the place where the Earth encounters the Quadrantids. The results showed that the Daytime Arietides (COOK, 1973) and the association No. 78 (KASHCHEJEV et al., 1967) with the radiant near α -Ceti as well as the Southern and Northern δ -Aquarides (COOK, 1973) could result from encounters of the Quadrantids stream with the Earth.

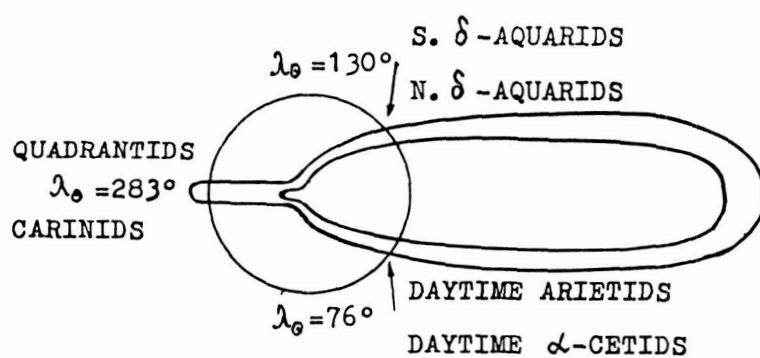


Fig. 3 The model Quadrantid stream cross-section in the ecliptic plane.

Theoretical shower radiants and velocities were obtained from calculations of secular perturbations of the Quadrantids mean orbit by the Halphen-Goryachev method.

Thus, the investigation of the Quadrantids meteor stream evolution and its comparison with observations give evidence of the supposed interrelations between the Quadrantids and δ -Aquirids (HAMID and WHIPPLE, 1963), on the one hand, and between the δ -Aquirids and Daytime Arietids on the other (COOK, 1973). The similarity in the heights of beginning, maximum brightness and end as well as in ablation coefficients and in indices of progressive fragmentation of the Quadrantids, δ -Aquirids and Daytime Arietids meteors (JACCHIA et al., 1965; VERNIANI, 1973) obviously given evidence that these showers are produced by the same stream.

A scantily studied question of the meteor stream dynamics is an estimate of the stream lifetime. The survival time of meteor particles seems to be better studied. Principal mechanisms of meteor stream disintegration are the Poynting-Robertson effect, the exhaustion by large planets and catastrophic collisions with sporadic meteoroids. The most effective mechanism is the last one (DOHNANNY, 1974; TOKHTASJEV, 1982).

Previously, on the assumption that the Geminids and Quadrantids have roughly equal width and thickness according to the calculations of the variation of orbital radii-vectors at the nodes, a conclusion was made that the observable periods of the corresponding showers are short (200-400 yr) (PLAVEC, 1950; BABADJANOV, OBRUBOV, 1980; HUGHES, WILLIAMS, MURRAY, 1980; FOX, WILLIAMS, HUGHES, 1983). In the light of new notions of the streams shape, one may conclude that the observable periods of the Geminids and Quadrantids can be comparable with the life-times of these meteor streams. Arguments in favor of such long observable periods are based on the ancient observations (IV-XII centuries) of fireballs with radiants in constellations of Gemini and Mural Quadrant during periods corresponding to the present active periods of the Geminids and Quadrantids (ASTAPOVICH, TERENTJEVA, 1968).

Thus, the results of investigation of the Geminids and Quadrantids meteor stream evolution show that under the influence of planetary perturbations, the stream may originally be flat but then thicken depending on the variation range of orbital inclinations. Eventually, due to planetary perturbations, a meteor stream may take such a shape as to cause the start of several active showers at different solar longitudes.

References

1. Astapovich I. S., Terentjeva A. K., 1960, in Physics and Dynamics of meteors, eds. Kresak L., Millman P., Reidel Pub. Co., Dordrecht, Holland, p. 308.
2. Babadjanov P. B., Obrubov Yu. V., 1979a, Dokladi Akad.nauk Taj. SSR, 22, 8, 46.
3. Babadjanov P. B., Obrubov Yu. V., 1979b, Dokladi Akad.nauk Taj. SSR, 22, 12, 730.

4. Babadjanov P. B., Obrubov Yu. V., 1980, in *Solid particles in the Solar system*, ed. Halliday I., McIntosh B., Reidel Pub. Co., Dordrecht, Holland, p. 157.
5. Babadjanov P. B., Obrubov Yu. V., 1983, *Highlights Astron.*, 6, 411.
6. Babadjanov P. B., Obrubov Yu. V., 1984, *Soviet Astron. J.*, 61, 5, p. 1005.
7. Cook A. F., 1973, NASA SP-319, p. 183.
8. Dohnany J. S., 1970, *J. Geophys. Res.*, 75, 17, p. 3468.
9. Fox K., Williams I. P., Hughes D. W., 1983, *Month. Not. R. Astron. Soc.*, 205, 3, p. 1155.
10. Jacchia L. G., Verniani F., Briggs R. E., 1965, SAO SR No. 175.
11. Hamid S. E., Whipple F. L., 1963, *Astron. J.*, 68, 8, p. 537.
12. Hughes D. W., Willimas I. P., Murray C. D., 1980, in *Solid particles in the Solar system*, eds. Halliday I., McIntosh B., Reidel Pub. Co., Dordrecht, Holland, p. 153.
13. Kascheyev B. L., Lebedinets, V. N., Lagutin M. F., 1967, *Meteoric phenomena in the Earth's atmosphere*, Nauka, Moscow.
14. Kresakova M., 1974, *Bull. Astron. Inst. Czech.*, 25, 1, p. 20.
15. Lidov M. L., 1961, *Iskusstvennie Sputniki Zemli*, 8, 5.
16. McIntosh B. A., Hajduk A., 1983, *Month. Not. R. Astron. Soc.*, 205, 3, p. 931.
17. Plavec M., 1950, *Nature*, 165, 4192, p. 362.
18. Radzievskij V. V., 1951, *Soviet Astron. J.*, 28, 5, 363.
19. Sekanina Z., 1976, *Icarus*, 27, 2, p. 265.
20. Tokhtashev V. S., 1982, in *Meteoric matter in interplanetary space*, eds. Belkovich O. I. et al., Moscow-Kazan, p. 162.
21. Verniani F., 1973, *J. Geophys. Res.*, 78, 35, 8429.
22. Whipple F. L., 1951, *Astrophys. J.*, 113, 3, 464.
23. Williams I. P., Murray C. D., Hughes D. W., 1979, *Month. Not. R. Astron. Soc.*, 189, 2, p. 483.

ELEMENTARY PROCESS AND METEOR TRAIN SPECTRA

O. G. Ovezgeldyev

Physical Technology Institute
Ashkhabad, USSR

Interaction of the atmosphere and meteors is a unique phenomenon out of a great number of elementary processes taking place in gases. Ionisation, recombination, attachment, ion-exchange reaction, diffusion, and other processes connected with the ionized component manifest themselves as ionized meteor trails that can be observed by radars. Excited atoms and molecules of meteor and atmospheric origin, in their turn, determine meteor radiation and make them visible.

The theory of meteor radiation and ionization founded by ÖPIK E.J. (1933, 1955, 1958) and HERLOFSON N. (1948) has made considerable headway. It has been generally established that meteor radiation includes several characteristic parts: coma, wake and train (ASTAPOVICH, 1958; CEPLECHA, 1964, 1968, 1973; MILLMAN 1935, 1962, 1963, 1872; HALLIDAY, 1958, 1960, 1963). The Coma is a gaseous sheath encircling the meteor body and consisting of a mixture of air and vaporized meteor atoms and molecules. The lion's share of meteor radiation comes from the coma. The wake content is practically the same and stretches behind the meteor body for up to one kilometer. In some meteors, luminous trains are sometimes visible with the naked eye but they can always be easily detected by radar.

In the formation of the wake and train, meteor fragmentation plays a certain part along with elementary processes. The process of meteor fragmentation into large pieces can be observed both visually and optically (BRONSHTEN, 1981; ASTAPOVICH 1958; KRAMER and SHESTAKA, 1983). Upon separation from the parent body, fragments continue to evaporate becoming an additional source of the elementary processes causing meteor phenomena. Therefore, even though complicating somewhat the pattern of wake and train formation, fragmentation of itself cannot serve as the clue to the problem of meteor phenomena.

The meteor (coma) radiation spectrum contains mainly lines of atoms and ions of chemical elements of meteor origin (FeI, MgI, NaI, CaI, NiI, CaII, FeII, SiII, etc. -- about 20 all told) and depends largely on velocity, composition and structure of a meteor body. Ionic spectra are often observed in fast meteor radiation with the share of atmospheric bands and lines in it being very small (no more than several percent). The wake spectrum is characterized by a far lower excitation potential than the meteor itself. While a great volume of observational data concerning meteor spectra is constantly reviewed in the literature (BRONSHTEN, 1981; ASTAPOVICH, 1958; SMIRNOV, 1977; CEPLECHA, 1968; MILLMAN 1963; HALLIDAY 1960, 1963), the problem of meteor radiation still remains a most complicated and scantily explored one. The present paper deals with findings of research into the problem and tries to formulate the most pressing tasks for further investigation in this very important field of meteor physics.

Elementary and diffusion processes of meteor train decay have been studied chiefly using results of observations of radio-echo duration over a wide range (from fractions of a second to several minutes) and characteristic changes in distribution trends. According to this, the main part in the meteor train decay is played by ambipolar diffusion, dissociative recombination,



recombination with electron stabilization,



electron attachment with neutral particles of atmosphere, and meteor



and atmospheric turbulent diffusion, (BRONSHTEN, 1981; KASHCHEEV et. al 1967; MANNING, 1958; FIALKO, 1961; BIBARSOV, 1979; TOKHTASJEV, 1976; POOLE and KAISER, 1967; NICHOLSON and POOLE, 1974; BAGGALEY and CUMMACK, 1974). The effectiveness of a particular process in the meteor decay is determined by its time-constant and probability as well as by the initial electron concentration in the trail. Specifically, the turbulent diffusion time constant is far greater than that of other processes, therefore it is typical only in long-lived meteor train decay. Ambipolar diffusion, on the contrary, plays the leading role at the beginning of a train. Various deionization processes accompanying meteor train decay cause intermediate breaks in the radio echo duration distribution.

Radar methods of observation, having a number of technical advantages, limit somehow the possibility of research into elementary processes of meteor wakes and trains for they are known to yield data bearing only on the electron component, usually giving no information about cross section and lengthwise distribution. The same can be said about ion and excited particle composition. Naturally, possessing so scanty experimental data, one cannot hope to definitely solve all the numerous problems of meteor physics.

The ion composition and role of various chemical reactions in the meteor trail decay was studied by BAGGALEY and CUMMACK (1974, 1976, 1979) using numerical simulation. Four kinds of metallic ions (Fe^+ 48.4%, Si^+ 33.9%, Mg^+ 10.4%, Na^+ 7.3%) were considered by them as initial data. Attachment and detachment, ion exchange reactions, radiation, dissociative recombination, and other processes were taken into account. Calculations were made for 70, 80, 90 and 100 km both for day and night. According to their results, the deionization process of meteor train decay is confined only to heights below 80 km. Along with metallic ions, their oxides and dioxides are present at all heights. The change in the ion composition from day to night is due largely to a diurnal change in O_2 atoms concentration. At 100 km, there was no significant difference between the day and night ion composition.

Radiation spectra contain plentiful information on elementary processes of meteor phenomena. For instance, CEPLECHA (1971) managed to detect a record number of nearly 1,000 spectral lines during a -12.5^m bolide flare.

Initial meteor train spectra were obtained in 1966 in Ashkhabad by NASYROV and NASYROVA (1966) using an optical system equipped with an octahedral prism. A meteor that produced this stable long-lived train belonged to the Leonid shower. But the system's insufficient linear dispersion made detection and identification of spectral lines difficult. Still, the analysis of radiation energy spectral distribution showed that meteor train luminescence was due mainly to the long-wave range of the spectrum ($\lambda > 5000\text{\AA}$). In addition, the train showed the signs of NaI ($\lambda 5895\text{\AA}$), MgI ($\lambda 5182\text{\AA}$) and OI ($\lambda 5577\text{\AA}$) lines.

Experimentally the task of registering meteor train spectra presents a rather complicated task needing a mobile optical system of great sensitivity and resolution and operating in the regime of very quick (fractions of a second) processes. It is only thanks to the progress of TV and electronic technology that this extremely difficult technical task has become a reality. First experiments using TV for meteor observations were held in Canada in the sixties (HEMINGWAY, et al, 1971; MILLMAN et al, 1971; MILLMAN and CLIFTON, 1975; SPALDING et al, 1961), and in the seventies they were started in the Soviet Union in Ashkhabad.

The theoretical sensitivity of modern TV equipment reaches stars of 14^m . It goes without saying that due to a weakening of optical signals within the dispersing elements, the limit is considerably lower. Nevertheless, in contrast to photographic methods, TV and optical electronics enable the use of shorter exposures so that it is possible to obtain separate spectra of coma, wake and trains as well as to study the temporal dependence of certain spectral line intensities. By way of example, Fig. 1 shows a spectrogram of a meteor of about -1.5^m obtained in Ashkhabad using an optical electronic image-tube having an exposure of 1.0s. The first frame gives the initial meteor spectrum, the second shows a spectrum of the meteor train with the lines MgI ($\lambda 5183\text{\AA}$), OI ($\lambda 5577\text{\AA}$), NaI ($\lambda 5890\text{\AA}$), Si II ($\lambda 6358\text{\AA}$), OI ($\lambda 7772\text{\AA}$), etc.

As was to be expected, the spectra of the wake and trains are much weaker than those of the coma and are characterized by lower excitation potentials.

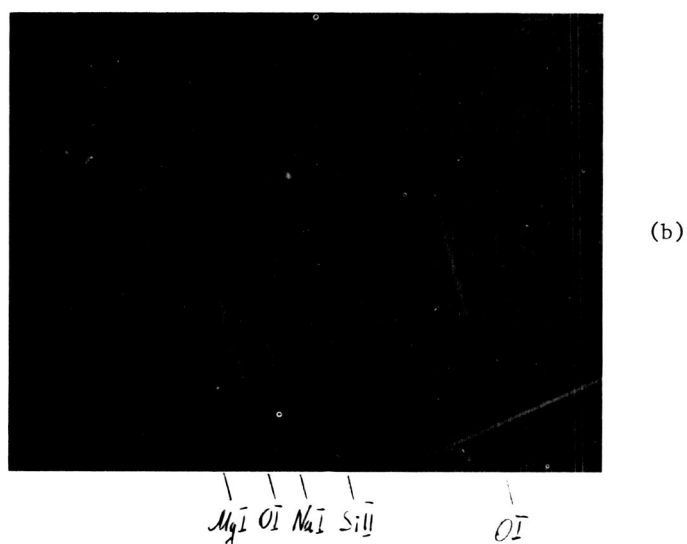
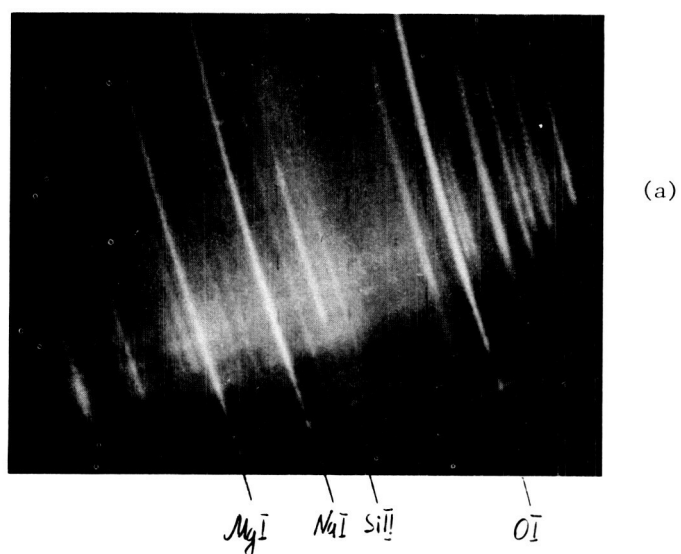


Fig. 1. Spectrogram of a meteor of ~ -1.5 m obtained in Ashkhabad. (a) is the initial meteor spectrum, (b) a spectrum of the meteor train.

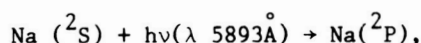
Table
Multiplets identified in the wake and train spectra.

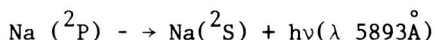
Numbers of Multiplets	
OI	1, 4, 3 (forbidden line)
NaI	1
MgI	1, 2, 3, 9
SiI	3
CaI	1, 2, 3, 4, 18, 19, 21
FeI	1, 2, 3, 4, 5, 16, 20, 21, 23, 41, 42, 43, 268
FeII	27, 28, 37, 38, 42, 48, 49
CaII	1, 2
SiII	2, 4
N ₂	1 positive lines system

The spectral composition of radiation consists mainly of multiplets of atoms and their ions. As to molecular lines, only the first positive system of N₂ has been positively identified as yet. An important peculiarity of meteor train radiation is the emission of the forbidden line OI (λ 5577Å) which is usually very bright and is characterized by a relatively long duration. The rate of spectral lines extinction is different. Multiplets 1, 2, 3, 13, 14 of FeI and the MgI (5183Å) lines last the longest.

Some elementary processes typical of meteor train radiation have been considered.

- a. Sodium radiation. While spectra of the meteor coma and wake reveal eleven multiplets of Na radiation, meteor trains, as it was noted above, appear to possess only the doublet of λ 5890Å and λ 5893Å as yet. The yellow doublet is known to be the strongest of the sodium lines and is also observed in spectra of night emission and twilight luminescence of the upper atmosphere. Besides, intensive resonance scattering by sodium according to the scheme:





has been widely observed in recent years by lidar probes of the upper atmosphere (KHROSTIKOV, 1963; BAGGALEY and CUMMACK, 1979).

The mechanism of NaD doublet excitation was studied by S. CHAPMAN, (1955) W. BAGGALEY (1976) and others. The excited atoms of Na responsible for the yellow doublet radiation turned out to be a product of oxidation reactions, namely:



An approximate numerical analysis of this catalytic cycle of Na considering diffusion is provided in BAGGELEY (1976) where it is shown that a meteor with brightness over -10^{m} can produce a luminescent trail of over one hour duration.

- b. Meteor Atoms and Their Ionic Radiation. Elementary chemical reactions producing metallic atoms and ions have been the subject of intensive study during the last few years. Just as with Na, the chemistry of these particles to a great extent depends on oxidation reaction with O_3 , i.e.,



At relatively low heights the process of oxidation may have the following stages:



Here X, Y are atmospheric molecules of O_2 , N_2 , with excited metallic atoms M^* appearing as a product of the dissociative reaction:



According to J. POOLE's estimates (1978, 1979b) radiation of certain multiplets of FeI, MgI, CaI in the meteor tail and trails can be explained by the chemical reactions (7-10).

The process of resonance charge-exchange of atom and molecular systems, that is



occupies an important place in the chemistry of meteor trails. X^+ ions of atmosphere molecules are a product of ionization, resulting from their collision:



J. POOLE (1979a) explains the appearance of the multiplet of H and K CaII lines, first positive line N_2 and separate multiplets of FeII by the processes (11, 12). The resonance H and K CaII lines are known among the brightest features of photographic meteor spectra. Most often these lines are observed in fast meteors. But when large meteor bodies enter the atmosphere with a flare, they show sharply increased lines of H and K CaII. J. RAJCHL (1972) when studying radiation of large meteor bodies came to the conclusion that, unlike the turbulent flow regime, flare-caused H and K CaII multiplets do not appear due to the resonant charge exchange, but as a result of radiative recombination of double-ionized CaIII. This process was subjected to a quantitative analysis by KRAMER and SHESTAKA (1983) of the H and K CaII lines in the wake of a bolide observed on August 13, 1974 by the instant exposure method.

- c. The Study of Atomic Oxygen Forbidden Green Line. This line appears at rather high altitudes at the starting point of luminescence of meteor bodies having a great velocity. It reaches its maximum about 0.1 s into a meteoroid flight. These peculiarities of the 5577A line radiation lead one to believe that excitation of OI responsible for this radiation is a result of ionization and recombination processes in the meteor wake and trains (BAGGALEY, 1976, 1977, 1978; OVEZGELDYEY et al., 1976; BAKHARAV, et al., 1970) according to which the excited $O(^1S)$ atoms, causing the green line emission, result mainly from two-phase chemical reactions:



Considering the possibility of $O(^1S)$ transformation from its 1D condition into a 3P condition and deactivation by collisions,



BAKHAREV et al (1970) derived an expression enabling them to determine the time dependence of the 5577A line relative intensity. That is,

$$\frac{I}{I_0} = 2 \exp(-At) - \exp(-kt) \quad (17)$$

The coefficient A depends on altitude, while coefficient K depends both on altitude and meteor body parameters at the level of E-region where A of the green line is about 2.7 s^{-1} .

The formula (17) makes it possible to account for the basic morphological peculiarities of the green line in meteor train spectra. It is in keeping with this formula that the 5577Å emission can be observed only at the start of meteor entry into the ionospheric E-region. The density at lower altitudes makes collision deactivation likely. If the coefficient A equals 2.7 s^{-1} at 100 km, it is about 100 s^{-1} at 80 km. The same effect explains the fact that this line is usually observed only in trains of fast meteors, the latter being known to start luminescence at higher altitudes than slower ones.

Thus, in this short review it is possible to see that considerable progress has been achieved in this area of meteor physics. The conventional observational approach to this study continues to make progress with hardware being extended and improved. In this context, special emphasis should be given to the TV and optical electronic methods from which unique data on faint meteors spectra and, what is more, spectra of their trains have been obtained.

Mechanisms of excitation of individual spectral line radiation have been studied experimentally and theoretically and it has been demonstrated that such processes as oxidation, resonant charge exchange, dissociative recombination and others play an important part in the chemistry of excited particles. The foundation has been laid toward simulating the elementary processes of meteor physics. Having a number of advantages and possibilities, this method is sure to find a wide use in the future. Speaking of future research, it must also be noted that the problem of further improving spectral observations and the methods of quantitative analysis is very important with a view to carrying out comprehensive radar, optical, optical electronics and TV measurements. Together these can help solve many problems facing meteor physics.

References

- Astapovich, I.S., 1958, Meteor Phenomena in the Earth's Atmosphere, Moscow, Phizmatgiz Publ., p. 640.
- Baggaley, W.J., CUMMACK, C.H., 1974, Meteor Train Ion Chemistry, J. Atmos. and Terrest. Phys., V. 36, No. 11, p. 1759-1773.
- Baggaley, W.J., 1976, The Chemical Reduction of Meteoric Metal Oxides as a Source of Meteor Train Emission, Bull. Astron. Inst. Czechsl., V. 27, No. 4, p. 244-246.
- Baggaley, W.J., 1976, The Quenching of Meteoric OI Forbidden Radiation, Bull. Astron. Inst. Czechosl., V. 27, No. 5, p. 296-300.

- Baggaley, W.J., 1977, The Velocity Dependence of Meteoric Green Line Emission, *Bull. Astron. Inst. Czechosl.*, V. 28, No. 5, p. 277-280.
- Baggaley, W.J., 1978, Observational Data Concerning the Meteoric 5577Å Emission, *Bull. Astron. Inst. Czechosl.*, V. 29, No. 1, p. 59.
- Baggaley, W.J., Cummack, C.H., 1979, The Duration of Long-Lived Meteor Trains, *Bull. Astron. Inst. Czechosl.*, V. 30, No. 3, p. 180-183.
- Bakharev, A.M., Nasyrova, L.I., Shodiev, U., 1970. A Meteor Train Spectrum Study, *Bull. Taj. Astrophys. Inst.*, No. 53, p. 14-18.
- Beghanov, M., Gulmedov, H., Polyakov, M., Mukhamednazarov, S., 1972, *Ibid.*, NO. 690, P. 6-7.
- Bibarsov R. SH., 1979, Neutral Meteor Particles Impact on Electron Concentration in Meteor Trails, *Repts. of Tajik SSR Acad. Sci.*, V. 22, No. 10, p. 592-595.
- Bronshiten, V.A., 1981, *Physics of Meteor Phenomena*, Moscow, Nauka Publishers.
- Cepplecha, Z., 1964, *Bull. Astr. Inst. Czechosl.*, V. 15, No. 3, p. 102-112.
- Cepplecha, Z., 1968, in: *Physics and Dynamics of Meteors* (Eds. Kresak, Millman), Dordrecht-Holland, D. Reidel Publ., p. 73-83.
- Cepplecha, Z., 1971, *Ibid.*, V. 22, 219-304.
- Chapman, S., 1955, in: *The Aurora and Airglow* (Eds. Armstrong and Dalgarno, Pergamon Press), p. 204.
- Dalgarno, A., 1965, Excited Molecules Oscillation in Atmosphere Reactions, in: *Elementary Processes in the Upper Atmosphere*, MIR Publ., Moscow, p. 71-78.
- Fialko E.I., 1961, *Radar Meteor Observations*, Moscow, Soviet Radio Publ.
- Gulmedov, H., Beghanov, M., Polyakov, M., Krushchev, L., 1971, TV Meteor Observations in Ashkhabad, *Astron. Circular*, No. 607, p. 6-7.
- Halliday I., 1958, *Astrophys. J.*, v. 127, No. 2, p. 245-252.
- Halliday I., 1960, *Ibid.*, v. 131, No. 1, p. 25-33.
- Halliday I., 1963, *Ibid.*, v. 25, No. 5, p. 47-57.
- Hemenway C.L., Swider A., Bowman C., 1971, Meteor Spectroscopy Using an Image Orthicon, *Canadian J. Phys.*, V. 49, No. 10, p. 1361-1364
- Herlofson N., 1948, *Repts. Prig. Physo.*, v. 11, p. 444-454.

Kashcheev B.L., Lebedinets V.I., Lagutin M.F., 1967, Meteor Phenomena in the Earth's Atmosphere, Moscow, Nauka Publ., p. 260.

Khvostikov, I.A., Physics of Ozonesphere and Ionosphere, Sov. Acad. Sci. Publ., 1963, Moscow, p. 663.

Kramer, E.N., Shestaka, I.S., 1983, Meteor Matter in the Earth's Atmosphere and Off-Sun Cosmic Space, Nauka Publ., Moscow.

Manning L.A., 1958, J. Geophys. Res., v. 63, p. 181-196.

Millman P.M., 1935, Ann Harvard Coll Obs., v. 82, No. 7, p. 149-177.

Millman P.M., 1962, J. RAS Canada, v. 56, p. 263-252, 263-267.

Millman P.M., 1963, Smiths Contr. Astrophys., v. 7, p. 119-127.

Millman P.M., Cook A.F., Hemenway C.L., 1971, Spectroscopy of Perseids Meteors with an Image Orthicon, Canadian J. Phys., V. 49, No. 10, p. 1365-1373.

Millman P.M., Clifton K.S., 1975, SEC Vidicon Spectra of Geminids Meteors, Ibid., V. 53, No. 19, p. 1939-1947.

Nasyrova L.I., Nasyrov G.A., 1966, Astron. Circular NO. 370, p. 1-2.

Nicholson T.F., Poole L.M.G., 1974, The Observed Characteristics of Radio Echoes from Overdense Meteor Trains, Planet. and Space Sci., V. 22, No. 12, p. 1669-1690.

Opik E.J., 1933, Acta et commentat. Univ. Tartu, v. 26, No. 2, p. 1-39.

Opik E.J., 1955, Proc. Roy. Soc., ser. A, V. 230, p. 463-501.

Opik E.J., 1958, Physics of Meteor Flight in the Atmosphere, N.J., Interscience Publ.

Ovezgeldyev O., Mukhamednazarov S., Gulmedov H., 1976, Oxygen Green Line in Meteor Train Spectra, I Repts. Taj. Acad. Sci., No. 4, p. 57-61.

Ovezgeldyev O.G., Berkeliev M., Lagutin M.F., Lebedinets V.N., Savrukhin A.P., 1983, Magnetosphere as a Natural Laboratory for Interplanetary Dust Izvestiya Acad. Scie. Taj. SSR, No. 1, p. 32-43.

Poole L.M.G., Kaiser T.R., 1967, The Duration Distribution of Radio Echoes Obtained from Under Dense Shower Meteor Trains, Planet. and Space Sci., V. 15, No. 7, p. 1130-1150.

Poole L.M.G., 1978, The Decay of Luminosity in the Trains of Moderately Bright Meteors, Planet. Space Sci., V. 26, No. 7, p. 697-701.

Poole L.M.G., 1979b, The Excitation of Spectral Lines in Faint Meteor Trains, J. Atmos. Terrest. Phys., V. 41, No. 1, p. 53-64.

Rajchl J., 1965, On the Possible Connection Between the Auroral Green Line in Meteor Spectra and the Head-Echo Phenomenon, Bull. Astron. Inst. Czechosl., V. 16, No. 5, p. 282-284.

Rajchl J., 1972, Shock Waves and Flares by Meteors, Bull. Astron. Inst. Czechosl., V. 23, No.6, p. 357-366.

Smirnov V.A., 1977, in: Historic and Astronomical Studies, Iss. 13, p. 235-274.

Spalding, J., Dugan J. F., Hemenway C.L., 1961, Experiments with High Sensitivity Image Orthicons, Astron. J., V. 66, No. 7, p. 296.

Tokhtashev V.S., 1976, EAO Proceedings, Iss. 41-42, p. 225-227.

THE ARCHIVING OF METEOR RESEARCH INFORMATION
NECHITAILENKO V.A.

Soviet Geophysical Committee
Moscow, USSR

As was noted in the GLOBMET Planning Document, the project has as its main aim intensification of research in the fields of meteor astronomy and meteor geophysics on the basis of recent achievements in these fields and expansion of international cooperation into meteor research.

The GLOBMET Project has become one of the most popular projects out of which fruitful international cooperation in meteor research is successfully developing. Our Symposium and participation in it of representatives of many meteor research centers give convincing evidence of this.

The author's intention is not to review the results obtained over the past years under GLOBMET but to discuss some of the problems the solution of which will guide further development of meteor investigation and international cooperation in this field for the near term. Of course, the main attention will be paid to problems which the meteor community itself can solve, or at least expedite a solution. Most of them are more or less connected with the problem of "information archiving"!

"Information archiving" deals with methods and techniques of solving two closely connected groups of problems. The first one concerns the analysis of data and information as an integral part of meteor research and dealing with the solution of certain methodological problems. The second deals with gathering data and information for the designing of models of the atmosphere/meteor complex and its utilization.

Essentially GLOBMET is a methodologically-oriented project. Following Fig. 1 which shows in a simplified form main components of scientific investigation and connections between them it can be said that to achieve its goals (theories and models) the project focuses attention on experiment, data gathering and analysis as the initial points.

There are at least two areas where joint efforts can produce the maximal possible effect. The first is expansion of meteor observation networks, installation of new observatories, modification of old ones, unification of soft- and hardware parameters and fitting them into an agreed unified series.

The second line along which international cooperation under GLOBMET should develop (and probably the more promising one) is connected with the creation of data bases and archives, as well as improvement of international data exchange and the "suppliers/users" interaction.

a) Gathering, processing and managing of data.

The concept of gathering, managing and exchange of data, as it was defined when the WDC system was created, has mainly a discipline-oriented character. Such approach does not secure solution of many tasks, in the first place that of compatibility of data belonging to different scientific disciplines. The modern approach to the interpretation of atmospheric and

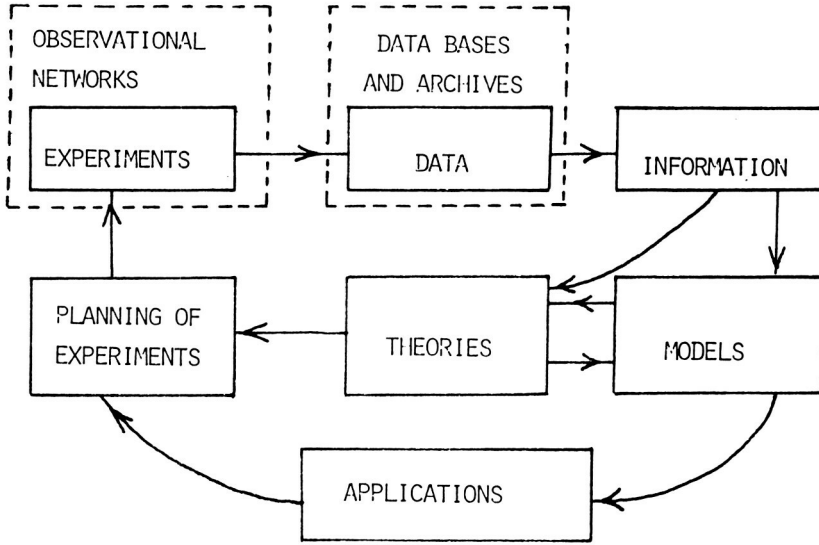


Fig. 1 Scientific investigation components and connections among them.

meteoric phenomena involves data obtained using a wide spectrum of measuring devices and installations. The problem of data compatibility seems to be one of the most important issues here.

Designing an effective data managing system presupposes solving, among others, the following problems:

- development of coordinated conceptional data models and their unification;
- designing of Integrated Data Processing System as an aggregate of data bases and software for checking, editing and processing of data interacting through a certain standard interface;
- ensuring of compatibility, homogeneity and representativity of data.

The Draft Manual on Meteor Radar Observations recommends as a first step a no more than 2- or 3-level structure of data so that future recommendations would not conflict with present protocols and software.

b) Data classification.

At present there is no unified meteor data classification (or Planetary Geophysics data, for that matter). Most common are a hierarchial approach to data exchange accepted by the WDC-A and WDC-B (1981) and the data classification used by the MAP Data Management Committee (1982).

The first approach deals with classification of data levels according to the type of data center. The second deals with the data representation level, i.e., data structure and formats.

The second approach corresponds to the classification proposed in the Fifth Edition of the ICSU Guide to International Data Exchange through the WDCs. This classification is based on processing, organization and analysis of data.

Level-0: Physical samples from which useful information is derived;

Level-I: Analog or digital observational/instrumental data in engineering units, e.g. radiosonde, telemetry, ionograms, etc;

Level-II: Scaled and calibrated observational data (Level-0 or Level-I) transformed into scientific units and variable parameters derived from a mix of observational data, e.g. cloud tracked winds, meteor radar winds, temperature profiles, etc.

Level-III: Analyzed fields, model output products, and special computational or processed results tailored to users requirements, e.g. hemispheric/global analyzed grid-point fields of wind direction/speed, etc.

c) Data accessibility.

When one works with data in the Center using some sort of soft- and hardware to implement searches by important classification parameters

(keyword), the level of technical accessibility of data becomes quite important.

Levels of accessibility of various kinds are compared in the Table with those defined by the MAP Data Committee as the Technical Status of data and are as follow:

First level (I-level) - data in machine-readable form presented in agreed formats of international data exchange (WDC's formats)

Second level (R-level) - data in machine-readable form presented in regional or/and individual formats (formats of regional data centers)

Third level (A-level) - analog data and hard copies.

Table I.

Data media	I	I	
Technical status of data according to MAP classification	I	I	
	I	I	
	I	I	Machine-readable
	I	I	(cards, tapes, discs, etc.)
	I	I	Others
	I	I	
Local individual formats	I	I	
	I	I	R-level
	I	I	
Formats of regional centers	I	I	
	I	I	
	I	I	A-level
	I	I	
International formats	I	I	I-level
	I	I	

The technical accessibility of data is only one of the parameters of logical and physical accessibility of data to users, but problems that need to be solved go far beyond those only of logical and physical accessibility.

Everyone knows that the development of research techniques, the use of more and more up-to-date means of measurement and observation, especially when carrying out comprehensive information-saturated experiments, lead to a situation when one needs more frequent access to data but utilization is found to be restricted by authors and owners of data. This restriction is intended to prevent uncontrolled copying, dissemination and use of data. The traditional WDC concept of free data exchange and dissemination does not guarantee author's sole rights to data and results of data analysis.

Further development of "suppliers/users" data exchange on an international scale should have the highest priority to accompany the existing WDC system (or as its integral part) with a special service providing the exchange of "non-free" data. Most such data are obtained during special observational campaigns or using unique devices. For convince sake, we shall use the term "project data" for any sort of data that are not free.

Each unit of such data included in the Data Archives is proposed to be accompanied with a special parameter, namely, the Copyright Level (CL). Values of the Copyright Level are defined below:

CL=1 free data (data for free dissemination),
 CL=2 data, distribution among project/campaign participants,
 CL=3 data which can be copied only by permission of the author/owner.

The CL=3 data should probably be stored at institutions where they are produced but Data Centers should also have a special service providing at least the description of the data in their directories and having them ready for eventual use in their archives and bases. Copying and distribution of these data is to be exercised only on the author's (owner's) request.

The authorship of each data level is to be ensured by:

- including the author's name in the description of the corresponding data sets;
- registering all the requests for data which have been filled;
- meeting requests for the CL=3 data only upon the author's consent. The author's (or Principal Investigator's) consent is also needed when a request on the CL=2 comes from persons (institutions) not included in the project/campaign participants list.

The CL=2 data are to be converted into the CL=1 data after a fixed time interval defined by the Principal Investigator (or Working Group in charge) of the project/campaign under which these data were obtained.

The CL=3 data are to be converted into CL=2 data by the author/owner of the data, but hopefully within a reasonable time frame.

d) Systems for information backing of meteor research

Soviet researchers of meteor phenomena attach great importance to solution of the problems mentioned above. Two of the eight initiatives of the National Program of the USSR participation in the GLOBMET (1984) (further on designated as GI-5 and GI-6) concern these problems.

The main aim of the GI-5 is to analyze typical tasks of meteor studies and processing algorithms and to develop a software system for meteor research (SMR).

The principal components of such system are shown in Fig. 2. Of primary importance here is an Integrated Meteor Data Processing System (IMPDS) which would form a component subsystem of the SMR.

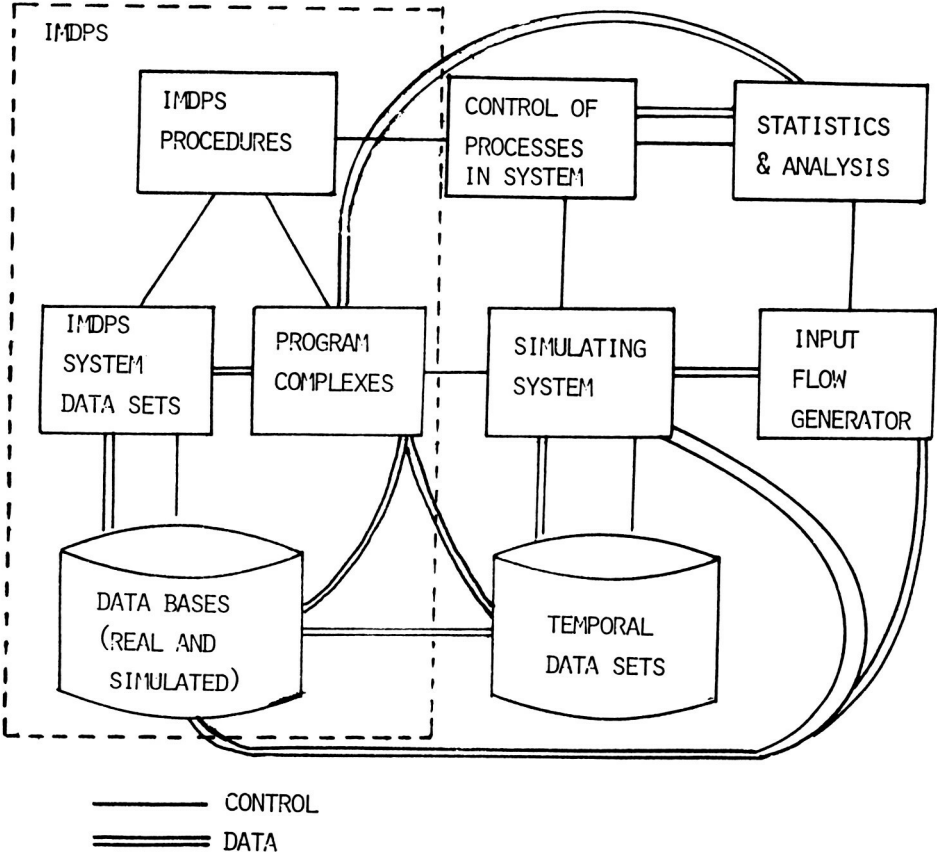


Fig. 2 Integrated meteor data processing system.

The IMPDS must become a basis for solving both the task of constructing the SMR as a whole and methodological tasks of GLOBMET as defined in Part III of the GLOBMET Planning Document.

Following the existing trends in the development of computer systems and networks, as well as data acquisition systems, the software components are being worked out under the GI-5 in order to be integrated into the local and distributed database management system.

The GI-6 is aimed at analysis of data and methods of observation with a view to developing indices adequately characterizing methods and results of observations and solving the problems of data and method comparability. An index here denotes a certain statistical generalization designed from space-and-time parameters of meteor observations and reflecting the most essential characteristics of a given group (complex) of observation.

e) Automated information-inquiry system

The experience gained in the course of joints efforts under the GI-5 has been used in the draft project of the Automated Information-Inquiry System (AIIS) that is now being developed at the Soviet Geophysical Committee. Fig. 3 shows the main parts of the AIIS and connections among them.

The AIIS architecture is optimized in such a way as to provide an effective preparation, in interactions mode, of inventories and directories on users' requests and standard processing of machine-readable data. The AIIS must include software means for the following tasks:

- work in interactive mode on the General Data Inventory, preparation of data inventories on request;
- work on the General Data Directory, preparation of data directories on request;
- standard procedures of processing, checking and editing of machine-readable data;
- users' procedures for processing Level-1 and Level-2 data;
- procedures for planning optimal experiments;
- procedures of situational simulation;
- users' applied procedures. These include interface modules through which users' programs can call the system data sets without any changes of the latter. All calls are registered;
- subsystem of international book exchange;
- subsystem of preparing formalized tasks by users and registering requests for copying data of all the three levels.

Prospects of information archiving of meteor research are obviously linked with creation of complex, all-embracing information backing system for Planetary Geophysics research under the GLOBAL CHANGE Project. It is

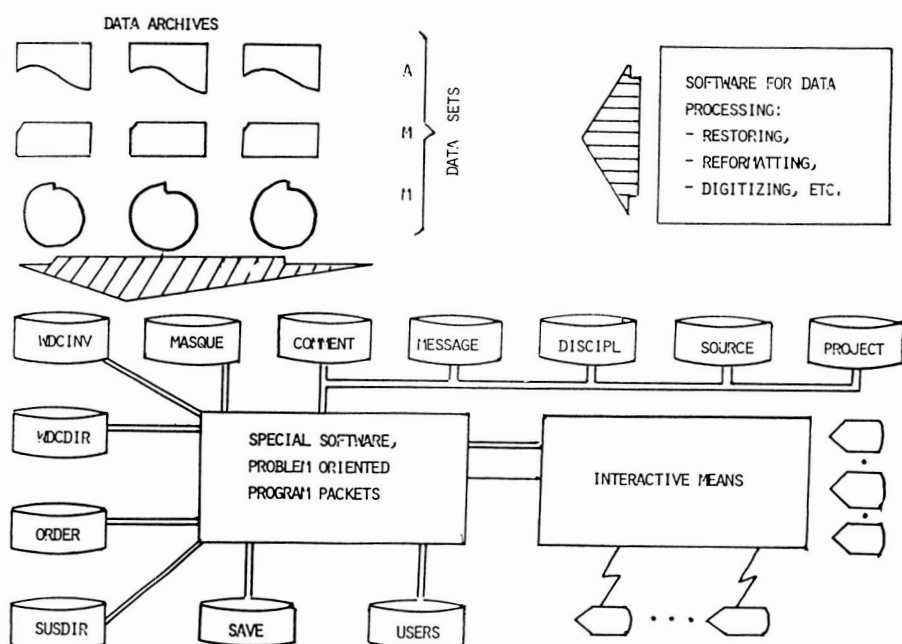


Fig.3 Proposed automated information-inquiry system.

WDCINV - data inventory, WDCDIR - data directory, MASQUE - set of data formats, COMMENT - commentary data set, MESSAGE - diagnostics, DISCIPL, PROJECT - descriptions of scientific disciplines and projects, ORDER - descriptors set, SUSDIR - data suppliers/user directory, SAVE - protocols, USERS - AIIS's user list.

proper to mention that the ICSU colloquium on IGBP stressed the importance of using new methods, especially for data processing and analysis, on an international basis, of large-scale data bases, meaning the creation, as the first step, of a rather complicated distributed information-inquiry system.

At this stage, it is impossible to give a complete picture of what is to be done. However, there is one thing worth considering right now.

Even though future research and observation program, initially under the GLOBAL CHANGE Project, mean extension of networks and application of mainly new methods and means of observation and analysis, the bulk of data to be analyzed will include either already existing data deposited in various centers and institutions or that obtained using existing observational means.

In such a case, the task of interpreting data appears to be by far more difficult than that of its collecting, despite the difficulties of the latter, which lie not only in the enormous amount of work to be involved in converting data into a machine-readable form and third-level representation status, but also in the lack of a necessary means of achieving data accessibility.

The development of a means of providing easy access to such a wide variety of geospheric and biospheric data present an extremely complicated task.

And yet, at least one part of it can be and must be solved as soon as possible by specialists of the corresponding disciplines. I have in mind the formulation of conceptional models, data structures and formats, a provisional but representative data index system, and standard processing algorithms, especially algorithms for converting Level -1 and Level-2 data into that of Level-3.

The task is very difficult. But we are hopeful it can be solved. The experience steadily gained by the meteor community allows one to be optimistic about the immediate solution of at least the "data-indices-algorithms" problem of meteor geophysics and astronomy.

References

1. GLOBMET Planning Document, 1982, MAP Handbook, Vol. 7, pp. 20-33.
2. Joint Report of WDC-A and WDC-B2, 12981, Moscow, December.
3. MAP Data Management Committee, Questionnaire No. 1982.
4. Soviet National GLOBMET Program, 1984, in: Global Meteor Observation System, VINITI Publ. House, Moscow, pp. 5-26 (in Russian).

THE CLIMATIC WIND REGIME IN THE LOWER THERMOSPHERE
FROM METEOR RADAR OBSERVATIONS

Yu. I. Portnyagin

Institute of Experimental Meteorology
Obninsk, Kaluga Region, USSR

The determination of climatic norms of wind regime parameters in the lower thermosphere requires some questions of a methodical and scientific character to be settled. Among those of a methodical character one can single out the following questions: how to properly construct climatic circulation models using limited experimental data obtained by various methods during different time periods and in different geographical regions. The most important questions of a scientific character are the following: what main dynamic structures characterize the wind regime and how are these structures related to various atmospheric parameters and to the dynamic structures in the overlying and underlying atmospheric layers.

Let us consider these questions:

1. Representativeness of sampling used for mean monthly value determination

Wind velocity measurements in the lower thermosphere as a rule are not carried out continuously. As a result, for the mean monthly value determination, some sample of the total wind field on consecutive days in the month, or on several days uniformly distributed throughout the month (e.g., on Wednesdays during meteorological rocket launchings), is used.

Continuous meteor radar measurements carried out in Obninsk and at Molodezhnaya station (Antarctica) during several years produced data from which one can estimate the degree of difference between such samples and the true mean. Let us consider as an example some results of various mean monthly value estimates based on continuous measurements from Molodezhnaya station (Antarctica). Similar estimates are obtained also for data from continuous measurements in Obninsk.

The results presented in Figures 1 and 2 show that if it is not possible to measure continuously it is necessary to carry out measurements on separate days uniformly distributed throughout the month. The estimates of mean monthly values obtained from such measurement data are close to the true monthly means.

2. The influence of interannual variability of estimates of monthly means.

Dispersion estimates of monthly mean velocity values caused by the interannual variability of mean monthly wind velocities is important in the construction of a mean perennial circulation model.

The knowledge of these dispersions makes possible an evaluation of the accuracy of mean monthly values pertinent to the model because it allows

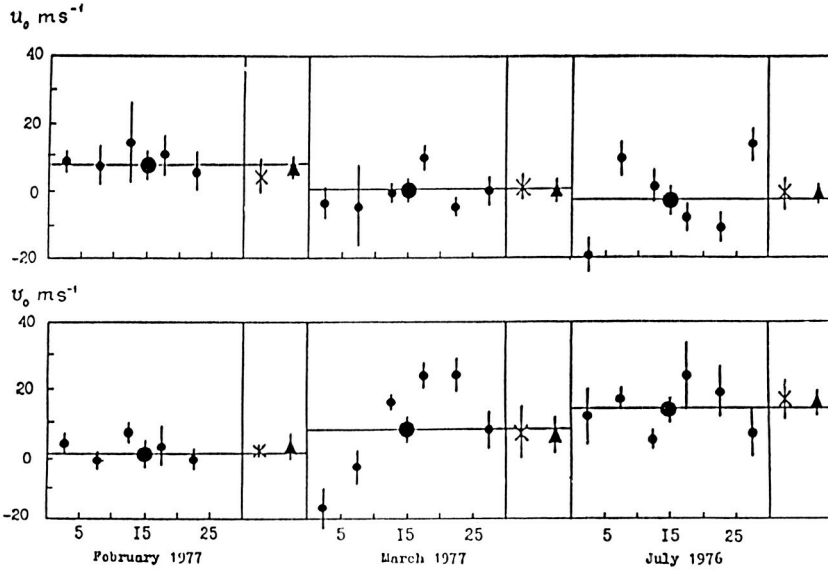


Fig. 1 Mean monthly velocity values of zonal v_0 and meridional u_0 wind: ϕ - selected mean five day values; $*$ - value averaged over 4 days equally distributed during the month; \uparrow - values averaged over 8 days equally distributed during the month; ϕ - true mean monthly values.

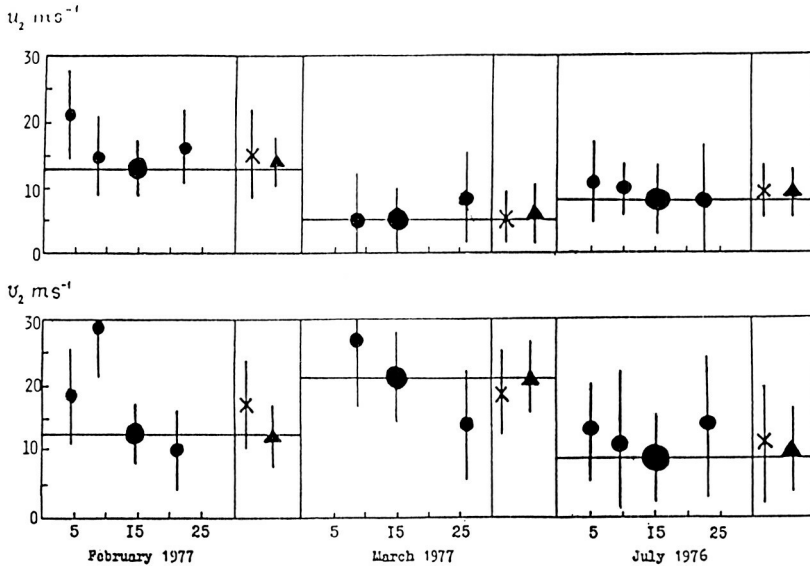


Fig. 2 Mean monthly amplitude values of zonal component v_2 and meridional component u_2 of a semidiurnal tide (symbols the same as in Fig. 1).

one to determine the confidence intervals inherent in the smoothing of model values in space and, hence, enables the drawing of realistically smoothed isolines of wind velocity.

Figures 3 and 4 are presented as examples of the interannual variation in mean monthly velocity values. These figures show year-to-year variations of mean monthly velocity for January and July from perennial measurement data from the Obninsk, Heiss Island and Molodezhnaya stations.

It is seen from these figures that in some cases the interannual variations of mean monthly values may cause wind velocity variations not only in value but also in sign. So, in January of different years on Heiss Island and in Obninsk the meridional wind can be northerly as well as southerly with mean perennial values for January close to zero (Figure 4). Such behavior of the meridional wind can be explained by the fact that the center of the winter cyclone, characteristic of the Northern Hemisphere circulation in January, may not be centered on the pole, but undergo periodic displacements from the pole. This would indicate that the resulting meridional wind has ageostrophic as well as geostrophic components. Similarly, the meridional wind in Antarctica may vary in sign in July. The zonal wind, while more stable in sign (Figure 3), may in some years vary in direction (e.g., in January at Molodezhnaya station). As seen from Figures 3 and 4, oscillations with periods of 3-5 years occur in the interannual variations of mean monthly values (according to our data, this conclusion is also valid for other months of the year). So, the most exact evaluation of mean perennial wind velocity values can be obtained by averaging observations over periods exceeding five years. Unfortunately, such long-term series of observations exist at a comparatively small number of geographic locations.

To quantitatively estimate the dispersions connected with interannual variability and the corresponding least square deviations, we used a data series obtained during many years at sites located at the high, moderate and subtropical latitudes of both hemispheres: on Heiss Island (1965-1981), in Obninsk (1964-1981), in Atlanta (1974-1978), Adelaide (1966-1972), and at Molodezhnaya station, Antarctica (1968-1981). Figures 5-7 show the values of root mean-square deviations σ_i (dispersion D_i) of the mean monthly values from mean perennial velocities for all months of the year; these deviations were estimated from measurements made at the above stations. It is seen from the figures that minimum σ_i^u and σ_i^v values (i.e., for meridional and zonal components respectively) are observed in Obninsk, which is located at a moderate latitude of the Northern Hemisphere. The σ_i values on Heiss Island are somewhat higher. The maximum σ_i values of about 15-20 m/s are observed at subtropical latitudes (Atlanta and Adelaide) during some months of the year. A definite seasonal σ_i dependence was not established. Moreover, even at one site but at different height levels (measurements in Atlanta and Adelaide were carried out by facilities which measure height variations) the character of the seasonal course of σ_i does not always coincide (Figures 6 and 7). However, results presented in Figures 5-7 give a rather clear presentation of the order of σ_i for different latitudes and allow one to estimate the root-mean-square errors of wind velocity values for different seasons of the year.

It should be noted that dispersion estimates connected with the interannual variability are maxima, as scatter in the mean monthly values

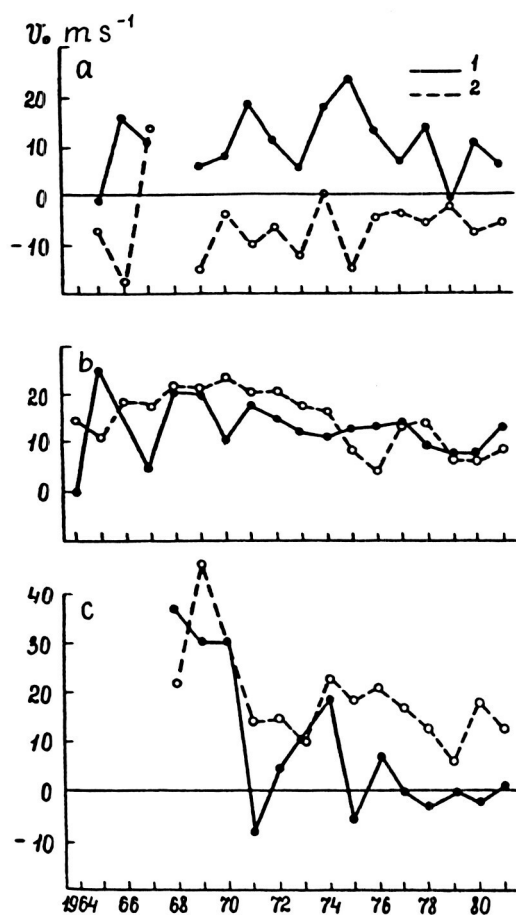


Fig. 3 Interannual variability of mean monthly zonal wind velocities for January and July from measurement data for many years on Heiss Island, in Obninsk and Molodezhnaya station. a) Heiss Island, b) Obninsk, c) Molodezhnaya station; 1 January, 2 July.

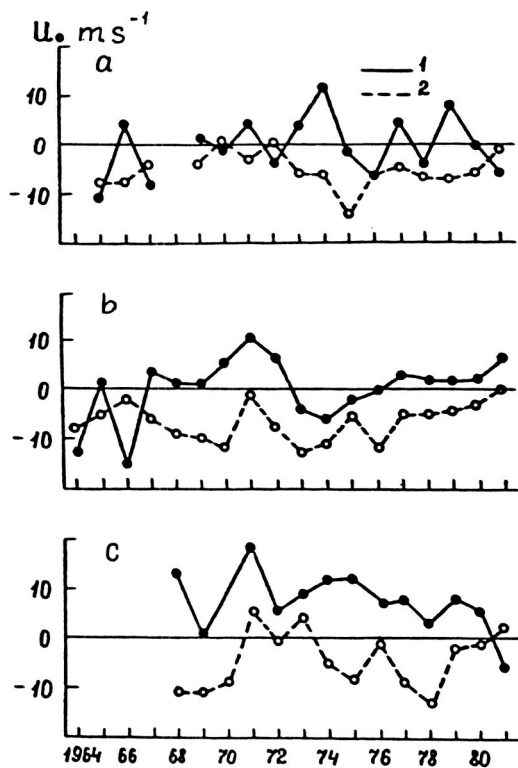


Fig. 4 Interannual variability of mean monthly meridional wind velocities for January and July from data of persistent measurements on Heiss Island, in Obninsk and at Molodezhnaya station. a) Heiss Island, b) Obninsk, c) Molodezhnaya station; 1 January, 2 July.

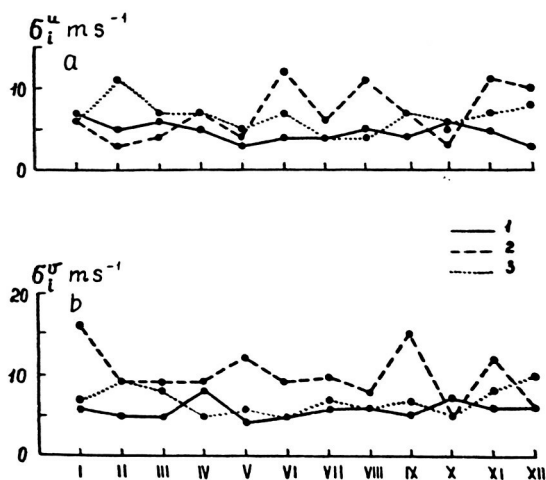


Fig. 5 Seasonal variations of root-mean-square deviations of mean monthly values of wind velocities from mean perennial for 95 km obtained during observations in Obninsk (1964-1981), at Molodezhnaya station (1968-1981), Heiss Island (1965-1981). a) meridional component, b) zonal component; 1-Obninsk, 2-Molodezhnaya station, 3-Heiss Island.

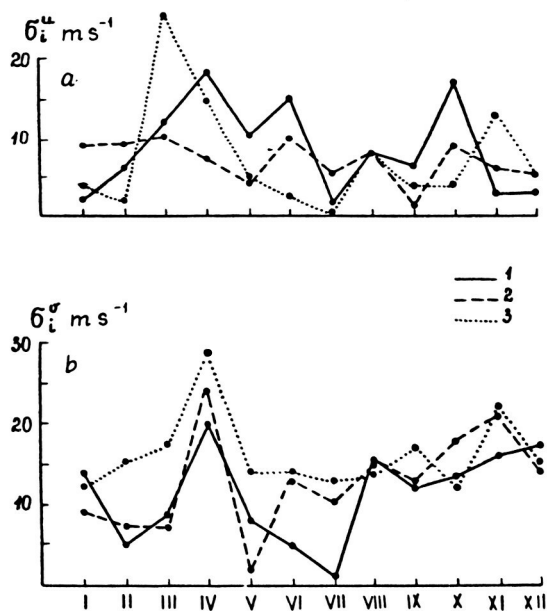


Fig. 6 Seasonal variations of root-mean-square deviations from observations in Atlanta (1974-1977) at 80, 92, 100 km. a) meridional component, b) zonal component; 1, 2, 3 - 80, 92, 100 km, respectively.

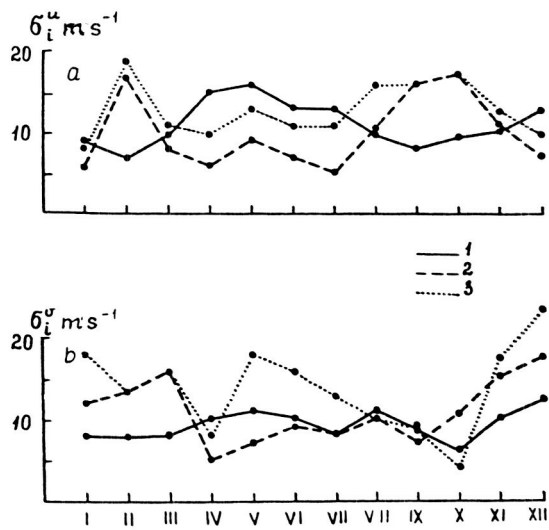


Fig. 7 Seasonal variations of root-mean-square deviations from observation data (1966-1972) at 80, 95, 100 km. a) meridional component, b) zonal component; 1, 2, 3 - 80, 95, 100 km, respectively.

was not excluded since continuous measurements from 1974 to 1983 were carried out only in Obninsk.

Figure 8 presents graphs of the mean perennial seasonal course of zonal and meridional prevailing wind velocities obtained by averaging the corresponding mean monthly values for the period from 1964 to 1981 from observation data in Obninsk, for 1965-1981 from data for Heiss Island and for 1968-1981 from data obtained at Molodezhnaya station. It is seen from this figure that the amplitude of a seasonal variation of prevailing wind velocities exceeds the errors associated with the mean perennial wind velocity values; the main features of the seasonal variation at each observation site are highly regular from year to year. At the same time, at different latitudes the seasonal variation of wind velocity has its own typical peculiarities. Differences in the seasonal variations of wind velocity are especially significant when comparing northern and southern hemisphere sites (it must be kept in mind that there is a shift of seasons equal to six months between hemispheres). These results show that when constructing a mean perennial circulation model for the meteor zone one can use data for different sites averaged over some years even though at these sites measurements were not continuous and the years over which the data were averaged do not necessarily coincide completely.

3. Longitudinal variability of wind regime parameters.

As is seen from the analysis, the dependence of mean monthly wind velocity values on longitude at moderate latitudes of the northern hemisphere is comparatively insignificant. Such a conclusion is confirmed by comparing the seasonal variation of zonal and meridional wind velocities at sites located at similar latitudes, but significantly different longitudes.

Figure 9 presents the mean monthly values of zonal and meridional wind velocities for sites located in two narrow latitudinal zones of the northern hemisphere 52-57°N and 45-50°N. (Stations in latitudinal zone 52-58°N are Jodrell Bank (2°E), Kuhlungsborne-Collm (12°E), Obninsk (38°E), Kazan (49°E), Tomsk (85°E), Badary (102°E) and Saskatoon (107°W); in the latitudinal zone 45-50°N, Budrio (12°E), Kiev (31°E), Kharkov (36°E), Volgograd (44°E) and Khabarovsk (135°E). It is seen from Figure 9 that difference in longitude between the sites does not significantly increase the dispersion of mean monthly values in comparison with dispersion of these σ_i values specified by their interannual variability (dispersion of wind velocity values resulting from their longitudinal variability σ_λ according to our estimates, is characterized by $\sigma_\lambda^v \sim 5$ m/s, $\sigma_\lambda^u \sim 5$ m/s). From this, we conclude that at moderate latitudes of the northern hemisphere the mean meridional wind is mainly of a geostrophic character. This is confirmed by comparison of the seasonal variation of wind velocities at high, subtropical and tropical latitudes of the northern hemisphere. (High latitudes: Heiss Island (80.5°N, 58°E), Kiruna (68°N, 10°E), College (65°N, 148°W); subtropical latitudes: Dushanbe (38°N, 69°E), Palo Alto (37°N, 122°W), Atlanta (34°N, 84°W), Kyoto (35°N, 136°E); tropical latitudes: Kingston (18°N, 77°W), Punta Borinken (18°N, 67°W), Waltair (18°N, 83°E)). So, it can be supposed that the dependence of the seasonal variation in wind velocity in the meteor zone on longitude is insignificant at all latitudes. Thus, when developing atmospheric circulation models, it is possible as a first approximation to use mean zonal winds in which only seasonal and latitudinal dependencies are taken into account.

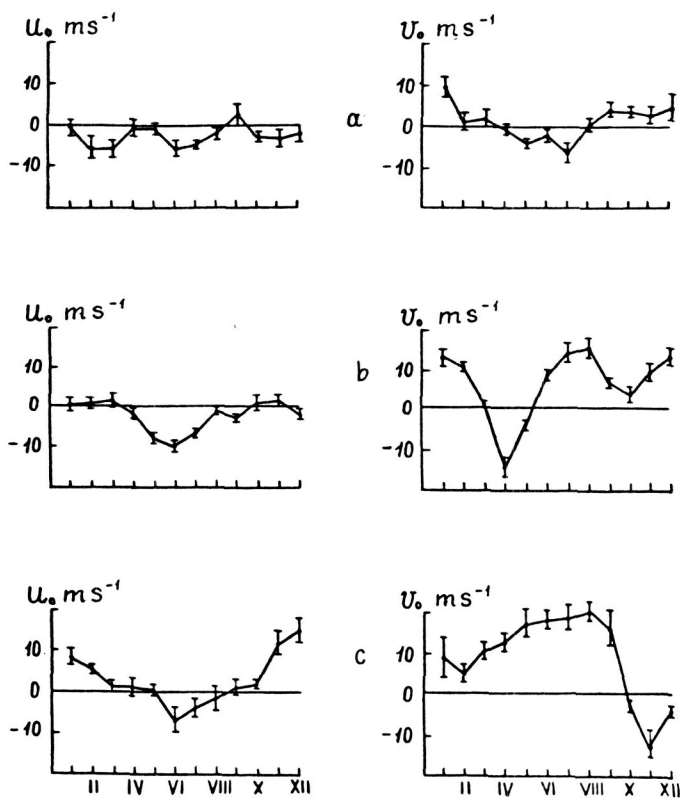


Fig. 8 Mean perennial seasonal course of meridional u_2 and zonal v_2 prevailing wind velocities from measurement data in Obninsk (1964-1982), on Heiss Island (1965-1982) and at Molodezhnaya station (1968-1982). a) Heiss Island, b) Obninsk, c) Molodezhnaya station.

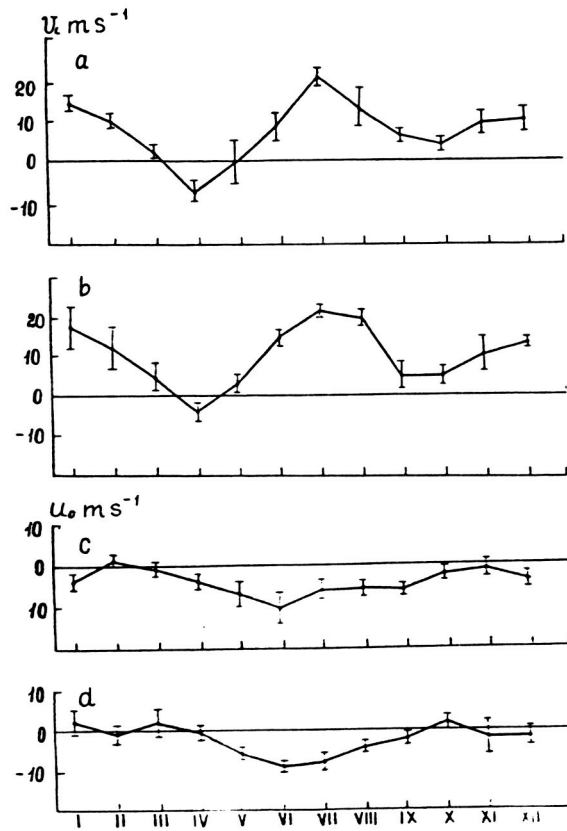


Fig. 9 Seasonal course of zonal v_o and meridional u_o prevailing wind velocity components at 95 km, averaged over different longitudes for two latitudinal belts: $52^\circ-57^\circ \text{ N}$ (a,c) and $45^\circ-50^\circ \text{ N}$ (b,d).

4. Regularities of zonal circulation in the region of the mesopause-lower thermosphere.

In constructing our model of zonal circulation in the mesopause-lower thermosphere, we used results obtained at 27 sites by meteor radars, and at six sites by the partial reflection method. Wind variations in both height and time have been measured at the following sites: Kiruna, 68°N; Saskatoon, 52°N; Garchy, 48°N; Atlanta, 35°N, Punta Borinken 18°N; Townsville, 18°S; Adelaide, 35°S; Birdlings Flat (Christchurch), 44°S). The analysis of results from all sites permits the construction of height-latitude cross sections of the mean zonal wind field for all seasons of the year. Over the 70-80 km height range, the radar wind results have been coupled with height-latitude sections constructed from meteorological rocket sounding data, with due regard given to the measurement errors associated with each technique. The experimental data used for construction of these sections at sites located at different longitudes are in good agreement with each other, and after smoothing and spatial interpolation, latitude-height cross sections of model mean values of zonal wind velocity for each month of the year were obtained.

These sections are presented in Figures 10-13. Let us consider, for example, sections of the zonal wind field for January and July (Figures 10 and 12). Dominant dynamical structures are clearly seen in these sections; for example, a region of easterly circulation in the northern hemisphere in July and in the southern hemisphere in January which is connected with the summer strato-mesospheric anticyclone; a region of westerly circulation in the northern hemisphere in January and in the southern hemisphere in July caused by penetration of the winter stratomesospheric cyclone into the meteor zone; a westerly circulation structure which is specific to the lower thermosphere for the summer hemisphere covering in height most of the meteor zone; and a region of low latitude easterly circulation and related to it the region of easterly circulation in the lower thermosphere of the winter hemisphere. Analysis of these cross sections shows that the global zonal circulation in the mesopause-lower thermosphere region is greatly influenced by dynamical processes in not only the strato-mesosphere, but also the thermosphere. It follows from Figures 11-13 that in both the southern and northern hemispheres, along with general regularities of global zonal circulation, there are great differences between the spatial location of mean circulation structures and the intensity of air mass movements in these structures.

Lastly, one can conclude that available experimental data on wind velocities in the mesopause-lower thermosphere can be analyzed to determine climatic regime parameters and to construct mean perennial circulation models. However, for further advances in detailed modeling, it will be necessary to increase the present station network, particularly in low latitudes, and to carry out long-term continuous measurements. A timely solution to this problem will require the combined efforts of scientists from many countries.

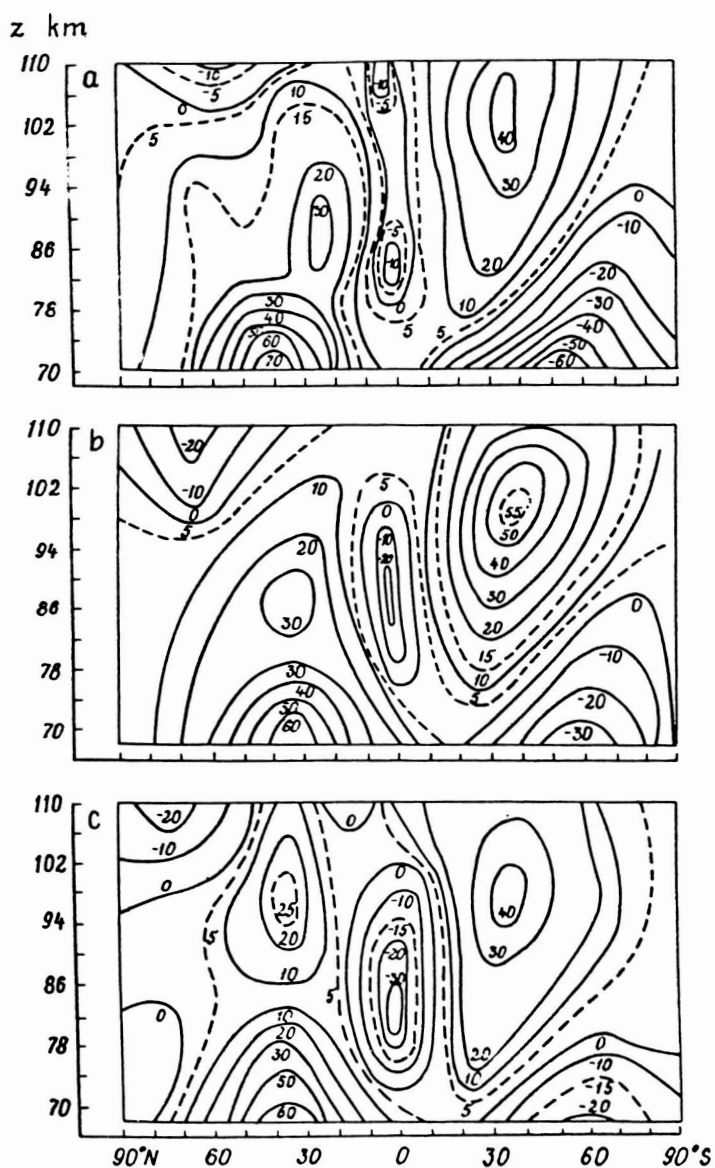


Fig. 10 Height-latitude structure of the zonal wind field (m/s), December-February. a) December, b) January, c) February; positive value - western wind.

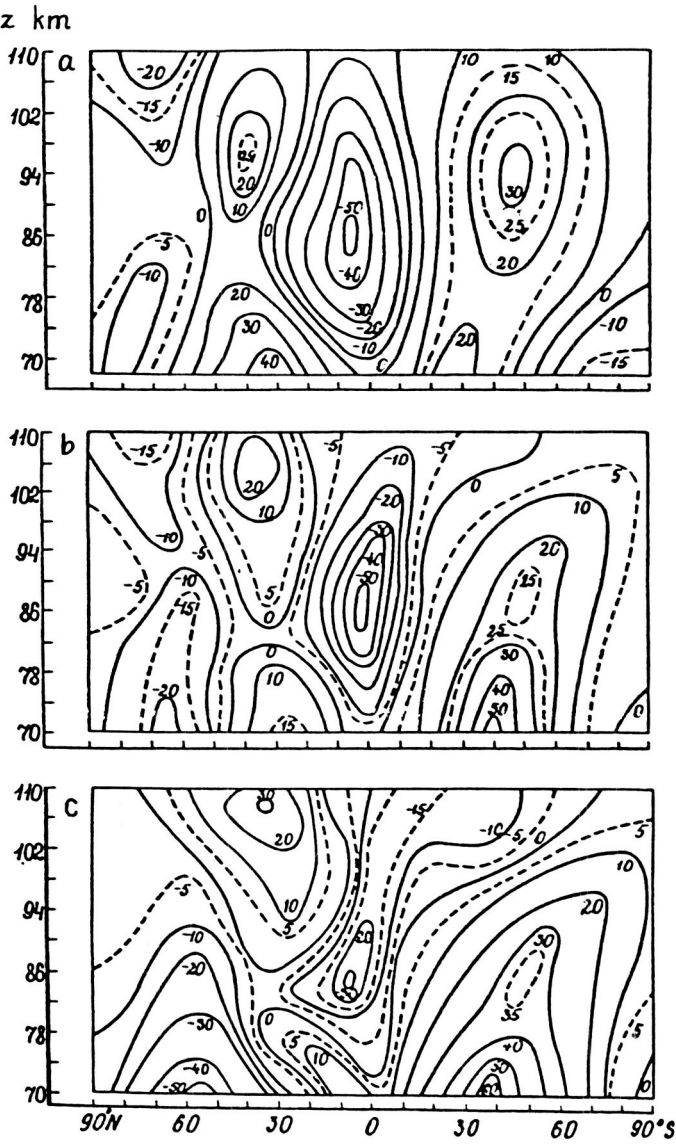


Fig. 11 Height-latitude structure of the zonal wind field (m/s), March-May. a) March, b) April, c) May.

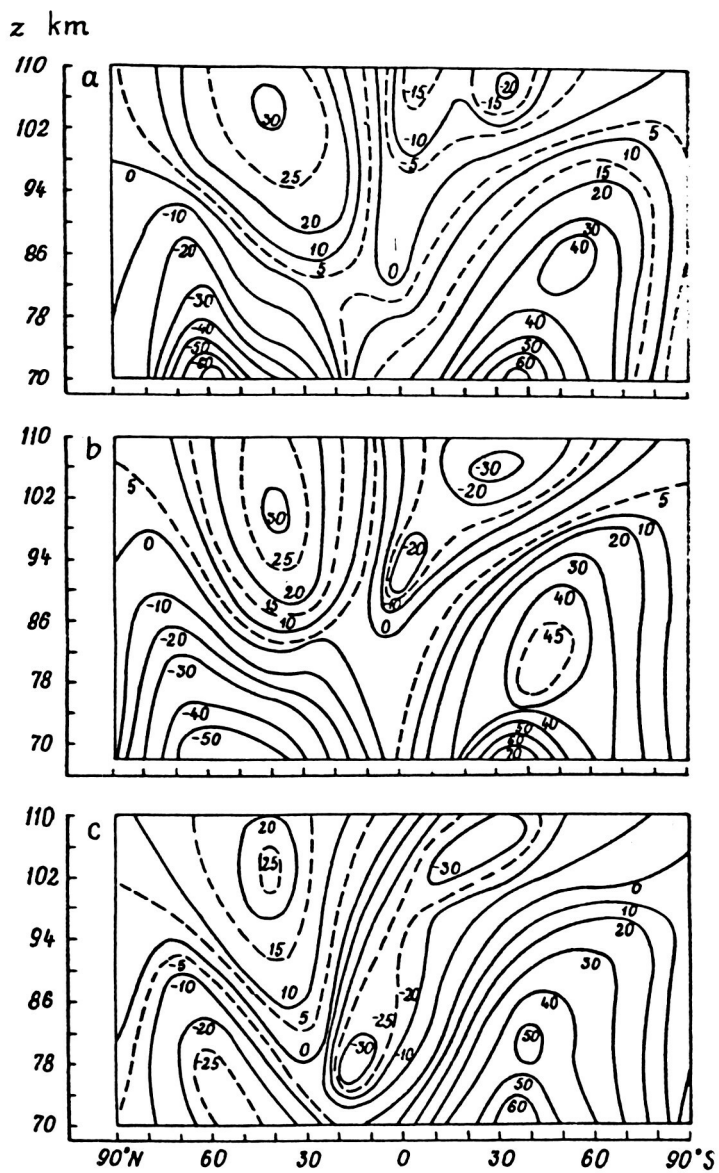


Fig. 12 Height-latitude structure of the zonal wind field (m/s), June-August. a) June, b) July, c) August.

METEOR OBSERVATION BY THE KYOTO METEOR RADAR

Susumu Kato and Toshitaka Tsuda

Radio Atmospheric Science Center,
Kyoto University, Uji 611
Japan

The Kyoto Meteor Radar is a monostatic coherent pulsed doppler radar operating on the frequency of 31.57 MH (Aso et al 1979). The system is computer-controlled and uses radio-interferometry for echo-height determination. The antenna, an improvement of the initial system, can be directed either to the north or the east.

The system has been in operation in Shigaraki (35 N, 136 E) since 1977, collecting data almost continuously in recent years as shown in Table 1. Winds at meteor heights are the main subject of the radar observation. The meteor echo rate has also been measured as illustrated in Fig. 1 where the echo rate distribution with height and the daily variation in height integrated echo rate are shown. These results are consistent with well-known meteor behavior (e.g. McKINLEY 1961). Fig. 2 shows the monthly mean of the echo rate. Note that the Kyoto Meteor Radar discards all echoes from over-dense meteor trails which are of no use for wind observation.

A large amount of wind data is now available. TSUDA and KATO (1981) were successful in deducing the lunar tides (both M2 and O1 components). Fig. 3 shows the spectrum of the observed wind varying with season. For instance, the two-day period wave is clearly enhanced in summer. Penetration of this wave into the ionosphere, giving rise to an ionospheric dynamo, has been discussed elsewhere (ITO et al 1985). Investigations of atmospheric tides are being pursued by cooperative observations between our meteor radar and the partial reflection radar in Adelaide (VINCENT, Private Communication, 1985). One example is illustrated in Fig. 4. A novel approach to the study of gravity waves has recently been attempted using our meteor radar which is able to detect the horizontal propagation of the waves by observing the changing phase through the region illuminated by the radar (YAMAMOTO et al 1986).

Whilst the MU radar is now in operation in Shigaraki, the Kyoto Meteor Radar is still playing a role because the latter is more suited for continuous observation throughout both day and night for longer periods.

References

1. Aso, T., T. Tsuda and S. Kato, Meteor radar observations at Kyoto University, *J. Atmos. Terr. Phy.* 41, 517, 1979.
2. Itoh, R., T. Tsuda and S. Kata, A consideration on ionospheric wind dynamo to be driven by planetary wave with two day period, *J. Atmos. Terr. Phy.* (in press)

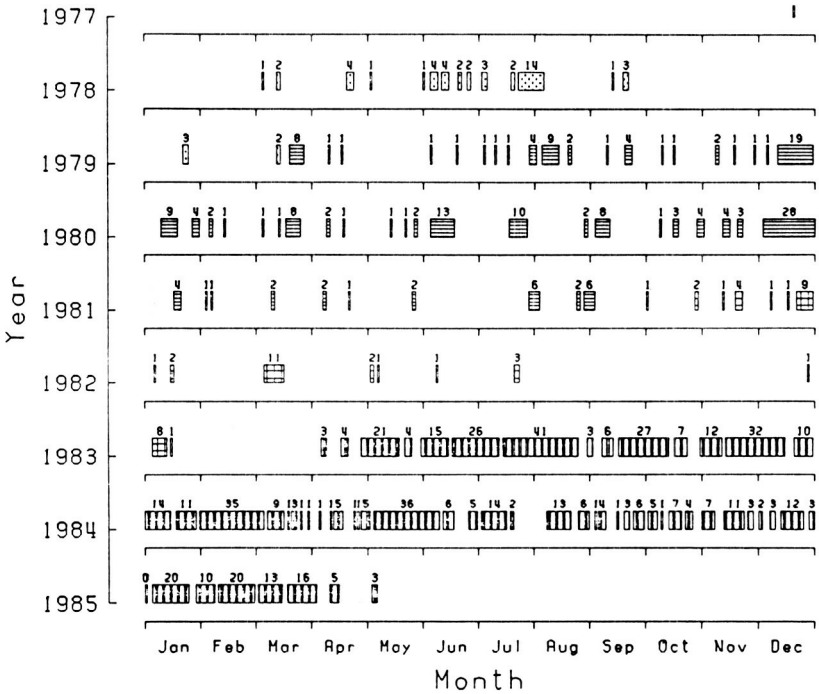
3. McKinley, D.W.R. Meteor Science and Engineering, McGraw Hill Book Co, N.Y., 1961.

4. Tsuda, T. and S. Kata, Lunar tides at meteor heights, Geophys. Res. Lett. 81, 191, 1981.

5. Yamamoto, M., T. Tsuda, and S. Kato, Gravity waves observed by the Kyoto Meteor Radar in 1978-1985 (submitted for publication).

Table 1

Kyoto meteor radar observation period.
The shaded area shows the observation period.



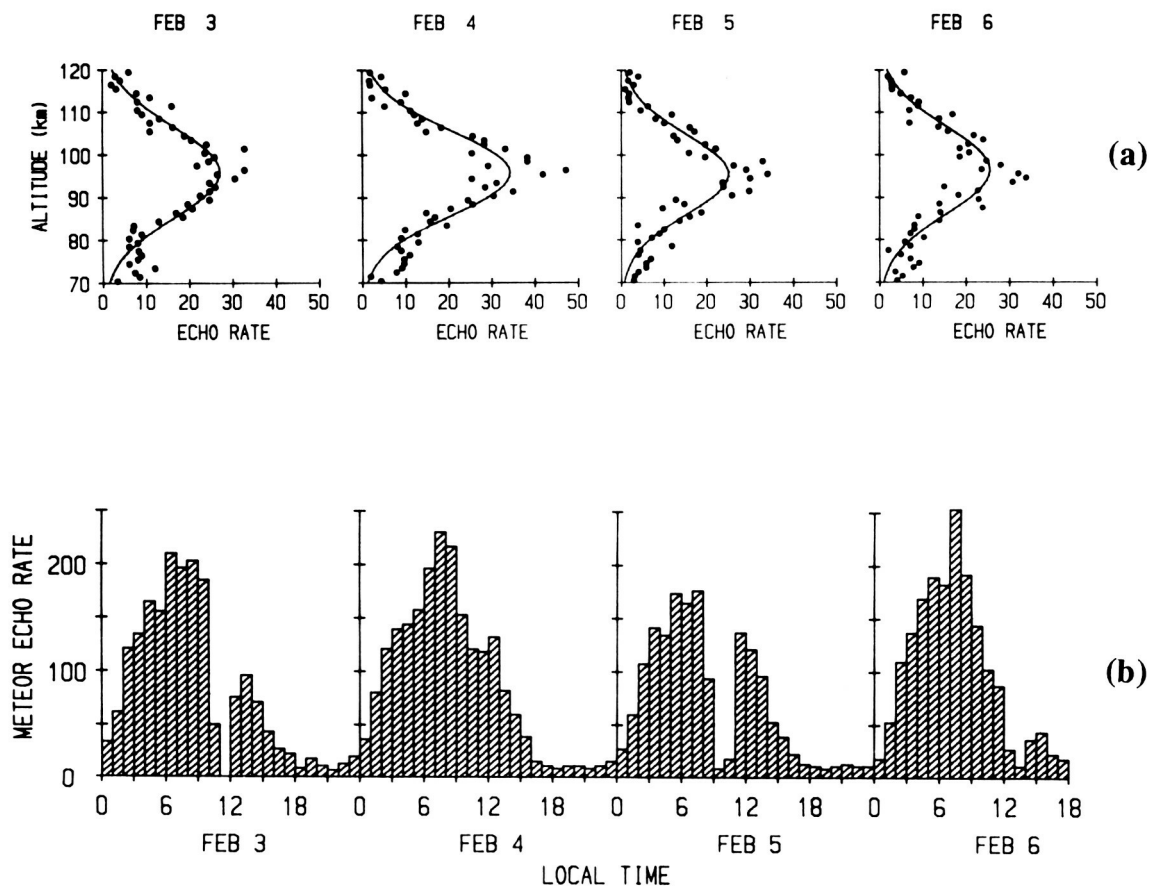


Fig. 1 (a) Meteor echo daily occurrence-frequency (per km during Feb. 1983) versus height.

(b) Meteor echo occurrence-frequency integrated over height in one hour.

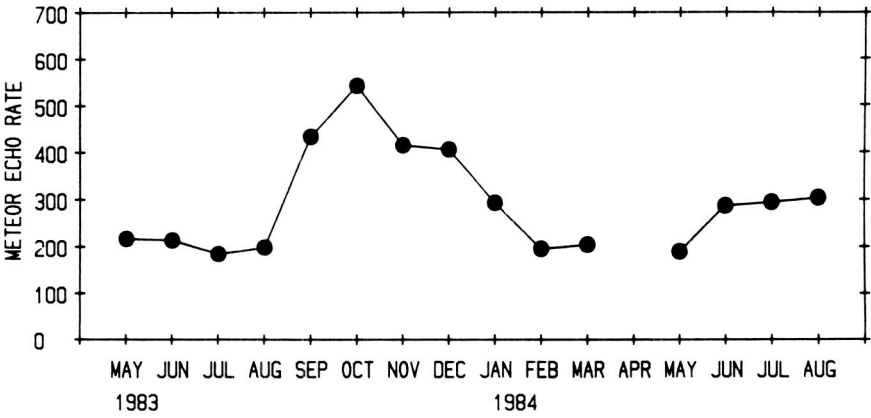


Fig. 2 Similar to Fig. 1 (b) except for monthly mean, in 1983.

DYNAMIC POWER SPECTRUM ,KYOTO METEOR RADAR

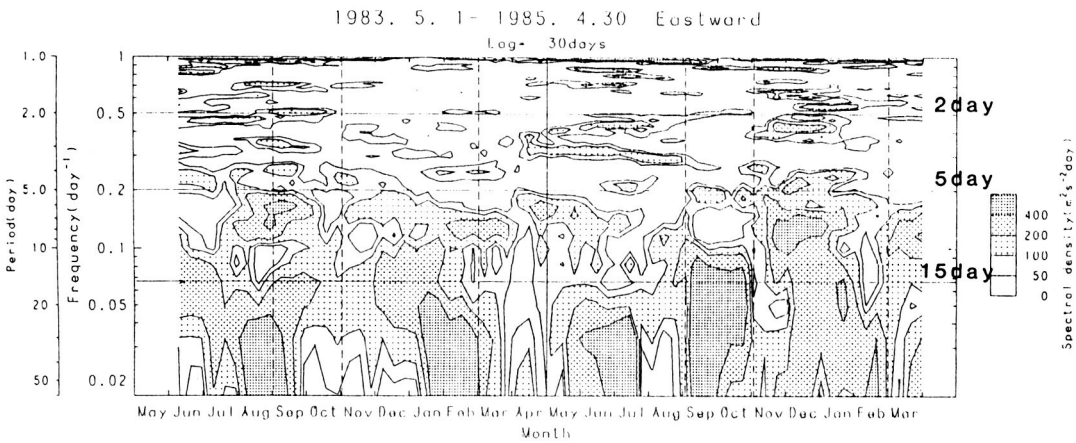


Fig. 3 Dynamic period spectrum of meteor wind in contour map.

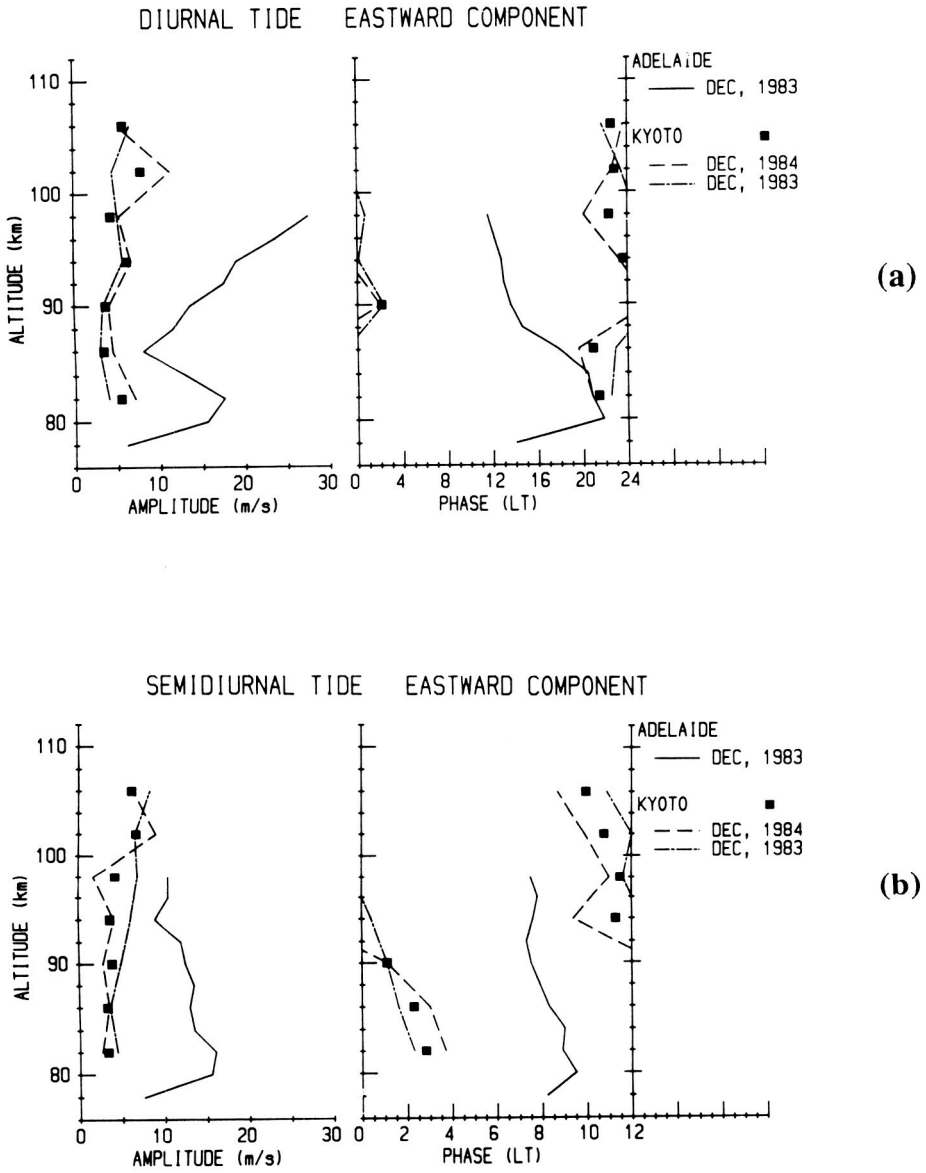


Fig. 4 (a) Diurnal tide in Kyoto and Adelaide.

(b) Similar to Fig. 4 (a) except for semidiurnal tide.

ATMOSPHERE DYNAMICS IN THE EQUATORIAL METEOR ZONE

B. L. Kascheev

Institute of Radioelectronics
Kharkov, USSR

The study of the atmospheric circulation of the earth from its surface to the altitudes of 100-110 km is essential for establishing atmospheric motion regularities with a view to perfecting weather forecasting.

Meteorological satellites, rocket soundings and radar tracking of meteor motion have been used for over 20 years, along with the more conventional methods of data acquisition.

The global network of meteorological observation stations is distributed very unevenly over the earth's surface. There are vast regions of the ocean, where observations are practically non-existent, particularly in the southern hemisphere. 90% of the stations carry out observations only in a thin layer above the earth; about 10% sound the air to altitudes of 30-40 km (aerological stations) and less than 1% conduct observations at the altitudes of 100 km and higher using meteorological rockets (LOSEV, 1985).

It should be noted that half of aerological stations are located between 30° N and 50° N in the zone covering only 16% of the earth's surface. Only 5% of the aerological stations are in the equatorial zone between 10° N and 10° S, which covers 35% of the planet's area. It must be stressed as well that the members of the MAP Study Group 6 who suggested an equatorial location for an observatory in May 1982, believe that such an observatory should be placed at no more than 5° off the equator.

Radiometeor stations are distributed still more unevenly, being mainly confined to middle latitudes of the northern hemisphere.

Several years ago, the middle atmosphere over the equator was studied by the Soviet equatorial meteor expedition (SEME), from August 1968, to July 1970. Observations of meteor trail drift, measurements of individual radiants and meteor numbers were carried out by SEME, for the first time ever, in Mogadishu, Somali (2° N, 45° E) (BABAJANOV et al., 1970; BABAJANOV et al., 1973). The observations were conducted during 326 full days. About 450,000 meteors were recorded, which is considered an adequate number for identification of meteor winds. The Manning method was used for 12 azimuthal directions, with 6-minute measurements in each, thereby determining, both components of the wind velocity.

The radio equipment consisted of an amplitude-phase altimeter ensuring altitude estimation with an error of $\pm(2...3)$ km (DUDNIK 1963). The overwhelming majority of meteors occurred at 80-105 km, the maximum being registered at 93-94 km. Most of the measurements, however, were carried out without an altimeter.

The diurnal variation was clearly marked over the equator, the quantity of meteors decreasing sharply at 16.00-20.00 local time. The hourly rate was observed to change by as many as 50-60 echoes over a day.

Despite the 15 years that have passed since the expedition nobody so far has carried out measurement over the equator. Some meteor trails drift research has been carried out since in Jamaica, India nad Puerto Rico, but in all these cases the radars were situated further from the equator, at approximately 18°N .

Here we present the main results of the SEME. A continuous 40-day cycle of measurements was carried out in September-October 1968. Considerable interdiurnal variation of the zonal component was observed. In particular, in the meridional component, the prevalence of a two day component was established in the equatorial meteor zone for the first time. it is worth noting the pronounced westward motion of the atmosphere over the equator. The measurements show eastward wind velocity values of 1-3 mps only for two months (December 1969 and June 1970) out of the 24 from August 1968 to July 1970. In all the other months the wind was clearly directed to the west, wind velocity reaching 40 mps in certain months. Average monthly mean values yield a semi-annual wind velocity with an amplitude of 15 mps. The semi-annual wave phase is such that maximum breaking of the atmosphere rotating with the earth takes place in March and September and the minimum - in June and December.

The meridional wind was essentially directed to the North over the biannual cycle of observation. The most common velocity of mid-month estimates exceeded ten mps only in three instances.

For the equatorial zone, as well as for the other zones, the presence of diurnal and semi-diurnal wind velocity components at the altitudes of 80-105 km is characteristic. However, the relation between these components over the equator is different from that at mid-latitudes. The zonal diurnal component is larger than the semi-diurnal in approximately 50% of the months measured, and for the meridional component, in 75%. The mean value of the diurnal component amplitude in both directions amounts to 13 mps, with the semi-diurnal somewhat less: for the zonal wind it equals 12.6 mps, and for the meridional, 9.9 mps.

Fig. 1 (a-b) shows an example of semi-diurnal variations of the prevailing wind (V), of semi-diurnal (V_{12}) and diurnal V_{24} fluctuations of wind velocity at 85, 93 and 97 km on May 7-8, 1970. At the same time, we note a tendency to variation of the zonal circulation direction in the upper part of the meteor zone as compared with the lower one. Studies carried out in 1977-79 in Puerto Rico and in France confirm such variation of direction (Fig. 2, taken from MASSABEUF et al., 1981).

A stable prevalence of the diurnal component of wind velocity over semi-diurnal is clearly observed for the considered period.

The initial stage of the semi-diurnal zonal component within the two-year period was more stable than that of the meridional component in the variations of which the semiannual period with a span of 180° was traced. The mean value of the initial stage of the semi-diurnal tide for the zonal component constituted 268° (9 hours) and for the meridional one - 215° (7 hours). During a year the horizontal vector of the semi-diurnal tide can rotate clockwise as well as counter-clockwise.

The SEME data analysis has shown that the meteor zone is characterized by flashes of intensity of IGW and turbulence at highest instability moments of atmosphere due to tidal motions.

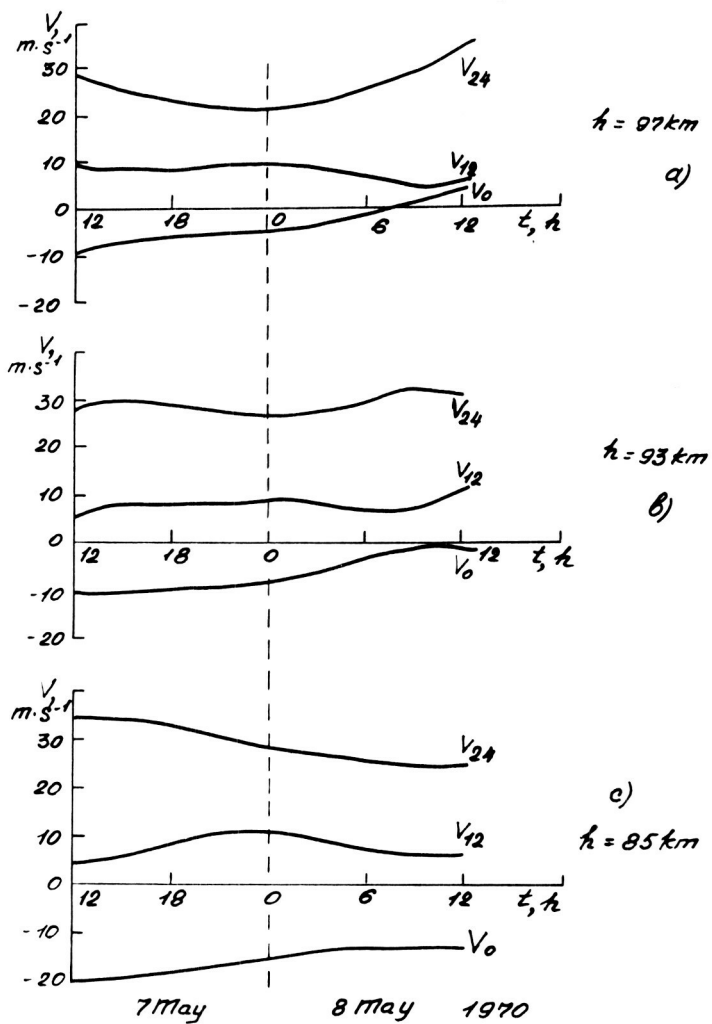


Fig. 1 Prevailing wind v_0 , and semidirunal v_{12} and diurnal v_{24} oscillations over Mogadishu (2°N, 45°E) on May 7 and 8, 1970 at a) 97 km, b) 93 km, and c) 85 km.

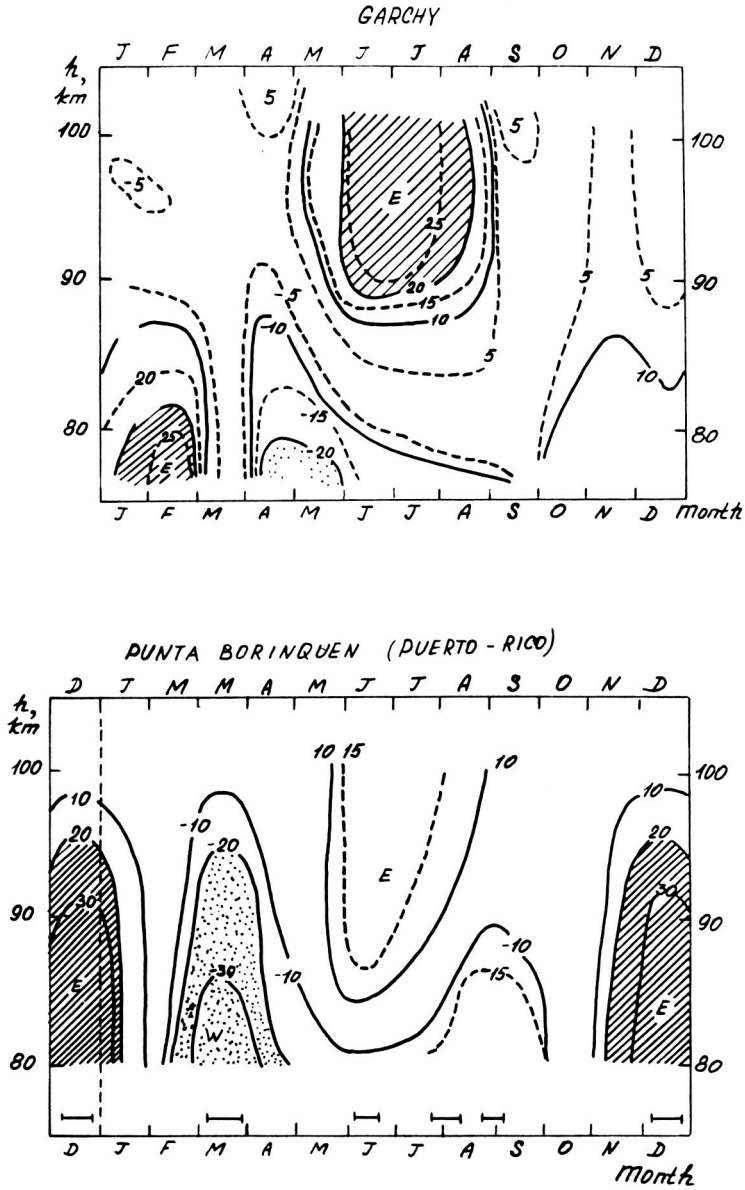


Fig. 2 Prevailing winds over Garchy, France, and Punta Borinquen, Puerto Rico, as determined from radio meteor data, 1977-1979.

Fig. 3 shows an example of the wind velocity spectrum variations of May 7-8, 1970, at 90 km. The local time is indicated over each curve. The spectra change greatly with altitude.

The harmonic analysis of the experimental data obtained during long-term continuous measurement cycles over the equator has shown that the presence of 3-4 and 8-day periods of the zonal component variation is characteristic of the altitudes of 80-100 km. The main component of the meridional wind velocity is a two-day wave, its amplitude generally exceeding those of both the diurnal and semi-diurnal components.

It is interesting to note that the direction of the steady component of the meridional wind for middle latitude stations and Mogadishu is often convergent: in middle latitudes wind is directed southward and over the equator - northward. The diurnal component amplitude analysis of the meridional wind velocity obtained from Mogadishu, Dushanbe and Kharkov shown similar variations during a year of observations (Fig. 4). There was no such similarity in the zonal component.

Meteorologists pay considerable attention to the epoch of the equinox. Such measurements were carried out in 1968-1970. Fig. 5 shows the diurnal variation of zonal and meridional components from data obtained in the epoch of the vernal equinox (March 1969), local time. The character of wind velocity variations in Mogadishu, Dushanbe and Kharkov in this epoch was practically the same, which is indicative of the global character of the dependence of atmospheric circulation on the tidal mechanism.

On the basis of data obtained in the above-mentioned locations an approximate scheme of atmospheric circulation in the meteor zone is given in BABAJANOV, et al., (1974) for March, June, September and December 1969, for low and middle latitudes.

References

1. Losev K. S., 1985, Climate: yesterday, today...and tomorrow?, Leningrad, Geometeoizdat Publ., p. 174.
2. Babadjanov P. B., Kalchenko B. V., Kashcheev B. L., Fedynsky V. V., 1970, Atmospheric circulation in the meteor zone over the equator, Bull. of Sov. Acad. Sci., No. 9, pp. 32-36.
3. Babadjanov P. B., Kalchenko B. V., Kashcheev B. L., Fedynski V. V., 1973, On the atmosphere motion in the lower thermosphere near the equator, Reports of Sov. Acad. Sci., Vol. 206, No. 6, pp. 1334-1337.
4. Babadjanov P. B., Kashcheev B. L., Nechitailenko V. A., Fedynsky V. V., 1974, Radar observation of the upper atmosphere circulation, Dushanbe, Donish Publ., p. 171.
5. Dudnik B. S., 1963, Phase-amplitude measurements at meteor heights, Kharkov State University Press, Meteors, Nos. 2, 3, pp. 8-13.
6. Massabeuf M., Benard, P., Fellous J. L., Glass M., 1981, Simultaneous meteor radar observations at Monpazier (France, 44°N) and Punta Borinquen (Puerto Rico, 18° N). Mean zonal wind and long-period waves. J. Atm. Terrest. Phys., Vol. 43, Nos. 5, 6, pp. 535-542.

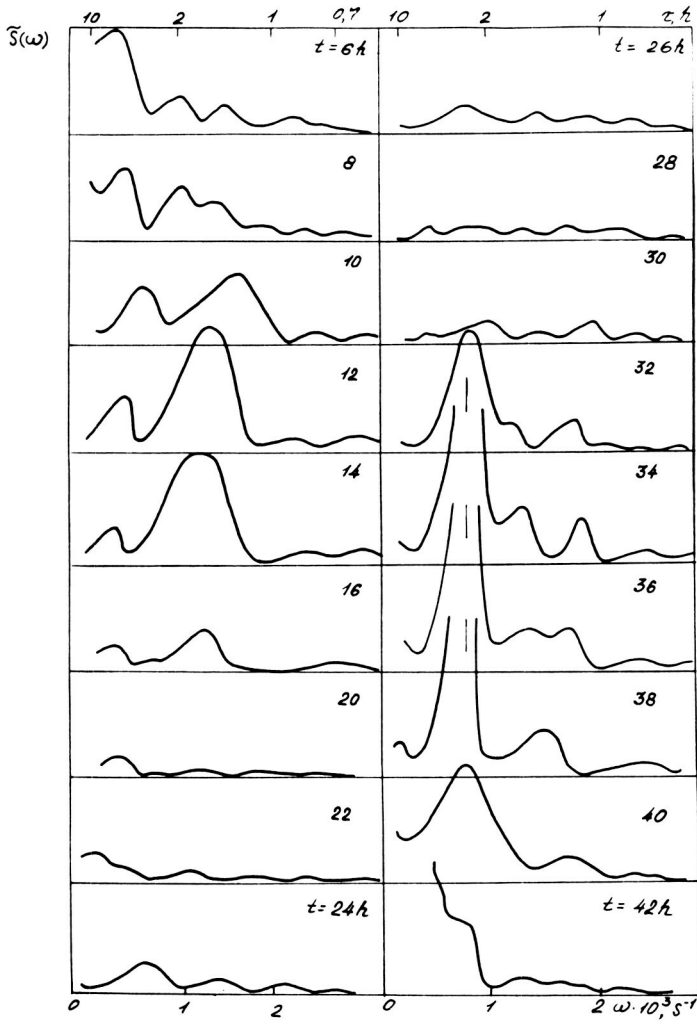


Fig. 3 Variation with local time t of the wind velocity spectrum at 90 km for May 7-8, 1970, over Mogadishu.

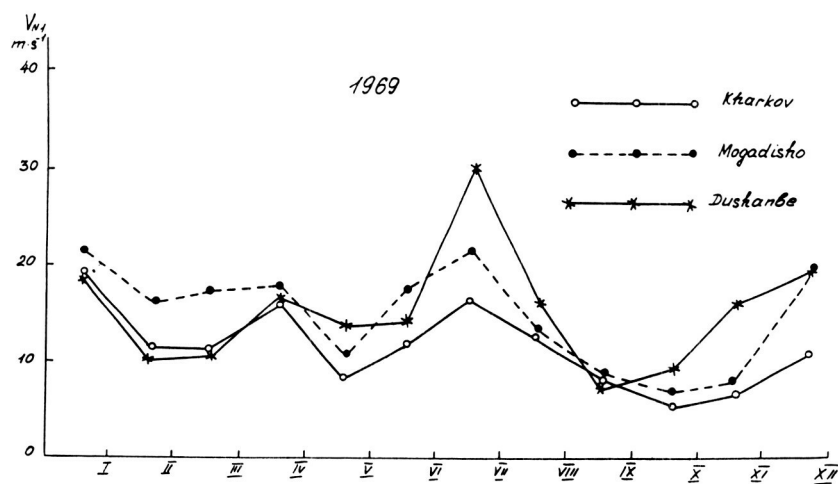


Fig. 4 Monthly mean meridional diurnal amplitudes for Kharkov, Mogadishu and Dushanbe in 1969.

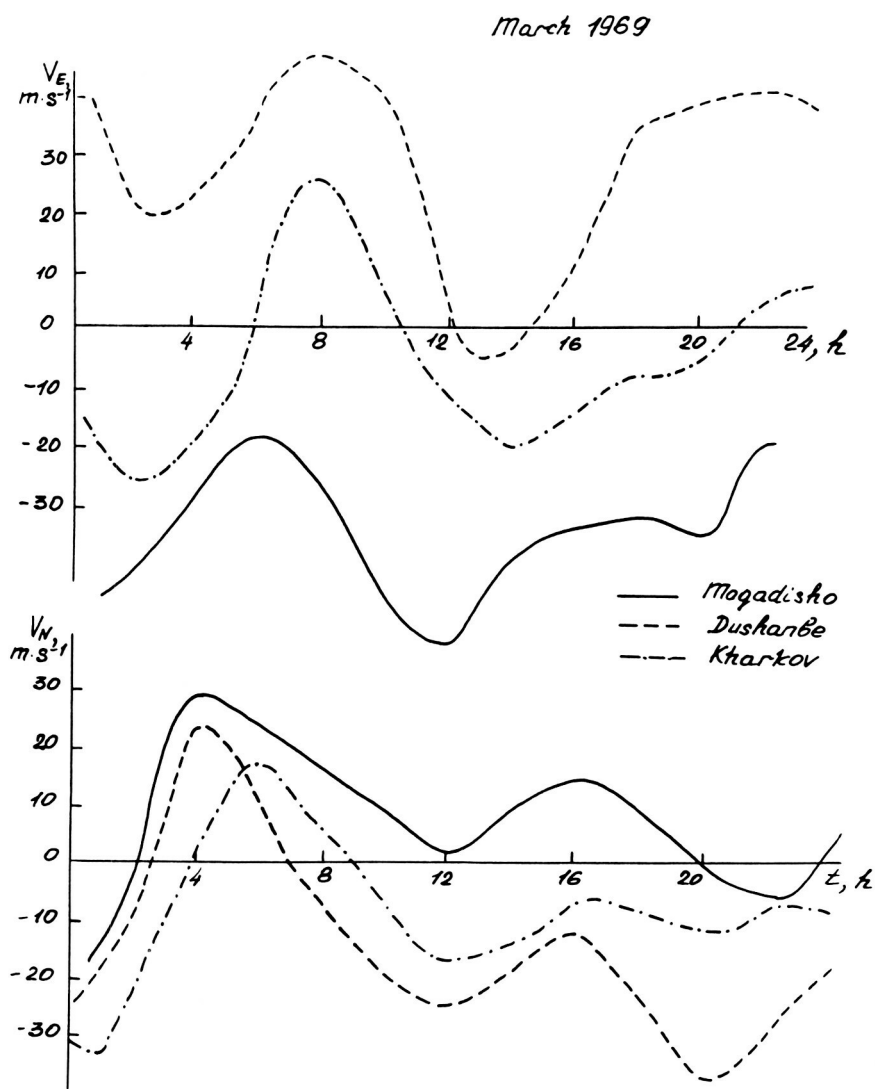


Fig. 5 Diurnal variation of zonal and meridional components obtained in the epoch of the vernal equinox (March 1969), local time.

LONG-PERIOD VARIATIONS OF WIND PARAMETERS IN THE
MESOPAUSE REGION AND THE SOLAR CYCLE DEPENDENCE

K. M. Greisiger,¹ R. Schminder,² and D. Kürschner²

1. Heinrich-Hertz-Institute of Atmospheric Research and Geomagnetism, Observatory of Atmospheric Research, DDR-2565 Kühlungsborn, G.D.R.
2. Collm Geophysical Observatory of the Karl-Marx-University, Leipzig DDR-7261 Collm, G.D.R.

A solar-cycle dependence of wind parameters below 100 km was found for the first time, by SPRENGER and SCHMINDER (1969) on the basis of long-term continuous ionospheric drift measurements in the l.f. range at the observatories in Kühlungsborn and Collm. They observed during the winter a positive correlation of the prevailing wind with solar activity, whereas the amplitude of the semi-diurnal tidal wind showed a negative correlation. This result was confirmed later on by radar meteor wind measurements (method D2) at Obninsk and further D1-measurements at Kühlungsborn and Collm (PORTNJAGIN et al., 1977) and, for the prevailing wind, by DARTT et al., (1983).

Prevailing wind: The continuation of D1-measurements at Collm and the beginning of continuous D2-measurements at Kühlungsborn in 1976 made possible the further investigation of such long-periodic variations in the middle atmosphere. During the years of maximum solar activity (1979-1981) we did not observe the expected large westerly wind velocities in winter; on the contrary, the velocities were as low as during the solar minimum of 1964/65. For the winter periods from 1975/76 to 1983/84, the correlation of the average prevailing wind V_0 (zonal component) with the 10.7 cm radio emission of the sun $F_{10.7}$ now became negative with correlation coefficients as high as -0.93 for D2 and -0.76 for D1-measurements (As winter we took the average of November, December and January).

For the meridional prevailing wind no significant variation was found in this investigation. The same comparison as for winter was done for summer (June, July, August) where the previous investigations gave no correlation. Now the D2 values, too, showed a significant negative correlation of the zonal prevailing wind with solar activity ($r = -0.83$) for the years 1976-1983. The D1-results of Collm have the same tendency but a larger dispersion due to the lower accuracy of the harmonic analysis because of the shorter daily measuring interval in summer (night-time measurements). The same sense of the long-term variation of V_0 in winter and in summer let us expect that it is rather a manifestation of an annual characteristic. Therefore we have estimated annual averages approximating the seasonal variation of V_0 by a mean value V_{00} and an annual and semi-annual harmonic which are the essential terms. The course of the variation of V_0 since 1964 (solar minimum) up to 1984 is reproduced in Fig. 1 in the upper part and compared with annual averages of the solar 10.7 cm radio flux $F_{10.7}$. Here we can see a positive correlation for the years from 1964 to 1973 and a negative one later on with an indication of new change in 1984. (The annual and semi-annual harmonics of the prevailing wind showed no distinct long-term variation as also found by

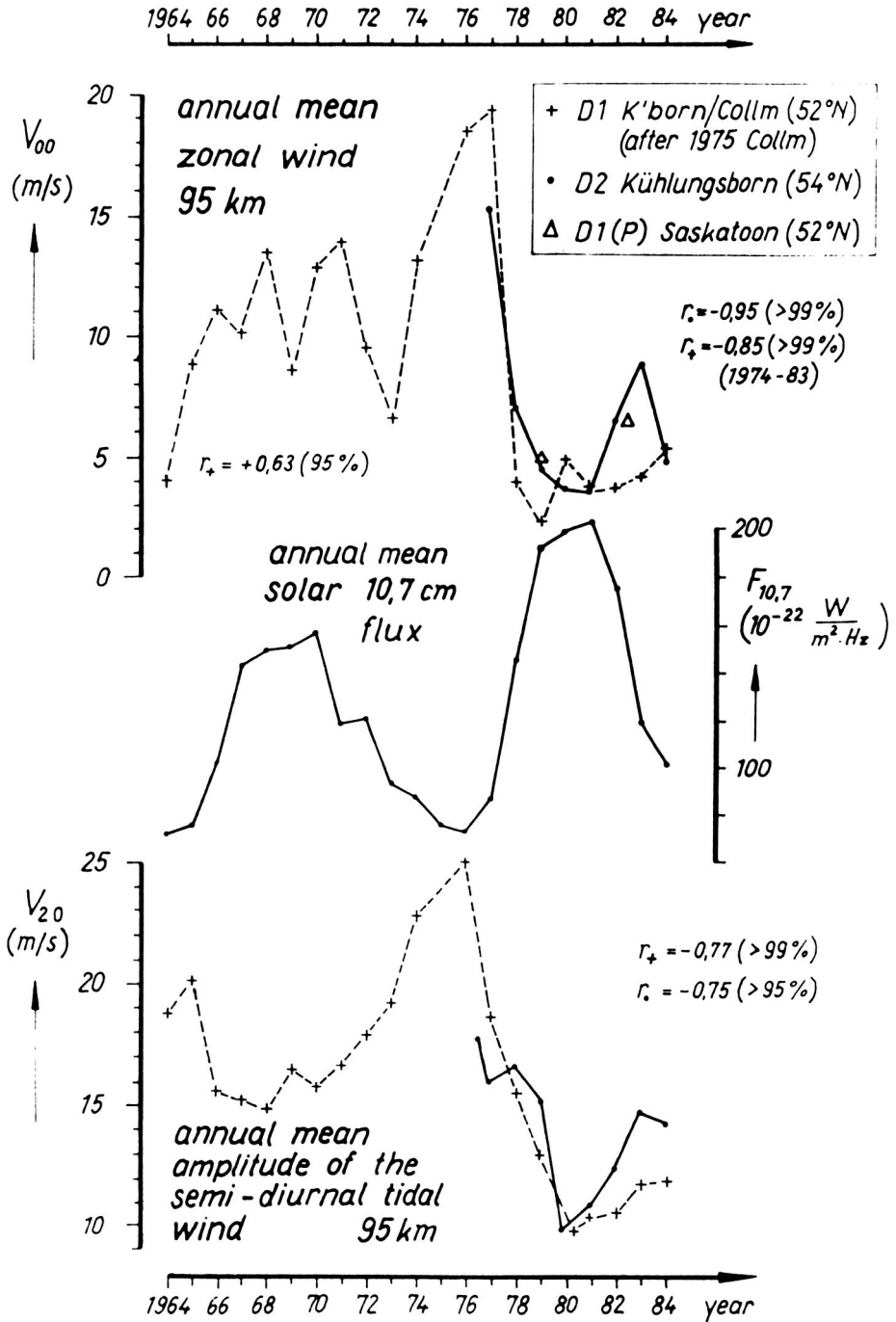


Fig. 1 Variation of annual means of the zonal prevailing wind, amplitude of the semi-diurnal tidal wind (both at 95 km and at medium latitudes) and solar 10.7 cm radio flux for 1964-1984.

DARTT et al., 1983). The corresponding V_{00} values of Saskatoon for 1979 and 1982/83 (taken from the literature and analyzed in the same way) confirm the low velocities during the last solar maximum found by the measurements at Kühlungsborn and Collm. Summarizing one can say that the average circulation (annual mean) of the upper mesopause region exhibits a distinct long-term variation which for some series of years seems to have close connections with solar activity variations. But, in reality, such an alternating mechanism of direct solar control seems to be very improbable. We therefore conclude that the long-periodic variations found in the prevailing circulation in 90-100 km at medium latitudes have essentially an internal atmospheric cause and are of climatic character with a time-scale of about 10 years. The source of these variations could be the recently intensively investigated mechanism of momentum deposition and generation of turbulence by breaking internal gravity waves (LINDZEN, 1981, MATSUNO, 1982, HOITON and ZHU, 1984). This mechanism is very likely the dominating factor for determining the strength and direction of the relatively weak prevailing circulation in the mesopause region.

Semi-diurnal tidal wind: In contrast to the prevailing wind variations we found for the semi-diurnal tidal wind no change in the dependence on solar activity. On the basis of the radar meteor wind measurements at Kühlungsborn we can now show that the same anti-correlation as in winter exists also in summer. The D1 results for summer have a large dispersion and give, as previously, no correlation. But from the D2 results one can suppose that the solar cycle dependence of the semi-diurnal tidal wind is not seasonal and should exist also for annual means. Concerning D1 results one can expect that the relatively short summer period with values of large dispersion will not qualitatively influence an annual characteristic. We estimate (as for the prevailing wind) by harmonic analysis of the seasonal variation an annual mean of the semi-diurnal tidal amplitude V_{20} as well as an annual and semiannual harmonic. In the lower part of Fig. 1 we see the course of V_{20} since 1964 from D1 results and since 1976 from D2 results. The comparison with the variation of the solar 10.7 cm flux shows a clear anti-correlation. The D1 results of V_{20} give a significant correlation coefficient $r = -0.77$ for almost two solar cycles (1964-1984). The D2 results confirm this with $r = -0.75$ for the last solar cycle.

Direct solar control of the amplitude of the semi-diurnal tidal wind which is a manifestation of the thermally excited solar semi-diurnal atmospheric tide seems to suggest itself. The thermal excitation takes place mainly by absorption of the solar UV in the wave length range 200-370 nm due to ozone in the stratopause region. But after recent satellite measurements we have only a weak enhancement of O_3 and UV (some percents) from solar minimum to maximum and, moreover, our observations show a decrease of the tidal wind amplitude with increasing solar activity. The semi-diurnal tidal wave may be influenced further by the propagation conditions between the excitation layer and the level of observations; that is by the temperature profile and the background zonal wind. As can be seen from recent numerical models of the semi-diurnal tide (WALTERSCHEID et al., 1980) these factors must have variations during the solar cycle of the same order as their seasonal ones in order to cause effects of the observed magnitudes (percent variation 50-100 %). But solar cycle variations of temperature and zonal wind in the upper stratosphere and mesosphere, found up to now, are too small and not in the right sense to explain our results.

Continuous wind observations in the upper mesopause region over more than twenty years revealed distinct long-term variations, the origin of which cannot be explained with our present knowledge. But, for a climatology of the middle atmosphere, they are of great interest. Further studies are therefore desirable, both theoretical and observational. It has been shown that lower ionospheric drift measurements and the radar meteor wind method are valuable tools for a continuous monitoring of the wind field at the top of the middle atmosphere over a time period of climatological extent.

References

1. Dartt, D.G. Nastrom, and A. Belmont, 1983, J. Atm. Terr. Phys. 45, pp. 707-718.
2. Holton, J.R., and Zhu Xun, 1984, J. Atm. Sci. 41, pp. 2653-2662.
3. Kaidalov, O.V., K.M. Greisiger, and K. Sprenger, 1977, Phys. Solaterr., Postdam, pp. 91-96.
4. Lindzen, R.S., 1981, J. Geophys. Res. 86, pp. 9707-9414.
5. Matsuno, T., 1982, J. Meteorol. Soc. Japan 60, pp. 215-226.
6. Sprenger, K. and R. Schminder, 1969, J. Atm. Terr. Phys. 31, pp. 217-221.
7. Waiterscheid, R.L., J. G. De Vore, and S. V. Venkatesvaran, 1980, J. Atmos. Sci. 37, pp. 455-469.

THE LOWER THERMOSPHERE WIND REGIME FROM
SIMULTANEOUS OBSERVATIONS OVER EUROASIA
(COLLM, DUSHANBE, FRUNZE)

R. Schminder, D. Kurschner,
Geophysical Observatory, Collm, DDR

K. A. Karimov, R. B. Bekbasarov,
Institute of Physics, Frunze, USSR

L. A. Riazanova,
Central Aerological Observatory, Dolgoprudny, USSR

R. P. Chebotarev, Kh. Nabotov
Institute of Astrophysics, Dushanbe, USSR

The circulation in the lower thermosphere as determined from the results of measurements in 1984 in Collm, Volgograd, Frunze and Dushanbe is considered in the present report. In Collm ionospheric drift measurements were taken using the method of spaced reception in the long wave range. The other three stations used the D_2 method. Average daily values of wind velocity were used. Discontinuity of measurements ranged from a day to a week. Preliminary data in Collm were reduced to the common average height of 93 km with the help of vertical profiles of wind velocity components.

Figures 1 and 2 present the results of measurements of zonal and meridional wind velocity components at the above mentioned stations. In Fig. 1 wind direction from west to east (westerly winds) corresponds to positive values. In Fig. 2 wind direction from south to north (southerly winds) corresponds to positive values.

Zonal circulation changes from westerly to easterly winds were observed in the winter, in periods of spring time reversal and during stratomesospheric rises in temperature. In January one local rise in temperature was observed. At the lower thermosphere level this rise in temperature caused a change in the sign of the circulation only over Collm. The other stations measured in this period only a tendency toward weakening of the westerly circulation. An especially powerful warming in the stratosphere was observed between the end of February and the beginning of March. Easterly winds were observed at all four stations. In the stratosphere, the pronounced cyclonic vortex was surrounded by a well developed zone of high pressure with two very active centers - over the Pacific and North Africa. They intensified almost simultaneously and the warming spread over a vast territory -- all over Euroasia and the polar region. As a result of the final warming and rapid destruction of the cyclonic vortex a baric and circulatory reversal occurred in the middle of March.

In the same period the spring time reversal process began in the lower thermosphere. The reversal processes were marked by the intensity of the easterly winds and their duration and dates. In the course of the whole year considerable uncorrelated variation in magnitude and direction of the meridional wind was observed.

In the summer in the lower thermosphere an ordinary summer circulation was observed. In the stratomesosphere, the cyclonic vortex had also a

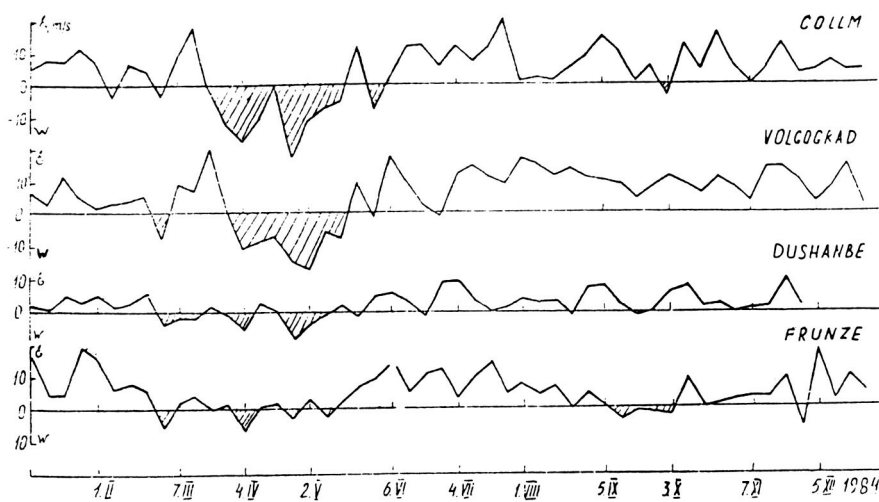


Fig. 1 Zonal winds at 93 km for 1984 from Collm, Volgograd, Frunze and Dushanbe.

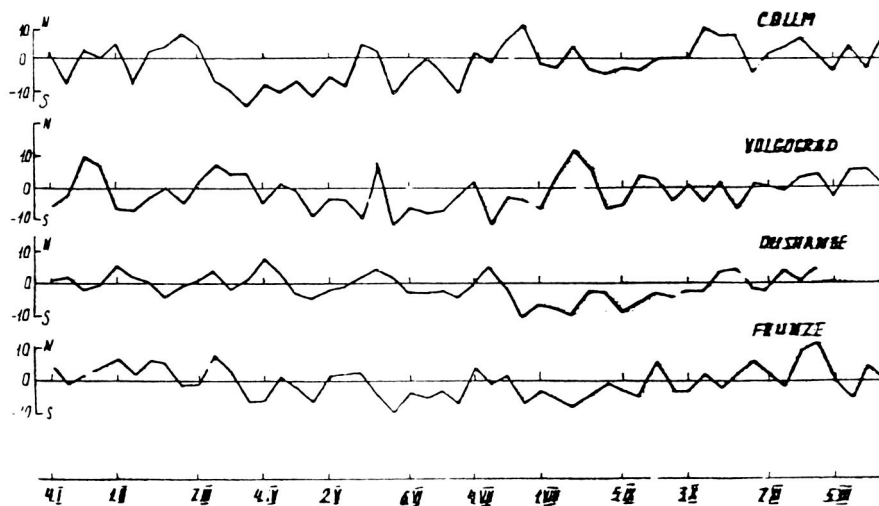


Fig. 2 Meridional winds as for Fig. 1.

normal average development. Tables 1 and 2 show the average values and their dispersions.

On the basis of the observational data, it can be noted that the connection of winter large scale processes in the lower thermosphere with those in the lower strata is different for Europe and Central Asia. This results in differences in intensity, duration and dates of spring reversals. According to the results of European and Central Asian stations, the synchronous reversal of zonal wind is connected with simultaneous activity of two centers in the stratosphere, in our case over the Pacific and North Africa.

Quasi-periodical variations were present in the meridional winds, but correlation between data of any pair of the stations considered is absent. The correlation of the zonal wind characteristics in the summer is also absent. Fig. 3 presents the dependence of the correlation coefficient of the zonal wind on distance during the winter. Fig. 3 shows that significant correlation in zonal wind occurs for distances of up to 2,000 km between stations. This confirms the well known observations from Kazan, Obninsk and Kharkov.

Table 1.

Zonal Wind	\bar{V}_{I-XII}	\bar{V}_{I-IV}	$\bar{V}_{VI-VIII}$	\bar{V}_{IV}	σ^2_{I-XII}	σ^2_{I-IV}	$\sigma^2_{VI-VIII}$
Collm	3,4	-0,3	7,6	-13,5	74	121	31
Volgograd	5,7	1,7	11,0	-10,2	69	74	25
Dushanbe	2,1	0	3,7	- 3,0	15	14	14
Frunze	4,4	4,5	7,2	- 1,5	35	50	17

Table 2

Meridional Wind	\bar{V}_{I-XII}	\bar{V}_{I-IV}	$\bar{V}_{VI-VIII}$	σ^2_{I-XII}	σ^2_{I-IV}	$\sigma^2_{VI-VIII}$
Collm	-1,1	-3,2	-1,2	39	47	32
Volgograd	-1,0	-0,8	-2,6	34	33	21
Dushanbe	-0,3	1,0	-3,6	20	16	17
Frunze	-0,3	0,5	-3,5	25	24	14

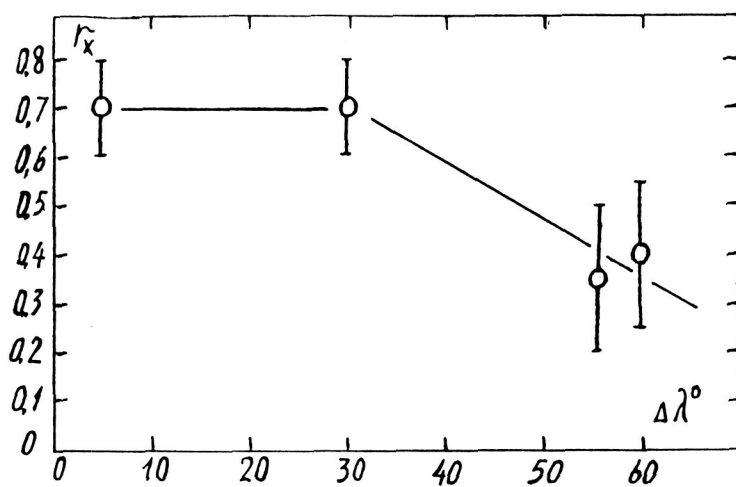


Fig. 3 Dependence of the correlation coefficient of the zonal wind with distance during the winter of 1984. $\Delta\lambda$ is degrees of longitude.

WIND REGIME PECULIARITIES IN THE
LOWER THERMOSPHERE IN THE WINTER OF 1983/84

I. A. Lysenko, N. A. Makarov, Yu. I. Portnyagin, B. I. Petrov¹,
K. M. Greisiger², R. Schminder, and D. Kurschner³

1. Institute of Experimental Meteorology, Obninsk, USSR
2. Hertz Institute of Atmospheric Sciences and Geomagnetism, GDR
3. Karl-Marx University, GDR

This report analyses temporal variations of prevailing winds at 90-100 km obtained from measurements carried out in winter 1983/1984 at three sites of the USSR (Obninsk, Volgograd and Khabarovsk) and two sites in the German Democratic Republic (Kuhlungsborn and Collm). These variations are compared with those of the thermal stratospheric regime.

Measurements in Obninsk, Khabarovsk and Kuhlungsborn were carried out using the drifts D2 method (meteor wind radar) and in Collm by the D1 method (ionospheric drifts). In Obninsk and Khabarovsk wind data were obtained simultaneously in for directions and in Volgograd measurements were carried out using the Greenhow method.

Temporal variations of zonal and meridional prevailing wind components for all of the five sites are given in Figures 1a, 1c,. Fig. 1a presents also zonal wind data obtained using the partial reflection wind radar in Saskatoon (Canada) (NAUJOKAT and LABITZKE, 1984). Wind velocity values (Fig. 1a) for Saskatoon were obtained by averaging data recorded at this site between 105 and 91 km altitude. Wind velocity data averaged in such a way can be related to about the same height interval to which the data obtained by the meteor radar and ionospheric methods at the other considered sites refer, i.e., to the mean height of the meteor zone (about 95 km).

Firstly, it is worth noting the good agreement between the temporal course of zonal and meridional prevailing wind components measured in the opposite directions (S-N, W-E) for Obninsk and Khabarovsk. This indicates that the spatial scales of synoptic wind field inhomogeneities in the lower thermosphere exceed significantly the distances between the opposite sounding regions which are spaced some 300-400 km apart.

The results presented in Fig. 1a and 1c show that there are significant fluctuations about the seasonal course of both zonal and meridional prevailing winds.

Many investigators consider that zonal wind disturbances observed in winter characterized by direction reversals or sudden decrease of wind velocity are often connected with stratomesospheric warmings. In this connection it is of interest to compare time variations of zonal prevailing wind with the thermal regime of stratosphere. With this aim in view we used temperature data near the pole at the level of 10 hPa as well as radiance in the infrared referred to the levels of 4 pHa and 1,7 hPa (NAUJOKAT and LABITZKE, 1984, (Fig. 1b).

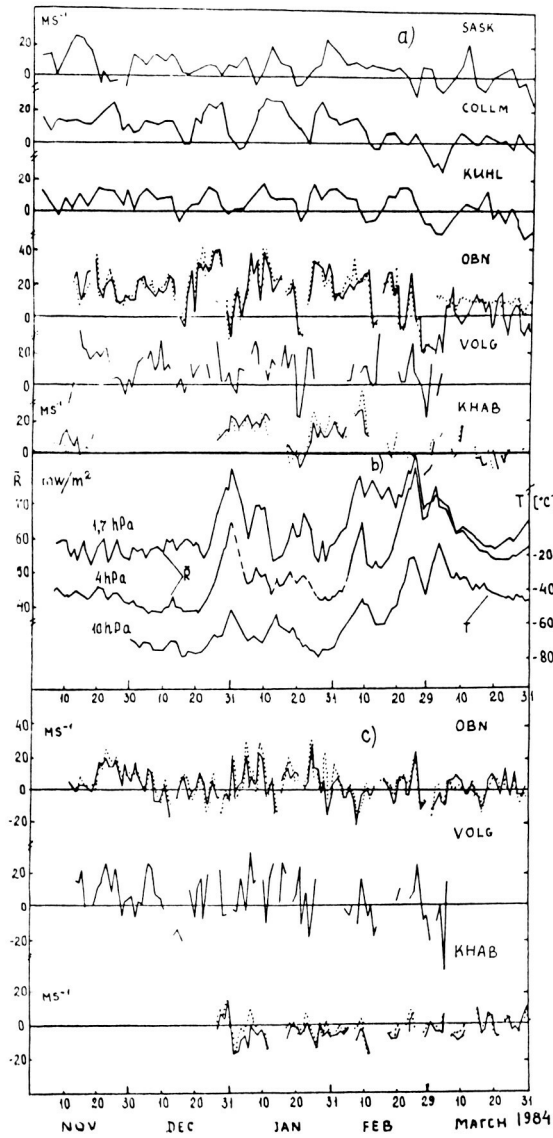


Fig. 1 Day-to-day variations of (a) zonal prevailing wind velocities (b) temperature near the pole at the level of 10 hPa and radiance in infra-red at 1,7 and 4 hPa and (c) meridional prevailing wind velocities.

According to the data from Obninsk (Fig. 1a), the first reversal of zonal wind occurred in the middle of December. At the same time easterly winds were observed in the lower thermosphere over Volgograd (Fig. 1a) and Collm. The decrease of westerly winds practically to zero was observed in Kuhlungsborn and Saskatoon. Due to the fact that all the observation sites are located in a narrow latitudinal interval one can conclude that in the middle of December there was a global disturbance of zonal circulation in the lower thermosphere with a slight dependence on longitude. The analysis of the vertical zonal wind profile from observation data from Saskatoon (NAUJOKAT and LABITZKE, 1984) shows that the boundary between easterly (above 105 km) and westerly (below 105 km) wind usually observed at 105 km in winter shifted to 97 km in the middle of December. At the same time, in the stratosphere at the level of 10 hPa at 60°N (NAUJOKAT and LABITZKE, 1984) there were no significant variations of the mean zonal westerly wind. Hence, the height gradient of the zonal wind in the mesosphere-lower thermosphere increased on the average. According to the thermal wind equation such an increase of the zonal wind gradient means that the latitudinal temperature gradient also increases. So, it can be stated that temperature has increased from middle latitudes to the pole (warming) and has decreased toward the equator.

Neither the temperature itself (Fig. 1b) nor the latitudinal temperature gradient (NAUJOKAT and LABITZKE, 1984) varied in the stratosphere during this period. This confirms the hypothesis that in winter in the mesosphere-lower thermosphere there may be warming (cooling) processes not connected with stratospheric warmings.

The first significant stratospheric warming occurred late in December-early January. As seen from Fig. 1a, the reaction to this warming in the lower thermosphere was non-zonal. While in Obninsk, Kuhlungsborn and Collm there was a significant decrease of zonal wind velocity and even reversal of its direction, in Saskatoon and especially in Khabarovsk the stable westerly winds were maintained. It can be hypothesized that during this period the longitudinal structure of the zonal wind in the lower thermosphere was characterized by a planetary wave with the zonal wave number $s = 1$.

The reaction of lower thermospheric winds to the second warming wave in the stratosphere observed in the third decade of January (Fig. 1a) was different. During this period there occurred a reversal to easterly winds at all the sites (Obninsk, Volgograd, Kuhlungsborn, Collm and Saskatoon). Hence, the zonal wind reaction in the lower thermosphere can be classified as global and non-longitude dependent. According to data from Saskatoon (NAUJOKAT and LABITZKE, 1984) the lower boundary of the easterly wind zone decreased to 90 km. It can be said that during this period the thermal structure of the lower thermosphere qualitatively varied in the same way as during the disturbance observed in mid-November.

Lastly, the final stratospheric warming late in February-early March was accompanied by a zonal wind reversal at practically all the sites (Fig. 1a) and this disturbance was similar to the previous one in character. However, the zonal wind gradient with height in the

mesosphere-lower thermosphere changed its sign (NAUJOKAT and LABITZKE, 1984), i.e., the latitudinal temperature gradient also changed its sign. Hence, unlike the previously considered disturbances, in this case temperature should decrease from moderate latitudes to the pole and increase toward the equator. Such height structure of the zonal wind and latitudinal temperature structure are typical of the spring circulation reconstruction which begins usually late in March.

The analysis of day-to-day meridional wind variability observed in the lower thermosphere over Obninsk, Volgograd and Khabarovsk (Fig. 1c) showed that there is no clear-cut correlation between variations of the meridional wind and the temperature in the stratosphere. The meridional wind behavior over Obninsk and Volgograd significantly differs from that over Khabarovsk. At the same time there is a definite correlation between long-period (about two weeks) variations of meridional wind over Obninsk and Volgograd. There is no connection between velocity pulsations with periods of 2-5 days either for meridional or zonal wind components over all the observation sites. It should be noted that meridional wind velocities averaged over the observation period in Obninsk and Volgograd differ from the corresponding averaged values for Khabarovsk in absolute value as well as in sign. Thus, significant longitudinal dependence of meridional wind can be observed in winter and should be taken into account when constructing non-zonal models of global circulation.

These results as presented, show that the winter period is characterized by three types of disturbance in the lower thermospheric circulation regime: a) non-longitude dependent disturbances with the wind gradient varying significantly with height; b) longitude-dependent disturbances; and c) non-longitude dependent disturbances with the wind gradient significantly varying with height.

References

1. Naujokat, B., Labitzke, K., 1984, The stratospheric-mesospheric circulation in winter 1983/1984, MAP Newsletters, Sept.
2. Portnyagin, Yu.I., Lysenko, I.A., 1983. Wind regime peculiarities in the meteor zone of moderate latitudes in winter 1978/79 - 1980/81, Meteorologiya i Gidrologiya, Moscow, No. 8, pp. 15-20.

ON THE INTERCONNECTION OF DYNAMIC PROCESSES IN THE LOWER
THERMOSPHERE WITH METEOROLOGICAL PHENOMENA IN
THE TROPOSTRATOSPHERE

A. N. Fakhrutdinova, A. M. Stepanov, and I. P. Perevedentsev

Kazan State University
Kazan, USSR

Nowadays the atmosphere is considered a single dynamic system governed by inner and outer factors, the separate layers of which (troposphere, strato-mesosphere, thermosphere) are in a state of interaction though they differ physically from one another in thermal stratification and energetic processes. There is now substantial acceptance of the point of view that disturbances of meteorological fields caused by baroclinicity and orography are transferred up from the troposphere to the stratosphere by the wave mechanism. This is substantiated not only theoretically, but also by the results of statistical studies of measured thermodynamic parameters.

This paper presents observational data of thermodynamic parameter connections in the troposphere-stratosphere-mesosphere-lower thermosphere height range. Data from radio and rocket atmosphere soundings over Heiss Island (80°3 N) and Volgograd (48°4 N) were used. Over Kazan (55°4 N), radiosonde data up to 30 km and meteor wind radar observations in the altitude range of 80-100 km carried out as part of the MAP/GLOBMET international program were analyzed. The trop-strato-mesosphere statistical characteristics obtained during the five year period at Heiss Island and Volgograd serve as a background for Kazan where observational results were used for analysis of the winter and summer period of 1984.

For all the above observation stations in winter and summer periods temperature field correlation coefficients pass through zero. As observed at the tropopause, this is a consequence of the antiphase nature of the thermodynamic field disturbances in the tropo- and stratospheres. In the stratosphere the correlations between the levels are higher and weaken more gradually as the distance between the levels increases.

In spring, the correlations obtained testify to the downward transmission of the reconstruction mechanism.

This report attempts to define the interconnection between the temperature field disturbances in the tropo-stratosphere and the dynamic regime in the lower thermosphere in winter and summer, as revealed by observations in Kazan. Characteristic analysis of prevailing wind influx in the meteor zone (on 10-31 of January and 8-16 of February, 24-29 of February, 1984) and the tropo-stratosphere temperature regime (on 1-8 of January, 24-29 of February, 1984) showed the presence of wave disturbances with time scales of 2-8 days. Reciprocal correlation analysis showed the presence of wind parameter disturbances in the meteor zone that propagated from the troposphere with a 1-6 day delay from altitudes of 30-10 km respectively. Curves of reciprocal correlation functions of temperature T , prevailing wind amplitude A_0 , semidiurnal influx $A_2(\rho_T, A_0, \rho_T, A_2)$ are presented in Figs. 1 and 2.

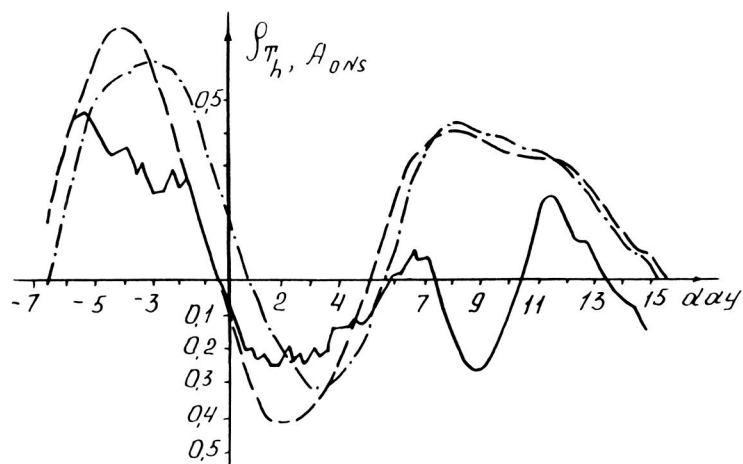
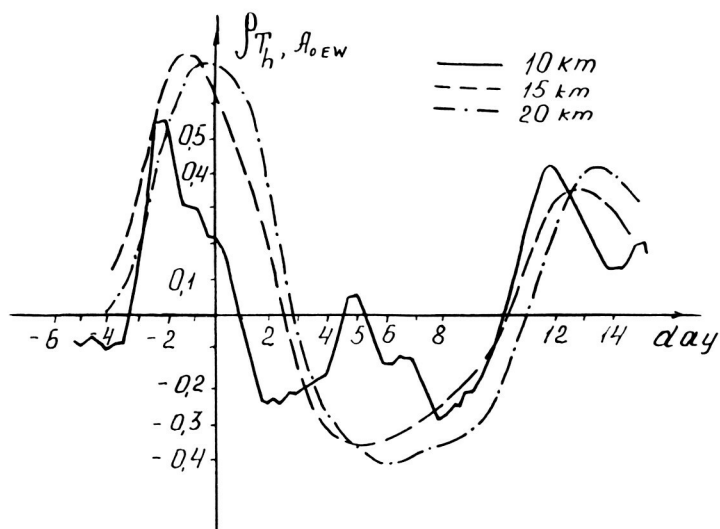


Fig. 1 Reciprocal correlation function of temperature T and amplitude of zonal A_{OEW} and meridional A_{ONS} prevailing wind component in the winter period.

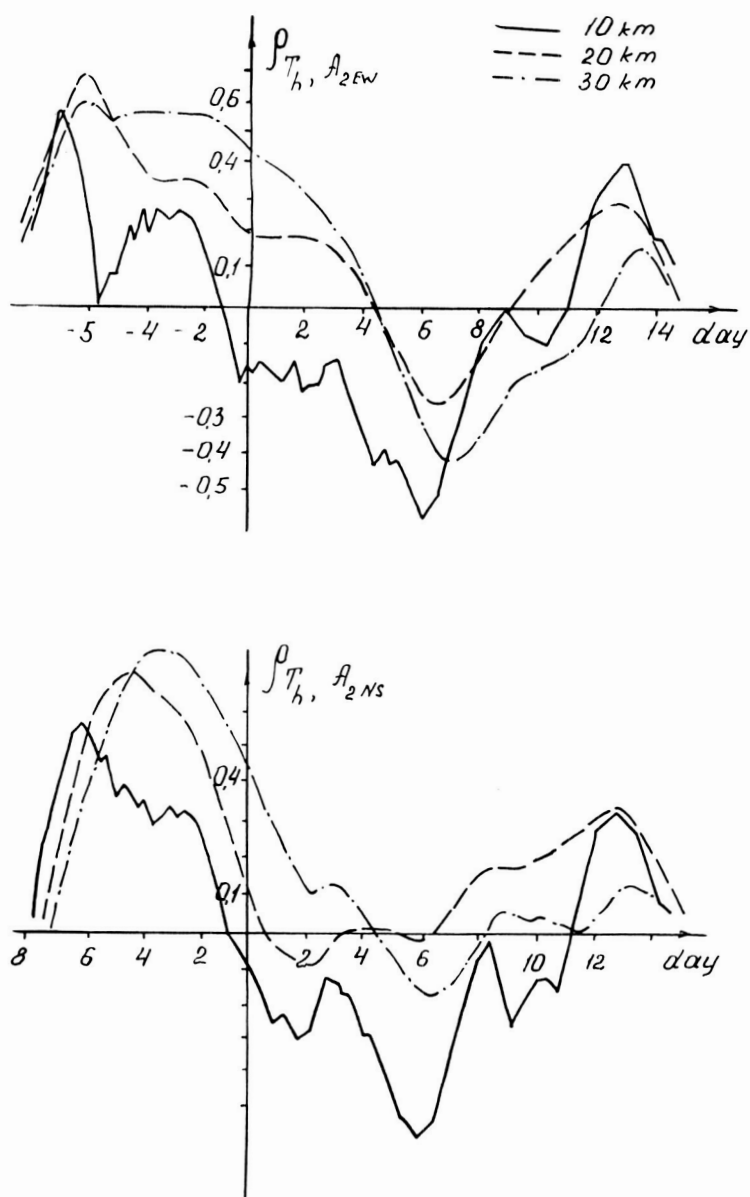


Fig. 2 Reciprocal correlation function of temperature T and amplitude of zonal A_{2EW} , meridional A_{2NS} semidiurnal influx component in the winter period.

A sharp reversal coinciding with the rise in temperature in the troposphere and the decreases of the prevailing wind vector on the stable wind position are more noticeable for the zonal component. The amplitude of the prevailing wind and the semidiurnal influx are modulated by a two-day wave.

In the summer period (July 16 - August 6, 1984) there were disturbances with time scales of about 2-8 days in the prevailing wind field, in the semidiurnal tide in meteor zone, and in the temperature field in the tropo-stratosphere. Reciprocal correlation function curves for the summer period are shown in Fig. 3 and 4. No process of successive transmission of temperature field disturbances from the troposphere-stratosphere to the lower thermosphere was revealed in the summer period.

Nevertheless the reciprocal correlation analysis shows the presence of a quasi-two-day wave in the meteor zone in the semidiurnal tide with a delay of about 4 days relative to the lower troposphere. In the prevailing wind a 4-day wave is traced along with a 2-day wave which is revealed in the meteor zone in the zonal component with a delay of about 4 days relative to the troposphere level. The reciprocal correlation function curves in summer reveal a maximum correlation of semidiurnal tide and temperature with a delay of 5-6 days observed between the troposphere and the meteor zone. It should be noted that the disturbance of the temperature field T at altitudes of 15-20 km is in antiphase with the 1-10 km level. The wind parameter disturbance at meteor heights (80-100 km) is in phase with the disturbance T in the 1-10 km layer and in antiphase with the 15-20 km layer.

When the change in the prevailing wind vector amplitude is strong in the summer period, the direction of the prevailing wind is stable except for the short lived reversals during the day on July 24 and 30 and August 3, corresponding to the minimum values of wind amplitude.

These results testify to the interconnection of thermodynamic parameter disturbances in the middle atmosphere, which are most clearly revealed in the winter period.

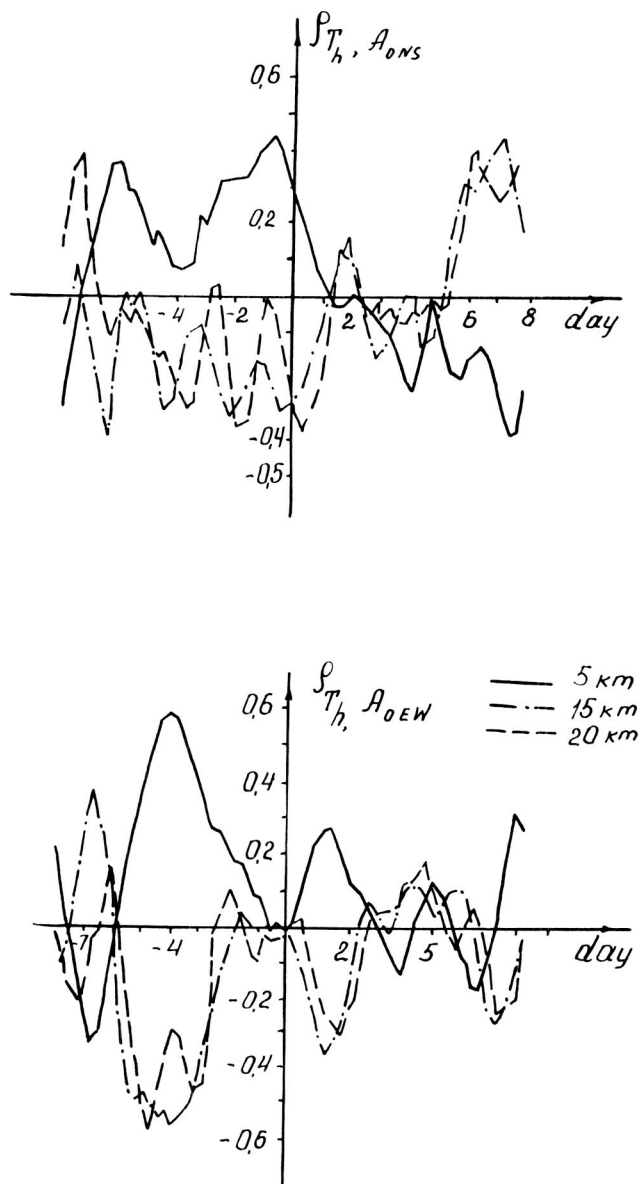


Fig. 3 Reciprocal correlation function of temperature T and amplitude of zonal A_{OEW} and meridional A_{ONS} prevailing wind component in the summer period.

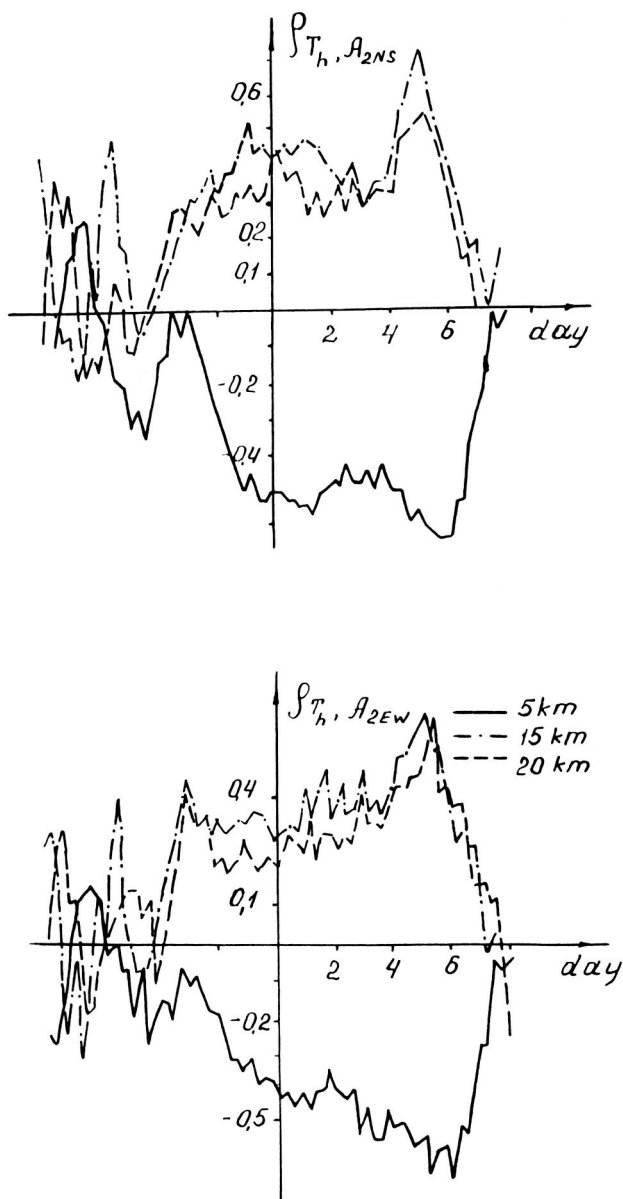


Fig. 4 Reciprocal correlation function of temperature T and amplitude of zonal A_{2EW} and meridional A_{2NS} semidurnal influx component in the summer period.

C-2

MEAN PRESSURE DISTRIBUTION AND GEOSTROPHIC CIRCULATION IN THE METEOR ZONE

Yu. P. Koshelkov

Central Aerological Observatory
USSR State Committee for Hydrometeorology
and Control of Natural Environment

BOUTKO et al., (1982) used available satellite radiometer data to estimate 0.1 mb constant pressure heights in the mesosphere and KOSHELKOV and KOVSHOVA (1984) derived, 0.1-0.005 mb or 0.1-0.001 mb layer thickness from which were compiled height fields of the 0.005 mb and 0.001 mb levels. The close relationship ($z \sim 0.95$) discovered between mean thicknesses (calculated for each month at various latitudes from CIRA (1972) and zonal values of atmospheric radiances (LABITZKE and BARNETT (1981)) observed in channel 3000 of the pressure modulated radiometer (PMR) on board the Nimbus-6 satellite in 1975-1978 was used (see Fig. 1). An analysis of the geopotential height fields in the lower thermosphere of the southern hemisphere was carried out by KOSHELKOV (1984) and KOSHELKOV and KOVSHOVA (1984). The present paper deals mainly with northern hemisphere patterns. The analysis was limited to regions north of 20°N due to poor reliability of the thickness estimates from the PMR data at low latitudes.

Monthly mean maps of the geopotential heights of the 0.005 mb and 0.001 mb surfaces in the northern hemisphere are presented in Fig. 2. The lower of these characterize pressure distribution at geometric heights of about 81 to 84 km while the upper level corresponds to 91-94 km, i.e., to the lower part of the meteor zone. In this layer, as Fig. 2 confirms, the main feature of the pressure distribution in summer is the presence of an anticyclonic system centered around the pole. In accordance with observational evidence, the polar anticyclonic vortex dominating the stratosphere and mesosphere attenuates with increasing height. It is markedly pronounced (though not so well as in the mesosphere (KOSHELKOV, 1984)) at the 0.005 mb level, while at heights greater than 90 km (0.001 mb level) it is limited to polar regions north of 65°N where the circular low pressure area is located.

It should be noted that contraction of the area dominated by anticyclonic circulation with increasing altitude in the lower thermosphere (between the 0.005 mb and 0.001 mb levels) progresses more rapidly in the northern than in the southern hemisphere. Actually, the latitudinal pressure patterns at the 0.001 mb level were similar in the two hemispheres, and at the 0.005 mb level the pressure minimum was marked in the southern hemisphere near 40-45°S while a monotonous decrease from the pole towards low latitudes was observed in the northern hemisphere.

The center of the anticyclonic vortex during the period of its maximum development (in June-July, according to the present analysis) was located near the pole. In the middle latitudes geopotential values were somewhat higher in the American and Pacific areas as compared to other sectors of the hemisphere. As a result, the asymmetry of the pressure distribution relative to the North Pole was a little higher than that recorded for the southern hemisphere (ENTZIAN and TARASENKO, 1971; MININA et al., 1977); one cannot exclude, however, the possibility that the observed asymmetry in summer is largely related to limitations of the map compilation technique or partly to the short period of observation.

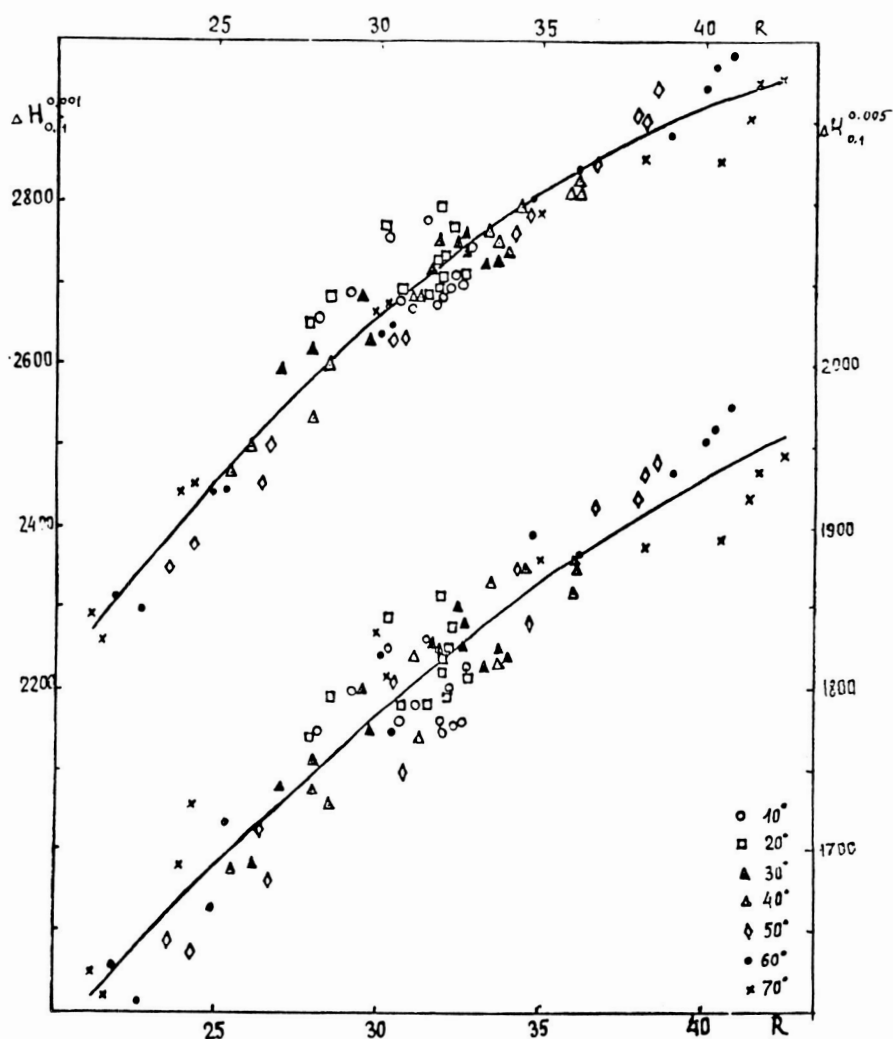


Fig. 1 Relationships between monthly mean PMR ch. 3000 radiances ($\text{W/m}^2 \text{ sr cm}^{-1}$) in 1975-1978 and monthly mean thicknesses (dm) of the layers 0.1-0.001 mb (above) and 0.1-0.005 mb (below), calculated from CIRA 1972 for various latitudes (10° to 70°N).

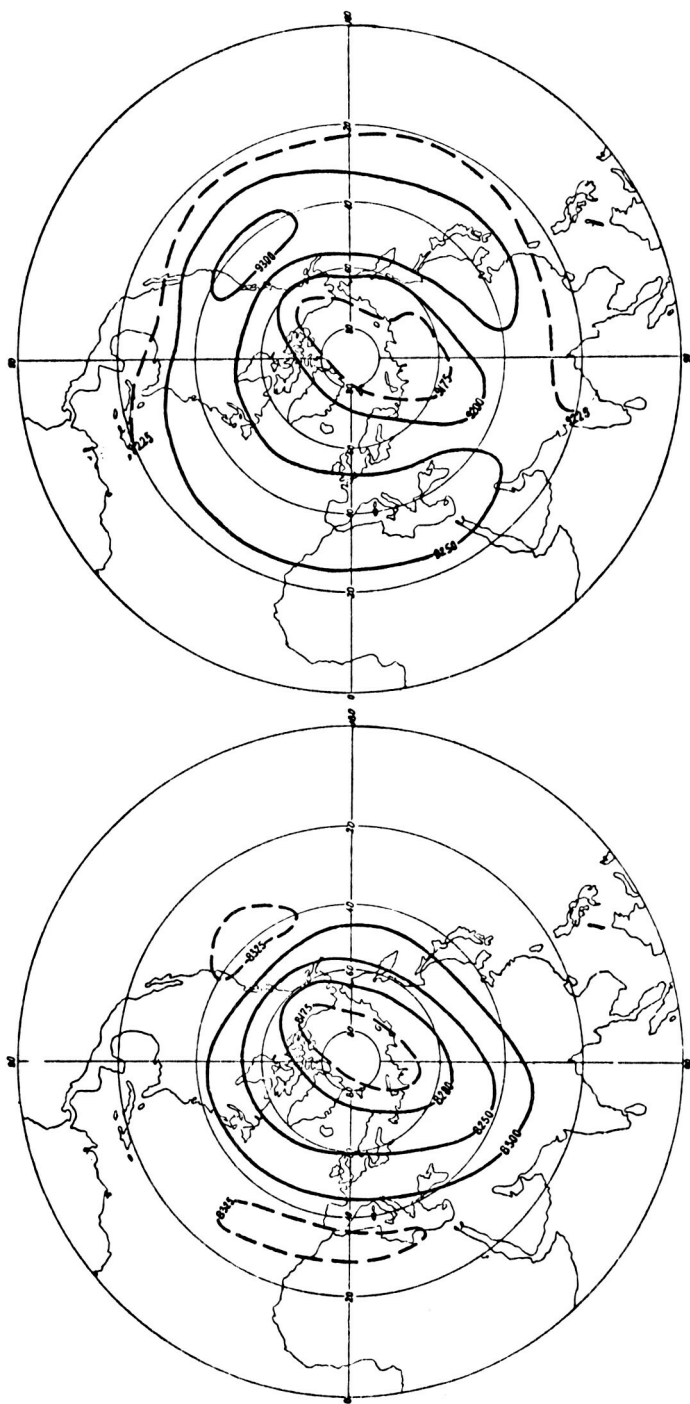


Fig. 2 Monthly mean maps of the geopotential height (dm) of the 0.001 mb (above) and 0.005 mb (below) levels in the Northern Hemisphere, January.

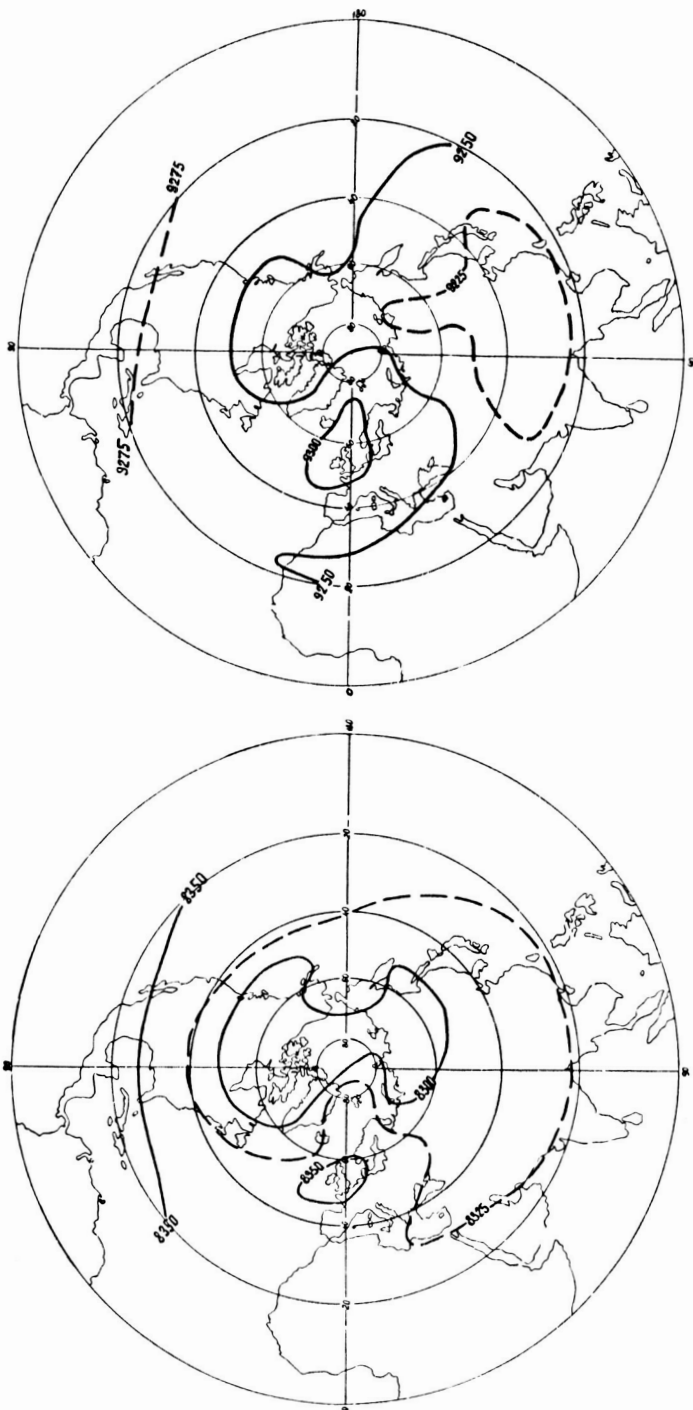


Fig. 2 (continued) March

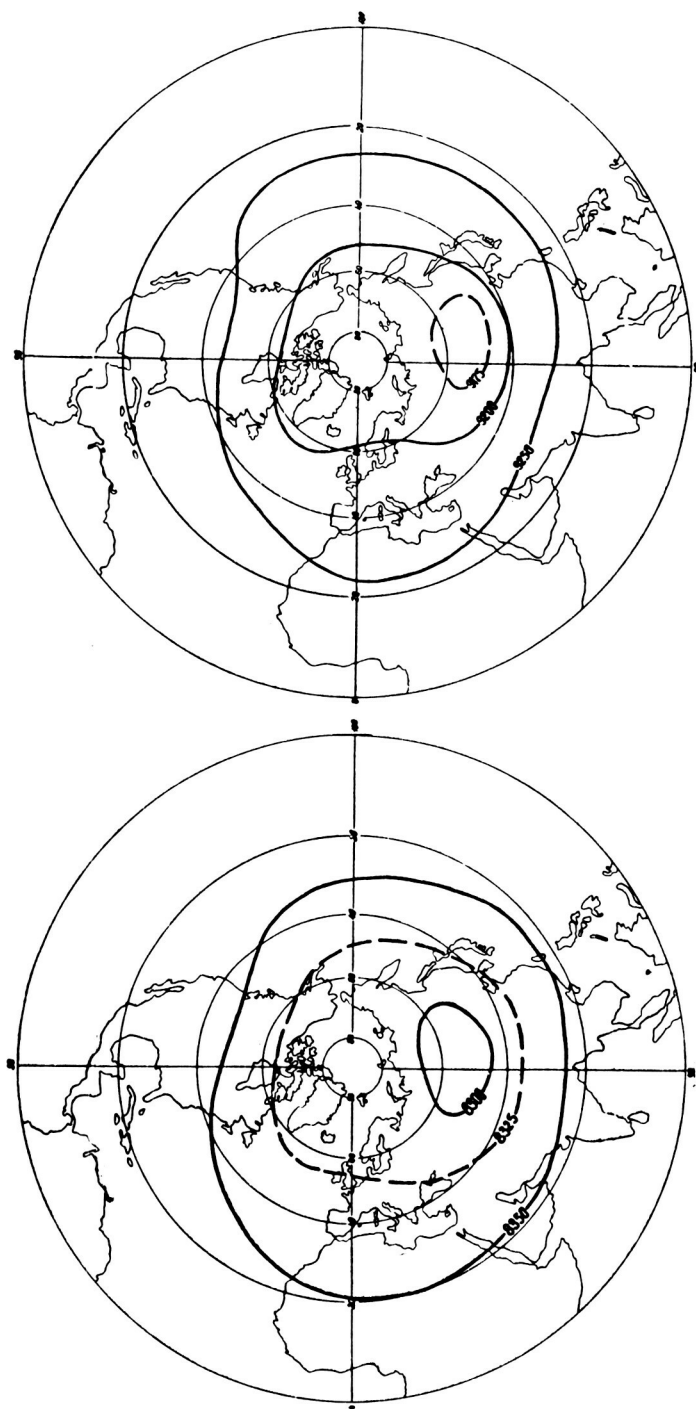


Fig. 2 (continued) April

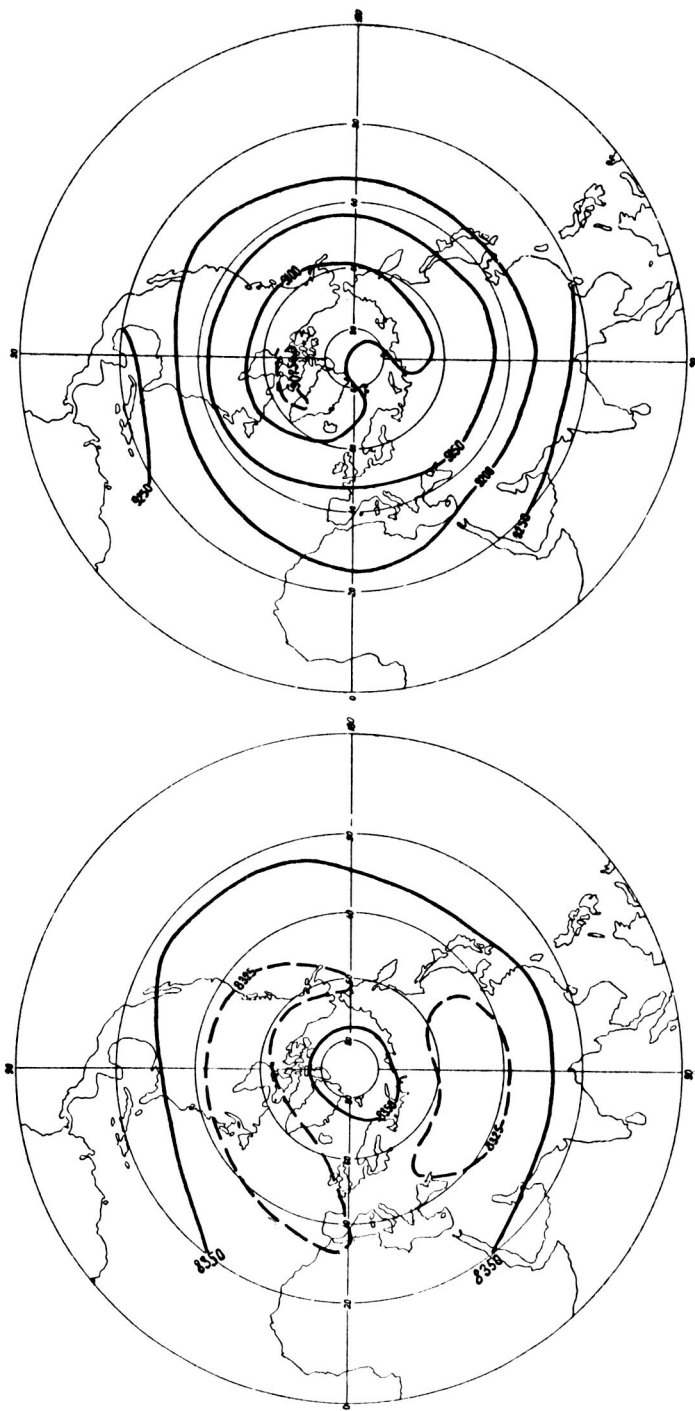


Fig. 2 (continued) May

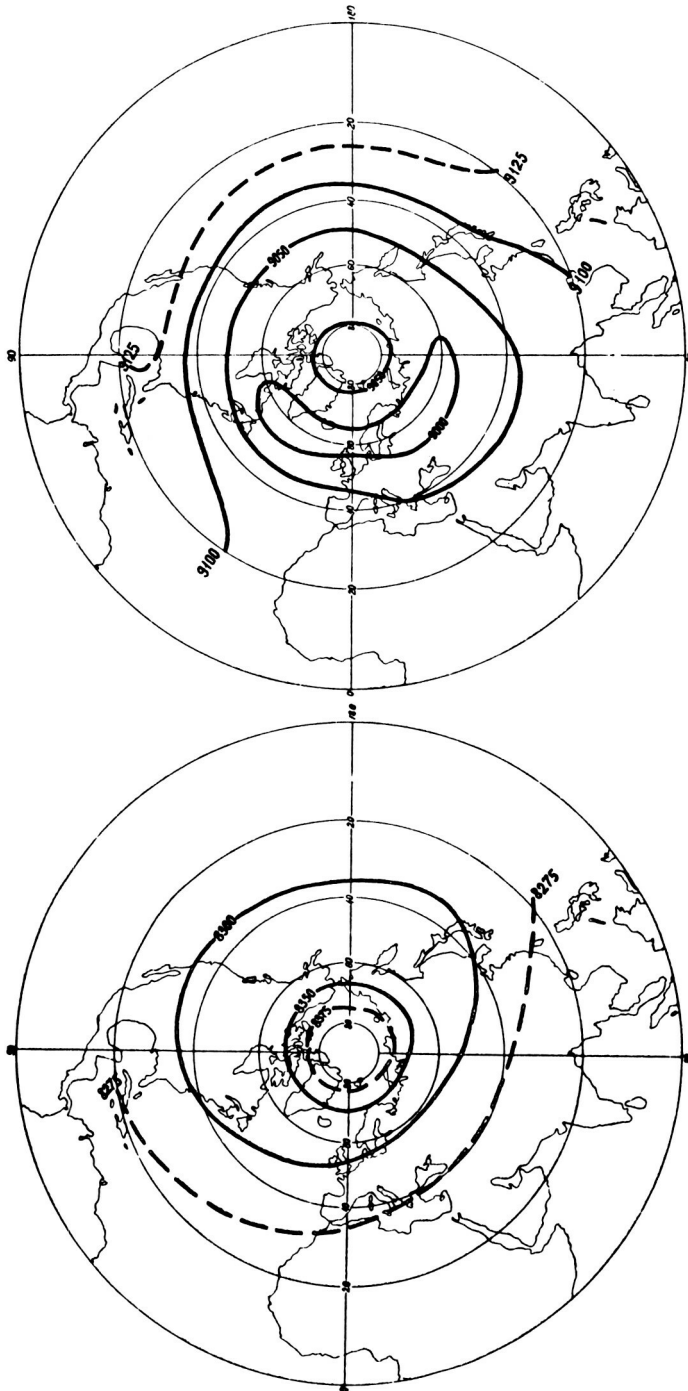


Fig. 2 (continued) June

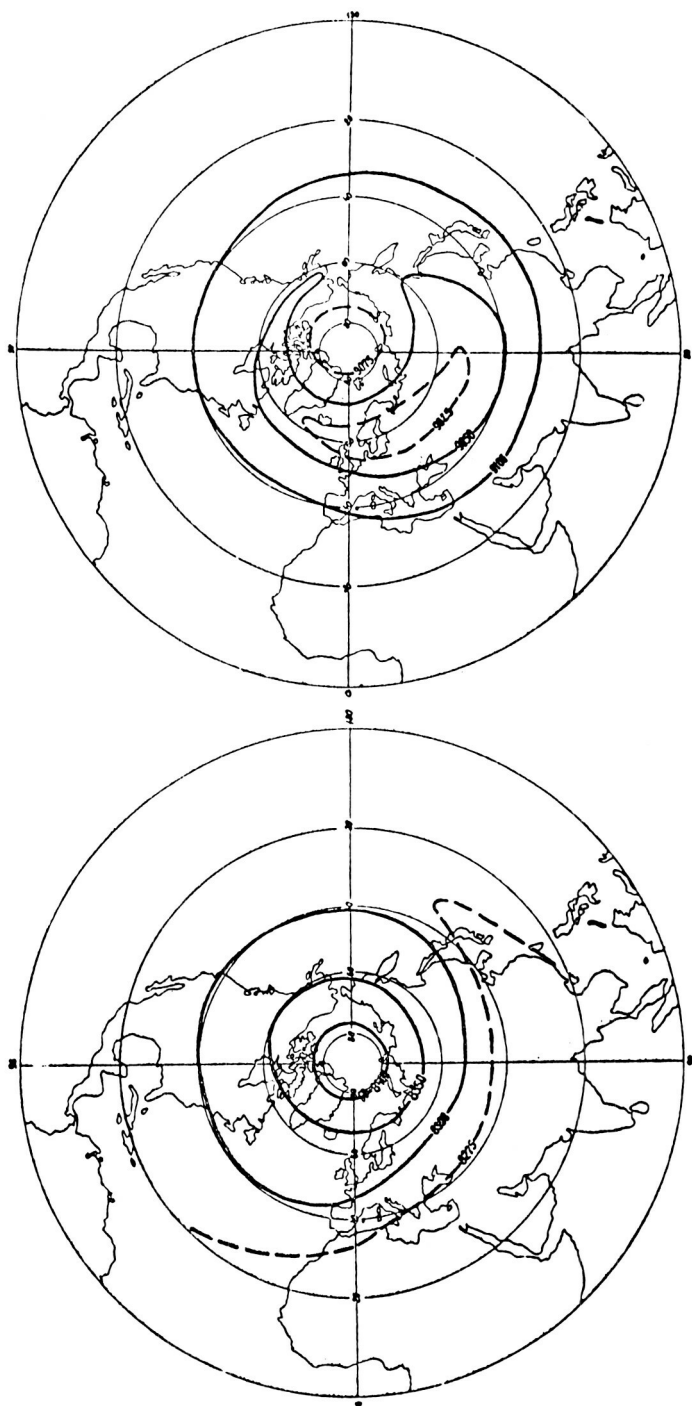


Fig. 2 (continued) July

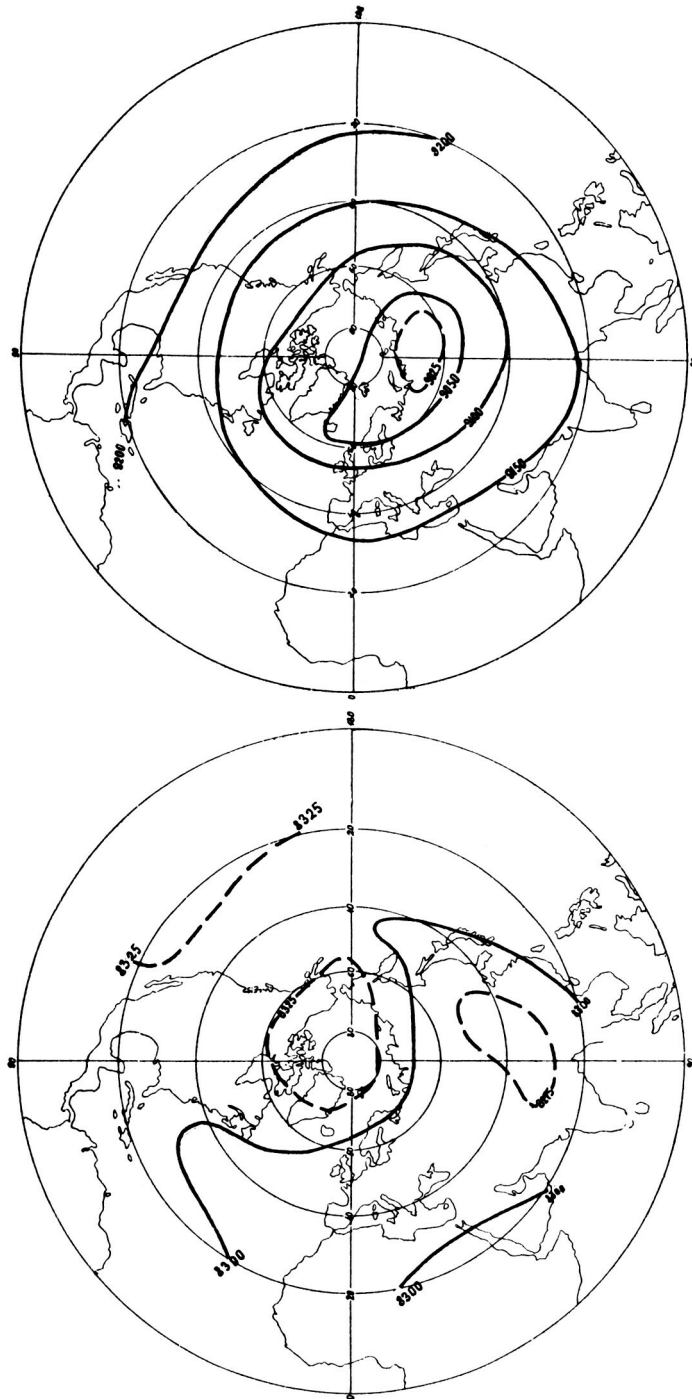


Fig. 2 (continued) August

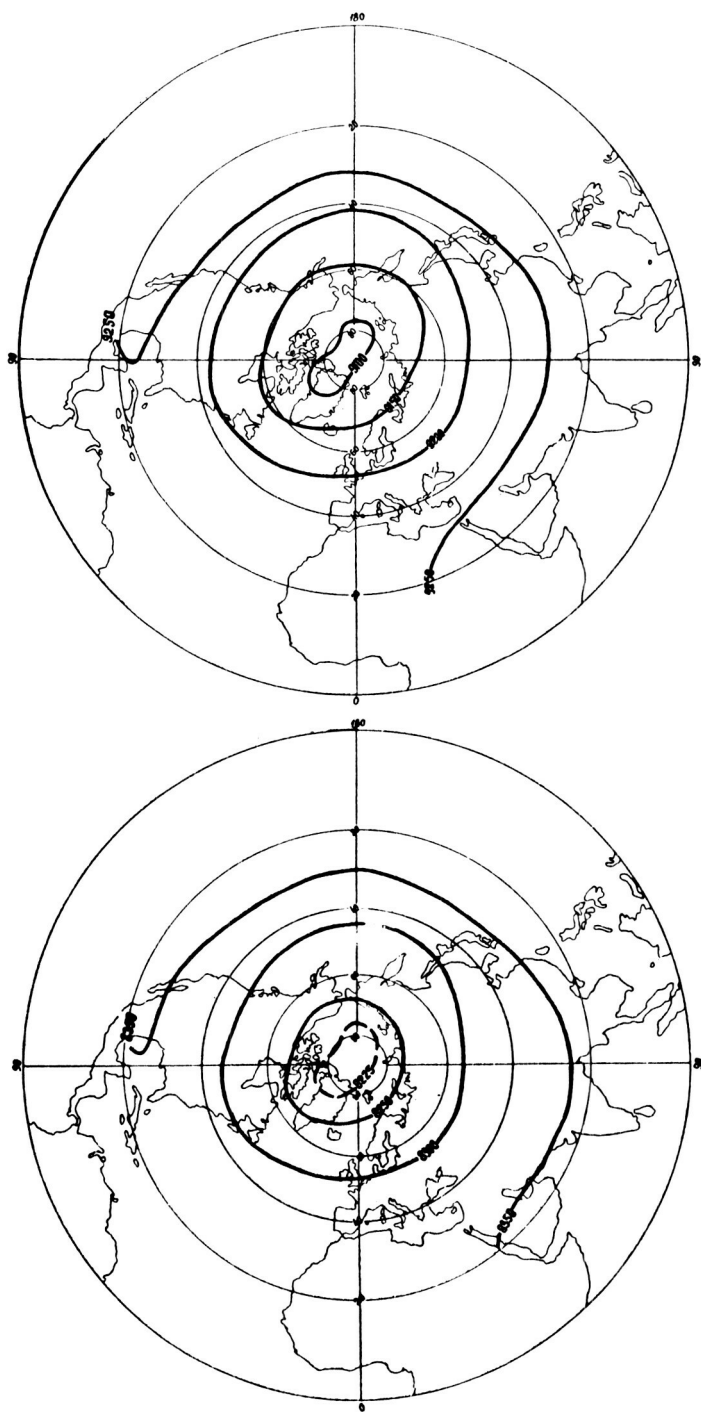


Fig. 2 (continued) September

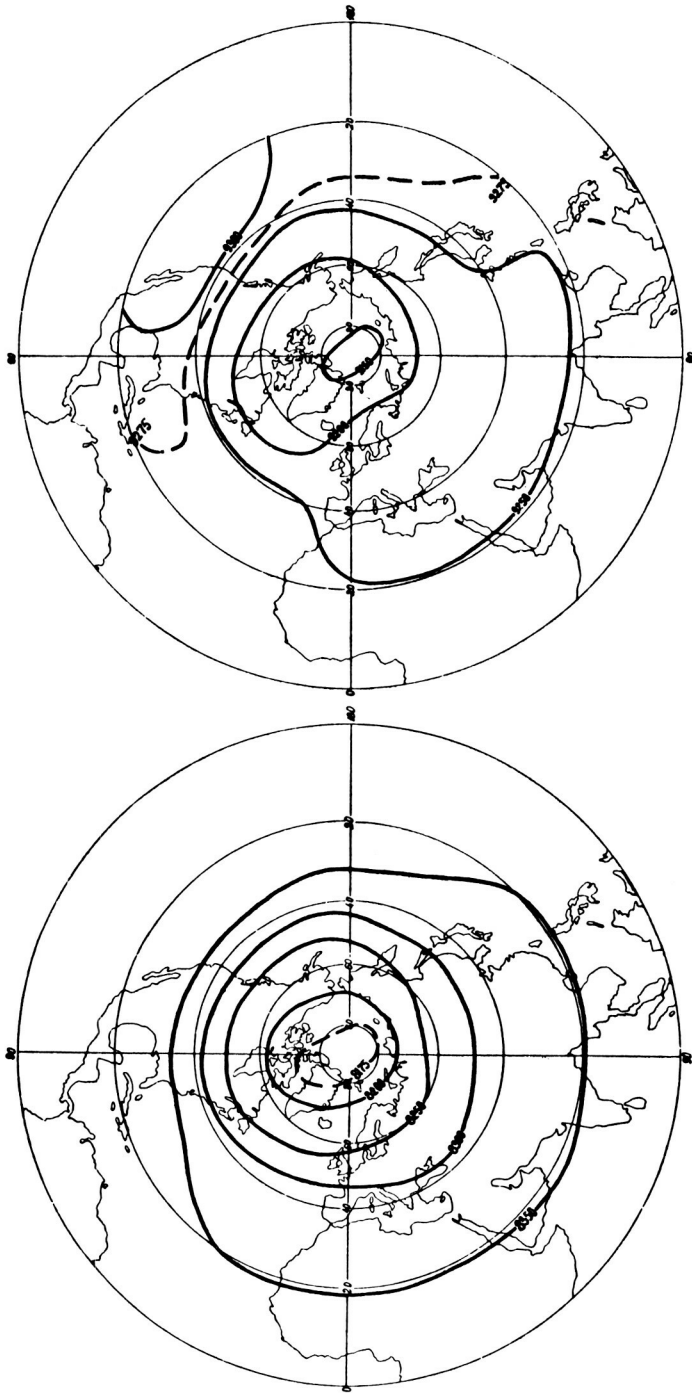


Fig. 2 (continued) October

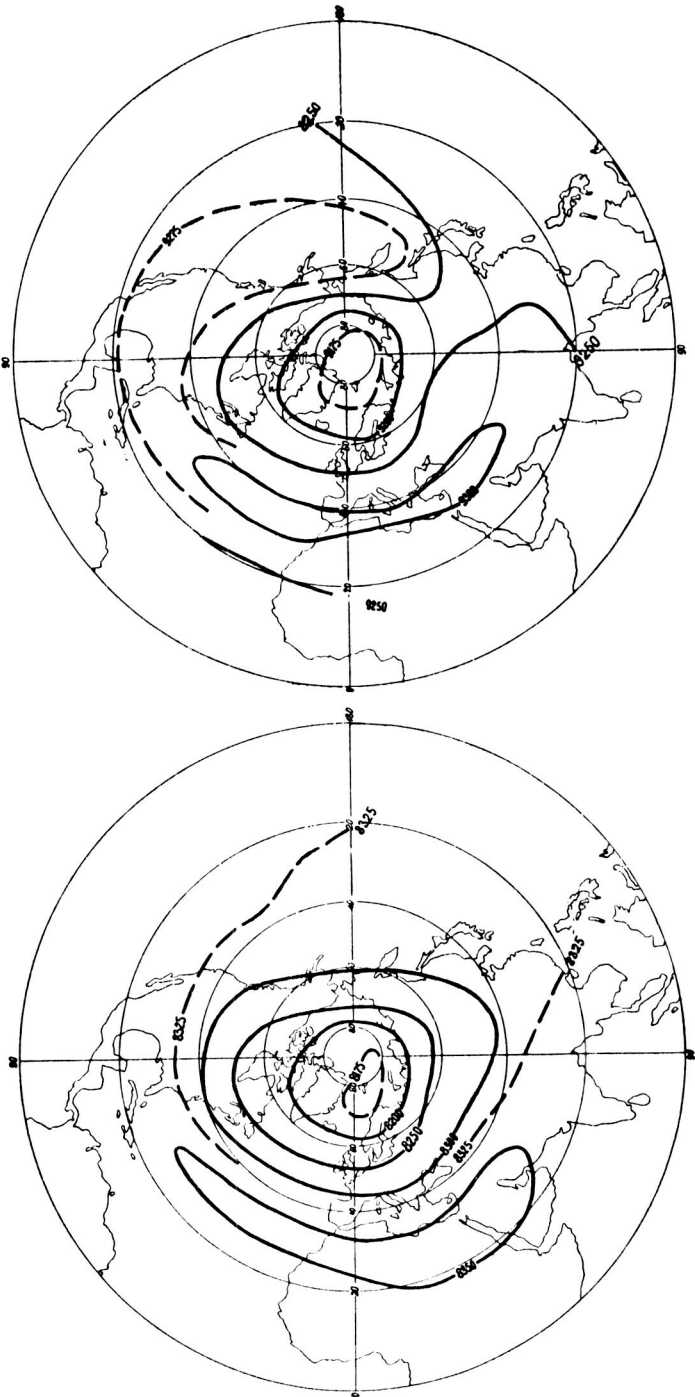


Fig. 2 (continued) November

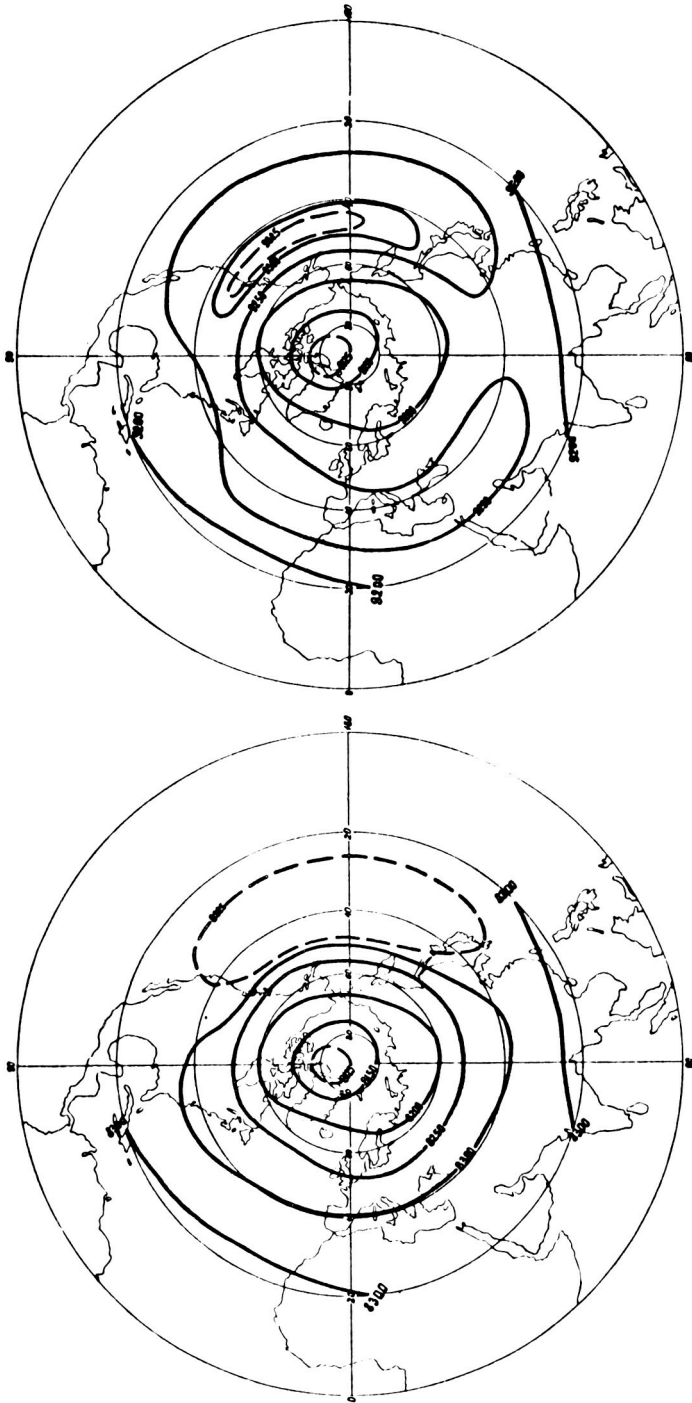


Fig. 2 (continued) December

Late in summer a destruction of the polar high takes place. In August, the center of the anticyclone which shifted to the Canadian sector of the Arctic could be traced only at the 0.005 mb level while in higher atmospheric layers it was not observed and a low pressure area could be seen arising over northern Asia. In September and October the latter occupied the polar region and deviations from the zonal pressure distribution were relatively small (two troughs appeared directed towards Greenland and northeastern parts of Asia). Some deformation of the cyclonic vortex (with troughs in the North American and Asian sectors) was also observed all through the winter months.

Beginning in November, the area of westerly flow within the cyclonic circumpolar vortex was contracting along with the appearance of a high pressure belt in the subtropics (near 30°N at the altitude of 83-84 km and 40°N at 93-94 km). The belt was pronounced until January and dissipated in February. In March two pressure ridges became active, stretching from lower latitudes towards northern parts of the Pacific and Atlantic oceans and forming a high pressure center near 60°N in the Atlantic region. In April, the available data for the years considered did not reveal further progress of the anticyclonic system (as may be the case in the climatological situation (MININA et al., 1977, 1981)), and only the May geopotential patterns showed the development of the polar high pressure area - better at the 0.005 mb level than at 0.001 mb.

It is known that the time of the seasonal reversals of meridional pressure gradients and the change of sign of zonal circulation in the meteor zone can vary significantly from year to year (ENTZIAN and TARASENKO, 1971; KAZIMIROVSKY and KOKOUROV, 1979; MININA et al., 1977). Thus the reliable climatological picture of seasonal variations in atmospheric pressure and geopotential heights of constant pressure surfaces in this zone may be determined only in the future, provided the duration of the period of satellite observations is long enough.

It is of interest to compare the satellite-based maps with the results of an earlier analysis (GAIGEROV, et al., 1983) of the 0.001 mb level geopotential fields based on other observational techniques. The comparison confirmed general similarity of pressure patterns depicted in the two series of maps, though the winter cyclonic system shown in that paper was significantly deeper than its counterpart in Fig. 2 of the present analysis.

The pressure patterns depicted for the lower thermosphere of the northern and southern hemispheres were found to have much in common, e.g., in seasonal change of polar cyclonic and anti-cyclonic vortices. Main hemispheric asymmetry (besides that shown above concerning the area of domain in the anticyclonic vortex at the 0.005 mb level) can be seen in the following; meridional gradients of geopotential height between the tropics and the pole in the winter season were generally weaker in the northern hemisphere; there was no evidence of a high pressure belt at 30-40°S similar to that visible at the northern hemisphere maps in November-January.

The presence of stationary waves in the mean geopotential fields was investigated by means of Fourier analysis applied at various latitudes. Amplitudes and phases of disturbances with zonal wave numbers $n=1$ and $n=2$ in the northern hemisphere are shown in Fig. 3 for the winter and spring

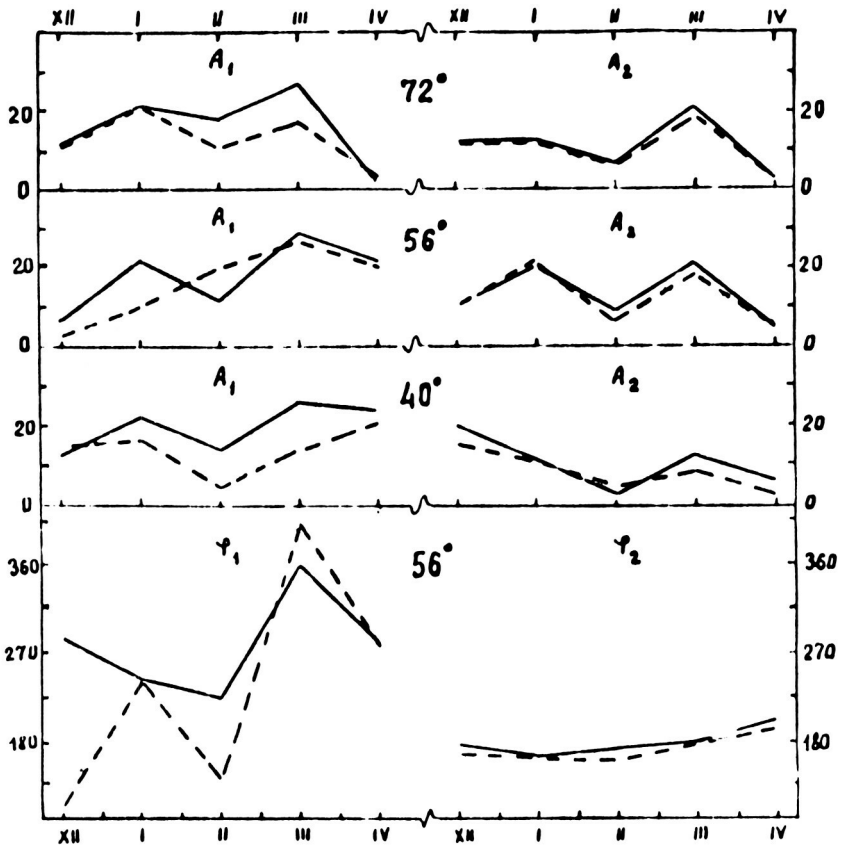


Fig. 3 Amplitudes (A , dm) and phases (ϕ , $^{\circ}\text{E}$) of zonal waves 1 (left) and 2 (right) of the heights of the 0.001 mb (solid line) and 0.005 mb (dashed line) levels at latitudes 40, 56, and 72°N.

seasons. The amplitudes are presented for 3 latitudes (40, 56 and 72°N) and the phases only for 56°N since the phase values have not revealed systematic change with latitude. It should be stressed that the amplitudes of the second harmonic were not much less than those of the first harmonic. This was not the case in the southern hemisphere where wave 1 was commonly much more significant than wave 2. The amplitude of the first harmonic in mid-latitudes of the northern hemisphere revealed some increase in early spring (March), but it was in general not as great as in high latitudes of the southern hemisphere. Thus the transition to the anticyclonic pattern via the development of ridges of high pressure in a certain region in spring was not so pronounced in the northern hemisphere during the years considered as it was in the southern hemisphere. This is corroborated by the high variability of phase in case of wave 1 in Fig. 3. Conversely, the phase of wave 2 was practically invariable during all months of the winter and spring period (the ridges near 0° and 180° long), with orientation of the troughs towards the continents. There was no definite trend in the magnitude of the amplitude of wave 2 during winter and spring; the values of the amplitude were not very different in the northern and southern hemispheres. In general, deviation from zonality in mean pressure fields in the lower thermosphere during the winter and spring periods considered were less pronounced in the northern than in the southern hemisphere. However, additional observations are needed to see if this hemispheric asymmetry is confirmed in the long run.

Variations of wave amplitudes in the lower thermosphere of the northern hemisphere with latitude were not substantial; however, the amplitude of wave 2 in some months was not as large at 40°N as at higher latitudes.

A comparison of the amplitudes in the thermosphere and mesosphere was made which showed that in winter (December) the amplitude of wave 1 in the mesosphere (BOUTKO et al., 1985) was greater than at higher levels. Similar reduction of the amplitude (with little change of phase) was found in the case of wave 2.

It is of interest to compare zonal mean values of the geopotential heights obtained from the maps to appropriate values from a reference atmosphere. It should be kept in mind that the maps described in this paper represent one of the first attempts to picture pressure fields at heights greater than 80 km with the help of satellite data and they are possibly neither very accurate nor representative since only crude estimates of the geopotential can be obtained from one-channel radiances and the period of the observation was limited. With this in mind, it seems encouraging to see (Fig. 4) good agreement of seasonal variations of the geopotential obtained from the maps and from CIRA 1972 data. The agreement is better in higher latitudes, so the compiled maps seem to be more reliable north of 25-30°N.

As for the seasonal variations of heights of the constant pressure surfaces, the curves of the seasonal course in Fig. 4 are generally similar in low latitudes for the two levels considered, while they reveal an out-of-phase relationship north of 50°N. This is reflected also in the distribution of the phases (Fig. 5) - in the case of the annual wave (which was dominant in all latitudes north of 30°N at the 0.001 mb level and north of 50-60°N at the 0.005 mb level) the phases at the two levels were close together in low latitudes and revealed an abrupt change of phase north of

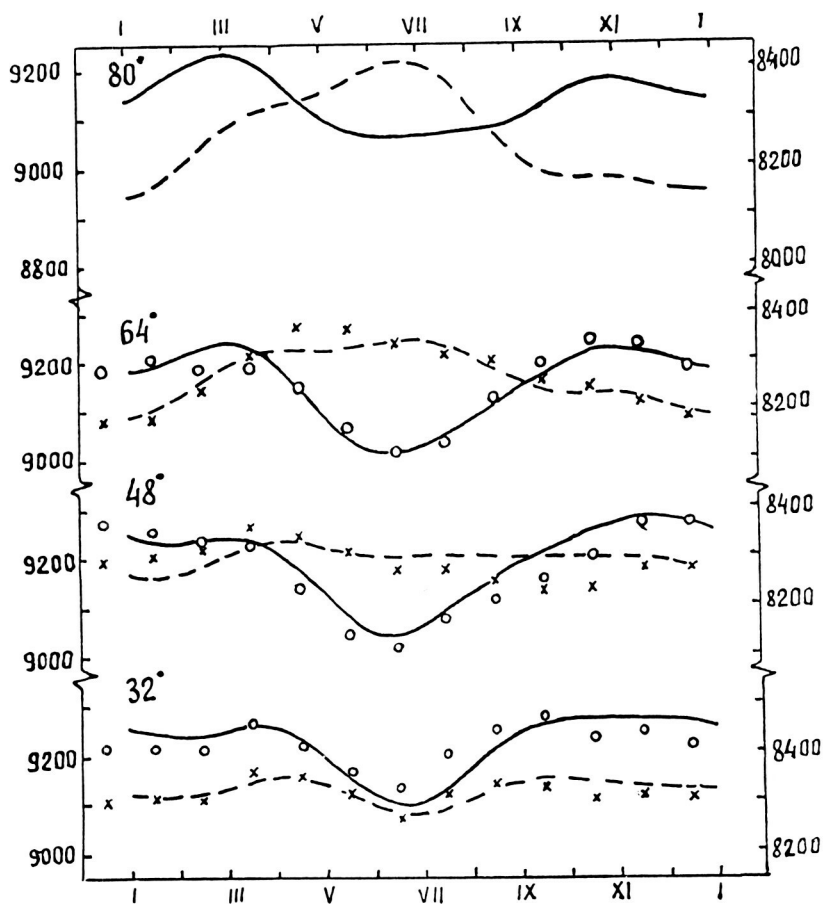


Fig. 4 Seasonal variation of heights (dm) of the 0.001 mb (solid line) and 0.005 mb (dashed line) surfaces in the Northern Hemisphere. (Circles and crosses 0.001 mb and 0.005 mb heights, respectively, calculated from CIRA 1972.)

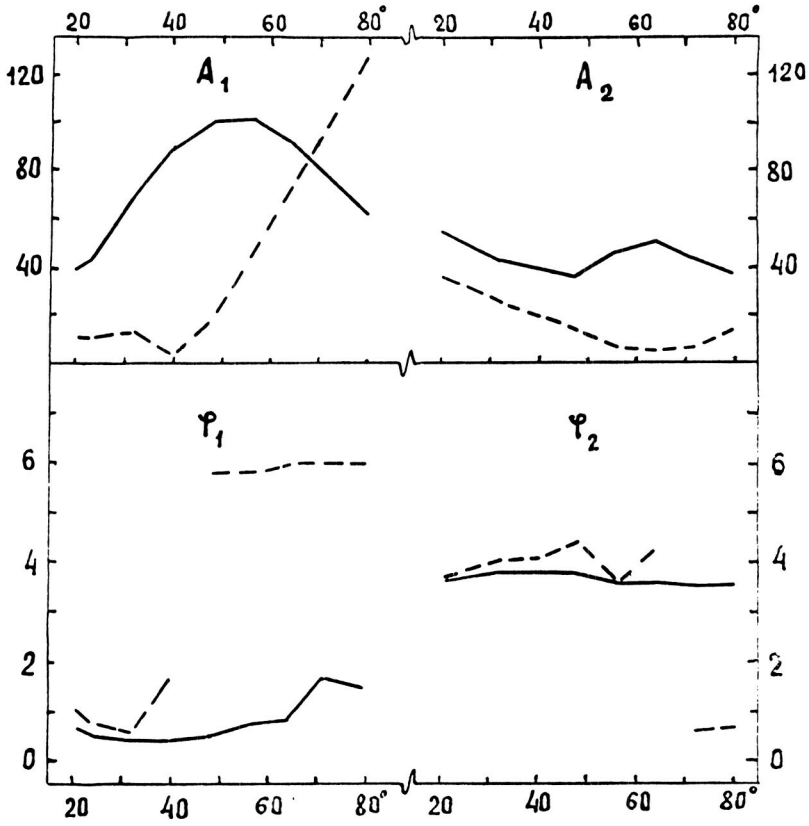


Fig. 5 Amplitudes (A , dm) and phases (ϕ , month) of the annual (left) and semiannual (right) variations of heights of the 0.001 mb (solid line) and 0.005 mb (dashed line) surfaces in the Northern Hemisphere ($\phi = 0$ on 15 December).

45°N (maximum in June at the mesopause level and in January at heights of about 93 km). Such shift of the phase of the annual variation with increasing height in the lower thermosphere of the Arctic and Subarctic from the middle to the beginning of the year is related to the attenuation of the polar anticyclone at heights greater than 90 km. It should be marked that the change of the phase of the annual wave with height in the 0.005-0.001 mb layer was not as rapid in the southern hemisphere over the Subantarctic. A specific feature of seasonal variations in the low latitude thermosphere is the simultaneous appearance of the annual wave maximum (in January) in the two hemispheres which is undoubtedly related to the corresponding phase of the annual temperature wave in the equatorial mesosphere (KOSHELKOV, 1984).

For most of the northern hemisphere the amplitude of the annual variation was greater at the 0.001 mb level, and only in the Arctic north of 70°N was the reverse proved to be true.

The comparison of the amplitudes of the annual variation in the two hemispheres confirmed that at levels close to the mesopause (0.005 mb) the amplitudes were significantly greater in the southern hemisphere. This is also true for the stratosphere and mesosphere (BOUTKO et al., 1985). The asymmetry is related to lower values of the geopotential in the southern hemisphere relative to the northern hemisphere in the winter season as well as to the similar phase of the annual wave (maximum in summer) in the extratropical latitudes of the two hemispheres. At the 0.001 mb level the geopotential height values in winter remained lower in the southern hemisphere (maximum in winter), and the amplitude was no longer greater in the southern than in the northern hemisphere.

The semi-annual wave in the lower thermosphere of the northern hemisphere was more pronounced at the 0.001 mb level than at the 0.005 mb level. The phase was almost independent of latitude (the first maximum in April). The amplitudes of the semi-annual and annual variations were comparable in low latitudes while the latter dominated at higher latitudes.

The constant pressure contour maps compiled for the lower thermosphere enabled an estimate of zonal mean geostrophic circulation to be made (Fig. 6). The geostrophic zonal wind speed was calculated with the help of zonal mean values of the geopotential heights, with some smoothing in latitude and time (using a 1-2-1 scheme). For the comparison with the geostrophic calculations, some recent results of radio wind measurements in the meteor zone are also presented in Fig. 6; these involve an empirical model (PORTNYAGIN, 1984) and wind analyzed data for 9 radiometeor and ionospheric stations in Europe, North America and Japan (MANSON, et al., 1984). The actual wind data were derived from the cross-sections presented in MANSON et al., (1984) and PORTNYAGIN (1984) at the geometric heights corresponding to the location of the 0.001 mb and 0.005 mb surfaces for each month. The wind values from PORTNYAGIN (1982) for the stations with similar latitudes were averaged during the preparation of Fig. 6.

The distributions of zonal geostrophic and actual wind speeds in Fig. 6 have much in common. In particular, a seasonal change of easterly and westerly flow has been recorded. Maximum values of both easterlies and westerlies were similar in both geostrophic and actual winds. The well-known decrease of zonal wind with increasing height in the lower thermosphere was confirmed. In accordance with this fact, the amplitude of

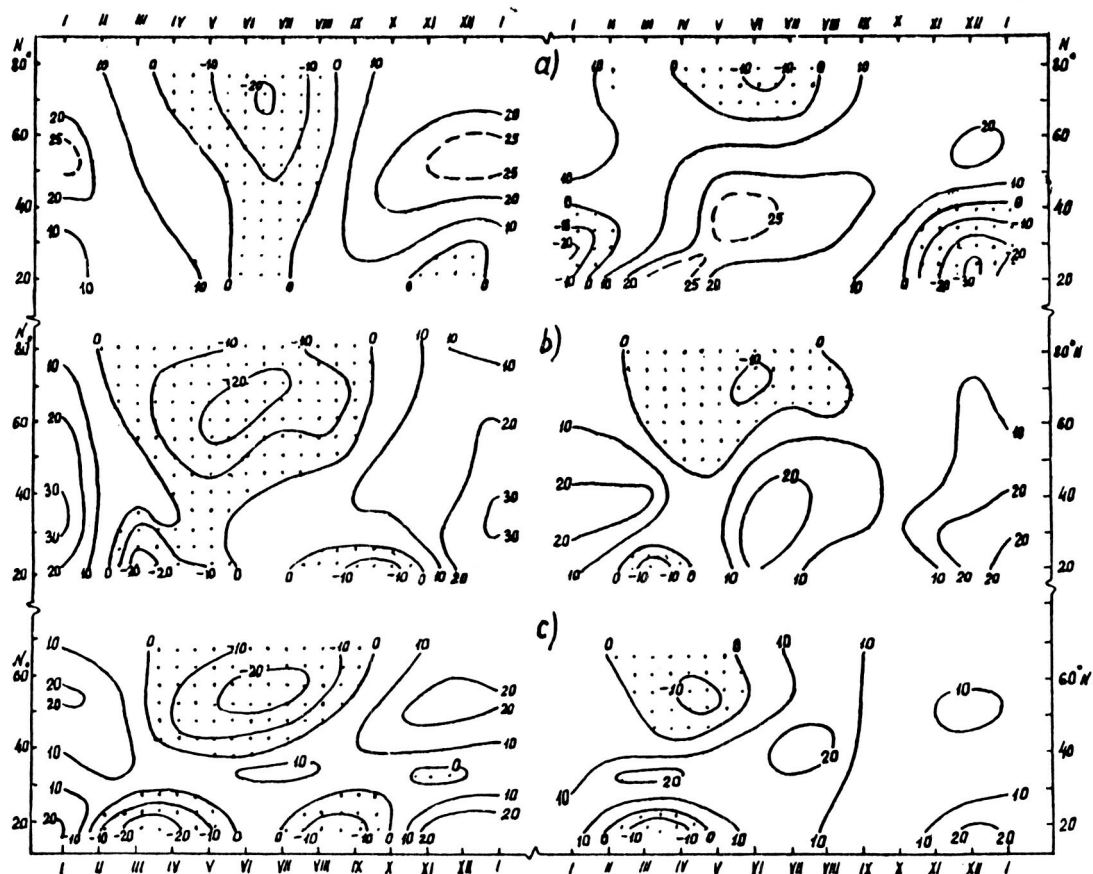


Fig. 6 Latitude-time sections of mean zonal wind (m/s) in the lower thermosphere of the Northern Hemisphere: a) zonal geostrophic wind speeds at the 0.005 mb (left) and 0.001 mb (right) surfaces, b) actual wind speeds at the 0.005 mb (left) and 0.001 mb (right) surfaces, compiled from PORTNYAGIN (1984), c) actual wind speeds at the 0.005 mb (left) and 0.001 mb (right) surfaces, compiled from MANSON ET AL. (1984).

the annual variation of geostrophic zonal wind (Fig. 7) north of 40°N was greater at the 0.005 mb than at the 0.001 mb level. At the 0.005 mb level the phase was reversed in low latitudes (maximum in summer).

The distributions of zonal geostrophic and actual winds in Fig. 6 also reveal substantial discrepancies. These are particularly serious in low latitudes, e.g., in the seasonal position of easterly and westerly flow areas. It is evident that in general actual wind measurements could provide a more reliable representation of prevailing winds than geostrophic estimates. Of special interest is, however, an area of easterly geostrophic flow south of 40°N in early winter at the 0.001 mb level, which is related to the development of a high pressure area in November-January in this region. The continuous appearance of the easterlies during a 30 month period seems to corroborate their reality. In this case the reason for this "anomalous" circulation might be attributed to specific features of the years considered, and so significant interannual variability of the prevailing flow might be a possibility in the subtropical lower thermosphere.

Certain derivations of geostrophic flow estimates from mean radiometer and ionospheric drift wind data also appear in Fig. 6 in the extratropical latitudes. In particular, it has long been known from actual wind measurements that the spring appearance of easterly circulation takes place earlier in the lower thermosphere than in the strato-mesosphere, and a semi-annual wind variation with westerly wind maxima in winter and summer is typical for the circulation in the meteor zone (ENTZIAN and TARASENKO, 1971; KAZIMIROVSKY and KOKOUROV, 1979; MININA et al., 1981; PORTNYAGIN, 1982).

This is not obvious in the case of the geostrophic calculations (Figures 6 and 7). The existence of the discrepancies is not surprising if one keeps in mind that, first, geostrophic wind estimates at high levels are probably not accurate; second, geostrophic winds may differ from actual; and third, satellite-based maps need to be improved.

It should be added that differences also exist between various analyses of actual wind measurements in the meteor zone. These can be seen in Fig. 7, e.g., in the duration of the period of easterly flow in spring and summer at the 0.001 mb level or in the latitudinal structure of the westerly flow in winter. So it seems without doubt that, with the continued progress of satellite observations, constant-pressure contour maps can contribute not only to characterizing pressure fields in the lower thermosphere but also to analyzing circulation in the meteor zone.

An attempt at comparison of the geostrophic zonal wind in the lower thermosphere of the two hemispheres was made which testified to generally higher values of westerly flow in the southern than in the northern hemisphere (Table 1). The differences are however noteworthy only in lower latitudes (near 30° lat.) while it follows from the actual wind analysis (PORTNYAGIN, 1984) that a difference of this kind may be observed in most latitudes. According to the geostrophic calculations, the axis of the winter westerly flow at levels close to the mesopause (0.005 mb) was located nearer to the equator in the southern than in the northern hemisphere ($35\text{--}40^{\circ}\text{S}$ and $50\text{--}55^{\circ}\text{N}$, respectively). Somewhat different values are given by the wind model of PORTNYAGIN, (1984), namely, 45°S and

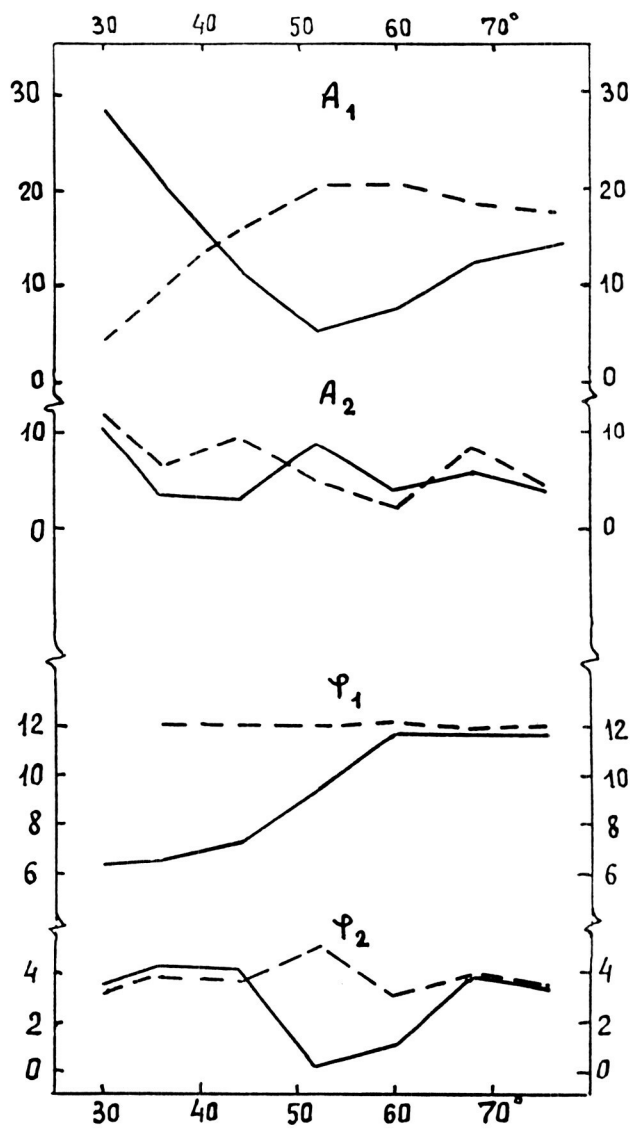


Fig. 7 Amplitudes (A , m/s) and phases (ϕ , month) of the annual (1) and semiannual (2) variations of the geostrophic wind speed in the lower thermosphere of the Northern Hemisphere. (0.001 mb, solid line; 0.005 mb, dashed line, zero phase on 15 December.)

Table 1

Mean differences in speed (mps) of the zonal geostrophic wind in the southern and northern hemispheres at the 0.005 mb level (81-83 km) (top) and respective differences for the actual wind (PORTNYAGIN, 1984) (bottom) for 3-month seasons.

Lat. :	Season			
	Winter	Spring	Summer	Autumn
70	5/18	-6/10	2/14	0/9
50	-2/27	8/21	4/13	18/18
30	41/9	14/25	15/18	22/9

Mean speeds of zonal geostrophic wind averaged for the two hemispheres are presented in Table 2. These values can serve to characterize the circulation in the lower part of the meteor zone as derived from satellite data irrespective of the hemisphere.

Table 2

Mean wind speeds (mps) of zonal geostrophic wind in the lower thermosphere (two hemispheres combined). 0.001 mb level (91-93 km) - top, 0.005 mb level (81-83 km) - bottom.

Lat. :	Month											
	1	2	3	4	5	6	7	8	9	10	11	12
70	$\frac{16}{20}$	$\frac{8}{10}$	$\frac{-4}{-1}$	$\frac{-2}{-6}$	$\frac{-1}{-9}$	$\frac{-4}{-15}$	$\frac{-4}{-16}$	$\frac{3}{-5}$	$\frac{11}{10}$	$\frac{12}{15}$	$\frac{16}{18}$	$\frac{19}{22}$
60	$\frac{12}{19}$	$\frac{1}{9}$	$\frac{0}{3}$	$\frac{5}{1}$	$\frac{8}{-4}$	$\frac{5}{-12}$	$\frac{4}{-14}$	$\frac{11}{-2}$	$\frac{14}{15}$	$\frac{17}{23}$	$\frac{17}{23}$	$\frac{18}{24}$
50	$\frac{7}{22}$	$\frac{0}{15}$	$\frac{4}{12}$	$\frac{16}{11}$	$\frac{23}{5}$	$\frac{20}{-4}$	$\frac{18}{-8}$	$\frac{20}{1}$	$\frac{22}{18}$	$\frac{23}{32}$	$\frac{23}{35}$	$\frac{18}{31}$
40	$\frac{7}{30}$	$\frac{7}{26}$	$\frac{11}{22}$	$\frac{22}{20}$	$\frac{31}{11}$	$\frac{31}{1}$	$\frac{27}{-1}$	$\frac{24}{6}$	$\frac{21}{18}$	$\frac{19}{32}$	$\frac{17}{39}$	$\frac{10}{38}$
30	$\frac{0}{26}$	$\frac{10}{30}$	$\frac{15}{24}$	$\frac{20}{17}$	$\frac{28}{9}$	$\frac{31}{4}$	$\frac{31}{6}$	$\frac{26}{12}$	$\frac{20}{18}$	$\frac{12}{22}$	$\frac{0}{25}$	$\frac{-7}{24}$

NOTE: Month 1 refers to Jan. N.H. and July S.H., 2 to Feb. N.H. and Aug. S.H., and so on.

35-40°N. It seems reasonable that a more detailed analysis of hemispheric asymmetry in geostrophic circulation may not be justified.

References

1. Boutko, A.I., Koshelkov Yu. P. and Tarasenko D.A., 1982, in Geophysical and Meteorological Effects in the Ionosphere, Alma-Ata, Nauka.
2. Boutko, A.I., Britvian R.A., Kovshova E.N., Koshelkov Yu. P. and Tarasenko D.A., 1985, in Meteorological Investigations in the Antarctic (Report of the II Symposium), Leningrad, Gidrometeoizdat.
3. COSPAR International Reference Atmosphere CIRA 1972, Akademie-Verlag, Berlin, p. 450.
4. Entzian G. and Tarasenko D.A., 1971, Meteorologia y Gidrologia, No. 5.
5. Gaigerov S.S., Kalikhman M.Ya., Fedorov V.V. and Zhorova E.D., 1983, Adv. Space Res., Vol. 3, No. 1, pp. 27-32.
6. Kazimirovsky E.S. and Kokourov V.D., 1979, Movements in the Ionosphere, Nauka, Novosibirsk, p. 344.
7. Koshelkov Yu. P., 1984, J. Atmos, Terr. Phys., Vol. 46, No. 9, pp. 781-798.
8. Koshelkov Yu. P. and Kovshova E.N., 1984, in Antarctica, Vol. 24, pp. 29-42.
9. Labitzke K. and Barnett, J.J., 1981, Planet Space Sci., Vol. 29, No. 6, pp. 673-685.
10. Manson A.E., Meek C.E., Massebeuf, M., Fellous J. L., Elford W. E., Vincent R.A., Craig R.L., Roper R. G., Avery S., Balsley B.B., Fraser G.J., Smith M.S., Clark R.R., Tsuda T. and Ebel A., 1984, preprint XXVth COSPAR, Graz.
11. Minina L. S., Petrosyants M.A. and Portnyagin Yu. I., 1977, Meteorologia and Gidrologia, No. 1.
12. Minina L. S., Petrosyants M. A. and Yu. I. Portnyagin, 1981, Meteorologia y Gidrologia, No. 9, pp. 5-11.
13. Portnyagin Yu. I., Meteorologia Y. Gidrologia, No., 1982, pp. 5-10.
14. Portnyagin Yu. I., 1984, in Handbook for MPA, Vol. 10, pp. 134-142.

CIRCULATION IN THE MESOSPHERE AND LOWER
THERMOSPHERE DURING THE MAP/WINE PERIOD

D.A. Tarasenko

Central Aerological Observatory
Moscow, USSR

One of the scientific programs in the MAP project "Winter in the Northern Europe" (1983-1984) involved an analysis of circulation processes in the middle atmosphere which characterized that winter period. For this purpose a series of rocket soundings was conducted in the USSR. At Heiss Island (polar latitude) and Volgograd station (middle latitude) the sounding was conducted twice a week from December to February. Besides this, four daily series were carried out (with 10 firings a day), two of them on December 9 and 19, one on January 18 and the last one on February 22.

Other data analyzed involved rocket sounding results obtained at a number of stations (Andoya and Lista, Norway; Ahtopol, Bulgaria; Riory, Japan; Thumba, India; Primrose Lake, Canada; Shemya, P. Kennedy, Antigua, P. Mugu and Kwajalein, USA; research vessels), as well as NOAA-7 data submitted by Great Britain. In order to investigate deviations of the mean winds for the MAP/WINE period from the circulation conditions of other winters, from CIRA 1972 (CIRA, 1972) and from the climatic norm (TARASENKO, 1969; GAIGEROV et al., 1981) rocket sounding data of Churchill and Barrow stations for many years were used as well as the "Pressure Modulated Radiometer" (PMR) channel 3000 data from the Nimbus-6 satellite for 1975-78 (LABITZKE and BARNETT, 1981), which enabled the author to compile geopotential fields and to calculate winds in the geostrophic approximation for comparison with the meteor winds. The maximum of the weighting function of channel 3000 occurs at an altitude of 80 km.

Let us analyze briefly the large scale processes of the winter of 1983-1984 which determined the circulation in the period of the experiment. The winter of 1983-1984 differed from other winter periods - a very deep cyclonic stratomesospheric vortex which reached its maximal development in January and early in February was present. A very high location of the lower boundary of the mesosphere (the stratopause) was also observed, sometimes as high as 58-60 in January.

The structure of the pressure field changed in late February due to a rapid intensification of the Pacific anticyclone and the shifting of its center to 70°N. The cyclonic vortex stepped away from the polar region toward Euroasia, and centered on 65°N. On February 22 the polar region was occupied by a high pressure area which came from the Pacific. A global change of the pressure field took place (Fig. 1). During the last several days of February the anticyclone shifted away from the Pole and the geopotential heights in its center decreased.

At the levels of the lower and middle mesosphere, large scale processes from December to mid-February were characterized by a well-

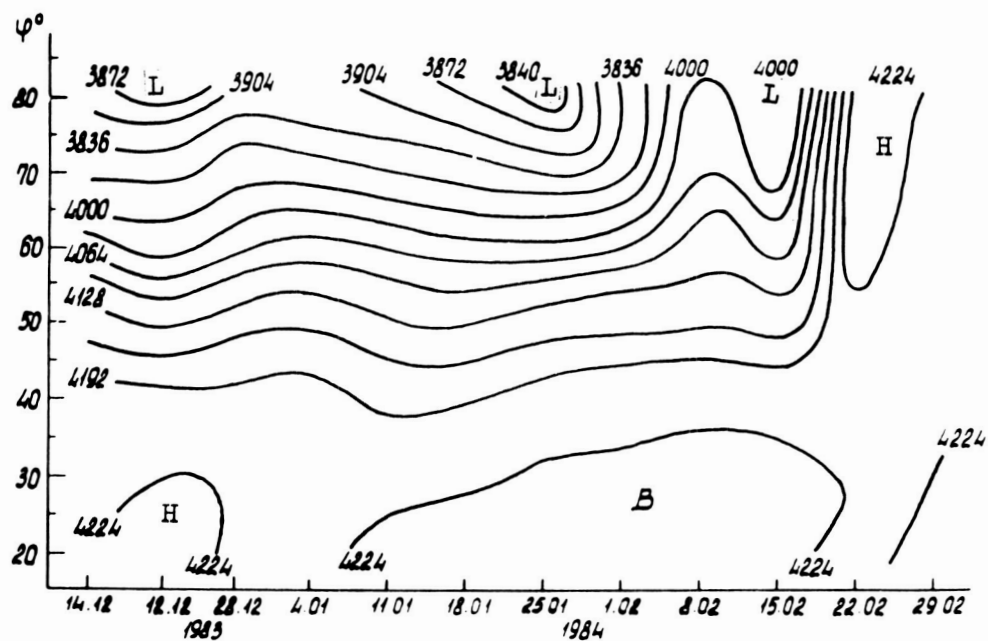


Fig. 1 Time-latitude section of zonal mean geopotential heights at 2 hPa (dm).

developed cyclone typical of the winter period. Late in February the pressure field was complicated and exhibited a four-cell structure.

Figures 2 and 3 present fields of the zonal and meridional components of geostrophic wind calculated from the geopotential field at a constant pressure surface located near the lower boundary of the mesosphere. The geopotential field at the 2-hPa level was obtained from rocket sounding data and PMR radiances on the NOAA-7 satellite.

Mean data for this period a weak easterly wind over the Greenland sea, since the center of the polar cyclone was displaced from the geographic pole to the European-Atlantic sector of the Arctic to a greater extent than had usually been observed. The observed asymmetry of the polar cyclone created large pressure gradients (greater than climatological values) over Central Europe and therefore caused large asymmetry in the zonal distribution of the wind field.

Thus, the westerly wind speeds reached greater values over Central Europe than over North America (80 mps and 30 mps, respectively). The stratospheric field of zonal wind (at 2 hPa) was characterized by the presence of an area of easterlies with speeds up to 7 mps over the Pacific regions. It should be noted that easterly winds are not observed each winter. Mean climatic data (GAIGEROV et al., 1981) reveal that in the Pacific Ocean area (north of 30°N) only a reduction of westerly flow (down to 5-7 mps) is observed due to the intensification and northern shift of the Pacific anticyclone on some days in the winter period. During the period considered here the low latitude stratosphere (south of 10°N) was occupied by area of easterlies which is in accordance with the normal climatic conditions. In the extratropical latitudes, with the exception of the Pacific Ocean and Greenland Sea, the wind was westerly which is also in agreement with the climatic conditions. The analysis of the fields of the meridional circulation showed that at the 2 hPa level two major meridional circulation cells were observed which stretched from the tropics to the Pole.

Eurasia was mainly occupied by southerly winds with their center over northern Siberia. Northerly flow dominated over eastern and central parts of the Pacific and America.

The meridional wind component is highly variable and reference atmospheric models existing now include only the zonal component (CIRA 1972).

Studies made earlier showed (TARASENKO, 1979; GAIGEROV et al., 1981) that maximum variability of zonal and meridional wind components in the lower mesosphere is recorded in winter. The summer time wind regime is relatively stable. At upper mesospheric and lower thermospheric levels, variations of meteorological parameters are of the same order of magnitude in winter and summer which is likely to be related to the penetration of planetary and gravity waves into these layers as well as to tidal effects. Results presented in Table 1 can serve as an example of the standard deviations of zonal wind with altitude.

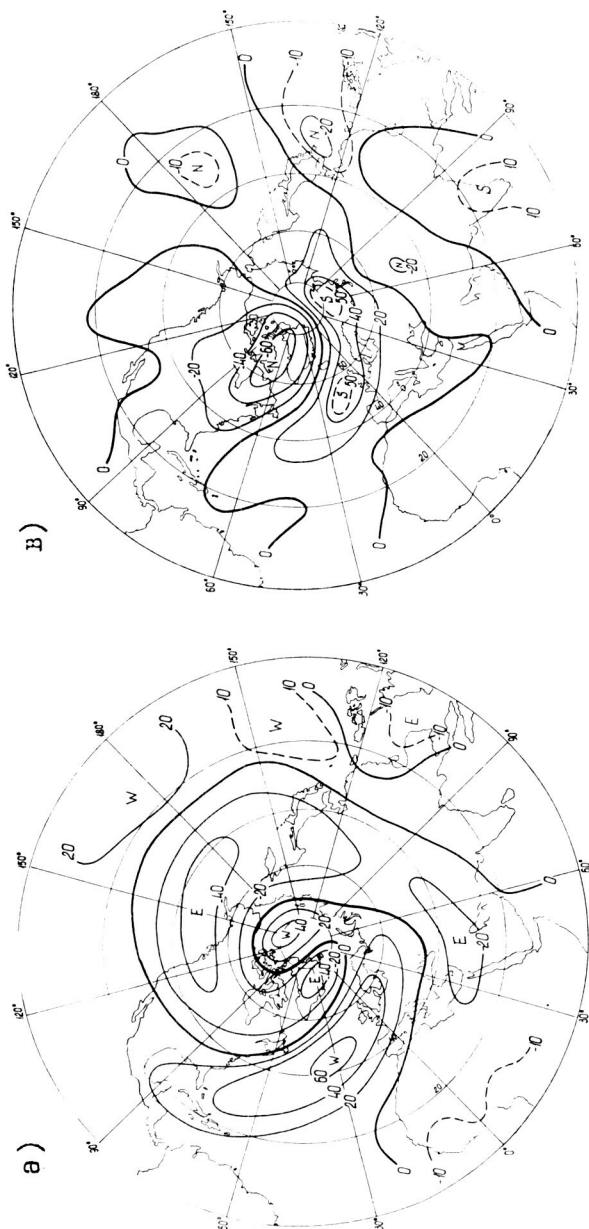


Fig. 2 Fields of zonal (a) and meridional (b) components of geostrophic wind speed (mps) at 2 hPa for February 22, 1984.

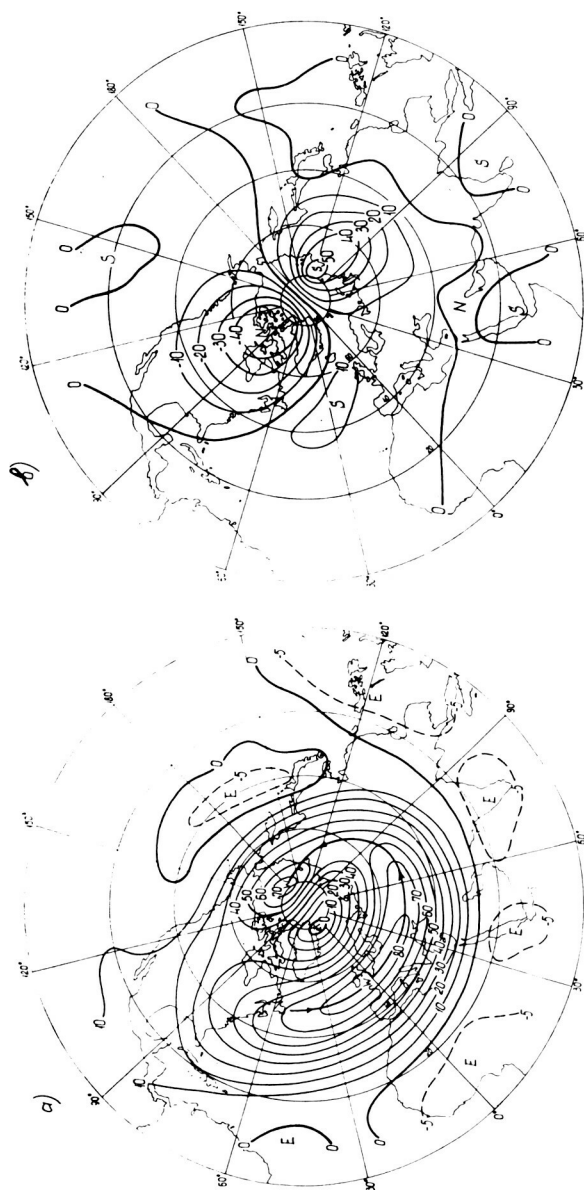


Fig. 3 Mean fields of zonal (a) and meridional (b) components of geostrophic wind speed (mps) at 2 hPa for the period from December, 1983, to February, 1984.

Table 1

Standard deviations (σ) of the zonal wind component
for various stations in winter.

H km	Barrow (71°N)	Churchill (59°N)
50	24.6	28.2
60	24.9	24.2
70	36.5	42.2
80	46.8	45.7
90	55.1	57.2

During the period of MAP/WINE, northerly winds of about 40 to 60 mps were observed above 60 km over Heiss Island. The zonal component in high latitudes, above 60 km, was more variable. Westerly winds changed several times into easterlies in the mesosphere and lower thermosphere, mainly due to the migration of the center of the "circumpolar cyclone" (Figs. 4 and 5).

In middle latitudes (Volgograd) easterly winds at lower mesospheric levels were recorded only during warmings accompanied by circulation reversals while in the upper mesosphere (above 70 km) and lower thermosphere they were frequently observed (Fig. 6).

It is possible that easterly winds in the upper mesosphere and lower thermosphere testify to the fact that the height of the winter strato-mesospheric cyclone in middle latitudes is less than in polar latitudes, and in some periods the upper boundary of the winter circumpolar vortex occurs at altitudes exceeding 70 km (Fig. 7).

Mean values of zonal wind in the geostrophic approximation as a function of latitude (ψ) and longitude (λ) and their zonal mean values for January in the middle mesosphere (0.1 hPa ~ 60-64 km) based on rocketsonde and satellite data and in the lower thermosphere (0.001 hPa ~ 90-95 km) based on rocketsonde, satellite, meteor trail and ionospheric observations are presented in Table 2.

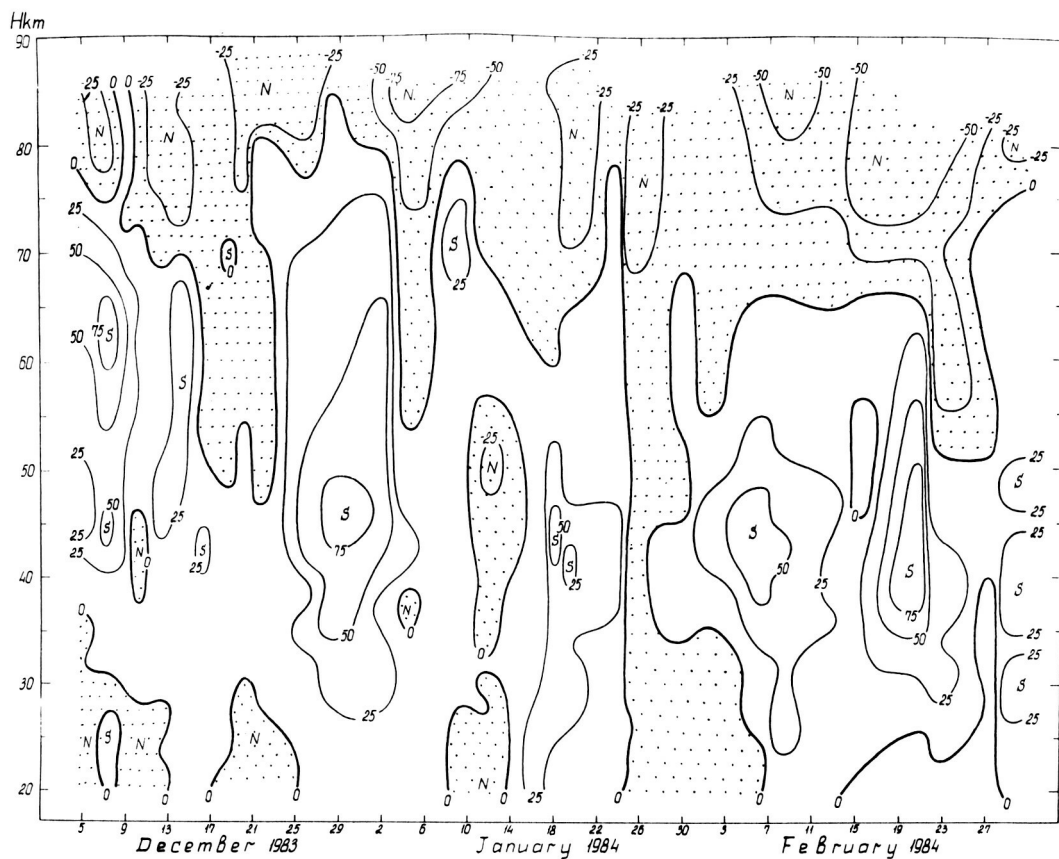


Fig. 4 Time-altitude section of meridional wind component (mps) over Heiss Island for the period of December 1983, - February 1984.

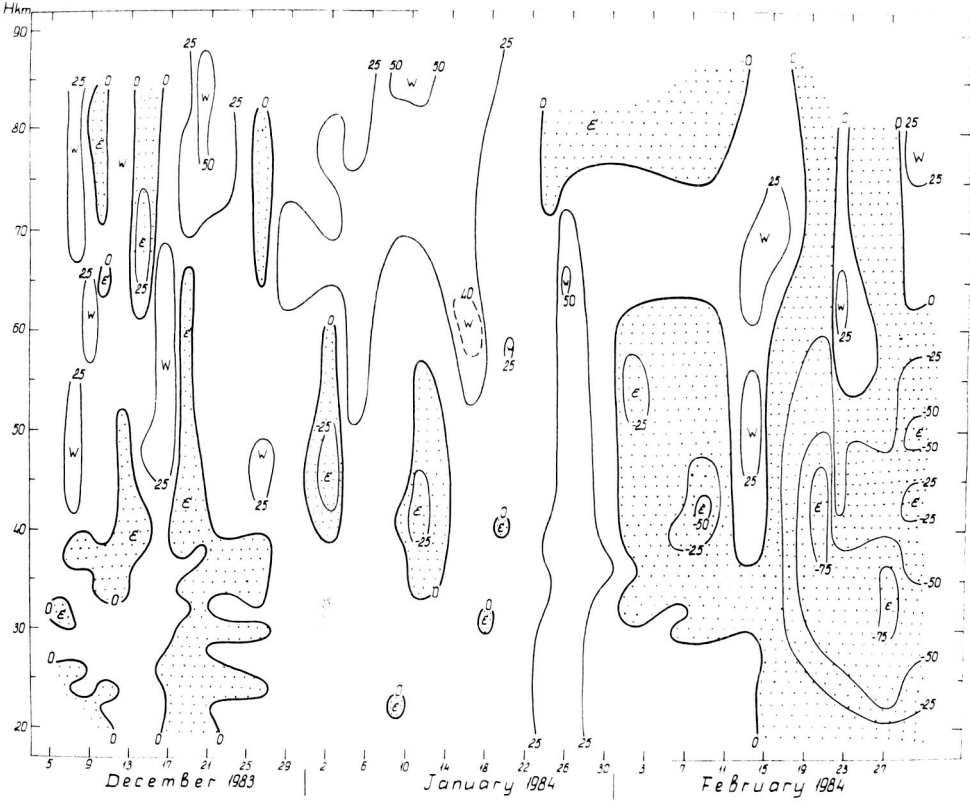


Fig. 5 Time-altitude section of zonal wind component (mps) over Heiss Island for the period of December 1983 - February 1984.

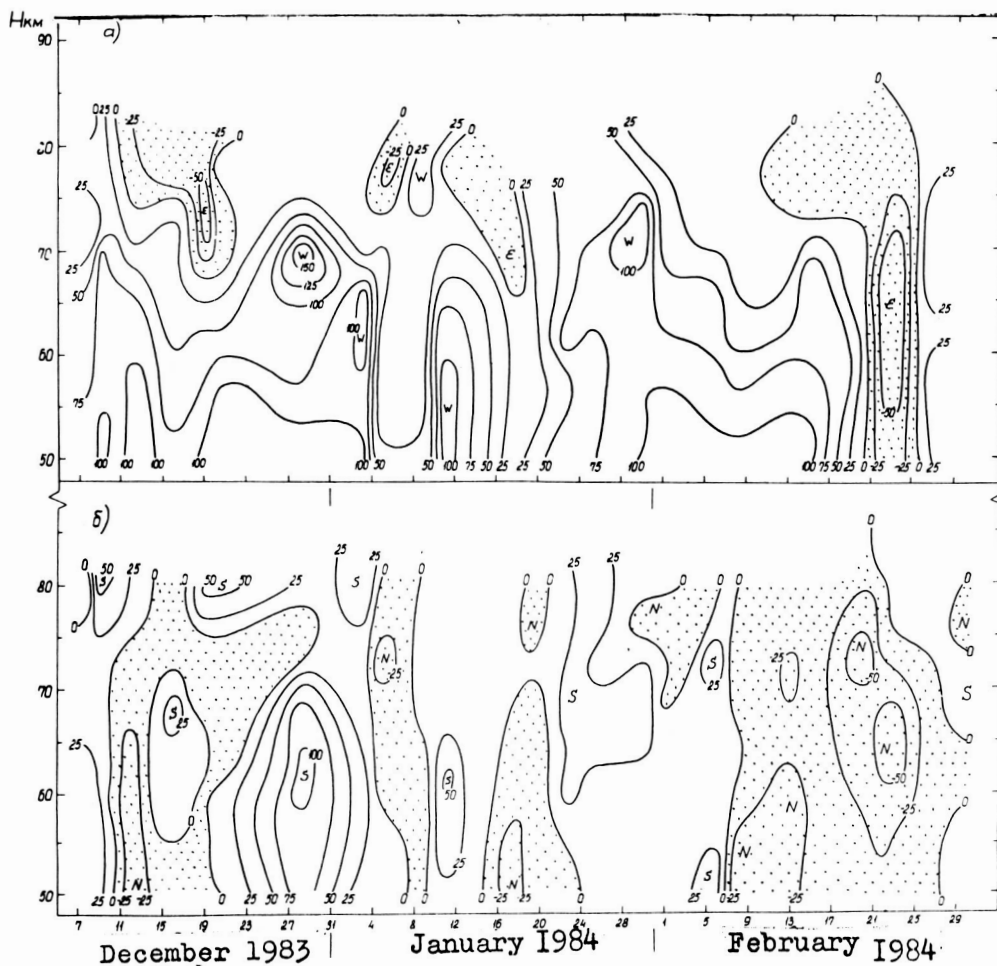


Fig. 6 Time-altitude section of zonal (a) and meridional (b) wind components (mps) over Volgograd station for the period of December 1983 - February 1984.

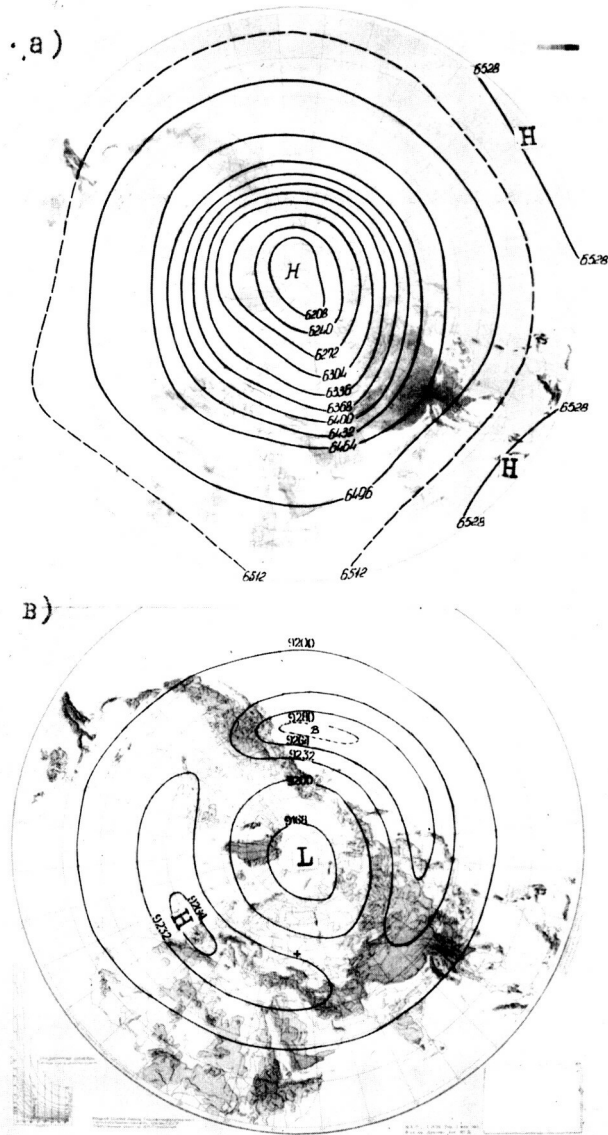


Fig. 7 Mean constant pressure chart at 0.01 hPa (a) and at 0.001 hPa (b) for January.

Table 2.

Mean values of zonal wind component (mps) over the European region, zonally averaged values of zonal wind and model values (CIRA 1972) at two constant-pressure levels and three latitudes.

AT	:	ψN	:	λE						:	\bar{U}	:	CIRA-72		
				:	:	:	:	:	:					:	:
0.1hPa		70		27	32	32	33	33	34	34		44		19	
		60		42	40	39	37	35	35	32		45		54	
		50		42	40	42	42	45	45	40		59		58	
0.001hPa		70		10	10	10	9	7	6	5		10		--	
		60		15	14	12	12	10	10	9		15		--	
		50		18	18	17	16	16	14	14		19		15	

References

1. CIRA 1972, Akademie-Verlag, Berlin.
2. Tarasenko D.A., 1979, Space Res., Vol. 19, pp. 135-139.
3. Gaigerov S. S., et al., 1981, Adv. Space Res., Vol. 1, pp. 151-155.
4. Labitzke K. and Barnett J. J., 1981, Planet. Space Sci., Vol. 29, No. 6, pp. 673-685.

CHARACTERISTICS OF ATMOSPHERIC DISTURBANCES WITH
A QUASI-TWO DAY PERIOD

B. V. Kalchenko

Institute of Radioelectronics
Kharkov, USSR

In 1968 the Soviet equatorial meteor expedition to Mogadishu (2°N, 45° E, July, 1968-July, 1970) measured for the first time at an altitude of 80-105 km wind velocity disturbances in the equatorial atmosphere with a quasi-two day period (KASHCHEYEV et al., 1971; KALCHENKO, BULGAKOV, 1973). An example of such disturbances is provided in Fig. 1, which shows time series of wind velocity in the meridional $V_N(t)$ and zonal $V_E(t)$ directions.

On September 10-17, 1968, the predominant meridional northward wind velocity was 9.1 mps and that of the predominant zonal westward wind - 38.3 mps. While the time series themselves show convincingly enough the presence of a quasi-two day period in the velocity variations, the results of an harmonic analysis of the time series are given below. This table shows that a significant anisotropy exists in the wind velocity disturbance, with a pronounced meridional maximum. During the period in question, $\bar{V}_{N48} = 64.6$ mps and $\bar{V}_{E48} = 19.3$ mps. The mean values of different harmonic components are compared in Table 1.

Table 1.

Average Values of the Velocity Harmonic Components During the Period
From September 10 Through 17, 1968

	V_0 $m \cdot s^{-1}$	V_{48} $m \cdot s^{-1}$	V_{24} $m \cdot s^{-1}$	V_{12} $m \cdot s^{-1}$	V_8 $m \cdot s^{-1}$	ϕ_{48} h	ϕ_{24} h	ϕ_{12} h	ϕ_8 h
Meridional Direction	9,1	64,6	16,6	9,0	13,9	30,0	16,4	11,9	4,6
Zonal Direction	-38,3	19,3	14,9	15,0	7,4	31,0	16,4	7,7	4,6

The table shows that in the meridional direction the amplitude of the two-day variations exceeds that of the diurnal component almost by a factor of four. In the zonal direction harmonics are commensurable but the two-day component exceeds the diurnal and semi-diurnal components by a factor of 1.3. These results convincingly show that one should take into account the velocity component with a quasi-two-day period when analyzing the wind at mesopause altitudes. The amplitude of the semi-diurnal component in the zonal direction is nearly double that in the meridional direction. The phase of these components is such that the velocity vector of the semi-diurnal tide rotates counter-clockwise. ($\phi_{N12} - \phi_{E12} = 3.2$ h).

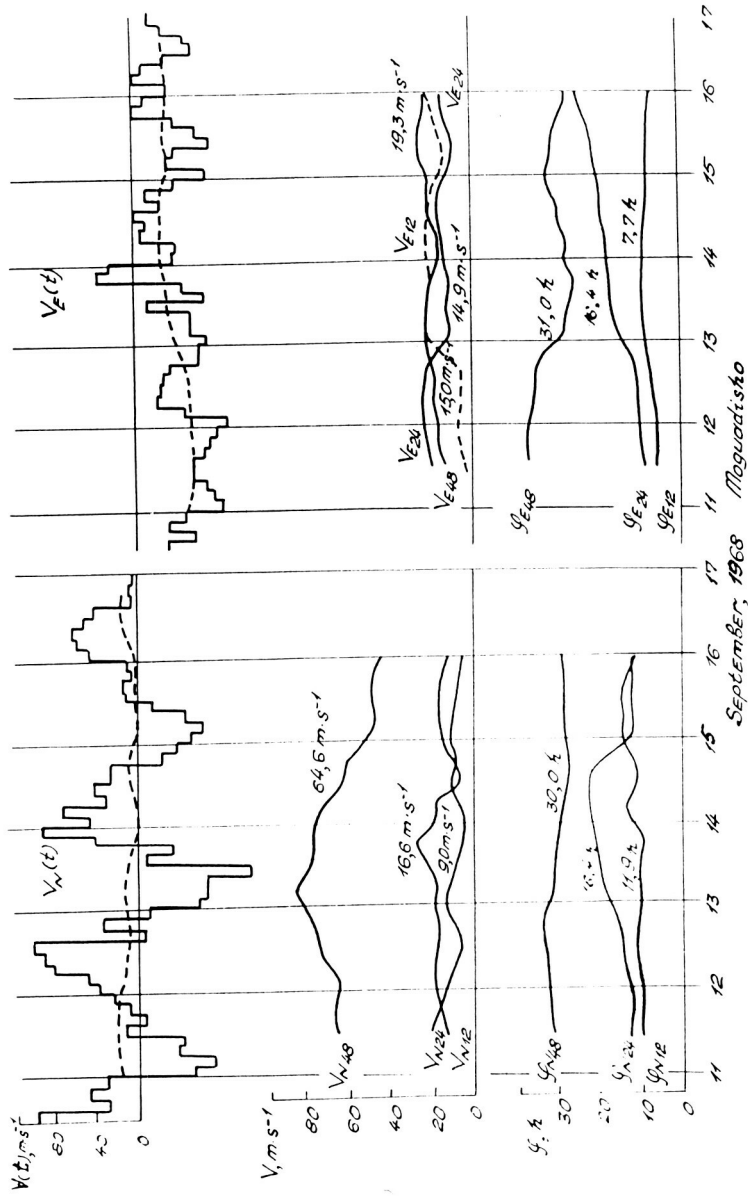


Fig. 1 Wind velocities in the meridional, V_N , and zonal, V_E , directions for the period September 11-17, 1968, over Mogadishu. Mean amplitudes and phases for each periodicity over the measurement interval appear on the curves.

The mean values of the diurnal component phase were the same for both the zonal and the meridional components.

Comparison of results obtained in the equatorial zone with those obtained in Kharkov and Dushanbe showed the global nature of the quasi-two day disturbances, with an amplitude maximum over the equator. The period of the discovered variations may be other than 48 hours. For example in July-August, 1981, $T_x = 44, 5$ hrs., while in July, 1971, $T_x = 52, 5$ hrs.

The experiments carried out in the equatorial zone using velocity measuring equipment revealed that the two-day disturbance amplitude is bigger in the upper layers of the meteor zone and the phase either decreases in the upper layers or remains unchanged. Fig. 2 shows the results of observations carried out in February-March, 1970. Three independent height ranges are presented, with average altitudes of 84.3 km, 92.7 km, and 100.8 km, with a distinct two-day wave dominating the highest altitude.

It was noticed that the appearance of quasi-two-day variations is close in time to the change of polarity of the interplanetary magnetic field (IMF). Moreover, the phase of the fluctuations depends on the sign change from "+" to "-" or vice versa.

Experimental data obtained in 1970-1976 (50°N), in 1968-1970 (2°N) and in 1972-1974 (67°S) were used in an analysis of the two-day variations at different latitudes and in different seasons of the year (Obninsk, 1976, iss. 7, 9, 10, 11). For each month the maximum amplitude of the two-day wave was chosen for both the meridional and zonal directions. The velocity values were averaged for each month using available data and the results obtained referred to the middle of each month. Thus, monthly mean values were obtained for an average year. A 10-year analysis carried out for 50°N for all the measured two-day disturbances yielded about the same results. The velocity values V_{48} are denoted by dots for the meridional direction and by circles for the zonal in Fig. 3. One can note that meridional and zonal components have nearly the same amplitudes (50°N and 67°S) and similar transformation laws. In the equatorial zone the meridional component is predominant and its annual variation differs slightly from that of the higher latitudes. The zonal component has the same half-year period just as at 50°N and 67°S. The maximum amplitude of the two-day disturbances is observed in July and January. The results also showed that two-day variations with a definite original phase and large amplitude occur with a sign change of the IMF provided that the polarity remains relatively constant for some days thereafter.

Simultaneous occurrence of quasi-two-day variations was observed more often in geographical points located on the same meridian; for points located at other longitudes such variations occur earlier in the east, i.e., the appearance of the wave moves from the east to the west. According to experimental data the wave number can have values from 3 to 5. Fig. 4 shows a case of quasi-two-day variations observed over Kharkov and Kharbarovsk, the longitude separation between these two points being 98.34°. It is obvious from Fig. 4 that the wind variations of August 17-21 over Khabarovsk are the same as those of August 19-23 over Kharkov. In this case processes observed over Kharkov repeated themselves over Khabarovsk

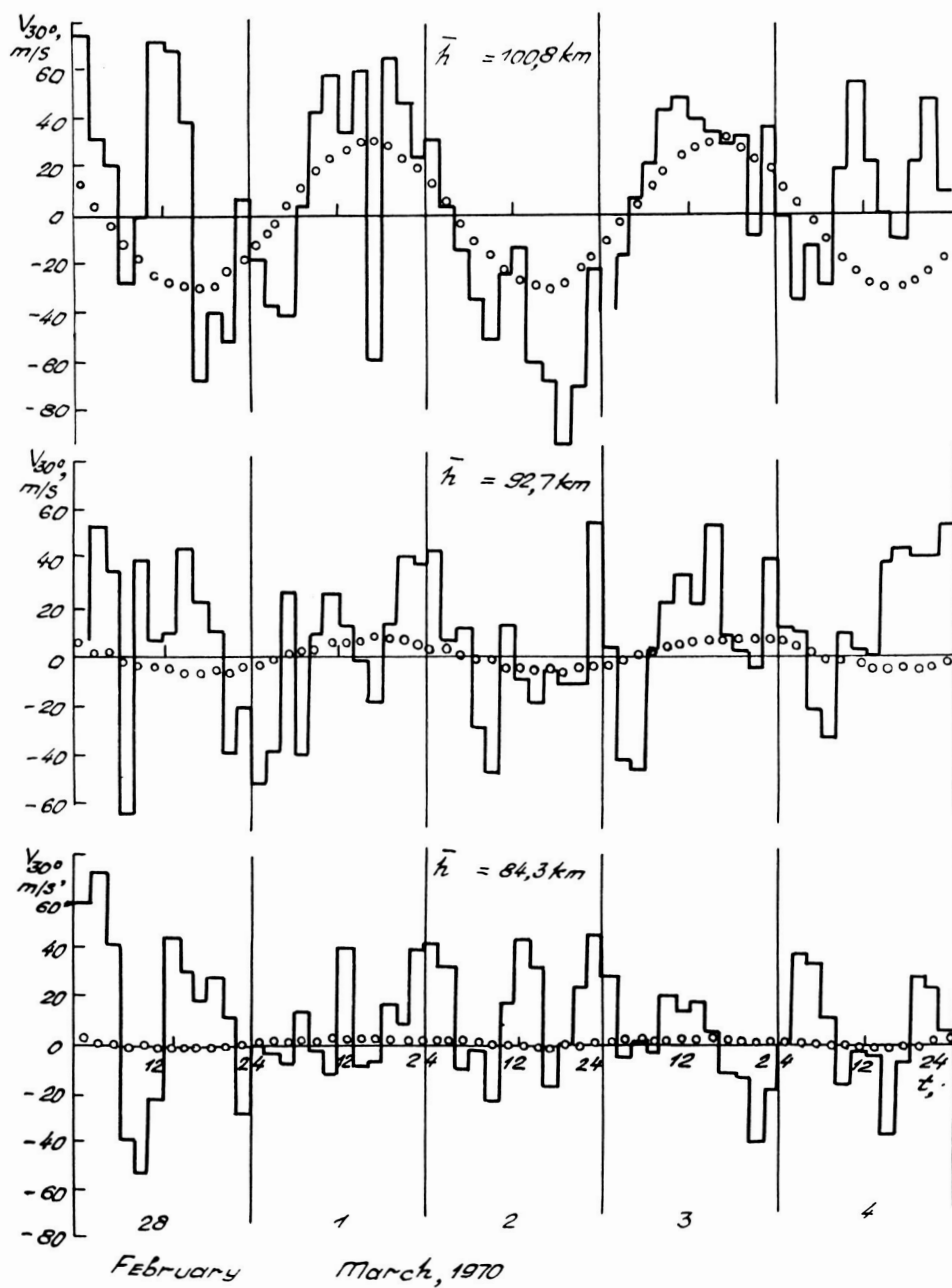


Fig. 2 The wind field at three heights for February 28 to March 4, 1970, with two day wave superimposed. Note the rapid increase in two day wave amplitude with height.

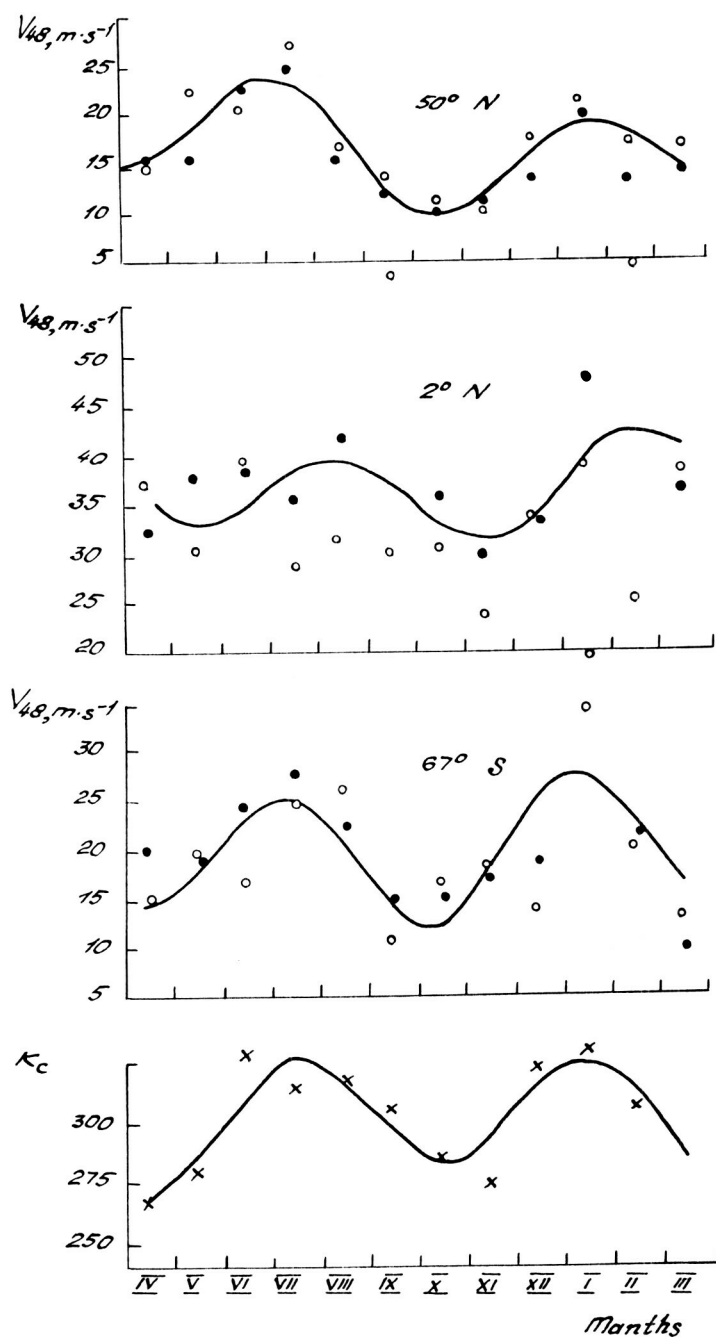


Fig. 3 Average maximum monthly amplitude of the two day wave from data measured at 95 km from Obninsk (50°N, 1970-76), Mogadishu (2°N, 1968-70) and Molodezhnaya (67°S, 1972-74), meridional ●, zonal ○; note the obvious correlation with K_c .

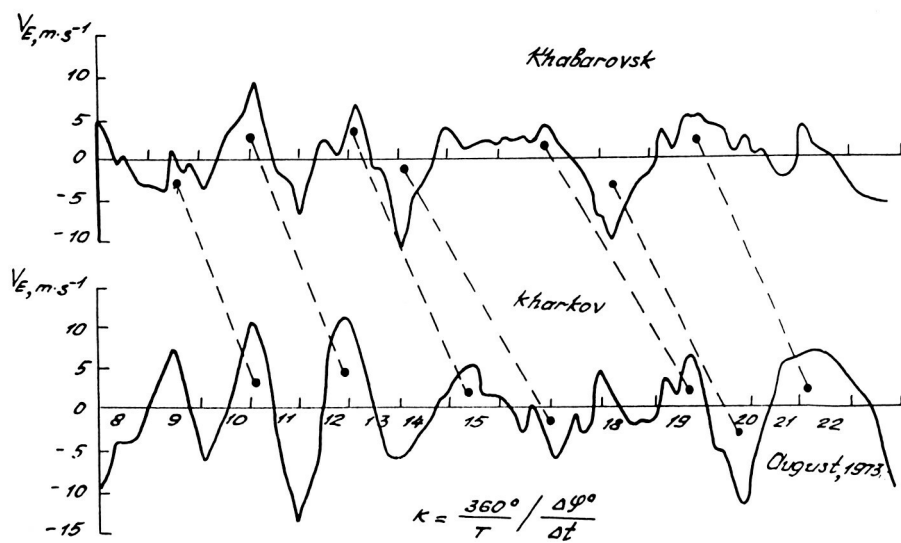


Fig. 4 Quasi two day variations observed simultaneously over Kharkov and Khabarovsk, separated by 98° in longitude. The phase lag of 62-65 hours corresponds to a zonal wave number of 5.

62-65 hours later which corresponds to a wave number $K \sim 5$. Similar results were obtained when comparing the measurements from two stations with $\Delta\phi = 12^\circ$ (Kharkov, Kazan) obtained from July 30 to August 9, 1978. From data obtained during January 15-27, 1978 over Obninsk and Kuhlungsborn ($\Delta\phi = 24.5^\circ$) $K = 4.7$.

The obtained results show that quasi-two diurnal variations are due to solar activity.

References

1. Kashchev B.L., B. V. Kalchenko, V. V. Lisogub, et al., 1971, In: 13th Plenary Session of the Committee on Comets and Meteors of November 1-15, 1971, Theses of the reports, Moscow, pp. 29-30.
2. Kalchenko B.V., S.B. Bulgakov, 1973, Geomagnetizm i aeronomiya, col. 13, No. 6, pp. 1125-1126.
3. Wilcos J.M., 1975, Solar Activity and the Weather, J. Atm. Terrest. Phys., Vol. 37, pp. 237-256.
4. Mardia K., 1978, The Statistical Analysis of Angle Observations, Science Publishers, Moscow, p. 239.
5. The Wind at the Altitude Range of 80-100 km, 1976, Obninsk, Iss. 7, 9.
6. Ibid., Iss. 10, 11.

VARIATIONS OF THE SEMI-DIURNAL TIDAL WIND IN THE
METEOR REGION WITH PERIODS OF ABOUT 27 AND 13.5 DAYS

K. M. Greisiger

Heinrich-Hertz-Institute of Atmospheric Research and Geomagnetism
Observatory of Atmospheric Research, DDR-2565 Kühlungsborn, GDR

Daily values of sunspot number and solar radio emission at 10.7 cm wavelength show a well known strong modulation with a period of 27 days, the sun's rotation period. Recent satellite measurements revealed the same modulation of the U.V. irradiance at wavelength below 300 nm (ROTTMANN 1983, LONDON et al., 1984). These U.V. variations, though relatively weak (a few percents), can influence the thermal heating of the ozone layer by altering the chemical composition (LONDON et al., 1984). Therefore, one can also expect a corresponding variation in the middle atmosphere of the semi-diurnal tide, which is thermally excited essentially by absorption of U.V. between 200 and 370 nm in the upper ozone layer.

We used results of radar meteor wind measurements at Kühlungsborn which were, for the most part, continuous since 1976. In order to detect a presumably very weak 27-day modulation within the natural and artificial noise of the daily values of the semi-diurnal wind amplitude (V_2) we chose the summer period with relatively steady conditions and the maximum amplitudes during the year (August, September). Further, by using the Bartels Rotation of the sun with a period of 27 days we applied the method of superposed epochs (or synchronization method). The result of this procedure by using the daily V_2 values of all Bartels Rotation periods in July, August and September from 1976 to 1983 for the zonal and meridional component, respectively, give a surprisingly distinct variation with dominant periods of about 27 and 13.5 days and a minimum to maximum change of about 20%. As was to be expected from the physics of the atmospheric tide, both components show a very similar behavior.

To test the significance of these results we investigated various subsets of the whole amount of data, for instance solar minimum and maximum years of every second year from the eight years 1976-1983. No essential differences of the amplitudes and phases of the 27 day- and 13.5 day-harmonics were found for the various data sets. That means that, especially, the deep minimum around the day 18 of Bartels Rotation is a persistent feature in the long-term mean behavior.

To remove the remaining doubts about the reality of this unexpectedly strong influence of the sun's rotation, a quantitative statistical test is necessary. For this purpose one can apply the "shaking test" after Bartels. This test gives the result that we have found a systematic 27-day variation at a confidence level of 95%. For other seasons than summer we haven't found any significant variation. This may be, above all, due to the noise introduced by natural wave processes in the same range of periods especially in winter.

Concerning a similar investigation for individual years, only the summer data of 1982 and 1983 were suitable because of only small gaps and

the high statistical significance of the data. Again, the already known picture from the many years average appears for these individual years but with a larger minimum change: about 50%. The "shaking test" shows the significance of this 27-day variation. There are some indications of an anticorrelation between solar activity and the amplitude of the semidiurnal tidal wind as was already found by GREISIGER et al., (this issue) for the 11-year solar cycle.

We have found a clear modulation of the semi-diurnal tidal wind amplitude in summer by the rotation of the sun. This amplitude variation exists for individual summer periods, but is present also in the average of several years (up to eight) with relatively persistent maxima and minima. We may speculate that on the sun a longitudinal activity variation exists which is persistent for several years. But a corresponding solar radiation modulation of this kind is not known up to now.

The modulation of the tidal amplitude was unexpectedly strong and seems to be in anticorrelation with solar activity. As for the 11-year solar cycle dependence of the tidal amplitude, the strength and the anticorrelation with solar activity of this 27-day variation also cannot be explained with current models of the semi-diurnal tide; the mechanism of this modulation has to be found yet.

References

1. J. London, G. G. Bjarnason and G. J. Rottmann, 1984, 18 Months of U.V. Irradiance Observations From the Solar Mesosphere Explorer Geophys. Res. Lett. 11, pp. 54-56.
2. G. J. Rottmann, 1983, 27-day Variations Observed in Solar U.V. (120-300 nm) Irradiance Plan. Space Sci. 31, pp. 1001-1007.

TIDAL ACTIVITY IN THE METEOR ZONE OVER BUDRIO, ITALY

G. Cevolani

FISBAT/CNR Institute
Bologna, Italy

Abstract: A brief survey is presented here of the variations with time and height of atmospheric tides observed at Budrio (45°N, 12°E) in the wind field between 80 and 110 km altitude during the 1978-82 year period. Variations of amplitude maxima mainly of the semidiurnal tide in the winter data of 1979 and 1980 show periodicities of a few days throughout the observing period. Upward propagation of tidal energy during a stratospheric warming in January 1982 is proposed to be inhibited because of instabilities in atmospheric conditions.

The CNR radar station at Budrio, near Bologna, first carried out observations in 1976, keeping records throughout these last years for time intervals varying between 2 days and 3 months. Records for 2-6 days were kept for every month in 1976; 4-7 days for every month in 1978; 2-3 weeks during the "special" periods (11-25 January, 14-18 March, 11-23 September) of the CTOP (Cooperative Tidal Observational Project) in 1979, and in the course of three observational campaigns jointly with the University of Sheffield in 1979 (26 July - 4 August) and in 1980 (16 July - 2 August and 7 November - 1 December) the latter within the EBC (Energy Budget Campaign) program; and for up to 2-3 months (Winters 1981-82, '82-'83 and '83-'84) in the course of the SWAMP (Stratospheric Warming Mesospheric Project) a sub-program of MAP (the Middle Atmosphere Program). In table 1 the time intervals of wind observations are presented: numbers represent the number of days of observation.

VERNIANI et al., (1980) have presented the first results obtained in the February 1976 - January 1977 year period from wind observations in the lower thermosphere. These results indicate the necessity of furthering the study of monthly and seasonal variations in amplitudes and phases of tides and the possible correlation between the long-period waves in the meteor zone and variations with the same periods in tropospheric parameters. Unfortunately, the recording method did not allow measurements of the height of the radio echoes, so that the wind data were referred to an average height of 96 km.

A new observational campaign was conducted at Budrio throughout all of 1978 aiming at studying the vertical propagation of gravity, tidal and planetary waves by using an interferometric system pointed eastwards and able to associate with every echo its real height. At the end of 1980, a second interferometer pointed northwards was constructed so as to allow the measurement of the southerly wind component. Consideration of the two systems for interferometric measurements indicate an accuracy in the height of the echo and the radial velocity measured with the Doppler effect is $\pm 2-3$ km and 3 m/s, respectively. For the results presented here, it has been assumed that the wind values depend only on time and height, and represent the components of the horizontal wind along the main axis of the antennae.

Table 1

Number of observational days at Budrio in the 1976-83 year period.

<u>31</u>	<u>7</u>	<u>7</u>	<u>12</u>	<u>10</u>		<u>10</u>	<u>8</u>		<u>12</u>			1983	
<u>30</u>			<u>10</u>	<u>8</u>		<u>24</u>			<u>13</u>		<u>24</u>	1982	
						<u>10</u>			<u>15</u>		<u>10</u>	1981	
		<u>55</u>			<u>14</u>	<u>15</u>		<u>9</u>	<u>14</u>	<u>24</u>		1980	
<u>15</u>		<u>15</u>	<u>3</u>	<u>4</u>	<u>10</u>	<u>10</u>		<u>15</u>	<u>13</u>	<u>4</u>	<u>10</u>	1979	
<u>5</u>	<u>4</u>	<u>3</u>	<u>3</u>	<u>3</u>	<u>3</u>	<u>4</u>		<u>4</u>	<u>3</u>	<u>12</u>	<u>3</u>	<u>5</u>	1978
<u>6</u>	<u>2</u>	<u>2</u>	<u>2</u>	<u>2</u>	<u>2</u>	<u>3</u>		<u>2</u>	<u>4</u>	<u>2</u>	<u>2</u>	<u>4</u>	1976
JAN	FEB	MAR	APR	MAY	JUN	JUL	AUG	SEP	OCT	NOV	DEC		

The data from 1976 and 1978 have been analyzed using the autocovariance function method; from 1979, use has been made of the Fourier transform and "maximum entropy" methods, the latter being employed for studying vertical profiles of the fine structure of the wind field (CEVOLANI and FORMIGGINI, 1981). For the data from 1979 onwards, the Fourier transform method has proven to be the best for studying the phenomena in question, and the inverse Fourier transform, centered on a suitable band of frequencies of the transform spectrum has been used to describe time variations of the amplitudes and phases of the most important oscillations.

Results of the 1978 observations - Average values of tidal parameters were obtained from observations of zonal winds carried out regularly at Budrio for a few consecutive days in each month of 1978. The normalized spectra of wind amplitudes, corresponding to each month and referred to an average height of 95 km are presented in Figure 1. The amplitudes and average phases of the diurnal, semidiurnal and terdiurnal tides have been obtained with a weighted least-squares method, while the frequencies have been deduced from the autocovariance function. Figure 2 presents the seasonal variations of a) the prevailing wind, b) the semidiurnal, c) the diurnal, and d) the terdiurnal tide in 1978 over Budrio. Comparison is made with results of 1976, and for prevailing winds only, with the values interpolated from the CIRA (1972) model for 45°N lat. From Figures 1 and 2, it appears obvious that the energy associated with the semidiurnal tide is the most important compared to that of other components. A salient aspect of the wind observations performed at Budrio in 1978 and previous years is that these exhibit not only systematic variations in the amplitude and phase of the tides throughout the year; but also that sometimes little coherence exists between results of the same month of different years and even in observations carried out in consecutive days of the same month. This observed variability of the tides is suggested to be linked with different contributions from their distinct modes which can interfere with each other with effects that vary with season, latitude and even with longitude.

Results of the 1979 observations - In order to study in detail the variability of the tides with height and time in the lower thermosphere, observations were conducted at Budrio in 1979 for zonal winds during three "special" periods (11-25 January, 14-28 March and 11-23 September) of the CTOP and between 26 July and 4 August within the joint project with the University of Sheffield. This series of observations had the dual aim of analysing tidal parameter variations on short and large time scales, showing up deviations from average structures even in long periods and studying more closely the seasonal variations of different tidal modes in the lower thermosphere (CEVOLANI and BONELLI, 1985). The Fourier transform and inverse transform method has been applied to time series of these data after sorting them into uniformly spaced height intervals with sampling at 5 km between 80 and 110 km. Figures 3 and 4 present the daily vertical profiles of zonal tidal amplitudes limited to 11-20 January and 27 July - 3 August 1979, together with profiles of phases obtained for three distinct days (11, 15 and 20) in January and (27, 30 and 3) in July - August 1979. For the semidiurnal tide only the average profiles of amplitudes and phases for altitudes between 80 and

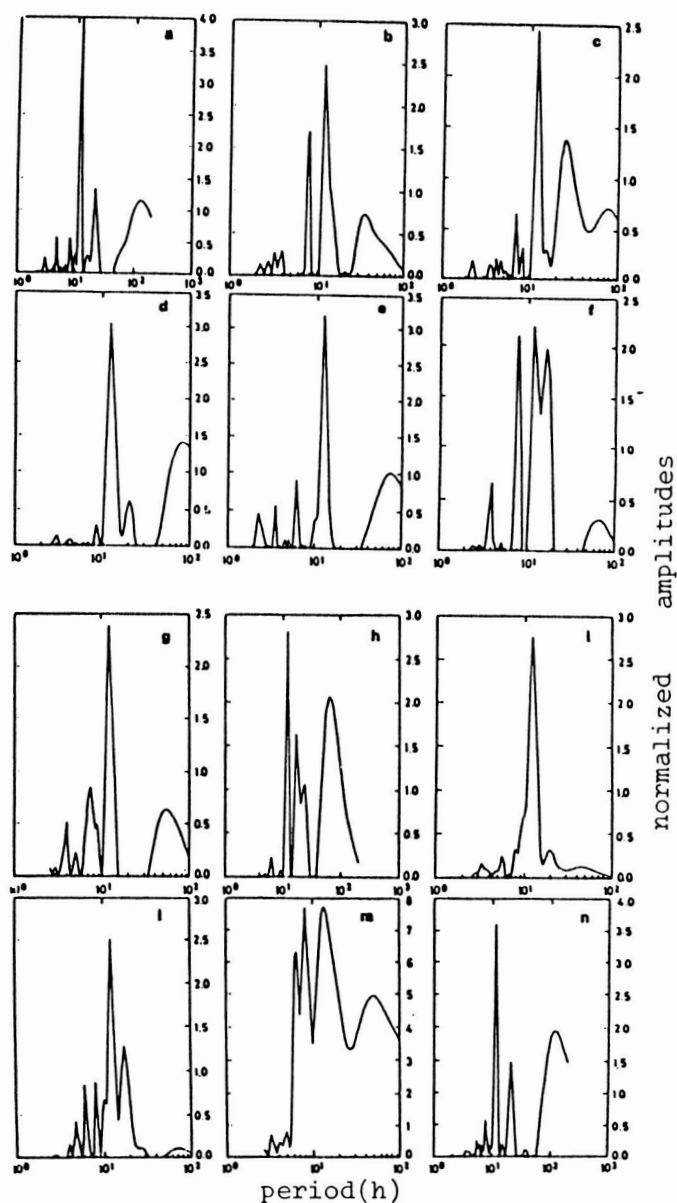


Fig. 1 Normalized amplitude spectra of the zonal wind observed at Budrio in the following periods: a) January 16-21; b) February 13-17; c) March 14-17; d) April 20-23; e) May 8-12; f) June 19-22; g) July 11-14; h) August 20-24; i) September 9-12; l) October 18-22; m) November 1-4; and n) December 14-19, 1978.

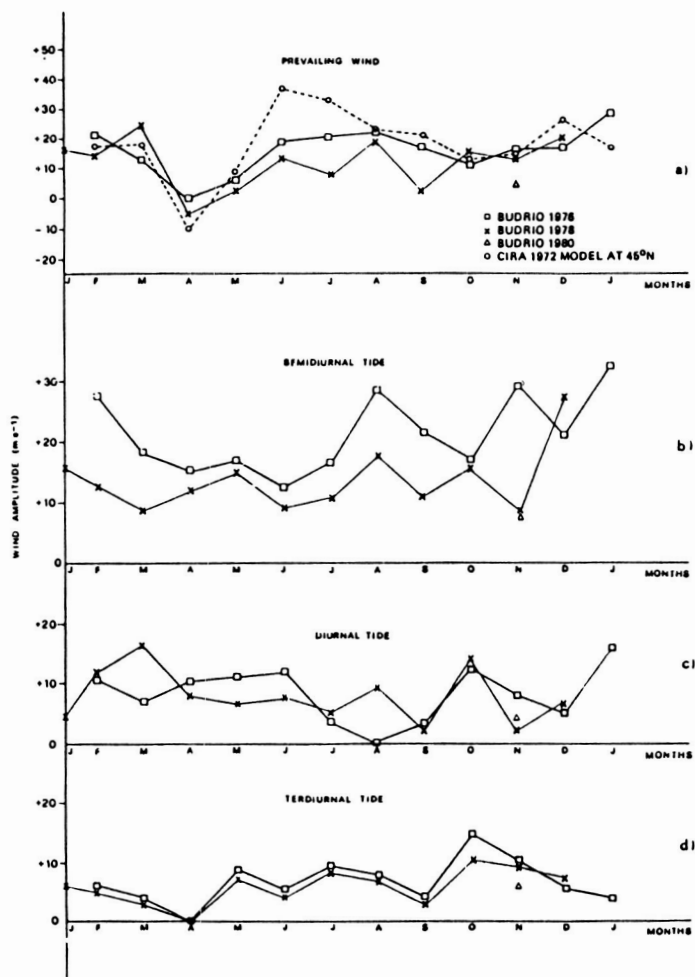


Fig. 2a-d Seasonal variations of: a) the prevailing wind; b) the semidiurnal tide; c) the diurnal tide; d) the terdiurnal tide in different years at Budrio.

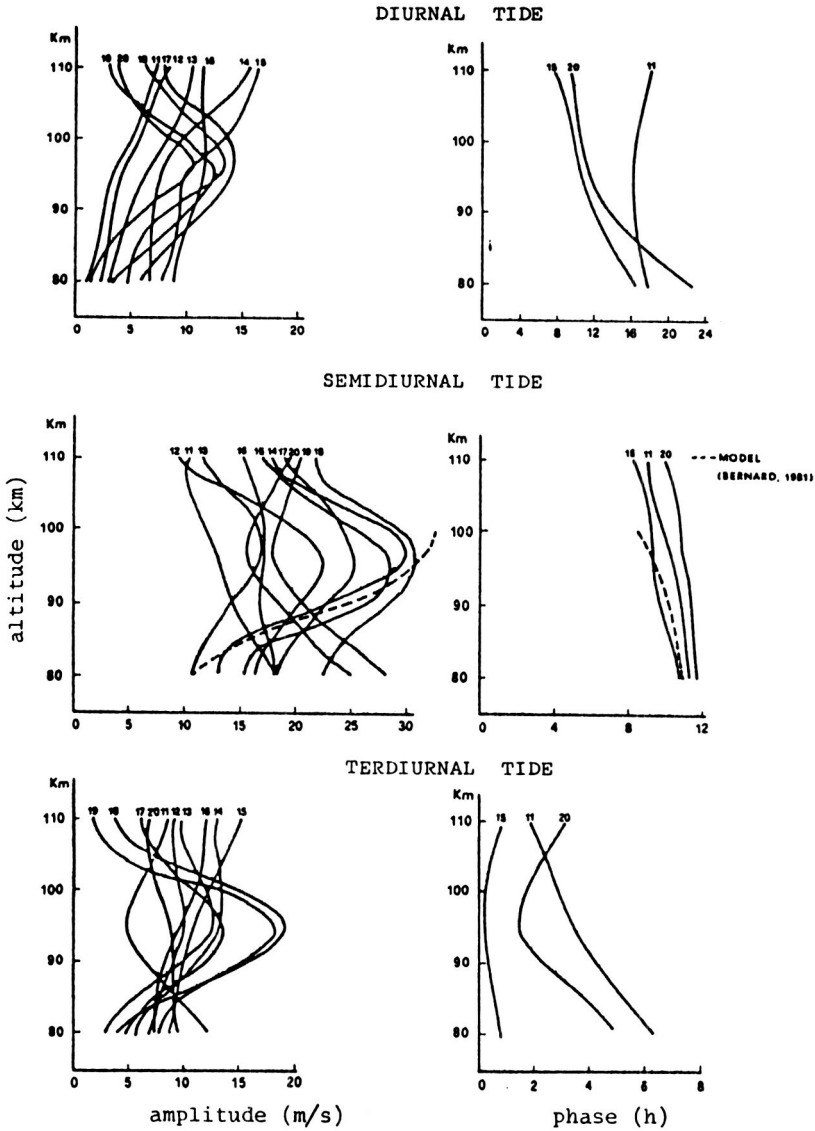


Fig. 3 Vertical profiles of: a) amplitudes and b) phases of the diurnal (D), semidiurnal (S) and terdiurnal (T) tide observed at Budrio between 80 and 110 km in the 11-20 January 1979 period.

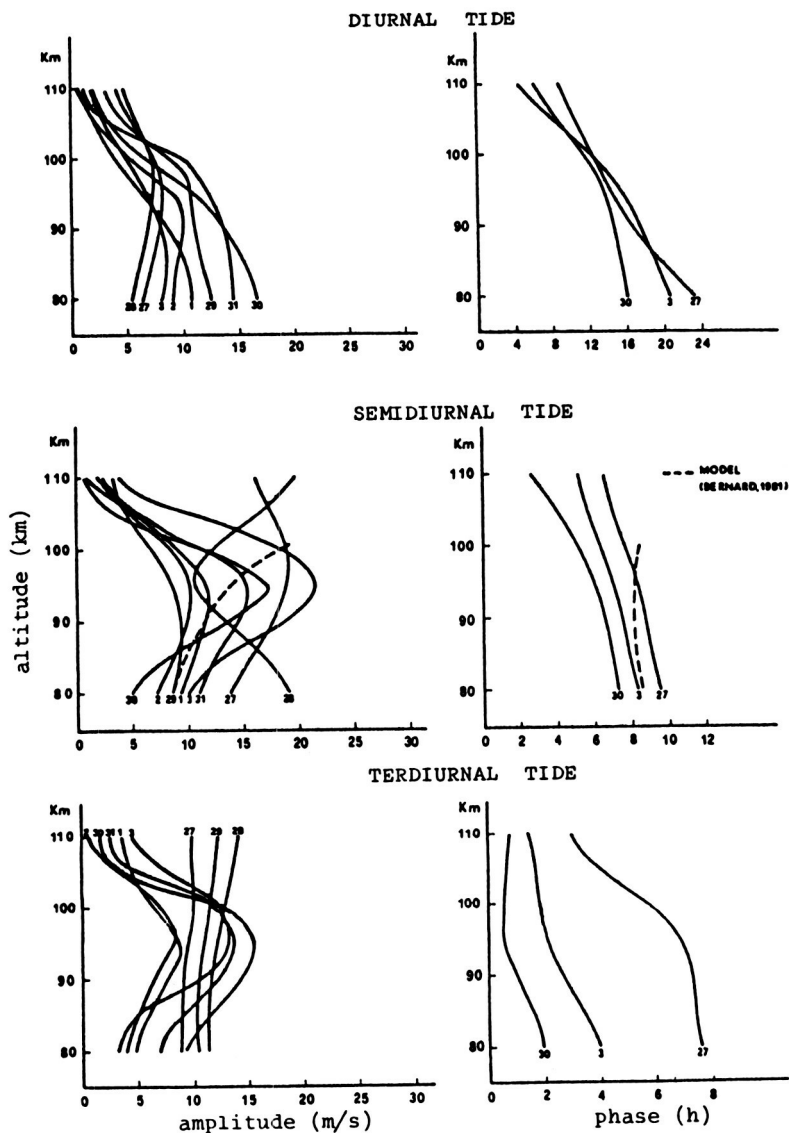


Fig. 4 Vertical profiles of: a) amplitudes and b) phases of the diurnal (D), semidiurnal (S) and terdiurnal (T) tide observed at Budrio between 80 and 110 km in the 27 July-3 August 1979 period.

100 km, deduced from a realistic tidal excitation model by ozone at the solstices (BERNARD, 1981), are presented for comparison. The inverse transform centered on peaks of the three tidal oscillations, whose frequencies are deduced by Fourier transform, give the time amplitude and phase variation for the whole observing period. In Figures 5 and 6 are presented the variations of amplitude maxima of the three tides in the periods 11-25 January and 26 July - 4 August respectively, for the altitude intervals: a) 75-90, b) 90-100, and c) 100-115 km.

The diurnal tide - The data from the 1979 observation periods show that the diurnal tide carries only a small part of the total energy of the wind in the lower thermosphere. Generally amplitudes have a tendency to increase with height in winter and decrease in summer. The maximum amplitudes are never above values of 15 m/s and are obtained in the two quoted periods at different heights. The trend with height of the observed phases is generally typical of the main mode (1,1) with vertical wavelengths $\lambda = 25-30$ km for altitudes below 95 km. Above this altitude, phase in winter diminishes less rapidly (on the 11th of January a slow progression is recorded) as one might expect in the presence of evanescent modes, that is of modes whose energy is exposed to reflection processes. In contrast, in summer phases diminish more rapidly above the height in question, indicating the possible importance of modes which propagate upwards with short wavelengths. The seasonal variations found in the average phases are not consistent and the amplitude maxima of the zonal wind are generally recorded eastwards at 95 km where phases vary from 1200 hrs local time in winter to 1400-1500 hrs local time in summer. This progression can be linked with variations of the average wind and temperature profiles which can influence modes of the diurnal tide. It can be interesting to examine the variability of amplitudes of the diurnal tide on short time scale, that is in the course of a few consecutive days. Figure 5 shows periodicities of a few days in variations of amplitude maxima observed in winter at high altitudes, whereas it appears more problematic to isolate such periodicities in summer (see Figure 6).

The semidiurnal tide - The data of the 1979 observing periods have emphasized the variability of this oscillation not only with height but also on large time scales (seasonal variations) and short ones (variations in a period of a few consecutive days). The amplitudes of this tide appear clearly higher in winter with respect to the ones recorded in summer (Figures 3 and 4). The phase profiles for the months of January and July-August indicate the presence of vertical wavelengths with $\lambda \geq 100$ km (typical of the main mode (2,2)) relative to oscillations which propagate upwards and eastwards. Average phases at 95 km vary from 1000 to 1100 hrs local time in winter, and from 0700 to 0800 hrs local time in summer. The deviations of the observed phase in summer from the theoretical (FORBES, 1982) can result from: a) reflection of the (2,2) mode in the thermosphere due to damping phenomena; b) interaction of the semidiurnal modes with average winds which can modify the propagation conditions. The data of the two quoted periods have revealed variability of this wave even on short time scales. The inverse transform method indicates that the tide is modulated in amplitude throughout the observing period. Figures 5 and 6 show the amplitude variations of maxima with time scales possibly of 3-5 days in winter and summer, at the three quoted height intervals. It is important to stress that in winter in the intermediate layer (90-100 km)

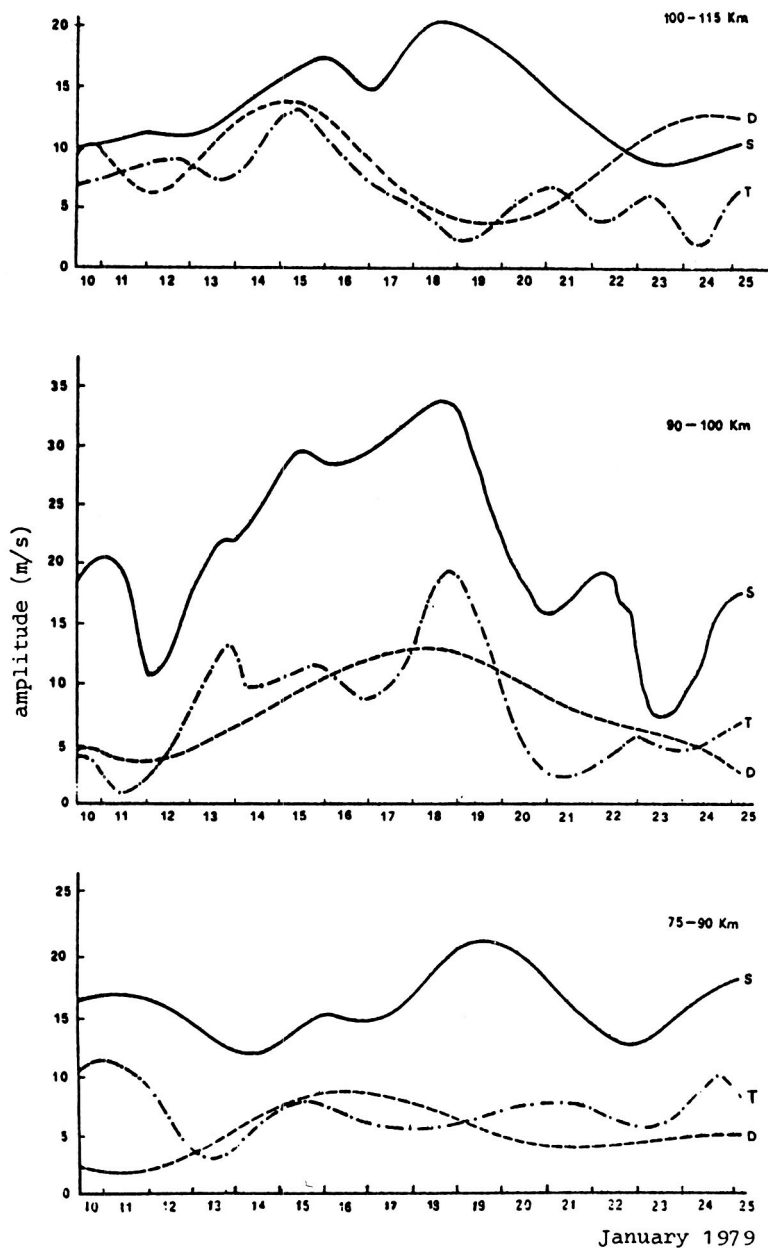


Fig. 5 Variations of amplitude maxima of the diurnal (D), semidiurnal (S) and terdiurnal (T) tide observed at Budrio in the 11-25 January 1979 period, for the height intervals: a) 75-90; b) 90-100; and c) 100-115 km.

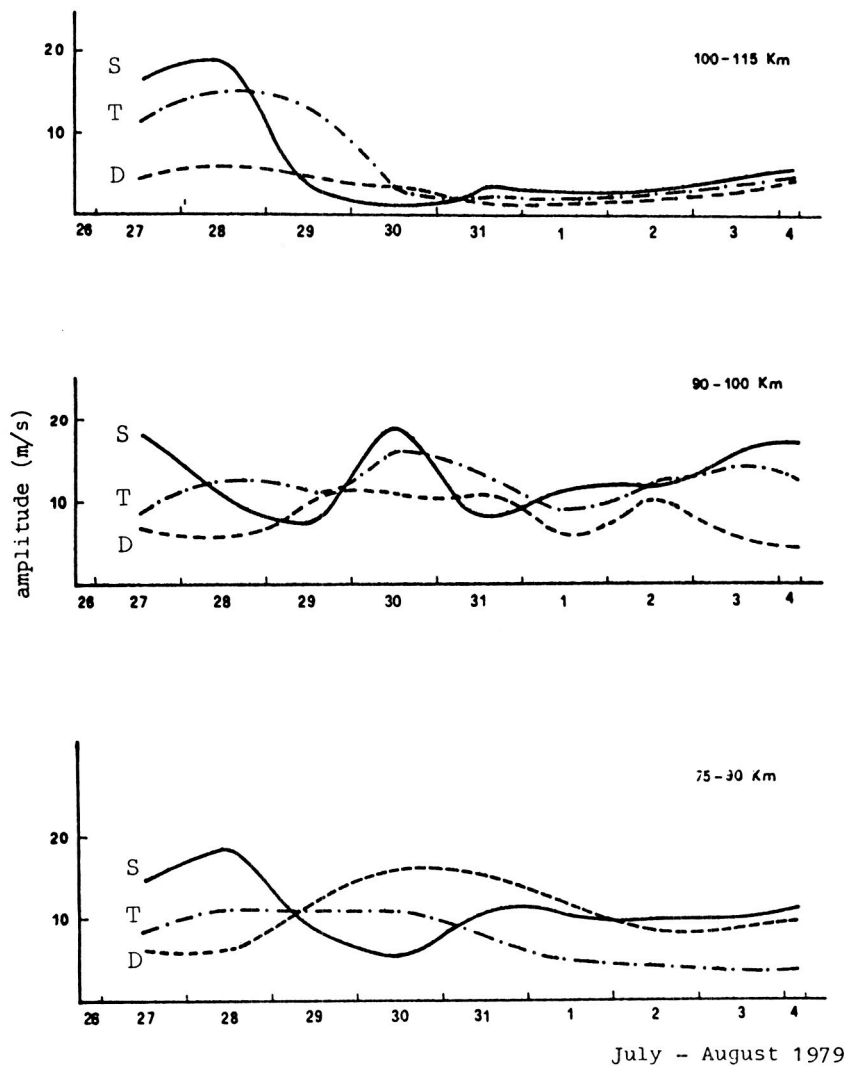


Fig. 6 Variations of amplitude maxima of the diurnal (D), semidiurnal (S) and terdiurnal (T) tide observed at Budrio in the 26 July-4 August 1979 period, for the height intervals: a) 75-90; b) 90-100; and c) 100-115 km.

the amplitude of the tide varies by a factor of 3 in the course of a week (12-18 January).

The terdiurnal tide - The results of the 1979 observations emphasize the lack of coherence of this oscillation, which nevertheless shows a normally pronounced peak around 8 hrs. The amplitudes are generally consistent (maximum values are about 15 m/s at 95 km) and more significant than the diurnal ones. These amplitudes do not perceptibly vary in winter and summer months in contrast to what was seen in the semidiurnal tide. Phase variations in the diurnal vertical profiles are quite large and do not allow any comparison with those of the two other tides. There appears to be a correlation between the temporal variability of this tide and the semidiurnal tide as observed in the two periods of 1979. Figures 5 and 6 show that short time scale variations (3-5 days) of the terdiurnal tide generally correlate closely with the corresponding ones of the semidiurnal tide. This correlation is more consistent in winter data and underlines the possible importance of the common excitation of both of the tides, mainly due to the absorption of solar radiation by ozone. The seasonal and short time scale variations of this tide suggest a possible link with variations in the thermal excitation of its source rather than with the effects induced by the presence of average zonal winds.

Results of the 1980-'82 year observations - A further observational wind campaign was carried out at Budrio in summer (July-August) 1980 jointly with the University of Sheffield, utilizing data from both Sheffield and Stornoway, in order to allow hour by hour comparison of tides and planetary waves in the meteor region at different latitudes (CEVOLANI et al., 1983). These three-station observations of the semidiurnal tide showed the mean tidal pattern to agree with the predicted main solar tide (Figure 7). Systematic differences existed, however in the amplitudes and phases recorded at different latitudes which may reflect local variations in the stratospheric wind and temperature fields. Variations in the amplitude and phase of the tides did not correlate with longer period planetary wave activity and the results suggest that in the upper mesosphere and lower thermosphere such interaction was not present and that the two kinds of waves existed independently. The possibility remains that the variations were caused by non-solar tidal modes (generated at lower altitudes by the interaction between the primary solar tide and travelling or quasi-steady atmospheric structures) which would account for the systematic variations between the stations.

Zonal wind observations were carried out at Budrio in the 7 November - 1 December period during an integrated ground based, balloon and rocket campaign - the Energy Budget Campaign (EBC) 1980 - planned for the study of energy inputs and outputs in the upper atmosphere (60-180 km) during geomagnetic disturbances. The meteor radar observations carried out at Budrio and different stations in middle latitudes during the EBC provide a comprehensive picture of upper atmosphere dynamics for that period (Fellous et al., 1985). The main wind component at all stations is outstandingly the semidiurnal tide. This oscillation is strongly modulated in amplitude and an important result is in evidence of the large horizontal extent of this phenomenon, as shown in Figure 8. The variations of semidiurnal amplitude over 8° in the latitude and 15° in longitude appear reasonably well correlated

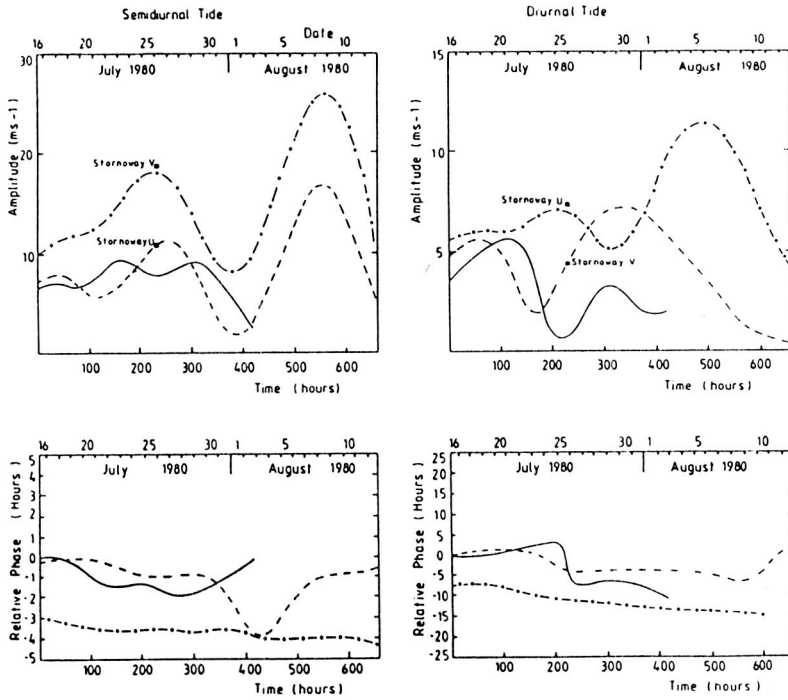


Fig. 7 Amplitude and phase variations of the semidiurnal and diurnal tide at 95 km during summer 1980 for Budrio zonal (—), Sheffield zonal (---), and Sheffield meridional (-●-) components. The average of six days of Stornoway zonal (U) and meridional (V) amplitudes are shown as square dots.

as measured by different instruments. It is recognized that the variation of the main tide over scales of several days and shorter time scale variations from place to place, relate to local effects. All tidal wind components as observed in late autumn at Budrio exhibit amplitudes generally lower than those measured in November of previous years. The daily variations in the amplitudes of the semidiurnal tide over scales larger than 5-6 days (Figure 8) suggest changes in the source, whereas the daily drift in the phase of this tide could indicate that its vertical structure is consistent with short vertical wavelengths. In the quoted period, the amplitudes of the diurnal and terdiurnal tides are not significant and the phases of these components exhibit non linear vertical variations. The complete description of these results awaits the formulation of a global model relating the energy input in the atmosphere and its distribution through dynamical processes.

Current meteor wind observations intended to monitor stratospheric warmings as part of the SWAMP campaigns, might well reveal the extent to which changes in stratospheric circulation influence the structure of tidal waves in the upper meso- and lower thermosphere. Information on the amplitude variation of tidal modes present in the meteor region at 95 km in the 11-22 December 1981 and 6 January- 2 February 1982 time periods, are shown in Figures 9 and 10 respectively, for zonal and meridional wind components. We can recognize the prominence of the amplitudes of the zonal tides with respect to those of the meridional ones. In December 1981 the tidal activity appears more intense and amplitudes up to 30 m/s for the semidiurnal tide and up to 15 m/s for the terdiurnal are recorded in the zonal wind structure. It is important to consider the persistence in the amplitude variation of the zonal tides of time scales of 5-6 days pointed out at Budrio in previous campaigns. A significant change in the pattern of the prevailing flow occurred between January 20 and 23, 1982: a reversal in the zonal flow was accompanied by a corresponding change in the meridional flow about the time of a temperature rise of 20-25 degrees in a few days observed at the 10 mb level by radiosondes in Central Europe. Figure 10 shows that at the time of the prevailing flow reversal, a strong weakening in the amplitudes of the tides was recorded in both wind component directions. On January 22-23, 1982, a minimum in the amplitude variation of the diurnal, semidiurnal and terdiurnal tides was generally observed, suggesting that the perturbation induced in the meteor region by the quoted temperature change during a minor stratospheric warming can also influence the tidal fields. It can be tentatively proposed that propagation of tidal energy at that time was seriously inhibited because of consequent irregularities and instabilities in atmospheric conditions, possibly accompanied by reflection and/or dispersion of energy through damping processes (CEVOLANI and DARDI, 1983).

References

1. Bernard, R., 1981, Seasonal Variation in Mesospheric Semidiurnal Tides. Comparison of Meteor Radar Observations and Results from an Excitation Source Model, *J. Atmos. Terr. Phys.*, 43, pp 101-109.

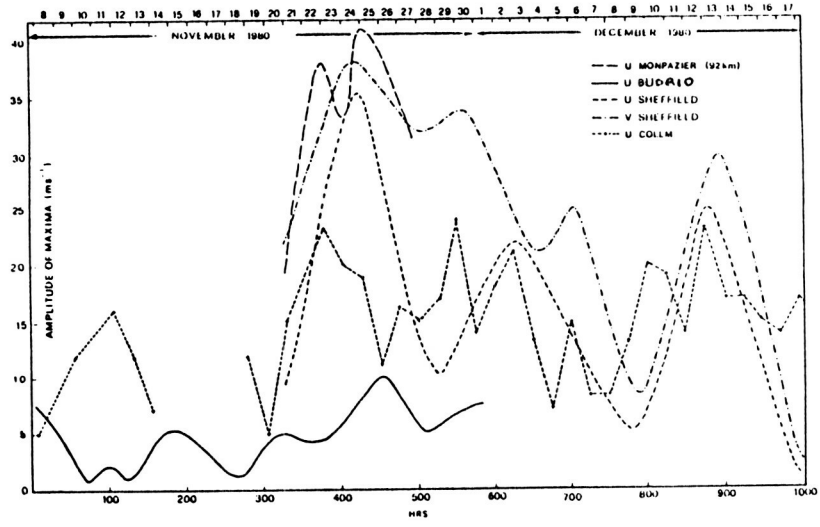


Fig. 8 Maximum amplitude variation with time of the 12 h tide at Budrio (zonal U), Sheffield (zonal U and meridional V), Monpazier (zonal U), and Collm (zonal U).

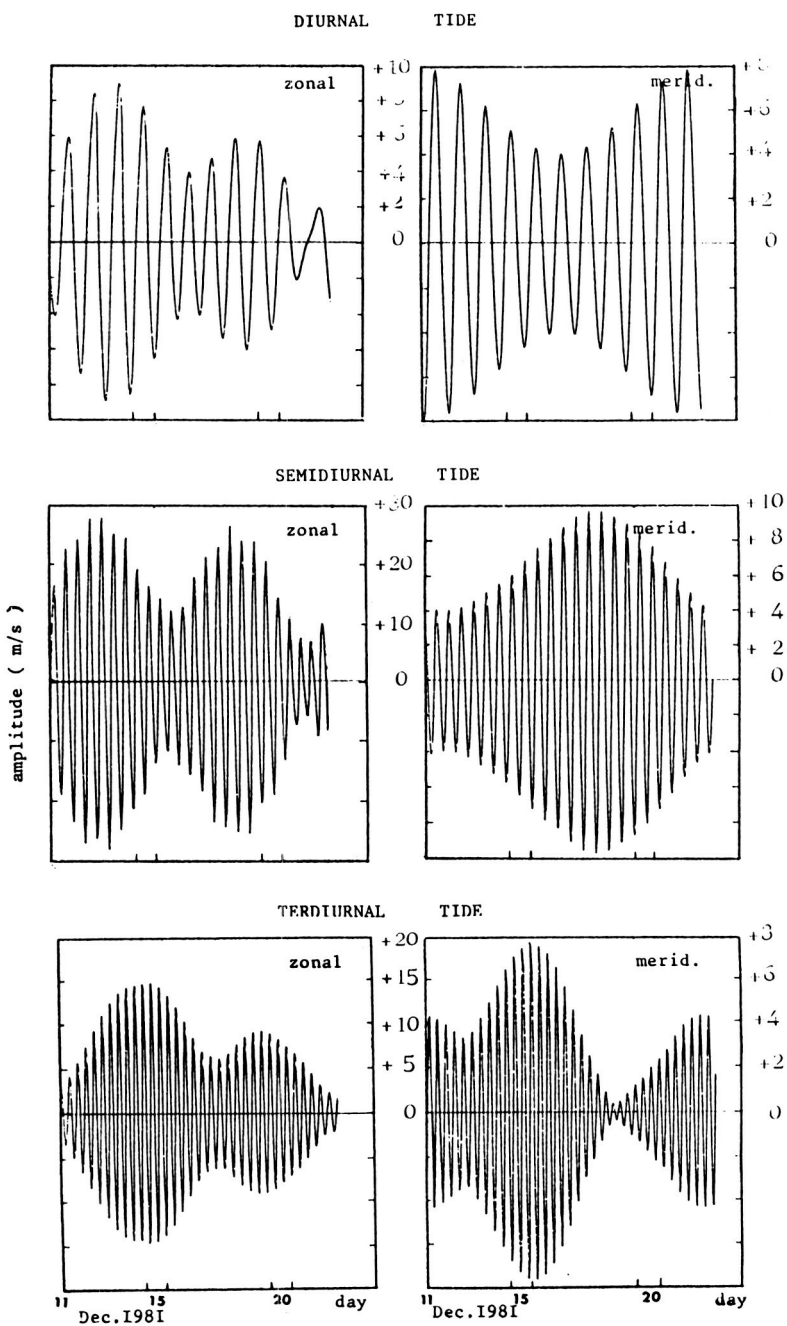


Fig. 9 Inverse Fourier transform of the 24, 12, and 8 h tidal peaks relative to zonal and meridional winds observed at Budrio at 95 km. Start time is 11.00 h LT, December 11, 1981.

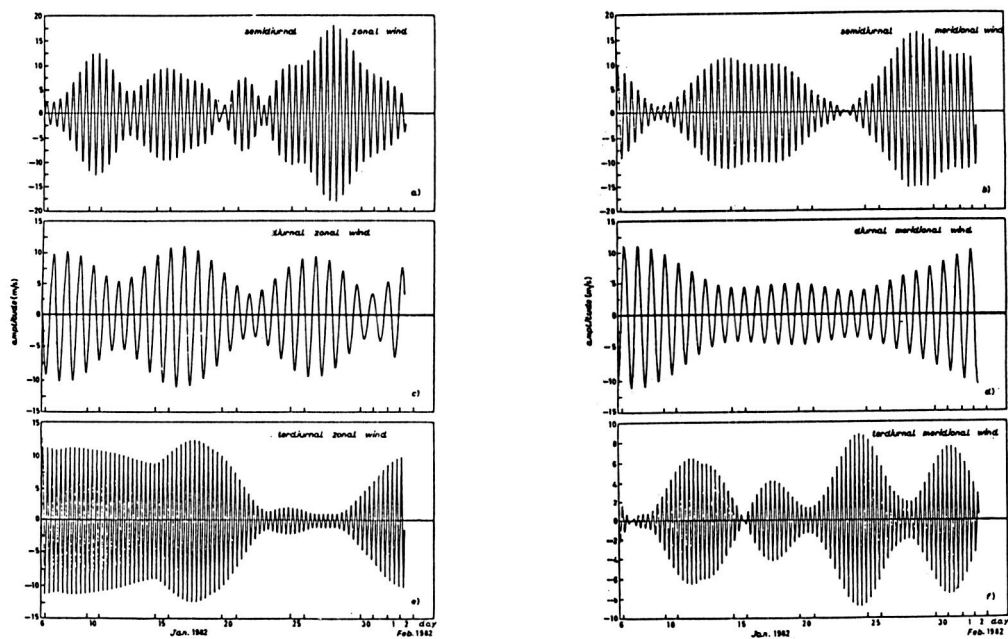


Fig. 10 Inverse Fourier transform of the 12, 24 and 8 h peaks in the Fourier transform relative to zonal (a, c, e) and meridional (b, d, f) winds observed over Budrio at 95 km.

2. Cevolani, G. and C. Formiggini, 1981, Evidence of Internal Gravity Waves in the Lower Thermosphere at Midlatitudes, *Il Nuovo Cimento*, 4C, pp 1-25.
3. Cevolani, G. and A. Dardi, 1983, A Coupling Phenomenon Between Mesospheric Wind Patterns and Midwinter Stratospheric Warmings: Preliminary Results, *Lettere al Nuovo Cimento*, 36, pp 177-187.
4. Cevolani, G., S.P. Kingsley and H.G. Muller, 1983, Three-Station Meteor Wind Observations in Northern Europe during Summer 1980, *J. Atmos. Terr. Phys.*, 45, pp 275-280.
5. Cevolani, G. and P. Bonelli, 1985, Tidal Activity in the Middle Atmosphere, in Press on *Il Nuovo Cimento C*.
6. Fellous, J.L., G. Cevolani, S.P. Kingsley and H.G. Muller, 1985, Atmospheric Dynamics Observed During the Energy Budget Campaign, *J. Atmos. Terr. Phys.*, 47, pp 233-241.
7. Forbes, J.M., 1982, Atmospheric Tides, 2. The Solar and Lunar Semidiurnal Components, *J. Geophys. Res.*, 87, pp 5241-5252.
8. Verniani, F., G. Cevolani, G. Grassi and F. Pedrini, 1980, Systematic Measurement of Northern Hemisphere Winds in the Meteor Region of 45 of Latitude, *J. Atmos. Terr. Phys.*, 42, pp 83-95.

MAIN RESULTS OF ATMOSPHERIC FINE STRUCTURE PARAMETER
OBSERVATION IN THE LOWER THERMOSPHERE

V. V. Sidorov, A. N. Fakhrutdinova, and V. A. Ganin

Kazan State University
Kazan, USSR

The capabilities of the radiometeor method of wind measurement increase with the increase of the transmitted power of radar stations fitted with goniometric systems which enables the observation of shower meteors along with sporadic background. In shower observations the meteor zone reflecting area narrows to the echo surface which is perpendicular to the flux radiant. Favorable conditions are created for singling out atmospheric disturbances in which the wave front is parallel to the echo surface which plays, in this case, the role of a frequency filter. For the first time ever this technique as, developed by TEPTIN and FAKRUTDINOVA, (1975) allowed wave disturbances with periods of ≥ 4 minutes to be measured, with about a 99% probability of exceeding the level of the turbulence noise, during the Geminid (1981,1983) and Perseid (1978,1984) showers. Maximum values of such wave disturbance amplitudes were about 15-20 m/s, with lifetimes up to 2 hours.

Long sequences of radiometer observations carried out in Kazan in 1978-1980 have made it possible to study wave disturbances in the time scale interval $T = (1-6)$ h. Analysis of the spectral density of the zonal and meridional component disturbances in the (N,S) and (E,W) observation areas averaged over the period from August 30 to September 9, 1978, for four time intervals during the day, showed a disturbance intensity increase in the second half of the day, especially in the period from 12:00 to 18:00 o'clock.

Fig. 1 presents spectral density curves for the winter period of observation (on January 19, 1979). The horizontal line shows the level of turbulent noise with the probability of about 99%. There are significant differences in the disturbance spectra of zonal and meridional circulation as well as in those of each component, the observation regions being spaced about 400 km from each other in the case of meteor zone sounding in the (N,S) and (E,W) directions.

The dependence of the disturbance intensity behavior on time of day and season has been investigated using the observational data of 1980. It was found that for the zonal and meridional components of wind velocity significant peaks in the spectral density curves are observed in all seasons. Diurnally, the disturbance intensity increase is observed in the second half of the day. Seasonally, there is a tendency for disturbance intensity to increase from January to June. Disturbances with time scales $T < 3$ h make deep mesometeorological minimum in the movements spectrum observed in the lower troposphere about one hour less pronounced in the lower thermosphere. This confirms our earlier (1969) observation results (SIDOROV and FAKHRUTDINOVA, 1981). Wave disturbances modulation is noted in the interval (period) of IGW disturbances on a meteorological scale.

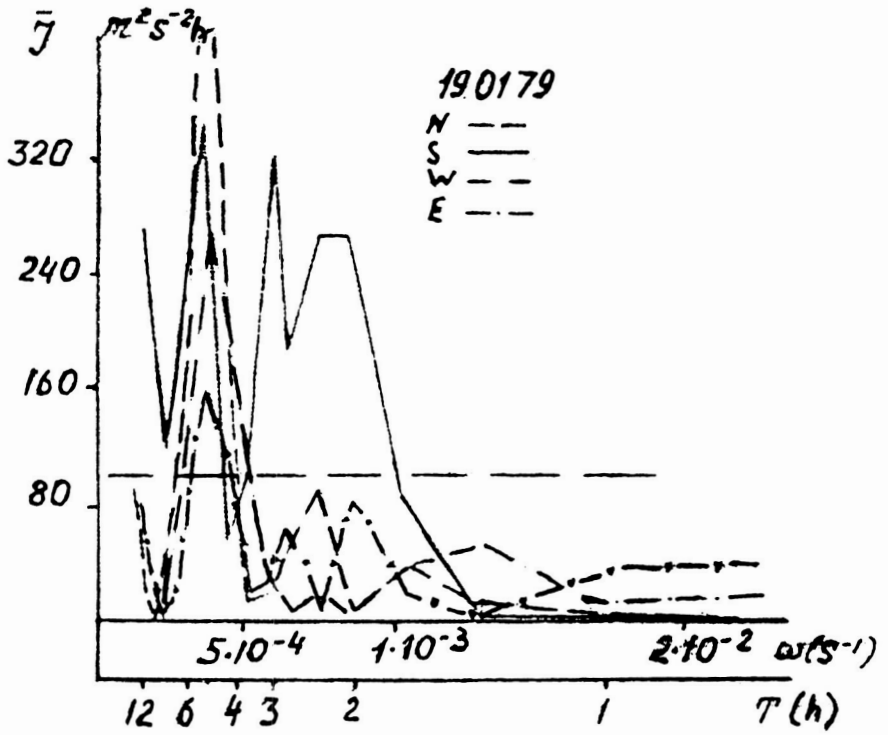


Fig. 1 Spectral density of prevailing wind disturbances for four areas of the meteor zone.

IGW singling out was done during observation periods using altimeter in summer (August, 1983) and winter (December, 1983). The spectral density change with height in the scale interval of 0.5-4 hours according to observations on August 11, 1983, (from 00.00 to 04 hours 30 minutes) is shown in Fig. 2. Disturbances with periods $T = 0.5, \sim 1$ h are given. Their intensity increase with height is well marked. The phase change with altitude is quasi-linear. The parameters of the singled out wave disturbances are as follows:

August 11, 1983.

$T \approx 0.5$ h, $\lambda_z \approx 11$ km, $\lambda_h \approx 150$ km, $V_z \approx 5$ mps, $V_h \approx 85$ mps
 $T \approx 1$ h, $\lambda_z \approx 12$ km, $\lambda_h \approx 360$ km, $V_z \approx 3$ mps, $V_h \approx 100$ mps

December 13, 1983.

$T \approx 1$ h, $\lambda_z \approx 9$ km, $\lambda_h \approx 360$ km, $V_z \approx 3$ mps, $V_h \approx 100$ mps

December 28, 1983.

$T \approx 3$ h, $\lambda_z \approx 27$ km, $\lambda_h \approx 450$ km, $V_z \approx 3$ mps, $V_h \approx 42$ mps

As a result, the disturbance intensity decrease has been found in the 90-94 km layer for $T = 1$ h (as revealed by observations on August 11, 1983) and in the 94-97 km layer for $T = 3$ h (from observations on December 28, 1983). This disturbance intensity behavior is presumably connected with wave energy absorption at the indicated altitudes.

Altitude profiles of the zonal and meridional prevailing wind components have been measured in both summer and winter periods. The zonal component data are presented in Fig. 3. The profiles show a considerable altitude wind inconstancy up to the wind reversal. It is significant that in the meteor zone there are layers moving in opposite directions stretching horizontally within the range of the measuring aerial polar diagram. Altitude gradient values reach 0.05 s^{-1} , increase with height and decrease with time from 0 to 4 o'clock in the morning.

The altitude profiles of ambipolar diffusion coefficient for summer and winter differ. This can be related to seasonal temperature changes. The change of the ambipolar diffusion coefficient with altitude from summer to winter is in keeping with a scale H height increase of the homogeneous atmosphere from 5.13 km up to 7 km. These changes of H can be accounted for by a possible temperature increase in winter in the lower thermosphere.

References

1. Sidorov, V.V., Fakhrutdinova, A.N., 1981, Quasi-two day periodicity of wind velocity measurements at meteor heights, Meteor Research, Radio in Svyaz Publishers, Moscow, No. 7, pp. 74-82.

2. Teptin, G.M., Fakhrutdinova, A.N., 1975, Determination methods and results of motion energy spectral density measurements in the upper atmosphere for the time interval of 5 minutes to 12 hours, in Radiowaves Meteor Propagation, Kazan, the Kazan State University Publishers, Nos. 10-11, pp. 42-48.

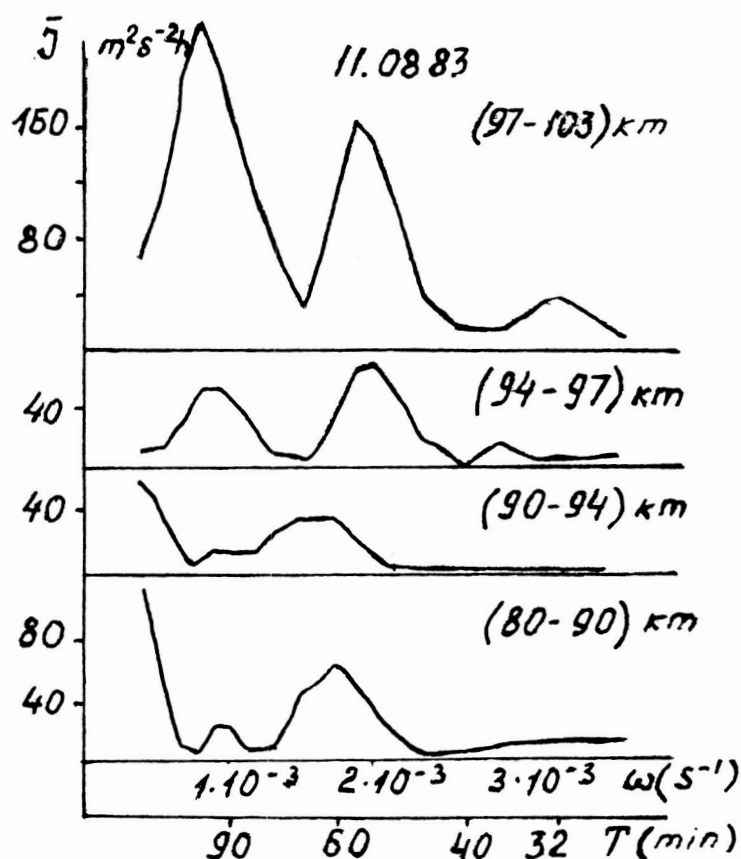


Fig. 2 Spectral density altitude variations.

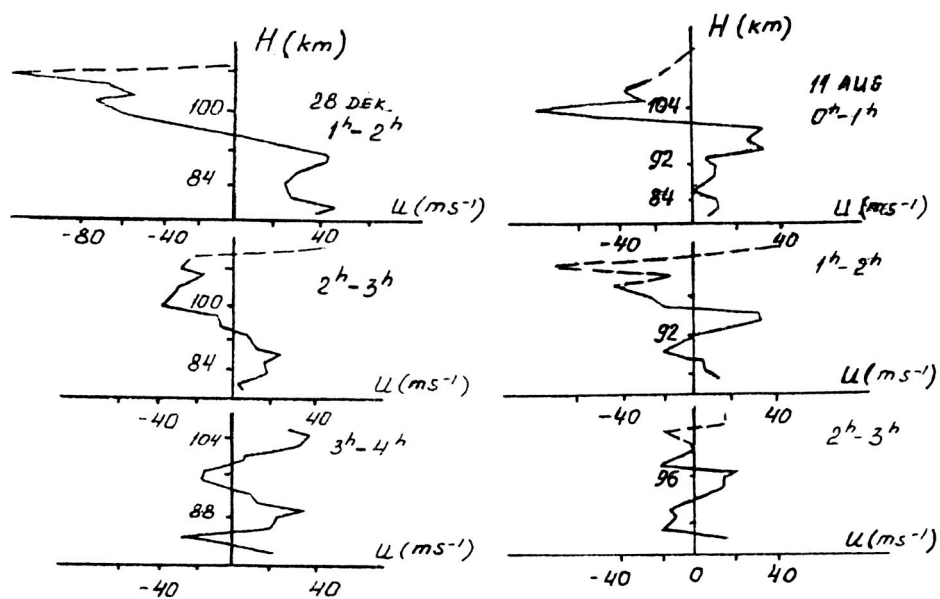


Fig. 3 Prevailing wind zonal component altitude variations in summer and winter.

ON CONNECTION BETWEEN EVOLUTION OF TROPOSPHERE FRONTS
AND CHANGES OF CIRCULATION REGIME IN METEOR ZONE

K. A. Karimov

Institute of Physics
Frunze, USSR

This report considers the interactions between the thermobaric fields at heights from 5 to 95 km at the beginning of a winter period, based on experimental radar measurements of meteor drifts obtained in Frunze in November-December, 1983. During this period the high atmosphere readily responds to even slight changes in the thermal regime of the stratosphere. The interdiurnal variations of average daily values of wind u , v , U , and azimuth ϕ are shown in Fig. 1.

Of particular interest here is the following - three of four days after a wind reversal from west to east in the meteor zone a powerful cold north-west intrusion took place in troposphere. The period considered witnessed five such intrusions, with a reversal of wind direction occurring in four cases. For example, intensive cold intrusions with transfer of arctic air were observed in the troposphere on November 18 and 26 and December 4. The main frontal division over Kirghizia at the time shifted from west to east. The temperature in the frontal division fell from $+15^{\circ}\text{C}$ to -3°C . The analysis of these tropospheric fronts were carried out using ground level weather maps for 3 to 4 days before their intrusion. The synoptic situation for all the three periods was similar: a cyclone existed over Europe, and an anticyclone over Middle Asia and Kazakhstan. The front was directed from north to south and stretched from the southern Urals to the south of Middle Asia and Turkmenistan.

The velocity of intrusion of these fronts was 55-60 km per hour and they advanced at a speed of 1,300 km a day. The ground weather maps for November 14 and 23, 1983, are given in Fig. 2. The maps of the 500 mb surface placed the frontal division practically parallel to that of the ground level weather maps. There was a hardly discernible trough above middle Volga and a ridge above northern Kazakhstan.

Most interesting here is the analysis of the pressure maps of the stratosphere at the 10 mb level for this period. The maps for November 14 and 23 are presented in Fig. 2. The stratospheric South-Asian anticyclone with its northern boundary reaching to $48-50^{\circ}\text{N}$ developed in the middle latitudes on November 14-15 and 22-23. Similar intrusion of subtropical anticyclone created a contrast in the temperature field of the cyclone with thermal overfall in the frontal zone ranging from $-(61 \text{ to } 63)^{\circ}\text{C}$ to -48°C .

The frontal division in the stratospheric temperature field occupied the area from Sverdlovsk to the south-west and further to the Caspian Sea parallel to the frontal division in the troposphere. It led to the formation of a high frontal zone in the upper atmosphere in the same direction. The intensification of stratospheric anticyclones gives rise to local warmings near the stratopause and to intensification of planetary

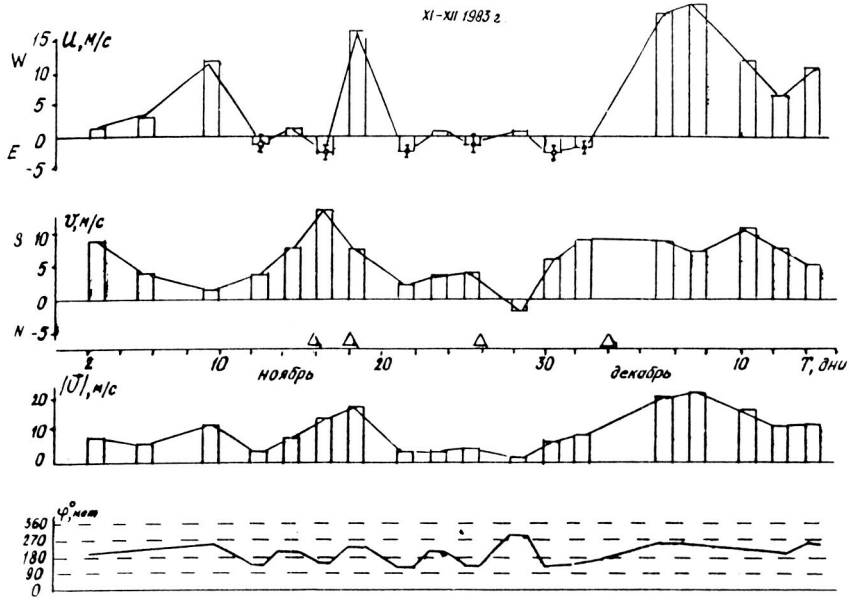


Fig. 1 Variation of zonal u , meridional v , and vector $|U|$, ϕ wind at 95 km over Frunze from November 2 to December 18, 1983.

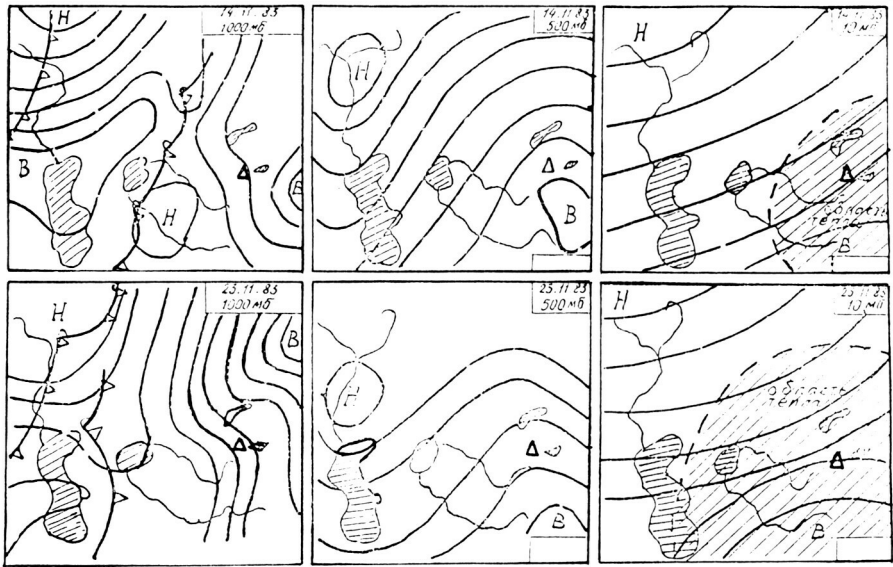


Fig. 2 1000, 500 and 10 mb maps over Central Asia (Frunze Δ) for November 14 and 23, 1983.

waves spreading from the troposphere to higher layers. The amplitudes of the planetary waves intensify owing to the blocking of western streams by anticyclones.

The waves spread upwards and upon reaching meteor heights cause reversal of the wind at 93 km above Middle Asia. The blocking processes in the tropospheric zonal wind stream during periods of local warming and the inverse reaction of higher layers produce intensification of frontal activity at ground level. Two and a half or three days after the anomalous wind reversal at the height of 93 km the troposphere over Kirghizia underwent a powerful intrusion from the north-west.

It is clear that the development in the stratosphere of the South Asian anticyclone leads to displacement of warm area to higher latitudes, from the center of the anticyclone to the north, bringing about a thermal reconstruction of the wind field at greater heights and even a reversal of wind direction at the height of 93 km.

The ridge that forms in the troposphere blocks the main western stream, a trough naturally appearing ahead of it. The frontal part of the trough serves as the frontal division and its projection on the ground forms the frontal line. The above front moved at a speed of 700-900 km a day and it took it 2.5-3 days to reach Kirghizia. These results would indicate, at least for the northern latitudes from which our observations were made, that the passage of a front at ground level is often preceded, by some 2.5 to 3 days, by a wind reversal at 93 kilometers.

A STUDY OF THE MECHANISM OF INTERNAL GRAVITY WAVE GENERATION BY QUASIGEOSTROPHIC METEOROLOGICAL MOTIONS

A. S. Medvedev

Leningrad State University
Leningrad-Petrodvorets, USSR

Numerous experiments on the detection of atmospheric waves in the frequency range from acoustic to planetary at meteor heights have revealed that important wave sources are meteorological processes in the troposphere (cyclones, atmospheric fronts, jet streams, etc.). A dynamical theory based on the works of OBUKHOV (1949) and MONIN (1958) include describing the adaptation of meteorological fields to the geostrophic equilibrium state. According to this theory, wave motions appear as a result of constant competition between the maladjustment of the wind and pressure fields due to non-linear effects and the tendency of the atmosphere to establish a quasi-geostrophic equilibrium of these fields.

Barotropic Atmospheric Model

To demonstrate the above, we consider an approximation of the atmosphere to be a two-dimensional liquid film located in the Coriolis force field. The equations for this model are obtained by averaging over height the equations of motion and continuity for a three-dimensional atmosphere (OBUKHOV, 1949). Then, passing over to dimensionless variables, we choose values corresponding to large-scale synoptic motions (OBUKHOV, 1949) by way of the scales of length L and velocity W . The natural scale $(2\omega_z)^{-1}$ corresponding to OBUKHOV's (1949) characteristic adaptation time will serve as the temporal scale. In the dimensionless variables we have equations:

$$\frac{\partial U}{\partial \tau} + R_0 \left(U \frac{\partial U}{\partial \zeta} + V \frac{\partial U}{\partial \eta} \right) - V = - \frac{\partial \Pi}{\partial \zeta} ; \quad \frac{\partial V}{\partial \tau} + R_0 \left(U \frac{\partial V}{\partial \zeta} + V \frac{\partial V}{\partial \eta} \right) + U = - \frac{\partial \Pi}{\partial \eta} ;$$

$$\frac{\partial U}{\partial \tau} + R_0 \left(U \frac{\partial \Pi}{\partial \zeta} + V \frac{\partial \Pi}{\partial \eta} \right) + \frac{D}{\beta^2} = 0 ; \quad D = \frac{\partial V}{\partial \zeta} + \frac{\partial V}{\partial \eta} , \quad (1)$$

where $2\omega_z$ is a Coriolis parameter; U, V are the wind velocity components; $\zeta = x/L$; $\eta = y/L$; $U = u/W$; $V = v/W$; $\Pi = c^2 x/2\omega_z WL$;

$$\tau = 2\omega_z t ; \quad x = \ln(p/p_0);$$

p is pressure, p_0 is a standard pressure near the earth. The dimensionless parameters of Rossby-Kibel $R_0 = W/2\omega_z L$ and $\beta = 2\omega_z L/c$ have been introduced into (1). To analyze the system (1), we use a small Rossby number for motions of the synoptic scale and apply the method of asymptotic series and multiple time scale successive approximations (BLUMEN, 1972; JEFFREY and KAWAHARA, 1982), according to which we introduce, apart from the "fast" dimensionless time $\tau = 2\omega_z t$, the "slow" dimensionless time $T = R_0 \tau = tw/L$ and change

$$\partial/\partial\tau \rightarrow \partial/\partial\tau + Ro \partial/\partial T$$

The zero-order system in Ro

$$\frac{\partial U_0}{\partial\tau} - V_0 = \frac{\partial \Pi_0}{\partial\zeta}; \quad \frac{\partial V_0}{\partial\tau} + U_0 = -\frac{\partial \Pi_0}{\partial\eta}; \quad \frac{\partial \Pi_0}{\partial\tau} + \frac{D_0}{2} = 0; \quad D_0 = \frac{\partial U_0}{\partial\zeta} + \frac{\partial V_0}{\partial\eta} \quad (2)$$

was investigated by OBUKHOV (1949). OBUKHOV showed that a complete solution of the nonlinear system (2) is the superposition of the non stationary waves and the stationary geostrophic components.

In the first-order approximation in Ro the system (1) takes the form:

$$\begin{aligned} \frac{\partial U_1}{\partial\tau} + \frac{\partial \Pi_1}{\partial u} - V_1 = & -\frac{\partial V_0}{\partial\tau} - U_0 \frac{\partial V_0}{\partial u} - V_0 \frac{\partial V_0}{\partial\eta}; \quad \frac{\partial V_1}{\partial\tau} + \frac{\partial \Pi_1}{\partial\eta} + U_1 = & -\frac{\partial V_0}{\partial T} - U_0 \frac{\partial V_0}{\partial u} - V_0 \frac{\partial V_0}{\partial u}; \\ \frac{\partial \Pi_1}{\partial\tau} + \frac{D_1}{\beta^2} - V_1 = & -\frac{\partial \Pi_0}{\partial T} - U_0 \frac{\partial \Pi_0}{\partial u} - V_0 \frac{\partial \Pi_0}{\partial\eta}; \quad D_1 = \frac{\partial U_1}{\partial u} + \frac{\partial V_1}{\partial\eta}. \end{aligned} \quad (3)$$

In the analysis of wave generation within the flux under the influence of nonlinear terms we consider the atmosphere in a quasi-adjusted state when the process of adaptation either has been completed and the wave component has already been scattered in space or the wave motion has not occurred at all due to the initial adjustment of the meteorological fields. Therefore, in what follows, we shall consider the zero-order terms in (3) to be purely geostrophic and independent of the "fast" time τ . Proceeding in the usual way we obtain from (3) equations for the vorticity

$$\Omega_1 = \partial V_1 / \partial\zeta - \partial U_1 / \partial\eta$$

and divergence D_1

$$\partial D_1 / \partial + \Delta \Pi_1 - \Omega_1 = -q_0; \quad \partial \Omega_1 / \partial + D_1 = -\partial \Omega_1 / \partial T - S_0; \quad \Delta = \partial^2 / \partial\zeta^2 + \partial^2 / \partial\eta^2;$$

$$q_0 = \frac{\partial U_0}{\partial\zeta}^2 + 2 \frac{\partial U_0}{\partial\eta} \frac{\partial V_0}{\partial\eta} + \frac{\partial V_0}{\partial\eta}^2; \quad S_0 = (\vec{v}_0 \nabla \omega_0) = U_0 \frac{\partial \Omega_0}{\partial\zeta} + V_0 \frac{\partial \Omega_0}{\partial\eta} \quad (4)$$

By excluding D_1 from the third equation of (3) and the second equation of (4), we obtain

$$\frac{\partial}{\partial\tau} (\Omega_1 - \beta^2 \Pi_1) = -\frac{\partial \Pi_0}{\partial T} + \frac{1}{\beta^2} \frac{\partial \Omega_0}{\partial T} + \frac{1}{\beta^2} (\vec{v}_0 \nabla \Omega_0) \quad (5)$$

In the right-hand side of (5) there is a function T , in the left-hand one there are functions τ and T . Therefore, to eliminate divergence in (5), according to the requirements of the method of multiple time scales, we assume that the right- and left-hand sides of (5) separately equal zero. By equating to zero the right-hand side of (5) we obtain the equation of slow quasi-geostrophic evolution of a potential vortex (BLUMEN, 1972). Then, from the condition of the left-hand side of (5) being zero, we obtain $\Omega_1 - \beta^2 \Pi_1 = 0$. Thus, the first order terms in R_0 in the expansion (5) are purely wave terms. Making use of the condition $\Omega_1 - \beta^2 \Pi_1 = 0$, it is possible to derive wave equations with a nonlinear forcing term on the right-hand side. For instance, the equation for Ω_1 has the form:

$$\frac{\partial^2 \Omega_1}{\partial \tau^2} - \frac{\Delta \Omega_1}{\beta^2} + \Omega_1 = q_0 \quad (6)$$

The expression on the right-hand side of (6) describes the rate of wave generation by the background quasi-geostrophic motions. This process exists owing to the nonlinear transfer of energy between motions of different types: slow quasi-geostrophic and fast waves.

Influence Functions of Tropospheric Meteorological Sources

We can obtain an equation for the spectral density of the vertical velocity W (GAVRILOV, 1985) for an isothermal three-dimensional atmosphere:

$$\begin{aligned} \frac{d^2 W}{d\zeta^2} + n^2 W &= F_w(\zeta, \omega, k_x, k_y); \quad \zeta^2 = \zeta/H; \quad k^2 = k_x^2 + k_y^2; \\ n^2 &= (N^2 - \omega^2)/(\omega^2 - \ell^2) k^2 H^2 + \omega^2 H^2 / C_s^2 - 1/4; \\ F_w &= \frac{iH^2}{\omega^2 - \ell^2} \left(\frac{1}{H} \frac{d}{d\zeta} - \frac{N^2}{g} \right) (\omega/Q - i\ell S) \exp(-\zeta/2); \quad (7) \end{aligned}$$

where N is the Brunt frequency; W , Q , and S are the Fourier transforms of the vertical components of wave velocity W and the source terms (4) q and s , respectively; ω , k_x , k_y are the frequency and horizontal projections of the wave vector, respectively. Analysis of (7) shows that the contribution of the source Q increases in the region of high frequencies. For the acoustic frequencies $\omega \gg 2\omega_z$ the main contribution to the generation of acoustic waves is made by Q , the expression for which coincides with that for the source of the sound generation by turbulence obtained by Lighthill (1952). For the low frequency IGW the contribution of the addendum containing s is essential whereas the values of Q and S are smaller and of the same order.

Using the condition of radiation $W \sim \exp(i\eta u)$ at $u \rightarrow \infty$ and being interested in a solution for large heights only, one can find the solution of (7) by the method proposed in KAMKE, (1976) and GAVRILOV (1985):

$$W = -e^{i\eta\zeta} I; \quad I = \int_0^{\zeta} \frac{\sin n\nu}{n} F_W(\nu) d\nu \quad (8)$$

Here the wave field of the vertical velocity W is the Fourier integral:

$$w = e^{\frac{\zeta}{2}} \iiint_{-\infty}^{\infty} \exp[i(\omega t - k_x x - k_y y + n\zeta)] \int_0^{\zeta} \frac{\sin n\nu}{n} F_W(\nu) d\nu d\omega dk_x dk_y \quad (9)$$

In (9) we proceed from integration over spectral variables Ω , k_x , k_y to integration over the natural variables t , x , y . With this in view, we use the theorem of the Fourier-transform of the convolution of functions and find the influence functions of the sources q and S :

$$G_i(\nu, \zeta, x, y, t) = \iiint_{-\infty}^{\infty} \frac{\sin n\nu}{n} \exp[i(\omega t - k_x x - k_y y + n\zeta)].$$

$$\frac{iH^2}{\omega^2 - 4\omega_u^2} \phi_i(\omega, \ell) d\omega dk_x dk_y; \quad \phi_1 = \omega; \quad \phi_2 = -i\ell \quad (10)$$

The expressions for W through G_1 and G_2 have the form:

$$\begin{aligned} -W(x, y, t, \zeta) e^{-\zeta/2} &= \int_0^u G_1 \theta \left(\frac{1}{H} \frac{d}{d\nu} \frac{N^2}{g} \right) q(\nu) e^{-\nu/2} d\nu + \\ &+ \int_0^{\zeta} G_1 \theta \left(\frac{1}{H} \frac{d}{d\nu} \frac{N^2}{g} \right) s(\nu) e^{-\nu/2} d\nu \end{aligned} \quad (11)$$

where the symbol θ denotes the convolution of functions in the variables x , y , t . It can be seen from (11) that the wave amplitudes increase exponentially with height. Therefore, of interest is the behavior of G_1 and G_2 at $u \rightarrow \infty$. To calculate the integral

$$= \iint_{-\infty}^{\infty} \frac{\sin n\nu}{n} \exp[i(n\zeta - k_x x - k_y y)] dk_x dk_y, \quad (12)$$

contained in (10) we use an asymptotic expansion by the stationary phase method (FELSEN and MARCUVITZ, 1973) at $\zeta \rightarrow \infty$. We obtain, for example, for G_1

$$G_1 = - \frac{(2\pi)^{3/2} H}{\sqrt{3Nt} R} (1 - \mu)^{2/3 - 1/4} \sin(\nu \frac{\zeta H}{2R} \frac{\mu^{2/3}}{1 - \mu^{2/3}}) \cos[Nt(1 - \mu^{2/3})^{3/2} - \frac{\pi}{4}]$$

$$- \frac{(2\pi)^{3/2} H c^*/R}{NR \sqrt{t}} (1 - \mu^2)^{-3/4} \sin(\nu \frac{\zeta H}{2R} \frac{N(1 - \mu^2)^{1/2}}{c^* \mu} R) \cos[c^* t/R \cdot (1 - \mu^2)^{1/2} + \frac{\pi}{4}]$$
(13)

where $\mu = R/(2HN)$; $R = \sqrt{x^2 + y^2}$; $C^* = 4R^2 \omega_z^2 + N_{\zeta}^2 H^2$.

The expression for G_2 is derived in a similar way but is omitted here because of its bulkiness. The first addendum in (13) describes the high frequency mode of IGW with the frequencies $\omega \sim N$, and the second addendum is the lower frequency waves with periods of the order of hours.

The described procedure of obtaining the Green's function was used in the calculation of the wave field of the vertical velocity W for a typical meteorological formation, such as the cyclonic vortex. The mathematical model of the latter is given by the expression

$$p = p_0 - \delta p \cdot \exp(-t^2/\tau_0^2 - x^2/a^2 - y^2/b^2);$$
(14)

where the cyclonic pit depth p changes with height

$$p(u) = p_n \exp[-(z - z_s)^2/h^2]$$

In (14) p_0 is the standard pressure at a given height; a , b are the scales of the vortex length along the corresponding axes, τ_0 is the vortex characteristic lifetime; z_s is the vortex maximum height; h is the vertical halfwidth of the source. In the calculations the values which correspond to mesoscale synoptical vortices of the moderate type were used: $a = 50$ km, $b = 100$ km, $h = 2$ km, $\delta p_m = 20$ m bar, $z_s = 8$ km, $\tau_0 = 3$ hrs. Fig. 1 shows the directional pattern of radiation in the p_0 plane x , y for the vertical velocity W . It can be seen that the maximum radiation intensity takes place along the semimajor axis of the vortex. The ratio of the radiation intensities along the main semiaxes increases in proportion to the square of the a/b ratio. Fig. 2 shows a horizontal cross-section along the x axis of the wave field of the vertical velocity W . It can be seen that the vertical velocity values reach tens of cm s^{-1} , and the decrease of the amplitude is due to the source attenuation with time. The temporal variation of W at the point $x = 1,500$ km, $y = 0.3$, $H = 100$ km is presented in Fig. 3. It can be seen that oscillations at a given point occur with a period $T \sim 80$ min and are modulated by a wave with the period $T \sim 16$ hrs.

References

Blumen W., 1972, Geostrophic adjustment, Rev. Geophys. Space Phys., 10, 485-528.

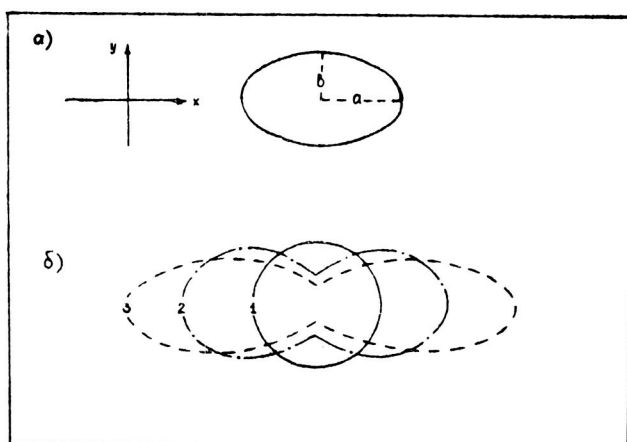


Fig. 1 Radiation orientation direction diagram (δ) by a vortex (α): 1 - for $a/b = 1$; 2 - for $a/b = 2$; 3 - for $a/b = 3$.

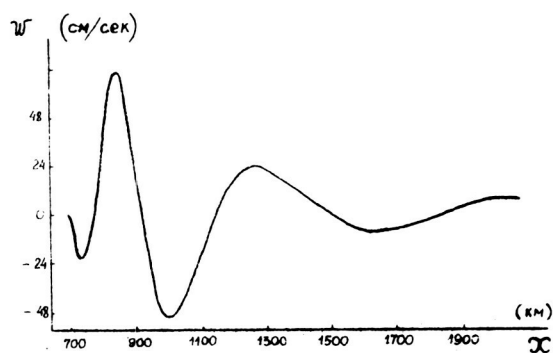


Fig. 2 A horizontal cross-section of vertical velocity wind field ω_w caused by a mesoscale vortex.

Felsen L.B., and Marcuwitu J., 1973, Radiation and Scattering of Waves, New Jersey, p. 576.

Gavrilov N.M., 1985, On the Mechanism of Meteorological Sources of Wave Motions in a Baroclinic Atmosphere, Iuvestiya Sov. Acad. Sci., in press.

Gossard E.E., Hooke W.H., 1975, Waves in the Atmosphere, Elsevier, Amsterdam.

Lighthill M.J., 1952, On Sound Generated Aerodynamically, I. General Theory, Proc. Roy. Soc., London, A211, No. 1107, 564-587.

Monin A.S., 1958, Pressure Variation in a Baroclinic Atmosphere, Iuvestiya Sov. Acad. Sci., Ser. Geophys., No. 4, 495-513.

Obukhov A.M., 1949, On the Geostrophic Wind, Iuvestiya Sov. Acad. Sci. ser. Geograph. Geophys., V. 13, No. 4, 281-306.

STUDY OF INTERNAL GRAVITY WAVES IN THE METEOR ZONE

N. M. Gavrilov

Leningrad State University
Leningrad-Petrodvorets, USSR

An important component of the dynamical regime of the atmosphere at heights near 100 km are internal gravity waves (IGW) with periods from about 5 min to about 17.5 hrs. which propagate from the lower atmospheric layers and are generated in the uppermost region of the atmosphere. As IGW propagate upwards, their amplitudes increase and they have a considerable effect on upper atmospheric processes: 1) they provide heat flux divergences comparable with solar heating (SHVED, 1977; GAVRILOV and SHVED, 1975, 1982; CHUNCHUZOV, 1978, 1982); 2) they influence the gaseous composition (GAVRILOV and POGORELTSEV, 1980) and produce wave variations of the concentrations of gaseous components and emissions of the upper atmosphere (KRASSOVSKI, 1972; WEINSTOCK, 1978; GAVRILOV and SHVED, 1982; GAVRILOV and YUDIN, 1982); and 3) they cause considerable acceleration of the mean stream (CHUNCHUZOV, 1971; GAVRILOV, 1976; GAVRILOV and SHVED, 1982), etc.

Considerable progress in IGW studies has been achieved in recent years in connection with the MAP and GLOBMET research programs. Interest in IGW studies has increased notably. This can be traced to the mathematical experiments on numerical modelling of the middle atmospheric circulation at 10-150 km altitude started in the 1980's. These experiments have revealed that the drag created by molecular and turbulent viscosity is insufficient for the formation of the meridional circulation observed, and therefore an additional source of acceleration must exist. It is proposed that IGW serve as such a source (HOLTON, 1982, 1983; MIYAHARA, 1984).

The considerable effect of IGW on middle atmospheric circulation has stimulated interest in IGW studies. At present IGW in the upper atmosphere are investigated by all the methods available, both new (MST radars; BALSLEY, 1983; BALSLEY et al., 1983; the use of surface industrial explosions; GOKHBERG, 1983) and traditional (rocket soundings, HIROTA, 1984; observations of variations in nocturnal airglows characteristics, KRASSOVSKI et al., 1978; MOLINA, 1983; SHEFOV et al., 1983; methods of incoherent scattering and partial reflections, VINCENT, 1984; radar location of meteor traces, etc.). These investigations have yielded ample information about IGW near the mesopause. Taking into consideration the specific subject of this Conference, we shall dwell on the results obtained making use of the radiometeor method.

IGW studies by the radiometeor method were started in France (SPIZZICHINO, 1969, 1972) and later continued in other countries. In the USSR this kind of research was started jointly by the scientists of Leningrad State University and groups of researchers in Kharkov and Frunze (GAVRILOV and DELOV, 1976; GAVRILOV et al., 1976). These groups continued their research (KARIMOV and LUKYANOV, 1979, KALCHENKO et al., 1985). Later similar investigations were carried out in Obninsk and Kazan (KAZANIKOV and PORTNYAGIN, 1981a, b; SIDOROV et al., 1983). The investigations differ in

the instrumentation and methods of statistical identification of IGW. Table 1 presents the IGW parameters measured by different scientists and the IGW characteristics calculated from the parameters measured. In early works (SPIZZICHINO, 1969; GAVRILOV and DELOV, 1976; GAVRILOV et al., 1976; KARIMOV and LUKYANOV, 1979) individual values of wind velocities for single meteors were averaged over the entire horizontal area of the meteor zone observed by the radar. Therefore, only the amplitude V , period τ_w and vertical wavelengths λ_z were measured in cases when the determination of echo height made it possible to divide the meteor zone into a number of layers according to height. KAZANIKOV and PORTNYAGIN (1981a, b) measured the wind simultaneously in four mutually perpendicular directions. The use of coherent analysis for spatially remote regions made it possible to determine the horizontal wavelengths, velocities and directions of propagation of IGW with large horizontal wavelengths $\lambda_h \gtrsim 700$ km.

In recent papers (KALCHENKO et al., 1985; GAVRILOV and KALOV, 1985) an algorithm for singling out IGW from radiometeor data has been used which was developed earlier by GAVRILOV (1981, 1984a). The algorithm is based on dividing the area observed by the radar into a number of subareas in the direction of the beam of vision of the antenna. Statistical analysis of the velocity spectra obtained for these areas makes it possible to discriminate IGW from the background noise and to determine the horizontal wavelengths λ_{11} of IGW along the axis of the antenna direction diagram. If the radar can measure echo height (KALCHENKO et al., 1985) it is possible to measure λ_z .

The radiometeor method is limited in the measurement of IGW parameters because of the necessity of average data over a large spatial area and the finite number of meteor echoes per time unit (GAVRILOV and DELOV, 1976; GAVRILOV, 1984a). As a rule, IGW with $\tau_w \gtrsim 0.5$ -1 h, $\lambda_{11} \gtrsim 100$ -200 km and $\lambda_z \gtrsim 5$ -30 km are accessible to measurement. In this connection, it is interesting to note an original method proposed by SIDOROV et al., 1983, for measuring IGW during meteor showers when a great number of meteor radioechoes located practically on the same plane makes it possible to measure IGW with periods of several minutes.

IGW in the meteor zone have small but markedly variable λ_z . Therefore, when measured at stations which do not measure echo height, they yield only rough, considerably smoothed estimates. The advent of automated height measuring radars with a large number of useable radioechoes and appropriate vertical resolution (KALCHENKO et al., 1985) has made it possible to measure the IGW vertical wavelengths and to improve the accuracy of the determination of wave characteristics. The results presented in the paper by KALCHENKO et al., (1985) appear to be, for the present, the most comprehensive and accurate estimates of the IGW parameters from radiometeor data; they are given in Table 2 and are in good agreement with the results of previous radiometeor measurements and data obtained using other methods.

It can be concluded that the periods, wavelengths, amplitudes and velocities of IGW propagation in the meteor zone are now measured quite reliably. However, for estimating the influence of IGW on the thermal regime and the circulation of the upper atmosphere these parameters are not as important as the values of wave fluxes of energy, heat, moment and mass.

Table 1

IGW parameters measured and calculated from radiometeor data.

Authors	Measured IGW Parameters	Calculated IGW Parameters
Spizzichino, 1969, 1972	$V, \lambda_z, \tau \gtrsim 1h$	F_z
Gavrilov and Delov, 1976	$V, \lambda_z, \tau \gtrsim 1h$	F_z
Karimov and Lukyanov, 1979	$V, \tau \gtrsim 1h$	
Kazanikov and Portnyagin, 1981a,b	$\lambda_h \gtrsim 1000 \text{ km}$ $V, A, \tau \gtrsim 1h$	F_z, F_{xz}, F_{yz}
Sidorov et al., 1983	$V, 8 \text{ min} \lesssim \tau \lesssim 1h$	
Kalchenko et al., 1985	$V, \lambda_z, \lambda_{11} \lesssim 1000 \text{ km}$ $\tau \gtrsim 0.5 \text{ h}$	
Gavrilov and Kalov, 1985	$V, \lambda_{11} \lesssim 1000 \text{ km},$ $\tau \gtrsim 0.5 \text{ h}$	$F_z, F_x, F_y, F_{xz}, F_{xy},$ $F_{Tx}, F_{Ty}, F_{Tz},$ F_{mx}, F_{my}, F_{mz}

Note: V is the amplitude, τ is the period, λ_h and λ_z are the horizontal and vertical wavelengths, λ_{11} is the length along the antenna horizontal axis, A is the azimuth of IGW propagation, F_i, F_{ij}, F_{Ti} and F_{mi} are the components of the wave fluxes of energy, moment, heat and mass, respectively.

Table 2

Values of IGW characteristics from radiometeor measurements (KALCHENKO et al., 1985) and estimations (GAVRILOV and KALOV, 1985).

Parameter	Range of values	Parameter	Range of values
τ	0.5-6 hrs	F_{xz}	$1-4 \text{ m}^2 \text{s}^{-2}$
V	$6-20 \text{ m s}^{-1}$	F_{yz}	$1-10 \text{ m}^2 \text{s}^{-2}$
λ_{11}	100-800 km	F_{xy}	$2-20 \text{ m}^2 \text{s}^{-2}$
λ_z	10-30 km	F_{Tx}	$1-20 \text{ erg cm}^{-2} \text{s}^{-1}$
\tilde{C}	$20-160 \text{ m s}^{-1}$	F_{Ty}	$1-200 \text{ erg cm}^{-2} \text{s}^{-1}$
F_z	$1-6 \text{ erg cm}^{-2} \text{s}^{-1}$	F_{Tz}	$1-6 \text{ erg cm}^{-2} \text{s}^{-1}$
\tilde{F}_x	$1-20 \text{ erg cm}^{-2} \text{s}^{-1}$	F_{mx}	$2-10 \cdot 10^{-8} \text{ kg m}^{-2} \text{s}^{-1}$
\tilde{F}_y	$1-10 \text{ erg cm}^{-2} \text{s}^{-1}$	F_{my}	$1-4 \cdot 10^{-6} \text{ kg m}^{-2} \text{s}^{-1}$
		F_{mz}	$1-3 \cdot 10^{-8} \text{ kg m}^{-2} \text{s}^{-1}$

The difficulty here is that to calculate the above mentioned wave fluxes, which require knowledge of the wave variations of pressure, density, temperature and vertical velocity, while the radiometeor method makes it possible to measure only the horizontal wind velocity. In a paper by GAVRILOV (1984b) a method is proposed for calculating the wave fluxes of energy, heat, moment and mass from radiometeor data using IGW theory. The method has been applied in GAVRILOV and KALOV (1985) to statistically analyze the Obninsk radiometeor measurements. Although no echo height information is available from Obninsk, a great amount of observational material (about 9,000 IGW harmonics) and application of statistical modelling has made it possible to obtain sufficiently reliable estimates for the monthly mean values of wave fluxes which are presented in Table 2 and which provide the evidence of the important contribution of IGW to the energetics and dynamics of the upper atmosphere.

Study of the IGW vertical structure has revealed that from 60 to 80% of the IGW harmonics in the meteor zone propagate upwards (KALCHENKO et al., 1985; VINCENT, 1984). The IGW amplitudes increase with height (Fig. 1a), the increase being influenced by the superposition of oscillations due to partial reflection of the IGW energy (SPIZZICHINO, 1969, 1972; GAVRILOV and DELOV, 1976; KALCHENKO et al., 1985). An interesting feature is a zone of increase of IGW decay at heights about 92 km which has been discovered by KALCHENKO et al., (1985). A decrease in the IGW amplitudes and a disturbance of the linear phase variation with height can be systematically observed in this zone (Fig. 1).

When the seasonal variation of IGW parameters in the meteor zone is discussed, the existence of an annual cycle with the maximum amplitude in winter and minimum in summer is mostly generally accepted. However, recent research has revealed a more complicated situation. Fig. 2a presents the seasonal and latitudinal distribution of the IGW intensities at 20-70 km obtained by HIROTA (1984) from the analysis of meteorological rocket soundings. It can be seen that from 40°N northwards an annual harmonic with a maximum in winter is predominant in the seasonal variation of the IGW intensity. However, at low latitudes a semi-annual variation with maxima in spring and autumn prevails. This kind of pattern is confirmed by observations at heights about 100 km from radiometeor data (GAVRILOV and KALOV, 1985; KARIMOV and LUKYANOV, 1979) and from observations of wave variations of the night airglow emission of atomic oxygen $O \lambda 5577A$ (GAVRILOV and SHVED, 1982), as is shown in Fig. 3.

In the annual variation of the IGW amplitudes V in Obninsk at 56°N (Fig. 2b) the annual harmonic prevails, whereas at stations located in more southward areas (FRUNZE, 43°N and ASHKHABAD, 38°N) the semi-annual variation of V appears with maxima in spring and autumn. The reasons for seasonal variations in the IGW intensity are supposed to be the changes in the activity of wave sources in the lower atmospheric layers and also changes in the filtering properties of the middle atmosphere due to seasonal adjustments of the circulation in the strato-mesosphere.

Interesting results have been obtained from radiometeor investigations of the intra- and inter-diurnal variations of the IGW energy. Fig. 3c shows the results of the analysis of the IGW energy variations E_w with τ_w 1-6 hrs from the data of field expedition measurements of the Kharkov group

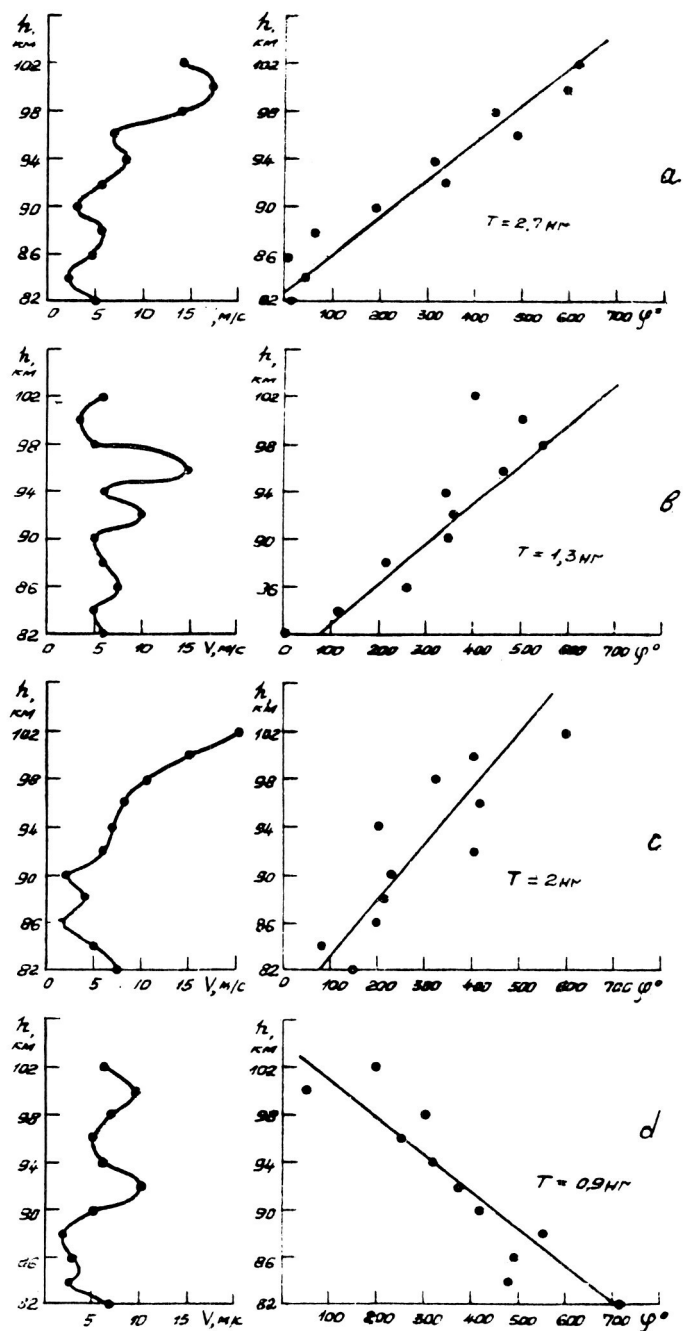


Fig. 1 Altitude variations of amplitudes (left) and phases (right) of period T IGW harmonics.

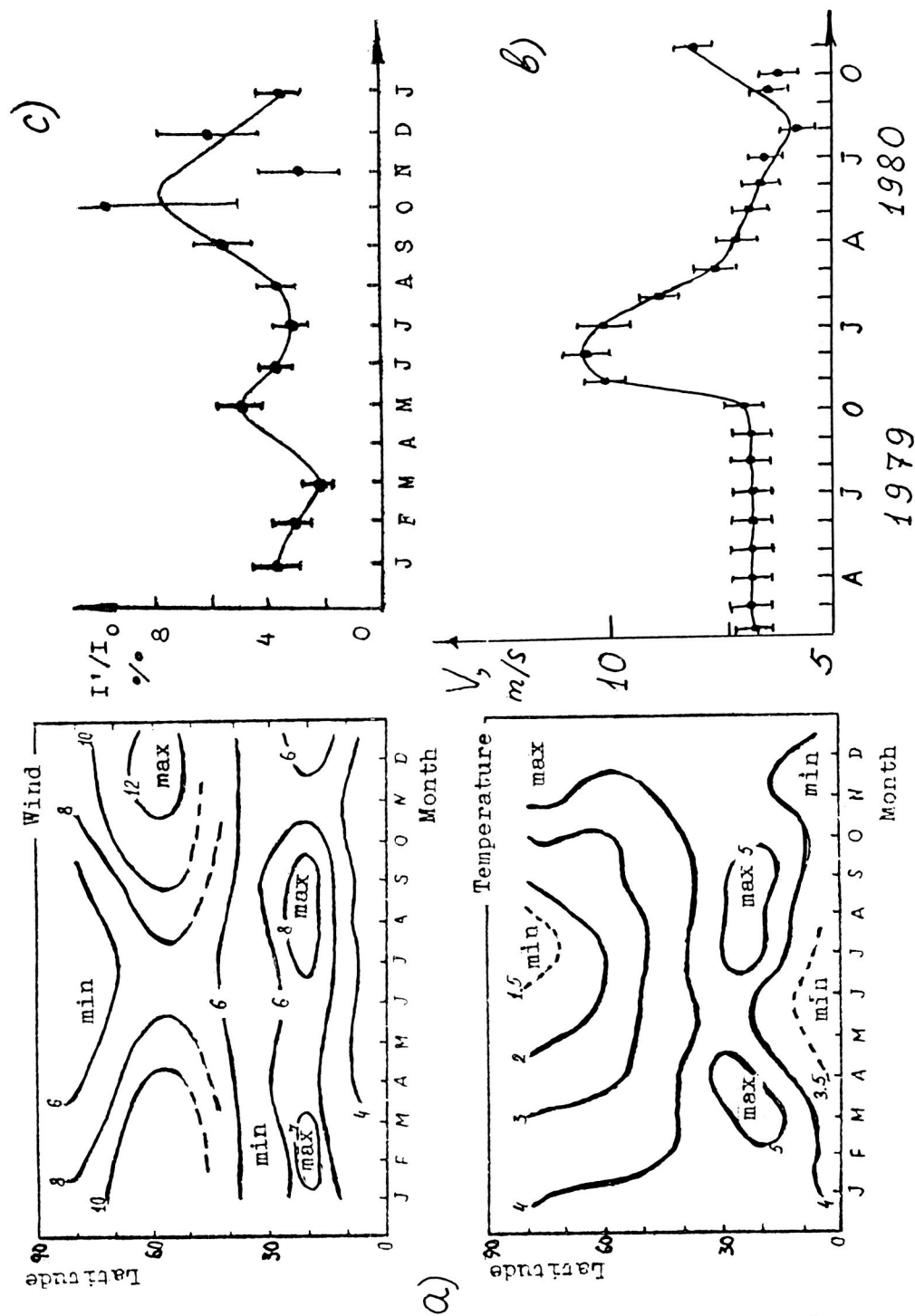


Fig. 2 Latitude and seasonal distributions of IGW amplitudes in the stratosphere (a) and seasonal variations of IGW amplitudes at 90-100 km over Obninsk (b) and Ashkhabad (c).

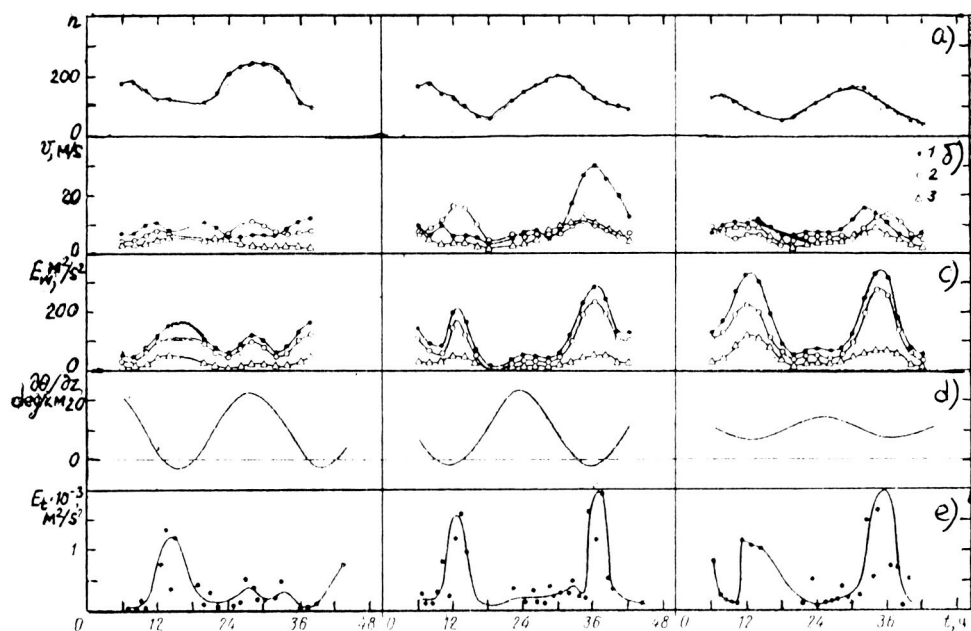


Fig. 3 Variations of meteor rates (a), IGW amplitudes (b), IGM intensity (c), potential temperature vertical gradient (d) and intensity of turbulence (e) at 85-90 km (left), 90-95 km (center), and 95-100 km (right) in the tropical meteor zone.

in the tropical zone on May 7-8, 1970 (GAVRILOV et al., 1981). The diurnal variations of E_w are quite obvious. Fig. 3d presents the calculated variations of the vertical gradient of potential temperature in the diurnal tide. It can be seen that the maxima of E_w coincide with the passage of the zones of convective instability of the tide. Similar diurnal and semi-diurnal variations of E_w have also been found at the middle latitudes (KALCHENKO et al., 1985; GAVRILOV and KALOV, 1985), the diurnal harmonic being dominant. In the middle latitudes the tidal amplitudes are smaller than in the tropics, and no convective instability appears. The cause of the diurnal and semidiurnal variations of E_w here is apparently the modulation of propagating ICW caused by the tidal fields of wind and temperature.

In recent years great attention has been paid to the study of tropospheric sources of acoustic gravity waves in the atmosphere. These are earthquakes, industrial explosions, mountains, displacement instabilities, convective motions, thunderstorm clouds, etc. However, all these are local in both time and space. In particular, mountains are not located everywhere and instabilities, earthquakes or thunderstorms in the troposphere do not always appear, whereas wave motions in the upper atmosphere are observed at all times and places. Hence, the problem arises of finding permanently active sources of wave motions in the atmosphere. Such a source is known: it is the non-linearity of the atmospheric hydrodynamic equations due to which any dynamical formation in the atmosphere (a turbulent or cyclonic vortex, jet, front, etc.) generates wave motions.

For the sake of simplicity, let us examine the case of a two-dimensional barotropic model. In consideration of fast waves, the natural time scale in $T_w = L/c$, where L is the horizontal scale of the stream and c is the sound velocity. When transformed to dimensionless coordinates, the hydrodynamic equations have two dimensionless parameters; $f = 1L/c$ (1 is the Coriolis parameter), and the Mach number M introduced as a perturbation parameter before the nonlinear terms. The conventional method of expansion of hydrodynamic variables into asymptotic series over the perturbation parameter M converges only if $fM < 1$, where $\tilde{t} = t/T_w$ is dimensionless time. In order to overcome this difficulty, we shall use the recently developed "method of multiple timescale successive approximations" (LEIBOVICH and SIBASS, 1977; SITENKO, 1977; JEFFREY and KAWAHARA, 1982) where time variables in the hydrodynamics equations are presented as asymptotic series $\partial/\partial\tilde{t} = \partial/\partial\tau + M \partial/\partial T + M^2 \partial/\partial\theta + \dots$, where $\tau, T, \theta \dots$ is a hierarchy of formally introduced temporal variables which are considered to be independent and which are chosen to ensure the convergence of the asymptotic series in M , with $\tau = O(\tilde{t})$, $T = O(M\tilde{t})$, $\theta = O(M^2\tilde{t})$, etc. In other words, the variable θ characterizes changes in the hydrodynamic fields with the scale of fast waves T_w ; the variable T characterizes the slow advective evolution with scale $M^{-1}T_w$, and the variable θ characterizes still slower changes with scale $M^{-2}T_w$, etc.

The use of the method of multiple timescale successive approximations yields, for the zero-order terms in M , a system of linear equations, the solution of which after the initial period of adaptation (when waves originated by the maladjustment of the initial conditions attenuate) tends to background fields independent of and satisfying the equation:

$$\beta U_0 = -\partial \pi_0 / \partial y ; \quad \beta V_0 = \partial \pi_0 / \partial x ; \quad D_0 = 0 ; \quad \beta \Omega_0 = \Delta \pi_0, \quad (1)$$

where U_0 , V_0 are dimensionless velocity components along the horizontal axes x and y ; D_0 and Ω_0 are the divergence and vorticity of the horizontal velocity; π_0 is the normalized relative variation of the near-Earth pressure. The absence of the dependence of π_0 , U_0 , V_0 , D_0 and Ω_0 on τ reflects the obvious fact that during the time of the run of the fast wave the background fields do not have time to change. A system of equations of the first order of the asymptotic expansion in M leads to the equation of change of the potential vorticity:

$$\partial(\Omega_1 - \beta \pi_1) / \partial \tau = -\partial(\Omega_0 - \beta \pi_0) / \partial T - \vec{V}_0 \cdot \vec{\nabla} \Omega_0 \quad (2)$$

where \vec{V}_0 is the velocity vector of the zero approximation; the subscript "1" marks the first-order values in M . The right-hand side of equation (2) is independent of τ . Therefore, to eliminate the divergence of the asymptotic series with the increase of τ , according to the method of multiple timescale successive approximations, we assume the zero-order values to be dependent on T and equate to zero the left- and right-hand sides of (2) separately, thus obtaining

$$\partial(\Omega_0 - \beta \pi_0) / \partial T = -\vec{V}_0 \cdot \vec{\nabla} \Omega_0 ; \quad \Omega_1 - \beta \pi_1 = 0 \quad (3)$$

The first, conventional equation for the evolution of the background potential vorticity, when added to (1), closes the system of equations for the background values in the quasigeostrophic approximation. It can be seen from (3) that, due to advection, the evolution of the background fields is a slower process than wave propagation and is characterized by the variable T with a scale of variation $M^{-1} T_w$ (see above). The second equation in (3) together with the other equations of the first approximation, yields a system of equations for D_1 , Ω_1 and π_1 of the type:

$$\frac{\partial^2 \pi_1}{\partial \tau^2} - \Delta \pi_1 + \beta^2 \pi_1 = G_0 ; \quad \frac{\partial^2 D_1}{\partial \tau^2} - \Delta D_1 + \beta^2 D_1 = -\beta \vec{V}_0 \cdot \vec{\nabla} \Omega ; \quad \Omega_1 - \beta \pi_1 = 0, \quad (4)$$

where

$$G_0 = (\partial U_0 / \partial x)^2 + 2(\partial U_0 / \partial y)(\partial V_0 / \partial x) + (\partial V_0 / \partial y)^2 \quad (5)$$

The two first equations in (4) are linear wave equations with inhomogeneous linear "forcing" terms on the right-hand sides which describe the generation of waves by the quasigeostrophic motions of (1) and (3). The equations in (4) present a quantitative interpretation of the qualitative theory of Obukhov-Monin (OBUKHOV, 1949; MONIN, 1969) of the generation of wave motions in the process of permanent maladjustment of the wind and pressure fields due to nonlinear effects and the tendency of the atmosphere towards reconstruction of the quasigeostrophic agreement between these fields.

The system of equations (1), (3) and (4) is simplified for small-scale motions where the Coriolis force may be neglected. In this case, the zero-order background motions are solenoidal and the wave fields are potential, the generation of waves being defined by a single value G_0 , i.e. in the limit, transition to the wellknown Lighthill's theory of emission of sound by small-scale turbulence takes place.

When small-scale turbulence in the atmosphere is investigated, the assumption is usually made of the solenoidal nature of the velocity field. According to (4), at $\beta \rightarrow 0$ the solenoidal component of turbulence constantly excites the potential constituent, the main contribution to which is made by the running waves. Therefore, one can speak about "wave" (or "potential") turbulence in the atmosphere which is caused by solenoidal turbulence. The basic property of "wave" turbulence is fast energy distribution with the group velocity. Therefore, wave packets brought about by solenoidal turbulence in the tropo-stratosphere perform an efficient transfer of energy to the upper atmosphere where a layer of intensive wave turbulence is formed which is observed as irregular wave noise.

All the above also applies to larger scale motions, for which the Coriolis force is essential and $\beta \sim 1$. The statistical regime of such motions can be treated as macroturbulence. The only difference is that the geostrophic constituent with a non-zero potential vorticity rather than the solenoidal is the background component here. For the wave component, the potential vorticity equals zero.

The periods and wavelengths of the waves generated depend on the scales of the synoptic and turbulent motions. The small-scale turbulence excites acoustic waves. The meso-scale turbulence is a source of IGW, while large-scale synoptic motions generate low-frequency inertial gravity and planetary waves.

Analysis of the qualitative regular features of the behavior of the wave source G_0 in (4) for mathematical models of vorticity with elliptical current lines⁰ and a rectilinear jet has shown that dynamical formations with lifetime $\tau \sim 1$ h produce the maximum of IGW radiation with period $\tau \sim 2.2$ hrs and horizontal wavelengths $\lambda_h \sim 160-2000$ km. Estimates of the vertical energy flux at heights of the order of 100 km from a rotation vortex with $\tau \sim 1$ h lie within $F \sim 1.6 \cdot 10^{-2}$ to $20 \text{ erg cm}^{-2} \text{ s}^{-1}$ for the values of $M_0 \sim 0.01-0.06$, where M_{max} is the maximum value of the Mach number M in a dynamical formulation. Thus, the intensities of the meso-scale vortices existing in the atmosphere can provide the observed values of the energy wave flux to the upper atmosphere.

The mechanism examined of the continuous generation of waves by meteorological and turbulent motions is apparently the basic mechanism in the formation of the background level of the wave disturbance in the upper atmosphere. Other wave sources in the atmosphere (see above) can produce local and short-term enhancement of the wave noise.

Observations using state-of-the-art meteor radars can be used for a detailed study of both the interaction between IGW and the mean flux and the sources of wave motions. IGW observations by a global network of

C-3

radiometeor stations are a pressing necessity for they can help to work out a season-latitude-longitude model of the IGW parameters and energy characteristics.

References

1. Balsley B. B., 1983, Radio Sci., 18, No. 6, pp. 1011-1020.
2. Chunchuzov E. P., 1971, Izvestia USSR Acad. Sci., Physics Atmos. Ocean, 7, No. 10, pp. 1090-1092.
3. Chunchuzov E. P., 1978, Ibid., 14, No. 10, pp. 1094-1097.
4. Chunchuzov E. P., 1982, Ibid., No. 10, 18, pp. 1095-1098.
5. Fritts D. C., 1983, Radio Sci., 18, No. 6, pp. 1053-1058.
6. Gavrilov N. M., 1976 Izvestia Sov. Acad. Sci., Physics Atmos. Ocean, 12, No. 11, pp. 1212-1213.
7. Gavrilov N. M., 1981, Ibid., 17, No. 7, p. 762.
8. Gavrilov N. M., 1984a, Coll. papers: Meteor Studies, No. 9, Moscow, pp. 106-112.
9. Gavrilov N. M., 1984b, Ibid., No. 11, Moscow, pp. 23-28.
10. Gavrilov N. M., Delov I. A., 1976, Geomagn. Aeron. (USSR), 16, No. 2, pp. 293-297.
11. Gavrilov N. M., Yudin V. A., 1982, Geomagn. Aeron. (USSR), 22, No. 3, pp. 444-449.
12. Gavrilov N. M., Kalov E. D., 1985, Coll. papers: Studies of Minor Gaseous Components and Dynamical Processes in Middle Atmosphere, VINITI, Moscow.
13. Gavrilov N. M., Kalchenko B. V., Kashcheev B. L., Shved G. M., 1981, Isvestiya Sov. Acad. Sci., Physics Atmos. Ocean, 17, No. 7, pp. 680-689.
14. Gavrilov N. M., Karimov K. A., Koksharov I. I., 1976, Trans. Kirghiz State Univ., Ser. Phys. Sci., iss. 7, pp. 29-36.
15. Gavrilov N. M., Pogoreltsev A. I., 1980, Geomagn. Aeron. (USSR), 20, No. 4, pp. 664-669.
16. Gavrilov N. M., Shved G. M., 1982, Ann. Geophys., 38, No. 6, pp. 789-803.
17. Gavrilov N. M., Shved G. M., 1975, Ibid., 31, No. 3, pp. 375-388.

18. Gokhberg M. B., 1983, Coll. papers: Active Exp. Space, Proc. Intern. Symp., Albach, May, 1983, Paris, No. 8, pp. 99-110.
19. Hirota I., 1984, J. Atmos. Terr. Phys., 46, No. 9, pp. 767-773.
20. Holton J. R., 1982, J. Atmos. Sci., 39, No. 4, pp. 791-799.
21. Holton J. R., 1983, Ibid., 40, No. 10, pp. 2497-2507.
22. Jeffrey A., Kawahara J., 1982, Asymptotic Methods in Nonlinear Wave Theory, Boston, Pitman.
23. Kazanikov A. M., Portnyagin Yu. I., 1981a Izvestia Sov. Acad. Sci., Physics Atmos. Ocean, 17, pp. 95-98.
24. Kazanikov A. M., Portnyagin Yu. I., 1981b, Geomagn. Aeron. (USSR), 21, No. 2, pp. 371-372.
25. Kalchenko B. V., Kashcheev B. L., Oleinikov A. N., 1985, Izvestiya Acad. Sci. (USSR), Physics Atmos. Ocean, 21, No. 2, pp. 123-130.
26. Karimov K. A., Lukyanov A. E., 1979, Izvestia Sov. Acad. Sci., Physics Atmos. Ocean, 15, No. 8, pp. 877-880.
27. Krassovski V. I., 1972, Ann. Geophys., 28, No. 4, pp. 739-746.
28. Krassovski V. I., Potapov B. P., Semenov A. I., Sobolev V. G., Shagaev M. V., Shefov N. N., 1978, Coll. papers: Aurorae Borealis and Nigh Sky Airglows, Moscow, Sov. Radio, No. 26, pp. 5-30.
29. Leibovich S., Sibass A. R., 1971, Coll. papers: Nonlinear Waves, Moscow, Mir Publ., pp. 113-150.
30. Miyahara S., 1984, Dynamics of the Middle Atmosphere, Tokyo, pp. 271-287.
31. Molina A., 1983, Planet. Space Sci., 31, No. 3, pp. 331-337.
32. Monin A. S., 1969, Weather Forecast as a Physical Problem, Moscow, Nauka Publ.
33. Obukhov A. M., 1949, Izvestia Sov. Acad. Sci., Geophys. Geograph., 13, No. 4, pp. 281-306.
34. Shved G. M., 1977, Coll. papers; Studies in Geomagnetism, Aeronomy and Solar Physics, Irkutsk, iss. 43, pp. 182-190.
35. Sitenko A. G., 1977, Fluctuations and Nonlinear Interaction of Waves in Plasma, Kiev, Naukova Dumka Publ.
36. Spizzichino A., 1969, Ann. Geophys., 25, No. 1, pp. 5-28.
37. Spizzichino A., 1972, Coll. papers: Thermospheric Circulation, Cambridge, MIT Press, pp. 120-177.

38. Vincent, 1984, J. Atmos. Terr. Phys., 46, No. 2, pp. 119-128.
39. Weinstock J., 1978, J. Geophys. Res., 83, p. 5175.

NUMERICAL MODELING OF TROPOSPHERE-INDUCED GRAVITY WAVE PROPAGATION

N. M. Gavrilov and V. A. Yudin

Leningrad State University
Leningrad-Petrodvorets, USSR

Sources of internal gravity waves (IGW) in the upper atmosphere are assumed to be meteorological processes in the troposphere. These sources are vertically and horizontally inhomogeneous and time-dependent. In order to describe the IGW propagation from such sources, a numerical solution of a system of hydrodynamical equations is required. In addition, it is necessary to take into account the influence of the altitude-latitude inhomogeneity of the temperature and wind fields on the IGW propagation as well as the processes of dissipation.

This paper proposes an algorithm for numerical modelling of the IGW propagation over a limited area from tropospheric local sources to the upper atmosphere. The algorithm takes into account all the above mentioned features. A spectral-grid method is used with the expansion of wave fields into the Fourier series over longitude. The upper limit conditions have been obtained from the requirement of a limited energy dissipation rate in an atmospheric column. The no slip (zero velocity) condition has been used at the Earth's surface.

Therefore, for the analysis of the vertical structure of steady-state oscillations, the IGW source is given in the equation for divergence as an inhomogeneous term

$$\phi = f \cdot \exp \left[- \left(\frac{z - z_0}{d} \right)^2 \right] \exp(ik_x x - i \sigma t), \quad (1)$$

where f characterizes the source intensity, d its vertical extension, z_0 is the height of the maximum, k_x and σ are the horizontal wave number and the IGW frequency, respectively. The values of $z_0 = 10$ km and $d = 1.5$ km have been used in the calculations, as well as the value of $f = 10^{-11} \text{ s}^{-2}$. The results obtained (see below) show that even this moderate value of f provides correct orders of magnitude of the IGW amplitudes in the upper atmosphere.

Wave equations are integrated over time after switching on the source (1) at a movement $t = 0$ prior to the transition of the solution to the stationary regime. For complete stabilization of the wave oscillations regime, a time $\Delta t \sim (60-80)\tau$ is required (τ is the IGW period).

Fig. 1 shows profiles of the variations of wave energy dissipation ϵ_w ; of the transmission of wave energy to the background wind ϵ_b and the wave acceleration of the background flux a as well as the rate of dissipation of wave energy into heat ϵ_α . All curves have maxima at the heights of the lower thermosphere.

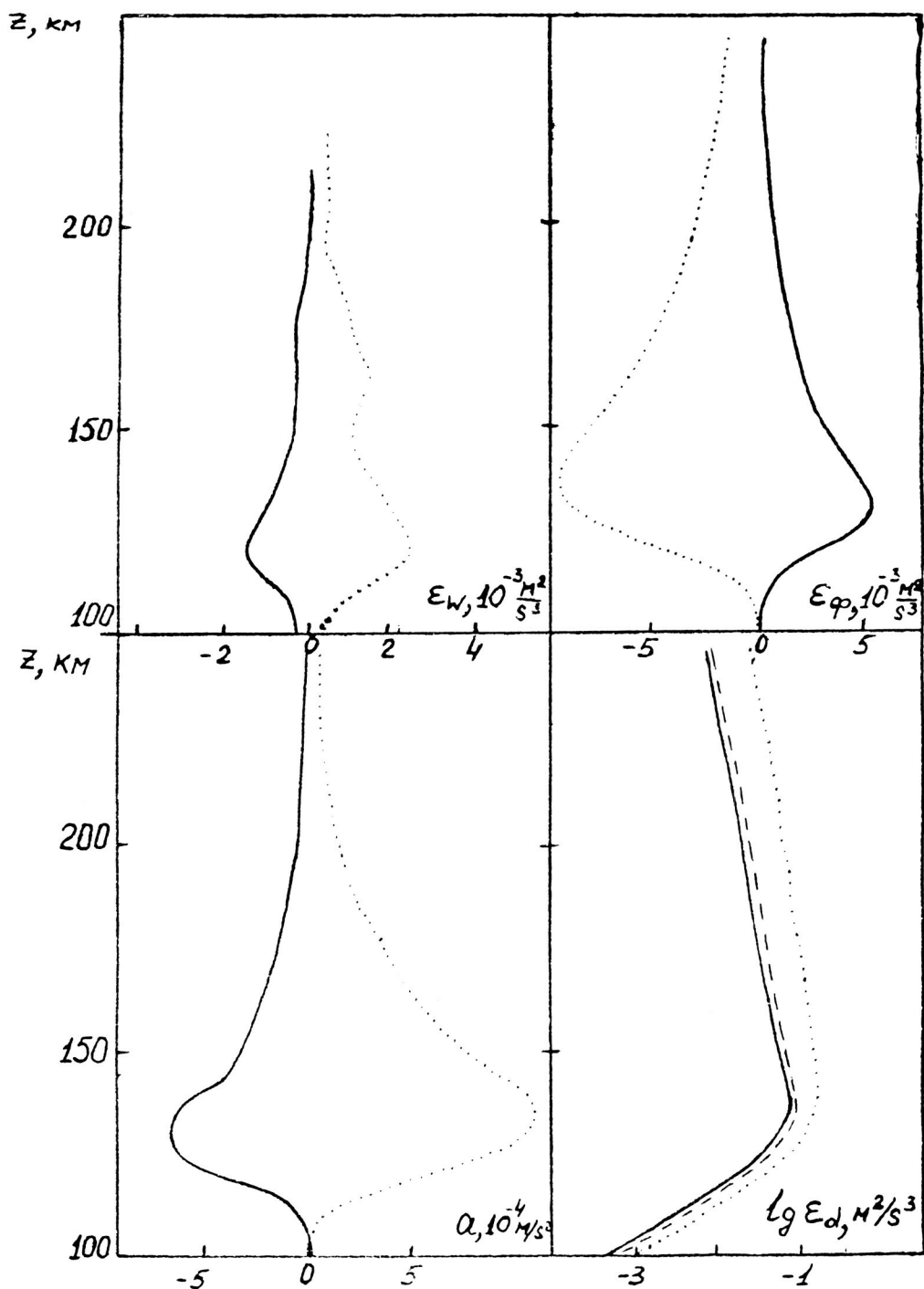


Fig. 1 Vertical Profiles of the ϵ_w , ϵ_ϕ , a , $\lg \epsilon_d$ for January and IGW propagating to the West (solid lines) and to the East (dotted lines).

Since for the stabilization of oscillations in the atmosphere time intervals of tens and hundreds of hours are required, as was mentioned above, real meteorological sources in the atmosphere cannot, usually, remain unchanged during such long time intervals. For modelling such a source the above-mentioned inhomogeneous term in that equation for divergence has been taken as

$$\phi(x_1 z_1 t) = f \exp[-(t - t_0)^2/\tau_0^2 - (z - z_0)^2/d^2 - ik_x x], \quad (2)$$

where τ_0 is the scale of variation of the wave source in time and t_0 is the time of its maximum. It can be considered that the source (2) generates a packet of IGW with the frequencies $-\omega \leq \omega \leq 2\pi/\tau_0$ which, with a given k_x , are propagated in both directions of the axis z with horizontal phase velocities $|C_x| \leq C_m = 2\pi/(\tau_0 k_x)$. Therefore, the values τ_0 and C_m have been used as parameters characterizing non-stationary sources. In (2) the following parameters for a tropospheric source are used:

$$f = 10^{-9} s^{-2}, \quad z_0 = 10 \text{ km}, \quad d = 5 \text{ km}$$

The results of calculations of the time variation of the integral over an atmospheric column of the wave energy E_{total} show that after the "switching on" of the source the wave energy quickly reaches its maximum values and then a slow process of attenuation begins which continues for $(20-40) \tau_0$. This can be accounted for by the fact that the main part of wave energy is concentrated in the tropo-strato-mesosphere and by the relatively low speed of its propagation to the thermosphere where dissipation of waves mostly takes place. The time lag of the wave energy maxima in relation to the $\tau_0/5$ moment t_0 for E_{total} is from $\tau_0/5$ to τ_0 and for local values of t_0 E increases for up to $(4-8) \tau_0$ at 100-150 km heights.

Fig. 2 shows the vertical profiles of the IGW parameters for January at various times for sources with $\tau_0 = 6$ hrs and different C_m . Analysis of Fig. 2 shows that after a time period $(4-8) \tau_0$ following the source function maximum a comparatively stable profile of E is formed with two maxima: in the troposphere and at the height of about 75 km. These maxima coincide with the regions of minima βH where β is the static stability parameter. The formation of the mesospheric waveguide is additionally influenced by the background wind profile which creates an increase of the wave flux F_z at the decrease of λ near the 75 km height. The formation of the waveguide leads to the lowering of the maxima of wave amplitudes and ϵ_z , ϵ_d and a in Fig. 2 in comparison with the stabilized regime. Curves K_{lw}^w and λ in Fig. 2 show that in the initial period the main reflection of wave energy takes place at 80-90 km due to the effect of the temperature profile and the maximum of turbulent dissipation in the lower thermosphere. As time passes, this barrier grows more transparent and another area of increased reflection is formed near the jet stream at a height of about 50 km.

In most cases the background wind in the strato-mesosphere leads to the enhancement of the harmonics of IGW coming from the opposite direction in comparison with those propagating in the same direction, and the resulting propagation of the IGW packets is directed towards the background flux. This determines the signs of accelerations a of the background flux by

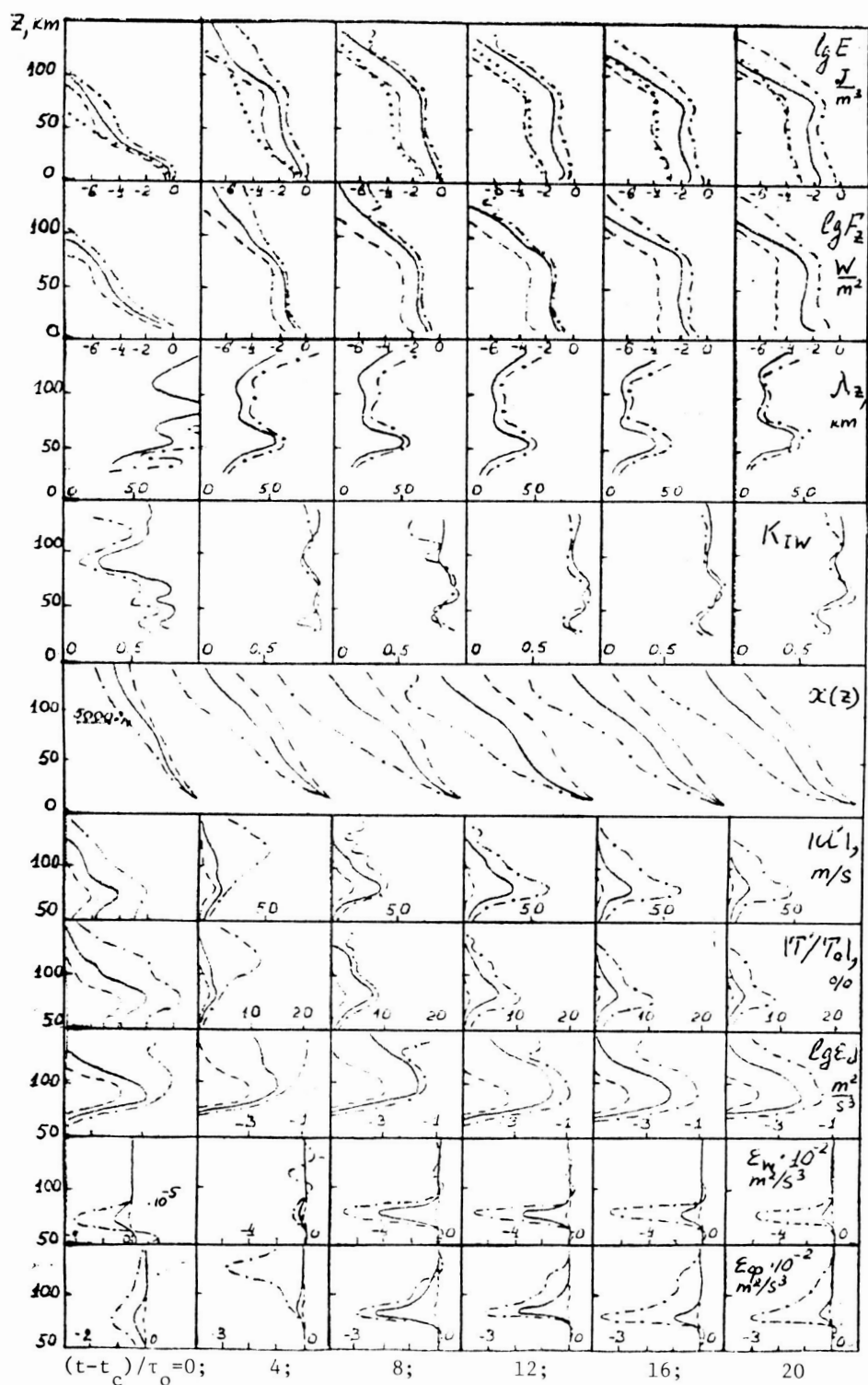


Fig. 2 Vertical profiles of IGW parameters for January at various times. Dashed, solid and dashed-dotted lines correspond to $c_m = 90, 150$ and 250 mps.

waves. In winter $a < 0$ (directed westwards); in summer, at its beginning and at heights less than 100 km, $a > 0$ (directed eastwards) although after a time (8-12) τ_0 after t_0 and above 100 km $a < 0$ occur. According to the present-day understanding (HOLTON, 1983), the effect of IGW drag is an essential mechanism of formation of the middle atmosphere circulation. The calculations presented in this paper, according to which the filter formed by the background wind, for the most part, transmits IGW propagating from the opposite direction, account for the mechanism of appearance of dragging wave accelerations.

Fig. 3 presents the dependence on $C_x = \sigma/k_x$ of the normalized wave energy $E_{\text{total}} C_0^2 / C_x^2$ integrated over an atmospheric column, where $C_0 = 150$ mps, and on the densities of wave energy E at different height levels. The solid curves in Fig. 3 reveal, for a windless atmosphere, the resonance peaks at the values $C_x = 310, 255$ and 180 mps which are very close to the values of atmospheric oscillations discussed by DIKIY (1969). The influence of the background wind leads to a bias in the resonance maxima for IGW coming from the direction opposite to the wind to $C_x = 295, 215$ and 125 mps, and for IGW propagating in the direction of the wind to $C_x = 335, 300$ and 235 mps, respectively. The bias of the resonance maxima in Fig. 3 is accompanied by a decrease in their values for IGW coming from the opposite direction and by an increase for those propagating in the same direction. Analysis of Fig. 3 (b through f) shows that, in the lower layers, the first resonance energy maximum prevails which corresponds to $C_x \sim 300-315$ mps. However, as the height increases it is attenuated and at $z \sim 100-150$ km the second resonance maximum prevails.

References

1. Holton, J.R., 1983, J. Atmos. Sci., 40, No. 10, 2497-2507.
2. Dikiy L.A., 1969, The Theory of The Earth's Atmospheric Oscillations, Gidrometeoizdat Publ., Leningrad, p. 196.

ORIGINAL PAGE IS
OF POOR QUALITY

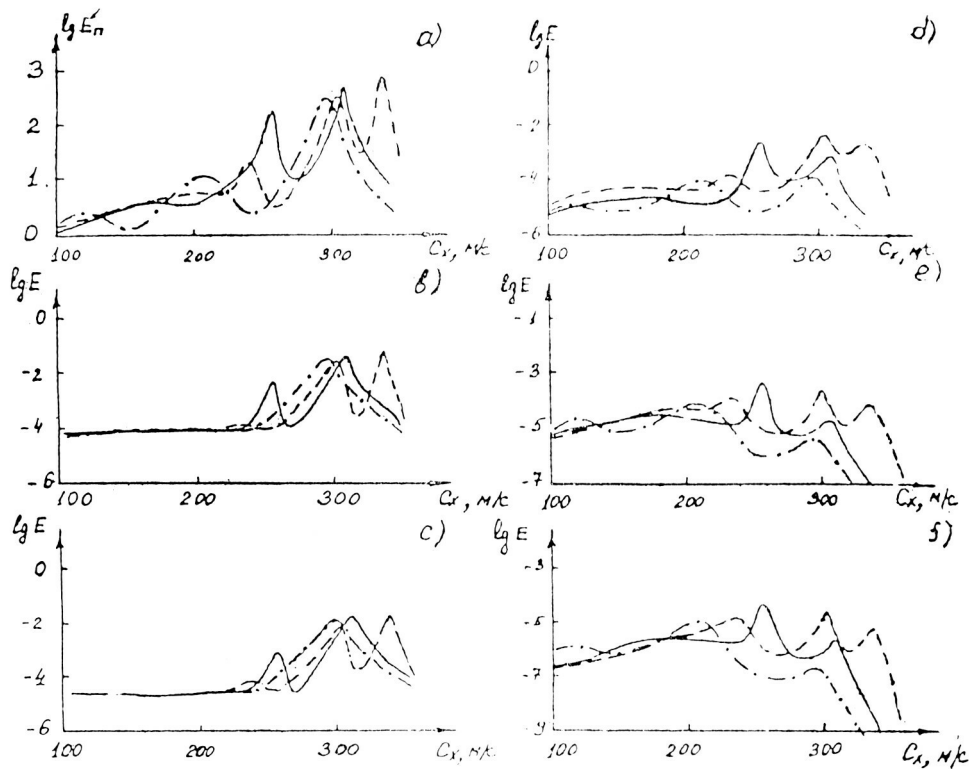


Fig. 3 Dependence on $c = \sigma/k$ of E_n (frame a) and E at the height levels 1, 10, 50, 100 and 150 km, (b) through (f).

A STATISTICAL STUDY OF VARIATIONS OF INTERNAL
GRAVITY WAVE ENERGY CHARACTERISTICS IN METEOR ZONE

N. M. Gavrilov and E. D. Kalov

Leningrad State University
Leningrad-Petrodvorets, USSR

Internal gravity wave (IGW) parameters obtained by the radiometeor method have been considered by SPIZZICHINO, (1975); GAVRILOV et al., (1976); GAVRILOV and DELOV, (1976); KARIMOV and LUKYANOV, (1979); KAZANIKOV and PORTNYAGIN, (1981) and KALCHENKO et al., 1983. This paper presents the results of the processing of regular radiometeor measurements taken during 1979-1980 in Obninsk (55.1°N, 36.6°E).

The Obninsk meteor radar takes simultaneous measurements in four areas of the meteor zone which correspond to antenna directions northwards, westwards, southwards and eastwards. The instrumentation used is described in PORTNYAGIN and SHIRENGER (1978), and the method of statistical data processing - in GAVRILOV (1984). The meteor station determines for each of the four directions a number of wind velocity values at random time moments at the average height of the meteor zone $z = 93$ km. To analyze the IGW horizontal structure, the area observed is divided in the direction of the antenna beam into horizontal subareas of width $x = 100$ km with the centers x_0 biased by $\Delta x_0 = 25$ km. For every group of meteor echoes in each of the horizontal subareas, a high frequency filtration (averaging over 10 minute intervals) and a low frequency filtration are performed (GAVRILOV, 1984), after which amplitude and phase spectral analyses of data over sliding 12-hour time intervals are carried out. The subsequent statistical analysis of the spectra obtained makes it possible to recognize the IGW spectrum from the background of noise (GAVRILOV, 1984), as well as to determine the values of projections of horizontal wave numbers k_h and phase velocities c_h of IGW to horizontal axes oriented along the antenna beams (see above).

Radiometeor data obtained in Obninsk for 582 days during the period from February 1979 to November 1980, were processed by the above-mentioned method.

Fig. 1 shows histograms of the distributions of IGW parameters for summer for all the sounded directions. They look alike and have maxima at the values of $c_h \sim 50-75$ mps, $V \sim 4-5$ mps and $k_h \sim (1-2) \cdot 10^{-2} \text{ km}^{-1}$. Of similar appearance are histograms of the distributions of IGW parameters for other seasons. Analysis of the IGW quantities propagating in various directions has revealed that IGW propagating southeastwards prevail in winter, whereas those propagating northwestwards prevail in summer. The same seasonal dependence of the prevailing directions of the IGW propagation was earlier found out from observations of night airglow wave variations (GAVRILOV, 1982). Causes for this regular feature can be seasonal variations in the location of IGW sources and those in the direction of the zonal flux in the stratosphere which influences the IGW propagation from tropospheric sources (GAVRILOV, 1982).

ORIGINAL PAGE IS
OF POOR QUALITY

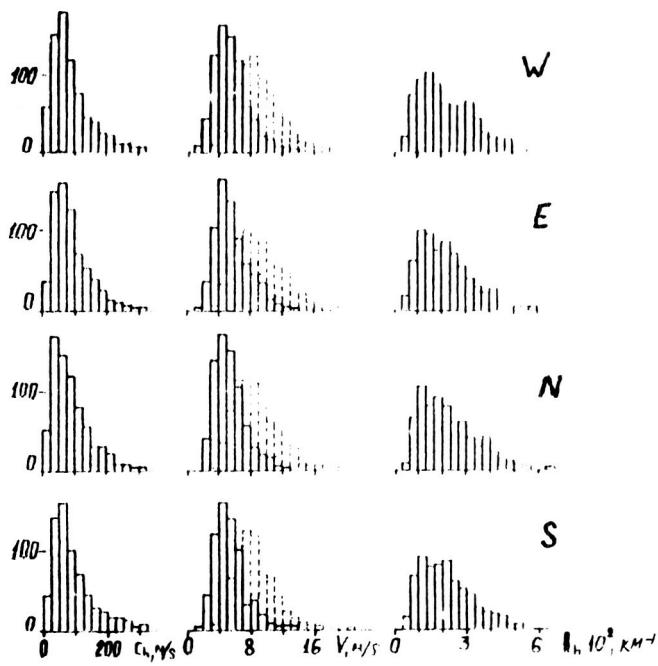


Fig. 1 Histograms of the distributions of the IGW parameters for all the IGW directions. Dotted lines correspond to the corrected values of V_{corr} .

Fig. 2 shows the mean values of c_h , V and k_h calculated separately for each month of the observation period and for the four groups of the IGW directions considered. It can be seen that c_h and k_h have no pronounced seasonal variations. The phase velocity of c_h changes within $c_h \sim 30-150$ mps and decreases with the increase of τ . The values of k_h lie within $(1.5 - 2.5) \cdot 10^{-2} \text{ km}^{-1}$ and are hardly dependent on τ at all. The most pronounced variation is observed only in the amplitudes of the velocity V ; for IGW propagating in all the directions and for all the frequency groups, the maximum of $V \sim 7-8$ mps is observed during the winter months (November to March), and the minimum of V 4-6 mps - in summer (Fig. 2). In Figs. 1 and 2 the histograms and V_{corr} are shown by dotted lines for the values corrected for the effect of the finite number of registered meteors (GAVRILOV, 1984). The mean winter values increase up to $V_{\text{corr}} \sim 12-15$ mps, and the mean summer ones - up to $V_{\text{corr}} \sim 8-9$ mps.

The components of the wave fluxes of energy F_i , heat F_{Ti} , momentum F_{ij} and mass F_{mi} are described by formulae of the type:

$$F_i = \langle p'v'_i \rangle + Ev_{io} ; F_{TC} = \rho_o C_p \langle T'v'_i \rangle ; F_{ij} = \langle v'_i v'_j \rangle ; F_{mi} = \langle \rho'v'_i \rangle , \quad (1)$$

where dashes denote the wave components and the subscript o the background components of pressure p , density ρ , temperature T , the wind velocity component v_i ; c_p is the specific heat capacity at constant pressure; E is the wave energy; the sign $\langle \rangle$ denotes averaging over the wave period; $i = x, y, z$ correspond to the x, y, z axes oriented eastwards, northwards and upwards. The value of p' , ρ' , T' and v'_i required for calculations according to (1) are found from the measured v'_x and v'_y by making use of hydrodynamics equations.

To perform the calculations, apart from the zonal wave number k_x , one must also know the meridional wave number k_y . Statistical analysis has revealed that in the meteor zone the "noise" of IGW coming from various incoherent sources is mainly observed, and that harmonics with identical periods are found in mutually perpendicular directions only occasionally. Therefore, it is impossible to calculate the values of (1) for individual harmonics.

However, considering the problem of the influence of IGW on the thermal regime and circulation of the upper atmosphere, not individual but long term averages of wave flux are important. The measured probability densities of the distributions of k_y (Fig. 1) and statistically reliable measurements data make it possible to use the methods of statistically modelling (Monte-Carlo) to calculate the mean values of (1). On a computer, by transformation of data from a random number generator, the random value k_y is modelled which has a probability distribution equal to the experimental. Wave fluxes (1) and their monthly mean values are calculated. To minimize the error, calculations are made for 10 different realizations of the random value k_y and the results are then averaged again.

Fig. 3 shows seasonal variations of the mean values of wave fluxes, all of which have a pronounced seasonal variation. The vertical energy flux F_z varies from $6 \times 10^{-3} \text{ Wm}^{-2}$ in winter to $1 \times 10^{-3} \text{ Wm}^{-2}$ in summer. The

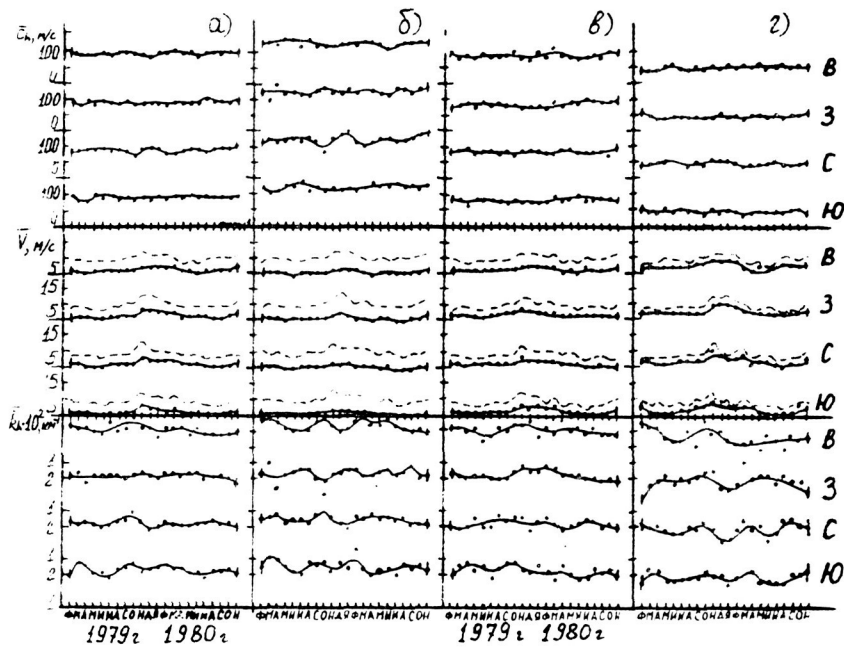


Fig. 2 Mean values of c_h , V and k_h for the groups of IGW propagating to the North (N), West (W), South (S) and East (E).

ORIGINAL PAGE IS
OF POOR QUALITY

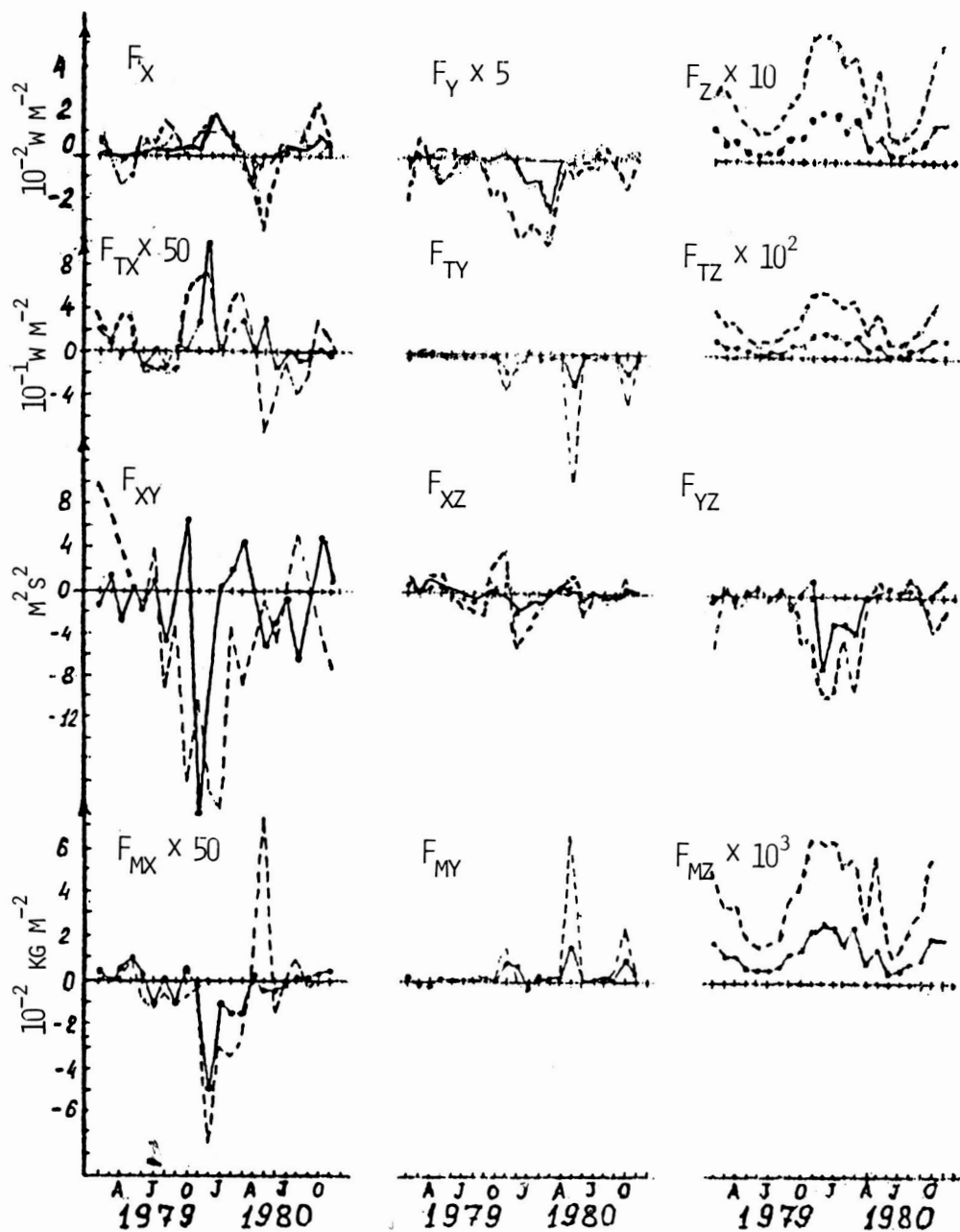


Fig. 3 Seasonal variations of the mean values of wave fluxes. Dashed lines correspond to the corrected values V_{corr} .

directions of F_x and F_y correlate fairly well with the signs of the background wind components V_x and V_y . The vertical mass flux F_z is always directed upwards and is maximal in winter. The variations of F_x and F_y are in antiphase with the variations of F_{Tx} and F_{Ty} . The velocity of the vertical wave transport of mass is comparable with the background vertical velocity. The vertical wave flux is of the type of $F_{Tz} = F_z$. The values and signs of the moment fluxes F_{xz} and F_{yz} in Fig. 3 correspond to wave accelerations in the zonal direction in winter of $-(80-100) \text{ ms}^{-1}/\text{day}$ westwards, and in summer $+(10-20) \text{ ms}^{-1}/\text{day}$ eastwards; in the meridional direction, to $+(10-50) \text{ ms}^{-1}/\text{day}$ in spring and autumn and $-(10-50) \text{ ms}^{-1}/\text{day}$ in winter and summer. This gives an experimental confirmation to the existing hypothesis that IGW in the upper atmosphere contribute to the drag of the zonal flux and the formation of meridional circulation. However, the values of wave accelerations obtained are somewhat lower than those used in numerical modelling (HOLTON, 1983), particularly for summer.

The variations of the IGW energy E with $\tau \sim 0.5-6$ hrs in the course of a 48-day cycle from July 8 to August 24, 1979, were investigated. The results of the spectral analysis of E and the background wind for four sounded directions in the period mentioned show that the main harmonics of the background wind are two day and semi-diurnal, whereas that of the wave energy is diurnal. The energy spectra of the wave variations of the meridional wind increase in the region $\tau \geq 2$ days in contrast to the spectra of E for zonal directions. Since tides in the middle latitudes are mostly stable, the main mechanism of the formation of diurnal and semi-diurnal variations of E is the modulation of IGW propagating from below under the influence of the vertical profiles of temperature and wind produced by tides. The diurnal tide in the meteor zone has much smaller vertical wavelengths than the semi-diurnal tide and a quasi-two diurnal variation. Therefore, it produces the largest amplitude of modulation of E .

The variations of E with 4 to 8 day periods can be accounted for by first possible modulation of the propagating IGW by planetary waves and second, meteorological processes in the troposphere with 4 to 8 day periodicity causing an enhanced generation of IGW propagating upward to the meteor zone.

References

1. Spizzichino A., 1975, in: Atmospheric Circulation, Moscow, MIR Publ., p. 120-174.
2. Gavrilov N.M., Karimov K. A., Koksharov I.I., 1976, Trans. Kirghiz State Univ., Ser. Phys. Sci., iss. 7, p. 20-36.
3. Gavrilov N.M., Delov I.A., 1976, Geomagn. Aeron. (USSR), 16, No. 2, p. 293-297.
4. Karimov K.A., Lukyanov, A.E., 1979, Izvestia Sov. Acad. Sci., Physics Atmos. Ocean, 15, No. 8, p. 877-880.
5. Kazanikov A.M., Portnyagin Yu. I., 1981, Geomagn. Aeron. (USSR), 21, No. 2, p. 371-372.

6. Kalchenko B.V., Kashcheev B.L., Oleinikov A.N., 1983, Abstracts of papers presented to I USSR Symp. on Middle Atmospheric Studies Alma-Ata, Febr.
7. Wind Measurement at Heights 90-100 km by Ground-Based Methods. Ed. Portnyagin Yu. I., Shirenger K.L., Leningrad Gidrometeoizdat Publ., p. 344, 1978.
8. Gavrilov N.M., 1984, in: Meteor Studies, Moscow, Soviet Geophys. Committee, No. 9, p. 106-123.
9. Gavrilov N.M., 1982, Izvestia Sov. Acad. Sci., Physics Atmos. Ocean, 18, No. 1, p. 8-17.
10. Holton, J.R., 1983, J. Atmos. Sci., 40, No. 10, p. 2497-2507.

ON THE DEPENDENCE OF THE LOWER THERMOSPHERIC
WIND REGIME ON THE SOLAR CYCLE

V. A. Djachenko, I. A. Lysenko and Yu. I. Portnyagin

Institute of Experimental Meteorology (IEM)
Obninsk, USSR

The lower thermosphere (80-100 km) occupies the intermediate position between the overlying thermospheric layers, for which direct correlation of its parameters with solar activity variations is well established, and the underlying ones, where this correlation is mainly of an indirect character. Therefore, for understanding the mechanism of solar-terrestrial correlations it is important to investigate the dependence of different atmospheric parameters in the lower thermosphere, and of wind regime parameters in particular, on the solar activity.

The paper by SPRENGER and SCHMINDER (1969) was among the first investigations in this field. Similar results were obtained in other papers (PORTNYAGIN et al., 1977; KAJDALOV and PORTNYAGIN, 1976; DARTT et al., 1983; and TEPTIN, 1971), but the limited temporal coverage of the experimental data used for the analysis did not allow the authors to investigate the interannual variations of wind regime parameters with periods over 11 years.

Since then there has appeared a considerable amount of evidences of an obvious effect upon the Earth's atmosphere of the 22-year solar cycle (see, for example, MC CORMAN, 1982). In this connection it is reasonable to investigate the dependence of lower thermospheric wind regime parameters on the 22 year as well as the 11 year solar cycle.

With this aim in view, the authors have used several series of observations which include the results of meteor radar wind velocity measurements carried out in Obninsk (1964-1983) complemented by the data obtained using the same technique at Jodrell Bank from 1953 to 1958 (GREENHOW and NEUFELD, 1961) and in Kharkov from 1960 to 1963 (LYSENKO, 1963; KASHCHEEV et al., 1967).

Until 1973 measurements in Obninsk were carried out every month for 7 to 10 days and in the ensuing years practically continuously; at Jodrell Bank and Kharkov measurements were carried out in cycles, 3-4 days every month. Monthly mean values of prevailing wind velocities and semi-diurnal tidal amplitudes were estimated from these measurements.

Fig. 1 presents the interannual variations of values averaged over these periods for prevailing wind velocities and semidiurnal harmonic amplitudes and also results for some separate months. It is seen that interannual variations with periods close to one or both main solar cycles are typical of all wind regime parameters. To determine amplitudes and phases of these variations the data presented in Fig. 1 were subjected to harmonic analysis with decomposition periods of 22, 11, 7 and 5 years. The Wolf numbers for the corresponding period were similarly analyzed. The analysis showed that the sum the squares of the amplitudes of the 22- and

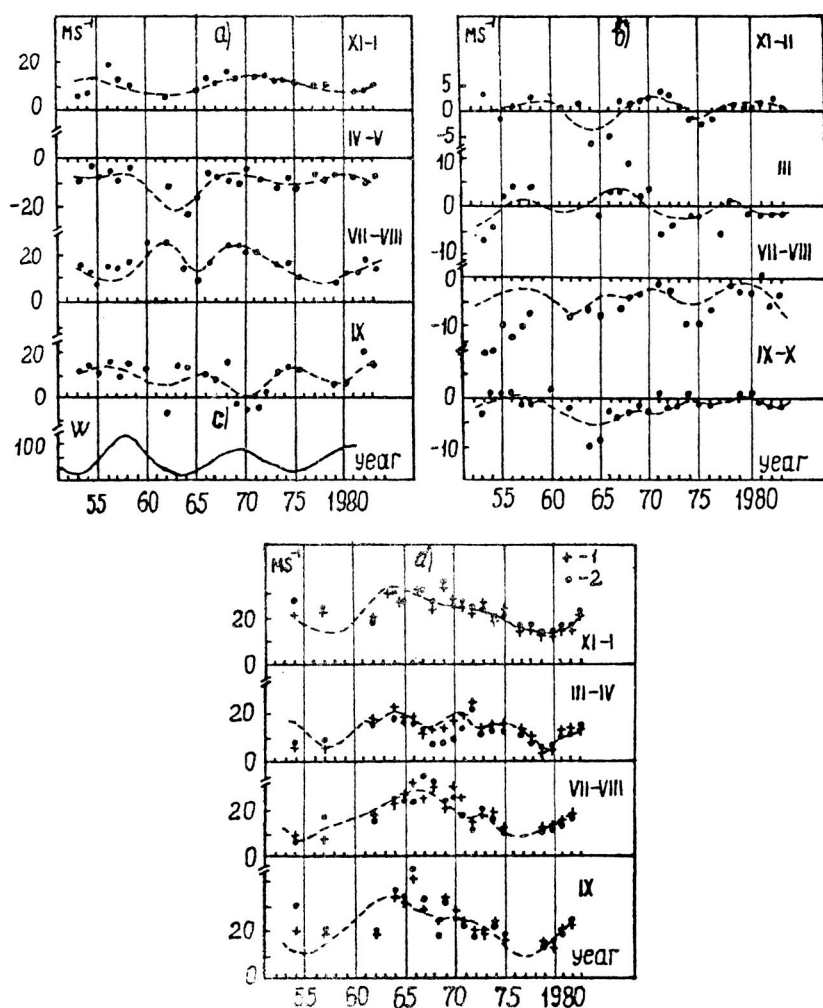


Fig. 1 Interannual variations of a) zonal and b) meridional prevailing wind velocities, c) mean annual values of the Wolf numbers, d) amplitudes of zonal (1) and meridional (2) components of the semidiurnal tide. Sums of the first five members of a Fourier series (semidiurnal tide only for the zonal component) are shown by broken lines.

11- year variations make up more than 70% of the total dispersion of the interannual wind regime parameter variations.

Results of the harmonic analysis are presented in Table 1. Here A_0 is the parameter value averaged over the whole observation period, A_{22} and A_{11} are the 22- and 11- year harmonics amplitudes, ψ_{22} and ψ_{11} are their phases (the time of the maximum of westerly and southerly winds for the prevailing wind, the time of the maximum of amplitudes of the semidiurnal tide and the time of the maximum of the Wolf numbers values). The root-mean-square errors of wind parameter estimations are also presented.

The mean values of the analyzed parameters and the amplitudes of the 22- and 11- year oscillations in the majority of cases exceed the corresponding root-mean-square errors. The harmonic analysis method requires, a priori, prescribed periods in the Fourier series; therefore, it was necessary to make sure that the considered experimental data really possess periodicities corresponding to the main solar activity cycles. The standard spectral analysis method proves unacceptable for this case due to the proximity of periods of the investigated oscillations to the entire duration of the data series.

The problem was solved by constructing the dependences of correlation coefficient values on test periods (of 18 to 26 years) that are given in Fig. 2. The analysis of these dependences showed that for all seasons (or months) for which the calculated A_{22} and A_{11} exceed the errors of their determination the maximum correlation coefficient values (0.4 to 0.9) correspond to periods close to 22 years for the interval of 18-26 years and close to 11 years for the interval of 7-15 years.

The results obtained show that the oscillations with periods of 22 and 11 years revealed experimentally are physically real and thus the corresponding solar cycles could be their real cause. Relations between interannual variations of prevailing wind velocities and semidiurnal tidal amplitudes with long-term solar activity variations are confirmed by the fact that the phases of these variations are connected with those of the corresponding solar cycles and can serve as an additional proof of this. In part, the phases of the 11- year harmonics of the zonal and meridional components of the prevailing wind are such that the maxima of their velocities fall in the years of 11- year solar cycles maxima. The maximum values of both amplitude harmonics of the semidiurnal tide are observed during the years of the minimum of the solar activity cycles.

The data show that the 22- year period variations dominate variations of zonal prevailing wind velocities in the winter and meridional winds in the autumn months. Meridional prevailing winds vary in November-February mainly with the 11- year cycle. In the other months of the year the amplitudes of the 22- and 11-year velocity variations of the prevailing winds are similar. Oscillations with a 22- year period prevail for the amplitude of the semidiurnal tide. It should be noted that the solar activity dependences of the zonal and meridional component amplitudes of the semidiurnal tide are quite similar whereas the character of corresponding dependences of zonal and meridional prevailing wind is different.

Table 1

Harmonic analysis results of mean monthly Wolf numbers, prevailing wind and semidiurnal tidal amplitude.

	A_0	A_{22}	A_{11}	Y_{22}	Y_{11}
W, Wolf numbers					
November-February	74±5	15±7,5	63±10	1958; 80±2,0	1959; 70; 81 ±0,5
March-April	73±4	14±7	65±7	1958; 80±2,0	1958; 69; 80 ±0,5
June-August	75±4	18±6	64±6	1957; 79±1,0	1959; 70; 81 ±0,5
September-October	79±7	17±9	70±10	1957; 79±2,0	1958; 69; 80 ±0,5
a_0 EW, zonal prevailing wind					
November-January	12±1	4±1	1±1	1971; ±0,8	1959; 70; 81 ±2,0
April-May	-11±1	4±1	5±2	1979; ±0,9	1957; 68; 79 ±1,0
July-August	17±1	5±1	4±1	1967; ±0,9	1960; 71; 82 ±1,0
September	11±1	7±1	6±1	1961; ±0,7	1961; 72; 83 ±1,0
a_0 NS, meridional prevailing wind					
November-February	0±0,5	1±1	3±1	1974; ±1,0	1958; 69; 80 ±0,5
March	1±1	4±2	2±2	1969; ±2,5	1958; 69; 80 ±3,0
July-August	-6±1	2±2	4±2	1968; ±2,0	1958; 69; 80 ±0,5
September-October	-3±1	3±1	1±1	1977; ±1,0	1959; 70; 81 ±1,0
a_2 EW, zonal semidiurnal tide					
November-January	22±1	7±1	3±1	1967; ±1,5	1953; 64; 75 ±0,5
March-April	15±1	4±1	3±1	1968; ±1,5	1952; 63; 74 ±1,0
July-August	19±1	9±2	0±1	1967; ±1,0	-
September	23±1	10±2	5±2	1966; ±1,0	1951; 62; 74 ±1,0
a_2 NS, meridional semidiurnal tide					
November-January	23±1	8±2	1±1	1968; ±1,0	1953; 64; 75 ±2,5
March-April	11±1	3±1	2±1	1968; ±2,0	1953; 64; 75 ±1,0
July-August	21±1	10±1	0±1	1967; ±0,5	-
September	24±1	9±2	4±1	1966; ±1,0	1953; 64; 75 ±1,0

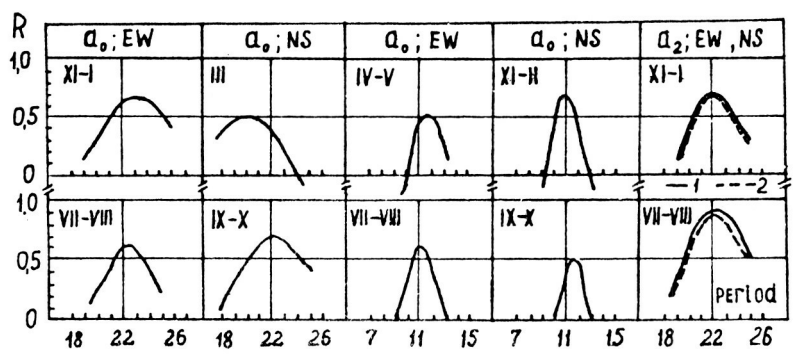


Fig. 2 Dependence of mutual correlation coefficients on period, 1) meridional component, 2) zonal component.

The results of this investigation show that when analyzing the dependence of the lower thermospheric wind regime parameters on solar activity it is necessary to take into account not only the 11- year, but also the 22- year cycle.

References

1. Sprenger K., Schminder R., 1969, Solar Cycle Dependence of Wind in the Lower Ionosphere, *J. Atm. Terr. Phys.*, Vol. 31, pp. 217-221.
2. Portnyagin Yu. I., Kaidalov O. F., Greisiger K. M., Sprenger K., 1977, Zur Abhangigkeir Der Wind Parameter Der Mesopausenregion Vom 11-Jahrigen Zzuyklus Der Sonneaktivitat, *Physica Solari-Terrestr.*, Potsdam, No. 5, pp. 91-95.
3. Kaidalov O. V., Portnyagin Yu. I., 1976, On the Connection of Solar and Geomagnetic Activity Parameters with Dynamical Processes at 80-100 km. *Physics of Upper Atmosphere, Proceedings of the IEM, Gidrometeoizdat, Moscow*, No. 5 (62), pp. 50-55.
4. Dartt D., Mastrom G., Belmont A., 1983, Seasonal and Solar Cycle Wind Variations, 80-100 km., *J. Atm. Terr. Phys.*, Vol. 45, No. 10, pp. 707-718.
5. Teptin G. M., 1971, Temporal Characteristics of Atmospheric Motion at 80-100 km. *Physics of Atmosphere and Ocean*, VII, No. 8, pp. 823-831.
6. *Solar-Terrestrial Relations, Weather and Climate*. Edited by McCorman, 1982, MIR Publishers, Moscow, p. 380.
7. Greenhow J. S., Neufeld E. L., 1961, Wind in the Upper Atmosphere, *Quart. J. Roy. Met. Soc.*, Vol. 87, No. 374, pp. 472-483.
8. Lysenko I. A., 1963, Air Streams in the Meteor Zone From Meteor Radar Observations, *Astron. Journal*, Vol. 40, No. 1, pp. 121-126.
9. Kashcheev B. L., Lebedinets V. N., Lagutin M. F., 1967, *Meteor Phenomena in the Earth's Atmosphere*, Nauka Publishers, Moscow.

LONGITUDINAL PECULIARITIES OF MERIDIONAL CIRCULATION
IN LOWER THERMOSPHERE AND MESOSPHERE

R. B. Bekbasarov, K. A. Karimov, and M. A. Takyrbashev

Institute of Physics
Frunze, USSR

Figure 1 presents average monthly longitudinal profiles of geostrophic wind in winter. Positive values correspond to meridional movements from north to south. The figure shows that the zonally averaged values of the meridional component of the wind velocity \bar{V} are close to zero. At the same time there are considerable meridional movements with average monthly speed maxima of 70-80 mps, especially at great altitudes and in high latitudes. The presence of sectors where meridional flows preserve their directions in the course of time comparable with a synoptical period is noted in all longitudinal profiles of the distribution of $V(\lambda)$. The sector boundaries are subject to insignificant monthly variations.

On the average mutually equivalent dispositions of sectors with prevailing meridional flows were observed each month on constant pressure surfaces. Fig. 2 shows an example of such a disposition of these sectors at the level of 0.4 mb. Sharp shifts of sector boundaries are normally limited to, and coincide in time with, stratomesospheric warmings.

Thus, it can be concluded that the normal longitudinal meridional circulation is characterized by the presence of sectors where meridional flows do not change their direction in the course of time comparable with synoptical periods.

Fig. 3 presents the longitudinal distribution of meridional wind in middle latitudes taken from the analysis results of radiometeor and ionospheric stations (Atlanta, Garchy, Dushanbe, Irkutsk, Kuhlungsborn and Frunze) observational data obtained in 1976-1980. Positive values correspond to winds from south to north. The winter period is divided into a relatively undisturbed period (November-December) and a disturbed period (January-February).

As is seen from the figure, meridional winds have a longitudinal variability that is equivalent to both the warm and cold half years. Annual variability of the meridional wind component as follows from the results obtained in Frunze and Atlanta is shown in Fig. 4. The results presented in Figures 3 and 4 show that large scale quasistationary disturbances of the circulatory regime that determine its longitudinal differences exist both in the lower thermosphere and in the stratomesosphere.

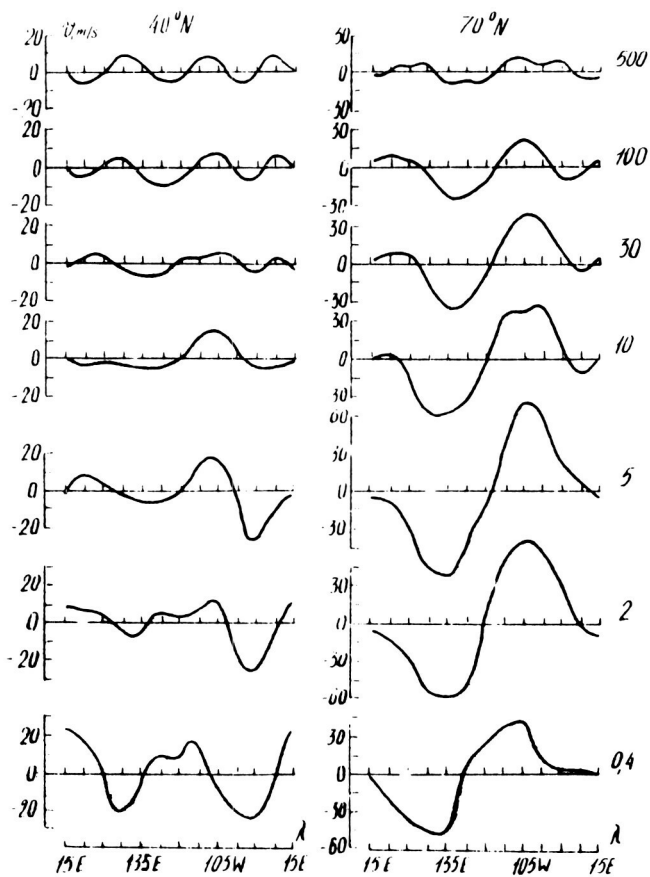


Fig. 1 Longitudinal variation of the monthly mean meridional geostrophic wind v for 500 to 0.4 mb surfaces at latitudes 40°N and 70°N . Positive values denote northerly winds.

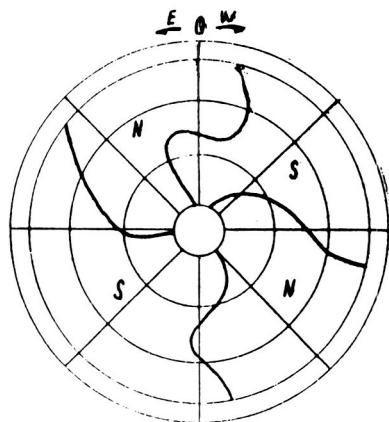


Fig. 2 Sectors of prevailing northerly N and southerly S flows over the northern hemisphere at 0.4 mb.

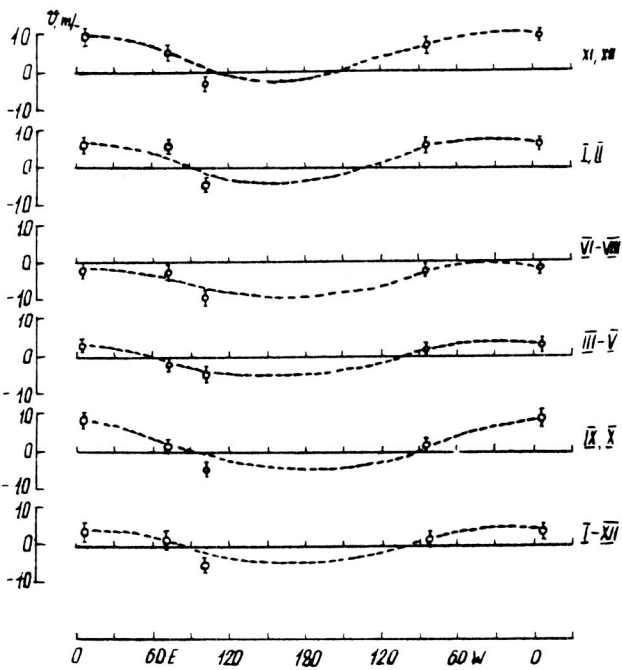


Fig. 3 Seasonal and annual means of average prevailing meridional wind at 95 km as measured at, from left, Garchy, Frunze, Irkutsk, and Atlanta for the year 1976-80. Positive values denote southerly winds.

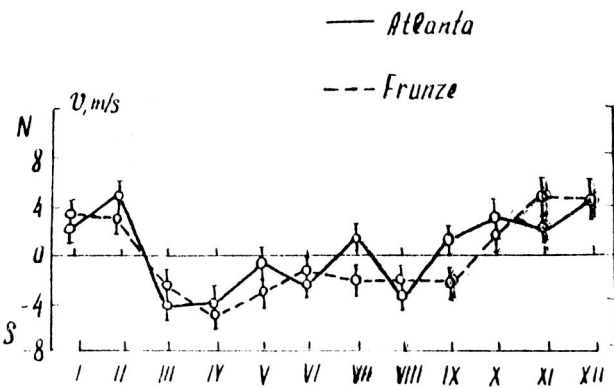


Fig. 4 Seasonal variation of mean meridional winds at 95 km over Atlanta and Frunze.

LOWER THERMOSPHERE WIND REGIME ACCORDING TO RADIOMETEOR MEASUREMENTS IN KAZAN

V. V. Sidorov, A. N. Fahrutdinova, and V. A. Makarov

Kazan State University
Kazan, USSR

Research in dynamic processes in the lower thermosphere has been carried out in Kazan using the meteor radar facilities of the Kazan State University under the MAP-GLOBMET international program.

This report presents experimental data on seasonal dependences of the wind for anomalous winter circulation periods, spring and autumn reconstructions and stable summer circulation from observations conducted in 1978-1984. Figures 1 and 2 show the prevailing wind parameters: zonal A_{QEW} and meridional A_{ONS} component amplitudes and A_0 and azimuth of the prevailing wind vector. Figures 3, 4, and 5 present the values of semidiurnal zonal A_{2EW} and meridional A_{2NS} tidal components, their correlation coefficient ρ and zonal component amplitude maximum time t_2 .

According to these observations, there are the following main regularities. The anomalous winter circulation period is characterized by frequent reversals of both zonal and meridional wind components, semidiurnal tidal amplitude disturbances and by increased random wind fluctuations. The summer period has a stable circulation with minimal turbulent motion. During the periods of spring and autumn reconstruction, transition from one to the other of the two main systems of circulation (summer and winter) is observed. In the meteor zone of the lower thermosphere a more pronounced zonal circulation is observed. The relation of prevailing wind zonal and meridional components amplitudes U_0/V_0 varies from about 7 to 75% in different years and seasons. The greatest interannual scatter of prevailing wind parameters is observed in winter, spring and autumn periods, interannual scatter being more pronounced for the zonal component.

In semidiurnal influx behavior there is observed the tendency of amplitude increase from summer to winter, common for all the considered years of observations when the values A_{2EW} , A_{2NS} change from about 10 mps to 30 mps, correspondingly. The greatest differences of disturbing processes affecting the semidiurnal influx are observed during the spring and winter period and they are manifested in seasonal variation of the parameter ρ and maximum time differences of semidiurnal influx zonal and meridional component.

Meteorological scale disturbances are observed in time variations of all wind parameters in meteor altitudes for all seasons, the seasonal wind parameters changes exceeding interannual scattering.

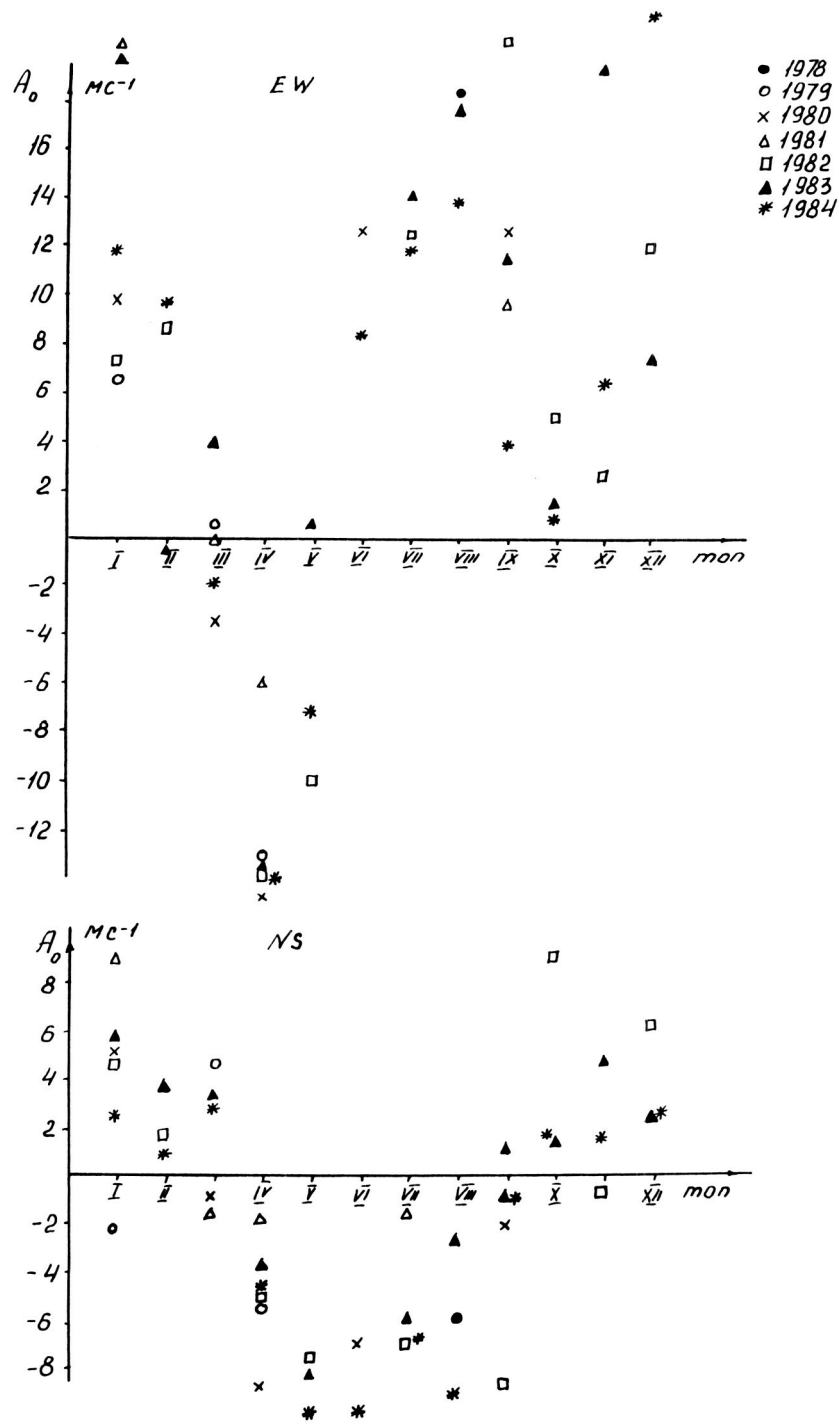


Fig. 1 Seasonal and interannual variations of the zonal A_{QEW} and meridional A_{OWNS} components of the prevailing wind.

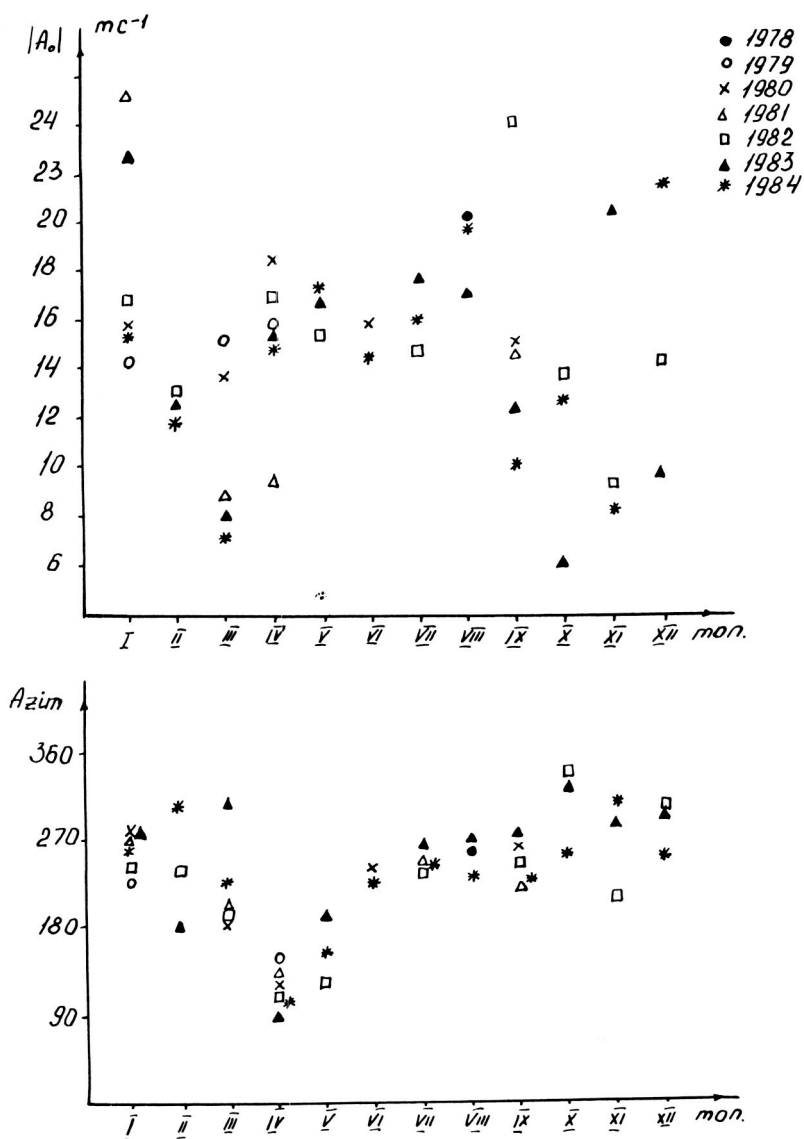


Fig. 2 Seasonal and interannual variations of the amplitude A_0 and azimuth of the prevailing wind vector.

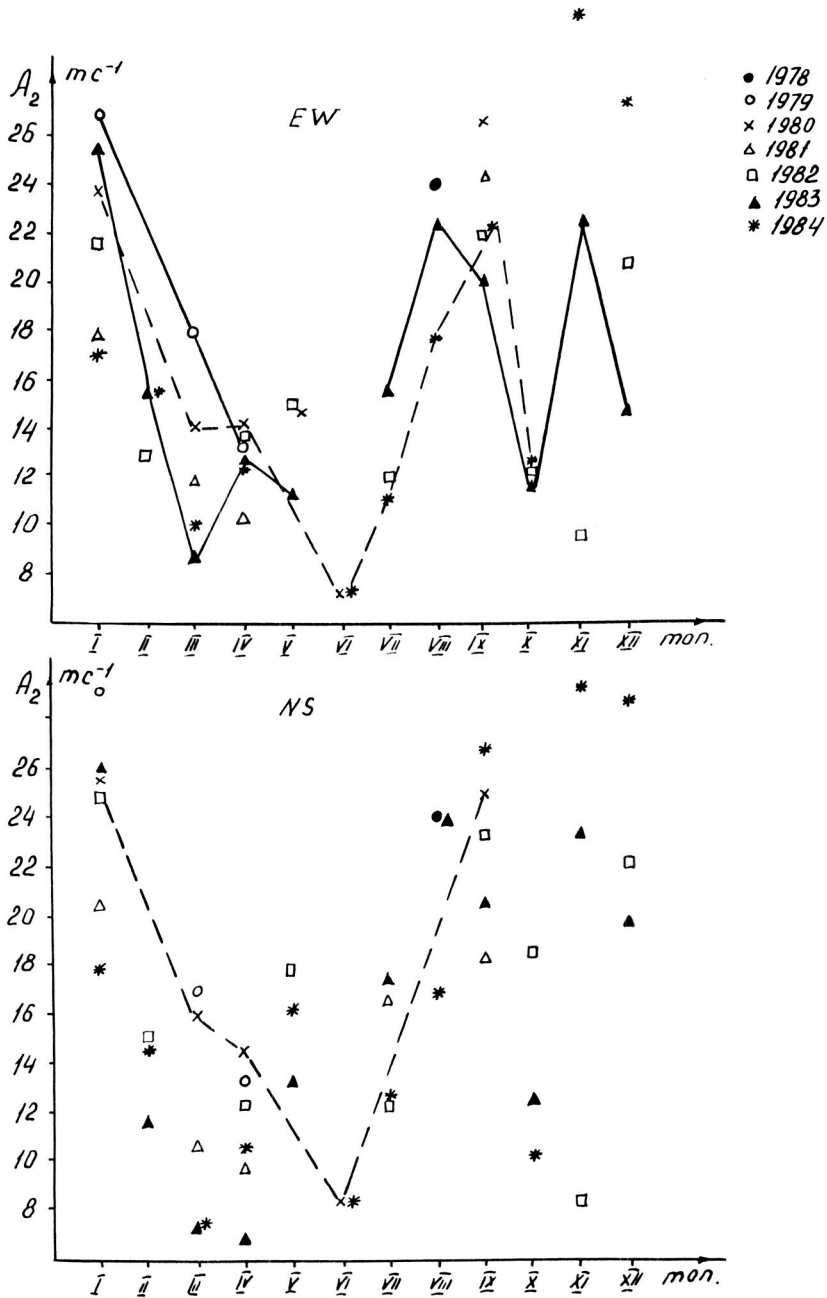


Fig. 3 Seasonal and interannual amplitude variations of the zonal A_{2EW} and meridional A_{2NS} components of the semidiurnal tide.

ORIGINAL PAGE IS
OF POOR QUALITY

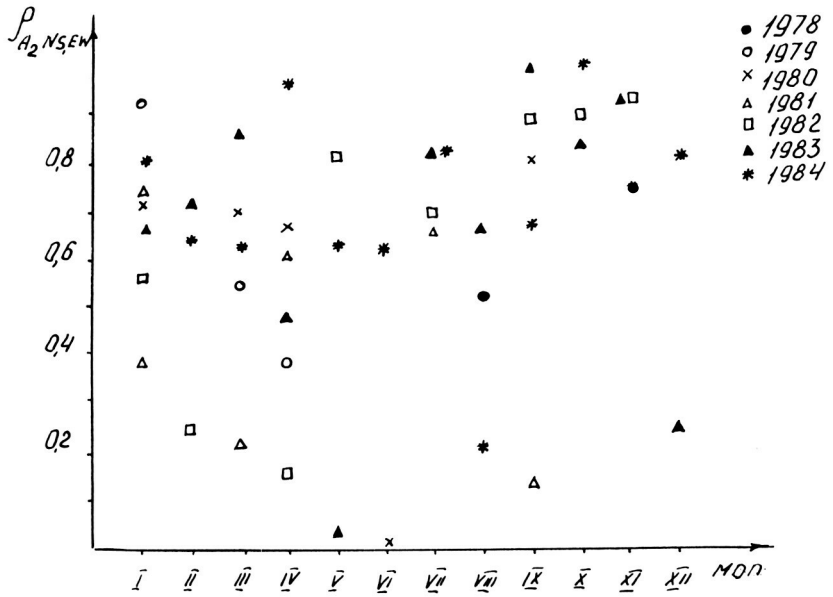


Fig. 4 Seasonal and interannual variations of the semidiurnal tidal zonal and meridional component correlation coefficient.

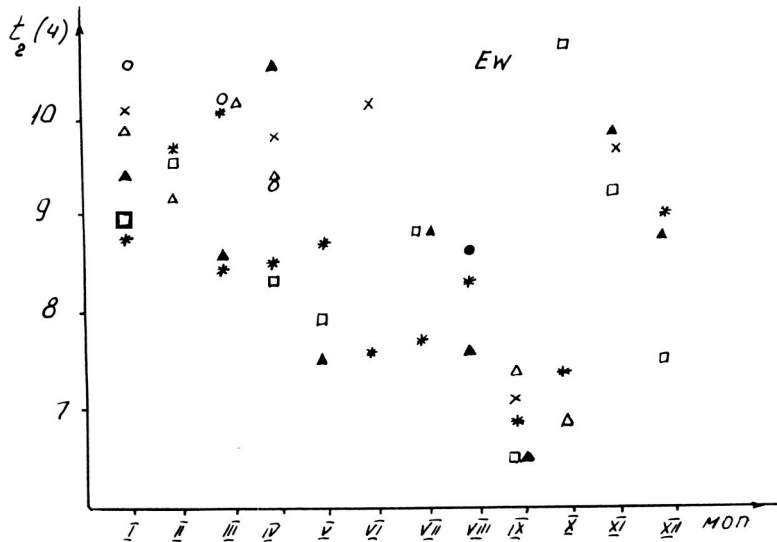


Fig. 5 Seasonal and interannual variations of the time of maximum amplitude of the zonal component of the semidiurnal tide.

ORIGINAL PAGE IS
OF POOR QUALITY

ATMOSPHERE DYNAMIC PROCESSES STRUCTURE AT 80-105 KM ALTITUDE

B. V. Kalchenko and A. N. Oleinikov

Institute of Radioelectronics
Kharkov, USSR

Determination of wind velocity by means of Doppler meteor radars is based on the assumption that an ionized meteor trail drifts together with the neutral atmosphere. From the Doppler frequency shift it is possible to estimate the radial velocity of the trail drift V_{Ri} .

Conversion of the recorded radial velocity to the true wind velocity vector in the given space region depends both on the radar technical parameters and the chosen atmospheric motion model. The best results can be obtained if the radar measures θ_i , the azimuth of the reflecting point i , ϵ_i , the reflection point elevation angle and h_i , the altitude of the reflecting point on the meteor trail for every meteor trail. Such a radar has been used by the authors (ZHUKOV, et al., 1978).

The wind velocity vector can be represented by its projections i.e., by meridional, zonal and vertical velocity components.

$$\vec{W}(t, h) = \vec{i}V_N(t, h) + \vec{j}V_E(t, h) + \vec{k}V_H(t, h)$$

Theoretical data on the velocity of vertical movement of atmospheric layers are contradictory (SEMENOVSKY, 1974; GUBIN V. I., 1972; KHANTADZE, 1979). In general, we shall consider models characterized by zero vertical velocity. Numerous experimental data obtained by different methods show the presence of significant vertical gradients in the horizontal wind dV/dh . Thus, the meridional and zonal components of wind velocity can be presented by the following formulae:

$$V_N(t, h) = V_{NO} + \frac{dV_N}{dh} (h_i - h_o);$$

$$V_E(t, h) = V_{EO} + \frac{dV_E}{dh} (h_i - h_o),$$

where V_{NO} , V_{EO} are mean values of the meridional and zonal wind velocity at the medium altitude h_o of a certain meteor measuring region.

The meteor zone is characterized by a wide wave motion spectrum and is generally turbulent. The spread of individual velocity values measured during an hour, has, characteristically, a standard deviation $\sigma = 30$ m sec⁻¹. Estimates of wind velocity are obtained using statistical methods. It is assumed in this case that during the averaged time (most commonly one hour) the parameters V_{NO} , V_{EO} , dV_N/dh , dV_E/dh and V_H do not change and characterize some mean value for the time Δt in the atmospheric layers located in the altitude interval Δh . The value of Δh is determined from measurement statistics. It is assumed that V_H does not change in the considered altitude region Δh .

When processing the observations made for December 13-27, 1983, acceptable intervals were $\Delta t = 1$ hour, $\Delta h = 6$ km, with aerials being directed northwards. In addition, the results for all the meteor echoes

were analyzed without separating them according to altitude. The average experimental altitude over the entire meteor zone was 92,5 km. In spaced six-kilometre intervals (84-90 km, 90-96 km and 96-102 km) the average altitudes were 87,3 km, 93,0 km and 98,5 km.

Fig. 1 shows the sliding average two day velocities of zonal, meridional and vertical wind in three altitude ranges. The data obtained show that the zonal circulation reversal began in the higher atmospheric layers first. The meridional and vertical velocities exhibit a tendency to inverse correlation, i.e., our results confirm the theoretical conclusions of GUBIN (1972) and KHANTADZE (1979).

Fig. 2 shows the day by day variations of the vertical gradient of the horizontal wind velocity in the zonal and meridional directions. Averaging over the whole of the meteor zone, the mean gradient of velocity in both directions amounts to $1 \text{ msec}^{-1} \text{ km}^{-1}$ and testifies to the presence of a nine-day wave whose phases for the two directions differ by $56,6^\circ$. The gradient value reached about $8 \text{ msec}^{-1} \text{ km}^{-1}$ when the height range was divided into six-kilometre intervals. The radar characteristics insure IGW identification with the following limiting parameters: $\lambda \geq 100 \text{ km}$, $\lambda_z \geq 8 \text{ km}$, $T > 30 \text{ min}$. In determining IGW parameters, the radio meteor observations undergo special processing, including spatial stratification of the meteor data, low and high frequency filtering of time series of horizontal wind velocity and spectral analysis. Identification of IGW oscillations is carried out from consideration of all of the above.

Using the above scheme, measurements over three intervals of meteor trails drift observations (December 17-19, 1978; July 23-August 2, 1982; December 13-27, 1983) have been processed.

In the meteor zone the spectra of meridional and zonal wind velocities were very unsteady both in time and in space. Several cases of a sharp change in the wind velocity spectrum above 90-92 km were observed. For most of the IGW the change of their amplitude with altitude, notwithstanding the general tendency for the amplitude increase, is oscillatory in character. Amplitudes of identified IGW fall within the limits of $5\text{-}30 \text{ m sec}^{-1}$, the mean value being $12\text{-}15 \text{ m sec}^{-1}$. The phase and altitude characteristics of IGW accompanied by a quasi-linear change of wave phase with altitude can be divided into three main types; increasing, decaying and broken. The phase changes with altitude and time of the waves indicates vertical wave energy propagation. The vertical wave length of over half of all the measured IGW varied within 8-30 km, the wavelength in 70% of the waves exceeding 20 km. Typical values of the meridional components of the horizontal wave length and the phase propagation velocity were 100-800 km and 20-140 m sec^{-1} respectively. Fig. 3 shows histograms of the distribution of frequency, meridional component amplitude, horizontal phase velocity, vertical wave length and the IGW vertical flux of energy.

Particularly noteworthy are cases of IGW behaviour at meteor heights revealed by the analyses of vertical profiles of wind velocity spectra and the wave amplitude and phase variations with altitude. These waves primarily decay, and are generated in the altitude interval under consideration.

Also observed were cases when the phase and amplitude of wind velocity disturbances with quasi-linear altitude change in the upper and lower

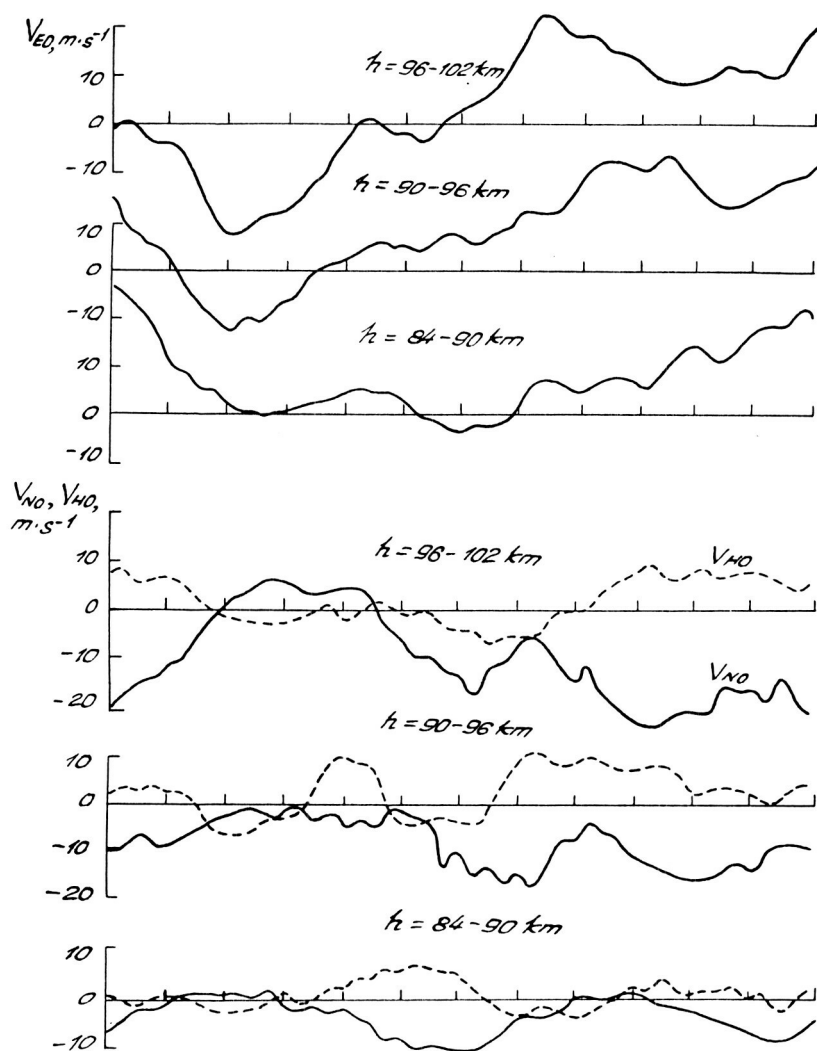


Fig. 1 Sliding two day mean velocities of zonal V_{EO} , meridional V_{NO} and vertical V_{HO} winds over Kharkov for December 13-27, 1983.

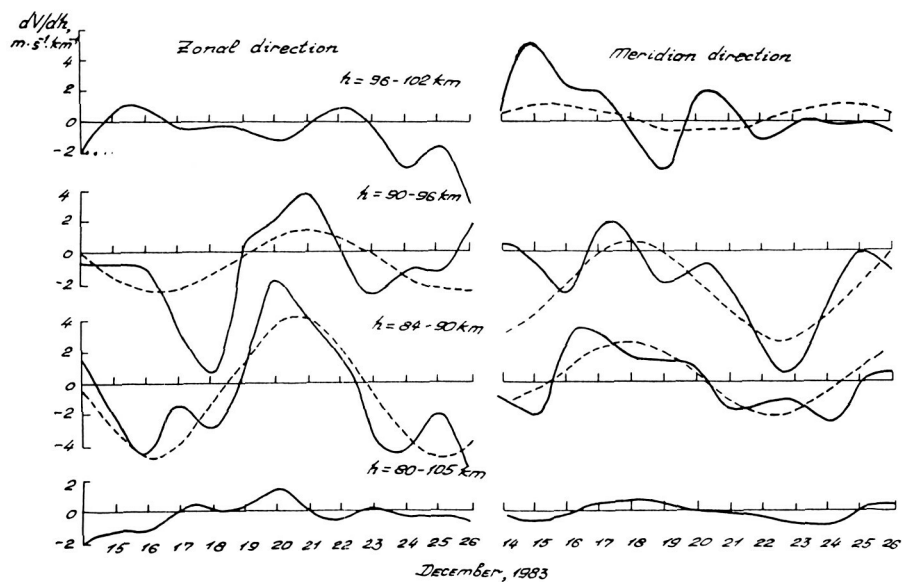


Fig. 2 Day-by-day variations of the vertical gradient of the horizontal zonal and meridional wind (—); the presence of a nine-day wave (---) is obvious.

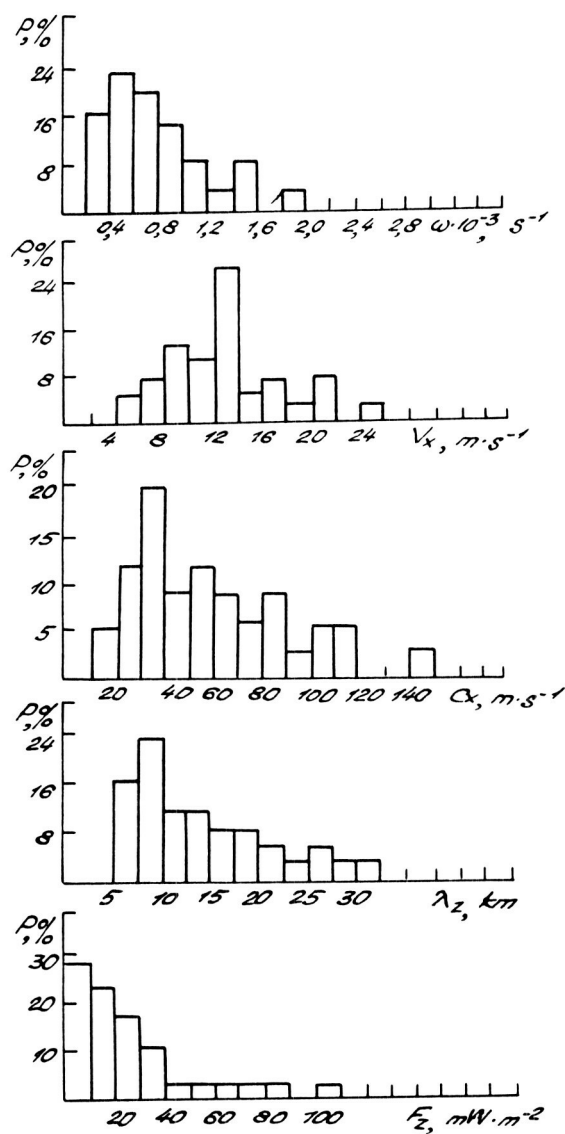


Fig. 3 Distribution of frequency ω , meridional component amplitude V_x , horizontal phase velocity C_x , vertical wavelength λ_z and the vertical flux of energy F_z of internal gravity waves in the meteor region over Kharkov, expressed as a percentage of occurrence.

meteor zone regions undergo a characteristic disruption in middle altitudes. Such behaviour of phase and amplitude characteristics is evidence of wave-wave interaction.

The cases of IGW decay and generation described above are typical of the meteor zone as we have observed it.

References

1. Zhukov V. V., Oleinikov A. N., Oleinikov V. N., 1978, Automatic Goniometer, Communication II, Signals pre-processing, in Collection Radiotekhnika, Kharkov, Vol. 47, pp. 9-14.
2. Semenovskiy Yu. V., 1974, Theoretical estimate of wind vertical velocity in the meteor zone, Transactions of the Institute of Experimental Meteorology, Moscow, Iss. 2, 47, pp. 42-46.
3. Gubin V.I., 1972, On wind velocity components, in Meteorologiya i Gidrologiya, Moscow, No. 7, pp. 3-6.
4. Khantadze A.G., 1979, On a mechanism of wind vertical velocity generation in ionosphere, in Geomagnetizm i Aeronomiya, No. 4, Vol. 19.

INTERNAL GRAVITY WAVES IN THE METEOR ZONE IN THE TBILISI REGION

Z. S. Sharadze, G. B. Kikhvilashvili, Z. L. Liadze, and N. V. Mosashvili

Tbilisi State University
Tbilisi, USSR

The study of wave disturbances (WD) in the upper part of the meteor zone (90-110 km) was made in the Tbilisi region. Observations were conducted using three ionospheric vertical sounders located at the corners of a triangle spaced from each other at a distance of 50 km, a four-azimuth electrophotometer by the method of spaced reception with a small distance (method D1) and a recording unit f_D .

Simultaneous round-the-clock observations using the three spaced ionosondes were carried out each season in 1980-83 and in January, 1984, and lasted for as long as 12-14 days. The stations operated in 1- or 5-minute averaging modes. Daily variations of the parameters f_{E_s} (blanketing frequency of the layer E), f_{E_b} (critical frequency of an ordinary ray in the layer E), Δf_E ($\Delta f_E = f_{E_b} - f_{E_s}$ is the semi-transparency of the E layer) were analyzed. WD of the layer E ionization caused by internal gravity waves (IGW) appear in the form of short-period fluctuations of the mentioned parameters shifted in time over the spaced points of observation.

The most intensive short-period variations of f_{E_s} , f_{E_b} and Δf_E are observed in summer near 90-110 km. Period (T), horizontal velocity (V) and wavelength (λ) of the IGWs were determined by the cross-spectral analysis of daily variations of f_{E_s} , f_{E_b} and Δf_E which were recorded simultaneously at the three observation points.

The IGW parameters (T, V, λ) for each season of 1980-1983 determined by quasi-periodic variations of f_{E_s} and f_{E_b} are shown in the form of histograms in Fig. 1. It is seen that IGW with periods of 10-20 and 70-90 min prevail. In spring and summer the most probable values of IGW periods lie within the intervals of 20-60 and 30-90 min, respectively. In autumn IGW with periods of 50-90 min dominate. In all seasons the prevailing velocities of IGW in the meteor zone are 25-100 mps and their wavelengths (excepting the summer season) are 50-100 km. In summer, IGW of greater wavelength lying in the interval of 50-250 km occur.

With the aim of finding daily variations of the direction of WD propagation for each season, velocity azimuths (ϕ) were grouped by six-hour intervals (00.00-06.00, 06.00-12.00, 12.00-18.00, 18.00-24.00 h LT) which are presented in the form of histogram in Fig. 1. In winter, in the daytime before noon WD propagate in the north-west direction, while in the afternoon they propagate in the southeast direction; at night, until midnight, WD move southwards. In spring, in the daytime until noon disturbances travel in the south-east direction and in the afternoon - in the north-west direction; at night, until midnight, disturbances propagate south-eastwards and, after midnight - south-westwards. In summer, in the daytime until noon disturbances propagate mainly in the south-west direction and, in the afternoon - in the south-east direction; at night,

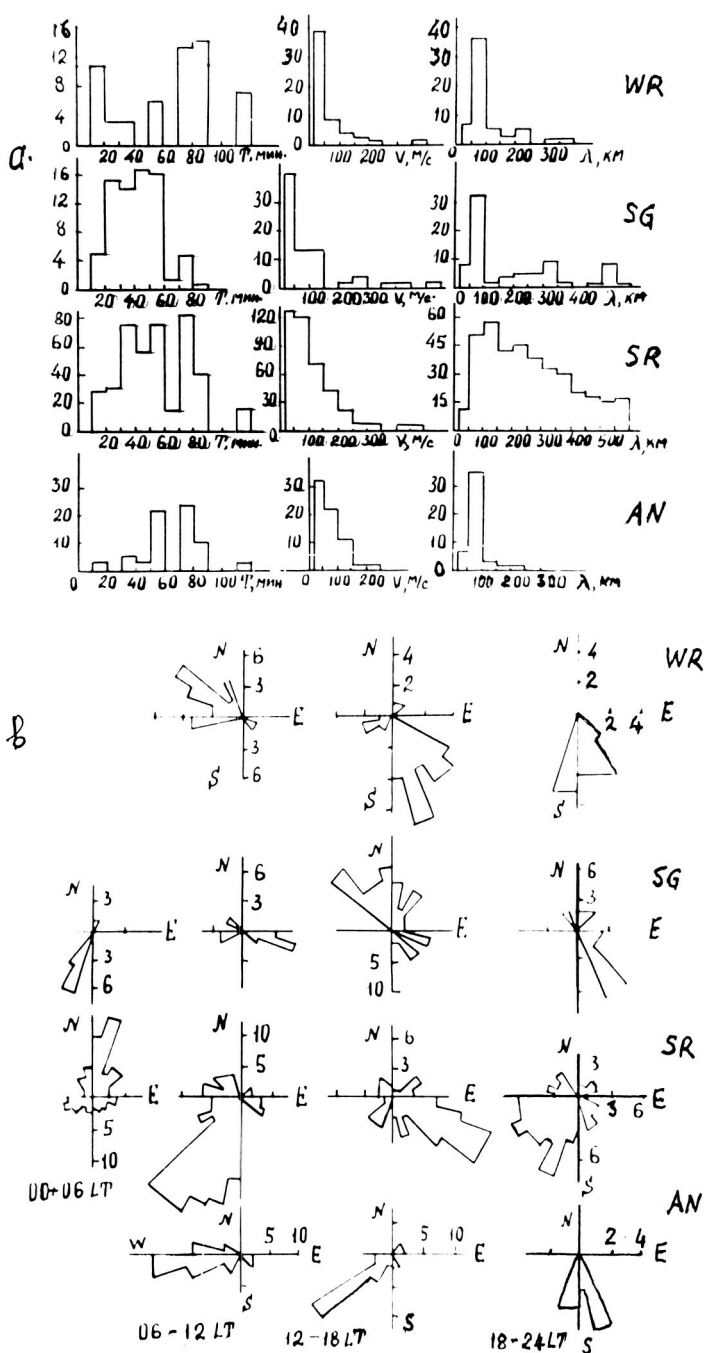


Fig. 1 The parameters (T , V , λ) of IGW for each season of 1980-1983 calculated by quasi-periodic variations of f_{oE_s} and f_{hE_s} , (a), and daily variations of WD propagation direction for different seasons of the year, (b). WR-winter, SG-spring, SR-summer, AN-autumn.

until midnight, WD propagation in the south-west direction prevails, and after midnight WD propagating in the north-east direction are mainly observed. In autumn, in the daytime, WD travel westwards and southwestwards; and at night, until midnight, disturbances travel southeastwards.

From variations of $\Delta f E_s$, we find that IGW with periods of 60-90 and 12-17 min occur most frequently. Horizontal velocities and lengths change mainly in the intervals of 12-100 mps and 25-125 km respectively. IGW propagate mainly in the south-west direction in the daytime and in the east-west or north direction at night.

Data obtained by simultaneous observations of WD and wind were used to study the dependence of WD propagation orientation on the background wind. WD propagate mainly crosswise to the wind, though there are cases when they propagate both crosswise and almost down the wind. Velocity values of WD and wind are of the same order while the prevailing directions differ by about 90-120°.

The parameters of medium-scale ($\lambda \leq 1,000$ km) WD in the meteor zone at night, calculated by variations of the emission intensity [01] 5577A, are given in Fig. 2. Measurements by means of a four-azimuth electrophotometer were performed in the winter period of 1980-1983. It is seen that disturbances propagating mainly in the west, south-west and south-east directions and having velocities of 200-400 mps prevail. The spectrum of measured WD has a linear character. The main harmonics have periods of 30-60 min, 7.5-10 min, and about 5 min. Horizontal wavelengths of the most frequently recorded disturbances lie within the interval of 50-200 km.

With a view to finding the role played by IGW in wind velocity variations near 100 km, long continuous (30-90 min and more) sessions of wind measurements were performed using the D_1 method. Wind velocities were determined by the similarity method every 1 or 5 min. In the wind, IGW appear first of all in the form of non-regular, short-period (~ 5 -180 min) variations of wind velocity imposed on regular wind velocity variations. The amplitude (root-mean-square deviation of wind velocity) of short-period variations of east-west ($V_x(t)$) and north-south ($V_y(t)$) components of wind velocity changes in the interval of 2.5-105 mps, with the most probable values in the interval from 10 to 45 mps. The most intensive variations of $V(t)$ are observed near 100-110 km where the critical value for IGW is expected.

The most intensive variations of the wind are accompanied by the appearance of E_s layers with the parameters $f_o E_s$, $f_h E_s$ and $\Delta f E_s$ changing periodically. The relation between variations of $V(t)$ and the E_s layer ionization confirms the reality of short-period variations of wind velocity in the geophysical sense and points to the fact that IGW disturbances influence the formation and development of E_s layers.

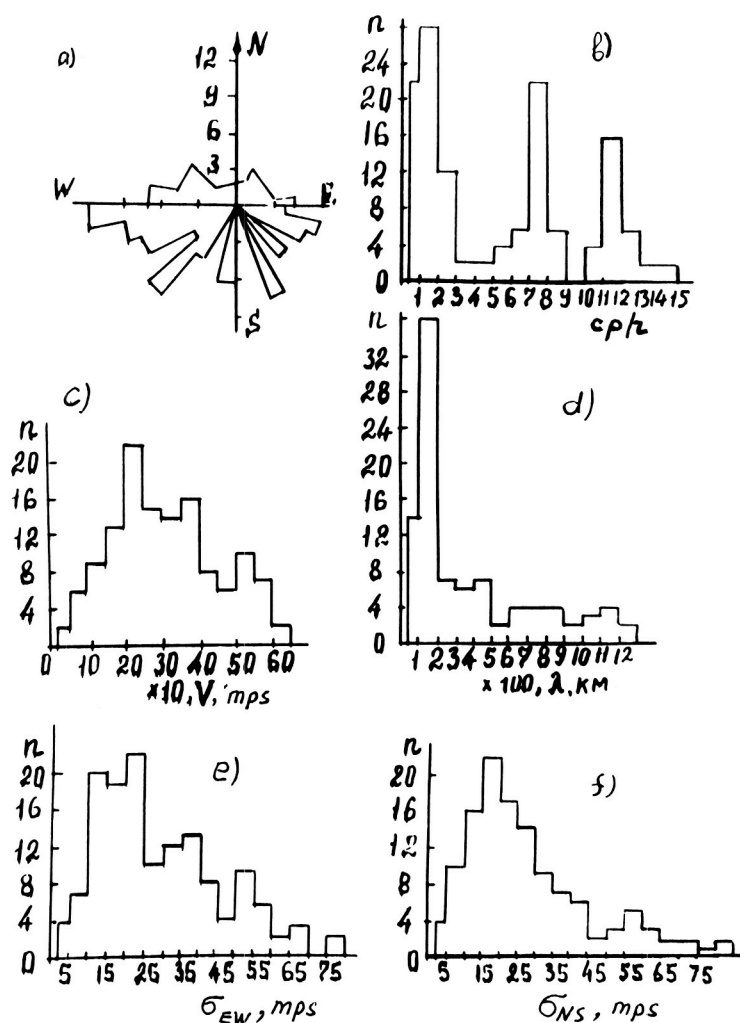


Fig. 2 The parameters of medium-scale WD determined by intensity variations of emission OI 5577 (a-d). Histograms of the distribution of root-mean-square deviations of zonal and meridional winds related to IGW (e,f).

MESOSCALE DENSITY VARIABILITY IN THE MESOSPHERE AND THERMOSPHERE:
EFFECTS OF VERTICAL FLOW ACCELERATIONS

D. O. ReVelle

Meteorology Program, Northern Illinois University
DeKalb, Illinois 60115 USA

A mechanistic one-dimensional numerical (iterative) model has been developed which can be used to simulate specific types of mesoscale atmospheric density (and pressure) variability in the mesosphere and the thermosphere, namely those due to waves (see below) and those due to vertical flow accelerations. i.e., quasi-static flow effects. The model was developed with the idea that it could be used as a supplement to the TGCMs (thermospheric general circulation models) since such models have a very limited ability to model phenomena on small spatial scales. The details of the model formulation can now be evaluated since observations indicate that quite large vertical flow accelerations exist in the disturbed high latitude thermosphere (ROBLE, 1983). The horizontal scales for which such effects are potentially possible have been calculated using the methods of SMITH (1980) and are equivalent to those developed by REVELLE (1987a). Depending on the thermal structure and on the mean horizontal winds, the mesoscale effects can influence a region approaching 500 km across under extreme conditions. More typically, however, the maximum horizontal scale where quasi-static conditions apply, are in the range from 50 to 120 km. Calculations for the mean troposphere using these methods indicate that the corresponding maximum values for the mesoscale regime are in the range from 1 to 50 km, with the latter being an extreme value.

The steady flow, inviscid model equations used satisfy the combined constraints of conservation of mass, linear momentum and of energy on a middle latitude f plane. They represent a set of equations similar to, but more general than, those developed by GHOSH (1970). As discussed in REVELLE (1987a), the equations developed apply not to wave effects on the hydrostatic mean flow, but rather to those of a vertically accelerated mean flow, i.e., a state of quasi-static balance. The corresponding effects of a noninteracting, linearized plane wave model have been calculated in REVELLE (1987b) in the internal acoustic-gravity wave part of the spectrum in the high and low frequency limits, respectively. In the latter, only wave amplitude was considered and wave sources were parameterized in the troposphere using a modified form of geostrophic adjustment theory.

The simplest case to consider was the integration upward through a time-averaged, height independent, horizontally divergent flow field. This situation was chosen in part because an analytic solution was derived for this case (in height coordinates) which could be used as a check on the validity of the numerical results. This was important since small vertical height steps were necessary in order to reliably integrate the resulting equations. Vertical winds were initialized at the lower boundary using the Ekman pumping theory over flat terrain.

The results of the computations can be summarized as follows:

a) Accelerating updrafts lower the air density (pressure) relative to the static case and vice versa. Nonaccelerated vertical flow does not influence the hydrostatically computed density (pressure) structure.

b) Unless vertical winds are very large, dynamical density (pressure) variations are virtually identical to each other. (See also e) below.)

c) The degree of density (pressure) change predicted with respect to the static reference state depends significantly on the local gas temperature. Vertical flow accelerations produce the maximum effect in regions of minimum atmospheric temperature (See also e) below.)

d) The minimum vertical wind speed necessary to significantly modify the density structure in the mesosphere and the thermosphere is about 50 m/s. For vertical winds approaching 250 m/s, density changes of about ± 20 percent maximum can occur.

e) An instability is predicted as the vertical wind approaches the isothermal acoustic wave speed. This could occur at the point where the vertical kinetic energy/mass equals or exceeds the atmospheric potential energy/mass in an inviscid fluid. Current observations indicate that the latter possibility is highly unlikely to occur.

In the current calculations, only mechanistic solutions were used, i.e., formal solutions of the energy equation were not used to constrain the results. Such constraints are necessary in general however so that vertical motions can compensate for any net heating/cooling effects in the steady flow limit. In this region of the atmosphere a combination of thermal conduction, radiation, joule heating, horizontal transport of heat and wave dissipation effects, etc. would need to be considered in any realistic thermal balance computation. Instead, the net heating/cooling rate necessary to maintain a steady state with vertical winds was determined. If this net heating/cooling field could be considered realistic in terms of values determined from various energy budget estimates (for example, during a substorm joule heating rates in excess of 1000 deg K/hr have been reported) then the effects of such accelerated flow on the statically computed reference state was considered reliable. Note that in a major heating event the static density (pressure) profile will also change significantly in general. Such effects have not been considered here. The reference state used was the U.S. Standard Atmosphere 1976 which is likely to differ from a mean disturbed state, but especially above about 150 km. Since in this latter region the changes predicted are relatively small due to the elevated gas temperatures, these static changes are probably not of great significance with respect to the currently predicted mesoscale quasi-static changes.

Although much work remains to be done, it would appear that the method is useful with regard to simulating density variability effects in the mesoscale range that cannot currently be addressed using either the TGCMS (see, for example, DICKINSON et al., 1981) or by using modified static diffusion models (see, for example, BARLIER and BERGER, 1983). This work was carried out in support of various NASA projects in this height regime including, but not limited to those of the shuttle, AOTV, Space Station, VARS, etc...

REFERENCES

1. Barlier, F. and C. Berger, A point of view on semi-empirical thermosphere models, *Planet. Space Sci.*, 31, 945-966, 1983.
2. Dickinson, R. E., E. C. Ridley, and R. G. Roble, A three-dimensional general circulation model of the thermosphere, *J. Geophys. Res.*, 86, 1499-1512, 1981.
3. Ghosh, S. N., Effect of motion on the altitude distribution of atmospheric density, *Ann. Geophys.*, 26, 795-799, 1970.
4. ReVelle, D. O., Estimation of dynamical density and pressure variability in the atmosphere: A one-dimensional vertical flow acceleration model, Submitted to *J. Geophys. Res.*, 1987a.
5. ReVelle, D. O., Dynamic density variability of the mesosphere and the thermosphere, Final Report, Universities Space Research Association, Boulder, Colorado, 1987b.
6. Roble, R. G., Dynamics of the earth's thermosphere, *Rev. Geophys. Space Phys.* 21, 217-33, 1983.
7. Smith, R. B., Linear theory of stratified hydrostatic flow past an isolated mountain, *Tellus*, 32, 348-364, 1980.

ON THE WAVE EXCITATION IN THE TURBULENT METEOR TRACE

G.V. Jandieri, G. Sh. Kevanishvili and V.I. Lenin

Polytechnical Institute
Georgia, USSR

The solution to the problem of excitation of longitudinal and transverse electromagnetic waves in randomly inhomogeneous media is reduced to the derivation of a complex effective dielectric constant (EDC) tensor which non-locally connects together the average values of field and current. When speaking about the average macroscopic electromagnetic fields in continuous media, we imply that the field values which are rapidly fluctuating on a microscopic scale in space and time become smoothed out in a specified way due to the inhomogeneous mixing of diffusion.

Mean field longitudinal wave propagation in a turbulent, incompressible plasma flow of cold electrons, with the perturbed values of electron density and velocity changing both in space and time, has been investigated in the hydrodynamic approximation, (GAVRILENKO and JANDIERI, 1981). A model describing the polarization in terms of a continuous dispersing medium consisting of a set of homogeneously distributed electric dipole-oscillators with random natural frequencies changing both in space and time is suggested in JANDIERI et al. (1986). Proceeding from the derived general expression for the EDC tensor new modes of longitudinal and transverse electromagnetic wave generation due to fluctuation in the parameters of the medium has been predicted. In this connection, it is of interest to investigate the peculiarities of electromagnetic longitudinal and transverse wave propagation in such randomly inhomogeneous media where, apart from the charged particle concentration change, the random spatial and temporal changes of natural frequency of closely located oscillators take place.

Suppose the inhomogeneous "system" possesses a natural oscillation frequency ω_0 prior to the passage of a body with a finite mass. After the meteor passage through the spatial region under consideration, the system becomes excited and begins to oscillate with a frequency which is, in the general case, a random fluctuation of spatial coordinates and time

$$\Omega^2(\vec{r}, t) = \omega_0^2 + \gamma^2(\vec{r}, t) \quad (1)$$

The latter term γ^2 , leads to a temporal polarization change and to the generation of longitudinal and transverse electromagnetic waves in the inhomogeneous turbulent meteor trace.

The initial system for the solution of the given problem is a closed one consisting of the electric field strength wave equation and the equation of a harmonic oscillator with randomly varying natural frequency $\Omega(\vec{r}, t)$:

$$\text{rot rot } \vec{E}(\vec{r}, t) \frac{1}{c^2} \frac{\partial^2 \vec{E}}{\partial t^2} = - \frac{4\pi \cdot \partial \vec{J}}{c^2 \partial t}$$

$$\ddot{\vec{S}}(\vec{r}, t) + \Omega^2(\vec{r}, t) \vec{S}(\vec{r}, t) = \frac{e_q}{m^*} \vec{E}(\vec{r}, t) \quad (2)$$

$$\vec{J}(\vec{r}, t) = e_q N(\vec{r}, t) \dot{\vec{S}}(\vec{r}, t)$$

where e and m^* are the oscillator "effective" charge and reduced mass, $\vec{S}(\vec{r}, t)^q$ is the "effective" charge displacement from their equilibrium positions, $N(\vec{r}, t)$ is the density of dipole-oscillators formed due to positive and negative "effective" charge displacements from their equilibrium positions by the local electric field $\vec{E}(\vec{r}, t)$ and $\vec{J}(\vec{r}, t)$ is the polarization current density.

Following the usual procedure of the perturbation method, we represent all the values as a sum of two terms - an average plus a fluctuating one. If it is further assumed that the perturbed parts (considered as small) of fields and currents are characterized by zero averages so that

$$\begin{aligned} \vec{E}(\vec{r}, t) &= \langle \vec{E}(\vec{r}, t) \rangle + \vec{E}_1(\vec{r}, t) = \vec{E}_1(\vec{r}, t) \\ \vec{S}(\vec{r}, t) &= \langle \vec{S}(\vec{r}, t) \rangle + \vec{S}_1(\vec{r}, t) = \vec{S}_1(\vec{r}, t) \\ \vec{N}(\vec{r}, t) &= \langle N \rangle + N_1(\vec{r}, t) = \vec{N}_1(\vec{r}, t) \end{aligned} \quad (3)$$

To find the EDC tensor of the randomly inhomogeneous medium under consideration, we use Kaner's method (KANER, 1959), while restricting ourselves to a case when the perturbed parts vary with time according to the harmonic law $\sim e^{-i\omega t}$.

In our further analysis of the derived EDC tensor, we use a correlation function having a Gaussian form $B(\rho) = e \exp(-\rho^2/\ell^2)$, where ℓ is the characteristic correlation radius of fluctuations of the frequency term $\gamma(\vec{r})$ and the electronic density of oscillators $N_1(\vec{r})$.

For the case of large-scale inhomogeneities, the full electromagnetic wave propagation in inhomogeneous medium is considered, its properties being described by an effective permeability $\epsilon_{ij}^{\text{eff}}(\omega, k)$. When the excited transverse wave frequency is close to the oscillator natural frequency ω_0 , the solution of the transverse wave dispersion equation $k^2 = \omega^2/C^2 \cdot \epsilon_{\text{eff}}^{\text{tr}}(\omega, k)$ results in two roots of the refractive index

$$n_{1\text{eff}}^{\text{tr}}(\omega) = \left(\frac{k\ell}{k_0} \right)^2 \sim \frac{\omega_p^2}{\omega_0^2 - \omega^2}, \quad n_{2\text{eff}}^{\text{tr}}(\omega) \sim \frac{3}{4} \omega_p^2 \frac{\omega^2 - \omega_0^2}{\langle \gamma^2 \rangle} \quad (4)$$

the first of them describes an ordinary transverse wave in the vicinity of the resonance (zero approximation), while the second takes into account the characteristic peculiarities of the inhomogeneous medium. Here ω_p stands for plasma frequency.

The longitudinal part of $\epsilon_{ij}^{\text{eff}}(\omega, k)$ may be calculated in a similar way. By solving the dispersion equation for longitudinal waves $\epsilon_{\text{eff}}^{\text{eff}}(\omega, k) = 0$, we may show that in the long-wave approximation, when $k_\ell C/\omega_p \ll 1$

$$\omega^2 = \Omega^2 - \frac{1}{3} \frac{\omega_p^2}{(\Omega^2 - \omega^2)^2} \left[\langle Y^2 \rangle - 2 \frac{\langle N_1 Y \rangle}{\langle N \rangle} (\omega_o^2 - \omega^2) + \frac{\langle N_1^2 \rangle}{\langle N \rangle^2} (\omega_o^2 - \omega^2)^2 \right] \left(\frac{k_e}{k_o} \right)^2 \quad (5)$$

where $\Omega^2 = \omega_o^2 + \omega_p^2$, $k_\ell^2 = k^2(1 + 1/k^2 \ell^2)$ is the new "effective" wave number. Assuming that $N_1 \neq 0$, we obtain the previously obtained result of JANDIERI et al., (1986).¹ With $\omega \approx \omega_o$, i.e. in the vicinity of the resonance, the density fluctuation contribution to the longitudinal wave excitation is negligibly small as compared with the frequency fluctuation. Taking into account absorption by means of formal substitution $\omega \rightarrow \omega - i J/2$ where J is the frequency correction for the attenuation of the oscillations of the oscillators proper, it may be easily proved by denoting real values of the wave vector $k \rightarrow k'$ and complex frequency $\omega = \omega' - i\omega''$ that the expressions for the group velocity and attenuation of propagating longitudinal waves are as follows:

$$\vec{V}_{gr} = \frac{\partial k_e \omega}{\partial k_\ell} = - \frac{1}{3} \frac{\langle Y^2 \rangle \vec{k}_e}{\omega_o k_o^2 \omega_\rho^2} \quad (6)$$

$$\text{Im } \omega = \frac{1}{6} J \frac{\langle Y^2 \rangle \Omega^2}{\omega_o^2 \omega_\rho^4} \left(\frac{k_e}{k_o} \right)^2 \quad (7)$$

Thus, we may conclude that in this case, the excited longitudinal waves are attenuated along the group velocity direction, the latter being anticollinear to the vector x direction.

According to (5), the presence of a correlation between the fluctuations of the charged particle density and the natural oscillation frequency, far from the resonance frequency, may change the direction of the excited longitudinal wave group velocity with respect to x , even to the extent of reversal. The latter may occur when the dispersions of the density and frequency fluctuations may turn out to be smaller than $\langle N_1 Y \rangle$. These relationships are valid only in case of weak absorption. Clearly, such plasma oscillations are characterized by dispersion.

The derived relationships may also be used to solve the inverse problem. By measuring the frequency and the wavelength of the propagating waves, we may obtain the characteristic scales of the fluctuations of the randomly inhomogeneous turbulent medium parameters.

References

1. Gavrilenko, V.G., Jandieri, G.V., 1981, Izvestiya VUSov (Radiophysics), Vol. 24, No. 10, p. 1211.
2. Jandieri, G.V., Gavrilenko, V.G., Gvelesiani, A.I., 1986, Physica Scripta (in press).

3. Kaner, E.A., 1959, Izvestiya VUSov (Radiophysics), Vol. 2, No. 5, p. 827.
4. Abramovich, B.S., Ryzhov, Yu, A., 1974, Izvestiya VUSov (Radiophysics), Vol. 17, No. 11, p. 1591.

METHODS AND FIRST RESULTS OF PLASMA NON-ISOTHERMAL
PARAMETERS MEASUREMENTS IN METEOR TRAILS

K. K. Kostylev and V. S. Tokhtashev

Kazan State University
Kazan, USSR

There is no reliable experimental evidence so far of either the presence or absence of non-isothermal effects in newly-formed meteor trails. Neither is there a common opinion on the most effective mechanism of electron cooling. According to the laboratory experimental data (BIDIN and DEMKOV, 1982), collisions of atomic and molecular particles of all kinds having velocities of $10\text{-}70\text{ km s}^{-1}$ often yields 1 eV electrons and not infrequently some have energies reaching several electron-volts. These highest energy electrons will be referred to as superhot electrons.

The mechanisms leading to electron energy losses in meteor trails are numerous (thermal conduction by ionospheric plasma electrons, diffusive cooling, elastic and non-elastic collisions of superhot electron with trail ions and neutral atmospheric particles), but each role is different. Diffusive cooling losses do not exceed 10-20% of the general electron energy. During the nighttime, thermal conductivity of ionospheric gas can be ignored. In meteor trails with linear electron densities $\alpha < 10^{12}$ el/cm, the plasma can be considered only slightly ionized and the electron cooling due to ion collisions may be ignored. If the conditions mentioned above are fulfilled, the energy balance equation for the electron component of the meteor trail plasma looks like:

$$\frac{3}{2} k n_e \frac{dT_e}{dt} = - \sum_n (L_{en}^o + L_{en}^*) \quad , \quad (1)$$

where n_e , T_e are concentration and effective temperature of electrons in trail, k is the Boltzman constant, and L_{en}^o , L_{en}^* is the electron cooling rate due to elastic losses and L_{en}^* is the non-elastic losses of energy through collisions with neutral atmosphere particles (atoms and molecules). Equation (1) was numerically solved for conditions covering the height interval of 80-115 km. The calculations included elastic collisions of electrons with N_2 , O_2 and O ; rotational and vibrational excitation of N_2 and O_2 molecules; electronic Δg and Σg excitation of O_2 molecules and D level of oxygen atoms as well as the O atomic fine structure excitation. The corresponding formulas for L_{en}^o and L_{en}^* are taken from STUBE and VARNUM (1972) and PRASAD and FURMAN (1973). Fig. 1 shows calculated results (over the height interval 90-100 km) for the electron thermalization time τ_T which is defined as the time required for the temperature to decrease from the initial value T_e down to a level 1.1 times greater than the neutral atmosphere particle temperature T_n . The numbers near the curves give the assumed value of electron temperature to neutral particle temperature ratio $a = T_e/T_n$ upon which calculations of τ_T were based. So, if $a = 50$, then at the heights of 90, 93, 95, 100 and 205 km, electron thermalization takes place in 3, 7, 9, 22.6 and 54 ms. The effective electron temperature decrease from $T_e = 50T_n$ to $T_e = 10T_n$ takes place very quickly with a time shorter than the ion thermalization time. Considerable moderation of trail plasma electron component cooling rate occurs when the values $T_e/T_n < 10$.

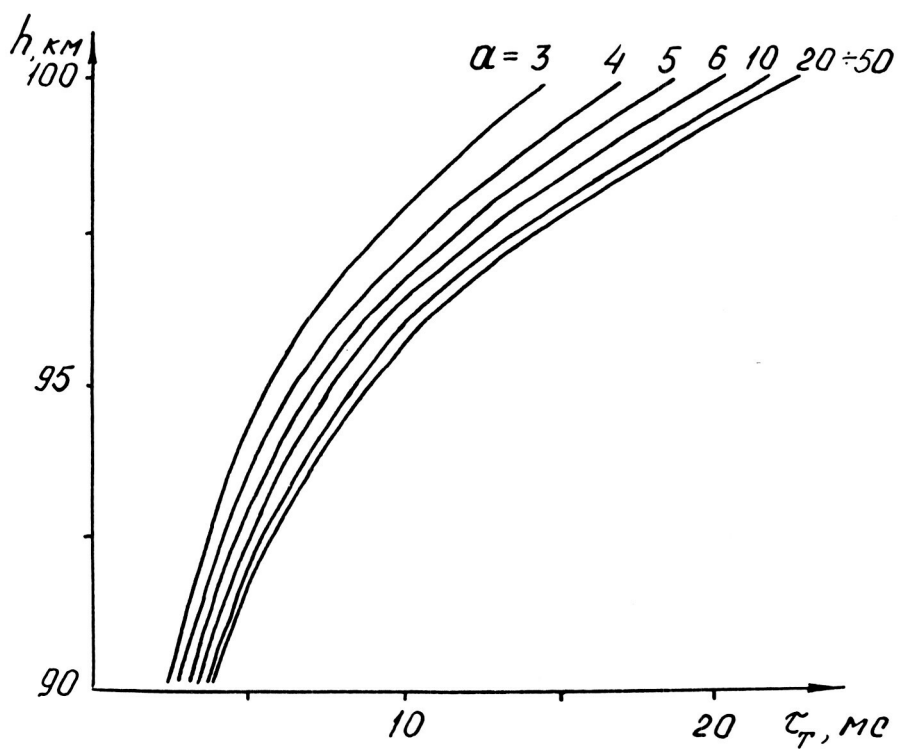


Fig. 1 Dependence of thermalization time τ_T on height and initial effective temperature α of electrons in a meteor trail.

Let us write down the signal power scattered by an unsaturated non-isothermal meteor trail as follows (AMINOV and TOKHTASJEVE, 1973; AMINOV et al., 1976):

$$P_r = P_{r_1} f(r_1) I^2 \quad (2)$$

where

$$I = \left| \frac{1}{\sqrt{2}} \int_{x_1}^{x_0} \frac{\alpha}{\alpha_1} \exp \left(i \frac{\pi}{2} x^2 - \left(\frac{4\pi r_0}{\lambda} \right)^2 \xi(t) - \left(\frac{2\pi r_0}{\lambda} \right)^2 \left[1 - \left(\frac{r_1}{r_0} \right)^2 \right] \right) dx \right|; \quad (3)$$

$$\xi(t) = \frac{D_{a0}}{r_0^2} \left[\frac{1}{2} t + \frac{1}{2T_n} \int_0^t T_e(\eta) d\eta \right]; \quad t = \frac{\sqrt{R_1 \lambda}}{2v} (x_0 - x); \quad (4)$$

$$f(r_1) = \exp \left[-2 \left(\frac{2\pi r_1}{\lambda} \right)^2 \right];$$

with α = linear trail electron density, P_{r_1} = signal power scattered from a trail when $\alpha = \alpha_1$ and calculated by the Lovell-Clegg formula; D_{a0} = coefficient of ambipolar diffusion in the isothermal meteor trace; r_{a0} = initial trail radius, R_1 = slant distance to the reflecting point in the trace, v = meteor body velocity, and λ = radar wavelength. The index 1 denotes the value corresponding to the reflecting point.

If the changes of α along the trail as well as the height dependence of D_{a0} , r_{a0} and ξ are all neglected, then the diffraction integral (3) is simplified:

$$I = \left| \frac{1}{\sqrt{2}} \int_{x_1}^{x_0} \exp \left[i \frac{\pi}{2} x^2 - \left(\frac{4\pi r_0}{\lambda} \right)^2 \xi(t) \right] dx \right| \quad (5)$$

To analytically calculate the diffraction pattern of the radioecho from unsaturated meteor trails, it is necessary to simplify the function $\xi(t)$. In order to do this, Equation (1) was replaced by two simple model differential equations having analytical solutions. One of the solutions gives a more rapid and another - a slower time decrease as compared with the results of the numerical solution Equation (1). For the first model we have

$$\left(\frac{4\pi r_0}{\lambda} \right)^2 \xi(t) = \frac{\tau_\phi}{\tau_D} (x_0 - x) + \frac{\tau_P}{\tau_D} \cdot \frac{\alpha^*}{2} \left(1 - \exp \left[- \frac{\tau_\phi}{\tau_P} (x_0 - x) \right] \right) \quad (6)$$

for the second

$$\left(\frac{4\pi r_0}{\lambda} \right)^2 \xi(t) = \frac{\tau_\phi}{\tau_D} (x_0 - x) + \frac{\tau_P}{\tau_D} \left(\frac{1}{1-C} - \frac{1}{1 - C \left[-\frac{\tau_\phi}{\tau_P} (x_0 - x) \right]} \right) \quad (7)$$

In the formulas (6) and (7), the following notations are introduced:

$$\tau_\phi = \frac{\sqrt{R_1} \lambda}{2v} ; \tau_D = \frac{\lambda^2}{16\pi^2 D a_0} ; \tau_P = \frac{1}{B} ; C = \frac{\sqrt{a^*} - 1}{\sqrt{a^*} + 1} ,$$

$a^* = T_e^*/T_n$. The physical meaning of the parameter B is defined below.

The influence of non-isothermal effects in a meteor trail plasma on the amplitude and form of radioecho depends upon the correlation of characteristic time of formation of the Fresnel first zone τ_ϕ , the electron effective temperature relaxation time τ and the time constant of the signal amplitude decrease L_D . When compared to the isothermal case, the diffraction pattern distortions increase with increasing reflecting point height. But when the reflection height and radar wavelengths are fixed, they increase with a decrease of the trail slant range.

Numerical integration of the formula (5) considering the dependence given by (6) was made to choose optimal conditions for detection of non-isothermal effects in meteor trails, which in turn allow measurement of the main parameters a^* and B for the non-isothermal plasma. The theoretical analysis permits the following conclusions. Despite the small values of the thermalization time τ_T of superhot electrons in newly-formed meteor trails, non-isothermal effects contribute to the considerable weakening of trail scattered signals and to specific diffraction pattern distortions. The first maximum of the diffraction pattern shifts slightly, but if its position is not used in amplitude and time characteristic processing (as is usually done), then errors in determining speed by all the other extremes are negligible and do not exceed 1-2%. The depths of the minima of the diffraction pattern all increase (Fig. 2). Fig. 3 (a, b, c) shows the amplitude ratios for several extrema as a function of $\Delta = \tau_\phi/\tau_D$ for both the isothermal (dashed curves) and non-isothermal solid curves) cases. It can be seen that relationships of the first and second maxima to the first minima possess a strong and rather characteristic dependence on Δ . The amplitude ratios, A/D and C/D, though not shown, are also characterized by a similar dependence on Δ .

The existence in the observational amplitude-versus-time characteristics of the mentioned peculiarities enables one to select those that are of interest for a more detailed analysis by optimization methods (KOSTYLEV and KOSTYLEV, 1980). Thanks to the sufficient accuracy of determining a whole range of meteor parameters, the use of these methods makes it feasible to estimate the main parameters of the non-isothermal electrons component in meteor trails - a^* and $q = B/100$ with a relative r.m.s. error of $\langle \sigma a^* \rangle / a^* \sim 25\%$ and $\langle \sigma q \rangle / q \sim 45\%$.

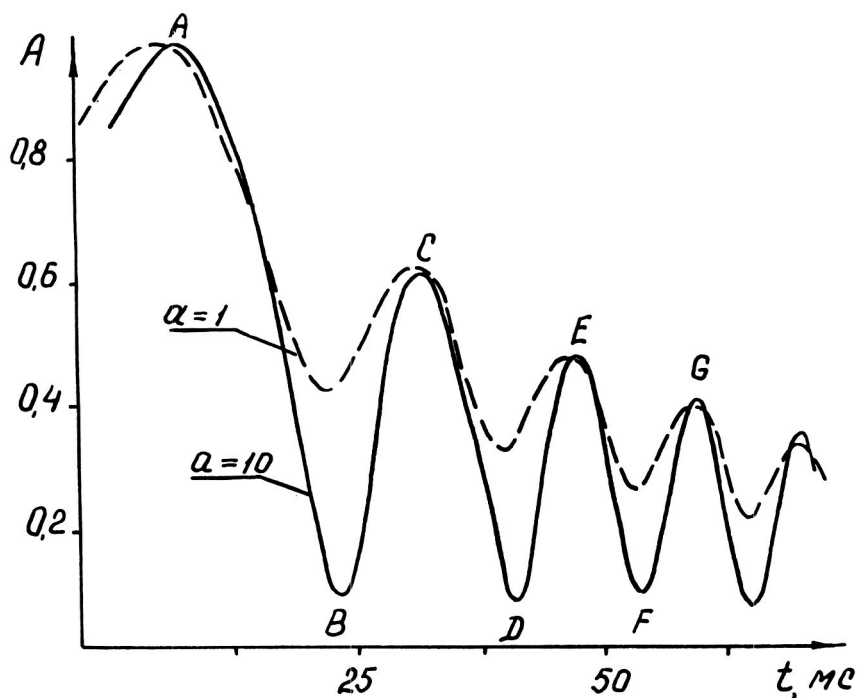


Fig. 2 Amplitude and time characteristics, with ($\alpha = 10$) and without ($\alpha = 1$) non-equilibrium temperature effects, calculated for the following parameters values:

$$D = 11.9 \text{ m}^2 \text{ s}^{-1}; \quad V = 40 \text{ km s}^{-1}; \quad Z = 33^\circ$$

$$r = 1.4 \text{ m}; \quad q = 4.34; \quad \lambda = 9.375 \text{ m}; \quad R = 185 \text{ km}$$

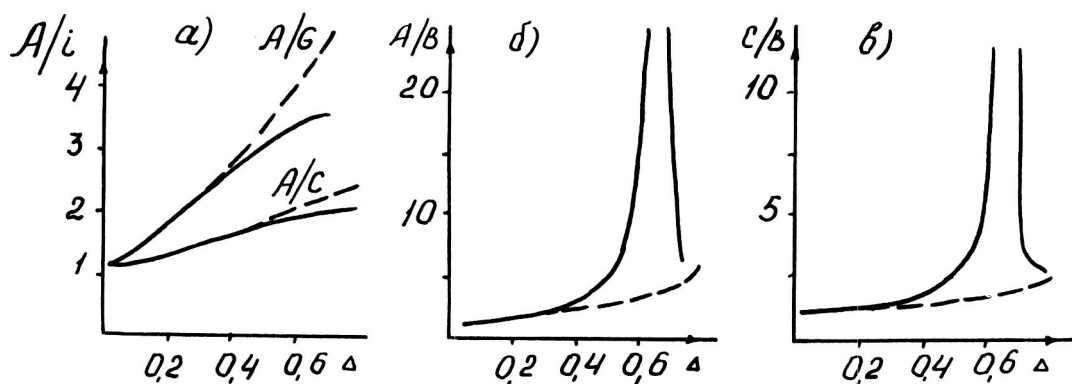


Fig. 3 Dependence of diffraction pattern extremum ratios on the parameter Δ with (—) and without (---) non-equilibrium temperature effects.

The model of meteor trail formation used in the calculations allows for variation of (a) the ambipolar diffusion coefficient and initial radius along the trail, (b) the position of the reflecting point on the ionization curve and (c) meteor body deceleration and seems adequate enough to describe real meteor phenomenon (KOSTYLEV, 1983).

Fig. 4 shows a histogram of the distribution of derived a^* values. Echoes recorded at night during the period of the Geminids in 1983 and Perseids in 1978 were selected for optimization methods processing. The mode of a^* shown by this distribution equals 4.7. The height dependence of the measured values of the number $q = B/100$ is shown in Fig. 5. Also shown is the theoretical dependence for mode (7) with $q = 0,014 \langle \delta \rangle v^{\circ}_{en}$, where $\langle \delta \rangle$ is the part of energy lost by superhot electrons per one collision with an atmospheric particle and averaged over the temperature interval $T < T < T$ and v°_{en} is the effective frequency of electron collisions with neutral atmosphere components with $T = T = 200^{\circ}\text{K}$. For the calculation $\langle \delta \rangle = 1,1 \times 10^{-3}$ was used. Using the derived value of the parameter q , we get the following values of v°_{en} : 1.4×10^5 and $1.2 \times 10^5 \text{ s}^{-1}$ at the heights of 94 and 96.5 km. The paper Middle Latitude Ionosphere Empirical Models, (Moscow, 1981), gives the v°_{en} values as 1.4×10^5 and $0.9 \times 10^5 \text{ s}^{-1}$ for the same altitudes. The coincidence is quite satisfactory.

In conclusion, it may be said that in trails produced by meteors with velocities of 35-60 kms, the initial effective temperature of electrons is at least 5 times as high as that of the neutral atmosphere particles. This provides a real possibility for radar measurement of an important structural parameter of ionosphere, the electron collision frequency, in the 90-105 km interval.

References

1. Aminov, A.N., Tokhtashev, V.S., 1973, in Meteor Radiowaves Propagation, Kazan State University Publishers, Iss. 9, pp. 30-37.
2. Aminov, A.N., et al., 1976, in Meteor Radiowaves Propagation, KSU Publishers, Issues 12-13, pp. 157-180.
3. Bidin, Yu. F., Demkov, Yu. N., 1982, Ph. Sci., Vol. 137, Iss. 3, pp. 377-414.
4. Kostylev, K.V., Kostylev, K.K., 1980, Astron. Bulletin, Vol. 14, No. 2, pp. 89-96.
5. Kostylev, K.V., 1983, In Meteor Radiowaves Propagation, KSU Publishers, Issues. 18, pp. 15-24.
6. Middle Latitude Ionosphere Empirical Models. Nauka Publishers, Moscow, p. 256, 1981.
7. Prasad, S.S., Furman, D.R., 1973, J. Geophys. Res., Vol. 78, No. 28, pp. 6701-6707.
8. Stube, P., Varnum, W.S., 1972, Planetary Space Sci., Vol. 20, No. 8, pp. 1121-1126.

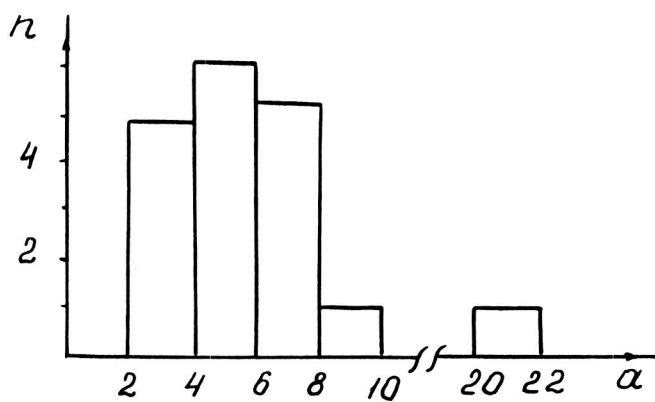


Fig. 4 Distribution of value $a^* = T_e/T_n$ for the Geminids - 83 and Perseids - 78.

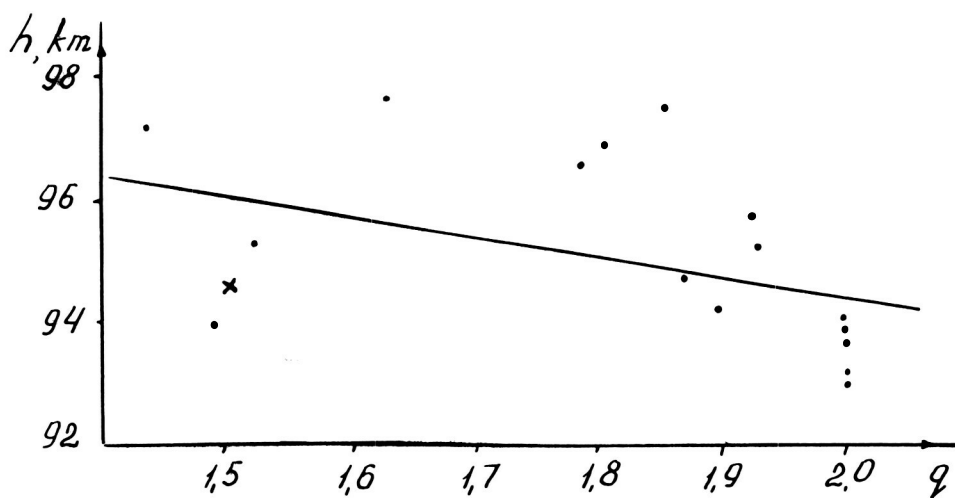


Fig. 5 Parameter q theoretically (—) and experimentally obtained dependence on height.

THE ROLE OF FRAGMENTATION IN INTERACTION OF METEORIODS
WITH THE EARTH'S ATMOSPHERE

P. B. Babadjanov, G. G. Novikov, V. N. Lebedinets, and A. V. Blokhin

Institute of Astrophysics, Dushanbe, USSR
Institute of Experimental Meteorology (IEM), Obninsk, USSR

As a rule, when analyzing the mechanism of quasi-continuous fragmentation (QCF) it is assumed that fragments separated from the parent meteoroid (PM) are of equal initial mass. In reality, this may not be so. A major difficulty is the lack of observational data on the function of the fragment initial mass distribution and so one must resort to theoretical modeling. Let us consider a discrete distribution which excludes to a certain extent some mathematical difficulties. We assume that during flight, fragments constantly separate from the PM forming several groups. In this case, the role of this distribution is reduced to mere addition of brightness from separate groups of fragments of the given weight factor. If M is the fragment mass maximum estimated by the formula (BABADJANOV and KRAMER, 1965) $M_0 \sim 4/3 \pi \delta x_0^3$ (where δ is the fragment density and x_0 is the depth of heating), then the rest of fragment masses will be $M_{oi} = M_0 / K^{i-1}$, where $K = 2$ or $\sqrt{10}$, or 10 . Let P_i be a part of the PM mass that became fragments with the particles mass M_{oi} , then the total number of fragments of each kind will be $N_i = M / M_{oi}$. (M_0 is the initial mass of PM). Thus, if $I_i(h)$ is the intensity at the height h of a definite kind of fragment i , then the meteor brightness curve taking into account the discrete distribution can be found by:

$$I_B(h) = \sum_{i=1}^n I_i(h) P_i \quad (1)$$

The calculation results (but without taking deceleration into account) are given below. To illustrate this, a slow fragmentation process has been considered when the lifetime τ_H of fragments separated at the moment when fragmentation began until their complete evaporation is less than that of the total PM lifetime τ_0 (BABADJANOV and KRAMER, 1968).

Meteoroid and fragment parameters were chosen as follow: $M = 3g$, $V = 30$ kms, $\cos Z_R = 0.6$, $H^* = 6$ km, $\Lambda = \Lambda' = 1$, $A = 1.5$, $A' = 1.21$, $\tilde{\rho}_0 = \delta_0 = 3.4$ g/cm³, $Q = 8 \times 10^{10}$ erg/s, $i = 5$, $P_1 = 0.1$, $P_2 = 0.2$, $P_3 = 0.4$, $P_4 = 0.2$, $P_5 = 0.1$, the height of fragmentation starting point is 90 km. Here V is the velocity of a meteoroid; H^* is the scale height; Z_R is zenith distance of the meteor radiant; Q and Q_p are the energies of evaporation and fragmentation respectively; Λ and Λ' are the heat transfer coefficient and shape factor of PM; Λ' , A' are the analogous values of a fragment; ρ_H is the atmospheric density at the height of meteor appearance; ρ is the atmospheric density at any point on the meteor trajectory; and δ_0 is density of PM. The table below shows this variation I_B of meteor brightness (in units of maximum magnitude) with the height h . For comparison, meteor brightness is also presented for the case of PM disintegrating into fragments of mass $m_{03} = M/10$ and labeled I_3 . As is seen from the table, the mass distribution has practically no effect on the shape of the brightness curve. The value of maximum brightness is roughly the same for different fragment masses and remains at about the same

height. The heights of meteor disappearance differ little from each other. If we consider P_i as some other function, the result will be essentially the same.

h km	90	88	86	84.64	84.41	83	81	79	77.89	77.6
I_B	0.00	0.730	0.960	1.00	0.996	0.941	0.630	0.145	0.00	-
I_3	0.00	0.774	0.958	0.988	0.992	0.902	0.607	0.103	7.10^{-3}	0.00

It is common knowledge that photographic observations using the instant exposure method give the most complete information on the process of meteor phenomenon origin. (BABADJANOV and KRAMER, 1965; BABADJANOV and KRAMER, 1968; BABADJANOV, 1983). Studying a succession of such meteor photographs, BABADJANOV and KRAMER (1965) concluded that during flight, a meteor coma might take different shapes, from a simple dot to a complete head and tail. A drop-like shape was the most typical. Since the question of the formation and further evolution of a meteor coma along its trajectory was of great interest, the quasi-continuous fragmentation theory was improved by including fragments deceleration (BABADJANOV et al., 1984).

This theory enables one to study not only meteor brightness curves and wakes, but also model the instantaneous images of the luminous coma along the whole of the visible trajectory of a meteor. The following simplifications were suggested: (a) PM deceleration is small; (b) all fragments are of equal initial mass m_o ; (c) the luminosity is due mainly to atoms and molecules evaporating from fragment surfaces, not from that of PM; (d) formulae of the simplest physical theory of meteors are true both for fragments and for PM (LEVIN, 1956); and (e) that the sizes of the PM and its fragments are much less than the distances between them so that all can be considered to be points. Given these assumptions, expressions for the total meteor intensity and brightness curve were derived as well as the visible intensity profile through the luminous coma.

The analysis revealed the dependence of I_B to be determined by physical parameters of PM and fragments through combinations of the special parameters γ , γ_1 , and λ as defined by BABADJANOV, et al. (1984).

$$\gamma = \frac{\Lambda A V^2 \rho_H H^*}{6Q_g (M_o \delta_o^2)^{1/3} \cos Z_R},$$

$$\gamma_1 = \frac{\Lambda' A' V^2 \rho_H H^*}{6(Q - Q_g)(M_{oi} \delta_o^2)^{1/3} \cos Z_R}, \quad \lambda = \frac{\beta \rho_H}{2V^2}.$$

These parameters can be obtained from comparison of theoretical and observed profiles of instantaneous meteor images. The figures show the evolution of instantaneous image profiles along the meteor trajectory for different times t . The parameters selected were as follow: $M_o = 30g$, $V =$

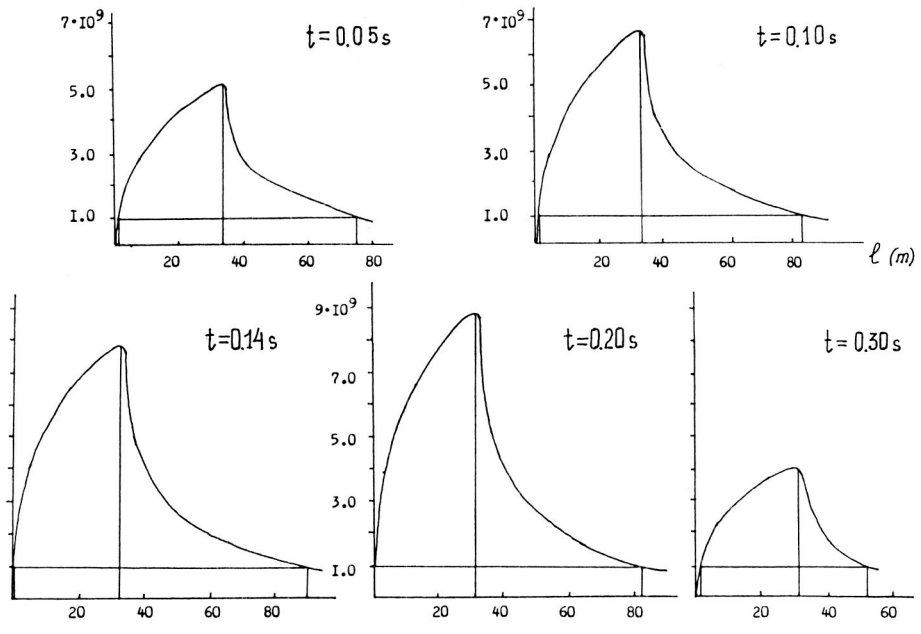


Fig. 1 The evolution of instantaneous image intensity (ergs/S) profiles along a meteor trajectory at different times t , for exposure times $5.6 \times 10^{-4} \text{ s}$.

60 km/s, $H^* = 6$ km, $\cos Z_R = 0.6$, $\lambda = 0.13$, $\gamma = 0.14$, $\gamma_1 = 1$. The intensity I_B is in erg/s (Y-axis) and distance in meters ℓ (X-axis). The exposure time $\tau_0 = 5.6 \times 10^{-4}$ s. The horizontal line gives the threshold brightness value equalling about 2×10^9 erg/s. Thus, we may conclude that the profile of a meteor instantaneous image evolves with time as does the visible size of the luminous coma. This is in good agreement with observational data obtained by instant exposure.

References

1. Babadjanov, P.B., Kramer, E.N., 1965, Sov. Astron. J., 42, No. 3, 660.
2. Babadjanov, P.B., Novikov, G.G., Lebedinets, V.N., Blokhin, A.V., 1984, The theory of the quasi-continuous fragmentation of meteor bodies accounting deceleration, pre-print, Physical Technology Institute, Leningrad.
3. Lebedinets, V.N., 1980, Dust in the Earth's atmosphere and cosmic space, Meteory, Leningrad, Gidrometeoizdat Publishers.
4. Levin, B.J., 1956, Physical theory of meteors and meteor matter in the solar system, Moscow, Soviet Acad. Sci. Publ.
5. Novikov, G.G., Lebedinets, V.N., Blokhin, A.V., 1984, Sov. Astron. J., No. 1, 10, 71.

ON THE METEOR TRAIL SPECTRA

O. G. Ovezgeldyev, S. Mukhamednazarov, R. I. Shafiev, and N. V. Maltsev

Physical Technology Institute
Ashkhabad, USSR

Meteor radiation appears as a result of collisions between evaporated meteoroid atoms and air molecules. Depending on duration, this radiation is usually divided into the following types:

- radiation of the meteor head itself with a typical duration of about 1 s,
- radiation of a 'coma' surrounding or immediately following the meteor head,
- radiation of a trail formed as a result of fragments lagging behind or by the afterglow of meteor matter atoms and ions and air caused by chemical processes,
- radiation of a meteor train forming from a 'tail' as a result of various chemical and dynamical processes.

To investigate physical processes caused by each of the above types, it is necessary to obtain the corresponding experimental data.

The lifetime of a trail is usually 10^{-3} - 10^{-1} s and that of a meteor train depending on brightness, height, velocity and atmospheric conditions, may be from 1 to 10^3 s.

The spectra of trails and short-period meteor trains were obtained by photographic cameras supplied with rotating shutters whereas determination of spectra of stable (long-period) trains remains a problem of meteor spectroscopy.

The television and optical electronics methods for meteor observations used at the Physical Technology Institute of the Turkmen Academy of Sciences since 1972 have opened up new possibilities of obtaining and investigating the spectra of trails and short-lived trains. Due to high sensitivity, these methods allowed spectrograms of meteors to be taken with exposures of 0.5-1.3 sec. The spectra of a head, trail and train are obtained as a separate series of photographs. Fig. 1 shows the photograph of a meteor spectrum and its train as two consecutive stills obtained on September 18, 1979 of the polar region of the sky, with the help of a TV frame-grabbing device. The first still shows the first half of a meteor head spectrum and the second one - its second half and the spectral lines referring to the train glow. The following spectral lines were identified in this meteor train spectrum: $5183.6^{\circ}\text{A}(\text{MgI})$, $5890.0^{\circ}\text{A}(\text{NaI})$, $7771.9^{\circ}\text{A}(\text{OI})$ and the forbidden oxygen line 5577°A . OVEZGELDYEV et al., (1976) investigated the peculiarities of the 5577°A line in the meteor trail spectra obtained with the help of a TV system. It was noted that this line usually appears at greater heights as compared with other lines of a meteor spectrum, i.e., at 100-120 km. However, further meteor observations with image-tubes revealed that the green oxygen line also appeared in a burst at 82-85 km. Fig. 2a shows a photometric tracing of a section of a meteor burst spectrum obtained during observations of the Perseids with an exposure of 1 sec on August 11, 1980. Fig. 2b shows a photometric tracing of the same spectrum region but in the meteor train. In Fig. 2a one can see only two bright lines referring to $\text{MgI}(5183.6^{\circ}\text{A})$ and $\text{NaI}(5890.0^{\circ}\text{A})$ and

ORIGINAL PAGE IS
OF POOR QUALITY

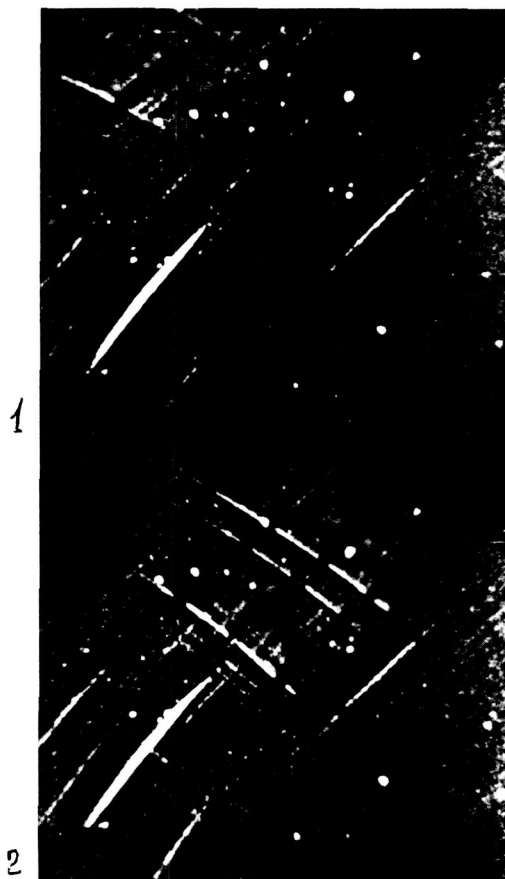


Fig. 1 Photograph of a meteor spectrum and its train in two consecutive stills, the first showing the beginning of a meteor path (upper left) the second - its end and the train spectrum (upper middle of frame). Dispersion goes from upper right to lower left.

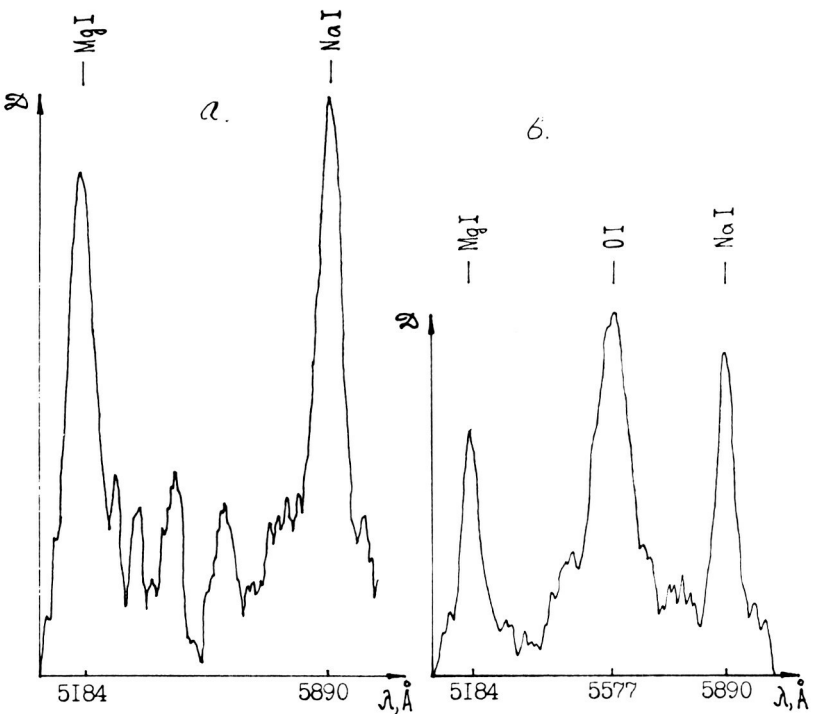


Fig. 2 a) Photometric record of a part of a Perseid meteor explosion spectrum,
 b) the same after the explosion (train).

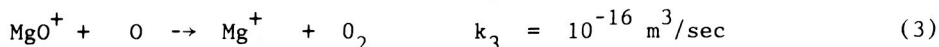
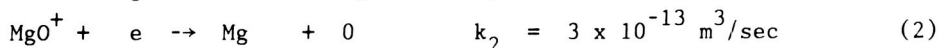
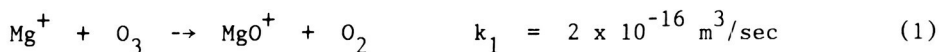
it is seen from Fig. 2b that the green oxygen line appeared in the trail spectrum after the explosion. Determination of height parameters for this meteor showed that the explosion was observed at 82.5 km. Apparently in this case, it was at the moment of explosion that the required linear density $O^+(^1S^o)$ reached the 10^{14} cm^{-1} needed for the green oxygen line radiation formation (according to the following reactions):



So, it can be clearly seen that the television and optical electronic methods allow investigation of meteor train spectra with high enough time resolution to allow the sequence of lines formation in a train and to investigate temporal variations of separate spectral lines. Fig. 3 presents typical temporal decay variations of lines $5183.6^\circ\text{A}(\text{MgI})$, $5890.0^\circ\text{A}(\text{NaI})$ and the red line $7771.9^\circ\text{A}(\text{OI})$ in apparent magnitudes as obtained from TV meteor observation data. The decay patterns of lines MgI and NaI are alike but that of OI(7771.9°A) proceeds more quickly. These diagrams allow one to determine the exponential decay of individual spectral lines in a meteor train. The analysis of such diagrams showed that exponential decay of MgI(5183.6°A) has time constants from 0.46 to 0.52 sec^{-1} and OI(7771.9°A) has time constants from 1.0 to 1.6 sec^{-1} . The lifetime of OI(7771.9°A) determined from TV observation data with no allowance for possible equipment persistence was 0.3 sec, a value that is in good agreement with observation data obtained by other methods.

If we assume that, as follows from KAISER (1963), the variation of meteor train brightness is proportional to the electron attachment rate (" k "), i.e. $dm/dt = 1.09k$, then the exponential decay dependences can help determine the speed of electron attachment in a meteor train. For example, " k " turned out to equal 0.21 for the MgI line.

In all probability, the decay of radiation of individual lines should be explained by a complex of chemical processes. For example, for MgI, the following reactions can be given:



Atoms of Mg as well as of O can be excited in reaction (2). As meteor trail spectra show, both these elements are the most frequently seen.

Radiation of the NaI line in meteor trains can be explained by the following reactions:



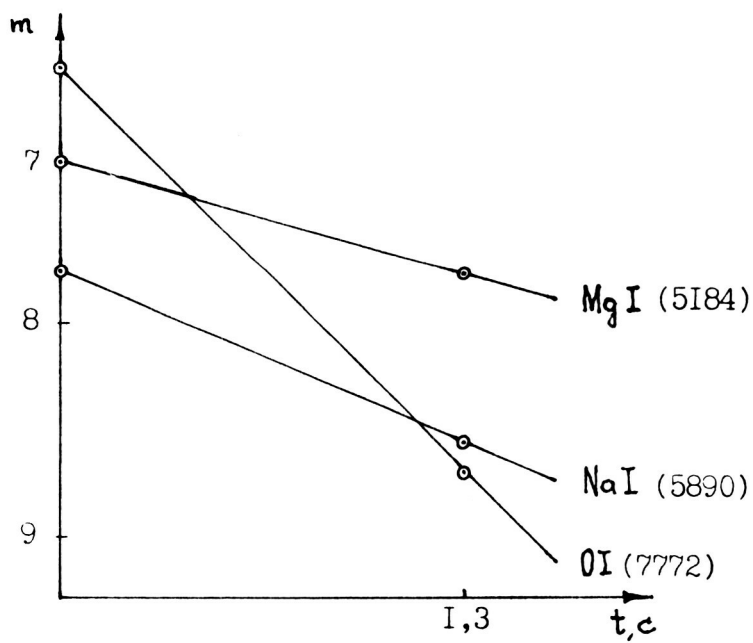


Fig. 3 Temporal dependences of spectral line decay in a meteor train.

Temporal variations of spectral lines of a meteor train obtained from our observations confirm the results of POOLE, (1978) where train radiation (L) is given as a number of photons per second, per one meter of meteor path length assuming dissociative recombination reactions is determined by the linear concentration of positive ions per cm^{-1} , as well as by electron, ozone and oxygen concentrations. Decay of the MgI line in a meteor train can be described by

$$\frac{dh_v}{dt} = L = - p b k_1 (O_3) \alpha(\text{Mg}^+)$$

where $\alpha(\text{Mg}^+)$ is the linear concentration of positive Mg ions per cm^{-1} in a meteor trail, p is the photon energy produced during recombination,

$$b = \frac{k_2[e]}{k_2[e] + k_3[O]} ; [e] = \frac{\alpha[\text{Mg}^+]}{4\pi D t}$$

Our meteor train spectra, also showed a number of weak lines: FeI (4046Å, 4064, 4272, 4308, 4326, 4384, 4405), CaI (4455Å, 4227) and the lines of atoms of SiI , ions of SiII , CaII , MgII as well as the neutral lines of atomic and molecular nitrogen.

References

1. Anisimov, V. F., Gulmedov H.D., Mukhamednazarov S., 1976, In: *Astronomichesky Vestnik*, No. 2, pp. 124-125.
2. Kaiser, T.K., 1963. *Negative Ions and Luminosity in Meteor Trails*, *Smithson. Contr. to Astrophys.*, Vol. 7, pp. 175-180.
3. Ovezgeldyev O.G., Mukhamednazarov S., Gulmedov H.D., 1976. In the collection *Izvestiya Akademii Nauk Tajikskoi SSR*, No. 4, pp. 57-61.
4. Poole L.M.G., *The Decay of Luminosity in the Trails*, *Planet. Space. Sci.*, 1978, Vol. 26, No. 7, pp. 697-701.

SOME ASPECTS OF METALLIC ION CHEMISTRY AND DYNAMICS IN THE MESOSPHERE AND THERMOSPHERE

J. D. Mathews

Electromagnetic Waves and Wave Propagation Group
Dept. of Electrical Engineering and Applied Physics
Case Institute of Technology
Case Western Reserve University
Cleveland, Ohio

The relationship between the formation of "sporadic" layers of metallic ions and the "dumping" of these ions into the upper mesosphere is discussed in terms of the tidal winds, "classical" (i.e., windshear) and other more complex, perhaps highly non-linear layer formation mechanisms, and a possible circulation mechanism for these ions. Optical, incoherent scatter radar, rocket, and satellite derived evidence for various layer formation mechanisms and for the metallic ion circulation system is reviewed. The results of simple one-dimensional numerical model calculations of sporadic E and intermediate layer formation are presented along with suggestions for more advanced models of intense or blanketing sporadic E. The flux of metallic ions "dumped" by the tidal wind system into the mesosphere is estimated and compared with estimates of total particle flux of meteoric origin. Possible effects of the metallic ion flux and of meteoric "dust" on D region ion chemistry are discussed.

I. Introduction

That meteors "burn-up" in the 80-110 km region of the atmosphere is unquestioned. However, the effect of this mass flux on the upper atmosphere and how the meteoric debris eventually settles to the ground is very much in question. The mass flux is estimated to be 10^{-16} gm-cm⁻²-s⁻¹ or 44 metric tons per day over the earth (HUGHES, 1978; HUNTEN et al., 1980) and, after meteor burn-up, is observable only in atomic neutral and ionized forms or as dust or "smoke" (HUNTEN et al., 1980) particles. The "budgets" or aeronomy of these two forms is unknown. It is the purpose of this paper to explore the budget issue for the atomic metal ions which form into narrow (in height) layers known as sporadic E and to introduce some possible new "clues" concerning dust in the meteor zone.

Numerous rocket borne mass spectrometer measurements (eg. AIKIN and GOLDBERG, 1973; Zbinden et al., 1975) have demonstrated the presence of atomic metal ions in sporadic E layers. These results have been confirmed by incoherent scatter radar measurements (eg. BEHNKE and VICKERY, 1975; TEPLEY and MATHEWS, 1985), by passive optical measurements (eg. TEPLEY et al., 1981 a) and by Lidar measurements (eg. GRANIER et al., 1984). Also Mg⁺ and Fe⁺ have been observed at F region altitudes (eg. GREBOWSKY et al., 1978; MENDE et al., 1985) leading to much speculation regarding the transport of these ions from the deposition region to these heights. MATHEWS and BEKENY (1979) have proposed an E/F region circulation mechanism involving tides, the equatorial fountain effect (HANSON et al., 1972), and "sporadic" layers which may explain some observations.

Sporadic E layers are transported to the lower thermosphere where chemistry (eg. 3 body recombination of the ions; SWINDER, 1984; BROWN, 1973) becomes dominant over transport (MATHEWS and BEKENY, 1979). Simple chemistry, such as the ion/neutral concentration ratio of a species, can be investigated experimentally. For example, neutral iron and calcium have been observed below 100 km altitude by passive optical means (TEPLEY et al., 1981 a,b) and LIDAR (GRANIER et al., 1984) respectively. However, the formation and growth mechanisms of dust or smoke particles which ultimately settle out of the atmosphere have proved much more difficult to investigate and evaluate in terms of overall effect on the mesosphere and D region. Dust quite probably plays a major role in noctilucent cloud formation (TURCO et al., 1982) and possibly modifies D region ion chemistry (eg. PARTHASARATHY, 1976).

In section 2 we explore some aspects of metallic ion transport at mid and low latitudes while section 3 emphasizes some aspects of metallic ion and dust chemistry. Section 4 forms a summary and discussion of the above topics from which we conclude that metals and dust should be studied via combined lidar and incoherent scatter radar instrumentation.

The basic veracity of the "wind shear" theory of layer formation (CHIMONAS and AXFORD, 1968; WHITEHEAD, 1971) is unquestioned (MATHEWS and BEKENY, 1979) as is the fact of metal ions (Fe^+ , Mg^+ , Ca^+ , Si^+ , etc.) within at least the 90-120 km layers.

II. Sporadic Layers and Metal Ion Transport

Figure 1 shows a typical time series of electron concentration profiles obtained with the Arecibo 430 MHz Incoherent Scatter Radar (ISR). All the major features of midlatitude "sporadic" layers appear in this sequence of profiles. In particular three layers (A,B,C) display the highly time coherent behavior that has been linked to the diurnal and semidiurnal tides (MATHEWS and BEKENY, 1979). More important to this paper is that layers B and C are the so-called intermediate layers (FUJITAKA and TOHMATSU, 1973) which descend from the F region into the E region where these layers join the sporadic E system.

Another idea of layer behavior observed at Arecibo is given in Fig. 2 where layer height is plotted versus time without regard to layer "strength" for three full days. The major features seen in Fig. 2 confirm those of Fig. 1. That is, intermediate layers descend from the F region, join the sporadic E layer system and finally descend to the "dumping" zone at 90 km altitude. This behavior is typical for Arecibo and two major points emerge. These are that ion layers are not sporadic but are almost always present and that the net vertical ion motion in the tidal wind is downward. That is, ions can move upward but only to the next descending convergent node (MATHEWS and BEKENY, 1979).

Figures 1 and 2 deal, by nature of the observing technique, only with vertical layer motion. We see that minimum layer "travel time" from 150 km to 90 km is about 18 hours where rates of 4-8 km/hr above 110 km and of 0.5 - 1 km/hr below 100 km correspond to semidiurnal and diurnal tidal phase speeds respectively.

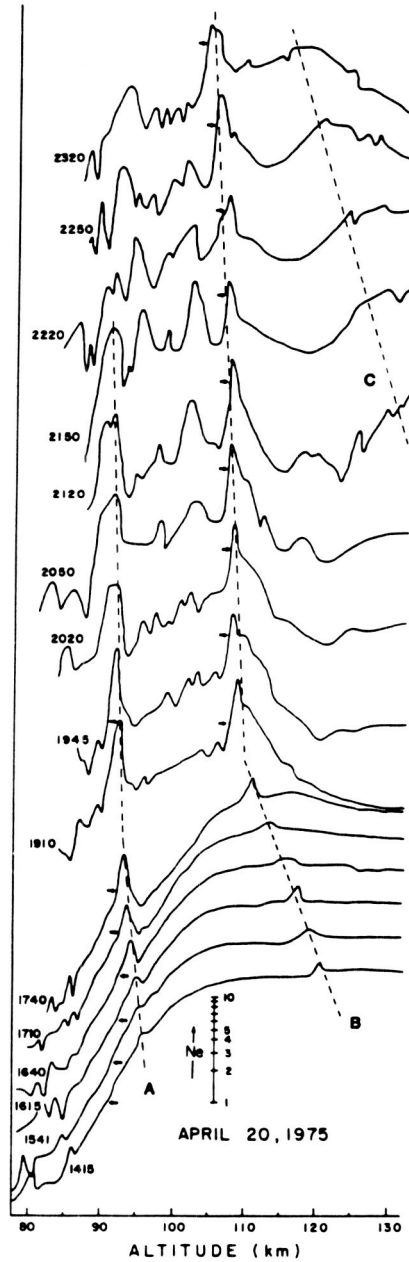


Fig. 1 Electron concentration is plotted on a logarithmic scale (ordinate) versus altitude (abscissa) and time (separate profiles arrayed along the ordinate with times ranging from 1415 through 2320 hours). These data were obtained with the Arecibo 430 MHz incoherent scatter radar and the arrows indicate the 10^4 el/cc level on each profile. Note the three separate long-lived layers (A,B,C) and the various descent rates. The early portion of layer B and layer C are known as intermediate layers. (Figures from MATHEWS and BEKENY, 1979).

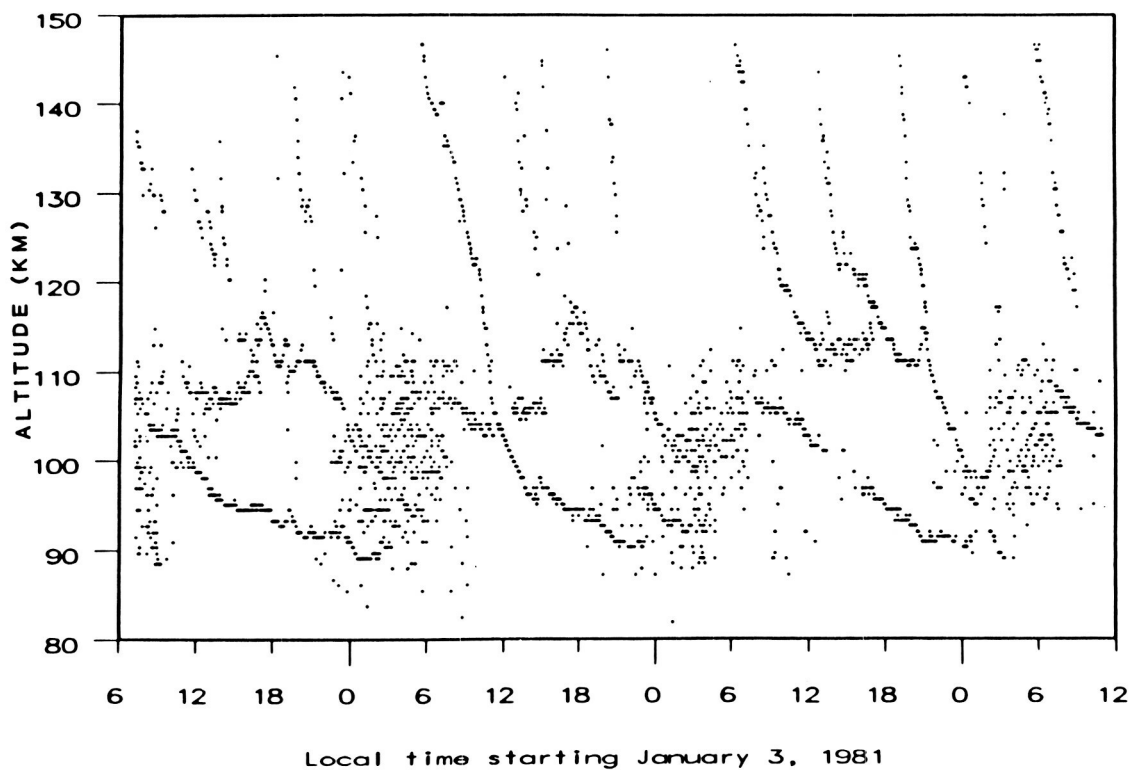


Fig. 2 The altitude of peak concentration of ion layers is plotted (for all layers) versus time for three days of Arecibo observations. The formation of layers and the rate of descent is controlled by the diurnal and semidiurnal tides. That several intermediate layers per day are observed indicates the presence of multiple semidiurnal modes.

Figure 3 summarizes the basis for layer formation via the $\underline{V} \times \underline{B}$ mechanism. That is, below about 130 km altitude ions are sufficiently coupled, via collisions, to the neutral atmosphere that a node in the zonal tidal wind system accumulates long-lived ions if the westward wind is above and eastward wind below. This "convergent" node in the zonal system also corresponds to maximum southward wind (northern hemisphere). Thus, the layers depicted in Figures 1 and 2 are being transported toward the equator at speeds of the order of 100 m/sec (MATHEWS, 1976; HARPER, 1977) or 360 km/hr. It is thus possible that these metallic ions are, at least at some longitudes, (the earth's spin and magnetic axes are not aligned) brought close enough to the magnetic equator to come under the influence of the combined polarization electric fields and $\underline{E} \times \underline{B}$ drifts which can lift them to the F region. This vertical transport effect is known as the equatorial fountain effect (HANSON et al., 1972) and is invoked in order to explain the metal ions observed in the F region at magnetic dip latitudes between $\pm 30^\circ$ (MENDE et al., 1985; FENSEN and HAYS, 1982).

The "fountain effect" is a two part process. The first part of the process is the lifting by the vertical polarization electric field of the minor constituent metal ions from the 90-110 km region to the lower F region. The second part of the process is the further lifting of these ions via $\underline{E} \times \underline{B}$ drift into the mid- and upper F region. The ions are then free to diffuse and fall along the B field lines to higher latitudes. This process is depicted in Fig. 4 (HANSON and MOFFETT, 1966).

The equatorial E region vertical polarization electric field arises from the fact that the vertical electron mobility is much larger than the corresponding ion mobility. Thus the primary zonal ("Pedersen") electric field gives rise to the "Hall" or vertical polarization E field. The Hall field produces a zonal current which combines with the original Pedersen current producing the eastward equatorial electrojet (Cowling) current (WOODMAN et al., 1977; VOLLAND, 1984; section 9.6). Note that this lifting mechanism only operates during the daylight hours. The reverse electrojet, which occurs from late afternoon through to sunrise, is characterized by a downward rather than upward polarization electric field.

The $\underline{E} \times \underline{B}$ lifting mechanism becomes dominant at about 160 km altitude where electron and ion collision frequencies become small relative to respective cyclotron frequencies and the vertical polarization field tapers off. The electric field is the "normal" daytime eastward E region field which is mapped along B field lines to the F region. (MARTYN, 1955; VOLLAND, 1984;; Section 9.7).

The total time for transport of metal ions from the equatorial E region to the higher latitudes (within $\pm 30^\circ$ magnetic latitude) of the F region must not exceed about 12 hours if the entire "circulation" process is to occur during the time the fountain effect is operative. This requirement seems unnecessary in that the "reverse fountain effect" which occurs when the daytime eastward E field reverses to the west is weaker than the daytime fountain (WOODMAN et al., 1977) thus leading to an apparent daily net positive flux of metal ions into the equatorial F region from the equatorial E region. Some evidence for this "pulsed" source of metal ions is found in the observed "clouds" of Mg⁺ reported by MENDE et al., (1985) and possibly by KUMAR and HANSON (1980).

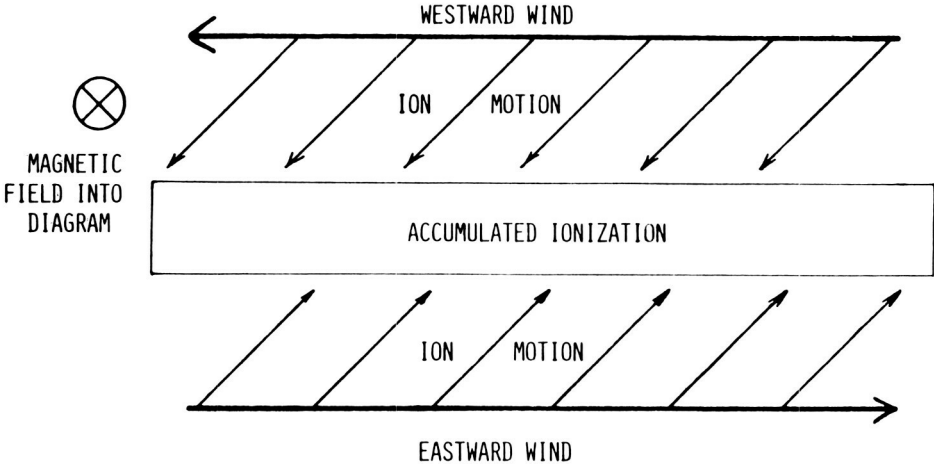


Fig. 3 A schematic representation of the "windshear" or $\underline{V} \times \underline{B}$ mechanism for layer formation. The earth's magnetic field \underline{B} is directed from south to north. Note that in the northern hemisphere the "convergent" node in the zonal tidal wind system corresponds to a maximum southward wind.

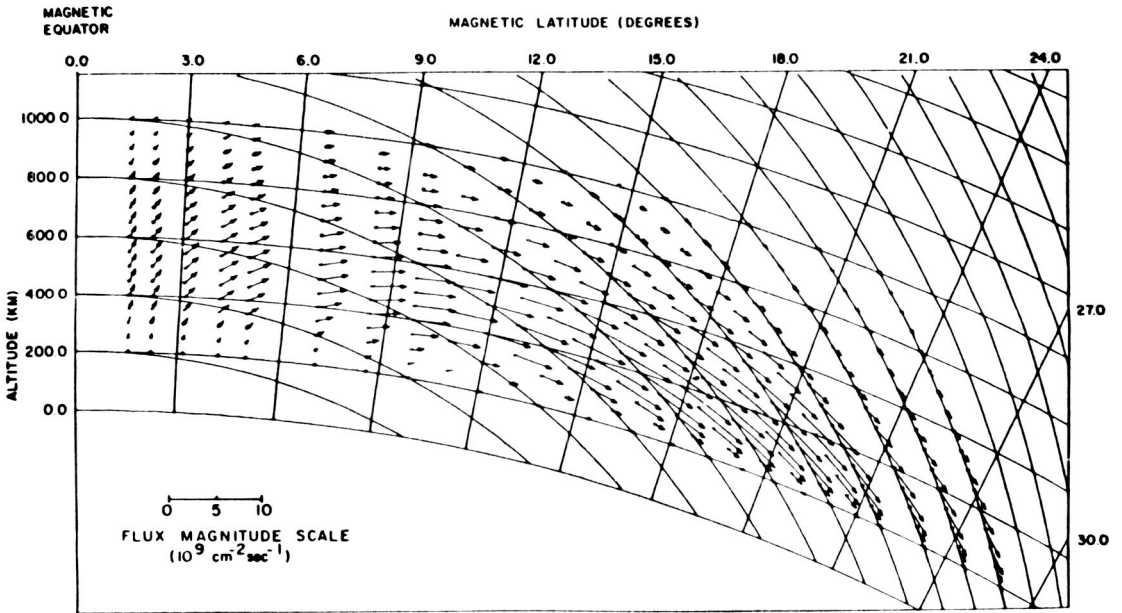


Fig. 4 The meridional plasma drift due to electric and gravitational fields. This drift pattern would carry metal ions from the equatorial F region to magnetic latitudes as high as Arecibo. The metal ions are transported to the equatorial F region via the "fountain effect". [after HANSON and CARLSON, 1977 and HANSON and MOFFETT, 1966].

Finally, we investigate some of the properties of the intermediate layer system shown in Figure 2. This system originates with the F region meridional winds (because the plasma is constrained to move parallel to the B field) where a northward wind above and southward wind below yields a "convergent node". At Arecibo, the F region winds are semidiurnal in character (HARPER, 1977). HARPER notes the twice-per-day formation of the intermediate layer at the "base" of the F region. (Note that Figure 2 shows a more complicated situation due apparently to multiple semidiurnal tidal modes.) He further notes that any metallic ions in the 120-250 km region will be swept into the nearest descending convergent node of the tidal wind system. The formation of intermediate layers in the F region is seen in Figure 8 of HARPER (1977) which is reproduced here as Figure 5.

In Figure 5, we see the basic features of the intermediate layer behavior. That is, winds are moving the F region up and down throughout the night with strong convergent nodes characterizing the actual intermediate layer. The "morning" intermediate layer is actually associated with the descent of the F layer which begins at about 0100 hrs. Also note that here again the 100 km sporadic layer descends and decays away through the night.

We conclude this section by asserting that any metal ions present at Arecibo latitudes in the F region will be swept into the E region by the wind system which forms the intermediate layer. This F to E region transport process then completes the hypothesized metal ion circulation system (MATHEWS and BEKENY, 1979).

III. Aspects of Layer Chemistry

SHEN et al., (1976) consider both photionization and transport in the formation of the intermediate layers observed in Arecibo. They conclude that these layers are not supportable in the 130-160 km E region without a production rate of $1\text{--}5\text{ cm}^3\text{--s}^{-1}$ and/or metallic ions. The suggested production rate is significantly higher than expected for scattered EUV (FUJITAKA et al., 1971) and, as noted in the last section, at least the continual presence of metal ions remains conjectural.

Thus, while the MENDE et al., (1985) results seem to indicate "clouds" of Mg^+ which extend from the E to F region and TEPLEY et al., (1981a) reports Ca^+ in an intermediate layer it is appropriate to further investigate standard (non-metallic) chemistry in the intermediate layer. WEBSTER (1981) has done this via a 2 ion, 1 dimensional chemical-dynamical numerical model of the 110-510 km ionosphere. This model, while simple, contains all the features necessary to investigate the formation, maintenance, and transport of the intermediate layer. The molecular ions NO^+ and O_2^+ are combined into a single effective molecular ion. The nighttime scattered EUV photoionization production sources for NO^+/O_2^+ and O^+ are based on the model of FUJITAKA et al., (1971) and all sources of either NO^+ , O_2^+ , or O^+ (eg N_2^+) are included. A proton-oxygen charge exchange source of O^+ based on the Young et al., (1979) results is also included as is a model of the Arecibo semidiurnal tide.

Results from this numerical model are given in Figure 6 which for display purposes is similar in format to Figure 5. In Figure 6 the

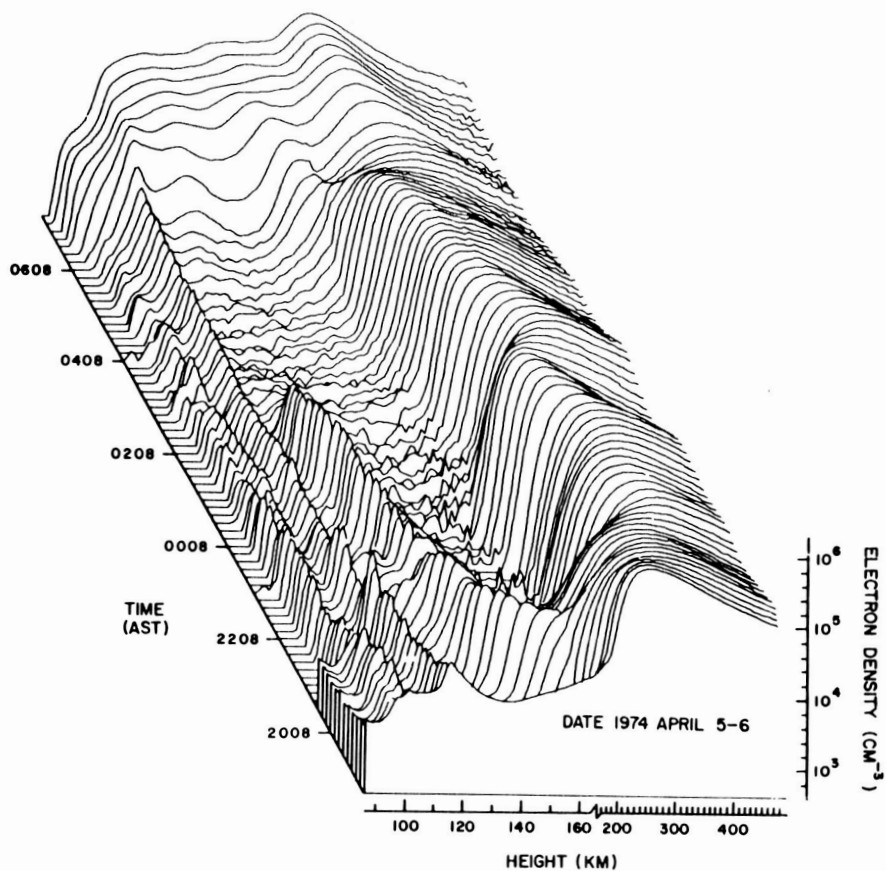


Fig. 5 A three-dimensional presentation of electron concentration plotted on a logarithmic scale versus height and time. Evening and morning intermediate layers are seen to form at the base of the F layer. Note the wavelike motions of the F layer. [From Figure 8; HARPER, 1977 and Figure 5; SHEN et al., 1976].

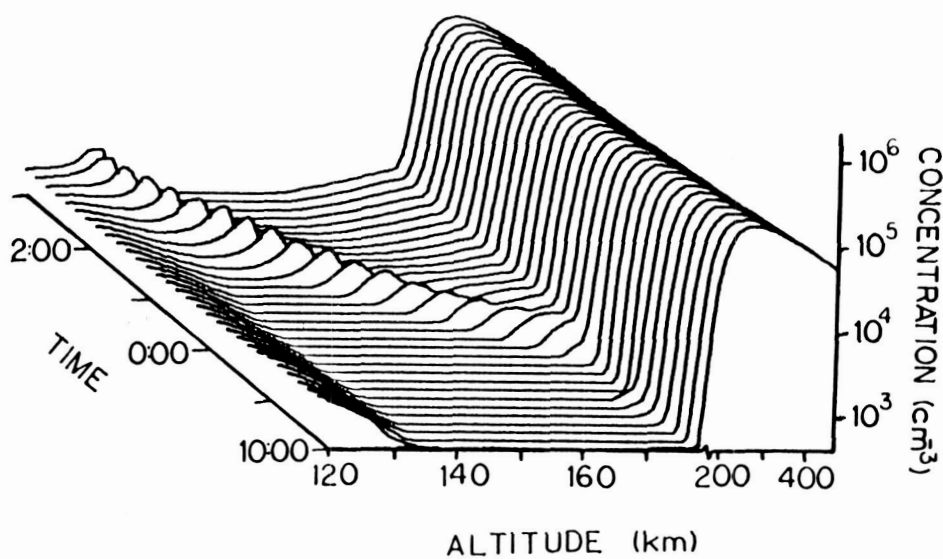


Fig. 6 Model calculations of the formation of an intermediate layer using the nighttime EUV production model of FUJITAKA et al., (1971) and an Arecibo-like semidiurnal wind. This model layer contains only NO^+/O_2^+ and O^+ ions as discussed in the text.

intermediate layer, which is composed of both NO^+/O_2^+ and O^+ , "detaches" from the base of the F layer (note the height scale change at 180 km) and descends to the nighttime E layer. This model intermediate layer has a peak electron concentration of 1000-2000 el/cc and a full width of about 10 km in altitude.

The basis for formation of this layer is that NO^+/O_2^+ ions have 1-2 hour lifetimes away from the layer. Thus convergent vertical ion "winds" of even 5m/sec can sweep ions into the layer from 25 km above or below the layer. Ion lifetime in the layer is less than 10 minutes at the layer peak.

The ion-electron production rate in this model calculation is essentially that shown in Figure 2 of FUJITAKA et al., (1971). That is a local maximum total production rate of $0.5 \text{ cm}^{-3} \text{ s}^{-1}$ at 180 km altitude, a local minimum rate of $0.2 \text{ cm}^{-3} \text{ s}^{-1}$ at 105 km altitude, and a peak rate of $2 \text{ cm}^{-3} \text{ fs}^{-1}$ at 105 km altitude. Thus these rates are sufficient to cause the formation of an intermediate layer which would be observable by the Arecibo radar. However, the more intense intermediate layers studied by SHEN et al., (1976) apparently require much larger production rates of metal ions. No sustained source for the high production rate is known, thus the Figure 6 model calculations suggest that indeed metal ions were present in the layers studied by SHEN et al., (1976).

Clearly metal ions could have been added to the model calculations just described resulting in even more intense intermediate layers. Then, however, the question of altitude distribution of metallic versus molecular ions within an intermediate or sporadic E layer arises. Specifically the long-lived metallic ions are swept to the center of the layer where the resultant increase in electron concentration would decrease molecular ion lifetime against recombination. Thus we expect the presence of metallic ions within layers to "sharpen" the layer peak and perhaps lead to more intense sporadic E.

The combined effect of metallic and molecular ions on layer formation in the 90-130 km altitude region has been investigated by TUCKER (1983) using a numerical model similar to that of WEBSTER (1981). This model also employed the EUV production model of FUJITAKA et al., (1971) while the wind system used was that of MATHEWS and BEKENY (1979). Figure 7 is a three dimension view (electron concentration versus height and time) of a two layer system superimposed on the "background" nighttime E layer. This results is "typical" for Arecibo in that the sporadic E layer appears at the lower heights while two intermediate layers form at the upper boundary, descend, and join. The broad distribution of ionization in Figure 7 is the normal nighttime E layer.

Chemical and dynamical effects in this model are better seen by plotting molecular and metallic ion concentration separately. This is done in Figures 8 and 9 which display the molecular and metallic ion profiles respectively, corresponding to Figure 7. From Figure 8 we see that at higher heights the intermediate layers are composed of molecular ions while at lower heights a "trench" in molecular ion concentration occurs at the layer peak. This "trench" corresponds to a maximum in metallic ion concentration as seen in Figure 9. This model was "started" with an even

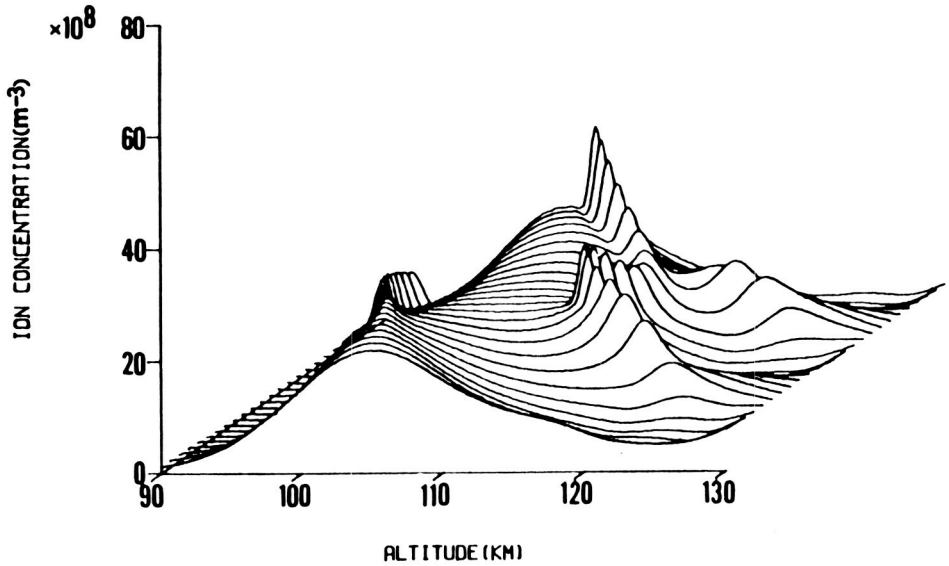


Fig. 7 Model electron concentration is plotted versus height and time. The FIJITAKA et al. (1971) nighttime production source and the MATHEWS and BEKENY (1979) diurnal and semidiurnal tidal wind system were used in these calculations which cover 26 hours with each contour separated by 4000 sec. The nighttime production source was used for the whole calculation so as to not mask layer dynamics for this presentation. Note the sporadic E layer at 105 km and below and the two intermediate layers which join at 110 km and at middle times.

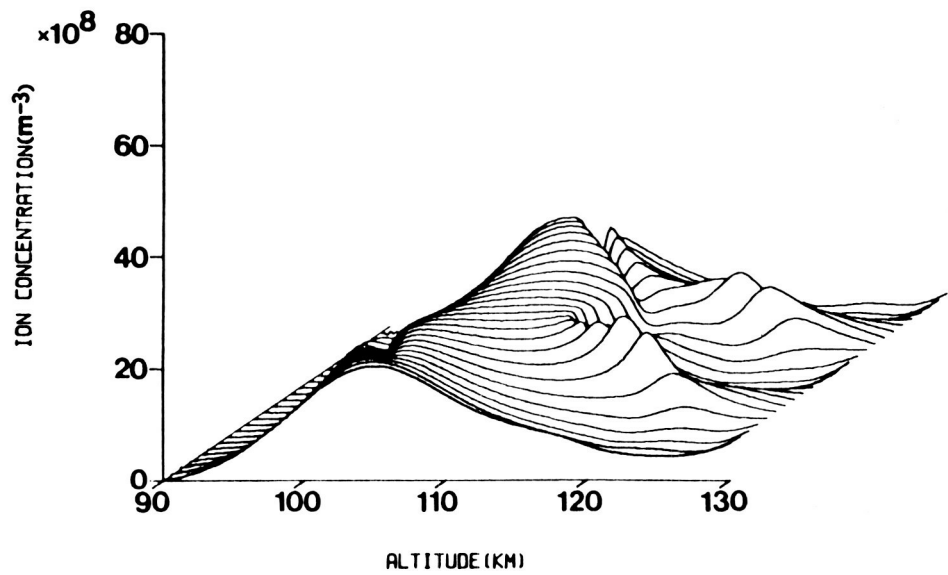


Fig. 8 The molecular ion concentration corresponding to the model results shown in Figure 7. Note that molecular ion concentration is depressed at the center of the large layers shown in Figure 7. This is due to the enhanced electron-molecular ion recombination rate in the layer.

ORIGINAL PAGE IS
OF POOR QUALITY

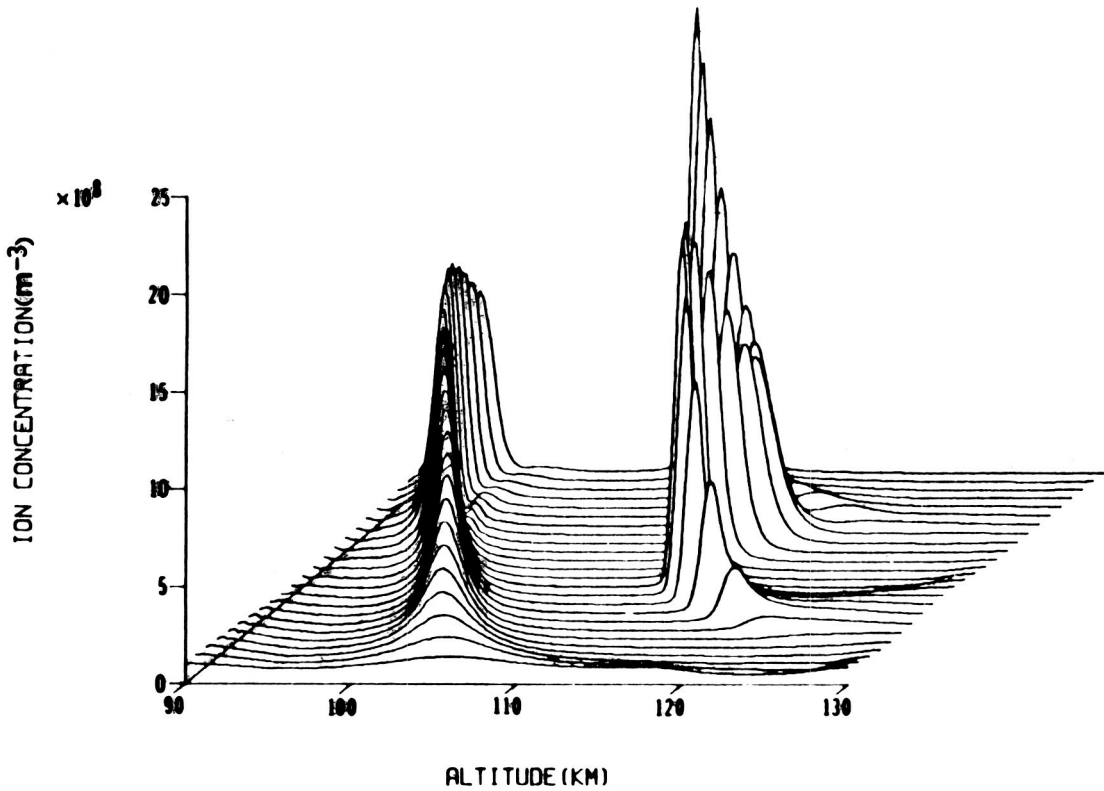


Fig. 9 The metallic ion concentration corresponding to the model results shown in Figure 7. The initial 100 metal ions per cc are seen to form into highly peaked "sporadic" layers.

distribution of metal ions (10^{22} cm^{-3}) so that once these ions accumulated in layers no additional metallic ions were available to, for example, enhance the peak concentration of the second intermediate layer.

An important result of these calculations is seen in Figure 10 which is a "cross-section" of Figure 7. From Figure 10 it is clear that the metal ion layers substantially depress molecular ion concentrations at the center of the layer. Also, the molecular ions at layer edges help support the layer against diffusion resulting in somewhat narrower and more intense layers when compared with the metal ion only case. However, this molecular ion enhancement of sporadic layers, in which metal ion diffusion is slowed by the molecular ion layer edges, in no way explains the very intense sporadic E events which are often observed at Arecibo and elsewhere. These events are apparently due to some other physical process (eg. local horizontal currents) which sufficiently counteract diffusive forces.

We have discussed the roles of chemistry and dynamics in the formation and maintenance of intermediate and sporadic E layers. These layers are a manifestation of the mechanism by which metallic ions maybe transported to, from, and across the meteor source region. We turn next to mechanisms by which metallic ions are finally lost from the 90 km and above region. An example of this loss process is seen in Figures 1, 2, and 5 where the very low lying sporadic layers are "dumped" at about 90 km altitude. This process is particularly evident in Figure 2 at 90 km and zero hours where on each day the diurnal tide dumps the layer.

The "dumping" of metallic ions into the 90 km altitude region is discussed by MATHEWS and BEKENY (1979) and occurs when the vertical ion velocity becomes less than the tidal phase velocity resulting in the layer being left behind as the tidal mode descends. The "dumped" layer then dissipates because of diffusion, electron-ion recombination, or possibly because of attachment of electrons to dust forming negative ions. Formation of stable molecular negative ions by the "usual" chemical paths is not thought to be effective above 85 km altitude even at night (eg. GANGULY, et al., 1979).

Recombination becomes an efficient loss mechanism when atmospheric pressure is high enough for three body (neutral reactant (eg. O), atomic ion, third particle) reactions (BROWN, 1973; BANKS and KOCKARTS, 1973; Section 9.2) to occur. Three body reactions lead to the formation of metal based molecular ions (eg. BROWN, 1973; Table 10) and are efficient below 100 km altitude. These ions can then recombine with electrons or participate in other chemistry.

Model calculations (MURAD, 1978; TEPLEY, 1981) indicate that concentration ratio of molecular metal ions (eg MO^+ , MN_2^+ etc.) to parent ion are small at all heights above 80 km altitude. That is while these ions form they are rapidly converted to neutral species via electron recombination (eg. $\text{MO}_2^+ + e^- \rightarrow \text{M} + \text{O}_2$) or to other ion forms. MURAD (1978) argues that detection of metal oxide ions by rocket mass spectrometric measurements (see MURAD for references) is probably invalid due to hydrocarbon contamination of the instruments. A further possibility that atomic or molecular metal ions attach directly to dust or meteoric smoke particles will be discussed shortly.

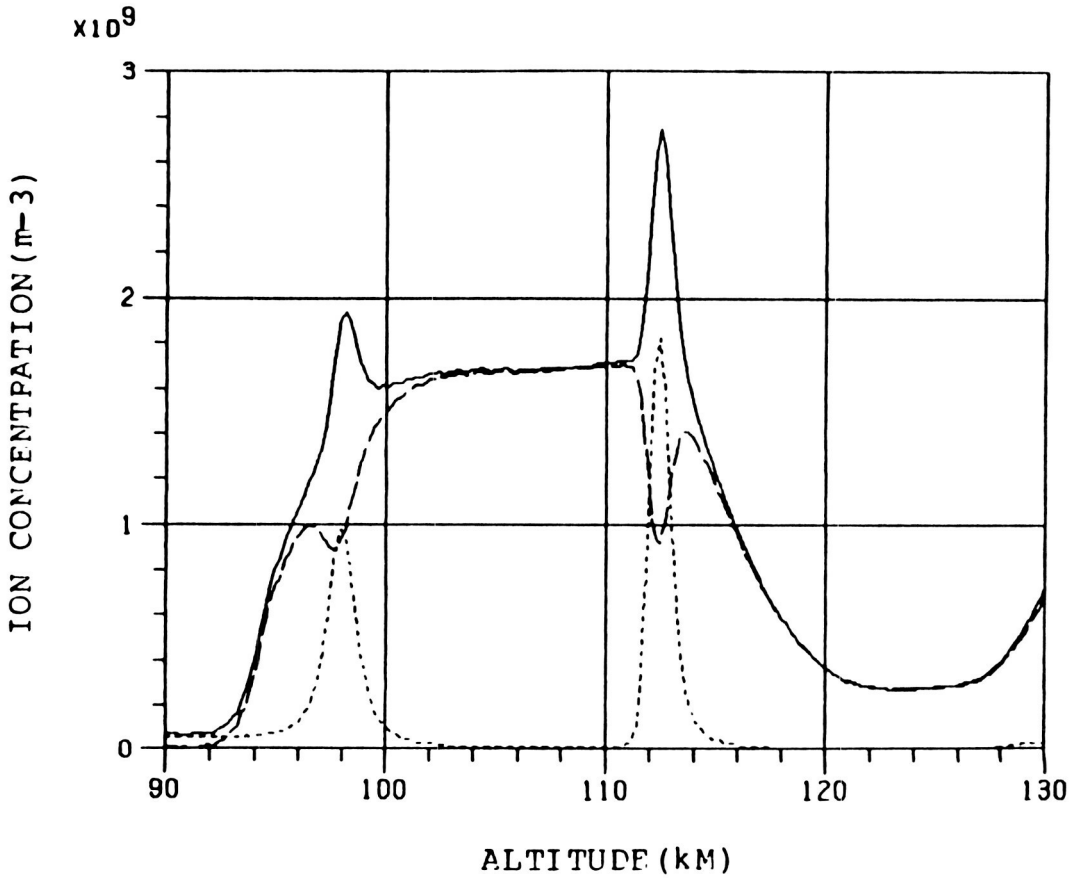


Fig. 10 Concentration cross-section of Figures 7, 8, and 9 at $t = 14.5$ hours. The short dashed line is the metal ion concentration etc. The presence of the molecular ions supports a somewhat narrower more intense (10-20%) metal ion layer that could exist otherwise.

Combined three body and two body reactions leading to neutral atomic metal and metal compounds then appear to be the major sink for atomic metal ions with the possible exception of direct attachment to dust. Fortunately ground based remote sensing of the metal ion-to-neutral ratio is possible. TEPLEY, et al. (1981 a,b) reports on separate Ca^+ and Fe concentration determinations via twilight resonant scattering of sunlight while GRANIER, et al., (1984) report almost simultaneous common value lidar measurements of Ca and Ca^+ concentration profiles. The GRANIER, et al. results are given in Figure 11.

All available evidence indicates that the atomic metal ion-to-neutral concentration ratio reaches one between 90 km and 100 km altitude and increases rapidly with increasing altitude. Also a modest "reservoir" of neutral atomic metals appears to be centered at 85-90 km altitude. Two important results seen in Figure 11 are the similar but displaced Ca and Ca^+ profiles and that the Ca concentration profile decreases sharply on the layer bottomside. The Figure 11 Ca^+ results are similar to those expected based on incoherent scatter radar total layer metal ion (i.e., electron) concentration measurements and the distribution of the elements in the average meteor. Lidar and combined lidar/incoherent scatter radar measurements will in the future add considerably to our knowledge of metal ion chemistry in the "dumping" region.

While the chemical mechanisms are probably many and uncertain it does seem clear that the neutral atomic metals become involved in reactions leading ultimately to the formation or growth of the meteoric "smoke" particles of HUNTEN, et al., (1980).³ HUNTEN estimates the concentration of the smoke particles to be $\sim 1000 \text{ cm}^{-3}$ and that this concentration falls off rapidly above 90 km altitude. As an estimate of the importance of meteoric mass appearing directly as smoke relative to ionized forms transported in layers we note that estimated meteoric mass influx of 44 metric tons per day corresponds to a particle flux of $\sim 10^6 \text{ cm}^{-2} \text{ s}^{-1}$ mass 57 amu atoms.³ The typical low lying sporadic layer has a peak concentration of $\sim 10^4 \text{ cm}^{-3}$ and a vertical speed of 10^2 cm/sec or a particle flux of $\sim 10^6 \text{ cm}^{-2} \text{ s}^{-1}$ also. The sporadic E layer arrives at 90 km altitude over only one or two hours per day. However, the point remains that at least sometimes meteoric ion flux in sporadic layers probably equals total meteor mass flux at 90 km altitude. The ion flux from sporadic layers may then influence the growth or even formation of the smoke particles while the dust or smoke particles possibly effect the ion chemistry.

HUNTEN takes the minimum size of the smoke particles to be a radius of 2A with a maximum density of 4 gm cm^{-3} corresponding to a particle mass of 80 amu. As the smoke particle grows it falls through the atmosphere until for a variety of reasons it is brought to the surface.

We are concerned with the role of meteoric smoke not only as a "sink" for atomic metals but also as an influence on the aeronomy of the meteor zone. Dust has long been considered important to the formation of noctilucent clouds at high latitudes. TURCO et al., (1982) extensively treats the problem of noctilucent cloud formation including effects of ion attachment to dust or ice particles. PARTHASARATHY (1976) has considered dust a direct "sink" for D region ionization. We will dwell on the latter

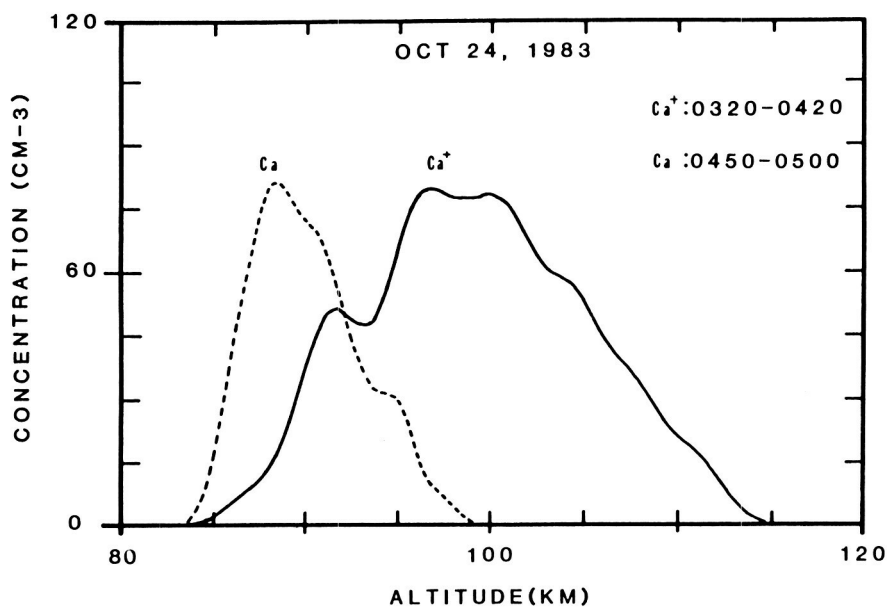


Fig. 11 Profiles of Ca and Ca^+ concentration obtained by LEDAR at the Observatoire de Haute Provence and reported by GRANIER et al., (1984).

as noctilucent clouds are not an aspect of low and mid-latitude D region aeronomy.

The role of dust in ion chemistry is of interest not only as a possible mechanism for growth of dust by accumulation of metals in both ion and neutral form but also because of associated possible effects on the "normal" molecular (NO^+ , O_2^+) and atomic metal ion chemistry near 90 km altitude. Dust particles presumably effect ion chemistry simply by successive capture of ions and electrons and possibly by photoelectric emission of electrons from the dust particles. Parthasarathy finds dust effects significant only if dust concentrations are large ($>> 1 \text{ cm}^{-3}$); however, he considers only very massive dust particles ($\sim 10^{10} \text{ amu}$).

HUNTEN et al., (1980; Figures 4 and 5) treat a spectrum of particle sizes. For initial smoke particles of radius 2A ($\sim 80 \text{ amu}$) peak dust concentrations of $5 \times 10^4 \text{ cm}^{-3}$ are predicted for 85 km altitude while for 10A radius ($\sim 10^4 \text{ amu}$) a peak concentration of $3 \times 10^3 \text{ cm}^{-3}$ is predicted for 80 km altitude. The corresponding surface areas per unit volume (A) of the dust are $10^{-9} \text{ cm}^2/\text{cm}^3$ and $7 \times 10^{-10} \text{ cm}^2/\text{cm}^3$ respectively. The mean time between collisions (Maxwellian velocity distribution) assuming uncharged dust and neutral atoms or molecules is $\tau = 4/A \sqrt{v}^2 = 8 \text{ kT/m}$, $k =$ Boltzmann's constant, $T =$ absolute temperature, $m =$ mass of colliding atom or molecule) or about two days at 90 km altitude. The mean time between attachment events for a single electron with dust would clearly be much faster (~ 15 minutes) using the above formula. However, the induced dipole moment would significantly increase the collision rate of electron and ions with uncharged dust.

We thus expect the dust or smoke particles to effect neutral atomic metals or metal compounds on the time scale of a day or two. For example at the peak Ca concentration of 10^{-4} cm^{-3} in Figure 11 the collision rate is $5 \times 10^{-4} \text{ cm}^{-3} \text{ s}^{-1}$. However, in a 90 km sporadic layer of peak electron concentration 10^4 cm^{-3} the ion collision rate with dust would be $5 \times 10^{-2} \text{ cm}^{-3} \text{ s}^{-1}$ and the electron collision rate would be $10^{-3} \text{ cm}^{-3} \text{ s}^{-1}$. The three body reaction producing metal dioxides (rate $2.5 \times 10^{-30} \text{ cm}^{-6} \text{ s}^{-1}$ for iron; BROWN, 1973) would have a reaction rate of $25 \text{ cm}^{-3} \text{ s}^{-1}$ at 90 km assuming $10 \text{ cm}^{-3} \text{ M}$ (assuming most metals have similar rates) concentration in the layer. Thus, if the HUNTEN et al., (1980) estimates of smoke and dust concentration at 90 km altitude are correct it seems plausible that the dust effects ion chemistry via at least electron attachment.

HUNTEN notes that the predicted dust content will Rayleigh scatter lidar signals much less than the atmosphere and thus not be detectable in this manner. However, there is some very preliminary evidence of charged dust (massive ions) effecting the incoherent scatter radar "ion line" spectrum.

MATHEWS (1984, 1986) describes incoherent scatter radar probing of the D region. In particular he describes the so-called ion line spectral shape as always being of Lorentzian shape for the collision dominated (diffusion limit) case and double humped for the wave limit. For the Arecibo 430 MHz radar the transition between the two regimes occurs between 90 km and 95 km altitude so that all D region spectra are in the diffusion limit. MATHEWS

(1984) also notes that the presence of negative ions broadens the spectrum in either limit as shown in Table 3 of that paper.

Figure 12 shows a sequence of Arecibo electron concentration profiles showing two different sporadic layers centered at 92 km and 112 km altitude. These layers are in every way normal when viewed in this manner and in Figure 13 the ion spectra of the lower layer are shown at one time (spectral and total power measurements are interleaved in time). The spectrum at 91.36 km is an example of the expected Lorentzian shape though its width is 13% narrower than the daytime molecular ion spectrum (TEPLEY and MATHEWS, 1985) because of the more massive metal ions characteristic of the layer. Most individual spectra are flat indicating no incoherent scatter signal.

Figure 14 shows that set of spectra measured next in sequence from those of Figure 13. Note that signal spectra occur only at the heights of those in Figure 13 but that the edges of the spectra are "turned up". These "events" are observed only occasionally but appear to be always associated with low lying sporadic layers and on the basis of Figure 13 to 14 like comparisons it seems certain that this phenomena is associated with the layer.

Use of a theoretical model of the incoherent scatter spectral shape indicates that these spectra are possible only in the transition region between the wave and diffusion spectral limits. Also and most importantly these spectra are consistent with 600-1000 amu ions having a negative ion-to-electron concentration ratio of about 3. These massive ions, if they exist, seem to occur only in horizontally small and vertically narrow "clouds" and do appear to be mixed (within the 600 m height resolution) with "normal" ions. Much more study remains concerning this possibly very important and just recognized phenomenon.

Again combined lidar and incoherent scatter radar studies of those layers might resolve the issue of massive versus "normal" ions. One straightforward indicator might be a dip in Ca^+ content in a layer which exhibits the unusual incoherent scatter spectra.

IV. Summary and Discussion

We have attempted to show that meteoric debris in the ionosphere and upper middle atmosphere form an interesting, pervasive, and diagnostically useful subject for study. We suggest that metallic atomic ions which form as meteors "burn up" in the 80-110 km region circulate in the low and mid latitude region due to tidal and electrodynamic effects. The suggested circulation system includes an E to F to E region path with the equatorial fountain providing the only E to F region transport mechanism. Metal ions are returned to the E region via intermediate layers. High latitude upward transport mechanisms (eg. GREBOWSKY and PHARO. 1985) have not been discussed here. Also, not mentioned are the various aspects of the "sodium problem" which is amenable to lidar studies [eg. RICHTER et al., 1981; BATISTA et al., 1985 and references of both]. While the aeronomy of sodium parallels that of the pure metals there are apparent differences which demand a separate detailed treatment which cannot be undertaken here.

C-4

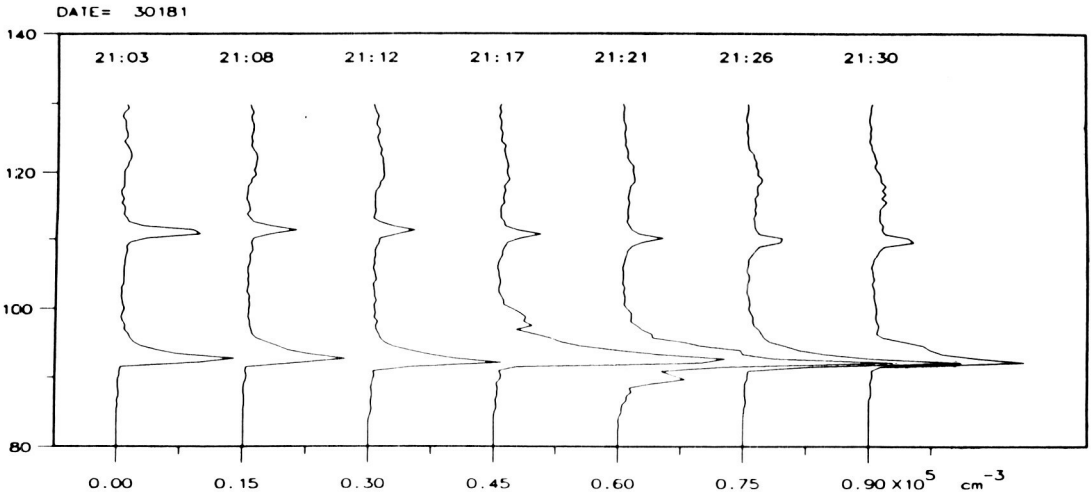


Fig. 12 Electron concentration profiles of a double layer sporadic E system at Arecibo. These profiles are unsmoothed in time or height and have 600 m height and 55 second time resolutions. The low lying layer has a peak concentration of 3×10^4 el/cc at 2121 hours and appears to perfectly "normal".

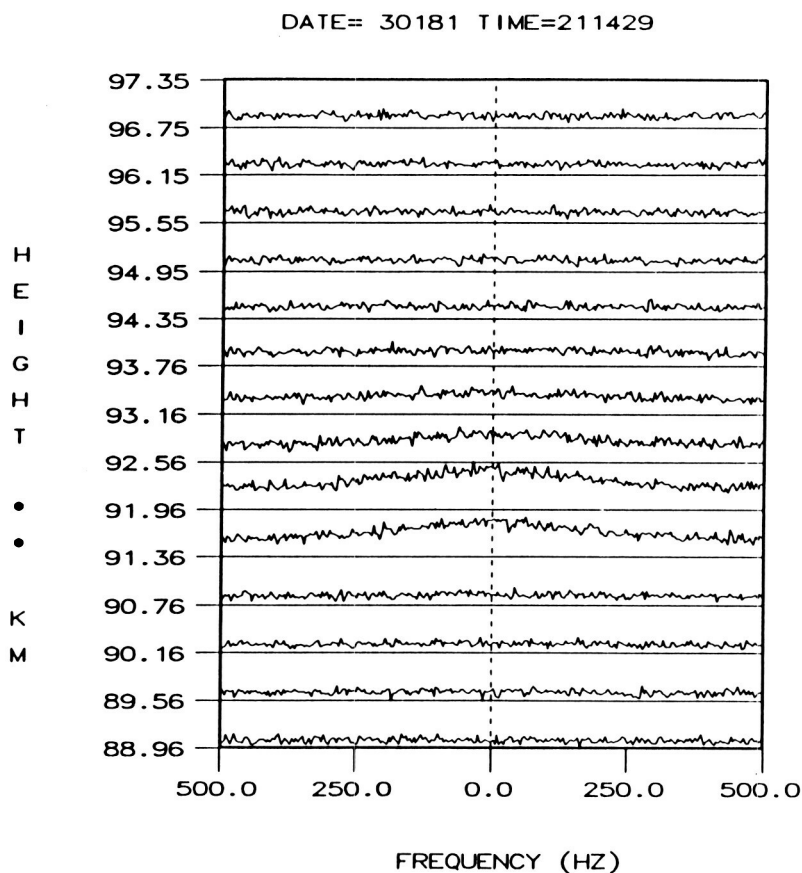


Fig. 13 A set of "normal" ion line spectra obtained between the 2112 and 2117 hrs profiles of Figure 12. The flat spectra indicate no signal while the Lorentzian shaped spectra correspond exactly in height to the lower sporadic layer in Figure 12.

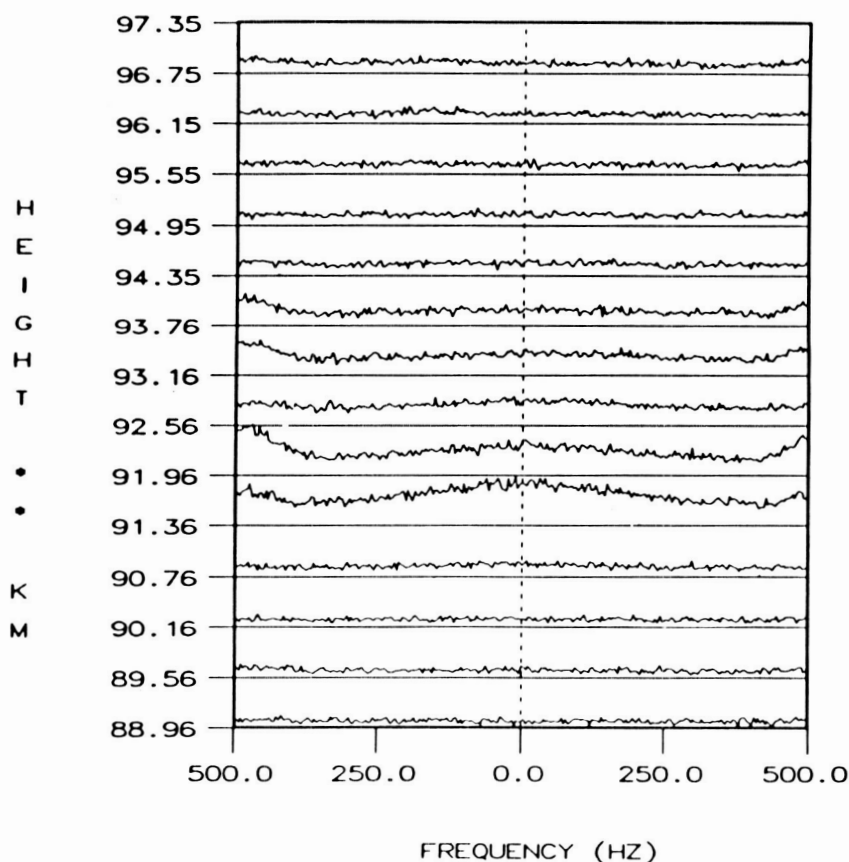


Fig. 14 Similar to and immediately following the spectra shown in Figure 13. Note that the signal or sporadic E spectra have additional "wind" features. The features have been tentatively been identified with 600-1000 amu ions with a negative ion-to-electron concentration ratio of ~ 3 .

ORIGINAL PAGE IS
OF POOR QUALITY

We have also discussed some details of intermediate and sporadic E layer dynamics and chemistry. We demonstrate that intermediate layers have significant molecular ion makeup and that metallic ions suppress molecular ion concentration in both intermediate and sporadic E layers. We note that no satisfactory explanation for intense (blanketing) sporadic E exists.

Also discussed are aspects of metal ion chemistry in the 90 km altitude "dumping" region. Included here is the role of these ions in the formation and growth of dust. If the HUNTEN et al., (1980) estimate of dust or smoke surface area is correct then this form of meteoric debris quite likely effects the ion chemistry of the region. The Arecibo incoherent scatter radar has possibly detected the massive (600-1000 amu) ions involved in this interaction.

We conclude that study of meteoric debris particularly in the 80-120 km region is vital to understanding at least the ion chemistry of the region. This study would also lead to much new information concerning the formation, growth, and effects of dust in the region. Common volume, simultaneous lidar and incoherent scatter radar measurements particularly if supplemented with rocket measurements of the D and E regions would yield the best data concerning these issues.

Acknowledgements

I would like to thank R. G. Roper, V. A. Nechitailenko, and the Soviet Geophysical Committee of the Academy of Sciences of the USSR for the opportunity to travel to Dushanbe and present this paper. I thank my academic department and the National Science Foundation (NSF) (via a grant to Georgia Institute of Technology) for travel support. Some data presented was obtained at Arecibo Observatory which is operated by Cornell University under contract with the NSF. The writing of this paper and incidental travel expenses were supported under NSF grant ATM84-18977 to Case Western Reserve University.

References

1. Aikin, A.C., and R.A. Goldberg, Metallic Ions in the Equatorial Ionosphere, J. Geophys. Res., 78, 734-735, 1973.
2. Banks, P.M., and G. Kockarts, Aeronomy, Part A, Academic Press, New York, 1973.
3. Batista, P.P., B.R. Clemesha, D.M. Simonich, and V.W.J.H., Kirchhoff, Tidal Oscillations of the Atmospheric Sodium Layer, J. Geophys. Res., 90, 3881-3888, 1985.
4. Behnke, R.A., and J.F. Vickrey, Radar Evidence for Fe^+ in a Sporadic -E Layer, Radio Sci., 10, 325-327, 1975.
5. Brown, T.L., The Chemistry of Metallic Elements in the Ionosphere and Mesosphere, Chem. Reviews, 73, 645-667, 1973.
6. Chimonas, G., and W.I. Axford, Vertical Movement of Temperate Zone Sporadic -E Layers, J. Geophys. Res., 73, 111-117, 1968.

7. Fensen, C.G., and P.B. Hays, Mg^+ Morphology from Visual Airglow Experiment Observations, *J. Geophys. Res.*, 87, 9217-9223, 1982.
8. Fujitaka, K., T. Ogawa, and T. Tohmatsu, A Numerical Computation of the Ionization Redistribution Effect of the Wind in the Nighttime Ionosphere, *J. Atmos. Terr. Phys.*, 33, 687-700, 1971.
9. Fujitaka, K., and T. Tohmatsu, A Tidal Theory of the Ionospheric Intermediate Layer, *J. Atmos. Terr. Phys.*, 35, 425-438, 1973.
10. Ganguly, S., J.D. Mathews, and C.A. Tepley, Thomson Scatter Radar Detection of D Region Negative Ions at Arecibo, *Geophys. Res. Lett.*, 6, 89-92, 1979.
11. Granier, C., J.P. Jegou, and G. Megie, Resonant Lidar Detections of Ca and Ca^+ in the Upper Atmosphere, Proceedings of the 12th International Laser Radar Conference, Provence, France, 13-17 August 1984.
12. Grebowsky, J.M., and H.C. Brinton, Fe^+ Ions in the High Latitude F Region, *Geophys. Res. Lett.*, 5, 791-794, 1978.
13. Grebowsky, J.M., and M.W. Pharo III, The Source of Midlatitude Metallic Ions at F-region Altitudes, *Planet. Space Sci.*, 33, 807-815, 1985.
14. Hanson, W.B., and H.C. Carlson, The ionosphere, Chapt. 5, The Upper Atmosphere and Magnetosphere, National Academy of Sciences, Wash. D.C., 1977.
15. Hanson, W.B., and R.J. Moffett, Ionization Transport Effects in the Equatorial F Region, *J. Geophys. Res.*, 71, 5559-5572, 1966.
16. Hanson, W.B., D.L. Sterling, and R.F. Woodman, Source and Identification of Heavy Ions in the Equatorial F Layer, *J. Geophys. Res.*, 77, 5530-5534, 1972.
17. Harper, R.M., Tidal Winds in the 100 to 200 km Region at Arecibo, *J. Geophys. Res.*, 82, 3242-3250, 1977.
18. Hughes, D.W., Meteors, Chapt. 3 in Cosmic Dust, Edited by J.A.M. McDonnell, Wiley, 1978.
19. Hunten, D.M., R.P. Turco, and O.B. Toon, Smoke and Dust Particles of Meteoric Origin in the Mesosphere and Stratosphere, *J. Atmos. Sci.*, 37, 1342-1357, 1980.
20. Kumar, S., and W.B. Hanson, The Morphology of Metallic Ions in the Upper Atmosphere, *J. Geophys. Res.*, 85, 6783-6801, 1980.
21. Martyn, D.F., Geomagnetic Anomalies of the F2 Region and Their Interpretations, in The Physics of the Ionosphere, pp 260-264, The Physical Society, London, 1955.
22. Mathews, J.D., The Incoherent Scatter Radar as a Tool for Studying the Ionospheric D Region, *J. Atmos. Terr. Phys.*, 46, 975-986, 1984.
23. Mathews, J.D., Measurements of the Diurnal Tides in the 80 to 100 km Altitude Range at Arecibo, *J. Geophys. Res.*, 81, 46712-4677, 1976.

24. Mathews, J.D., and F.S. Bekeny, Upper Atmosphere Tides and the Vertical Motion of Ionospheric Sporadic Layers at Arecibo, *J. Geophys. Res.*, 84, 2743-2750, 1979.
25. Mathews, J.D., Incoherent Scatter Radar Probing of the 60-100 km Atmosphere and Ionosphere, *IEEE Trans. Geosci. Remote Sensing*, in Press, 1986.
26. Mende, S.B., G.R. Swenson, and K.L. Miller, Observations of E and F Region Mg⁺ from SpaceLab I, *J. Geophys. Res.*, 90, 6667-6673, 1985.
27. Murad, E., Problems in the Chemistry of Metallic Species in the D and E Regions, *J. Geophys. Res.*, 83, 5525-5530, 1978.
28. Parthasarathy, R., Mesopause Dust as a Sink for Ionization, *J. Geophys. Res.*, 81, 2392-2396, 1976.
29. Richter, E.S., J.R. Rowlett, C.S. Gardner, and C.F. Sechrist, Jr., Lidar Observations of the Mesospheric Sodium Layer Over Urbana, Illinois, *J. Atmos. Terr. Phys.*, 43, 327-337, 1981.
30. Shen, J.S., W.E. Swartz, D.T. Farley, and R.M. Harper, Ionization Layers in the Nighttime E Region Valley Above Arecibo, *J. Geophys. Res.*, 81, 5517-5526, 1976.
31. Swider, W., Ionic and Neutral Concentrations of Mg and Fe Near 92 km, *Planet. Space Sci.*, 32, 307-312, 1984.
32. Tepley, C.A., and J.D. Mathews, An Incoherent Scatter Radar Measurement of the Average Ion Mass and Temperature of a Nighttime Sporadic Layer, *J. Geophys. Res.*, 90, 3517-3519, 1985.
33. Tepley, C.A., J.D. Mathews, J.W. Meriwether, and J.C.G. Walker, Observations of the Ca⁺ Twilight Airglow From Intermediate Layers of Ionization, *J. Geophys. Res.*, 86, 7781-7786, 1981 a.
34. Tepley, C.A., J.W. Meriwether, J.C.G. Walker, and J.D. Mathews, Observations of Neutral Iron Emission in Twilight Spectra, *J. Geophys. Res.*, 86, 4831-4835, 1981 b.
35. Turco, R.P., O.B. Toon, R.C. Whitten, R.G. Keesee, and D. Hollenback, Noctilucent Clouds: Simulation Studies of Their Genesis, Properties and Global Influences, *Planet. Space Sci.*, 30, 1147-1181, 1982.
36. Whitehead, J.D., Difficulty Associated with the Windshear Theory of Sporadic E, *J. Geophys. Res.*, 76, 3127-3135, 1971.
37. Woodman, R.F., R.G. Rastogi, and C. Calderon, Solar Cycle Effects on the Electric Fields in the Equatorial Ionosphere, *J. Geophys. Res.*, 82, 5257-5261, 1977.
38. Young, E.R., D.G. Torr, and P.G. Richards, Counterstreaming of O⁺ and H⁺ Ions in the Plasmasphere, *Geophys. Res. Lett.*, 6, 925-928, 1979.
39. Volland, H., Atmospheric Electrodynamics, Springer-Verlag, Berlin, 1984.

40. Zbinden, P.A., M.A. Hidalgo, P. Eberhardt, and J. Geiss, Mass Spectrometer Measurement of the Positive Ion Composition in the D- and E- Regions of the Ionosphere, Planet. Space Sci., 23, 1621-1642, 1975.

Reference is also made to the following unpublished material:

41. Tepley, C.A., An Investigation of Temperature and Metallic Composition of the Lower Ionosphere, Ph.D. Thesis, Department of Electrical Engineering and Applied Physics, Case Western Reserve University, Cleveland, Ohio, 1981.
42. Tucker, T., A Computer Model of Sporadic Ion Layers in the E-region of the Ionosphere, MS Thesis, Department of Electrical Engineering and Applied Physics, Case Western Reserve University, Cleveland, Ohio, 1983.
43. Webster, R.B., The Development of a Numerical Model of the Nocturnal F Region, M.S. Thesis, Department of Electrical Engineering and Applied Physics, Case Western Reserve University, Cleveland, Ohio, 1981.

THE END HEIGHT OF FIREBALL AS A FUNCTION
OF THEIR RESIDUAL KINETIC ENERGY

D. O. ReVelle

Meteorology Program
Northern Illinois University
DeKalb, Illinois, U.S.A.

Abstract

Previous analyses of meteoroid compositional groupings have utilized the end height of fireballs as a diagnostic tool. From an observational perspective this definition is straight forward, but from a theoretical viewpoint there are problems with using this operational definition. These include:

- a) Dependence of end height on slant range due to extinction for long optical paths;
- b) Minimum mass sensitivity effects due to ablation, gross fragmentation, etc.;
- c) Limiting wavelength and amplitude detection due to sky brightness, response of the emulsion, etc.;
- d) Theoretical predictions of an optically thick radiation field at low altitudes for high velocity entry (Biberman et al., 1980).

In order to realistically assess the estimated geometric uncertainty of + 1km in the observed end height, a theoretical definition of the end height of meteoritic fireballs is proposed using the results from the integral radiation efficiency model of REVELLE (1980). Three photographed and recovered meteorites, Pribram, Lost City and Innisfree are used as a calibration for this proposed definition. These three fireballs were calculated as having about 99% of their pre-atmospheric kinetic energy removed prior to the dark flight phase. Assuming that a fixed fraction of the initial kinetic energy will remain at the end height, a prediction of the theoretical end height can be made directly.

This definition has been used to evaluate the end height of all fireballs that were deduced by WETHERILL and REVELLE (1981) as being "meteoritic". In almost all cases the theoretical values are lower than the observed values, in some cases being as much as 5km lower. A preliminary summary table of results is given below.

This work was supported by Universities Space Research Association while the author was a Visiting Scientist at NASA/MSFC, Huntsville, Alabama.

Evaluation of fireball end heights with $\sigma = 0.02^2/\text{km}^2$, $H = 8 \text{ km}$ and $D_e = 4.60$.

Fireball Name/Number	I_m (g)	$\cos Z_R$	v_∞ (km/sec)	v_e (km/sec)	z_e (km)	Observed end Height (km)
PN39113A	$7.4 \cdot 10^3$	0.93	14.9	8.0	21.7	26.6
PN39409	$7.2 \cdot 10^2$	0.74	31.7	6.6	52.1^2 (40.8)	39.9
PN39499	$6.2 \cdot 10^3$	0.23	12.4	7.0	31.0	36.6
PN40503	$2.7 \cdot 10^6$	0.62	20.9	11.7	16.0	21.5
PN40590 (Lost City)	$6.0 \cdot 10^4$	0.62	14.2	3.5	19.3	19.9
PN40617	$1.0 \cdot 10^4$	0.52	13.2	4.6	24.3	26.3
Pribram	$1.4 \cdot 10^6$	0.69	20.89	7^3	18.4	13.3
Innisfree	$2.0 \cdot 10^4$	0.92	14.54	2.59	19.6	19.9

Legend

- 1 Mass values have been assigned by either the entry model values given in REVELLE (1979) (Lost City, Innisfree and Pribram), by photometric mass given in CEPLECHA and MCCROSKY divided by 13 (WETHERILL and REVELLE, 1981) (40503), or by three times the initial dynamic mass given in WETHERILL and REVELLE (1981) (39113A, 39409, 39499 and 40617).
- 2 Alternative value assuming $\sigma = 0.01$ at high velocity for large bodies (BIBERMAN et al., 1980).
- 3 Originally estimated as $10 \pm 7 \text{ km/sec}$ (see REVELLE, 1979).

REFERENCES

1. L.M. Biberman, C. Ya. Bronin and M.V. Brykin: Motion of a Blunt Body Through the Dense Atmosphere Under Conditions of Severe Aerodynamic Heating and Ablation, Acta Astronautica, 7, 53-65, 1980.
2. D.O. ReVelle: A Predictive Macroscopic Integral Radiation Efficiency Model, J. Geophys. Res., 85, 1803-8, 1980.
3. G.W. Wetherill and D.O. ReVelle: Which Fireballs are Meteorites?, A Study of the Prairie Network Photographic Meteor Data, Icarus, 48, 308-28, 1981.
4. D. O. ReVelle: A Quasi-Simple Ablation Model for Large Meteorite Entry: Theory Versus Observations, Journal of Atmospheric and Terrestrial Physics, 41, 453-73, 1979.

OZONE FORMATION DUE TO INTERACTION OF METEORIDS
WITH EARTH'S ATMOSPHERE

R. Sh. Bibarsov

Institute of Astrophysics
Dushanbe, USSR

In the previous paper (BIBARSOV, 1985) it was shown that concentration of atomic oxygen in overdense meteor trails may exceed that of the normal atmosphere by a factor of several hundred times. This may lead to the formation of meteoric ozone. Therefore, it is imperative to estimate the concentration of ozone in the trails of meteor bodies with different masses.

In the atmosphere, ozone is formed by Chapman's reaction:



where M is a particle of air or of meteoric matter.

Simultaneously other reactions occur that lead to the loss of O_3 and O :



The reactions (1)-(4) support the chemical balance of atmospheric particles.

The interaction of meteoroids with the Earth's atmosphere leads to a disturbance of the chemical balance of atmospheric particles in some air volume along the trajectory. This and subsequent dissociation of oxygen molecules by evaporated atoms of the meteoroid. While balance is recovered again through the reactions (1)-(4), the relative concentration of particles becomes different.

The concentration of newly formed ozone at the initial stage of meteor trail existence can be estimated.

The atomic oxygen concentration n_1 resulting from dissociation of oxygen molecules is $n_1 = 2\gamma n_m$ where γ is the dissociation coefficient of O_2 and n_m is the concentration of the evaporated meteor atoms. Both γ and n_m may be determined from the formulas:

$$\gamma_s = 2.82 \cdot 10^{-2}(V - 9.5) \text{ for stone meteor bodies} \quad (5)$$

$$\gamma_i = 1.82 \cdot 10^{-2}(V - 9.5) \text{ for iron meteor bodies} \quad (6)$$

$$n_m = \frac{4}{g\pi r_o^2} \cdot \frac{M_o \cos Z_R}{m \cdot H} \quad (7)$$

where V is the meteor velocity in kms, r_0 is the initial radius of a meteor trail, M_0 is the mass of meteoroid, z_R is the zenith angle of a radiant, m is the mean mass of meteor atoms in g (for stone meteoroid $m = 4.5 \cdot 10^{-23}$ g, for iron $m = 9.4 \cdot 10^{-23}$ g), and H is the atmospheric scale height ($H \leq 6$ km).

The balance of production and loss of ozone molecules per unit volume n'_3 , according to reactions (1) - (3) is constrained by the following equation:

$$\frac{dn'_3}{dt} = k_1 n_1 n_2 n - I n'_3 - k_3 n_1 n'_3, \quad (8)$$

where k_1 and k_3 are the rate constants of the reactions (1) and (3), n_1 is the concentration of oxygen atoms in meteor trails, n_2 is the concentration of oxygen molecules, n is the concentration of all the neutral particles in a trail, I is the photodissociation rate of O_3 .

Now, assuming that $dn'_3/dt = 0$, we shall consider the case of photochemical balance where

$$n' = \frac{k_1 n_1 n_2 n}{I + k_3 n_1} \quad (9)$$

The equations (5) - (9), data on atmospheric particles for different heights (PEROV and KRGIAN, 1980), and rate constants of reactions (1) and (3) (PEROV and KHRGIAN, 1980; SHIMAZAKI, 1984) allow one to calculate the maximum concentration of ozone formed in a meteor trail.

Figures 1 and 2 show, on a logarithmic scale, the dependence of predicted meteor ozone concentration ratio to that of atmospheric ozone in the daytime on the log of mass of stone and iron meteors as calculated for altitudes of 70, 80, 90, 100 km. It is assumed here that $\cos z_R = 2/3$ and the values of V and r_0 for these heights are taken from Baggaley, (1970).

According to the figures, the predicted meteor ozone concentration in the trails of meteor bodies with masses more than 10^{-2} g may exceed that of atmospheric ozone by a factor of several dozen times.

It seems that meteoric ozone must be taken into account when studying the balance of ionization in the meteor trails formed by particles with masses more than 10^{-2} g. The predicted levels of atomic oxygen and ozone seem sufficient to greatly influence the rate of meteoric plasma deionization.

References

1. Baggaley W.J., 1970, Mon. Not. R. Astr. Soc., Vol. 147, No. 3, p. 231.
2. Bibarsov, R. Sh., 1985 Reports of Tajik Academy of Sciences, Vol. 28, No. 8.
3. Perov, S.P., 1980, Khrgian, A. Kh., Present-day Problems of Atmospheric Ozone, Gidrometeoizdat, Leningrad.
4. Shimazaki, Tatsuo, 1984, J. Atmos. Terr. Phys., Vol. 46, No. 2, p. 173.

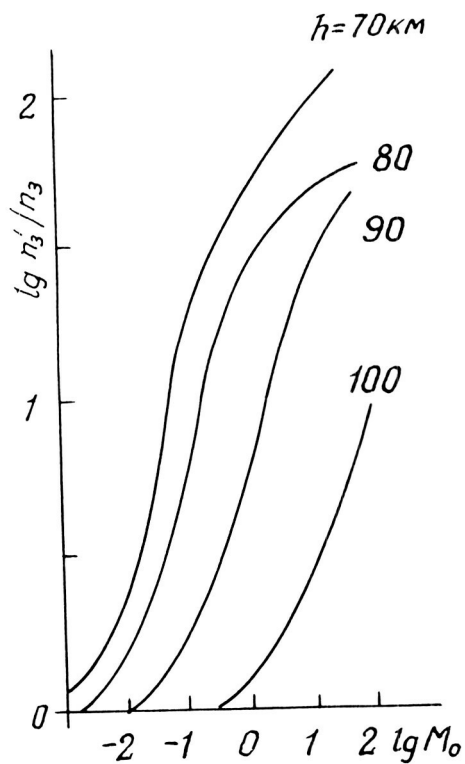


Fig. 1 Predicted daytime dependence of meteor zone concentration in meteor trails of atmospheric ozone for stony meteors at altitudes of 70, 80, 90, and 100 km.

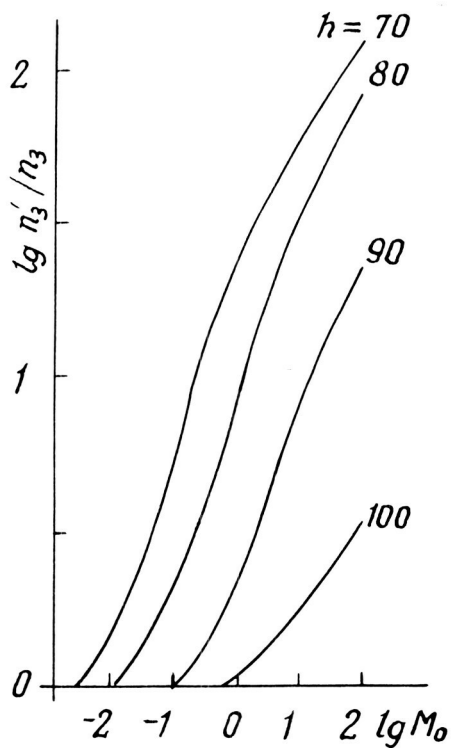


Fig. 2 Same as Fig. 1 except for iron meteors.

METEOR MATTER INTERACTION WITH THE EARTH'S ATMOSPHERE
AND THE IONOSPHERIC E-REGION STRUCTURE

O. Alimov

The Tajik Academy of Science Institute of Astrophysics
Dushanbe, USSR

The exploration of the ionospheric E-region is a pressing problem both in the applied and fundamental studies. A lot of previous work was dedicated to the problem. However, up to now it remains unsolved. The present paper presents results of an investigation a) to estimate the meteor ionisation contribution to the night-time E-layer and influx; b) to study the phenomenon of intensive sporadic layer formation following cessation of meteor stream activity; and c) to access the role of metallic ions of meteor origin in the diurnal and seasonal variations in the occurrence probabilities of mid-latitude E_s .

Examination of ionosonde vertical probing data shows that in the most cases, the night-layer diurnal appearance and the maximum number of weak sporadic meteors observed on $\lambda = 15-17$ m wavelength coincide in time and occur at 6 a.m. local time. Using well-known data on ion formation rates from two different sources (CHASOVITIN and NESTEROV, 1975; and JOFFE and RUBTSOV, 1980), we evaluated the contribution of meteor matter, Lyman radiation and corpuscular particles to the electron concentration of the night E-region. The table shows ratios of equilibrium electron concentrations $N_{em}/N_{eL\alpha}$, $N_{em}/N_{eL\beta}$, N_{em}/N_{ep} (N_{em} - caused by meteors, $N_{eL\alpha}$ - by Lyman radiation, $N_{eL\beta}$ - by corpuscles) as a function of height.

h, km	$N_{em}/N_{eL\alpha}$	$N_{em}/N_{eL\beta}$	N_{em}/N_{ep}
90	0.43	20.0	20.0
95	1.75	16.6	16.6
100	3.33	3.33	2.22
105	7.55	2.22	2.66
110	13.6	3.00	4.80

It follows from the table that the ionization of the night E-layer is most probably caused by meteor particles.

The ionosonde vertical probing data also often shows a simultaneous appearance of several types of sporadic E (E_s). In these periods of maximum probability, the appearance of several types of E_s is 1.5 to 2.0 times more probable than in quiet periods. Meteor streams are not homogeneous in their structure. They have bodies of different density. It is clear that bodies of different density produce ionisation at various heights that, in its turn, may bring about meteor-induced ionisation at several height maxima. The simulation and analysis indicates that the inhomogeneous density structure of meteor streams might be responsible for the creation of the stratified structure of the sporadic E-layer.

When analysing vertical ionosphere probe data obtained in Dushanbe and Ashkhabad, it was found out that after stoppage of the active stage of the Lyrids and η -Aquarids some delay in the formation of intensive E_s with $f E_s \geq 4$ MHz is observed. Fig. 1 presents the variation of probability of E_s appearance in 1964 and 1971 for Dushanbe and in 1966 for Ashkhabad. The X-axis shows the dates and Y-axis gives the percentage of E_s appearance probability. The arrows show the dates of meteor streams maximum activity. It can be seen that a marked increase of the number of cases of E_s appearance with $f E_s \geq 4,0$ MHz is really observed following 10-12 days after the stoppage of the meteor streams' active stage.

Now for the physical interpretation of the observed phenomenon. It is common knowledge that metallic ions of meteoric origin play an important part in the formation of narrow sporadic layers in mid-latitude ionosphere. According to the theory of wind shear, the maximum value of electron concentration in the E_s layer is determined by equilibrium concentration of metal ions of meteor origin. During the period of meteor streams activity the Earth's atmosphere receives a great number of meteor matter in the form of neutral atoms. Then these atoms, owing to change exchange with the atmospheric ions NO^+ and O_2^+ and photoionisation become ionized. Obviously, the active influence of meteor matter on the upper atmosphere brings about primary accumulation of these ions M^+ . These species disappear mainly due to the reaction $M^+ + O_2 \rightarrow MO_2^+ + h\nu$. Proceeding from the data on effective periods of meteor ion life times and reaction constants (MAC-EWAN M. and PHILLIPS, 1978) the value of time delay $T \approx 9$ days was obtained which is in keeping with the observations.

The influx of metal ions into the Earth's atmosphere is due mainly to sporadic meteor matter and shows diurnal and seasonal variations. Of interest here is the problem of influence of such variations on behaviour of metal ions. If N_1 and N_2 are the atomic and ionic concentrations, the differential equation of these values within the framework of equilibrium photochemistry are as follows:

$$\frac{dN_1}{dt} = Q_a - \frac{N_1}{\tau_1}; \quad \frac{dN_2}{dt} = \frac{N_1}{\tau_1} - \frac{N_2}{\tau_2} \quad (1)$$

where Q_a is the function of atoms of meteor origin formation; τ_1, τ_2 are effective periods of metal atoms and ions respectively. The solution of these equations with a model distribution Q_a shows that the diurnal variation of metal ions is of extreme character. The time of maximum ionization for different kinds of ions is different. Since $f E_s$ is determined by the maximum value of electron concentration which, according to the wind shear theory, depends in turn on the distribution of metal ions variations cannot be ruled out.

Considering the problem of seasonal behavior of N_1 and N_2 values we can assume that $dN_1/dt = \phi$ and $dN_2/dt = \phi$ and thus

$$N_1 = Q_a \tau_1; \quad N_2 = Q_a \tau_2 \quad (2)$$

Consequently, the equilibrium of metal ions concentration depends on only the seasonal variations of the number of sporadic meteors. Fig. 2 shows the seasonal variations of the monthly average number of appearances of E_s with $f E_s \geq 5,0$ MHz as revealed by vertical probing over Tajikistan. The variations of meteor numbers are also given there. It can be seen that

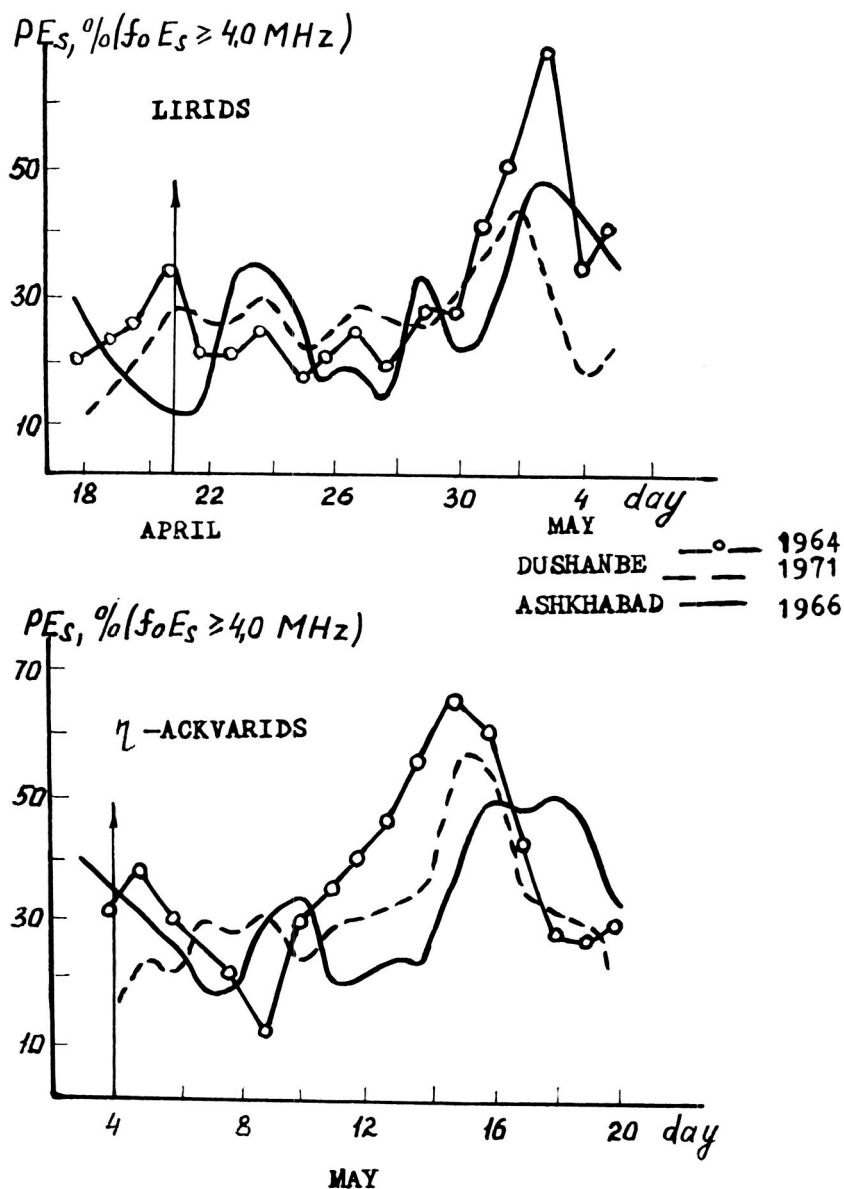


Fig. 1 The variation of the probability of occurrence of E_s in 1964 and 1971 for Dushanbe, and in 1966 for Ashkhabad, and the possible connection to the Lyrid and η Aquarid meteor showers.

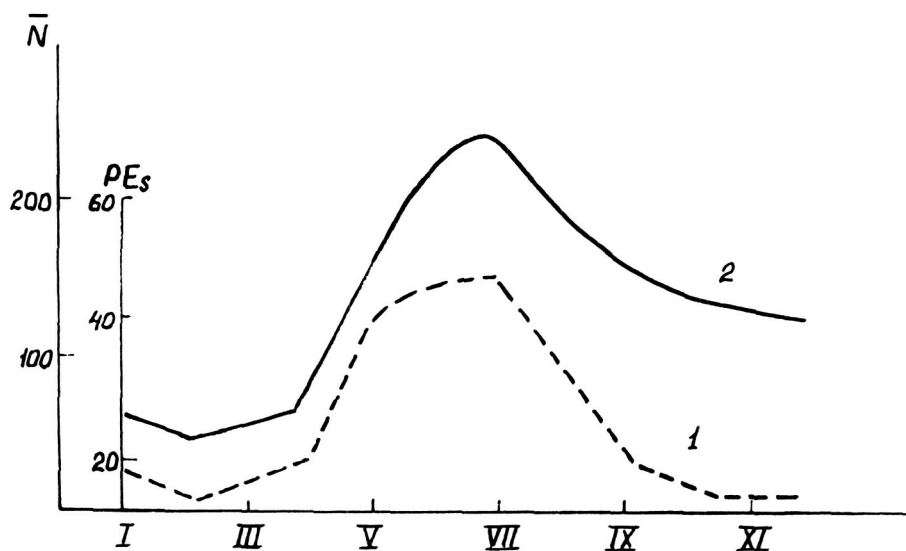


Fig. 2 The seasonal variation of the monthly average number of occurrences of E_s with $f_oE_s \geq 5.0$ MHz from vertical incidence soundings over Tajicistan (1), together with the daily average hourly radio meteor count (2).

these values are well correlated, and such correlation becomes quite understandable if we take into account the fact that the probability of mid-latitude E_s layer formation is determined by the metal ions concentration whose seasonal change depends on the seasonal influx of sporadic meteor matter into the Earth's atmosphere.

References

1. Alimov O., Novikov G.G., Rubtsov L.N., 1981, Geomagnetism i Aeronomiya, Vol. 21, No. 4, p. 720.
2. Chasovitin U.K., Nesterov V.N., 1975, IEM Proceedings, Vol. 3 (55), Moscow.
3. Joffe Z.M., Rubtsov L.N., 1980, in The Meteor Matter in the Interplanetary Space, Moscow, p. 240.
4. McEwan M., Phillips F., 1978, Chemistry of the Atmosphere, the Mir Publishers, Moscow.

THE NONLINEAR THERMODYNAMICS OF METEORS, NOCTILUCENT CLOUDS, ENHANCED
AIRGLOW AND GLOBAL ATMOSPHERIC CIRCULATION

J. Rajchl

Astronomical Institute
Ondrejov, Czechoslovakia

Abstract

Two types of fundamental topological junctions of elements are deduced from a nonlinear thermodynamical model. Using this scheme we examined the possibility of a causal relation between fireballs and faint meteors as nonlinear sources on the one hand, and noctilucent clouds (NLC) and Hoffmeister's enhanced airglow (EA) as complementary formative processes in the middle atmosphere and ionosphere, on the other hand. The principal role of the global atmospheric circulation in this relation is demonstrated. Such circulation in the mesosphere appears to prevent the neutral dust dissipated by fireballs from becoming an efficient agent in NLC generation. In this case, the behavior of ionized material deposited by both the bright and faint meteors is more probably controlled, as shown from the annual variation of the E_s layer by the darkness of lunar eclipses and the global circulation of the lower thermosphere. The role of fireballs and neutral dust might be more significant as a source of the EA phenomenon.

Details of this investigation will be published in the Bulletin of Astronomical Institutes of Czechoslovakia.

From a recent investigation by the author of coincidences between very bright meteors -- fireballs and noctilucent cloud (NLC) occurrence, it appears that practically no such coincidences exist (Paper II, RAJCHL, 1985). The question arises, what might be the cause of this negative result?

To answer this question, we have used a more general approach. From the author's thermodynamic model of meteors, published in Paper I (RAJCHL, 1979), it follows that an intimate connection does exist between the so-called compound thermodynamic system and the Clifford algebra representation. This leads to the conclusion that it is not only in the dissipative phase of meteor interaction that the role of the atmosphere is crucial. However, especially in the following formative phase, when deposited meteor material acts on the atmosphere, it is the dynamics of the atmosphere, represented in the model by vector products (namely, rotors contained in the Clifford product (CASANOVA, 1979)), and realized to the first approximation by the global circulation of the mesosphere and lower thermosphere, which is of fundamental importance (Paper II.)

It is widely accepted that the nucleation process leading to NLC generation in middle latitudes is nonhomogeneous and of a nonlinear nature (GADSDEN, 1982). Therefore, the nonlinear extension of our former thermodynamic approach, as used in Paper II, is necessary. Two forms of such extension are used: the network thermodynamics representation with bond graphs (OSTER et al., 1973) and the time derivative of the original

linear compound system of Paper I; thus, for such a nonsecond form of extension this means that the overall change of entropy production in such a nonlinear compound system S becomes proportional to the sum of terms $\dot{X}J$, $X\dot{J}$, $\dot{X}J^*$, and $X^*\dot{J}$; X and J are the forces of interaction with the atmosphere and the flow of meteor matter, respectively (represented e.g., by the mean velocity) in the dissipative phase of the meteor -- atmosphere interaction, and X^* and J^* are the same quantities for the formative phase. In other words, the formative process in the atmosphere, as induced by meteors, is represented by the response of the atmosphere to the dissipation of meteor matter as a source. The nonlinear compound system contains two different types of dissipative and formative terms.

Both above-mentioned thermodynamic nonlinear representations contain fundamental topological features in the form of serial (s) and parallel (p) junctions of sources and responses. From Paper I it follows that the following are acceptable nonlinear sources: fireballs and faint meteors. The atmosphere is considered global: both the northern and southern hemispheres are included.

From observational data collected by the European Network for fireball photography in the northern hemisphere (CEPLECHA, 1977), and those published in the SEAN Bulletin (1976-1980), we found that the maximum of a number of fireballs is in winter in the northern hemisphere. As no systematic fireball observation data exist for the southern hemisphere, we used an intimate analogy between fireballs and meteorites to estimate their approximate number in this hemisphere. A recent study by HALLIDAY and GRIFFIN (1982) shows that the maximum of fireballs (if analogous to meteorites) would occur in the southern hemisphere a half year later than in the northern. Thus, it seems that fireballs manifest -- in respect to both hemispheres -- a nonsimultaneous, i.e., serial junction of maxima of occurrence.

On the other hand, faint meteors represented by radar meteors (ELFORD, 1965) show their number maxima simultaneously in winter and in summer in both hemispheres, therefore in a parallel junction.

From Paper III (RAJCHL, 1985), it is apparent that possibly two adequate responses to the above-mentioned two sources may be observable in the form of NLC and the so-called enhanced airglow (EA) phenomenon (HOFFMEISTER, 1958). Both phenomena constitute a complementary s-p system, analogous to the system of sources. That is to say, the NLC are present only in the summer season in both hemispheres (GADSDEN, 1982), i.e., in a serial configuration, while EA are observed simultaneously in both the northern and southern hemispheres, therefore in a p-junction.

Now, if we introduce the global circulation of the mesosphere and lower thermosphere connected with subsequent vertical transport, we obtain throughout the whole year a situation demonstrated schematically in Table I (global circulation) and Table II (vertical transport) (ILICHOV and PORTNYAGIN, 1977, Papers II and III). According to NECHITAIENKO (1979), the direction of vertical transport is the same for natural and ionized material only for heights < 80 km. Higher in the atmosphere it is mutually opposite for both species.

Table I.

Season		winter	summer	summer	winter
Hemisphere		north.	south.	north.	south.
Height in km	> 80	W E W	W E W		
	< 80	W	E	E	W

W - cyclonic type of global circulation
E - anticyclonic type of global circulation

Table II.

Season		winter	summer	summer	winter
Hemisphere		north.	south.	north.	south.
Height in km	> 80	↑ ↓	↑ ↓	↑ ↓	↑ ↓
	< 80	↑	↓	↓	↑
Observed Phenomena		EA	EA NLC	/EA/NLC	/EA/

/EA/ means the EA of smaller intensity.

↑ means transport of neutral material
↓ means transport of ionized material

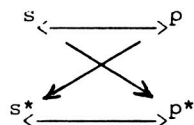
The Tables show that the majority of fireballs, which deposit ablated material (neutral dust and ions) at altitudes lower than the NLC level, is, because of the prevalent downward global transport in summer, incapable of directly influencing the NLC nucleation process. This conclusion is confirmed also by the minimal dust concentration in the whole atmosphere up to the 120-km height level in summer, as deduced from lunar eclipses photometric observations (LINK, 1955). Moreover, if we estimate the mean velocity of vertical transport from the delay between the global circulation reversal and the subsequent change of dust content in the atmosphere, we find a value of ~ 4 cm/s, i.e., the same value as obtained by other methods.

The meteor material transported upwards to the 120-km level in winter is more likely to be involved in the EA phenomenon, while the downward transport of ionized material, deposited mainly by faint meteors in heights about 100 km, it probably the source of NLC nuclei. This result seems to be substantiated also by the observed downward transport towards the E_s layer in summertime (ROYRVIK, 1983). Another fact may support the ions as the main cause of NLC nucleation: the short break in the global circulation of the lower thermosphere caused by the spring type of circulation result in upward ion transport. The return of the thermospheric circulation to westerly at the end of May, or the beginning of June, renews the downward transport of ions into the NLC level. This time coincides very closely with the beginning of the season of NLC observations in midlatitudes. Thus, it seems that in addition to the low temperature, this onset of downward transport of ions may be another important condition for the occurrence of NLC.

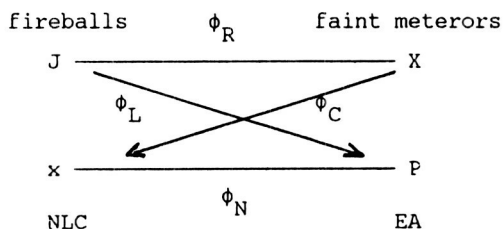
Thus, we may conclude that: 1) Even though such "local" processes as turbulence, internal gravity waves, etc. may be of higher intensity than the relatively fainter global-circulation-induced transport processes, to a first approximation, the global circulation may lead to consequences of fundamental importance relating meteors to atmosphere phenomena.

2) It seems that deposition of meteor ions is connected with NLC initiation, and neutral dust with EA phenomena.

3) If secondary relations are omitted, the fireballs (s-sources) are connected with EA (p^* -phenomena) and faint meteors (p-sources) with NLC (s^* -phenomena); so that some type of a cross-complementarity s - p^* , p - s^* arises. For the principal interactions (the secondary ones are omitted) we obtain the following nonlinear thermodynamic scheme:



An analogous scheme is known also in network thermodynamics (OSTER et al., 1973); when adapted to our problem, it is of the following form:



where X, J, x and P are forces, flows, displacements and impulses, respectively. $\phi_R, \phi_L, \phi_C, \phi_M$ are individual connections, represented in the form of the so-called constitutive relations:

$$\phi_R(X, J) = 0, \phi_L(J, P) = 0, \phi_C(X, x) = 0, \phi_M(P, x) = 0$$

It is apparent that both schemes are interrelated. Combining the results of the present paper with those of the network thermodynamics of OSTER et al. (1973), we may obtain some additional conclusions:

4) The sources, in the same way as energetic transactions, are characterized by the constitutive relation $\phi_R(X, J) = 0$, or by dissipation $(X, J) \neq 0$. The product $(P, x) \neq 0$ is typical for responses. Connections between sources and responses are then realized, in general, by the (X, x) , i.e., virial and (J, P) -impulse products. Applying this knowledge to our case, we find that the connection between faint meteors and NLC (scheme II) is of the form of this virial, especially as it applies to the NLC nucleation, as widely accepted. On the other hand, the impulse interaction is valid for the fireball-EA connection. Unfortunately, no more can be said about the precise mechanisms of either the virial or the impulse interactions from this scheme alone.

5) The quantities that are constant are the flows J for fireballs and forces X for faint meteors; for NLC there are displacements x ; for EA impulses, P . A comparison with individual terms of the nonlinear compound system implies that the quantities conjugate to the above-mentioned constants, i.e., X to J for fireballs, J to X for faint meteors, etc. can change with time. Therefore, from the schemes (I) and (II) and the nonlinear compound system terms all combined together with observations, we may infer that, e.g., $\dot{X}J$ corresponds to fireballs and the s-junction and $X\dot{J}$ to faint meteors and the p-junction, and so on.

References

1. Casanova, G., 1979, Vektornaya algebra, Mir Moskva.
2. Cepelch, Z., 1977, Bull. Astron. Inst. Czech., 28, 328.
3. Elford, W. G., 1965, Smithson. Contr. Astrophys., 11, 121.
4. Gadsden, M., 1982, Space Sci. Rev., 33, 279.
5. Halliday, I., and A. A. Griffin, 1982, Meteoritics, 17, 31.

6. Hoffmeister, C., 1958, Veroff. Sternw. Sonnebg., 3, No. 4.
7. Ilichov, Yu, and Yu. I. Portnyagin, 1977, Meteorol i Gidrol., 8, 3. No. 635.
8. Link, F., 1955, Mem. Soc. R. Sci. Liege, XV, 35.
9. Nechitailenko, V. A., 1979, Statistical Theory of Meteor Wind Radar Observation, Nauka Moskva. In Russian.
10. Oster, G. F, A. S. Perelson, and A. Katchalsky, 1973, Quart. Rev. Biophys., 6.
11. Rajchl, J., 1979, Paper I, Bull. Astron. Inst. Czech., 30,70.
12. Rajchl, J., 1985, Papers II and III, submitted to Bull. Astron. Inst. 1985 Czech., (in print).
13. Royrvik, O., 1983, Planet. Space Sci., 31, 253.
14. SEAN Bull., Scientific Event Alert Network Bull., Smithson. Inst.

A PROCESSING METHOD AND RESULTS OF METEOR SHOWER RADAR OBSERVATIONS

O. I. Belkovich, N. I. Suleimanov, and V. S. Tokhtashev

Kazan State University
Kazan, USSR

Studies of meteor showers permit to solve some principal problems of meteor astronomy:

- to obtain the structure of a stream in cross-section and along its orbits;
- to retrace the evolution of particle orbits of the stream taking into account gravitational and non-gravitational forces and to discover the orbital elements of its parent body;
- to find out the total mass of solid particles ejected from the parent body taking into account physical and chemical evolution of meteor bodies;
- to use meteor streams as "natural probes" for investigation of the average characteristics of the meteor complex in the solar system.

Many works in meteor astronomy are confined only to the analyses of recorded meteor rates and very often are not made thoroughly enough. We believe the preliminary analysis must contain the following stages: a) estimation of equipment sensitivity and instability; b) reduction of the recorded number of meteors to meteor rates; c) separation of shower rates from the sporadic background. After that one can draw the shower activity curve i.e., shower meteor rates as a function of the solar longitude, the meteor rates being taken from the same hour of every day of observations (for showers lasting several days), or hourly meteor rates being reduced to some reference hour (BELKOVICH, et al., 1984). This procedure eliminates the diurnal variation of shower rates due to the diurnal shift of the stream radiant in relation to the aerial beam.

Analysis of the activity curve can give only qualitative characteristics of a stream - the shape of the curve, its variations from year to year and positions of maxima of the shower activity for different detection levels.

A much wider scope of problems can be solved if flux densities $Q(m)$ of meteor bodies with masses greater than some mass m and the mass exponent s are known to be functions of the solar longitude λ_0 .

A simple and effective method of determining the flux density and s parameter has been worked out at the Engelhardt Astronomical Observatory. The main idea of the method is that two modes of detection are chosen for a average sensitivity radar. The first mode is an amplitude one. The meteor echo rate N_0 is counted at this threshold level. The rate N_0 corresponds to all meteor trails which have their electron line densities α at maximum ionization greater than α_0 , i.e., minimum electron line density detected by the radar in a given direction. Meteor echoes with durations greater than T are related to the second mode, that of duration. Selection

is restricted to echoes from overdense trails only where maximum electron line density is greater than α_T .

Let the shower radiant position on the celestial sphere be such that the echo plane intersects an aerial beam in the direction of its maximum sensitivity. Then the incident flux densities of meteor bodies $Q(\alpha_0)$ and $Q(\alpha_T)$ generating trails with $\alpha > \alpha_0$ and $\alpha > \alpha_T$ respectively are

$$Q(\alpha) = \frac{N_0}{\Sigma_0}, \quad Q(\alpha) = \frac{N_T}{\Sigma_T}$$

where Σ_0 and Σ_T are the corresponding effective collecting areas on the echo plane of the radar. The values of Σ_0 and Σ_T depend on the mass exponent s only in this particular case. Then one can determine the value of s by solving the equation

$$\frac{N_0}{\Sigma_0(s)} = \left(\frac{\alpha_T}{\alpha_0} \right)^{s-1} \cdot \frac{N_T}{\Sigma_T(s)} \quad (1)$$

using iteration. An equation similar to (1) can be written for any position of the shower radiant in relation to the aerial beam direction. The method for computing the effective collecting areas Σ_0 and Σ_T is considered in the papers of BELKOVICH and TOKHTASJEV (1971, 1974).

This method of meteor flux density determination has a number of advantages. On the one hand, different models of radio wave reflection from meteor trails (underdense and overdense ones) can be used which carry out an internal verification of the method. On the other hand, the parameters Q and S are determined in a rather wide mass interval (2-3 orders of magnitude). The method is very sensitive to the choice of physical parameters such as the value of the meteor trail initial radius, ambipolar diffusion coefficient and ionization coefficient as functions of the height and velocity. But the dependence of evaporation heights of meteor bodies on the velocities and masses is the most vulnerable. The first application of the method to the Quadrantids meteor shower has shown a complete failure of the classical theory, which in turn led to development of a new theory. Its difference from the classical one is independence of ionization height on meteor body masses that are less than a certain threshold value (BELKOVICH and TOKHTASJEV, 1974). The modified theory was confirmed recently by experimental data obtained from TV observations (SARMA and JONES, 1985).

The method was applied by us for a number of years during Geminids and Quadrantids observations (BELKOVICH et al., 1982; BELKOVICH et al., 1984). The main structural parameters were obtained for both the showers: the flux density $Q(10^{-3} \text{ g})$ of meteor bodies with masses over 10^{-3} g and the mass exponent s as functions of the solar longitude λ_0 . Comparison of the results has been carried out for different years of observations. It was found that the shapes of the curves are rather stable and the relative flux density fluctuations in the shower maxima do not exceed 15 per cent. Then we combined the results obtained in different years to form average curves of $Q(10^{-3} \text{ g})$ and s . The assumption that the value of s does not depend on the mass of meteor bodies makes it possible to determine the change of the flux density of particles with masses greater than the threshold mass.

This is necessary for comparison of observational results obtained by different methods.

Logarithms of the Geminids flux densities for different minimum masses normalized to the maximum are shown in Fig. 1. The peculiarities of the curves are their significant asymmetry and the linear variation of the logarithm of the flux density vs the solar longitude on both sides of the maximum. This means the flux density $Q(m)$ is an exponential function of λ_0 . It must be noted that the exponent index of the left branch of the curves and the flux maximum position both depend on the mass m .

The variations of logarithm of the flux density $Q(10^{-3} \text{ g})$ obtained from radar observations of the Quadrantids (solid line) and the logarithm of the visual meteor rates (dashed line) versus solar longitude are shown in Fig. 2. One can see more symmetrical shapes of the curves than for the Geminids and a sharp change of the slopes in both left and right wings of the curves.

The maximum flux densities as function of the minimum mass a.e shown in Fig. 3a and b from radar and visual observations of the Geminids and Quadrantids showers. All the results are presented on a comparable mass scale. Good agreement can be noted between our results and those derived from visual observations. Differences between the results of radar observations obtained by different authors can be explained by differences in processing methods and the physical parameters used.

It has been shown for the Geminids that the exponent index of the left wing of the activity curve is similar to that of the flux density curve. The following equation was found:

$$m_0 = [(0.5 \tau_0^*)^8 - 0.04]^{-1} \quad (2)$$

where m_0 is the minimum detected mass and

$$\tau_0^* = \Delta \lambda_0 / \Delta \ln Q$$

This equation can be used to determine the m_0 for any kind of observation (radar, photographic, visual, TV).

A mathematical model of the flux density through the plane normal to the velocity vector and crossing the descending node was derived on the basis of the flux and s variations along the solar longitude in the form

$$Q \cdot pm(x, y) \cdot p(m) \cdot$$

Here Q is the total flux through the plane;

$$Q = 1.24 \cdot 10^{18} \text{ g} \cdot \text{s}^{-1}, \quad p(m) = m_{\min} \cdot m^{-2}$$

(where m_{\min} is the minimum mass of the shower particles in grams),

$$pm(x, y) = \frac{p(1 - \beta^2 \tau^2)}{2\pi \tau^2} \cdot \exp - \frac{\sqrt{(x - r_x)^2 + p^2 y^2}}{\tau} - \beta (x - r_x) \quad (3)$$

$$p = 1.86, \quad \tau = 0.52^{-0.12}, \quad \beta = 1.47 m^{0.12}, \quad r_x = -0.116 m^{-1/3}.$$

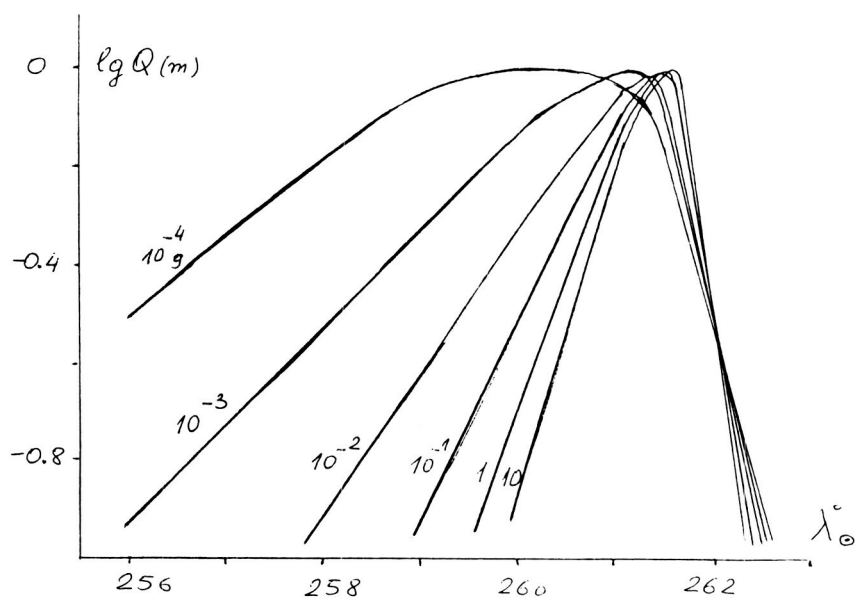


Fig. 1 The Geminids flux density variations of solar longitude for different minimal masses.

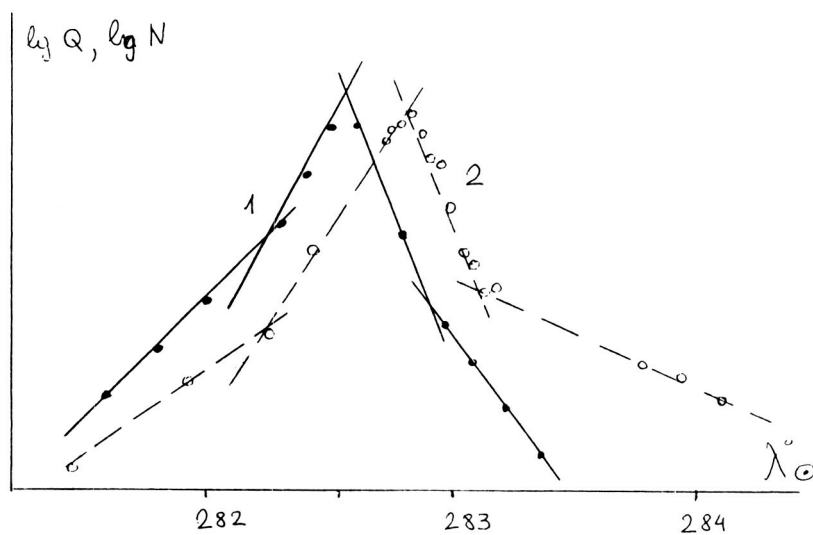


Fig. 2 Flux density logarithm for meteor bodies over $10^{-3}g$ (1) and the hourly meteor rate logarithm (2) for visual observations (HINDLEY, 1972) of the Quadrantids (in relative units) depending on solar longitude.

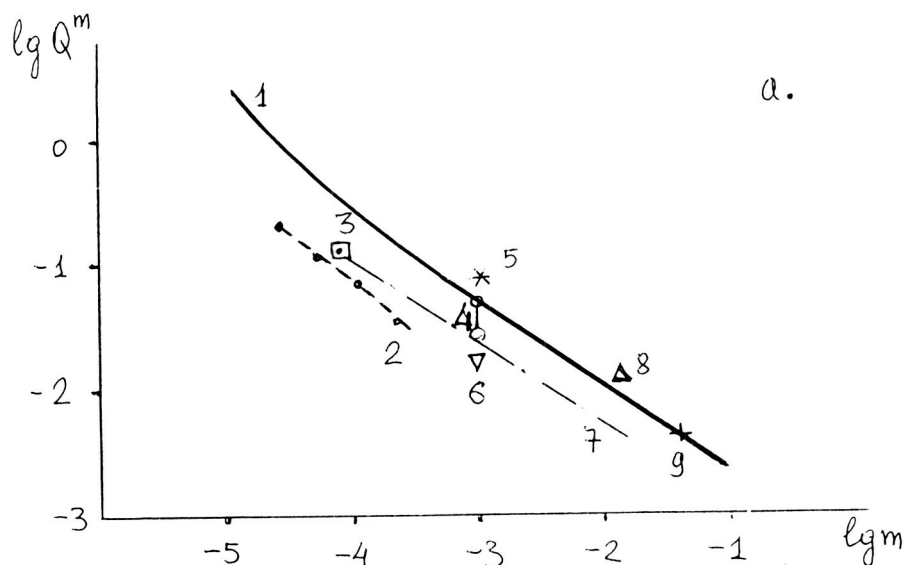


Fig. 3a The Geminids flux density variations in maximum depending on minimal mass: 1-EAO data, 2-HUGHES (1974), 3-LEBEDINETS (1970), 4-KOSTYLEV and SVETASHKOVA (1977), 5-TKACHUK (1982), 6-ANDREEV et al., (1982), 7-ANDREEV and RYABOOVA (1982, 8-LEVIN (1956), 9-PORUBCHAN and STOHL (1979).

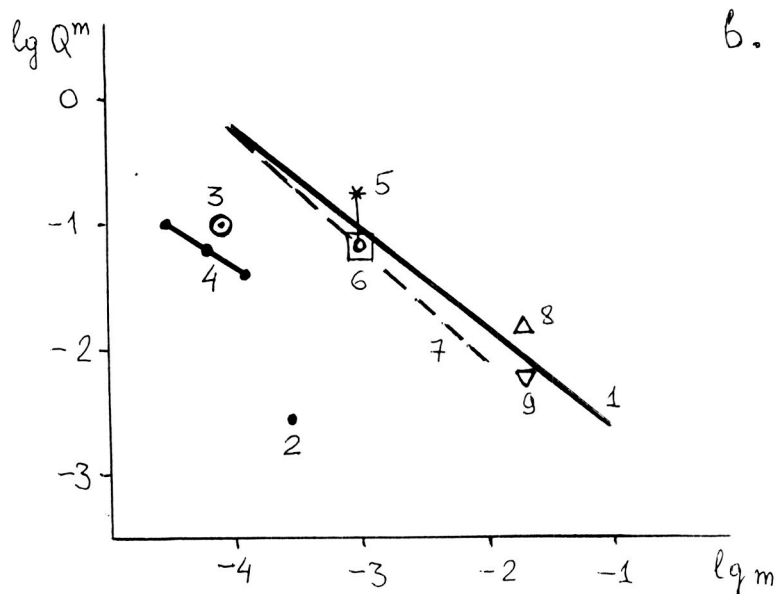


Fig. 3b The Quadrantides flux density variations in its maximum depending on the minimal detected mass: 1-EAO results, 2-WEISS (1957), 3-LEBEDINETS (1970), 4-HUGHES (1974), 5-TKACHUK (1982), 6-ANDREEV et al., (1982), 7-ANDREEV and RYABOVA (1982), 8-PRENTICE (1953), 9-HINDLEY (1972).

The coordinates in the plane are as follow: OX is the line of the normal plane intersection with the plane of the mean stream orbits, the positive direction of the axis is outside the orbit, the coordinate origin corresponds to the point of intersection of the mean orbit of the biggest stream particles with the normal plane. The projection of the Earth's orbit (equinox of 1950.0) on the normal plane is

$$y = -0.50 x - 0.15$$

The scale is chosen so that one unit equals 1° of the Earth's orbit arc or 0.0158 a.u. It follows from the model that the flux density of meteor bodies with fixed mass decreases exponentially in the normal plane from the maximum point to the periphery.

The following equations for the mean values of the Geminids orbit elements as functions of the mass of meteor bodies have been found from radar and photographic observations (BABADJANOV and KRAMER, 1963; BABADJANOV et al., 1969; KASHCHEEV et al., 1960; WHIPPLE, 1954; CEPLECHA, 1957; JACCHIA and WHIPPLE, 1961; HAWKINS and SOUTHWORTH, 1961):

$$\Omega = 261^\circ 593 - 0.0698 m^{-1/3}$$

$$a = 1.411 - 0.0146 m^{-1/3}$$

$$e = 0.9000 - 0.0009 m^{-1/3}$$

The inclination of the orbit $i = 23^\circ 4$ and the argument of the perihelion $\omega = 324^\circ 413$ practically do not depend on the mass m .

The values of the node longitude of the flux density maximum Ω , the semimajor axis a , the eccentricity e , the perihelion and aphelion distances q and q' , the period of partial revolution around the orbit T , and the extra atmospheric velocity of the Geminids particles V_∞ are given in the Table as functions of mass.

Table

$m(g)$	Ω	$a(a.u.)$	e	$q(a.u.)$	$q'(a.u.)$	$T(year)$	$V(km\ s^{-1})$
∞	261.59	1.411	0.900	0.141	2.681	1.676	36.24
1	261.52	1.396	0.899	0.141	2.651	1.649	36.18
10^{-1}	261.44	1.380	0.898	0.141	2.619	1.620	36.08
10^{-2}	261.27	1.343	0.896	0.140	2.546	1.557	35.88
10^{-3}	260.90	1.265	0.891	0.138	2.392	1.422	35.41
10^{-4}	260.09	1.097	0.881	0.131	2.063	1.148	34.20
10^{-5}	258.35	0.733	0.858	0.104	1.362	0.628	29.30

Apparently the mass of particles $\sim 10^{05}$ g is the minimal one in the Geminids because further decrease of mass is accompanied by a sharp decrease of the semi major axes.

Orbital elements of the Geminid's parent body can be found by increasing the mass m to the infinity in the equations (4):

$$\Omega = 261^{\circ}.593, \quad a = 1.411, \quad e = 0.9000, \quad w = 324^{\circ}.413, \quad i = 23^{\circ}.4$$

The total mass of the entire stream can be estimated using this mathematical model. For the Geminid stream, it turned out to be 0.9×10^{15} g. It corresponds to a spherical body 1.2 km in diameter assuming a particles density of 1 g cm^{-3} . Of course, one has to consider these values as minimal because of the disappearance of some particles due to catastrophic collisions and decrease of individual particle masses through loss of volatile elements.

The proposed method was recommended by the IAU Commission 22 (PATRAS, 1982) for the processing of meteor shower observations.

References

1. Andreev G.V., et al., 1982, in: Meteor matter in interplanetary space, Moscow, p. 188.
2. Andreev G.V., Ryabova G.O., 1982, *ibid.*, p. 129.
3. Babadjanov P.B., Kramer E.N., 1963, Methods and some results of photographic meteor observations, Sov. Acad. Sci. Publ., Moscow.
4. Babadjanov P.B., Getman T.I., Zausajev A.F., Karaselnikova S.A., 1969, Bull. Taj. SSR Inst. Astroph, No. 49, p. 3.
5. Belkovich O.I., 1971, Statistical theory of meteor radiolocation, Kazan State University, Kazan.
6. Belkovich O.I., Tokhtashev V.S., 1974, Bull. Astron. Inst. Czechosl., Vol. 25, No. 2, p. 112.
7. Belkovich O.I., Tokhtashev V.S., 1974, Bull. Astron. Inst. Czechosl., Vol. 25, No. 6, p. 370.
8. Belkovich O.I., Suleimanov N.I., Tokhtashev V.S., 1982, in: Meteor matter in Interplanetary space, Moscow, p. 88.
9. Belkovich O.I., Suleimanov N.I., Tokhtashev V.S., 1984, Bull. Astron. Inst. Czechosl., 35 No. 2, p. 123.
10. Cepplecha Z., 1957, Astron. Bull. Inst. Czechosl., Vol. 8, NO. 3, p. 51.
11. Hawkins G.S., Southworth R.B., 1961, *Ibid.*, Vol. 4, No. 3, p. 85.
12. Hindley K.B., 1972, Sky and Telescope, Vol. 43, No. 3, p. 162.

13. Hughes D.W., 1974, Space Research, Vol. XIV, p. 709.
14. Jacchia L.G., Whipple F.L., 1961, Smithsonian. Contrib. Astrophys., Vol. 4, No. 4, p. 97.
15. Kaiser T.R., 1955, in: Meteors, ed. Kaiser T.R., London, p. 119.
16. Kashcheev B.L., Lebedinets V.N., Lagutin M.F., 1960, in: Meteors Kharkov State University Press, No. 1, p. 25.
17. Kostylev K.V., Svetashkova N.T., 1977, Sov. Astron. J., Vol. 11, No. 3, p. 154.
18. Lebedinets V.N., 1970, Comets and meteors, No. 19, p. 25.
19. Levin B. Yu., 1956, Physical theory of meteors and meteor matter in solar system, Sov. Acad. Sci., Publ., Moscow.
20. Prentice J.P.M., 1953, J. Brit. Astron. Assoc., Vol. 63, No. 5, p. 175.
21. Porubcan V., Stohl J., 1979, Bull. Astron. Inst. Czechosl., Vol. 30, No. 2, p. 65.
22. Sarma T., Jones J., 1985, Bull. Astron. Inst. Czechosl., Vol. 36, No. 1, p. 9.
23. Tkachuk A.A., 1982, in: Meteor matter in interplanetary space, Moscow, p. 67.
24. Weiss A.A., 1957, Austral. J. Phys., Vol. 10, No. 3, p. 397.
25. Whipple F.L., 1954, Astron. J., No. 6, p. 201.

PHOTOGRAPHIC FIREBALL NETWORKS

Z. Ceplecha

Astronomical Institute of the Czechoslovak Academy of Sciences
2 51 65 Ondrejov Observatory, Czechoslovakia

This year is the centennial of the taking of pictures of meteor phenomenon. The first meteor ever photographed (by L. WEINEK in Prague in November 1885) belonged to the meteor Andromedid shower, the famous protrusion of the periodic comet Biela. For the first 50 years, photographic meteor programs gave rather scanty results. The second fifty years started with the Harvard patrol cameras being equipped with rotating shutters for measuring the meteor velocities, and they were operated continuously by F.L. WHIPPLE (1938, 1954) from 1936 to 1951. This was the first classical double-station program for photographing meteors, which gave enough results (144 published meteor trajectories and orbits) for a better understanding of the meteoroids and the atmosphere and their mutual interaction at "cosmic" velocities. The second large program of double-station meteor photography was the program active on a systematic continuous schedule at the Ondrejov Observatory in Czechoslovakia from 1951 to 1977 (CEPLECHA 1957, CEPLECHA et al. 1959). Eight years after the start of this program, a very bright fireball of -19 maximum absolute magnitude was photographed on April 7, 1959. Four meteorites were found near Pribram in Czechoslovakia in an area predicted from the double-station data on the fireball (CEPLECHA, 1961). This first photographing of a meteorite fall gave rise to the idea of systematic observational programs for photographing fireballs and eventually also meteorite fall was photographed, pointed to the fact that many stations over a large area each with cameras covering the whole sky, would be required to graph fireballs and meteorite falls.

Almost simultaneously in the fall of 1963, the first stations of two networks were put into operation, in Czechoslovakia and in the U.S.A. The Czechoslovak network, which later on, after being joined by European countries, became known as the European network, used one all-sky camera operating at each station. The spacing of the stations was 90 km on the average. The equivalent focal length of the stations all-sky camera in the classical mirror arrangement was only 6 mm, but the precision was usually good, because deep penetrating fireballs at heights below 40 km were still rather close to two or three stations. The number of stations operating in Central Europe nowadays is oscillating around 50. During the last 10 years the Czechoslovak part of the Network was modernized by using fish-eye cameras with a focal length of 30 mm. The extremely good optical quality of the Zeiss Distagon objectives enables the derivation of position from one photograph of the whole sky hemisphere (the diameter of the image is 80 mm) with a precision of one minute of arc. The camera is a small handy box (25 x 20 x 20 cm) weighing 4 kg, an instrument prepared for any type of field work and for easy automation. The Czechoslovak part of the Network has the prospect of another decade of operation.

The Prairie Network in the U.S.A. with 250 km spacing between adjacent stations, used 4 cameras with 1552 mm focal length and 90° field of view at each station. The large distances between neighboring stations were very

unfavorable for recording trajectories below 40 km. Usually only one station was close to the lower part of the fireball trajectory. The number of stations was 16 and the operation of the Prairie Network terminated in 1975.

In 1971, the Meteorite Observation and Recovery Project known as MORP began routine photographic observations in Canada. Each of 12 stations is equipped with 5 cameras having 50 mm focal length. They record about 100 fireballs per year, for which about 7 drop a total mass of at least 100 grams on the ground. The operation of the MORP Network will terminate this year, but the reduction of the data will continue.

The details on all three fireball networks and references can be found in a survey paper by Halliday (1971). The only change since that time, the use of fish-eye cameras in the Czechoslovak part of the Network, I have already mentioned. The areas covered by the Networks are about a million square kilometers for each. Future programs with automatic fish-eye cameras should cover bigger areas than that.

From all the networks, data on about 700 fireballs are available at the moment. Data on Prairie Network Fireballs were published in survey papers by McCROSKY et al. (1976, 1977). The data on individual European Network Fireballs were published in the Bull. Astron. Inst. Czechosl. and in the SEAN Bulletin. Meteoritics and the Journal of the Royal Astron. Soc. of Canada contain data on some MORP fireballs, but most of the European and Canadian fireball data are available only in the original computer files. Thus data used by other investigators than those directly involved with the observational program were usually the data on the Prairie Network fireballs.

The Prairie Network produced data on on meteorite fall, the Lost City meteorite (McCROSKY et al. 1971). The MORP Network was successful in obtaining data for one meteorite fall, the Innisfree meteorite (HALLIDAY et al. 1978, 1981). Altogether 3 meteorite falls have been photographed globally up to this time.

Except for the hope of repeating the photographic records of a meteorite fall after the Pribram success, the main objective of the networks was aimed at relations of the meteoroids, i.e. bodies before entering the Earth atmosphere, to meteorites, the recovered rests of ablated meteoroids on the ground. At the start of operation of the fireball networks, there were almost no precise data available on bodies with initial masses over 1 kg. The fireball networks gave data on bodies up to 1000 kg with a few cases as high as up to 100 tons. The initial idea was based on speculations that "friable" meteoroids, which were assumed to be cometary in origin, should become an insignificant population among the bigger bodies. If bigger bodies would be mostly solid asteroidal meteoroids, then fireball data might help in calibrating the luminous efficiencies and other quantities in the physical theory of meteors poorly known for smaller bodies. Then the properties by hypothetical cometary material would be better understood. But this proved false just with the first results of the networks. There were more bright fireballs than predicted by simple extrapolation, which simply said that the decrease in numbers slowed down with increasing mass. But there were fewer fireballs

penetrating very deeply into the atmosphere or, in another words, less predicted meteorite falls than expected from extrapolations. The problems in connection with searches for small meteorites in predicted areas made the discrepancy between the number of fireballs and of meteorite falls even larger.

The explanation of this situation was found in the existence of different populations of big meteoroids. Even if the whole problem was dealt with by statistical methods, it is useful to visualize the huge difference using individual representatives of various populations as it is shown in Table I. In the Table there are fireballs of approximately the same velocity, the same maximum and integrated brightness, the same inclination of the trajectory to the horizon, but widely differing

Table I. Example of PN-fireballs with comparable velocity, inclination of trajectory and brightness, but with differing terminal heights.

No. of PN-fireball	39276	39406B	40425	39533	39450
V (km/s)	25.8	23.3	25.6	23.5	25.6
M_{\max} (absolute magnitude)	-10.6	-10.6	-10.5	-8.6	-11.7
$\log \left(\int_{t_B}^{t_E} I dt \right)$	13.55	13.44	13.79	13.51	14.23
$\cos z_R$.626	.881	.640	.623	.963
h_E (km)	68.9	57.1	41.7	35.1	32.3
assigned type	IIIB	IIIA	II	I	I

terminal heights. Between the most solid bodies and most friable bodies, the air density at the terminal point of the luminous trajectory differs by a factor of 1000. The classification of fireballs into individual groups is based on such a huge difference of 3 orders in air densities, which represents the combined effect of the different ablation and different bulk density of the meteoroids, and should be connected with different structure and composition.

Details on the four different populations of big meteoroids can be found elsewhere (CEPLECHA and McCROSKY 1976, CEPLECHA 1977, CEPLECHA 1985, SEKANINA 1983, WETHERILL and REVELLE 1981 a,b). Four independent methods gave results differing in detail, but the existence of four groups of fireballs according to the various ablation rates of their bodies, as found by CEPLECHA and McCROSKY, had been confirmed. Here I give only a very brief summary of the fireball groups. Group I fireballs have the lowest

ablation rate and the greatest bulk density; among them are the Pribram, Lost City and Innisfree meteorite falls. Group I was proposed to be similar to ordinary chondrites. This classification was done before the Innisfree meteorite fall. Group II fireballs belong to meteoroids of somewhat lower density and greater ablation rate than the Group I meteoroids. It is proposed that the Group II fireballs belong to the carbonaceous bodies, which most disintegrate in the atmosphere; only the least friable members of their population can reach the ground as carbonaceous chondrites of CI and CM types. This material may be both of asteroidal and cometary origin, but recent work of WETHERILL and REVELLE (1981b) based on orbital definition of cometary origin, prefers the cometary source. The average ablation coefficient of a type I fireball is $0.014 \text{ s}^2/\text{km}^2$, while the value for a type II fireball is $0.042 \text{ s}^2/\text{km}^2$ (CEPLECHA, 1983).

Group IIIA contains bodies with a high ablation rate and small bulk density of somewhat less than 1 g/cm^3 . The cometary origin of these meteoroids is evident, because cometary shower meteors belong to this group. Also the two systems of orbits i.e. the short-period ecliptically-concentrated system and the long-period randomly-inclined system (IIIA) exist among fireballs of Group IIIA, in complete analogy to cometary orbits.

The fourth group of fireballs is denoted IIIB. Bodies of this group have the highest known ablation rate and the smallest bulk density of a few tenths of g/cm^3 . Fireballs of the Draconid meteor shower belong to this group. The cometary origin is also evident. It is surprising that this group contains relatively more bodies among fireballs than among fainter meteors.

We have detailed knowledge of meteorites from laboratory studies but little information of their orbits. The three directly photographed meteorite falls are quite insufficient in this respect. The classification of fireballs by statistical methods applied to the whole bulk of data cannot avoid the problem of a significant statistical admixture of non-meteorite fireballs. WETHERILL and REVELLE (1981a) proposed four criteria in answering the more specific question: Which fireballs do belong to meteorites? They found 27 Prairie Network fireballs comparable to or greater than Lost City in bulk strength and density. Most of them should be ordinary chondrites. Thus the statistics of orbits of ordinary chondrites increased by one order of magnitude. The orbits are ecliptically concentrated: the highest inclination found was 38° , but the majority of them have inclinations of less than 10° . Their perihelia exhibit a concentration close to 1 A.U. in accordance with a previous study of WETHERILL (1969) based on the time-of-fall and radiant distribution of meteorites from visual observations. Semimajor axes spread over a wide range, but some indication of clustering around 1, 2 and 2.5 A.U. is in evidence. The largest semimajor axes are 2.56 A.U. (The value of 4.2 A.U. for PN39057 comes from a wrong value of initial velocity). Aphelia of 4 A.U. are quite frequent, and Pribram is not an exception in this respect as well as in respect to the other orbital elements.

Recently WETHERILL (1985) presented a theoretical model of the orbital evolution of ordinary chondrites, assuming that they are injected with

rather small velocities into the 3:1 Kirkwood gap at 2.50 A.U. He assumed that such bodies can become Earth-crossing on a time scale of a million years, as a result of being injected in the chaotic zone discovered by WISDOM (1983) in connection with the 3:1 resonance. The computed distribution closely matches the distribution of orbits of ordinary chondrites derived from Prairie Network observations. Also the predicted fluxes of meteoroids and the time scales are in agreement. WETHERILL proposes as a source of the majority of the ordinary chondrites surfaces of S asteroids in this very limited region of the asteroidal belt, where the largest bodies are 11 Parthenope, 17 Thetis and 29 Amphitrite.

Recently HALLIDAY et al. (1984) published a study of the frequency of small meteorite falls on the Earth's surface based on the Canadian MORP data. They used the dynamically determined terminal masses and found 43 events in 9 years of continuous operation of the MORP network (29 percent of the night hours with clear sky) they have dropped meteorites from 0.1 to 12 kg. They use a previous study of HALLIDAY et al. (1982) on relative variations of meteorite falls for corrections and they gave the flux per year and per million square kilometers as $\log N = -0.689 \log m + 2.967$, where N is the number of events exceeding m grams. This is the first time instrumental data have been used for deriving the influx rate of meteorites on the Earth's surface. The authors then used REVELLE's (1979) theoretical work and converted the fluxes to masses of pre-atmospheric meteoroids. The result agrees in population index with the previous result of MCCROSKY and CEPLECHA (1969) on PN fireballs, but the MORP distribution line for pre-atmospheric masses is lower by 0.94 in $\log N$. The PN data contain all fireballs in contrast to meteorite dropping fireballs selected from the MORP data. This makes about a factor of 3 and the remaining factor of 3 is presumably accounted for by the low value of the luminous efficiency used in the PN reductions, which led to an overestimate of the masses (REVELLE, 1980). WETHERILL (1985) used the results of HALLIDAY et al. (1984) and computed the annual flux over the entire Earth in the mass range from 14 g to 140 kg as 3.9×10^4 kg on the surface. This corresponds to a pre-atmospheric mass range from 100 g to 1000 kg, if we assume a typical initial velocity of 14 km/s and an ablation coefficient $0.02 \text{ s}^2/\text{km}^2$. The total pre-atmospheric flux of ordinary chondrites inside this mass range before entering the atmosphere and counted over the entire Earth per year is 2.8×10^5 kg.

The interaction of the atmosphere with a big body is still quite regularly described by equations of the so called "single body theory", even if sometimes a rather modified version (REVELLE 1979; BRONSHTEN 1980). The problem of fragmentation of big bodies is quite serious for strong chondritic material penetrating deep into the atmosphere and this problem is decisive for understanding the motion and luminosity of IIIA and IIIB types of fireballs high in the atmosphere. The problem of luminous efficiency leading to overestimates of photometrically derived masses has already been successfully dealt with by REVELLE (1980). On the other hand, the proposed mechanism calls for strong continuum radiation at smaller velocities, which was not observed in spectral records of fireballs down to a height of 30 km and velocity of 7 km/s.

Table II

type	Ceplecha (1977,1983)		ReVelle (1983)	
	density g/cm^3	ablation coeff. s^2/km^2	density g/cm^3	ablation coeff. s^2/km^2
I	3.7	0.014	3.7	0.020
II	2.1	0.042	1.9	0.040
IIIA	0.6	0.13	0.9	0.08
IIIB	0.2	0.20	0.34	0.22

Recently REVELLE (1983) also accounted for the different hypothetical porosity of meteoroids of different types. The schematic model, which applied to PN fireballs, yielded values of ablation coefficients close to those values previously from a simpler model by CEPLECHA (1977, 1983), but the bulk densities for type II and especially for types III resulted in somewhat bigger values. (Tab. II).

Basic dynamical data derived from fireball photographs consists of distances along the trajectory, l (obs.), and heights, h (obs.), measured at each shutter time-mark, t . Due to lack of knowledge of the relation $l = l(t)$, even in the scope of single body theory, only least-squares fits of $l(\text{obs})$ and $h(\text{obs})$ were usually done by interpolation formulae. Also, the "observed" velocities, $v(\text{obs})$, were derived from numerical differentiation of $l(\text{obs})$ and the fit was done using a theoretical formula $v = v(h)$. PECINA and CEPLECHA (1983, 1984) derived a new integral $l = l(t)$ in a closed analytic form. This formulation, when applied to PN fireballs, gave much more precise values of initial velocity and ablation coefficient than those published before, when the simple interpolation formula was used. The inherent precision of the PN-fireballs (McCROSKY, 1971 and 1984) is significantly higher (up to one order) than the published solutions (McCROSKY et al. 1977) that have been obtained by means of the interpolation formula. Moreover, the new analytical solution $l = l(t)$ can be used for the entire, rather long trajectory of a fireball with one constant ablation coefficient (the total ablation coefficient). Fireballs penetrating deep into the atmosphere are usually photographed also after they reach the point of maximum deceleration. Significant terminal mass is typical for such cases. The velocity and deceleration at the terminal point of the luminous trajectory of such a fireball is necessary for determining the meteorite search area. The interpolation formula used for the extrapolation below the maximum deceleration point gives an unrealistically higher value of deceleration and a lower value of velocity.

The problem of predicting an impact point for a meteorite fall from its photographic fireball data arose first with the Pribram meteorite fall. The luminous trajectory terminates due to insufficient heat influx, when the velocity becomes too small (about 3 km/s). After the terminal point, the body moves without ablation in a dark-flight trajectory. The motions

of a body with constant mass in a resisting medium, the density distribution of which is known, is a classical problem. The numerical computations in a realistic atmosphere depend on the observed terminal velocity and deceleration, on the air density profile, and on the wind field. A knowledge of the mass of the body is not necessary. Also the unknown shape of the body enters only into the assumption of the relative change of the drag coefficient with decreasing velocity. Of course, exotic shapes may give enormous lift forces to the body and then any prediction of an impact point is necessarily fictive. The Pribram, Lost City and Innisfree experiences indicate a precision of better than 1 km for such predictions, if the dark-flight of a meteorite mass of several kilograms is computed. In any case, the method of PECINA and CEPLECHA (1983, 1984) yields more precise values of velocity and deceleration at the terminal point as derived from the photographic observations of fireballs, and these values are necessary for the predictions of meteorite impact point and impact area.

The greatest trouble in this business is the meteorite search itself. The actual conditions of the countryside inside the predicted search area may be very diverse. Usually at least part of the land is unfavorable for finding anything at all! The search method simply requires looking; it does not matter if one is walking, driving, flying or snowmotoring. To search for bodies of a few hundred grams is almost hopeless, but a few kilogram meteorite fresh fallen on the smooth surface of a spring field can be recovered almost with certainty. The number of searches done in all three fireball networks is close to 50. With 3 meteorites found so far, you need searches for about 15 different meteorite fireballs to recover something. Anybody in a search group should accept the fact that the probability of recovering a meteorite is less than 1 percent for one searcher after spending two or three weeks of intense work in the predicted area of fall.

From the recent study of HALLIDAY et al. (1984), it is also possible to estimate how many searches were necessary on an average to recover each of the two photographic meteorites with well determined terminal masses during the whole operation of all three networks. Innisfree needed about 12 searches for bodies with computed terminal mass of 5 kg and bigger, while the Lost City meteorite need about 6 searches for bodies of computed terminal mass of 20 kg and bigger. During the whole operation of all three networks, only searches for bodies with computed terminal mass of 200 kg or bigger (they never occurred) would yield an almost certain meteorite recovery. It is clear that the actual meteorite search is the weakest point in acquiring photographic data on recovered meteorites.

The initial interest and enthusiasm in big meteoroid studies and in the operation of photographic fireball networks has diminished during the last few years. But still more theoretical studies of the interaction of big meteoroids with the atmosphere as well as more systematic observations of fireballs are needed to solve definitely the questions of the relationship between meteorites and meteoroids before atmospheric entry. Activity in this field is now going on in USSR and in Czechoslovakia. The possibility of continuing this work and creating new interests and methods has been increased by plans for multilateral cooperation between the

socialist countries, where this topic should be studied at least during the next five year period.

References

1. Bronshten, V.A.: 1980, *Astronomiczeskij vestnik* 14, 25 (in Russ.)
2. Ceplecha, Z.: 1957, *Bull. Astron. Inst. Czechosl.* 8, 51.
3. Ceplecha, Z.: 1961, *Bull. Astron. Inst. Czechosl.* 12, 21.
4. Ceplecha, Z.: 1977, in *Comets, Asteroids, Meteorites*, ed. A.H. Delsemme, The University of Toledo (USA), p. 143.
5. Ceplecha, Z.: 1985, *Fireball Information on Meteorids and Meteorites*, *Bull. Astron. Inst. Czechosl.* 36, (in press).
6. Ceplecha, Z.: 1983, in *Asteroids, Comets, Meteors*, ed. C.I. Lagerquist, H. Richman, *Astron. Obs. Univ. Uppsala (Sweden)*, p. 435.
7. Ceplecha, Z. and R.E. McCrosky: 1976, *J. Geophys. Res.* 81, 6257.
8. Ceplecha, Z., J. Rajchl and L. Sehnal: 1959, *Bull. Astron. Inst. Czechosl.* 10, 204.
9. Halliday, I.: 1971, in *Evolutionary and Physical Properties of Meteorides*, ed. C.L. Hemenway, P.M. Millman, A.F. Cook, NASA SP-319, Washington (U.S.A.).
10. Halliday, I., A.T. Blackwell, and A.A. Griffin: 1978, *J. Roy. Soc.*
11. Halliday, I., A.T. Blackwell, and A.A. Griffin: 1984, *Science* 223, 1405.
12. Halliday, I., and A.A. Griffin: 1982, *Meteoritics* 17, 31.
13. Halliday, I., A.A. Griffin, and A. T. Blackwell: 1981, *Meteoritics* 16, 153.

A METHOD OF LONG-TERM RADAR SHOWER DATA ANALYSIS

M. Simek

Astronomical Institute of the Czechoslovak Academy of Sciences
Ondrejov, Czechoslovakia

Long-term radar observations of any meteor shower yield good data for a study of the features of its cross-section structure in detail. The hourly rates of meteor echoes represent usually the basic data from which shower characteristics are derived. Unfortunately, the hourly rate does not depend only on the activity of the shower in question but also on the position of the shower radiant (i.e., its zenith distance), on the mutual radiant-antenna position and, on the parameters of the radar system. We know that the knowledge of the response function of the radar is necessary for good interpretation of the hourly echo counts.

The response function introduced by MCINTOSH (1966) corresponds to the radar sensitivity for different radiant zenith distances. It varies with meteor mass, slightly with the population exponents and with the meteor velocity. In most cases we do not know the response function well enough and, therefore, many authors use, for shower activity analysis, daily rates (or a fraction of a day, say 6, 8, 10 or any other number of hours of observation which repeats every day). Then a knowledge of the response function is irrelevant, but, every day of observation is then represented by only one value on the activity curve. The fine structure of the shower activity is then lost.

The basic idea for using the hourly echo counts without knowing the response of the radar is based on the fact that the same diurnal variation of geometrical observational conditions repeat every day. We are neglecting here the daily motion of the radiant and the four minutes a day difference between siderival and standard time. Let us suppose that the cross-section patterns of the shower do not change drastically from year-to-year except for the activity level. This is the case for the Geminids, Perseids, Quadrantids and other meteor streams.

Previous studies by several authors covered often only one or at best a few years of observation from one station only; these results do not yield a homogenous view on the stream and its structure. Radar observations and their lack of dependency on weather conditions enables complete analysis when satisfactorily long time series of data are available. We must also not forget that the shower radiant will not be above the observer's horizon for the whole 24 hours period, and that the antenna characteristics will permit observations only for some fraction of the day. It is very worthwhile to supplement the data set, using the results of other radars situated on different geographical longitudes.

When dealing with overdense echoes the condition of identical transmitting powers for the radars is not very serious. The wavelength should not be very different, within, say, some 20%, which is satisfied by most meteor radars operating in the wavelength range of 8 - 10m.

Particular difficulties, however, arise when combining the data from radars with different antenna characteristics.

We start the analysis using a preliminary model of the cross-section patterns of the shower. The model is usually just a rough estimation of the behavior of the activity within at least 48 hours of the shower observation. After subtraction of the sporadic background, the data are organized as a series of sets for each individual year. One set of data in a particular year is represented by measured hourly echo shower rates with respective solar longitude for say 8 - 9 hours through all days of shower observation. One set must necessarily contain at least two members. Similarly, we have another set for 9 - 10 hours and so on. In this way the shower rates for every single year are organized. The same equinox must be used. Each set is then normalized to the sum of the model data at the appropriate solar longitudes. We then obtain a new model of the shower pattern. This process is repeated for a sufficient number of times until the last resulting model is identical with the previous one. The convergence usually occurs after 4 to 6 iterations. As a by-product of this method we also obtain the response function of the radar system without a knowledge of its antenna characteristics. The method is described in more detail in SIMEK (1985).

This whole procedure has been applied to the Swedish Perseid observations from 1953 to 1978, and published by LINDBLAD and SIMEK (1985). The data was first divided into two parts: daytime observations and night-time observations (see LINDBLAD and SIMEK, 1983). Results were, in general almost identical. The cross-section patterns for combined day and night observations for echo durations ≥ 1 s are presented in Fig. 1. The scale is here normalized to 100 at the maximum.

Canadian Perseid observations were carried out in the period 1958 to 1974. The same method was applied and the resulting cross-section patterns for echo durations ≥ 1 s are presented in Fig. 2. Detailed analysis is presented by SIMEK and MCINTOSH (1986).

The Czechoslovak meteor radar program covered the Perseid activity for 11 years between 1958 and 1984. As with recent Swedish and Canadian data analysis, we concentrated our interest on the ≥ 1 s echo duration group.

The Swedish, Canadian and Czechoslovak data all show very similar features for the fine mean structure of the Perseid meteor stream activity. When combining all three resulting patterns together, each individual point at a particular solar longitude was averaged using a weight inversely proportional to its standard deviation. The observed shower data base contains some 300000 meteor echoes with durations ≥ 1 s. The position of peak activity was found at a solar longitude of $139.20^\circ \pm 0.02^\circ$ (equinox 1950.0). It should be understood that the stream shows slightly different features in the cross-sectional patterns from year to year. Therefore, the histogram in Fig. 3 describes the most probable pattern of the stream along the Earth's path. The peak is less pronounced than for a single year's observation, and is slightly flatter. Note that, because of the 6 hour shift per year in the diurnal cycle, peak activity cannot be observed from one station in those years when it appears around the time of the radiant culmination.

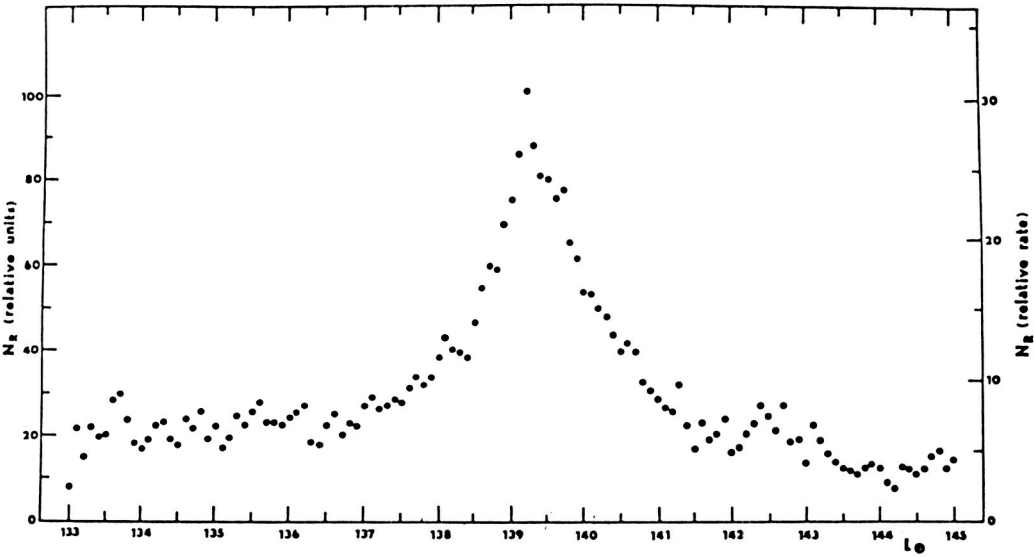


Fig. 1 Relative Perseid meteor flux producing meteor echoes having durations ≥ 1 s as a function of solar longitude L (epoch 1950.0). Swedish observations.

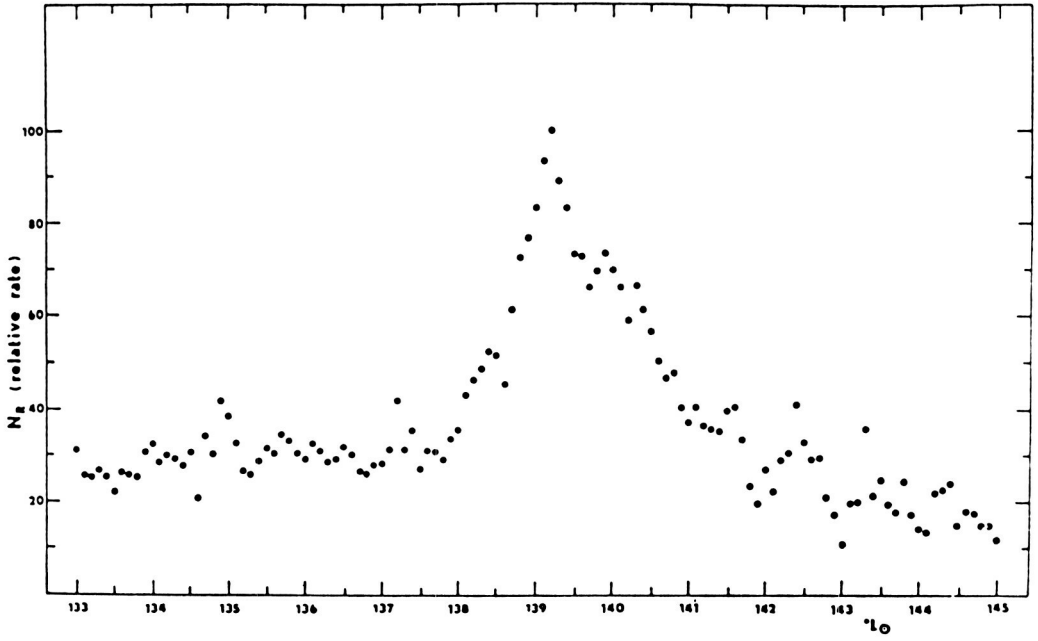


Fig. 2 Relative Perseid meteor flux producing meteor echoes having durations ≥ 1 s. Canadian observations.

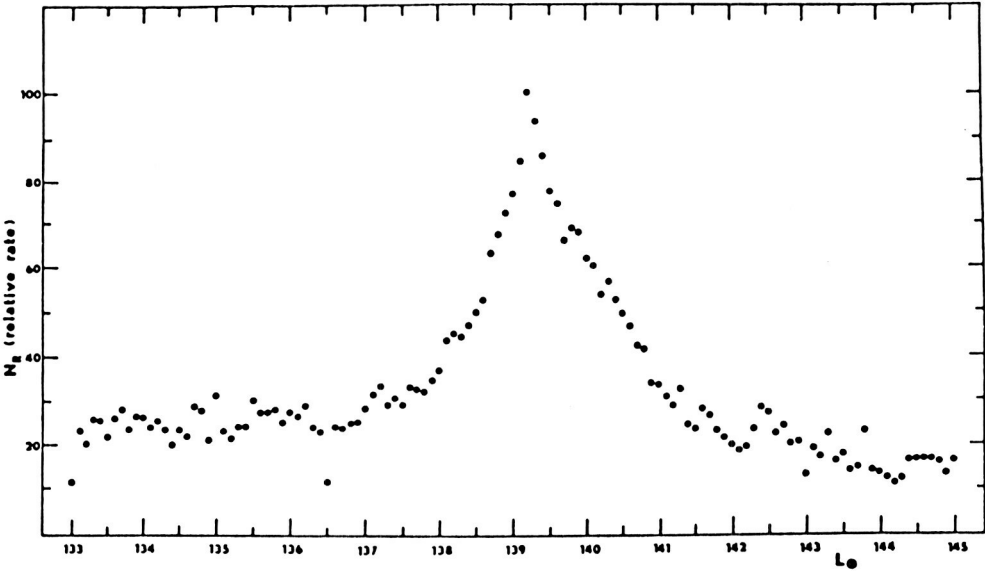


Fig. 3 Relative Perseid meteor flux producing meteor echoes having durations ≥ 1 s. Resulting histogram of Swedish, Canadian and Czechoslovak observations.

One would expect that the activity patterns should reach zero level on both wings of the histogram. This is contrary to our result in Fig. 3. Residual shower activity before and after the central part of the histogram result from one sided normalization of the data when negative shower rates were discarded.

In addition to the response function of each radar, the variation of shower activity from year-to-year was determined. Long series of observations of the sporadic meteor complex yield very good data for the analysis of solar activity cycle and its influence on upper atmosphere phenomena.

Final detailed conclusions concerning the complete set of long-term Perseid radar observations from different stations require further analysis, which will be published later. Colleagues who are interested in contributing their own data from Perseid radar observations are invited to participate in this project. We plan to concentrate our interest in the future also on other meteor streams such as the Quadrantids and the Geminids.

References

- Lindblad B. A. and M. Simek, 1983, in Asteroids, Comets, Meteors, ed. C.-I. Lagerkvist and H. Rickman, p. 431.
- Lindblad B. A. and M. Simek, 1985, in Asteroids, Comets, Meteors II, Uppsala symposium (in print).
- McIntosh B. A., 1966, Can. J. Phys. 44, p. 2729.
- Simek M., 1985, Bull. Astron. Inst. Czechosl. 36 (in print).
- Simek M. and B.A. McIntosh, 1986, Bull. Astron. Inst. Czechosl. 37 (in print).

INCIDENT METEOROID FLUX DENSITY

P. B. Badadjanov, R. Sh. Bibarsov, V. S. Getman, and V. M. Kolmakov

Institute of Astrophysics
Dushanbe, USSR

Complex photographic and radar meteor observations have been carried out at the Institute of Astrophysics since 1957. Using the available observational data we have tried to estimate the density of incident flux of meteoroids over a wide mass range of 10^{-5} to 10^2 g.

To avoid the influence of apparatus selectivity a special technique was applied. Its main characteristics are:

1. An integrated meteoroid mass distribution on a logarithmic scale defined as

$$\log N(m) = \log B - (S-1) \log m \quad (1)$$

where $N(m)$ is the number of meteoroids of mass greater than m which intersect a fixed area within a fixed time and B and S are parameters to be determined.

If we assume B and S to be constant then (1) can be fitted as a straight line equation. B will be constant only in the case of stable effective interception area. If this condition is met for meteoroids whose masses exceed m_0 , and a linear trend in the integral distribution (1) is obtained, it means that all the meteoroids of $m \geq m_0$ are recorded and the effective area for these meteoroids is indeed constant at least on average or for the given radiant.

2. It is supposed that for sporadic meteors, the parameters are constant or vary little over the range of meteor velocities.

3. Since we wish to determine the average density, the average parameters of both apparatus and meteors are used.

The meteoroid incident flux density was determined by:

$$N_0(m) = \frac{N(m)}{\sigma t k} \quad (2)$$

where $N(m)$ is the number of meteoroids of mass greater than m , recorded for the time t ; σ is the average effective area, k is the correction coefficient depending on the type of apparatus and method of observation used.

Only meteors corresponding to the linear part of the cumulative distribution (1) were selected.

To estimate the incident flux density using radar observations, we selected data on sporadic meteors producing overdense trails of duration $T > 0.1$ s that corresponded to masses greater than $m = 1.4 \cdot 10^{-3}$ g. Some 226,000 meteors of that type were recorded during 6,800 hours.

Taking into account the meteoroid density distribution and correcting for the attachment of electrons to neutral particles in meteor trails (when $T > 10^{-2}$ s), S is found to be 2.1 for meteoroids with masses from 10^{-5} to 10^2 g.

The average effective area σ for the mean radiant is estimated by:

$$\sigma = \frac{(S - 1) \cdot 1.8 \sqrt{R\lambda} \ell}{(S - 1.25) \cos Z} \quad (3)$$

Here R is the average range of meteor registrations, λ is the radar wave length ($\lambda = 8\text{m}$), Z is the zenith distance of the mean reflecting point, ℓ is the length of the horizontal line drawn between the ends of the aerial orientation diagram, through the mean reflecting point and made perpendicular to the main axis of the diagram at a distance of R from a radar.

Equation (3) uses the average effective length factor $(S - 1) 1.8\sqrt{R\lambda}/(S - 1.25)$ instead of the average length of the meteor trail, because in order to scale mass according to duration, one observes only a fraction of the trails which have reflecting points close to the ionization maximum. From observations with our interferometer we have found that on average $R = 146\text{ km}$, $\ell = 150\text{ km}$, $\cos Z = 0.643$. These observations also showed that all meteors whose radiants were in an area of 0.6 of a sky hemisphere were recorded. Therefore, for radar observations the adopted value for K is 0.6.

Our final solution for sporadic meteors with masses of from 10^{-3} to 10^2 g is

$$\log N_0(m) = 0.13712 - 1.1 \log m \quad (4)$$

where m is in g, and $N_0(m)$ in $\text{m}^{-2} \text{s}^{-1} (2\pi \text{ ster})^{-1}$.

The incident flux density was also estimated using double photographic observations of bright meteors carried out by the Dushanbe meteor patrol in 1957-1967.

Pre-atmospheric meteoroid masses were determined by:

$$m = \frac{2}{\tau v^2} \int_{-\infty}^{+\infty} I dt$$

where $\tau = \tau_0 v$ is the luminous efficiency, v the velocity of a meteoroid, I the luminous intensity.

Meteors having masses of 0.02 to 160g were recorded. The mass range of meteors corresponding to the linear part of the cumulative distribution was 16-160g. In this mass range S was found to be 2.1. The effective area covered by meteor patrol cameras at the height of 100 km was of the order of 10^4 km^2 . During 1,000 hours of observation 170 sporadic meteors were recorded with the result that we detected 0.78 of all the meteors whose radiants were in an area of 0.85 of the celestial hemisphere. Thus, for photographic observations K was assumed to be 0.68.

The solution for our photographic observations was

$$\log N_0(m) = -13.689 - 1.1 \log m \quad (5)$$

As an average from (4) and (5) we may adopt

$$\log N_0(m) = -13.7 - 1.1 \log m$$

For comparison, this method was also used to analyze Super-Schmidt data on faint meteors (MCCROSKY, et al., 1961). For their sporadic meteor sample we obtained.

$$\log N_o(m) = -13.913 - 1.12 \log m \quad (6)$$

If we adopt a more extreme model for the luminosity coefficient ($\tau \propto v^{-5}$) then for their bright meteor data we get

$$\log N_o(m) = -13.39 - 1.1 \log m \quad (7)$$

while for their faint meteors the result is

$$\log N_o(m) = -13.698 - 1.12 \log m \quad (8)$$

The fact that in (5), (6), (7), and (8), S is constant confirms indirectly the assumed lack of a meteor velocity dependence.

Since (4), (5), and (8) are in best agreement we suggest that for bright meteors the luminous efficiency is indeed proportional to the meteor velocity but for faint meteors the extremal model $\tau \propto v$ is more suitable.

Analogous calculations were made for the Perseides using observation data obtained in Dushanbe. Meteoroids of masses of 0.025 up to 25 g were recorded. The linear portion corresponded to masses of 1 to 10 g with

$$S = 1.67 \text{ and } \log >_o(m) = -14.2 - 0.67 \log m.$$

The calculation using the extremal model value of luminous efficiency yielded

$$\log N_o(m) = -13.6 - 0.67 \log m$$

where for meteor showers $N_o(m)$ is measured in $m^{-2} s^{-1}$.

These results may be compared with those of other authors. Thus, LEBEDINETS (1970) obtained $N_o(m) = 1.1 \times 10^{-10} m^{-2} s^{-1} (2\pi \text{ ster})^{-1}$ from radar observations of sporadic meteors with $m \geq 2 \times 10^{-4} \text{ g}$. For the same mass and using (4) we obtain $N_o(m) = 1.1 \times 10^{-10} m^{-2} s^{-1} (2\pi \text{ ster})^{-1}$. PECIAN (1984) from radar observations of overdense meteor trains with $T \geq 0.6 \text{ s}$ for $m \geq 10^{-2} \text{ g}$ obtained $N_o(m) = 3.7 \cdot 10^{-12} m^{-2} s^{-1} (2\pi \text{ ster})^{-1}$. For the same mass, using (4) we derived $N_o(m) = 3.2 \cdot 10^{-12} m^{-2} s^{-1} (2\pi \text{ ster})^{-1}$. According to LINDBLAD (1967), for $m \geq 10^{-3} \text{ g}$, $N_o(m) = 3.2 \times 10^{-11} m^{-2} s^{-1} (2\pi \text{ ster})^{-1}$, and for $m \geq 1 \text{ g}$, $N_o(m) = 1.26 \cdot 10^{-10} m^{-2} s^{-1} (2\pi \text{ ster})^{-1}$. For the same mass range using (4) and (5) we have $N_o(m) = 4 \times 10^{-11} m^{-2} s^{-1} (2\pi \text{ ster})^{-1}$ and $N_o(m) = 2 \times 10^{-14} m^{-2} s^{-1} (2\pi \text{ ster})^{-1}$ respectively.

In other references too numerous to mention, one can find the results of one or two orders of magnitude less than the results cited here. As shown by LEBEDINETS (1970), these differences can be explained by the fact that various factors of meteor detectability are not properly taken into account. If this is done the results obtained by different authors using different techniques agree well.

References

1. Lebedinets, V. N., 1970, Kometry, I. Meteory, No. 19, pp. 25-30.
2. Lindblad, B. A., 1967, Smiths. Contr. To Astrophys., Vol. 11, p. 1967.

3. McCrosky, R. E., Posen, A., 1961, *Smiths. Contr. to Astrophys.*, Vol. 4., No. 1.
4. Pecian, P., 1984, *Bull. of the Astron. Inst. of Czechoslovakia*, Vol. 35, No. 1, pp. 5-14.

MODELS OF SPORADIC METEOR BODY DISTRIBUTIONS

V. V. Andreev and O. I. Belkovich

Kazan State University
Kazan, USSR

The distributions of orbital elements and flux density over the celestial sphere are the most common forms of representation of the meteor body distribution in the vicinity of the earth's orbit.

The determination of flux density distribution of sporadic meteor bodies according to

$$QP(v, \epsilon, \psi) = QP_{\epsilon}(v)P(\epsilon, \psi) \quad (1)$$

where ϵ is the elongation angle from the earth's apex and ψ is the angle measured from the ecliptic plane upward to its northern pole, has been worked out at the Engelhardt Observatory. The distributions $P(v)$ (it was assumed that v and ψ are independent) are taken directly from meteor orbits catalogues corrected for selectivity of observational method while $QP(\epsilon, \psi)$ is obtained by the PUPYSHEV (1965) method from radar observations with step-by-step rotating aeriels. In this method, the number of recorded parameters is minimal as only events exceeding a threshold level are used and therefore the observational selectivity is minimal too, which makes processing easier. There is also no need to know the radiant distribution for determination of the velocity distribution. (The radiant distribution is usually obtained from catalogues of radar observations which for elongation angles over $100-110^\circ$ are often unreliable). As a rule from observation one can obtain a meteor flux having some measured parameter (brightness, echo amplitude) greater than a certain threshold level. This process of changing an apparent sporadic meteor flux density to that of the real meteor body density taking selectivity into account is described in ANDREEV and BELKOVICH (1975).

Catalogues of meteor orbits compiled on the basis of radar observations over the equator (Catalogue of WDC B-2, 1975, 1977) and maps of the flux density distribution over the celestial sphere obtained by PUPYSHEV et al., (1980) have been used as observational data. The dependence of ionised meteor trail properties on meteor height and mass as obtained by TOKHTASJEVE (1975) has also been used.

The velocity distributions $P(v_{\infty})$ reduced for selection and radiant density distribution $P(\epsilon)$ were analyzed. The velocity distributions $P(v_{\infty})$ given in ANDREEV et al. (1982) have been used as the first approximation for determination of radiant density distribution $P(\epsilon)$ in order to take into account observational selectivity.

The transformation of geocentric velocity and radiant distributions of heliocentric ones have been carried out by the method described in ANDREEV, et al. (1982) and ANDREEV and BELKOVICH (1978). This transformation is required because of the influence of the earth's motion and gravitation on the apparent incident flux of sporadic meteor bodies.

Actual heliocentric velocity distributions $P(v_h)$ and heliocentric radiant density distribution $P(E)$ are plotted by solid lines in Figs. 1 and 2 respectively.

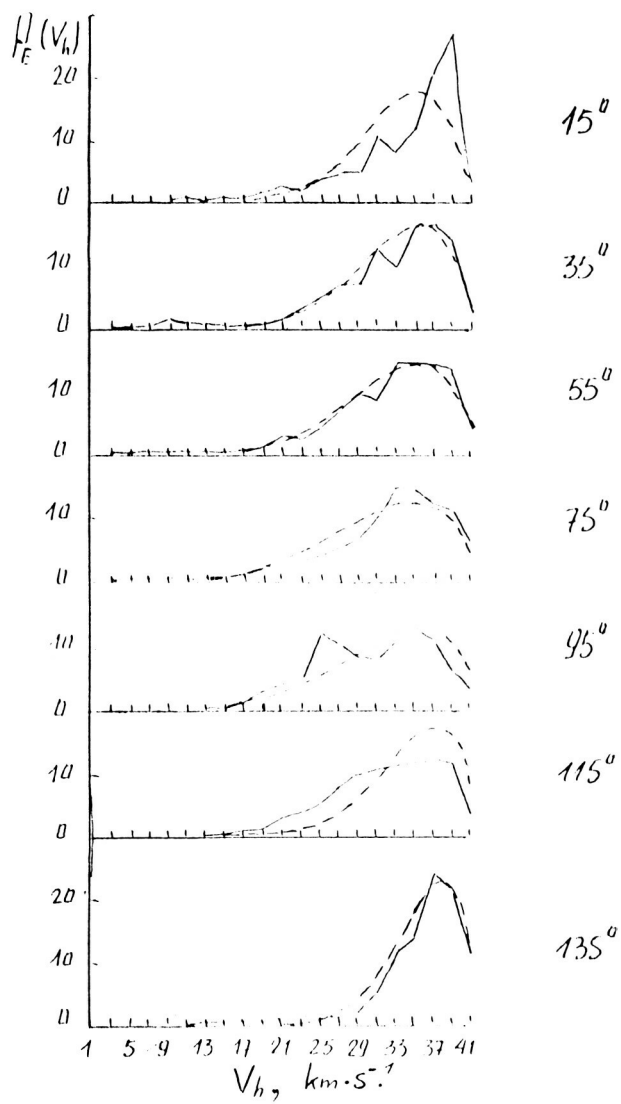


Fig. 1 Distributions of heliocentric velocities $P_E(v_h)$ of meteor bodies.

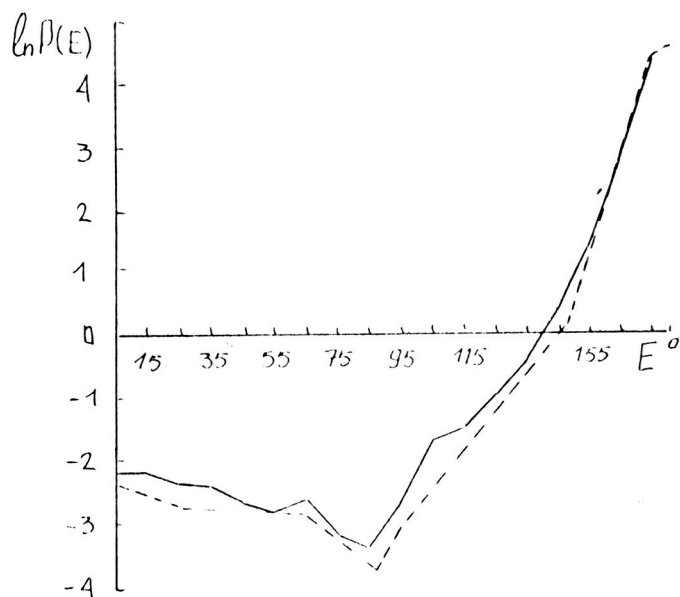


Fig. 2 Distributions of heliocentric radiant density $P(E)$ of meteor bodies.

The theoretical distributions of heliocentric velocities were written as

$$P_E(v_h) = B^{-1}(p, q) (v_h/v_o) (1 - \alpha)^{p(E)} \alpha^{q(E)} \quad (2)$$

where $v_o = 30 \text{ km s}^{-1}$ is the earth's orbital velocity,

$$\alpha = 0,5(2 - (v_h/v_o)^2), B(p, q) = \Gamma(p + 1) \Gamma(q + 1) / \Gamma(p + q + 2), \Gamma(y)$$

is the Gamma function, $p(E)$ and $q(E)$ are parameter derived by fitting the distribution equation (2) with observational data. The values p and q depend on heliocentric elongation angle E in complete interval as

$$\begin{aligned} p(E) &= \begin{matrix} 4.17 & - & 1.95E, \\ -7.26 & + & 5.33E, \end{matrix} & \text{for } \begin{matrix} 0^\circ \leq E \leq 90^\circ \\ 90^\circ \leq E \leq 180^\circ \end{matrix} \\ q(E) &= \begin{matrix} 2.07 & - & 0.809E \\ -0.471 & + & 0.809E \end{matrix} & \text{for } \begin{matrix} 0^\circ \leq E \leq 90^\circ \\ 90^\circ \leq E \leq 180^\circ \end{matrix} \end{aligned} \quad (3)$$

The heliocentric radiant density distribution $P(E)$ was approximated as

$$\begin{aligned} P(E) = \exp & \begin{matrix} -2.29 & -1.003E & \text{for } 0^\circ \leq E \leq 25^\circ \\ -2.69 & -0.215E & 25^\circ \leq E \leq 65^\circ \\ -0.0782 & -2.47E & 65^\circ \leq E \leq 87^\circ \\ -12.54 & +5.73E & 87^\circ \leq E \leq 94^\circ \\ -8.79 & +3.45E & 94^\circ \leq E \leq 148^\circ \\ -23.18 & +9.02E & 148^\circ \leq E \leq 175^\circ \\ -2.64 & +2.29E & 175^\circ \leq E \leq 180^\circ \end{matrix} \end{aligned} \quad (4)$$

In the expressions (3), (4) E is in radians. The results using expressions (2), (4) are plotted by dashed lines in Figs. 1 & 2 respectively.

Distributions of the geocentric radiants and velocities calculated from the mathematical model equations (2) - (4) in order to verify its accuracy. The coincidence of observational distributions with modelled ones is quite good with an exception of cases where velocities were less than 20 km s^{-1} .

A somewhat modified method of modeling sporadic meteor body velocity and radiant distributions has been worked out to achieve a closer approximation of the observations.

It is generally believed that comets and asteroids are the main sources of meteoric matter, but some authors differ in estimation of relative contribution of both sources.

Division of meteor orbit data into three parts was taken as the basis for the modeling method. A similar division was made for photographic meteors in MCCROSKY and POSEN (1961).

The selectivity of the photographic method of observations was taken into account ANDREEV et al., (1983).

As classifying parameters those of the Tisserand criterion

$$T = a^{-1} + 2 \cdot A^{-3/2} \cdot a(1 - e^2) \cos i \quad (5)$$

of the restricted circular three-body problem of Sun-Jupiter-particle were used. Here a , e , i are semi major axis, eccentricity, and orbit inclination refer to the meteor body and A is a semimajor axis of the disturbing planet. A value of $T = 0.5767$ corresponding to the Jovian orbit MCCROSKY and POSEN (1961)⁰ was taken as the dividing value of the Tisserand constant.

Meteor bodies with any i and $T < T_0$ were assigned to the first component. The orbits of these resemble those of long-period comets. Meteor bodies with $T \geq T_0$ were divided into two more components. The one contains meteor orbits with $i \leq 90^\circ$ (these are asteroid-like orbits) and the other contains meteor orbits with $i > 90^\circ$ representing a class of orbits not usually found among comets and asteroids.

Since the third group contained only 15 meteors from the catalogue (ANDREEV et al., 1983), this group was not subjected to further analysis. The preliminary result shows that the number of meteors of the third component increases with decreasing of masses of observed meteor bodies.

The heliocentric velocity distributions $P_E(v_h)$ of meteor bodies of the first and second components are plotted by solid and dashed lines in Fig. 3 respectively. They are completely different. One can see that the velocity distributions for each component do not depend on the elongation angle E .

Obviously, the observed dependence on elongation angle E of the heliocentric velocity distributions $P_E(v_h)$ of the total complex of meteor bodies and obtained from (3) and in ANDREEV et al. (1982) is really due to the superposition of the corresponding distributions of each of the three components.

The main advantage of this modified simulation method is the possibility of using traditional astronomical data for interpretation of observation and modeling results.

References

1. Pupyshv Yu. A., 1965, in: Results of researches under the IGY program, No. 14, Moscow, Nauka Publishers.
2. Andreev V. V., Belkovich O. I., 1975, Distribution of meteor bodies radiants and velocities, Soviet Astron. J., 9, No. 4.
3. WDC B-2 Catalogue of Meteor Rates and Orbits (based on equatorial observations), Soviet Geophysical Committee, 1975.
4. The same, 1977.
5. Pupyshve Yu. A., Filimonova T. K., Kazakova T. V., 1980, Maps of distribution of visible radiant density of sporadic meteors over the celestial sphere, in: Meteor radiowave propagation, No. 15, Kazan.
6. Tokhtashev V. S., 1975, Meteor bodies ablation in the earth's atmosphere, in: Interaction of meteor matter with the earth and

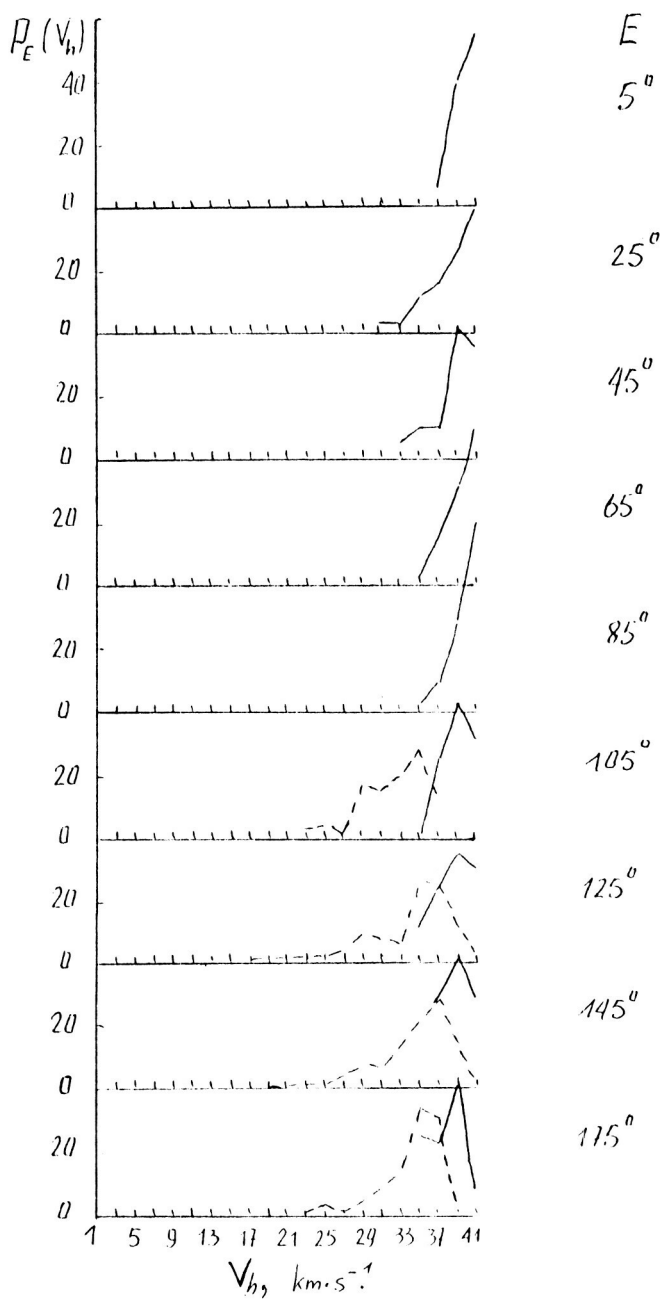


Fig. 3 Distributions of heliocentric velocities $P_E(v_h)$ of meteor bodies of the first and second components.

evaluation of meteor matter influx onto the Earth and Moon, Dushanbe, Donish Publ.

7. Andreev V. V., Belkovich O. I., Zabolotnikov V. S., 1982, The structure of the meteor complex in the vicinity of the earth's orbit, in: Meteor matter in interplanetary space, Kazan, Moscow.
8. Andreev V. V., Belkovich O. I., 1978, On sporadic meteor bodies influx, VINITI Publishers, Moscow.
9. Andreev V. V., Belkovich O. I., Tokhtashev V. S., 1983, Selectivity effect in photographic meteor observations, Soviet Astronom. J., 17 No. 4.
10. McCrosky R. E., Posen A., 1961, Orbital elements of photographic meteors, Smiths. Constr. Astrophys., 4, No. 2.
11. Kresak L., The discrimination between cometary and asteroidal meteors, Bull. Astron. Inst. Czechosl., 20, No. 4, 1969.

ON METEOR STREAM SPATIAL STRUCTURE THEORY

G.V. Andreev

Research Institute of Applied Mathematics and Mechanics
Tomsk University
USSR

The classical spatial representation of meteor streams is an elliptical torus with variable cross-section. The position of this torus in space is determined by the mean orbit elements that may be obtained directly from observations of individual meteor stream particles when crossed by the earth. Since the orbits of individual particles of a stream differ from each other, the distance between them on a plane normal to the mean orbit of elliptical torus forms some area, i.e., a cross-section. The size and form of these cross-sections change with the change of the direction among the mean orbit and are completely defined by the dispersion values of the orbit elements in a stream.

This paper deals with an attempt to create an analytical method that would permit description of the spatial and time parameters of meteor streams, i.e., the form and size of their cross-sections, density of incident flux and their variations along the mean orbit and in time. In this case, the stream is considered as a continuous flux rather than a set of individual particles.

The solution to this problem lies in creation of a model of a stream structure that depends on the type of parental matter decay and the stage of a stream evolution. We suggest the following three models giving analytical descriptions of the spatial structure of a meteor stream (ANDREEV 1984a, 1984b).

1. The stream is comparatively young and perturbations have not yet changed its structure. It is clear that in such a model all the orbits intersect at the ejection point.

2. The stream is comparatively old and the perturbations now show up as changes of the meteoroid orbit elements with their orbits intersecting, not at the ejection point but along some arc.

3. The stream is so old that it is impossible to distinguish the common area of crossing orbits but a distinct meteor stream is still spatially defined.

Since the analytical developments of the above models are about the same and the final formulas in some cases are rather bulky, we shall confine our exposition of the elements of our spatial structure theory using as an example only the first model.

Suppose the stream is formed by means of the parental body decay within an infinitesimal volume of its original orbit. Let a , e , i , Ω , ω be Kepler's orbit elements of parental matter having the velocity V at the decay point. Analysis shows that convenient formulas for estimating the velocity increment of particle orbital elements as compared with the comet orbit may be obtained, if the comet orbit plane is taken as the main plane

and the apex of comet motion is taken as the main direction. Let u be the velocity vector magnitude of matter ejection directed at an angle β to the main plane with a projection on the plane of the comet orbit making an azimuthal angle α with the direction to the apex. Vector addition of velocities gives the following variation of the velocity magnitude and its direction

$$\frac{\Delta V}{V} = \left(1 + \frac{U^2}{V^2} + 2 \frac{U}{V} \cos \alpha \cdot \cos \beta\right)^{1/2} - 1, \quad (1)$$

$$\sin \Delta\psi = U(V^2 + U^2 + 2UV \cos \alpha \cdot \cos \beta)^{-1/2} \cdot \sin \alpha \cdot \cos \beta \quad (2)$$

In the formula (2), $\Delta\psi$ is the change of angle of ψ between the radius-vector of r and the velocity vector of V .

Using the expressions (1, 2) we obtained the following correlations for estimating the variation of orbit elements:

a) increments connected with reorientation of the velocity vector in the orbit plane:

$$\Delta a = 2 \frac{a^2}{\mu} V \cdot \Delta V,$$

$$\Delta e = 2 \frac{\Delta V}{V} (e + \cos v) + \frac{r}{a} \Delta\psi \cdot \sin V, \quad (3)$$

$$\Delta\omega = 2 \frac{\Delta V}{eV} \sin V - (2e + \cos V + e^2 \cos V) (1 + e \cos V)^{-1} \cdot \frac{\Delta\psi}{e},$$

b) increments connected with the reorientation of the orbit plane:

$$\Delta i = \frac{r}{\sqrt{\mu p}} U \cdot \cos (V + \omega) \cdot \sin \beta,$$

$$\Delta\Omega = \frac{r}{\sqrt{\mu p}} U \cdot \sin (V + \omega) \cdot \operatorname{cosec} i - \sin \beta = \tan (V + \omega) \cdot \operatorname{cosec} i \cdot \Delta i, \quad (4)$$

$$\Delta\omega = - \frac{r}{\sqrt{\mu p}} U \cdot \cot i \cdot \sin (V + \omega) \cdot \sin \beta = - \Delta\Omega \cdot \cos i$$

The formulas given in the systems (3 and 4) enable one to analyze easily the orbit elements changes at ejection.

The formulas (1, 2, 3, 4) give the change of an individual particle orbit. For formation of a stream of particles, it is necessary to vary these relations using different values of u , α , β (depending on the required peculiarities of stream formation) and to find the stream's mean orbit and the dispersion of orbit elements. Suppose particles are ejected so that the relative velocities of particles and their directions are within the intervals of $U \pm \sigma u$, $\alpha \pm \sigma \alpha$, $\beta \pm \sigma \beta$. Then the elements of the mean orbit of a stream are ($U \ll V$)

$$\bar{a} = a + \frac{2a^2}{\mu} UV \cdot \cos \alpha \cdot \cos \beta,$$

$$\bar{e} = e + 2 \frac{U}{V} (e + \cos V) \cos \alpha \cdot \cos \beta + \frac{rU}{aV} \sin V \cdot \sin \alpha \cdot \cos \beta,$$

$$\bar{i} = i + \frac{rU}{\sqrt{\mu p}} \cos (V + \omega) \cdot \sin \beta,$$

(5)

$$\bar{\omega} = \omega + \frac{2U}{eV} \sin V \cdot \cos \alpha \cdot \cos \beta - \frac{U}{V} \left(1 + \frac{\cos E}{e}\right) \sin \alpha \cdot \cos \beta - \frac{rU}{\sqrt{\mu p}} \cdot$$

$$\frac{\sin (V + \omega)}{\tan i} \cdot \sin \beta,$$

$$\Omega = \Omega + \frac{rU}{\sqrt{\mu p}} \sin (V + \omega) \cdot \operatorname{cosec} i \cdot \sin \beta, \quad \cos E = (e + \cos V)(1 + e \cos V),$$

and the orbit element dispersions in the stream are defined by means of differentiation of (5) with respect to u, α, β .

If the ejection is considered isotropic rather than directed then the formulas for determining the root-mean-square dispersions of the orbit elements will look like:

$$\sigma_a = \frac{a^2}{\mu} V(U^2 + \sigma^2 U)^{1/2}, \quad \sigma_e = \frac{1}{2V} (V^2 + \sigma^2 U)^{1/2} [4(e + \cos V)^2 + r^2 a^{-2} \cdot$$

$$\sin^2 V]^{1/2},$$

$$\sigma_i = \frac{r}{\sqrt{\mu p}} \cdot \frac{(\sigma^2 U + U^2)^{1/2}}{2} \cdot \cos (V + \omega), \quad \sigma_\Omega = \tan (V + \omega) \operatorname{cosec} i \cdot \sigma_i,$$

$$\sigma_\omega = \frac{1}{2} (U^2 + \sigma^2 U)^{1/2} \left[\left(2 \frac{\sin V}{Ve}\right)^2 + \left(\frac{e + \cos E}{Ve}\right)^2 + \frac{r^2}{\mu p} \cdot \sin^2 (V + \omega) \cdot \right.$$

$$\left. \cotan^2 i \right]^{1/2},$$

and the mean orbit will coincide with that of the parental body.

The formulas (1-5) make it possible to model analytically any matter ejection out of a parental body, and to estimate the mean orbit and the orbit element dispersions about it. However, to study the meteor stream evolution as a whole, it is necessary to have the appropriate analytical formulas to calculate the mean orbit evolution and orbit elements dispersions. For the mean orbit, this calculation is not difficult. In studying the evolution of meteor streams during long time intervals, only secular perturbations that generate systematic change of stream

characteristics are of interest. For numerical investigation of the secular evolution of the mean orbit, one can apply the well-known Halphen-Goryachev method. But it is very difficult to calculate the secular evolution of the orbit element dispersions. However, as our investigations have shown, this problem may be solved by means of intermediate calculations using the Halphen-Goryachev algorithm for each step in time. Indeed, if the initial values of orbit elements and their dispersions are denoted by the zero subscript, new values of the Keplerian elements at the time $t = t_0 + \Delta t$ will equal $x(t) = x_0 + \Delta x$, where x is any of the elements. It is not difficult then to conclude that the value of the dispersions of element x by the moment of t can be found from the expression:

$$\sigma x(t) = \left| \frac{\partial \Delta(t)}{\partial x_0} \right| \sigma x = \left| 1 + \frac{\partial(\Delta x)}{\partial x_0} \right| \sigma x_0 \quad (6)$$

where particular derivatives related to orbit elements can be easily found by the Eulerian equations.

The next step is to obtain the analytical dependences of the form and size of cross-sections and their changes in space and time. The derivation of these formulas depends entirely on the model of stream origin and the evolutionary stage at which it occurs (ANDREEV, 1984). In particular, for a stream arising as a result of a "point" decay, the formula for determining the cross-sectional area may be obtained on the basis of independence of relative distance between orbits in the mean orbit plane and the plane orthogonal to it, i.e.,

$$S = \pi \cdot A \cdot B = \pi \cdot \Delta r \cdot \sin \psi \cdot r \cdot \Delta \phi \cdot \sin(V + \omega - c), \quad (7)$$

where $A = \Delta r \cdot \sin \psi$ is the size ("width") of the cross-section in the orbit plane, $B = r \cdot \Delta \phi \cdot \sin(V + \omega - c)$ is the stream's "thickness", c is an angular distance of decay point from the ascending node and $\Delta \phi$ is a dihedral angle between extreme orbits at the ejection point. The radius-vector variation in an arbitrary direction may be obtained by means of the expression:

$$\Delta r = \left[\left(\frac{\partial r}{\partial a} \sigma a \right)^2 + \left(\frac{\partial r}{\partial e} \sigma e \right)^2 + \left(\frac{\partial r}{\partial \omega} \sigma \omega \right)^2 \right]^{1/2}, \quad (8)$$

where radius-vector partial derivatives related to elements occur provided that $v(a, e, \omega) = \text{const.}$ Representative values $\Delta \phi$ and c may be obtained both analytically and by analyzing orbit catalogues. In particular, applying Delambert's formulas we have

$$\tan^2 \frac{\Delta \phi}{2} = \frac{\tan^2 \frac{\sigma \Omega}{2} \cdot \sin^2 i + \sin^2 \frac{\sigma i}{2}}{\tan^2 \frac{\sigma \Omega}{2} \cos^2 i + \cos^2 \frac{\sigma i}{2}}, \quad \tan c = \tan \frac{\sigma \Omega}{2} \cdot \sin i \cdot \operatorname{cosec} \frac{\sigma i}{2}.$$

Upon substitution of (7) and (8) we shall have

$$(v) = \pi r^2 \Delta \phi \left| \sin \psi \cdot \sin(v + \omega + c) \right| \left[\left(\frac{\sigma a}{a} \right)^2 + (e + \cos E)^2 \left(\frac{\sigma e}{1-e} \right)^2 + \cotan \psi \cdot \sigma \omega \right]^{1/2}$$

The formula (9) makes it possible to determine the cross-section. The mean orbit elements and their dispersions are calculated in the expression (9) according to expression (5) or are determined from existing orbit catalogues. Application of the above relations permits investigation of the stream evolution as a whole. If it is supposed that the number of particles in a stream does not change over time and denote the incident flux density by Q , we have the following explicit expression:

$$\frac{Q(v_1 t_1)}{Q(v_1 t_2)} = \frac{S(v_1 t_2)}{S(v_1 t_1)} \cdot \frac{a^{3/2}(t_2)}{a^{3/2}(t_1)} \quad (10)$$

which makes it possible to estimate the flux density change not only along the orbit (when it is constant) but in time as well. That is the main factor for estimating the meteor stream dynamics as a whole rather than just its individual orbits. It is clear that the space structure and dynamics of comparatively young meteor streams or streams of a common origin but which are only slightly susceptible to perturbations can be investigated by means of the above expressions. It can be expected that among modern meteor streams there are those to which the above method can be applied. To this end, only those streams have been considered which have sufficient orbit statistics. It turns out that the majority of modern active meteor streams are characterized by signs of parent body decay within a relatively small vicinity of their mean orbits.

Table 2 presents the ecliptic coordinates (λ_c , B_c) of the common "point" of orbit crossing, the nodal distance value C , radius-vector of this point r_c , and its true anomaly v_c .

Table 2.
Coordinates of common range of crossing orbits
for some meteor streams

	Perseids	Geminids	Orioids	S-Taurids
λ_c , degree	80 ± 5	190 ± 11	307 ± 3	130 ± 10
B_c , degree	74 ± 2	-22 ± 1	15 ± 7	5 ± 1
C , degree	77 ± 2	-72 ± 10	82 ± 8	79 ± 6
V_c , degree	-74 ± 4	-40 ± 10	0 ± 10	-40 ± 12
r_c , a.u.	1.5 ± 0.1	0.16 ± 0.01	0.6 ± 0.3	0.4 ± 0.1

It should be noted that in spite of insufficient accuracy of the present orbit catalogues, the errors in determining the point C are insignificant and the arc length, where the supposed decay of a parent body occurred, does not exceed 0.1 per cent of the orbit length for the showers under

consideration. Hence, knowing from observation the structure peculiarities of the above meteor streams, a space model for these streams can be constructed for a given moment by means of the relations (1-10). The main direction and ejection rate of matter from their parent bodies can be determined and the evolution of these streams as affected by gravitational and nongravitational forces can be traced.

References

1. Andreev G. V., 1984a, On the theory of spatial meteor structure of comet origin, in Meteor bodies in interplanetary space and Earth's atmosphere, Dushanbe, Donish Publisher, pp. 3-4.
2. Andreev G. V., 1984, The influence of astronomical selection on structural characteristics of meteor showers, Astronomical Vestnik, Vol. 18, No. 3, pp. 240-248.

DENSITY VARIATIONS OF METEOR FLUX ALONG THE EARTH'S ORBIT

N.T. Svetashkova

Tomsk State University
Tomsk, USSR

No model of distribution of meteor substance is known to explain the observed diurnal and annual variations of meteor rates, if that distribution is assumed to be constant during the year. A prediction of diurnal variation of rates carried out using statistical modeling (KOSTYLEV and SVETASHKOVA, 1977) for the meteor radar station in Mogadishu on the assumption that the distribution of the flux density of meteor bodies does not change during the year gives nearly the same average rates for all the different months. The analysis of the results of actual observations obtained from Mogadishu shows that the actual average rate of meteors reaches its maximum in July and minimum in March with the ratio of 5.7. Such a difference between the results of observations and the prediction leads to the conclusion that the density of the orbits of meteor bodies changes with the motion of the Earth along its orbit.

In the present paper, the distributions of the flux density over the celestial sphere are obtained by the method described previously (SVETASHKOVA, 1984). The system of equations of the form $Ax = \bar{u}$ are constructed on the basis of the observational results and adequately formulated prediction equations, where A is the matrix whose elements are hourly rates for separate areas of the celestial sphere obtained as a result of prediction; \bar{u} is the vector of the observed rates; x is the unknowns vector whose elements represent the meteor bodies flux density normalized for the assigned density in the prediction model. The solution of systems with inaccurately assigned u components and the unknown coefficient matrix is performed by the Tikhonov regularization method. Radar observations in Mogadishu covering the interval from December 1968, to May 1970, are used. The observations are taken for four azimuths (0° , 90° , 180° , 270°) with the time step of $\Delta t = 30$'s. The celestial sphere is subdivided into 76 areas. In the prediction algorithm of the meteor rates, a physical model of interaction of the meteor body with the Earth's atmosphere suggested by Tokhtasyev is employed. The distribution of the flux density parameter S over the celestial sphere is determined by the Pupyshev formula: $S(\epsilon) = 1.0 + 0.12\epsilon + 0.01\epsilon^2$ where ϵ is the elongation angle from the apex in radians and the geocentric and heliocentric distributions of velocities are taken from the paper by ANDREEV et al., (1982). It is supposed for simplicity that half of the meteor bodies have the mean density of 2 g/cm^3 while the other half - that of 0.2 g/cm^3 .

Variations of the average for the celestial sphere flux density of meteor bodies with masses over 10^{-3} g are in the geocentric system of coordinates and the flux density changes about four times a year, the minimum values being observed in March: $Q(10^{-3} \text{ g}) = 4.67 \times 10^{-4} \text{ km}^{-2} \text{ h}^{-1} \text{ sr}^{-1}$; the maximum - in July: $Q(10^{-3} \text{ g}) = 1.83 \times 10^{-3} \text{ km}^{-2} \text{ h}^{-1} \text{ sr}^{-1}$. The character of hourly rate variation is determined completely by the variations of the geocentric flux density during the year. This conclusion can only be valid provided the physical model of a meteor phenomenon and models of mass and velocity distribution over the celestial sphere remain invariable when the results of homogeneous observations for different months are interpreted. The average annual value of the influx in the interval of masses from 10^{-12} g to 10^2 g is 10 tons a day. The average annual flux density reduced

to the mass $M = 5 \times 10^{-6} \text{ g}$ ($1.80 \times 10^{-9} \text{ m}^{-2} \text{ s}^{-1}$) agrees well with the estimates of ELFORD (1967) ($2 \times 10^{-9} \text{ m}^{-2} \text{ s}^{-1}$) and Pupyshev ($6-9 \times 10^{-9} \text{ m}^{-2} \text{ s}^{-1}$). The estimates of other authors obtained on the basis of radar observations are of the order of 10^{-8} or 10^{-10} .

The minimum of the flux density in the heliocentric system of coordinates shifts to February, the maximum being observed in September-October. The maximum-minimum ratio is 3.6.

1. Distribution of the flux density over the ecliptic longitude.

a) The geocentric system of coordinates. The region of highest flux density is in the interval of longitudes from $\lambda - \lambda_0 = 165^\circ$ to $\lambda - \lambda_0 = 15^\circ$, where the flux density value varies within the limits of approximately one order of magnitude reaching the maximum value at $\lambda - \lambda_0 = 225$ to 255° . A characteristic feature is the lowering of the flux density in the immediate proximity to the apex (with the exception of August-September). The region of the lowered flux density lies within the interval of longitudes $\lambda - \lambda_0 = 45$ to 135° . The ratios of the flux density in the regions of the apex and anti-apex are 10^2 to 10^3 . The results show that the geocentric distributions of the flux density over ecliptic longitude can be considered symmetrical to the plane of the ecliptic for all months except March and the period of July to November.

b) The heliocentric system of coordinates. Taking into account (according to the Levin technique) the motion of the Earth around the Sun, we obtain the distribution of the flux density in a heliocentric system of coordinates (Fig. 1). The regions of the maximum heliocentric flux density are actually located near the geocentric anti-apex. Though right at that point ($\lambda - \lambda_0 = 105$ to 135° in Fig. 1) there is for many months, a flux density reduction comparable in value with the minimum that now appears in the geocentric apex direction. The average annual distribution of the heliocentric flux density near the plane of the ecliptic can be imagined in the form of two petals about 60° wide, the maxima falling on $\lambda - \lambda_0 = 45^\circ$ and 165° . The ratio of the mean values of the heliocentric flux density in the geocentric anti-apex region to the geocentric apex regions is about 3×10^2 . The asymmetry of distributions over the plane of ecliptic is especially noticeable in January and in the period of July to October. In August to October, the heliocentric flux density in the geocentric apex region of the Northern hemisphere is only about one order of magnitude higher than in other months and therefore the excess number of orbits with direct motion is 10 to 40, which is below what is considered normal. In the Southern hemisphere, a rise in heliocentric flux density of about one order of magnitude is observed in January and July. Thus, the distribution of the flux density over ecliptic longitude is not constant during the year. For sporadic meteors, a heliocentric component in the geocentric anti-apex direction near the ecliptic plane is thus always present. In January and July, the Earth similarly crosses a complex of meteors with retrograde motion whose radiants are located in the geocentric apex hemisphere at ecliptic latitudes 0° to 20° . In the Southern hemisphere meteor bodies going from the geocentric apex also have a high flux density in June, August and February. In August-October an analogous component of meteor bodies is present in the latitudes of 0° to 20° .

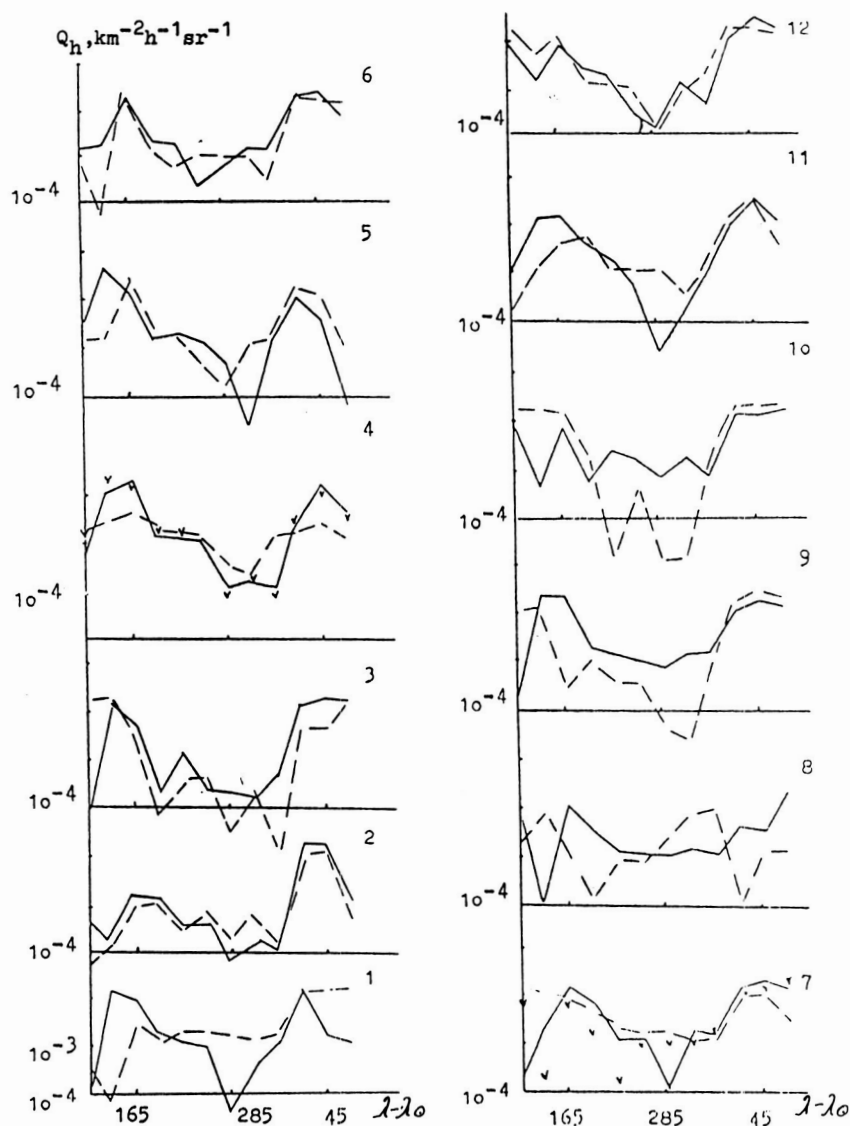


Fig. 1 Distribution of the heliocentric flux density of meteoric bodies with the masses greater than 10^{-3} g over the ecliptic longitude. The figures denote the number of a month. The continuous line shows distributions for latitudes 0° to 20° and the dashed lines represent 0° to -20° . A v symbol represents distributions with seasonal latitudinal variations of the density of the atmosphere being taken into account.

2. Distribution of the flux density over the ecliptic latitude.

Heliocentric distributions of the latitudinal flux density are presented in Fig. 2. In different months, 70-80 percent of meteor body orbits are located in the ecliptic latitudes $|\beta| < 35^\circ$ and less than 10 percent in the latitudes $|\beta| > 50^\circ$. The maximum flux density is observed near the ecliptic plane in the interval of latitudes $|\beta| < 20^\circ$. Distributions over latitude can be considered symmetrical to the plane of ecliptic only for two months - namely December and January. Assymetry becomes particularly apparent in February, April and May when the flux density of particles in the Northern hemisphere is 1.7, 1.9 and 1.7 times respectively higher than in the Southern one. On the contrary, in October, the Southern hemisphere is 1.5 times more active than the Northern one. Geocentric distributions of the flux density over latitude are also shown in Fig. 2. It can be seen that the Earth's motion along its orbit distorts the heliocentric distributions considerably.

The known seasonal and latitudinal variations of atmospheric conditions does not appear to significantly affect the value of the mean flux density of meteor bodies and the matter influx onto the Earth.

The analysis of the data obtained over the equator makes it possible to draw a conclusion that variations of meteor activity of the celestial sphere during the year are a reflection of variations of the meteor body flux density along the Earth's orbit.

References

1. Kostylev, K.V., Svetashkova, N.T., 1977, The method of statistical modeling of radar observations of a meteor shower, *Astronomicheskyy Vestnik*, No. 1, pp. 53-59.
2. Svetashkova, N.T., 1984, Determination of sporadic meteor flux density, *Astronomy and Geodesia*, Tomsk, No. 10, pp. 167-174.
3. Andreev, V.V., Belkovich, O.I., Zabolotnikov, V.C., 1982, Structure of meteor complex in the vicinity of the Earth's orbit, *Meteor Matter In Interplanetary Space*, Moscow, pp. 8-27.
4. Elford, W.G., 1967, Incidence of meteors on the Earth derived from radio observations, *Smithson. Contrib. Astrophys.*, vol. 11, pp. 121.
5. Ramasov, A.A., Sikharulidze Yu, G., 1979, The Model of Seasonal latitudinal variations of the density of the Earth's atmosphere, pre-print of the USSR Academy of Sciences Institute of Applied Mathematics, Moscow, No. 72, p. 30.

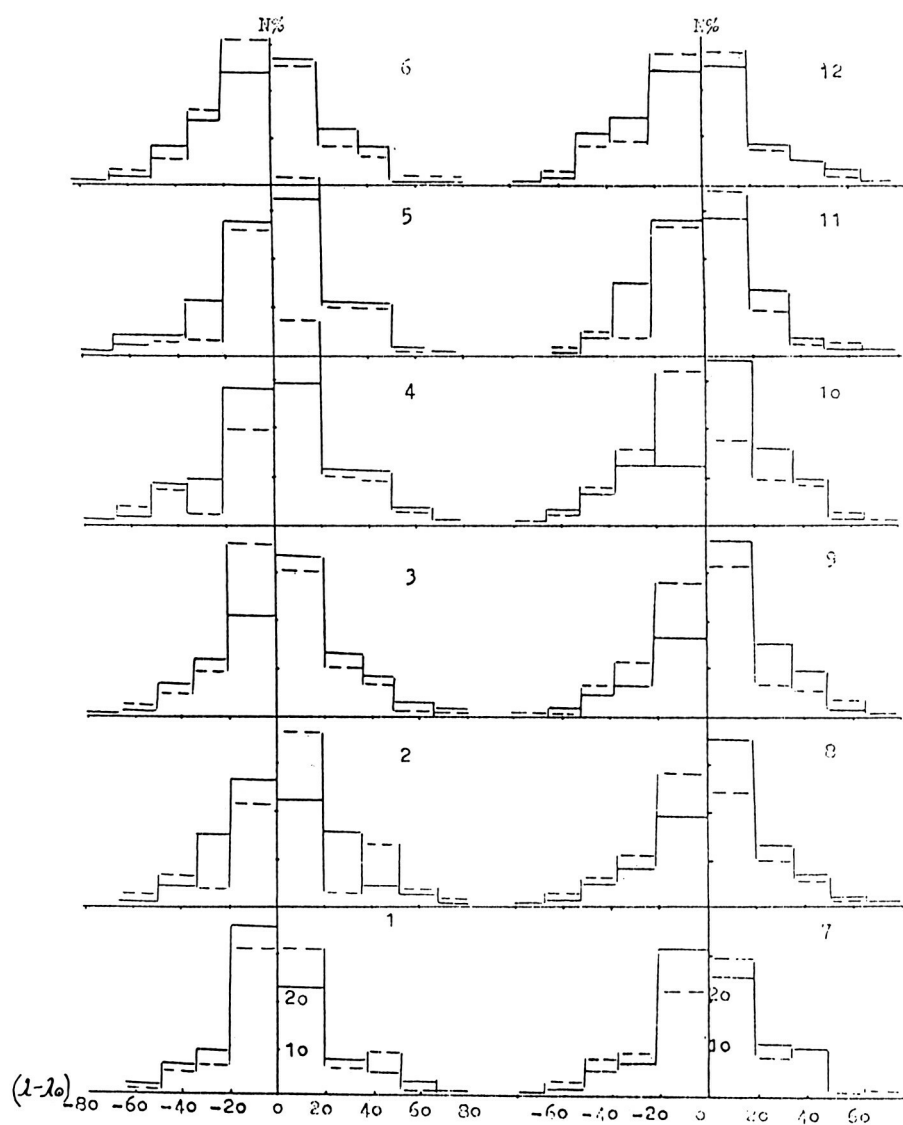


Fig. 2 Distributions of the flux density of meteoric bodies with masses greater than 10^{-3} g over the ecliptic latitude. The continuous line represents the geocentric distributions; the dotted line shows the heliocentric distributions.

METEOR VELOCITY DISTRIBUTION AND AN OPTIMUM MONITORING MATHEMATICAL MODEL

N. G. Volkov and O. N. Salimov

Moscow Physical Engineering Institute
Moscow, USSR

There are not many papers devoted to an optimization of meteor observations. For example, the optimization of the azimuth of antenna orientation of a 2 or 3-station network is given in MALYNJAK (1982). Optimization methods also have been used to determine the main parameters of a meteor body and the atmosphere in the meteor zone in KOSTYLEV (1982). At present, there are a great number of radio meteor, ionosphere and rocket observation data for the altitude range of 80-100 km which indicate the existence of large scale circulation systems in the mesopause-low thermosphere range which change regularly with season and latitude. But the existing observation network and observation programs are not optimal for revealing the main factors forming the circulation mode at these altitudes.

This paper offers for consideration a generalized optimum monitoring mathematical model. The model input data are distribution density, response function, individual measurement root mean square uncertainty and detection effectiveness function. The minimization of the prediction variance due to upper atmosphere ionization and impacts by sporadic meteors may also serve as the effectiveness function (SALIMOV et al., 1979). In the latter case, the results of a previously developed meteor thermal fragmentation model and laboratory data may be used (KOSTYLEV, 1982; LEBEDINETS et al., 1967; LEBEDINETS et al., 1968; MALYNJAK, 1982; SALIMOV, et al., 1979). The model makes it possible to obtain the observation distribution density, the minimal possible dispersion and optimized system effectiveness.

Suppose that $n(X)dX$ is the number of observed value (OV) magnitudes in the interval OV $(X, X + dX)$ ($\int n(X) dX = N$) that is connected with some effect by the relation $h = f(X)$. The purpose of monitoring is to achieve a certain value of the function $h(X)$ (denoted H)

$$H = \frac{1}{N} \int f(X) n(X) dX$$

by means of OV detection with sampling of the fixed size M . Let $m(X) dX$ be the monitoring sampling size ($\int m(X) dX = M$). The problem of monitoring optimization is to find the $m(X)$ function which achieves the least dispersion in the assessment of the value H .

It can be easily proved that dispersion of the value H with fixed $m(X)$, M and $f(X)$ is

$$D_H = \sigma_H^2 = \frac{1}{N^2} \int \left(\frac{df}{dX} \right)^2 \sigma_x^2 \frac{n^2(X)}{m(X)} dX,$$

where σ_x^2 is the dispersion of the OV measurement. The minimization of this expression on condition that $\int m(X) dX = M$ leads to an $m(X)$ function of the following form

$$m(X) = \frac{M}{\int \left| \frac{df}{dX} \right| n(X) \sigma_x dX} \left| \frac{df}{dX} \right| n(X) \sigma_x$$

When the $f(X)$ function has some inherent uncertainty then this formula is valid. Only the minimum value and optimization effectiveness are changed.

The relation for the minimum dispersion of the H value assessment of optimized system is

$$D_{Hmin} = \frac{1}{M} \left(\int_0^{\infty} \left| \frac{df}{dX} \right| w \sigma_x dX \right)^2$$

where $w = w(X)$ is the distribution density (i.e., weights) of OV. The parameter for characterizing optimization effectiveness is

$$E = \frac{D_H}{D_{Hmin}} = \frac{\int \left(\frac{df}{dX} \right)^2 \sigma_x^2 \frac{w^2}{m_n} dX}{\left(\int \left| \frac{df}{dX} \right| w \sigma_x dX \right)^2}$$

Two cases were considered: $m_n = \text{const}$ and $m_n = w$ where m_n is the observation distribution for the unoptimized system.

For the case of a power law response function $f = \alpha X^\beta$ and a constant relative error of measurement (not depending on OV) δ we have

$$m_n = \begin{cases} 1/(X_M - X_m) & X_m < X < X_M \\ 0 & X < X_m, X > X_M \end{cases}$$

$$m \sim X^\beta w, \quad E = a_\beta (X_M - X_m) / m_\beta^2$$

$$\text{where } a_\beta = \int_{X_m}^{X_M} (X^\beta w)^2 dX, \quad m_\beta = \int_{X_m}^{X_M} X^\beta w dX$$

X_m and X_M are the minimum and maximum magnitudes of OV respectively.

For the case $m_n = w$ and a log normal OV distribution density

$$\ln E = \beta^2 \sigma^2, \quad E = \exp(\beta^2 \sigma^2)$$

The relative error of effectiveness determination in this case is calculated as follows:

$$\delta_E = 2(\beta^2 \delta_\beta + \sigma^2 \delta_\sigma),$$

$$\delta_E = \frac{dE}{E}, \quad \delta_\beta = \frac{d\beta}{\beta}, \quad \delta_\sigma = \frac{d\sigma}{\sigma}.$$

$$\text{So } E = \exp(\beta^2 \sigma^2) [1 \pm 2(\beta^2 \delta_\beta + \sigma^2 \delta_\sigma)].$$

To implement the derived relations for real meteor observations, the radio meteor data obtained from Obninsk in 1967 - 1968 and which were published by the World Data Center B in 1981 - 1982 were analyzed (LEBEDINETS et al., 1967; LEBEDINETS et al., 1982). The results of observations during one full year were processed. The number of detected meteors in different months varied from 10^2 in September to $3.3 \cdot 10^5$ in December of that year. The distribution density of meteor body extra-atmospheric velocities was recorded.

Suppose that the OV is the meteor body velocity and the predicted effect is the atmospheric ionization at a certain altitude. To simplify the problem for the sake of demonstration, we shall consider $\beta = 6$ and assume that the effect does not depend on other variables except velocity. The distribution density of the number of measurements was calculated using the following formulae:

$$\bar{v}_i = \frac{v_i + v_{i+1}}{2}, \quad N = \sum N_i, \quad m_\sigma = \sum \bar{v}_i^\sigma w_i; \quad m_i = \frac{\bar{v}_i^\sigma w_i}{m_\sigma},$$

$$M = N/E, \quad E = \frac{ka_\sigma}{M_\sigma}, \quad a_\sigma = \sum (\bar{v}_i^\sigma w_i)^2, \quad k = \frac{v_m - v_{\bar{m}}}{\Delta v}, \quad M_i = M m_i.$$

The results of the calculations are given in the Table.

Table 1

Observation distribution density.

NN	$v_i - v_{i+1}$ kms	\bar{v}_i kms	w_i	$m_i \Delta v$	N_i	M_i	M_i/N_i
1	12-17	14.5	0.014	0.0000	131	0	0.00
2	17-22	19.5	0.064	0.0002	599	1	0.00
3	22-27	24.5	0.068	0.0006	636	2	0.00
4	27-32	29.5	0.072	0.002	674	7	0.01
5	32-37	34.5	0.125	0.009	1170	31	0.03
6	37-42	39.5	0.129	0.022	1207	76	0.06
7	42-47	44.5	0.087	0.030	814	103	0.13
8	47-52	49.5	0.069	0.045	646	155	0.24
9	52-57	54.5	0.108	0.125	1011	430	0.42
10	57-62	59.5	0.127	0.248	1188	853	0.72
11	62-67	64.5	0.096	0.304	898	1046	1.16
12	67-72	69.5	0.035	0.174	328	599	1.83
13	72-77	74.5	0.004	0.030	37	103	2.78
14	77-82	79.5	0.001	0.011	9	38	4.22

$$k=14 \quad \sum w_i = 0.999 \quad \sum m_i \Delta v = 1.001, \quad \sum N_i = 9348, \quad \sum M_i = 3444$$

$$N = 9358 \quad E = 2.72, \quad M = 3440$$

The effectiveness in this case is 2.7. This means that the number of observations can be reduced 2.7 fold without reducing the accuracy of the predicted results. When $v > 52$ kms the optimum observation distribution density becomes greater than the OV distribution density. When $v > 62$ kms, the number of meteors needed for each velocity range exceeds the number of detected meteors (the boundary of sampling and complete monitoring). The $N_i = N_i(v)$ function is bimodal and had two maxima (with 40 and 60 kms). The $M_i = M_i(v)$ function has one maximum when $v = 64$ kms. The M_i/N_i ratio is the monotonically increasing function of velocity.

If we consider the dependence of velocity on space coordinates and time we can derive recommendations concerning the observational distribution in space and time. For the cases when the predicted effect depends not on one but two (velocity and mass, for example), a multiple variable calculation is carried out in a similar way for such 2-dimensional or multi-dimensional problems. The described approach may be implemented for other effectiveness functions, such as wind speed determination at an altitude of 80-100 km through meteor observations.

References

1. Global meteor observation system. Ed. by Nechitailenko V.A., 1984, Soviet Geophysical Committee of the Academy of Sciences of the USSR, p. 47, Moscow.
2. Ioffe, Z.M., Rubtsov, L.N., 1982, In: meteor Matter in Interplanetary Space, Moscow-Kazan: Kazan State Univ., pp. 240-243.
3. Kostylev, K.K., 1982, In: Meteor Matter in Interplanetary Space, Moscow-Kazan; Kazan State University, pp. 203-207.
4. Lebedinets, V.N., Korpusev, V.N., Manokhina, A.V., 1981, Radio Meteor Investigations in Obninsk, Orbit Catalogue (September-December, 1967), Moscow, Materials of the WDC-B, p. 195.
5. Lebedinets, V.N., Korpusev, V.N., Manokhina, A.V., 1982, Radio Meteor Investigations in Obninsk, Orbit Catalogue (January - August, 1968), Materials of the WDC-B, p. 136.
6. Malynjak, M.I., 1982, In: Meteor Matter in Interplanetary Space, Moscow-Kazan: Kazan State Univ., pp. 248-252.
7. Salimov, O.N., Konstantinov, I.E., Mikheenko, S.G., 1979, Aston. News Letters, Vol. 13, No. 1, pp. 50-55.
8. Zelenin, V.N., Konstantinov, I.E., Mikheenko, S.G., Salimov, O.N., 1978, Aston. News Letters, Vol. 12, No. 2, pp. 84-87.
9. Zelenin, V.N., Kachanov, A.V., Konstantinov, I.E., Salimov, O.N., Sipailo, I.P., 1981, Physics and Chemistry of Materials Treatment, No. 4, pp. 47-50.
10. Zelenin, V.N., Konstantinov, I.E., Mikheenko, S.G., Salimov, O.N., 1982, In: Meteor Matter in Interplanetary Space, Moscow-Kazan: Kazan State Univ., pp. 203-207.

11. Zelenin, V.N., Konstantinov, I.E., Mikheenko, S.G., Salimov, O.N., 1982, Astron. News Letters, Vol. 16, No. 3, pp. 174-182.
12. Malynjak, M.I., 1982, In: Meteor Matter in Interplanetary Space, Moscow-Kazan: Kazan State University, pp. 248-252.
13. Salimov, O.N., Konstantinov, I.E., Mikheenko, S.G., 1979, Thermal Decay of Meteors, Astron. News Letters, Vol. 13, No. 1, p. 50-55.

THE "VALEC" FIREBALL AND PREDICTED METEORITE FALL

Z. Ceplecha and P. Spurný

Astronomical Institute of the Czechoslovak Academy of Sciences
Ondrejov Observatory, Czechoslovakia

After 22 years of continuous operation of the Czechoslovak part of the European Network for photographing fireballs, we succeeded in taking pictures of an object with a luminous trajectory below a height of 20 km (Ceplecha and Spurný, 1984). On Aug. 3, 1984, at 21^h05^m53^s UT, seven Czech stations photographed this slow-moving fireball, which traversed 94 km of luminous trajectory in 9.2 seconds and terminated its visible flight at a height of 19.1 km. The computed dark-flight trajectory intersected the surface close to Valec, a small village 40 km west of Brno. The "Valec" fireball was not only the lowest fireball photographed in our European program, but also the lowest photographed fireball ever. The only exception, the Příbram fireball photographed in the year 1959, terminated its luminous trajectory at a height of 13 km, but the photographs of its trajectory were taken only down to 22 km, where the trajectory went off the field of view of the camera system. The "Valec" fireball was photographed by fish-eye cameras with Zeiss-Distagon objectives f/3.5, f=30 mm, field of view 180°. The positional precisions of all our records were within the range of 1 to 2 minutes of arc. The closest station to the fireball trajectory was only 41 km from it and its picture (Fig. 1.) shows 109 measurable breaks spaced by about 0.08 seconds. Our rotating shutter is close to the focal plane. All measurements on all photographic plates were done by J. Bocek and this activity comprised more than 1600 points to be measured using a Zeiss Astroecorder. All computations were done by the authors of this paper using the FIRBAL program, a set of almost 4000 Fortran statements (Ceplecha et al., 1979) run on an EC 1040 computer at the Ondrejov Observatory, which is our standard procedure used for every fireball photographed by at least two stations. We tried to get our results as soon as possible, to be ready for a meteorite search before the harvest season was over. The average computed mass at the terminal point, i.e., the predicted mass of the biggest meteorite, was 16 kg. This number is based on the dynamical data at the terminal point solely (velocities and decelerations). We also collected visual data from occasional observers and it became clear from them that, except for the main mass, about 10 fragments reached the surface.

The fireball was a slow moving object, which enhanced the probability of a meteorite fall. The luminous trajectory started at a height of 84 km over the Austrian town of Heidenreichstein and terminated at a height of 19.06 km over a point slightly east of Jaromerice and Rokytou (Table 1). The absolute maximum brightness was almost -10 stellar magnitudes at a height of 54 km. The maximum of the light curve was very flat and the brightness stayed close to -9.5 magnitude in the height interval from 58 to 24 km. The initial velocity of 12.7 km/s changed only slightly down to the point of maximum brightness, where it reached 12.3 km/s. The initial photometric mass of about 380 kg changed only by 20 kg at this point with about 360 kg remaining. Thus the body was predetermined to penetrate very deeply and retain enough rest mass to reach the surface. At a height of

ORIGINAL PAGE IS
OF POOR QUALITY.

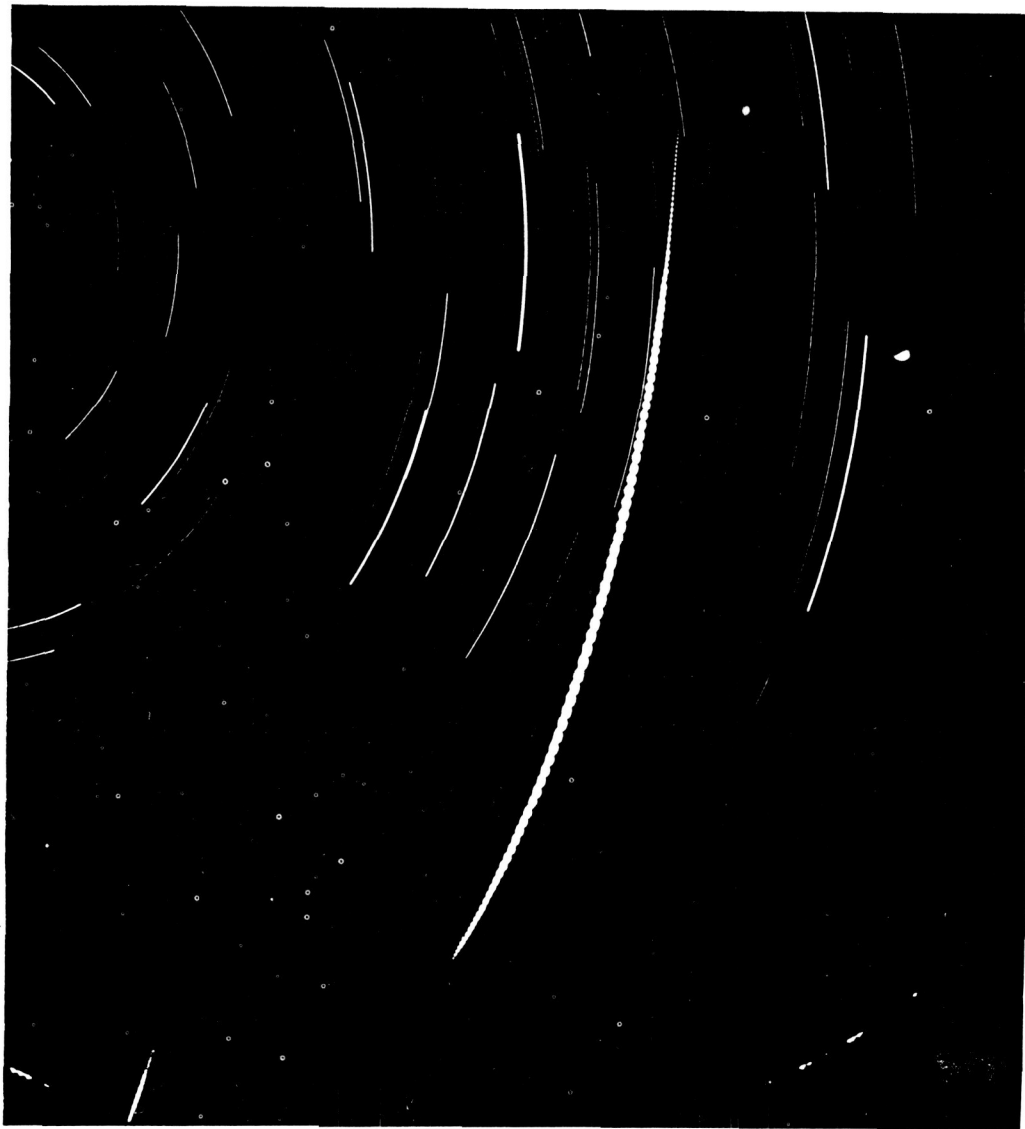


Fig. 1 Photograph of the "Valec" Fireball from station No. 15, Telc, by fish-eye Zeiss-Distagon $f/3.5$, $f=30$ mm, field of view 180° . The time marks (breaks on the fireball trail) are spaced by about 0.08 s. The curvature of the fireball trail is due to projection properties of the fish-eye objective. Direction of the flight: from up to down.

Table 1

	Beginning	Maximum Light	Maximum Deceleration	Terminal	Impact
Velocity km/s	12.69 ±.03	12.301 ±.014	5.58 ±.03	2.55 ±.08	0.088
Height km	83.79 ±.04	53.9 ±.2	22.47 ±.27	19.06 ±.28	0.5
Latitude N	48.8391° ±.0005°	48.971° ±.002°	49.111° ±.003°	49.1265° ±.0032°	49.1561° ±.0087°x)
Longitude E	15.1466° ±.0006°	15.520° ±.003°	15.922° ±.004°	15.9663° ±.0040°	16.0712° ±.0177°x)
Deceleration km/s ²	-0.032 ±.003	-0.275 ±.011	-3.04 ±0.03	-1.48 ±.03	-
Absolute Magnitude	-1.0 ±.2	-9.9 ±.4	-9.1 ±.4	-0.4 ±.2	-
Photometric Mass (terminal included) kg	377.	360.	102.	16.	16.
z _R	46.33° ±.11			46.94° ±.11	2.1°

x) standard deviations of the impact point include errors in the wind data

22.5 km, where the body reached its maximum deceleration of 3.0 km/s^2 , it was still of -9.1 absolute magnitude. All the data on velocities, decelerations and masses are given in Table 2.

The "Valec" fireball terminated its luminous trajectory with velocity only 2.5 km/s . The rest mass of about 16 kg landed at $49.1561^\circ \pm 0.0087^\circ\text{N}$ and $16.0712^\circ \pm 0.0177^\circ\text{E}$. Several criteria used for classification of the "Valec" fireball gave the same result: it was type I fireball, i.e. the same as Příbram, Lost City and Innisfree. Thus an ordinary chondrite was the most probable meteorite to be recovered. The penetration ability was somewhat larger than for type I, and an iron meteorite was not completely excluded since there is no experience with fireballs belonging to iron bodies.

Taking into account all uncertainties, we were reasonably sure that a multiple fall of meteorites followed the fireball and that the biggest piece was over 10 kg in mass. The complete footprint of all remnants was predicted as having a rather large area and is given in Table 3.

The radiant and orbit are given in Table 4. The orbit was almost in the ecliptic and the Earth met the body almost at its perihelion point, a little bit farther from the Sun than 1 A.U. The aphelion point was close to the 3:1 Kirkwood gap (WETHERILL, 1985). The orbit was typical for the meteorite fall published by WETHERILL and REVELLE (1981) and by HALLIDAY et al., (1984).

In the late summer of 1984, we searched for 3 weeks for meteorites in the predicted area, which mostly proved to be farmed land. Some less accessible places were left until autumn 1984 and spring 1985. Altogether a little over 2 km^2 were searched through, but no meteorites were found. We also instructed farmers and all interested people in the vicinity of the area that meteorites could be recovered. A small part of the area contained a water reservoir, but the probability that the main body fell there is rather low.

We used the "Valec" fireball to study the changes of ablation coefficient during the terminal parts of its luminous trajectory. We applied the method of PECINA and CEPLECHA (1984, 1985) and computed the "total ablation coefficient" for different height intervals. The result is in Fig. 2. From a height of 28 km to a height of 21 km the ablation coefficient increased 20 times (from 0.009 to $0.18 \text{ s}^2/\text{km}^2$) and seemed to level off at this high value. This change was associated with a sudden fragmentation shortly before the maximum deceleration point at a height of 28 km , and a possible fragmentation at a height of 26 km . Taking into account the terminal increase of the ablation coefficient, the major remnant should still have been quite large, of more than 6 kg , with the revised search area overlapping that actually searched. Considered against the statistical data recently published by HALLIDAY et al., (1984), it is no wonder that the search activities proved negative even in this very favorable case of a deeply penetrating fireball: on the average, about 10 searches were necessary for different fireballs with the same properties as the "Valec" fireball, to recover meteorites. But there is no doubt that all data on the "Valec" fireball are also data on a meteorite fall. (WETHERILL and REVELLE, 1981)

Table 2

Time s	Height km	Velocity km/s	Decleration km/s ²	Absolute Magnitude	Photometric x) Mass kg
0.00000	82.951	12.688±0.031	-0.034±0.003	-2.40±0.14	377
0.47999	78.760	12.669±0.029	-0.046±0.004	-2.83±0.13	377
1.03983	73.882	12.638±0.027	-0.065±0.005	-4.45±0.10	377
1.51974	69.712	12.602±0.025	-0.087±0.006	-5.35±0.12	377
1.99964	65.557	12.553±0.022	-0.118±0.007	-5.94±0.14	377
2.47954	61.422	12.487±0.019	-0.159±0.009	-7.45±0.21	376
3.03940	56.633	12.381±0.015	-0.225±0.011	-9.4 ±0.3	371
3.51928	52.569	12.255±0.013	-0.304±0.012	-9.9 ±0.4	358
3.99916	48.555	12.084±0.012	-0.410±0.013	-9.3 ±0.3	346
4.47906	44.609	11.855±0.015	-0.554±0.014	-9.3 ±0.3	335
5.03897	40.122	11.484±0.020	-0.786±0.014	-9.7 ±0.4	317
5.51898	36.310	11.108±0.005	-1.129±0.003	-9.6 ±0.4	300
5.99909	32.694	10.421±0.006	-1.758±0.003	-9.5 ±0.4	278
6.47931	29.450	9.409±0.006	-2.449±0.006	-9.5 ±0.4	246
7.03972	26.140	7.850±0.008	-2.954±0.014	-9.5 ±0.4	192
7.36000	24.521	6.896±0.012	-2.968±0.017	-9.3 ±0.4	155
7.60022	23.443	6.305±0.024	-2.97 ±0.03	-8.9 ±0.3	133
7.84045	22.469	5.58 ±0.03	-3.04 ±0.04	-9.1 ±0.4	102
8.00059	21.891	5.10 ±0.04	-2.98 ±0.04	-8.6 ±0.3	77
8.24082	21.074	4.41 ±0.05	-2.74 ±0.04	-8.1 ±0.3	36
8.40096	20.625	3.98 ±0.05	-2.53 ±0.04	-6.0 ±0.2	21
8.56108	20.220	3.60 ±0.06	-2.29 ±0.04	-3.60±0.10	17
8.64114	20.044	3.42 ±0.06	-2.17 ±0.04	-2.40±0.11	16
(9.11820	19.058	2.55 ±0.08	-1.48 ±0.03	-0.41±0.21	16)

x) terminal mass included

Table 3

Boundary of the whole strewn-field predicted.

Latitude N	49.168°	49.161	49.122	49.095	49.106	49.130	49.148°
Longitude E	16.089°	16.096	16.021	15.936	15.899	15.907	15.980°

Table 4

Radiant and orbit. (1950.0)

α_R	$242.10^\circ \pm 0.16^\circ$	a	1.821 ± 0.016 A.U.
δ_R	$17.17^\circ \pm 0.09^\circ$	e	0.443 ± 0.005
v_∞ (km/s)	12.74 ± 0.04	q	1.0135 ± 0.0001 A.U.
α_G	$230.97^\circ \pm 0.22^\circ$	Q	2.63 ± 0.03 A.U.
δ_G	$3.81^\circ \pm 0.19^\circ$	ω	$184.78^\circ \pm 0.11^\circ$
v_G (km/s)	6.57 ± 0.07	Ω	$131.2512^\circ \pm 0.0008^\circ$
v_H (km/s)	35.52 ± 0.06	i	$3.92^\circ \pm 0.07^\circ$

Suffixes: R ... observed radiant, ∞ ... initial no-atmosphere velocity,
 G ... geocentric radiant and velocity, H ... heliocentric velocity.

Elongation from apex: geocentric radiant: $157.61^\circ \pm 0.23^\circ$
 heliocentric radiant: $175.96^\circ \pm 0.07^\circ$

ORIGINAL PAGE IS
OF POOR QUALITY

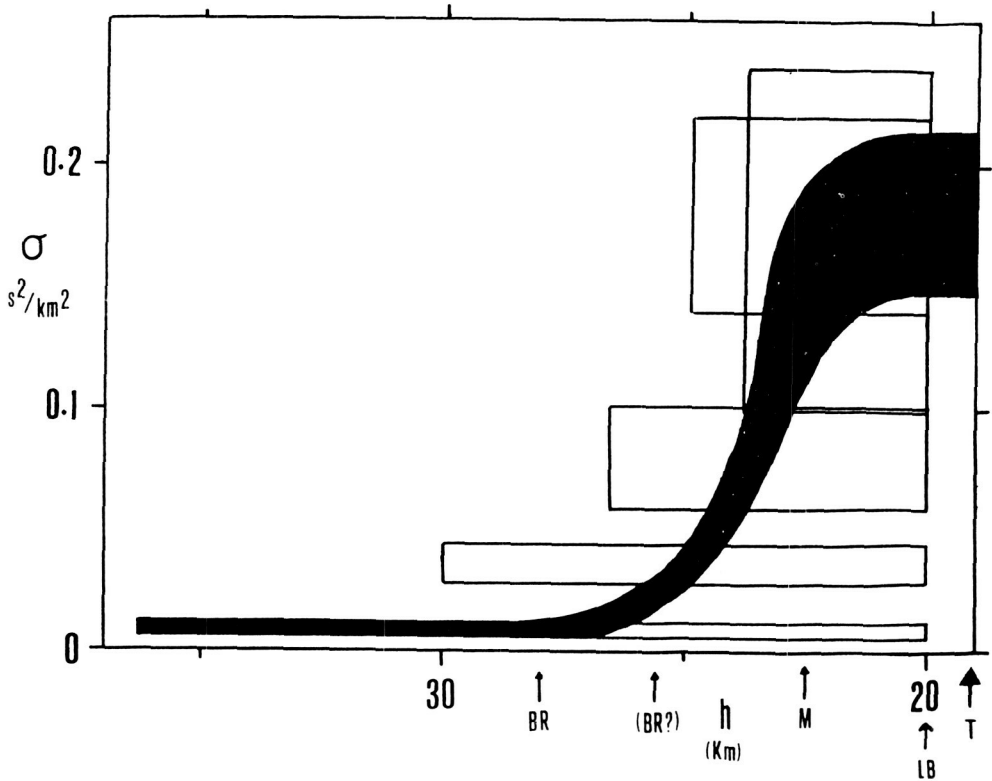


Fig. 2 The change of the ablation coefficient σ during the terminal portion of the "Valec" Fireball trajectory plotted against height h . Rectangles: area of standard deviations of solutions for total ablation coefficient σ in different height intervals. The thick curve covers the area of the most probable values of σ . BR...point of breakage, M...point of maximum deceleration, LB...last measured break, T...terminal point.

References

1. Ceplecha Z., J. Bocek, and M. Jezková, 1979, Bull. Astron. Inst. Czechosl. 30, p. 220.
2. Ceplecha Z., and P. Spurny, 1984, SEAN Bull. 9, No. 8.
3. Halliday I., A.T. Blackwell, and A.A. Griffin, 1984, Science 223, p. 1405.
4. Halliday I., and A.A. Griffin, 1982, Meteoritics 17, p. 31.
5. Pecina P., and Z. Ceplecha, 1983, Bull. Astron. Inst. Czechosl. 34, p. 102.
6. Pecina P., and Z. Ceplecha, 1984, Bull. Astron. Inst. Czechosl. 35, p. 120.
7. Wetherill G.W., 1985, Asteroidal Source of Ordinary Chondrites, Meteoritics (in press).
8. Wetherill G.W., and D.O. ReVelle, 1981, Icarus 48, p. 308.

N88-14548

RESULTS OF OBSERVATIONS OF THE ETA AQUARID
AND ORIONID METEOR SHOWERS IN 1980-1984

A. Hajduk

Astronomical Institute
Slovak Academy of Sciences
Bratislava, Czechoslovakia

Abstract

The main characteristics of meteor showers associated with Comet Halley have been derived from the most recent radar observations carried out at the Ondrejov Astronomical Observatory during the periods of May 1-10 and October 15-30. The activity variations, the positions of activity maxima, the size distribution of particles, the particle flux variation within the stream and other characteristics have been determined and compared with other results.

1. Introduction

The International Halley Watch has included in its program the observations of meteor showers connected with Comet Halley. The main goals expected from these observations lay in the determination of the stream structure with high resolution, the dust production and the dynamical evolution of the dust particles as well as the determination of the physical properties and composition of the particles. It is supposed that most of the observations within the IHW program will be carried out during the comet return in 1985-1986. Some results of observations have been published earlier in a series of papers (HAJDUK 1970, 1973, 1981, BABADZHANOV et al., 1977, 1979, HAJDUK et al., 1983, 1984, HAJDUK and CEVOLANI, 1981, CEVOLANI and HAJDUK 1984, HAJDUK and BUHAGIAR 1982, and others) including simultaneous and long-term observations mainly from Ondrejov, Springhill, Hissar, Budrio and Perth observatories.

The data presented in this paper contain the results of the most recent observations, including preliminary results of observations of the Eta Aquarids in 1985 and show the structural features of the stream cross section immediately before the comet return. The data allows one to predict the most effective observational periods for the IHW observations during the next shower returns.

2. Observations and data

Figures 1 and 2 show the mean hourly rates of meteors during the Orionid and Eta Aquarid shower periods, respectively, in the years 1980-1984 and the preliminary data for the Eta Aquarids in 1985. Two categories of meteor echoes are presented: all echoes and echoes with duration $\tau > 1$ sec. The values (marked in the Figures by dots and circles) are deduced mainly from 5 hour intervals including the radiant transit of the meridian. The 1985 Eta Aquarid data are for 1 hour intervals only, corresponding to the radiant culmination.

It is obvious, as with previous results, that there is neither a significant, let alone an extraordinary increase in meteor activity, connected with the approach of the comet. Rather, some decrease in activity is observed in the last observations. This is in agreement with the shell model of the stream, suggested by MCINTOSH and HAJDUK (1983), according to which we observe, especially in the central parts

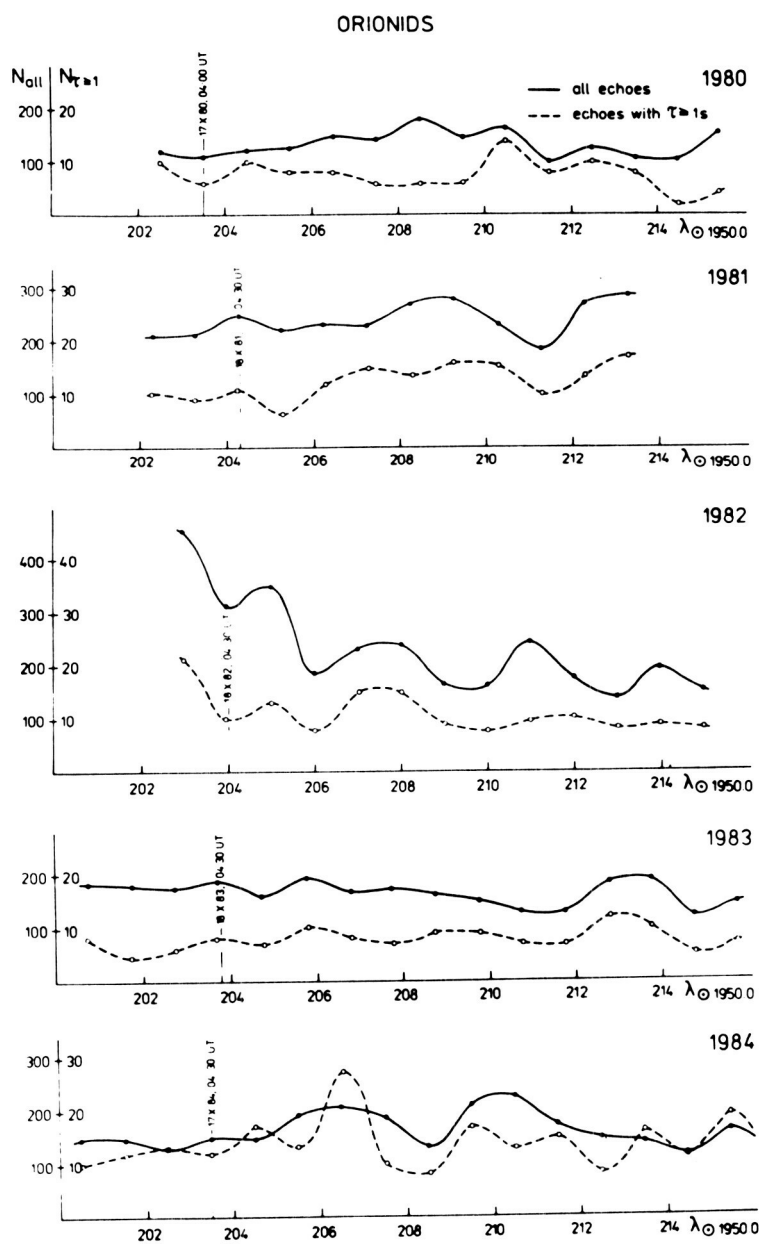


Fig. 1 Mean hourly rates of meteors during the Orionid shower period in 1981-1984.

C-5

ETA AQUARIDS

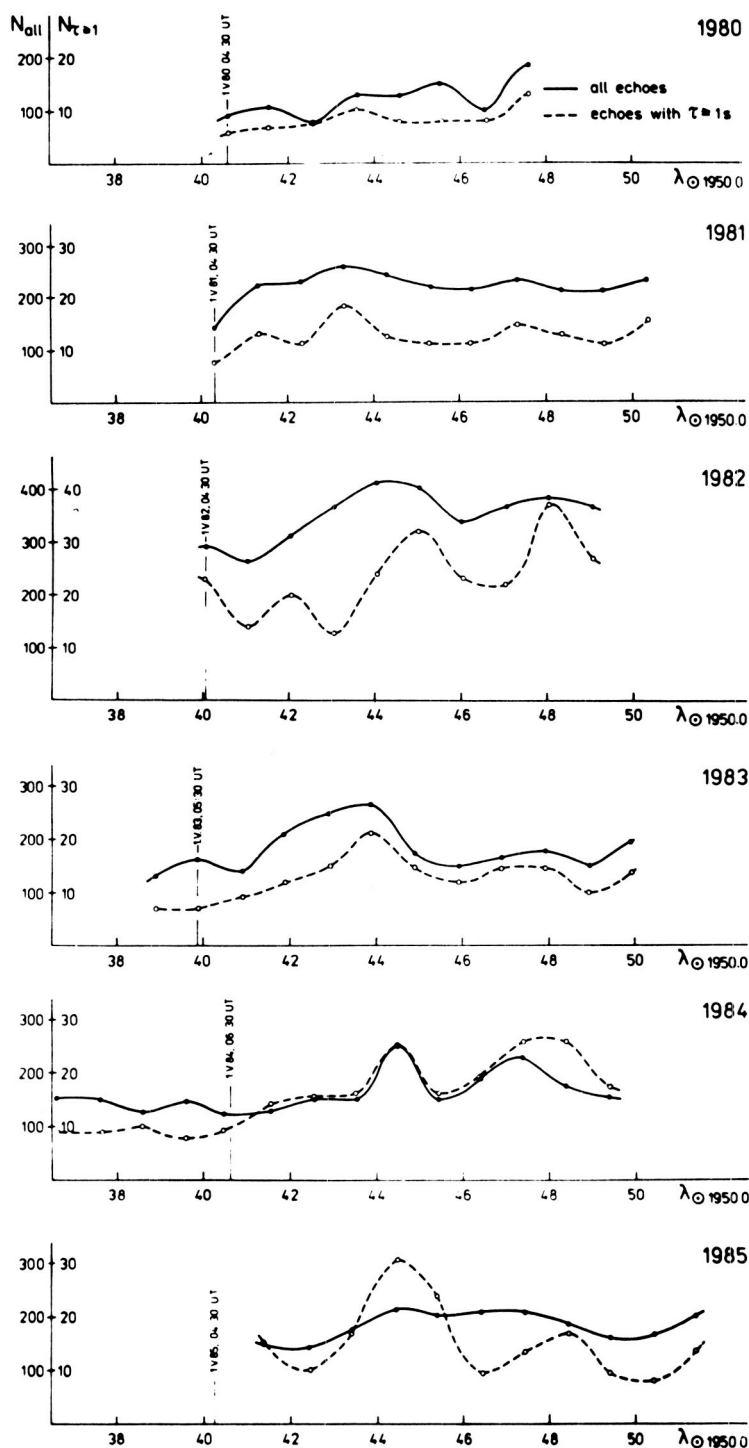


Fig. 2 Mean hourly rates of meteors during the Eta Aquarid shower period in 1980-1985.

of showers, particles ejected from the comet hundreds of revolutions ago. The quasi-diffusion of meteor particles is a very slow process and we cannot observe fresh ejecta of large particles in the mass range of observed meteoroids.

However, we may observe relatively young meteoroids, ejected from the comet during the last millenia and orbiting close to the previous orbits of the comet, crossing the Earth's orbit near the solar longitudes at about 38° and 203° (corresponding to April 28/28 and October 16/17). The orbit of P/Halley has crossed the Earth's orbit between 530 and 607 A.D. at its descending node in the case of the Eta Aquarids and between 836 and 763 B.C. at its ascending node in the case of the Orionids (YEOMANS and KIANG 1982, HAJDUK 1983). Of course, we cannot expect even at these solar longitudes very high meteor rates with the comet's return, but it is of great importance to observe the differences in the mass distribution of particles for the separate belts of particle orbits, as they represent the key to the determination of the evolution of the stream and through it to the evolution of the comet itself.

Planetary perturbations are the main source of the spread of orbital parameters of the comet and at the same time also of the ejected particles. As was shown by MCINTOSH and HAJDUK (1983), the spread in the position of the nodes and of the periods may produce a local and temporal mass concentration in the stream, resulting in the observed shifts of meteor shower maxima in solar longitude. It is difficult therefore to predict the exact time of the shower activity maximum for a particular year. However, the observed shifts are sometimes stable enough to recognize the tendency of such a shift for the next year. Figures 3 and 4 show the observed shower maxima during the last 27 years, based mainly on radar observations from Springhill, Ondrejov, Hissar and Budrio observatories. The positions of the maxima are given here in solar longitudes for the common equinox 1950.0. It can be deduced from these data that the highest activity of the 1985 Orionids may be expected on October 14, October 21 and October 27 and the highest activity of 1986 Eta Aquarids on April 30, May 5 and May 8, with an approximate error of 1 day. When some restrictions have to be made on the total period of observations the dates mentioned above are recommended. This prediction of shower maxima dates differ in the case of the Orionids from that of Oct. 24.2 based on the basis of the closest approach of the Earth's and P/Halley's present orbit. In the case of the Eta Aquarids - the closest approach on May 8.5 coincides satisfactorily with one of our maxima.

The mass distribution function of the Eta Aquarids and Orionids has been deduced from the number distribution in different echo duration categories, and also from the amplitude distribution of the echoes. The background rate was assumed to be constant during the shower period in all years. With an adopted value of the mass distribution factors for the sporadic meteors of $s = 2.5$, we obtained values of the mass distribution factor for shower meteors in the range between $s = 2.2$ (Eta Aquarids 1981 and Orionids 1981) and $s = 1.8$ (Eta Aquarids 1984 and Orionids 1984). The mass function gradually decreased in the period from 1981 to 1984; however, the preliminary results for the 1985 Eta Aquarids give $s = 1.9$. Previous radar results yield $s = 2.08$ and $s = 1.95$ for the underdense and overdense Orionids respectively (HAJDUK

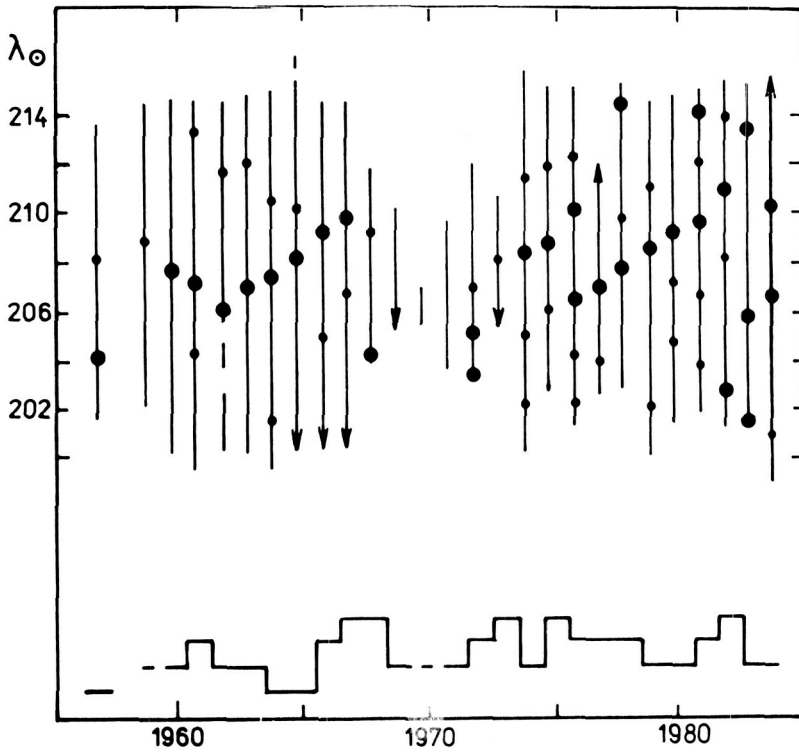


Fig. 3 The position of the Orionid shower activity maxima and secondary maxima (dots) in solar longitudes (1950.0) observed during last 27 years. The total shower activity in a particular year is given below in four levels.

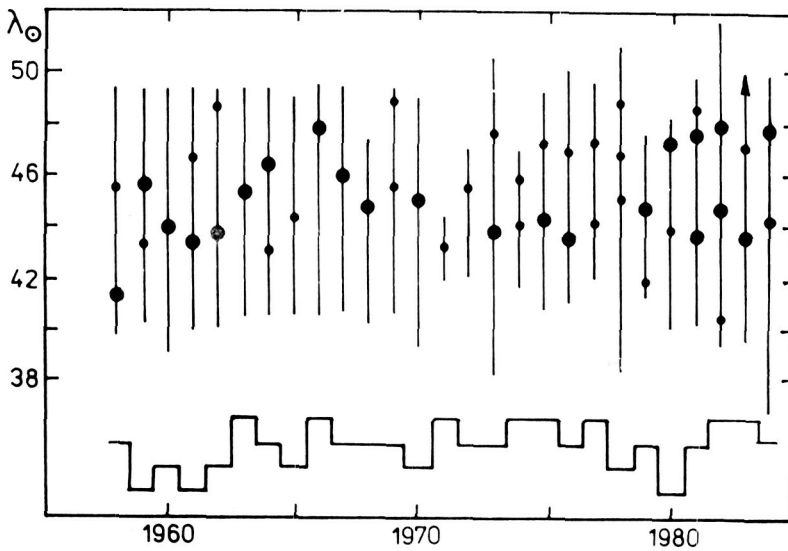


Fig. 4 The position of the Eta Aquarid shower activity maxima during the last 27 years. Other text as in Fig. 3.

1968), and previous visual observations give $s = 1.95$ for the Eta Aquarids and $s = 2.15$ for the Orionids (KRESAKOVA 1966).

Calculation of meteor flux ϕ yield values between the limits $10^{-11} \text{ m}^{-2} \text{ s}^{-1} < \phi < 5.10^{-11} \text{ m}^{-2} \text{ s}^{-1}$ in different years and shower periods for particles up to 7.25 magnitude, or 10^{-6} kg .

The study of the faint structure of the Halley stream during the IHW program should contribute substantially to our knowledge of the comet-meteor relationship. In addition, observations of the faintest meteors by means of optical and radar techniques may contribute significantly to the space missions sent to the comet. As was shown recently (HAJDUK 1985), the particle distribution in the vicinity of the comet yields at least one order higher risk for the space probes than that calculated before, and especially that the probability of the complete success of Giotto is considerably reduced. Telescopic or other optical and special radar observations of the particle size or mass distribution can improve the calculation of the risk to the space probes for given trajectories during the closest approach of the probes to the comet.

References

1. Babadzhánov, P.B., Chebotarev, R.P., Hajduk, A.: 1977, Bull. Astron. Inst. Czechosl. 28, 286-288.
2. ———: 1979, Bull. Astron. Inst. Czechosl. 30, 225-227.
3. Cevolani, G., Hajduk, A.: 1984, Il Nuovo Cimento Serie 1, 7C, 447-457.
4. Hajduk, A.: 1968, Bull. Astron. Inst. Czechosl. 19, 338-343.
5. ———: 1970, Bull. Astron. Inst. Czechosl. 21, 37-45.
6. ———: 1973, Bull. Astron. Inst. Czechosl. 24, 9-13.
7. ———: 1981, Contrib. A.O. Skalnatè Pleso 10, 125-133.
8. ———: 1985, in Asteroids, Comets, Meteors II, Uppsala; in press.
9. Hajduk, A., Cevolani, G.: 1981, Bull. Astron. Inst. Czechosl. 32, 304-310.
10. Hajduk, A., Buhagiar, M.: 1982, Bull. Astron. Inst. Czechosl. 33, 262-266.
11. Hajduk, A., Hajduková, M., Babadzhánov, P.B., Chebotarev, R.P.: 1983, Acta Astronomia et Geophysica Univ. Comen VIII-IX, 39-45.
12. Hajduk, A., Cevolani, G., Formiggini, C., Babadzhánov, P.B., Chebotarev, R.P.: 1984, Bull. Astron. Inst. Czechosl. 35, 1-5.
13. Kresàková, M.: 1966, Contrib. Astron. Obs. Skalnatè Pleso 3, 75-112.

14. McIntosh, B.A., Hajduk, A.: 1983, Mon. Not. Roy. Astron. Soc. 205, 931-943.
15. Yeomans, D.K., Kiang, T.: 1981, Mon. Not. Roy. Astron. Soc. 197, 633-646.

MONTE CARLO MODELING AND METEOR SHOWERS

N. V. Kulikova

Moscow Physical Engineering Institute
Moscow, USSR

Prediction of short-lived increases (by several orders of magnitude) in the cosmic dust influx, the concentration in lower thermosphere of atoms and ions of meteor origin and the determination of the frequency of micrometeor impacts on spacecraft are all of scientific and practical interest and all require adequate models of meteor showers at an early stage of their existence. A statistical probability (Monte Carlo) model of meteor matter ejection from a parent body at any point of space was worked out by BABADJANOV et al., (1980) and KATASEV and KULIKOVA, (1971) on the basis of the hypothetical appearance of meteor matter in space due to cometary nucleus disintegration. The direction and magnitude of the rate of meteor particle ejection from the parent body at a given point were modeled. The orbital element deviations from the elements of the parent comet orbit were then estimated and mean statistical orbit of a meteor stream formed by meteor particles ejected with specified velocities defined. Statistically reliable calculations were compared with the actual orbital element set of the particular meteor stream under study. This allowed evaluation of the general trends of orbital element changes taking place during meteor stream formation. (These become more obvious the further the ejection point gets from the parent orbit perigee point.) It also served to set limits to possible ejection velocities responsible for the formation of a particular meteor stream and to define more accurately the orbit region where the process was most likely to occur.

According to the scheme described, the formation of ten well known meteor streams was simulated and the possibility of genetic affinity of each of them with the most probable parent comet was analyzed. Some of the results are presented in Table 1.

Table 1

Name (Shower-Comet)	Orbital Region	Ejection Rate (m/s)
Draconids - Giacobini Zinner	0 - 90°	5-50
Leonids - 1866 I	0 - 30°	0, 25-1, 0
Taurids - Encke	80 - 90°	~ 350
Perseids - 1862 III	30°	~ 100
Lyrids - 1861 I	0°	> 150 - 160
Andromedids - Biela	0°	> 1,000
Orionids - 1910 II (Halley)	0°	> 350
η - Aquarids - 1910 II (Halley)	0°	< 5
Ursids - 1939 X	0°	for $\delta\alpha$ 150-200?
	0°	for angular > 1,000
α - Capricornids - 1954 III	0°?	> 1,000

To gain a better agreement of real and modeled calculations for large time intervals, the effect of a variety of gravitational and non-gravitational effects should be considered. To eliminate a number of restrictions, a statistical probability version of our algorithm was proposed to take into account the effect of solar radiation re-emission by the spinning spherical particle. This made it possible to investigate the behavior of meteor particles with both direct and retrograde rotation and to estimate the solar infall time of these particles.

It has turned out that the theoretically expected removal of meteoroids with direct axial rotation away from the Sun for particles with a radius of no more than k cm does not occur. Such meteoroids merely decelerate their falling into the Sun as compared with meteor particles of retrograde rotation. It is only at very close distances to the Sun (about 0.01 a.u.) that this effect appears comparable in value to other effects caused by solar radiation.

When comparing cometary and meteor stream orbits, it should be kept in mind that both single and successive matter ejections result in an impulse which affects the cometary nucleus in the direction opposite to the outflowing substance motion. This effect has been supposed to be the cause of the observed irregular changes observed in certain cometary orbital elements, no matter what the nature of the outflowing substance. A mathematical algorithm to calculate the perturbing acceleration components in three mutually perpendicular coordinates was suggested by SEKANINA (1968) for an arbitrarily rotating spherically-symmetric nucleus with a fixed rotation axis relative to the orbital plane. However, his derived solutions appear rather complicated and call for very accurately chosen initial assumptions.

A statistical probability variation of the algorithm was developed that helps to determine the outflow direction cosines by means of a combination of random numbers and variation (within specified limits) of mass of the ejected matter. The ejection velocities used here follow from the conditions of a particular meteor stream formation and its connection with a given comet. They were obtained through the ejection simulation described above. The calculations were made for comets Giacobini-Zinner and Encke with $r \leq 2$ a.u. and for comets 1954 III and 1910 II, in particular for the case when ejection occurred at cometary orbit perigee. Maximal deviation of orbit elements from their original element system caused by the ejection impulse are given in Table 2.

The cometary motions changes thus obtained, even though they define more accurately a part of the divergencies existing between orbital elements of parent comets and meteor streams, cannot really account for them. This is particularly true of angular elements. The orbital semi-major axis is subjected to the greatest changes under the dynamical effect. The eccentricity is less affected. The spatial orientation of cometary orbit when the affinity of a particular meteor stream and comet is ascertained is sometimes considered invariable. However, ejection effects may not be solely responsible. There are also non-gravitational changes in cometary motion. For instance, EVDOKIMOV (1984) reported non-gravitational changes₃ in semi-major axis for comet Giacobini-Zinner of $-0,12 \times 10^{-3}$ a.u., $0,1 \times 10^{-3}$ a.u. for 1972 and 1979 respectively. To make these results agree with the modeled ones, meteor matter ejection must be assumed to occur in the perigee region for 23 days non-stop, a duration which seems hardly possible.

Table 2

Comet in Perigee	Eject- ion rate (m/s)	δa (a.u.)	δe	$\delta \Omega$ (rad.)	δi (rad.)	$\delta \omega$ (rad.)
Encke	400	$0,4303 \times 10^{-4}$	$0,2967 \times 10^{-5}$	$0,2529 \times 10^{-6}$	$0,6074 \times 10^{-6}$	$0,1234 \times 10^{-5}$
Giacobini-Zinner	25	$0,3638 \times 10^{-6}$	$0,2834 \times 10^{-7}$	$0,1845 \times 10^{-8}$	$0,6433 \times 10^{-8}$	$0,1444 \times 10^{-7}$
1954 III	600	$0,4307 \times 10^{-4}$	$0,2662 \times 10^{-5}$	$0,6353 \times 10^{-7}$	$0,2103 \times 10^{-6}$	$0,2414 \times 10^{-5}$
1910 II	100	$0,2513 \times 10^{-3}$	$0,4575 \times 10^{-6}$	$0,2690 \times 10^{-6}$	$0,3225 \times 10^{-7}$	$0,3351 \times 10^{-6}$

There is no doubt that this method of research is convenient and useful. The possibility of developing new models, more elaborate and even better simulation of the natural processes makes it possible to tackle the solution of problems that cannot be resolved otherwise.

References

1. Babadjanov, P.B., Sausaev, A.F., Obrubov, Yu. V., 1980, Investigation of possible relationship of meteor streams and comets, Bull. Astroph. Inst., Tajik SSR, No. 69-70, pp. 45-53.
2. Katasev, L.A., Kulikova, N.V., 1971, On the theory of meteor stream formation, Proceedings of IEM, Gidrometeoizdat Publishers, No. 24, pp. 114-121.
3. Sekanina, Z., 1968, Non-gravitational effects in cometary motion and the model of arbitrarily spinning nucleus. In: Problems of Cosmic Physics, Kiev, Visshaja Shkola Publishers, iss. 3, pp. 82-97.
4. Evdokimov, Yu.V., 1984, Non-gravitational effects in Giacobini-Zinner comet motion, Cometary circulation letter No. 327, Kiev.

ON THE SPATIAL STRUCTURE OF THE PERSEIDS METEOR STREAM

G. V. Andreev, L. N. Rubtsov, and I. I. Tarasova

Institute of Astrophysics
Dushanbe, USSR

The paper deals with the analysis of radar observations of the Perseid meteor stream conducted at the ionospheric laboratory of the Astrophysics Institute of the Tajik Academy of Sciences in the period from 1964 to 1981.

The Perseids meteor rates were determined by the fluctuation method (ANDREEV and LAZAREV, 1979). Analysis of their hourly distributions showed that the stream maximum position is different for different years, i.e., the stream nodal position is constantly changing. Assuming the effect as real, the observed apparent nodal "regression" could be accounted for by the stream's complex structure (LEVIN, 1958). As for the true regression, it can be found only upon long-term observations. Later we shall show that the long-term Perseids nodal regression is very small, indeed. With due account taken of planetary perturbations, it amounts to something on the order of $2 \cdot 10^{-4}$ deg. yr⁻¹ for the last 15-20 millenia, which is confirmed by visual data (HUGHES, 1973). Therefore, since the narrow central condensation of the stream has been observed for at least a century we may conclude that this compact part is distributed all along its orbit but with a width that is obviously less than 1°. Consequently the thickness and width of this core are 0.016 a.u. and 0.0028 a.u. respectively.

The mean value of the solar longitude of the observed rate maximum has been $139.0 \pm 0.2^\circ$ for all the years of observation. It agrees well with most of the recent data obtained elsewhere. It is necessary to note that regardless of radioecho duration (i.e., particle mass) over a range from 1 to 20 sec, the maximum rate falls on the same solar longitude.

About 80 individual values of the mass index S have been found for this stream using the radio signal duration in the range of 0.7 to 60 sec. These are plotted in Fig. 1 as a function of the solar longitude (epoch 1950.0). It should be noted that the standard deviations in S for the Perseids are a little greater than for the Geminids and Quadrantids (ANDREEV et al., 1984 and ANDREEV et al., 1985). We believe a great portion of the spread in $S(\lambda_0)$ is due to a systematic mass index increase of about 0.01 a year (1964 to 1981). This increase can be explained by the ejection of mainly small particles from the comet surface during the last perihelion passage. The mean minimum value of S equals 1.94 ± 0.2 for the longitude of $139.0 \pm 0.2^\circ$.

We found the Perseid flux density $Q(m)$ by the modified Kaiser Belkovich method (ANDREEV et al., 1984). The physical model of the meteor phenomena selected was that of BELKOVICH et al., (1982). The particle density was taken as equalling 0.3 g cm^{-3} . For $m \geq 10^{-3} \text{ g}$, Fig. 1 gives the smoothed curve $Q(m, \lambda, 1950.0)$ obtained by averaging individual values with the step of about 0.9° in the solar longitude. Fig. 1 shows that the flux density maximum $q(10^{-3}) = 3 \cdot 10^{-3} \text{ particles km}^{-2} \text{ h}^{-1}$ coincides with that of large particles. For $m \geq 10^{-3} \text{ g}$, the stream width at half maximum density is 1.8° . Analysis of the $Q(m, \lambda_0)$ shows that there is no

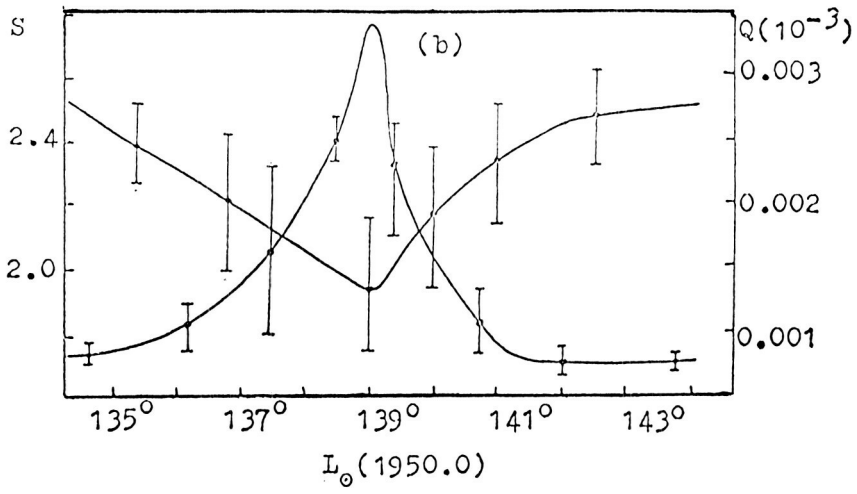


Fig. 1 Flux density $Q(10^{-3}g)/km^{-2}h^{-1}$ and index S versus solar longitude (epoch 1950.0).

displacement of the stream flux density position₂ in the Perseids for the mass particle variation in the range of 10^{-4} to 10^2 g.

On the basis of the obtained values of $Q(m)$ and index S the meteor matter influx on the Earth during the Perseids activity time was estimated. For the range of masses from 10^{-5} to 10^3 g the total influx amounted to 0.42 ton, half that amount striking the longitude range of 138 to 140° .

To define the total particle number in the stream and the stream mass, we derived the equation of the projection of the Earth's path on the nodal cross-sectional plane and determined the shower density distribution of particles with different mass along this projection. Studying these data, we discovered that the shower density distribution was asymmetrical to the mean orbital plane. It means that the area between equal density lines above the mean orbital plane are greater than the analogous area below it. The angle between the projection of the Sun direction and the major semi-axis of the cross-section is 27° . Hence, known gravitational and non-gravitational forces could not have caused this effect. The only possible explanation is a peculiarity of stream formation. The estimate of the total number of particles intersecting the cross-section of the Perseid stream at its node was obtained by integration of the flux density with the help of the ANDREEV and SUKHOTIN (1982) method. For the masses from 10^{-3} to 10^3 g, the particle flux through the cross-section appeared to amount to $1.6 \cdot 10^{12} \text{ h}^{-1}$ while the total number of particles in the stream was $1.7 \cdot 10^{18}$ and the stream mass less than $14 \cdot 10^{16}$ g.

The Perseid stream formation is usually connected with the decay of comet 1862 III. Taking into account the orbital size, one may assume that the decay of this comet was taking place mainly close to its perihelion. In this case, it should be expected that there must exist a common intersection region of individual meteor orbits. The analysis of 356 photographic meteor orbits showed that the ecliptic coordinates of this region are $\lambda_c = 84.4 \pm 4.5^\circ$; $\beta_c = 62.5 \pm 1.7^\circ$; $r_c = 1.51 \pm 0.09 \text{ a.u.}$; and its true anomaly $V_c = 274.284.1 \pm 4.4^\circ$. These data confirm the hypothesis of Perseid stream formation due to a comet decay on a rather small arc of the orbit.

Since individual meteor orbits cannot be used for solution of the problem of the Perseid formation and evolution, we considered the comet orbital evolution first and selected possible favorable moments for its decay. Fig. 2 gives the results of the comet evolution calculations by the Halphen-Goryachev method (ANDREEV and SUKHOTIN, 1982) under the following conditions: a) the orbits of the disturbing planets Jupiter, Saturn and Uranus are constant; b) secular perturbations up to the first order by these objects are taken into account; c) the same as in b) but with perturbations due to Neptune added; d) the same as in c) but with perturbations produced by the Earth added; e) the same as in d) but with periodic perturbations at the epoch of close approaches to the planets were considered using numerical methods. Fig. 2 shows that subsequent comet evolution depends primarily on integration conditions. The analysis shows that the main evolutionary transformations of the comet orbit were caused by the close approaches to Saturn (the first was up to 1.07 a.u. in 1859.9 and later - one for every 33 revolutions) and one catastrophic approach to Jupiter some 25 millenia ago. Discussing Fig. 2 we came to the conclusion

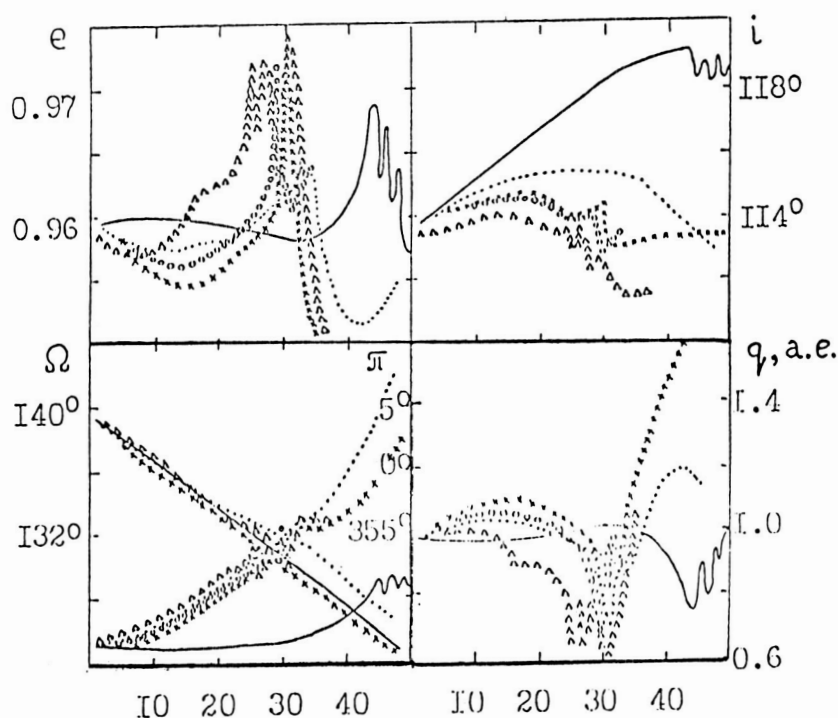


Fig. 2 Evolution of the comet 1862 III orbit. The curves correspond to the following integration conditions detailed in the text: a(---), b(●●●), c(xxx), d(ooo), and e(△△△).

that the comet 1862 III decay occurred most probably at the start of the comet onto its present orbit, i.e., 25 millenia ago. Special attention should be paid to the secular change of the true anomaly V of the common "point" in the Perseids orbits' approach. Irrespective of the integration conditions at the moment of approach to Jupiter, $V_c = 150 - 180^\circ$. It means that for an interpretation of decay near the c perihelion, the modern coordinates of λ_c, β_c are quite the opposite of the true ones.

In order to determine the decay velocities from the comet surface, various decay types (directed, isotropic, with different distribution of velocities and masses) were simulated. But none of the results satisfies either the observed deviation between the comet orbital elements and the elements of the stream's mean orbit nor the variance of the comet's modern orbital elements and the Earth's path length. Agreement with these decay models is possible only under the following conditions: a) if upon ejection practically all the particles pass through the sphere of influence of Jupiter (25 millenia ago) or Saturn (10-12 millenia ago); b) if the comet decayed near aphelia $\sim 20-025$ millenia ago and was of a collisional nature.

References

1. Andreev G.V., Lasarev R.G., 1979, Astronomy and Geodesy, No. 7, pp. 41-45, Tomsk.
2. Andreev G.V., Sukhotin A.A., 1982, In: Meteor Matter in the Interplanetary Space, pp. 175-176, Moscow.
3. Andreev G.V., Episheva A.E., Mugruzina O.A., Rubtsov L.N., 1984, In: Meteor Matter in the Interplanetary Space and Earth's Atmosphere, pp. 7-8, Dushanbe.
4. Andreev G.V., Episheva A.R., Rubtsov L.N., Tarasova I.I., 1985, Izvestiya Akademii Nauk Taj. SSR, No. 3, pp. 37-50.
5. Belkovich O.I., Suleimanov N.I., Tokhtashev V.S., 1982, In: Meteor Matter In the Interplanetary Space, pp. 88-101, Moscow.
6. Levin B.U., 1958, The Physical Theory of the Meteor and Meteor Matter In Solar System, p. 487, Moscow.
7. Hughes D.W., 1973, M. N. Roy. Astron. Soc., No. 2, Vol. 161, p. 113.

SOME MODELS OF THE GEMINIDS METEOR STREAM FORMATION

O. I. Belkovich and G. O. Ryabova

Kazan State University,
Kazan, USSR

Further development of methods of investigations of meteor shower structure and a great deal of observational data have made it possible to obtain a precise flux density profile along the Earth's orbit for the Geminids meteor shower. This curve proved to be adequately described by an exponential law. The information obtained by ground observations is insufficient for construction of the exact picture of the flux density distribution in a stream cross-section. But we can make some assumptions. Namely, in a normal cross-section plane of Geminids, the lines of equal flux density (for particles with fixed mass) will be represented by a family of nested ellipse-like curves. The curves are stretched more toward the inside of the stream orbit. The flux density decreases exponentially from the maximum point to the periphery.

In this connection it is interesting to find out the following:

1. Which ejection model will fit the observed shower structure: a single ejection, an ejection over a certain orbital arch of the parent comet, a destructive impact, etc; and
2. To what extent the subsequent process of evolution modifies the formed structure.

Ejection from cometary nucleus.

The ejection from a cometary nucleus was modeled for particles of equal mass and size (radius = 0.1 cm, density = 0.8 g/cm³). A sample of 5,000 particles was enough for construction of a qualitative picture of the stream cross-section in the ecliptic plane. The ejection speed of the dust was determined by the Whipple's formula (Whipple, 1951). The effect of radiation pressure was also taken into account (Burns et al., 1979).

The ejection at a certain point of the cometary orbit and around this orbit was simulated. Such models were considered by Fox, Williams and Hughes but for other purposes. The mean orbit of the Geminids from Fox et al., (1983) was chosen as a reference.

The model Geminids cross-section in the ecliptic plane with ejection at perihelion is shown in Fig. 1b. A distinctive ellipse was obtained. The size and compression of the ellipse changes depending on the true anomaly of the ejection point at the orbit of the parent comet but the qualitative picture is the same. It is clear that this model does not represent reality.

The second model simulates ejection around the cometary orbit. (See Fig. 1a). Ejection points are distributed around the orbit at random [rectangular distribution]. The ejection speed is fixed at every point. As we can see, the stream cross-section is of a rhombic rather than an

ORIGINAL PAGE IS
OF POOR QUALITY

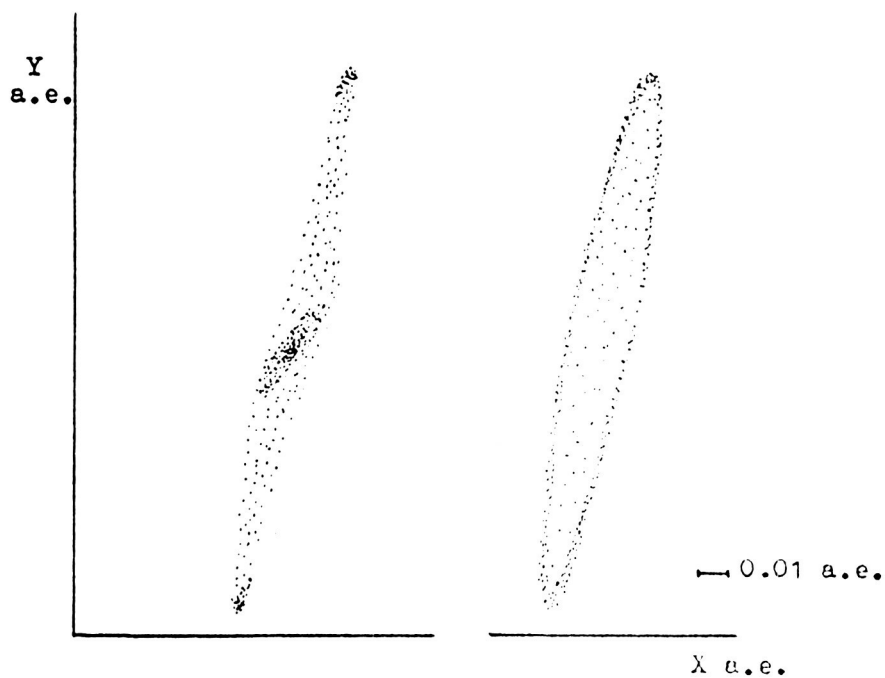


Fig. 1 Models of the Geminid cross-section in the elliptic plane. a) The ejection points are distributed randomly and uniformly around the orbit, b) The ejection from the perihelion point.

elliptical shape. A dense central core and distinctive concentrations at edges, so-called "wings", can be clearly seen.

Integrated rate curves, which are defined as the number of cross-section particles on some straight line (usually the X or Y axes of the standard heliocentric ecliptic frame), can be used for a qualitative study of the cross-sections. Fig. 2 shows the integrated curve along the X axis for ejections all around the orbit. An exponential density variation becomes apparent here.

1) Velocity distribution variation effects

The fixed ejection velocity for the given orbital point is an idealization. The gas flow speed (according to Whipple's model) is considered as a mean speed. It cannot be the same all over the cometary nucleus. Moreover, real particle cross-sections are different because of their irregular shape and this leads to variations in the ejection speeds. Therefore, it is more appropriate to study models where the ejection speed is distributed according to a certain law. Certainly, in the case of a destructive impact of the parent body, the notion of a velocity distribution must necessarily be applied.

Assuming a Gaussian distribution of ejection velocities we have obtained the following results:

1. In ejection all around the orbit there were the following changes: The "wings" vanished, while the exponentially grew more pronounced (Fig. 2).
2. But ejection only at perihelion produced striking changes as compared with the case of the fixed but random ejection velocity (Fig. 3). The structure of the cross-section in the ecliptic plane became similar to those observed in ejection all around the orbit. However, for this to occur the value of σ (the parameter of Gaussian distribution) must be no less than $0.4c$, where c is the mean ejection velocity.

We have also examined the case of a random [rectangular] distribution of ejection velocity. Fig. 4 shows the integral rate curve along the X-axis for the isotropic ejections at perihelion and for a rectangular distribution of the ejection velocities in the interval from 0 to 1.33634 km/s. A detailed study of this curve leads to the conclusion that the density decrease from the cross-section center appear to depart from one that is strictly exponential. The integral curve for ejection around the orbit did not change appreciably. However, we have every reason to assume that the exponential dependence was also disturbed here and so this case requires further study.

The previous models have been considered in the assumption that the ejections take place during one comet revolution. When ejections occur during several revolutions, it is easy to foresee the resulting cross-section structure. The new integral rate curve, for example, can be obtained by adding several single revolution sets shifted along the axis, one towards the other. The width of the stream increases by 1.5 times for 100 years.

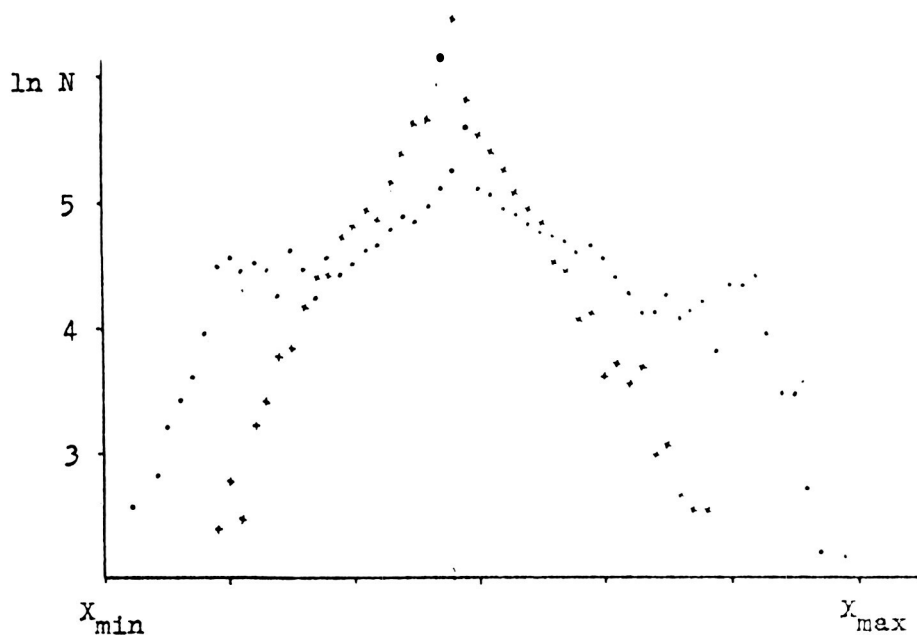


Fig. 2 The integral rate curves. The curve for the ejection around the orbit with the fixed ejection velocity is shown by dots, and the one with the Gaussian distribution of ejection velocities by crosses.

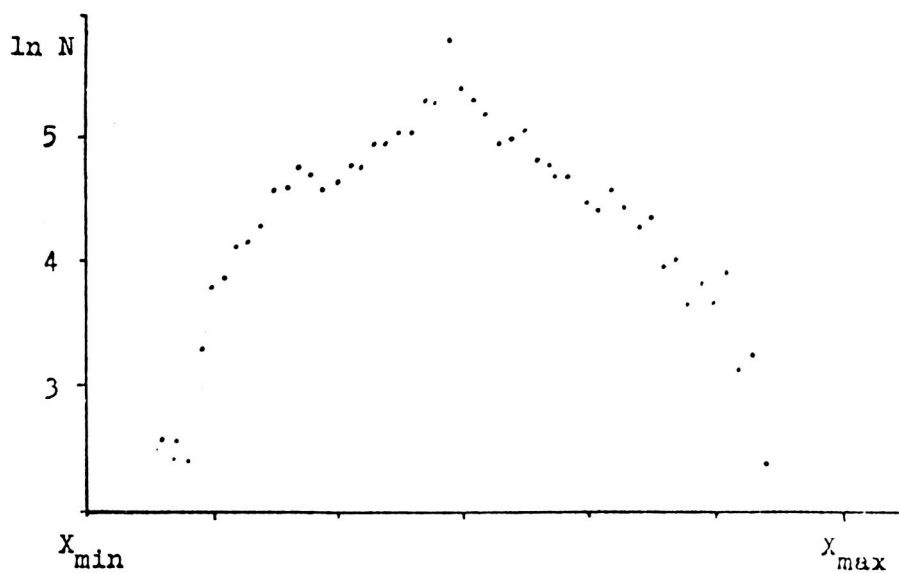


Fig. 3 The integral rate curve. The ejection at a perihelion. Ejection velocities are distributed by the Gaussian law.

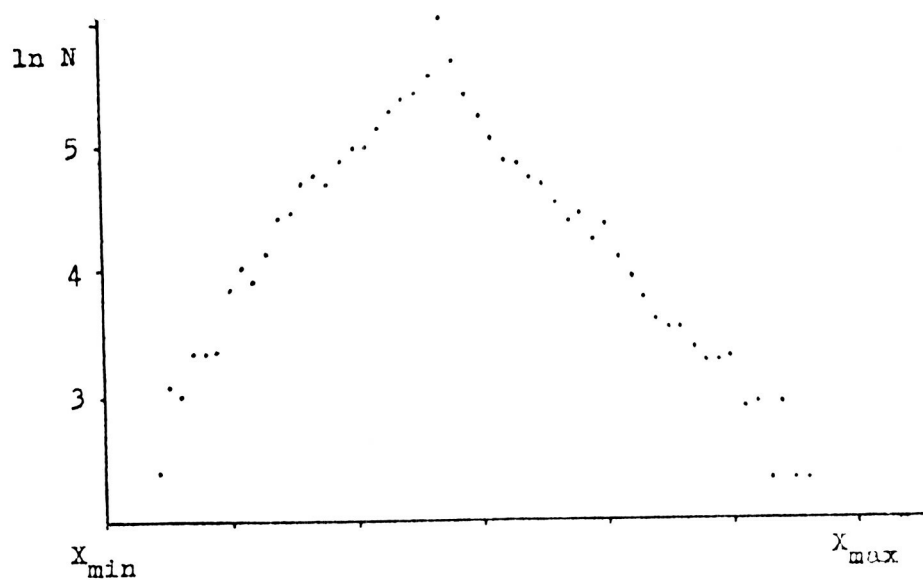


Fig. 4 The integral rate curve. The ejection at a perihelion. The distribution of the ejection velocity is uniform in the interval from 0 to 1.33634 km/s.

2) Cross-section changes due to the secular gravitational perturbations

A simple model to reveal the influence of secular gravitational perturbations on the cross-section structure changes is considered. A sample of 5,000 particles was ejected from the parent body around its orbit at random and rectangularly. The ejection velocity was determined by the Whipple's formula (WHIPPLE, 1951). The particles crossing the ecliptic plane along semi-major and semi-minor axes of the cross-section ellipse were chosen (Fig. 5, $t=0$). Then we traced the orbital evolution of those chosen (Fig. 5, $t=0$). Then we traced the orbital evolution of those particles for 8,500 years ahead by the Halphen-Goryachev method. It is sufficient to consider Jupiter's influence only on this model. The previously obtained ellipse-like shape of the stream cross-section is maintained for no more than 1,500-2,000 years (Fig. 5). The initial ellipse deforms gradually with the extension into the stream orbit increasing. The stream width remains about the same but due to stretching along the semi-major axis the mean space density of the stream decreases with time. However, the central core persists.

Thus, we can draw the following conclusions:

1. When studying the mechanism of formation of meteor streams, it is necessary to take into consideration the velocity distribution of particles that have been ejected from the parent body.
2. On the basis of the observed density variations, it is impossible to determine (at any rate at present) what kind of ejection takes place: a single ejection or that around an orbital arch.
3. The original structure of the Geminids cross-section persists for no more than 1,500-2,000 years.

References

1. Whipple, F.L., A Comet Model II., 1951, Physical relations for comets and meteors, *Astrophys. J.* Vol. 113, No. 3, pp 464-474.
2. Burns, T.A., Lamy Ph. L., Soter S., 1979, Radiation Forces on Small Particles in the Solar System, *Icarus*, Vol. 40, No. 2, pp. 1-48.
3. Fox K., Williams I.P., Hughes D. W., 1983, The rate Profile of the Geminides Meteor Shower, *Mon. Not. Roy. Astron. Soc.*, 205, No. 3, pp. 1155-1168.

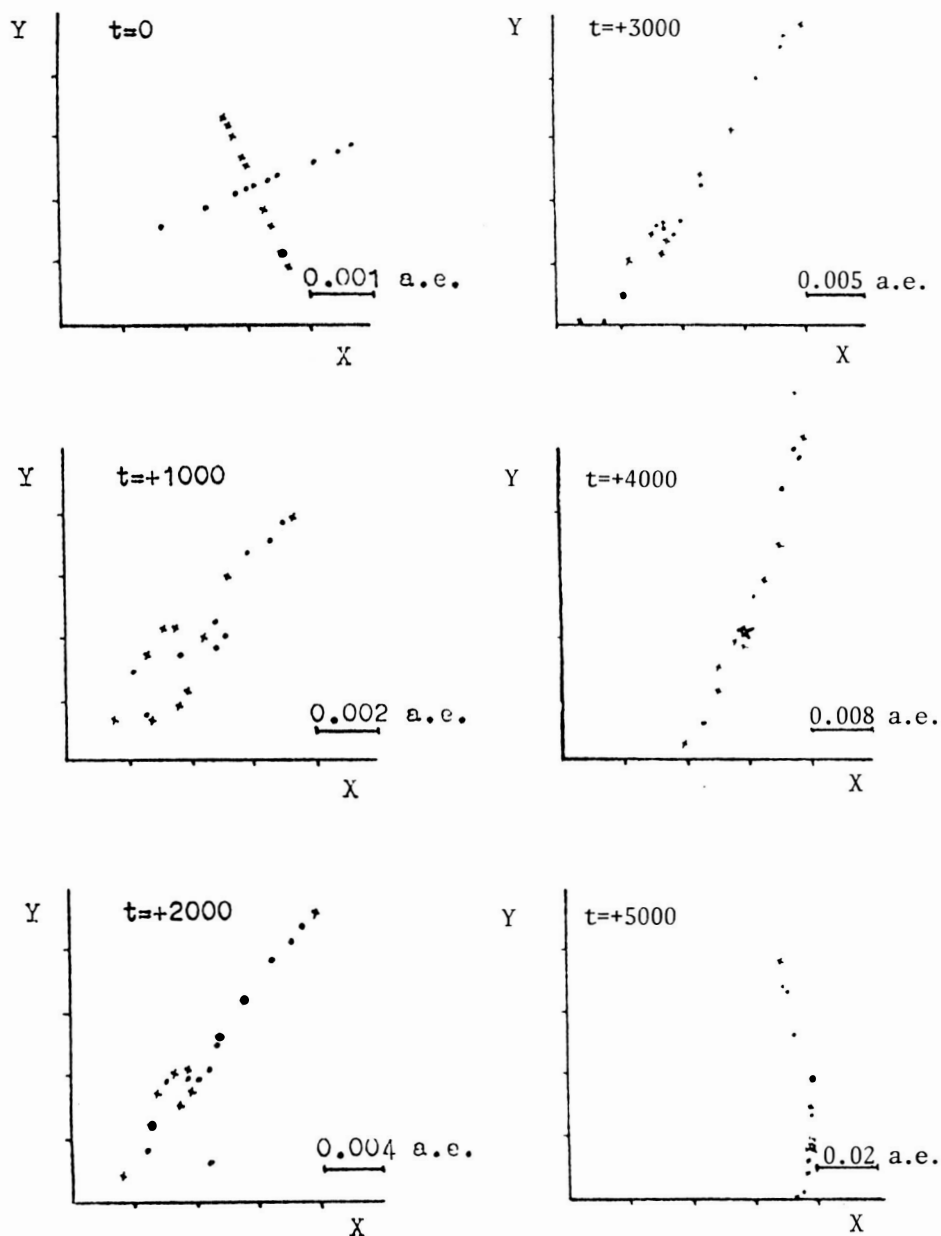


Fig. 5 The influence of secular gravitational perturbations on the shape of the Geminid cross-section in the ecliptic plane.

STRUCTURAL PECULIARITIES OF THE QUADRANTID METEOR SHOWER

SH. O. Isamutdinov and R. P. Chebotarev

Tajik Academy of Sciences Institute of Astrophysics
Dushanbe, USSR

Systematic radio observations to investigate the Quadrantid meteor shower structure are regularly carried out in Tajikistan. They have now been conducted annually in the period of its maximum activity (January 1-6) by the Gissar Observatory since 1966.

The paper provides the latest results of these investigations on the basis of 1981-1984 data obtained using new equipment with a limiting sensitivity of $+7.7^m$ which make it possible to draw some conclusions on the Quadrantids shower structure both for transverse and lengthwise directions.

Since 1981, meteor radar observations in Dushanbe have been carried out by using the MIR-3 radar whose principal parameters are: wavelength 8m, repetition frequency 500 pps, pulse duration 40 μ s, passband of receivers 50 kcs, peak pulse power in each of two directions 15-20 kW, and minimal detection level 4 μ v.

Identical transceiving antennas - five-element arrays oriented simultaneously westward and southward with a maximum gain coefficient of $G_r = G_T = 13$ at an elevation angle of 45° are used.

As on-line M-6000 computer records average hourly rates of radiometers as well as their durations and range distributions along with the individual levels of each parameter in each direction.

Fig. 1 shows the variations of the number of radiometers on the nights from January 1 to 2, 3 to 4 and 5 to 6, 1984. Considering radiometers recorded on the nights of January 1 to 2 and 5 to 6 as a purely sporadic background, the activity of the Quadrantids on January 4 is clearly marked within the period of 20:00-03:00 UT in the westward direction while for the southward direction it is in the intervals are obtained by simple subtraction of the extrapolated rate of sporadic meteors from the total meteor number.

Fig. 2 gives the 1966-1984 curves of the hourly rate variation of all Quadrantid radiometers with a reflection duration $\tau \geq 0.01$ s and of meteors with $\tau > 1$ sec as a function of solar longitude.

A rather symmetric shape of the curves and discrepancy between the maximum of the combined meteor rates ($\lambda = 282^\circ$, 62) and that of radiometers with $\tau > 1$ sec ($\lambda = 282^\circ$, 76) is of great interest. The latter, just as with the Geminids occurs a little later than the total rate maximum does.

To study the cross-structure of the Quadrantid meteor shower, solar longitudes corresponding to the maximum density of meteor flux of a certain radio magnitude were determined for those years when a sharp peak of activity occurred within the middle of a radio observation interval. The

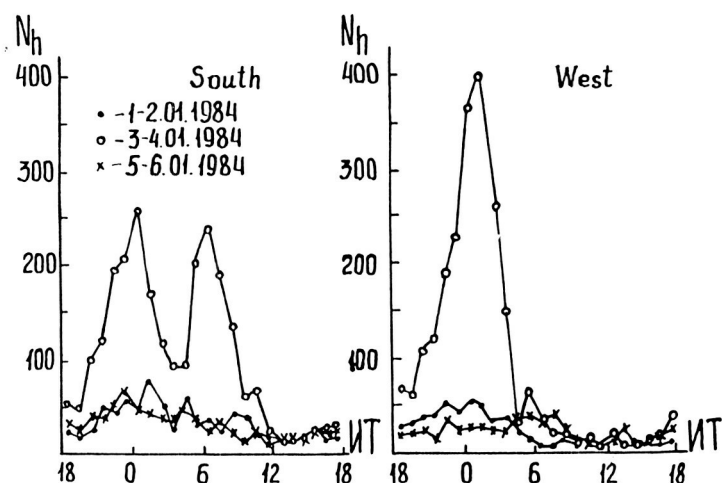


Fig. 1 The radiometer rate variation at the epoch of the Quadrantid shower activity on January 1-2, 3-4, 5-6, 1984.

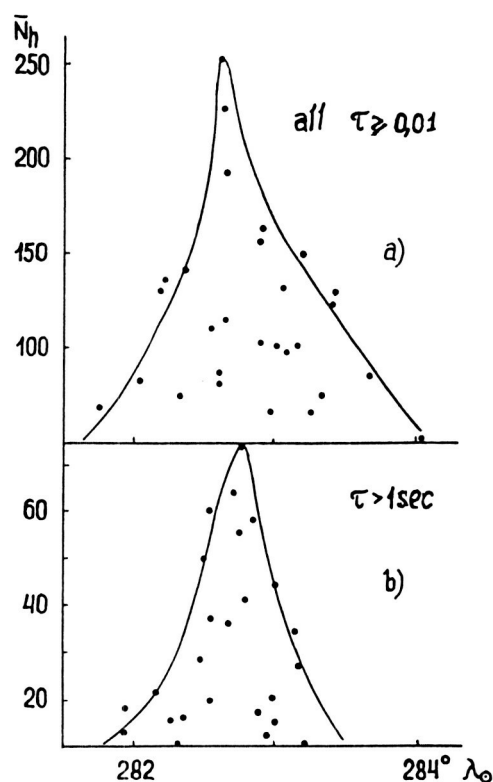


Fig. 2 The curves of the Quadrantid maximum activity for 1966-1984 (minus sporadic background).

resulting dependence is presented in Fig. 3 and correlates well with a similar finding by ISAMUTDINOV (1983). In the linear approximation, this dependence can be expressed as

$$L_0 = 282^\circ,71 - (0^\circ,02 \pm 0,01) M_r$$

where L_0 is the solar longitude and M_r the radiometeor magnitude.

Two more dependences characterizing the shower's cross-structure are given in Fig. 4. It represents the dependence of the average over a number of years of the flux density of particles $Q \text{ km}^{-2} \text{ h}^{-1}$ (with a mass over 10^{-3} g) and the parameter "s" (index of mass flux) on solar longitude. The dependences were derived by taking into account known ionic quenching processes. The derived values $Q (> 10^{-3} \text{ g}) = 0.1 \text{ particle km}^{-2} \text{ h}^{-1}$ exceed by about one order of magnitude similar values obtained from radar observations in LEBEDINETS (1970), HUGHES and TAYLOR, (1977), and ANDREEV, et al., (1982) but within 10 per cent of the value obtained by BELKOVICH, et al., (1982). The maximum flux density of the particles falls at solar longitude $\lambda_0 = 282^\circ,62$ and the parameter "s" minimum - occurs at $\lambda_0 = 282^\circ,76$, which is in good agreement also with the results of Hughes and Taylor, (1977).

A considerable variety of values Q and "s" for the same solar longitude proved to be caused by the annual variations i.e., by the length-wise inhomogeneity of the stream. Therefore, based on the analysis by HUGHES and TAYLOR (1977), we assumed that the Quadrantides stream revolution period is 4.4 years. This was done in order to estimate the stream structure along its axis and investigated the variations of parameters Q and "s" on the basis of our 18-year observations. The interval of solar longitudes covered was from $282^\circ 0$ to $283^\circ 3$.

Fig. 5 (where $360^\circ = 4.4 \text{ years}$) gives the changes of the averaged values of Q and "s" along the orbit stream. The averaging was performed for areas of $20^\circ \times 0.06$ for Q and $20^\circ \times 0.4$ for "s" parameter. It is worth noting that each area had 3 or 4 values of both Q and "s", and the deviations from the average value did not exceed ± 0.02 to ± 0.13 along the ordinate and $\pm 10^\circ$ along the abscissa. It is clearly seen that the variation of stream parameters along the orbit occurs with periods of about 4.4 years and 1 year. The maximum deviation from the average value is $\pm 50\%$ for Q and $\pm 7\%$ for "s". Although measurement errors are possible, inhomogeneous particle distribution along the stream orbit may also be the cause. This is all the more so, since the increase of particle flux density in 7 out of 9 cases corresponds to the parameter "s" decrease (usually observed in streams). Besides, it is necessary to note that since the stream orbit is close to that of Jupiter, a deflection of orbit stream with a period of 1,077 years is possible. Probably this is just the phenomenon that we seem to observe.

References

1. Belkovich O. I. et al., 1982, The analysis of the structure of the Quadrantides meteor stream made according to radar and visual observations, Meteor matter in the interplanetary space, Moscow-Kazan, pp. 121-129.

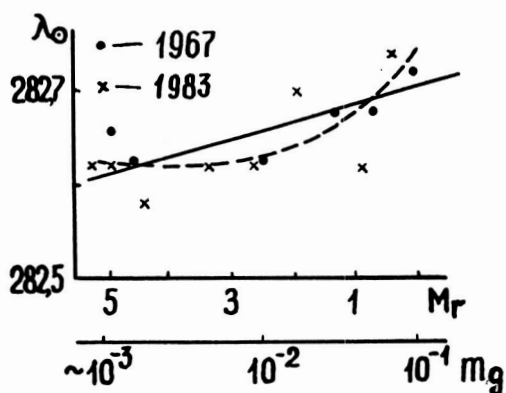


Fig. 3 The dependence of the particle flux density maximum of Quadrantides on solar longitude and radio-magnitude. • ---- 1967, x ---- 1983.

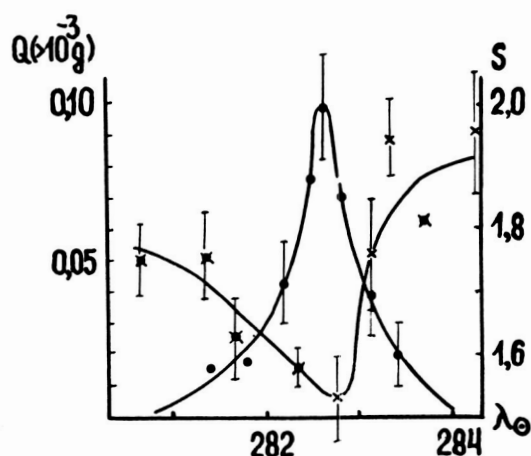


Fig. 4 The dependence of the Quadrantid flux density of particles over 10^3 g and the "s" parameter of mass distribution of meteor bodies on solar longitude.

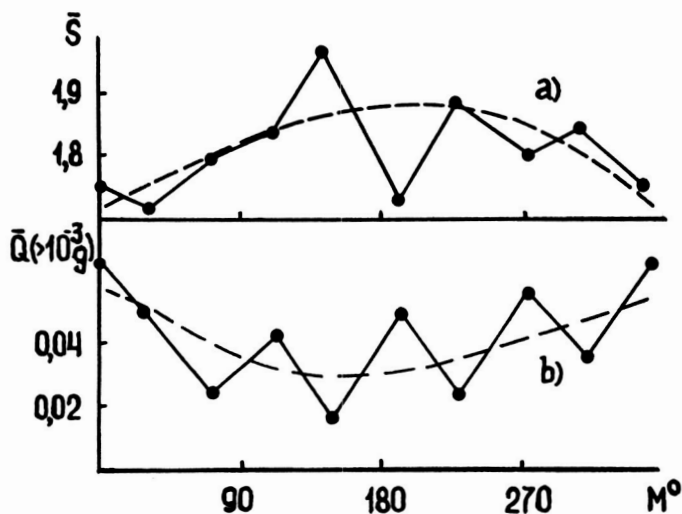


Fig. 5 The observed length-wise structure of the Quadrantid shower. a) parameters " \bar{s} ", b) particle flux density $\bar{Q}(m > 10^{-3} \text{ g})$.

2. Lebedinets V. N., 1970, The density of meteor body stream obtained by radar observations of meteors, Comets and Meteors, Dushanbe, No. 19, pp. 25-30.
3. Hughes D. W., Taylor I. W., 1977, Mon. Not. Roy. Astron. Soc., Vol. 181, No. 2, p. 517.
4. Andreev G. V., et al., 1982, The density and influx matter of the Geminides, Quadrantides and Leonides meteor showers according to observations conducted in Dushanbe, Meteor matter in the interplanetary space, Moscow-Kazan, pp. 118-120.

ON THE POSSIBLE ORIGIN OF METEOROID GENERATING ASTEROID ORBITS

A. M. Kazantsev and L. M. Sherbaum

Kiev State University
Kiev, USSR

A mechanism to replenish the Apollo and Amor groups by resonant asteroid-orbit transformation is suggested.

As is well known, the semi-major axes of resonant orbits oscillate periodically about a value corresponding to the exact commensurability with eccentricities oscillating out of phase. The periods and amplitudes of such librations depend on the initial value of eccentricity e , longitude of the perihelion π and on the initial position of the asteroid and Jupiter. We suggested a characteristic parameter M^* (KAZANTSEV and SHERBAUM, 1984) which connects the position of the asteroid on the orbit with the position of its line of apsides vis-a-vis Jupiter. Numerically it equals $\Delta\sigma$ - the oscillation amplitude of libration argument introduced by SCHUBART (1968). The value of M^* (or $\Delta\sigma$) defines the size of the libration for a and e . This characteristic parameter changes from 0° to 180° : for $M^* = 0$ the libration amplitude of a is minimum, for $M^* = 180^\circ$ it is maximum. According to SHARLJE, (1966) $\Delta\sigma$ is an integral of motion in the circular, limited three-body problem. It is clear that in the most general case, $\Delta\sigma$ is not constant. However, numerical calculations carried out by us as well as by different authors have revealed no changes of $\Delta\sigma$. According to SCHUBART's (1982) results, $\Delta\sigma$ remains invariable for the interval of up to 10^4 years. Besides short-period librations, the eccentricities undergo long-period changes with the same period as that of the perihelion longitude. The rates of these changes (de/dt and $d\pi/dt$) are determined by the value of M^* . The dependences $de/dt(M^*)$ and $d\pi/dt(M^*)$ are reproduced in Fig. 1 for the commensurability $1/3$, $e_0 = 0,3$ for different values of π . These were obtained using numerical calculations for the interval of 500 years. By dividing these dependences into pairs, the function $|de/d\pi|(M^*)$ for each value of π is obtained (Fig. 2). The gap of these functions in the region of $M^* = 100^\circ - 120^\circ$ is explained by the existence of orbits for which secular changes of the perihelion longitude practically equal zero whereas secular changes of eccentricities differ appreciably from zero. This peculiarity is true of all commensurabilities regardless of the values for e and π . In other words, the eccentricities of the orbits in the range of $\Delta\sigma$ from 100° to 120° can reach the largest values. Since the value $\Delta\sigma$ changes, even though very slowly, all the resonant orbits will, sooner or later, find themselves in favorable conditions for reaching large eccentricities. Some of these asteroids could become members of the Apollo and Amor groups.

Among the numbered minor planets there are only two known asteroids with orbits librating in commensurability $1/3$ with Jupiter. These are Alinda (887) and Quetzalcoatl (1915). Their orbital elements are $e = 0,55$, $\pi = 100^\circ$ and $e = 0,58$ and $\pi = 150^\circ$ respectively. The changes of the elements given in Fig. 3 were obtained using our calculations of their evolutions. The mean rate of change of π for Alinda is nearly zero, the eccentricity increasing only slightly. This is the real confirmation both of the existence for a break in the function $|de/d\pi|(M^*)$ and the reaching of large eccentricities by resonant orbits. The orbit of the minor planet, judging by its characteristics, is in the very center of the gap.

ORIGINAL PAGE IS
OF POOR QUALITY

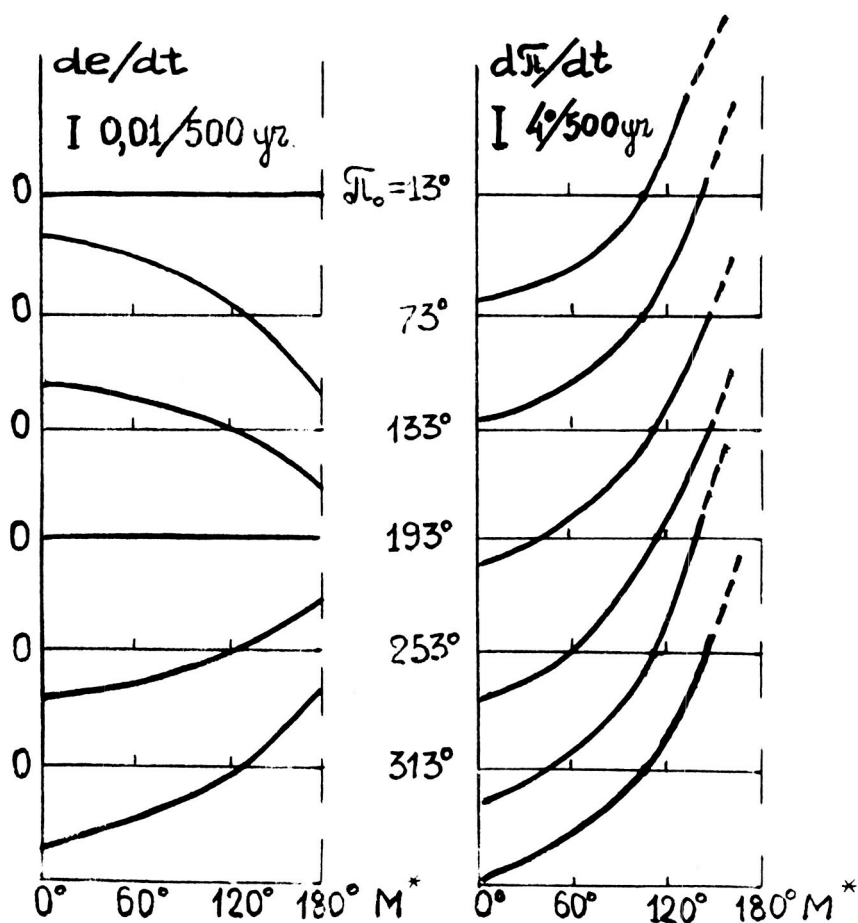


Fig. 1 Velocity dependences of M^* for long-period changes of eccentricity (de/dt) and longitude of perihelion ($d\pi/dt$) having different π_0 ($a_0 = -2, 50 \text{ a.u.}$, $e_0 = 0,3$).

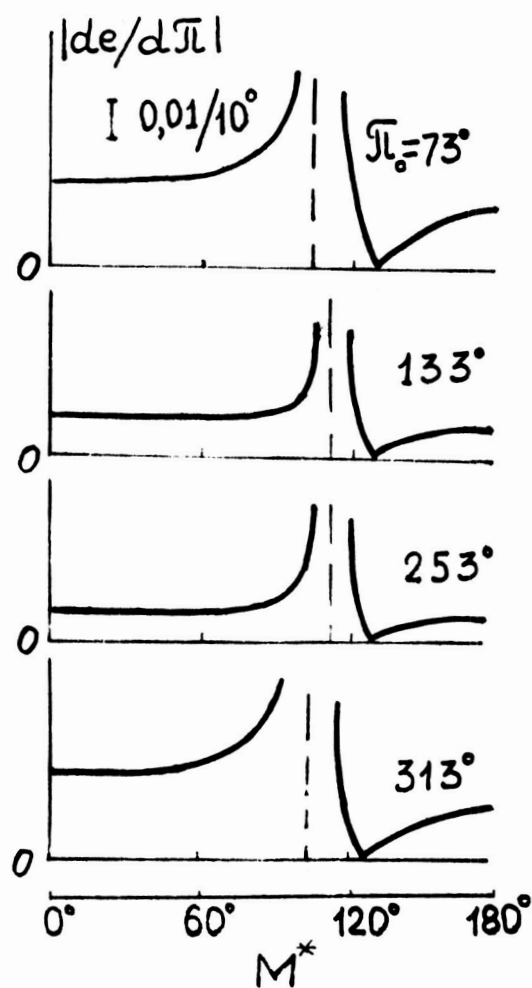


Fig. 2 Dependence $|de/d\pi|$ of M^* for different π_0 ($a_0 = 2,50$ a.u. $e_0 = 0,3$).

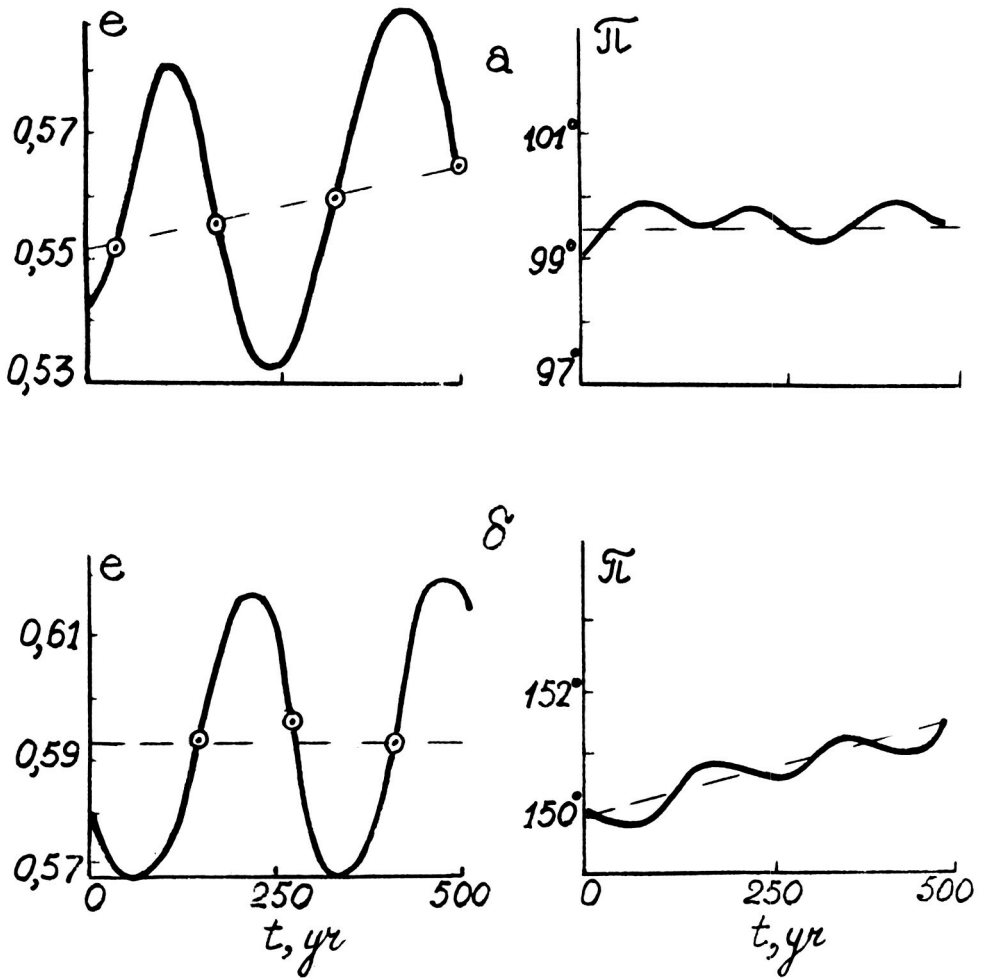


Fig. 3 Evolution of e and π elements for asteroid orbits:
 a - No. 887, b - No. 1915 (o - $a = a_c$).

The perihelion longitude of asteroid No. 1915 slightly increases (by nearly 1.5° in 500 years), the eccentricity practically not changing (this is perhaps explained by π being so close to 193° , the value at which the condition $de/dt = 0$ is fulfilled). The characteristic parameter M^* for this orbit is 130° which is at a distance of about 10° from the gap of the function $|de/d\pi|(M^*)$ with $e = 0.6$, $\pi = 164^\circ$ (Fig. 4). (Out of our numerous model orbits, these are the nearest to orbit elements of the minor planet No. 1915).

In MARSDEN's (1970) work, the results of calculations are given for an orbital evolution of the asteroids No. 887 and No. 1915. The calculations were carried out using a more exact program than ours for a time interval of 1,400 years.

According to both Marsden's and our calculations, the asteroid orbit is at a distance of no more than 8° from the gap of the function $|de/d\pi|(M^*)$. Consequently both orbits have just the very values of M^* which, according to our conclusions, ensure large eccentricities (the range of definition of M^* is 180°). The majority of Apollo and Amor asteroid orbits have the value $a < 2.5$ a.u. Large eccentricities of these orbits can be reached, in principle, by consideration of cases other than $1/3$ resonances with Jupiter.

References

1. Kazantsev A.M., Sherbaum L.M., 1984, *Astron. News Letters*, Vol. 18, No. 1, pp. 29-34.
2. Sharlje K., 1966, *Celestial Mechanics*, Moscow, Nauka Publishers, p. 627.
3. Marsden B.G., 1970, On the Relationship between Comets and Minor Planets, *Astron. J.*, Vol. 75, No. 2, pp. 206-217.
4. Schubart, J., 1968, Long-period Effects in the Motion of Hilda-type Planets, *Astron. J.*, Vol. 73, No. 2, pp. 99-103.
5. Schubart J., 1982, Three Characteristic Parameters of Orbits of Hilda-type Asteroids, *Astron. and Astrophys.*, No. 114, pp. 200-204.

N88-14554

METEOR DETECTION ON ST (MST) RADARS

S. K. Avery

University of Colorado
Boulder, Colorado

The ability to detect radar echoes from backscatter due to turbulent irregularities of the radio refractive index in the clear atmosphere has lead to an increasing number of established mesosphere - stratosphere - troposphere (MST or ST) radars. Humidity and temperature variations are responsible for the echo in the troposphere and stratosphere and turbulence acting on electron density gradients provides the echo in the mesosphere. The MST radar and its smaller version, the ST radar, are pulsed Doppler radars operating in the VHF - UHF frequency range. They provide nearly continuous wind measurements in real time in the troposphere and lower stratosphere and during daylight hours in the mesosphere. Several new radars have been proposed including a network in the United States that will replace the national rawinsonde network for operational use. The majority of the new radars will be the smaller ST radar which probes only the troposphere and lower stratosphere. The ST radar is much less expensive than the more powerful MST radars (\$150,000 vs \$1,500,000, excluding labor, real estate, and operations and maintenance). For those people interested in upper atmosphere dynamics, the ST radar is not a very useful tool due to the limited height of usable echo returns. However, the presence of strong meteor echoes in the upper mesosphere has been noted on ST radars (AVERY et al., 1983). These echoes can be used to determine upper atmosphere winds at little extra cost to the ST radar configuration. In addition, the meteor echoes can supplement mesospheric data from an MST radar. In this paper I will describe the detection techniques required on the ST radar for delineating meteor echo returns.

A basic radar schematic for the ST/MST radar is shown in Figure 1. The radar is very similar to the more traditional meteor radars and the major differences between the two systems are the antenna configuration and the echo detection and processing of the data. Narrow antenna beamwidths are required in an ST/MST radar. Consequently these systems use large antenna arrays and are generally more expensive. Coherent detection of the received signal from three antenna beam directions gives a measure of the complete wind field. Coherent integration and FFT techniques are used to determine the Doppler frequency which gives a measure of the radial velocity. Temporal resolution is approximately one minute with a possible height resolution of 150 m.

Meteor echoes observed with a ST/MST radar have a well defined location due to the narrow beam width of the ST/MST radar as compared with the wide beams of the more traditional meteor radars. The problem with using meteor echo returns, either on a meteor radar or a ST/MST radar is in finding the Doppler frequency using a fairly short time series. Pulse pair processing is usually done to determine the Doppler frequency (STRAUCH et al., 1978). Due to the narrow beamwidth and antenna pointing directions meteor echo rates are lower on the ST/MST radar than a meteor radar. However, there are a sufficient number of echoes to determine the winds and tidal harmonics of the wind over time intervals greater than a week.

ST RADAR SCHEMATIC

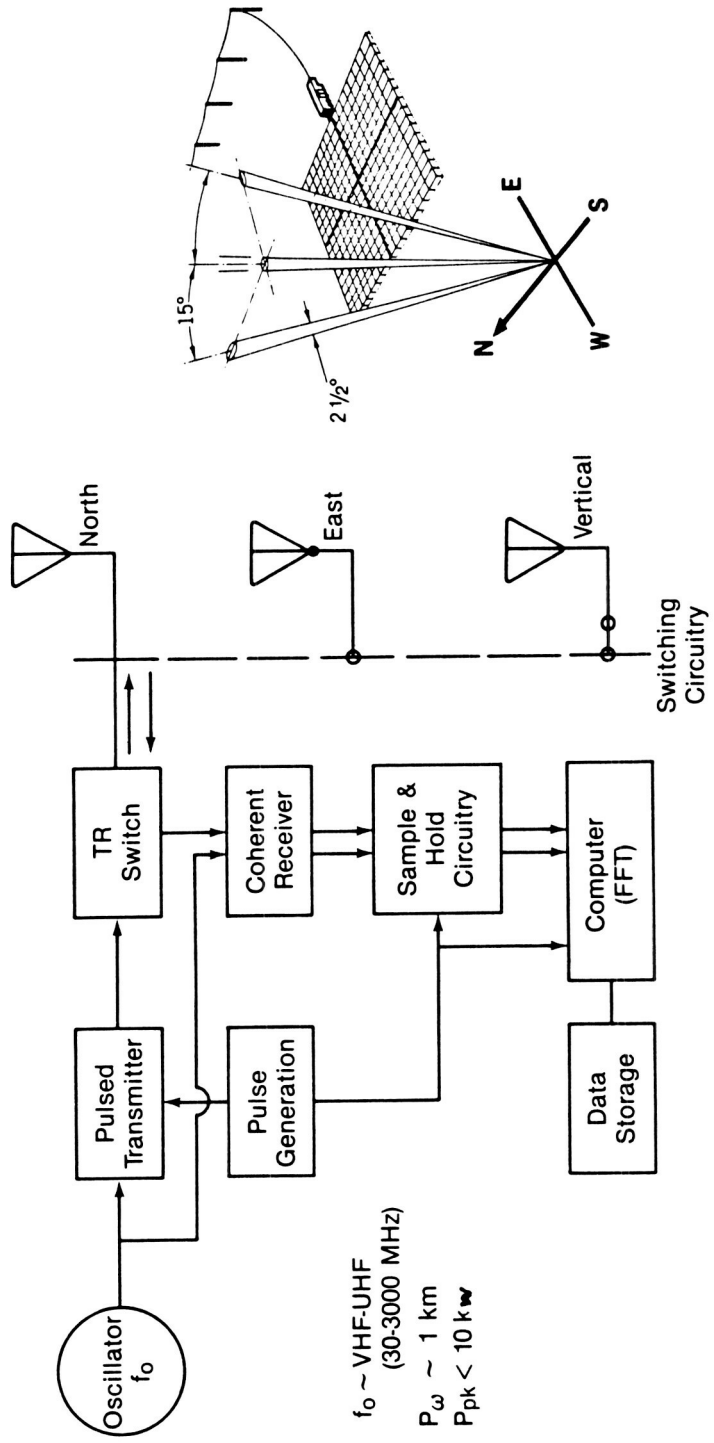


Fig. 1 Basic ST/MST radar schematic.

The existence of meteor echo returns is shown in the backscattered power profiles shown in Figure 2. These plots are from a recent experiment we performed using the Jicamarca Radio Observatory in Peru which is designed primarily for ionospheric research. The top plot shows a well defined meteor echo at 83 km. The presence of the echo is clearly seen in the power spike on the two-dimensional plot. The three dimensional plot shows the height and temporal evolution of the meteor echo. The echo lasted for 10 pulses which corresponds to a time interval of 67 milliseconds. The shape of the power plot as a function of time is generally gaussian. The bottom plot shows a meteor echo that spills over into several range (height) bins. This echo began in a range bin of 98 km and as time progressed moved down into the adjacent height bins. The general shape of the power curve is still gaussian with time.

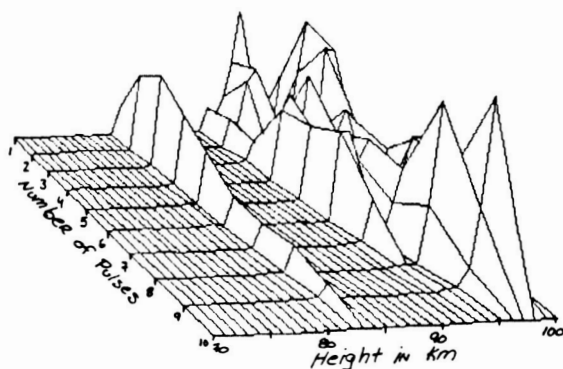
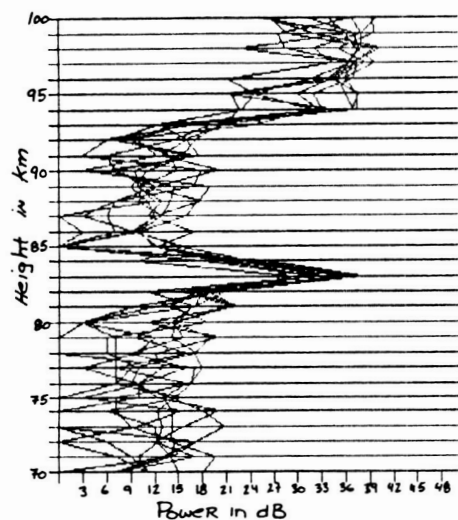
In routine operation of a ST/MST radar, a meteor echo appears; superimposed on the background echoes due to turbulent scattering. Consequently, depending on the length of the coherent averaging interval, a meteor echo can be lost in the background power level due to its short duration. Longer enduring meteor echoes can be selected from the combined data records which include meteor and turbulent echo returns using a post processing algorithm based on spatial and temporal properties of meteor echoes. This was done by AVERY et al., (1983) using the Poker Flat, Alaska MST radar. Based on their selection criterion, meteor echo rates were determined. Figure 3 shows a plot of the meteor echo count and the turbulent echo count as a function of height for three months at Poker Flat. Below 75 km, the meteor echo rate is almost constant with height. If the echoes selected by the algorithm were mostly noise and/or strong bursts of turbulent echoes, then we would expect, by symmetry, a double-peaked meteor distribution, corresponding to both the topside and bottomside of the turbulent echo region. Since the meteor echo profile shows only one peak, we conclude that the algorithm does indeed select, in the majority, true meteor echoes rather than noise spikes or intermittent turbulent echoes.

The profiles of meteor echo rates are, in comparison with the turbulent scatter profiles, much less variable, as seen in Figure 4. The meteor echo profile exhibits a stable, well-defined peak at about 92 km. The location and width of this peak is independent of the behavior of the turbulent scatter profile except during the summer months. During these months, near-continuous presence (80%) of strong turbulent echoes at Poker Flat masks virtually all the meteor echoes present. This is evident by the notch between 70-90 km in the echo height distribution during July. The echo rate corresponding to the peak in the echo height profile varies from about 2.2 echoes/hour in the summer to about 3.8 echoes/hour in the spring. The height of the peak is a minimum in the winter, while gradually rising in the spring and dropping in the fall.

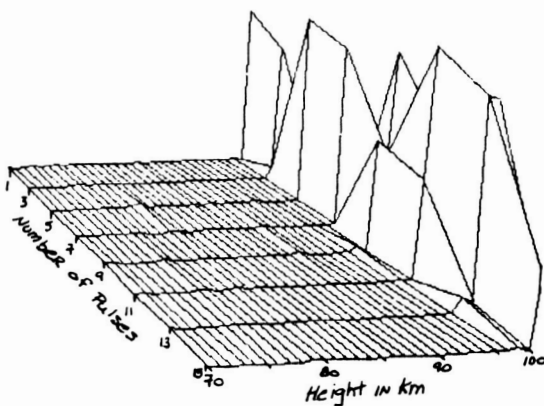
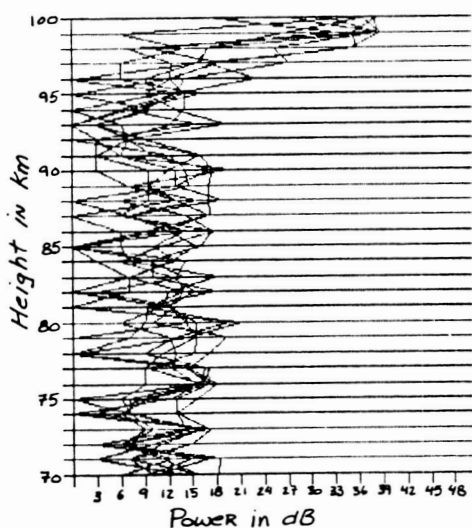
The echo rate is clearly a function of power and antenna size as shown in Figure 5. This figure is a plot of the echo rate for the month of October over several years. During the first year, only one fourth of the antenna was in use and the power was 400 kw. In 1983 the power was brought up to maximum (3.2 Mw) and the full antenna was used. Still the echo rate is low compared to a normal meteor radar because in part, the echoes are not being selected in real time.

In our experiment at Jicamarca, we collected meteor echo return data in real time. This was done using computer software only. The detection and data collection algorithm uses a thresholding criterion for determining

JICAMARCA
Radio Observatory



ECHO TIME 8:35:22
MARCH 26, 1985



ECHO TIME 2:3:24
MARCH 26, 1985

Fig. 2 Example of meteor echo returns from Jicamarca Radio Observatory, Peru.

ORIGINAL PAGE IS
OF POOR QUALITY

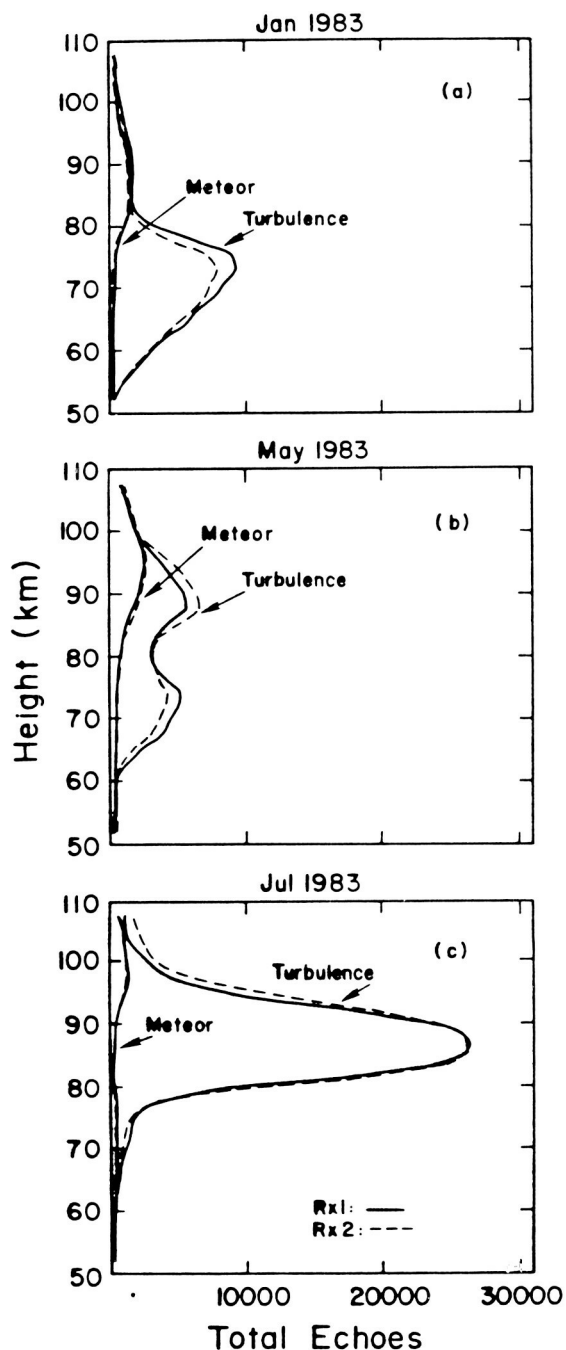


Fig. 3 Histograms of meteor echo and turbulence echo counts as a function of height at Poker Flat. Echoes determined from post processing criterion (from TETENBAUM and AVERY, 1986).

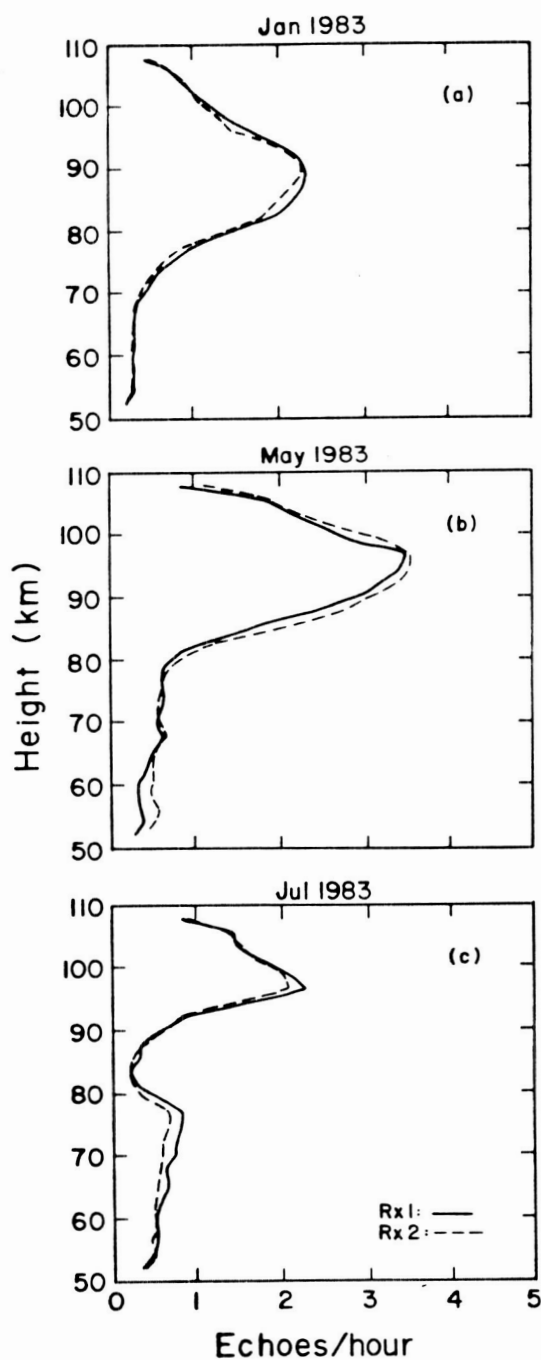


Fig. 4 Meteor echo rate as a function of height at Poker Flat. Echoes determined from post processing criterion (from TETENBAUM and AVERY, 1986).

Height Distribution Of Meteor Echoes - October

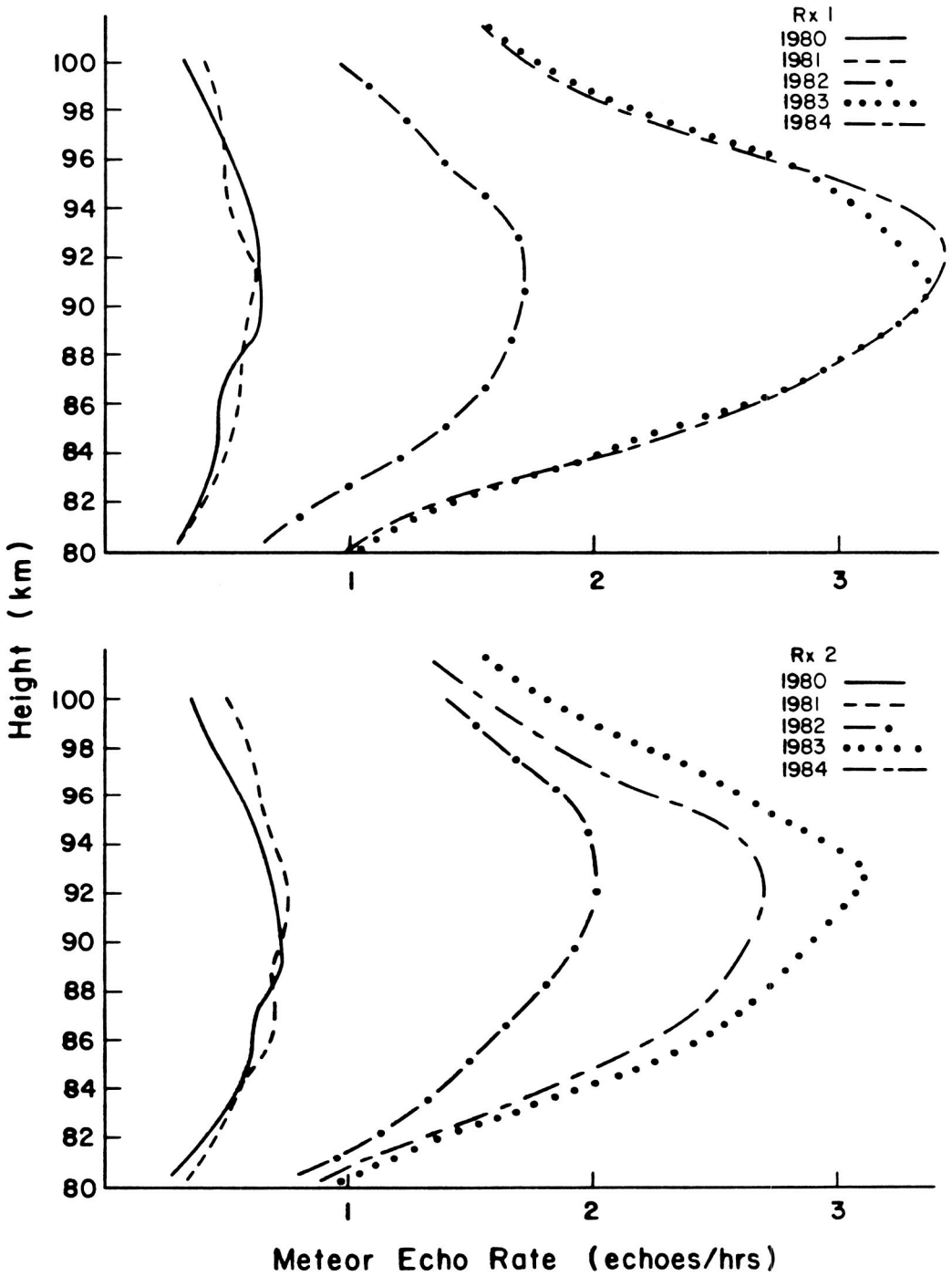


Fig. 5 Height distribution of meteor echoes in October for several different years (from TETENBAUM and AVERY, 1986).

the existence of a meteor echo. The threshold level, selected by the experimenter, is a fixed amount of dB above the background power level.

For the Jicamaraca experiment the threshold value was 9 dB. The background power level is determined at each range bin by a running average of the backscattered power from the previous 32 pulses. This is updated every pulse. Once a meteor echo is detected in a certain range bin, it must persist for at least 4 pulses (27 msec) but for no longer than 213 pulses (1.4 sec). In addition, the range bins on either side of the meteor echo range bin are checked. If the main echo power goes below the threshold value but appears in an adjacent range bin with a power level above the threshold value, we continue to take data in the new range bin. If this criterion is met, then the quadrature signals, range bin, and time of echo occurrence are recorded. Due to computer memory limitations, only the raw data was collected. We were unable to determine velocities in real time. Obviously this is less than ideal if there are a large number of echoes. Real time velocities could be calculated if a small personal computer was available and could be dedicated to the task of calculating Doppler frequencies.

A histogram of meteor echo count versus height is shown in Figure 6. The height profile peaks at higher altitudes than at Urbana, Illinois or Poker Flat, Alaska. This could be due to the equatorial location and position of the antenna beam, which was approximately 4 degrees off vertical. The equatorial atmosphere is more dense than the higher latitude atmosphere. Hence, meteors will ablate at higher altitudes. In addition, our thresholding algorithm may be preferentially deleting meteor trails that reach lower altitudes due to the length of the echo coming from that trail. More work needs to be done on refining the software algorithm. The temporal variation of echo count peaks in the early morning hours as expected.

The average echo duration as a function of height and time is also shown in Figure 6. In general, the echo duration, measured in number of radar pulses, is constant with time and height. We would expect this result given the random distribution of densities of sporadic meteors.

An alternative meteor detection scheme is being worked on at the University of Colorado. This scheme uses new technologies in hardware to incorporate the same detection ideas used in the software technique described above. The meteor echo detection and collection (MEDAC) system can be attached to many ST/MST radars and will operate in parallel with the normal data collection of turbulent echoes. A basic block diagram of the system is shown in Figure 7 (WANG, 1985).

Data is directly obtained from the radar receiver outputs and routed to the meteor system's own analog to digital converters. The system is completely independent of the ST/MST data acquisition system. The meteor selection criterion is now implemented in real-time rather than separating data after collection. The system is a two processor system. A foreground processor is dedicated to the task of echo detection. The processor performs dynamic thresholding on incoming echoes as they enter the system. A meteor will be detected if incoming echoes are above a certain threshold value. Threshold values are dynamically maintained and updated for every signal. The Texas Instrument's TMS32010 microprocessor is the thresholding processor. The FIFO Data Collection subsystem shown in the diagram performs data collection of a meteor when one is present. The main components of the FIFO data collection subsystem are the MK4501 512 by

ORIGINAL PAGE IS
OF POOR QUALITY

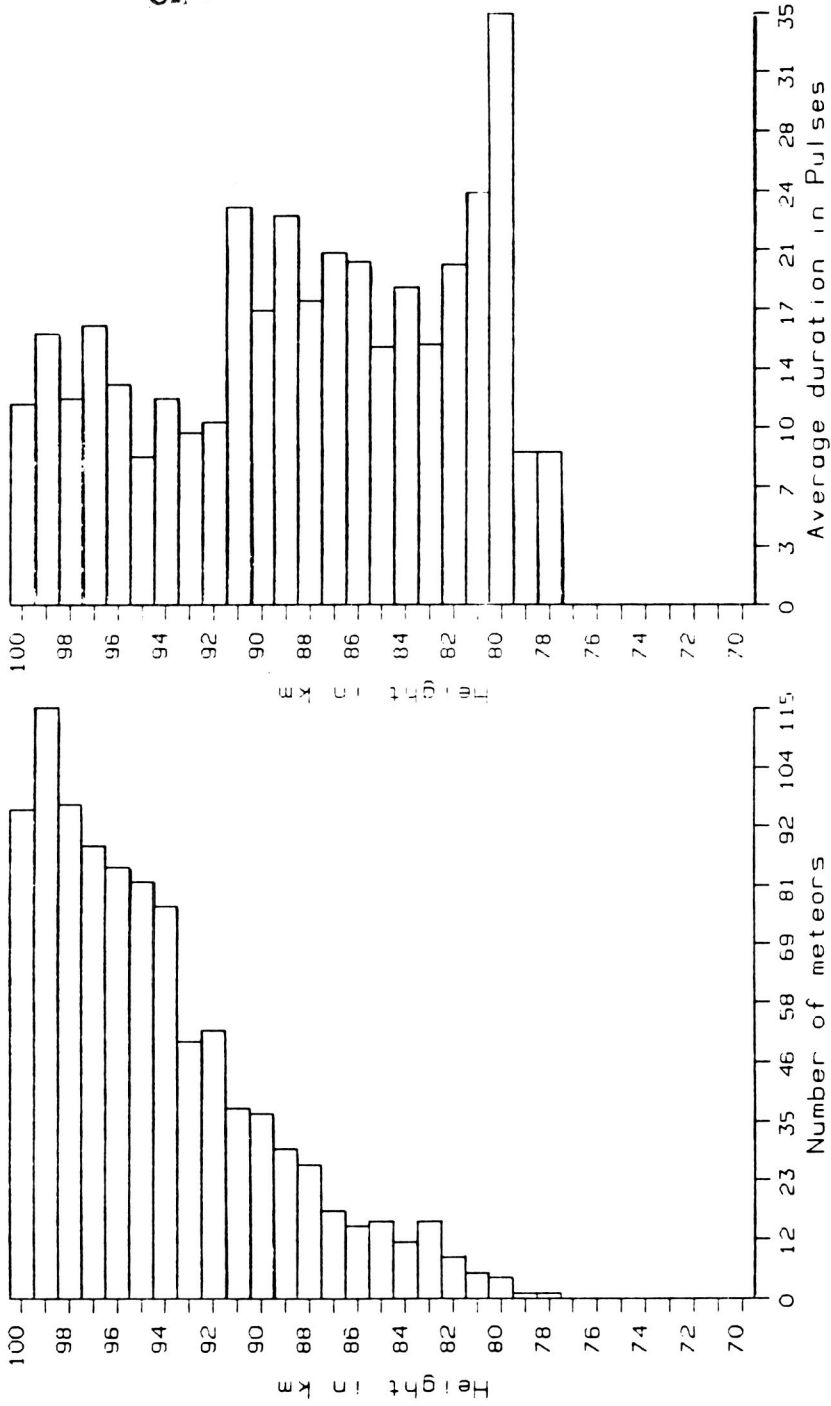


Fig. 6 Histograms of meteor echo count versus height and average echo duration versus height from Jicamarca.

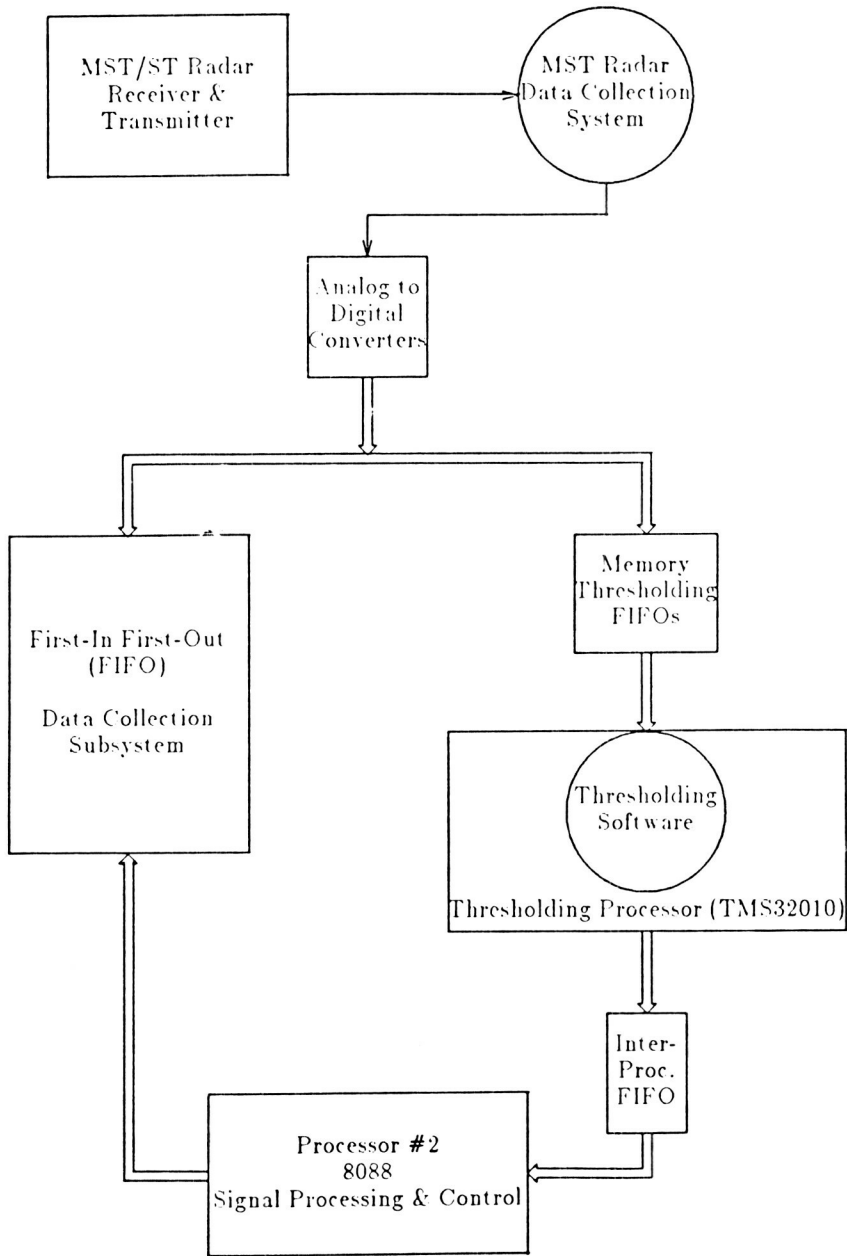


Fig. 7 Block diagram of MEDAC-system.

9-bit parallel input, output, first-in-first-out (FIFO) memory chips. Once a meteor has been found, the range bin and receiver number of the meteor is sent to the second processor through a shared memory between the processors. During operation the second processor is used for signal processing and data analysis of incoming meteors, as well as FIFO management.

A sample of winds determined from the Poker Flat post processing selection scheme is shown in Figure 8. The plot shows the winds determined from meteor echo returns with those determined from turbulent echoes. Clearly the agreement is good. Figure 9 shows a typical least squares sinusoidal fit to the wind determined from meteor echoes. The fit was done to a time series of 30 days of data of overlaying hourly wind averages from the 30 days into a single 24 hour period. Similar fits were done over shorter data sets with equally good results. From this type of data analysis, the tidal amplitude and phase structure can be calculated. Examples of the seasonal structures of the meridional semidiurnal tide from Poker Flat are shown in Figure 10. Because of the extensive data base provided by the Poker Flat, Alaska radar, seasonal changes in the winds and tides can be examined. Also shorter time scale variabilities can be assessed. Figure 11 shows the monthly mean wind climatologies which were determined from the Poker Flat MST meteor echoes.

Meteor echoes can be detected on ST/MST radars. If the radar is powerful (1 MW), enough meteor echoes can be selected from the turbulent echoes generally observed by the radar, to determine the winds and tides over monthly time scales. Using the less powerful ST radars, software or hardware detection schemes can be implemented to determine the mesospheric winds. The potential advantage of using meteor echo returns from ST radars is that it provides a relatively inexpensive way to obtain a measure of upper atmosphere winds. With the implementation of a network of these radars, we would have a significant number of upper atmosphere wind measurement stations. The cost for implementing the software algorithm would basically be the cost of a small computer. Two personal computers would be required to collect and analyze the meteor data for winds in real time. The hardware configuration we are developing will cost approximately \$6,000. This is small compared to the \$150,000 cost estimate for a ST radar.

REFERENCES

1. Avery, S. K., A. R., Riddle, B. B. Balsley, 1983: The Poker Flat, Alaska, MST Radar as a Meteor Radar, *Radio Sci*, 18, pp. 1021-1027.
2. Strauch, R. G., R. A. Kropfli, W. B. Sweezy, W. R. Moniger, and R. W. Lee, 1978: Improved Doppler Velocity Estimates by the Poly-Pulse-Pair Method, *Proceeding of 18th Conf. on Radar Meteorology*.
3. Tetenbaum, D. and S. K. Avery, 1986: Observations of Mean Winds and Tides in the Upper Mesosphere During 1980-1984 Using the Poker Flat, Alaska, MST Radar as a Meteor Radar, Submitted to *J. Geophys. Res.*
4. Wang, S. T.-H., 1985: The Design of a Microprocessor-Based System for Meteor Echo Detection and Collection on a MST Radar, M.S. Thesis, Dept. of Electrical and Computer Engineering, U. of Colorado, Boulder.

POKER FLAT MST RADAR 23 August 1980

— Winds from meteor echoes.
 +-+ Winds from "turbulent" echoes.

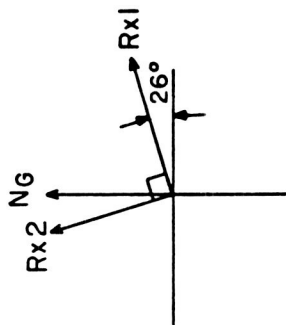
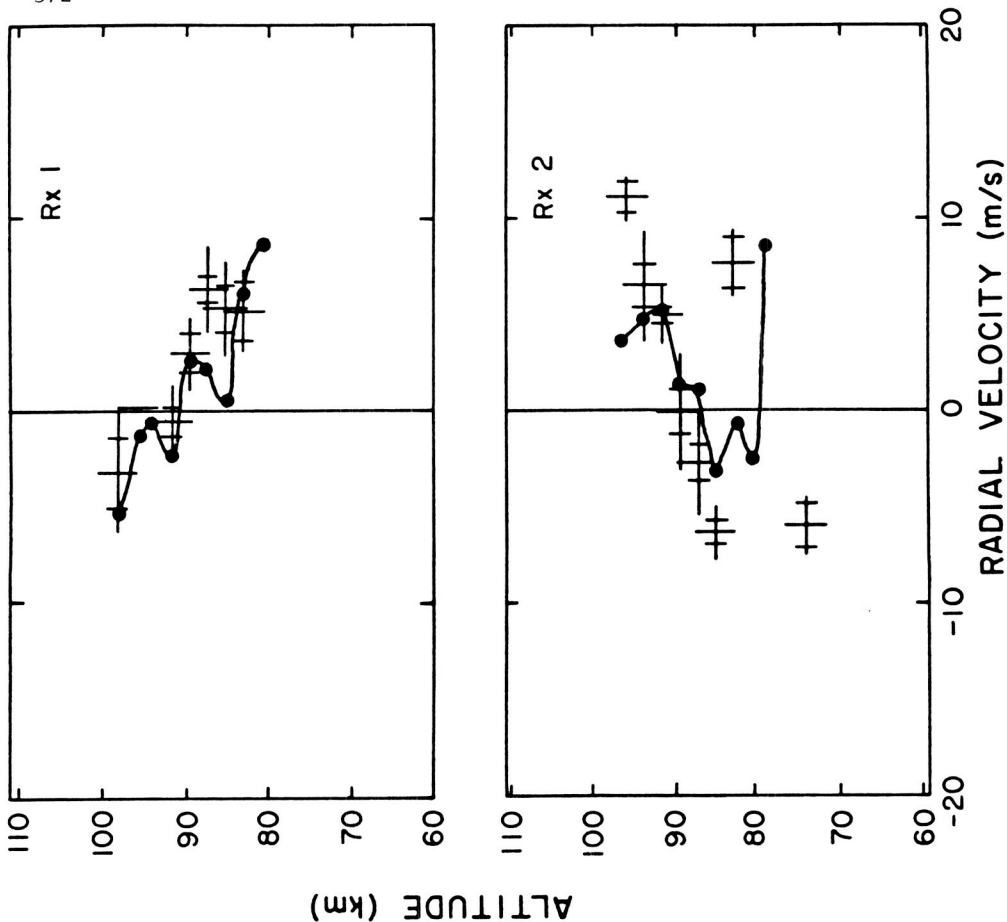


Fig. 8 Comparison of winds determined from meteor echoes with those obtained from turbulent echoes (from AVERY et al., 1983).

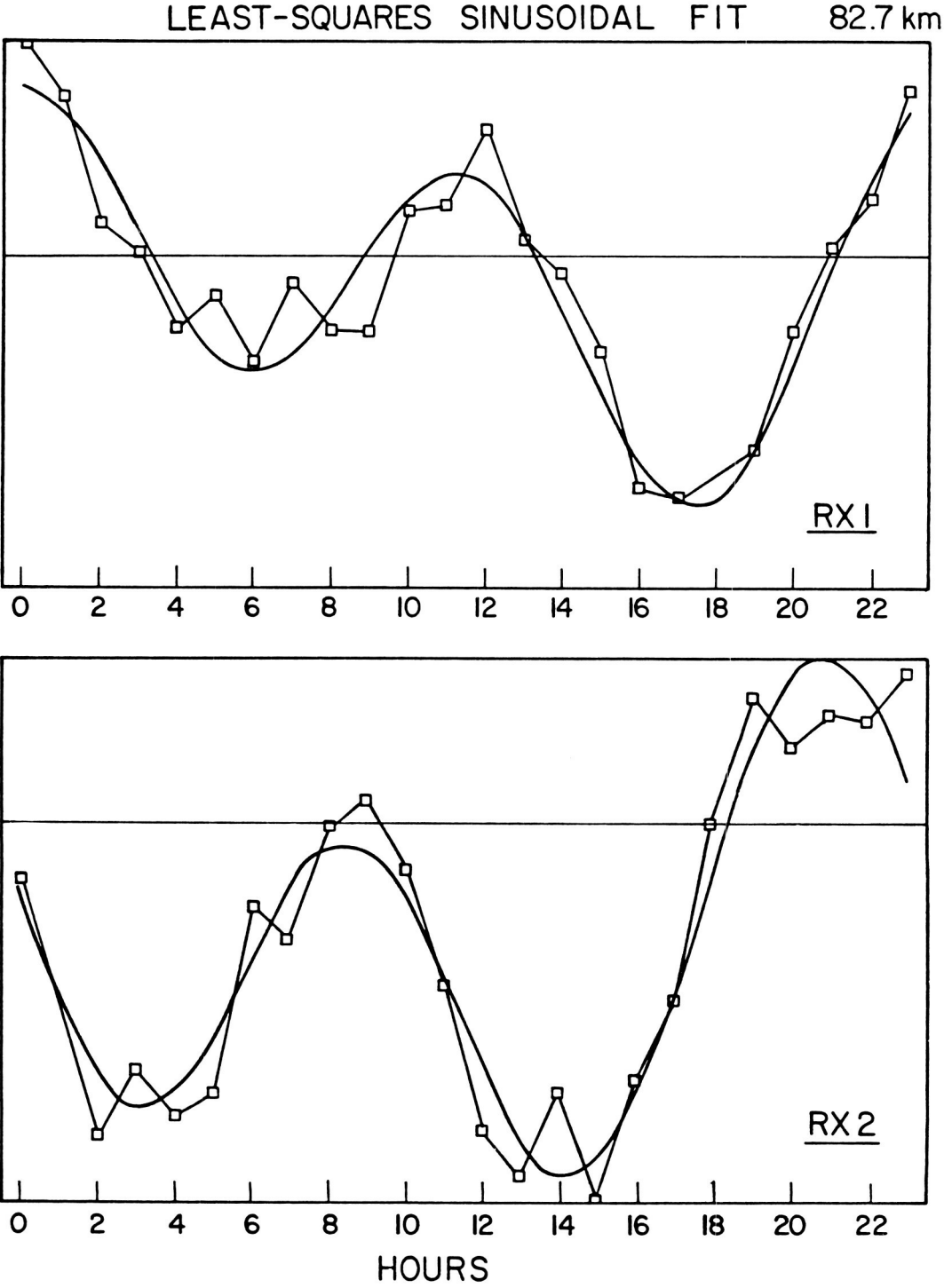


Fig. 9 Examples of least squares sinusoidal fits to Poker Flat data.

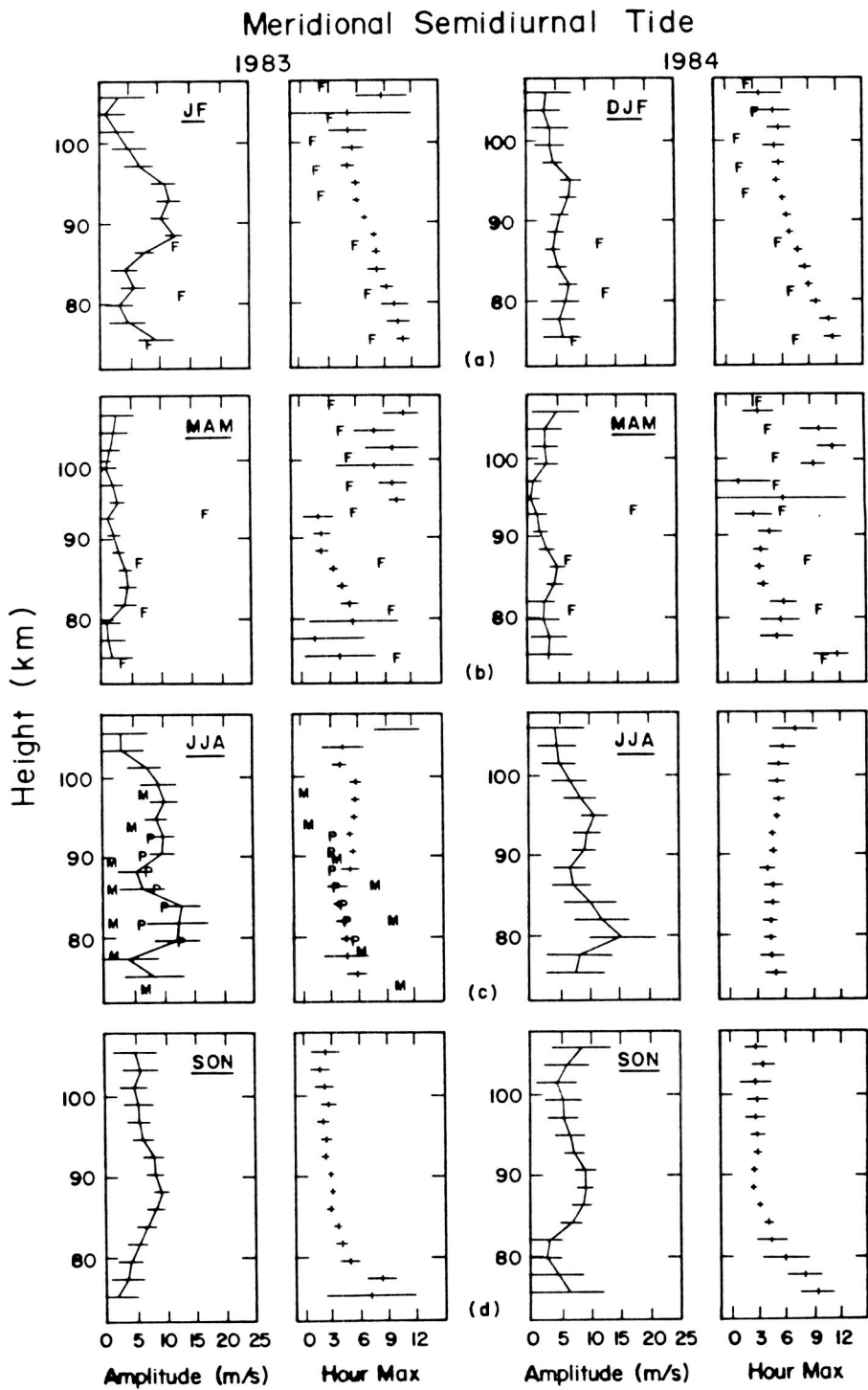


Fig. 10 Seasonal structures of the Poker Flat meridional semidiurnal tide (from TETENBAUM and AVERY, 1986).

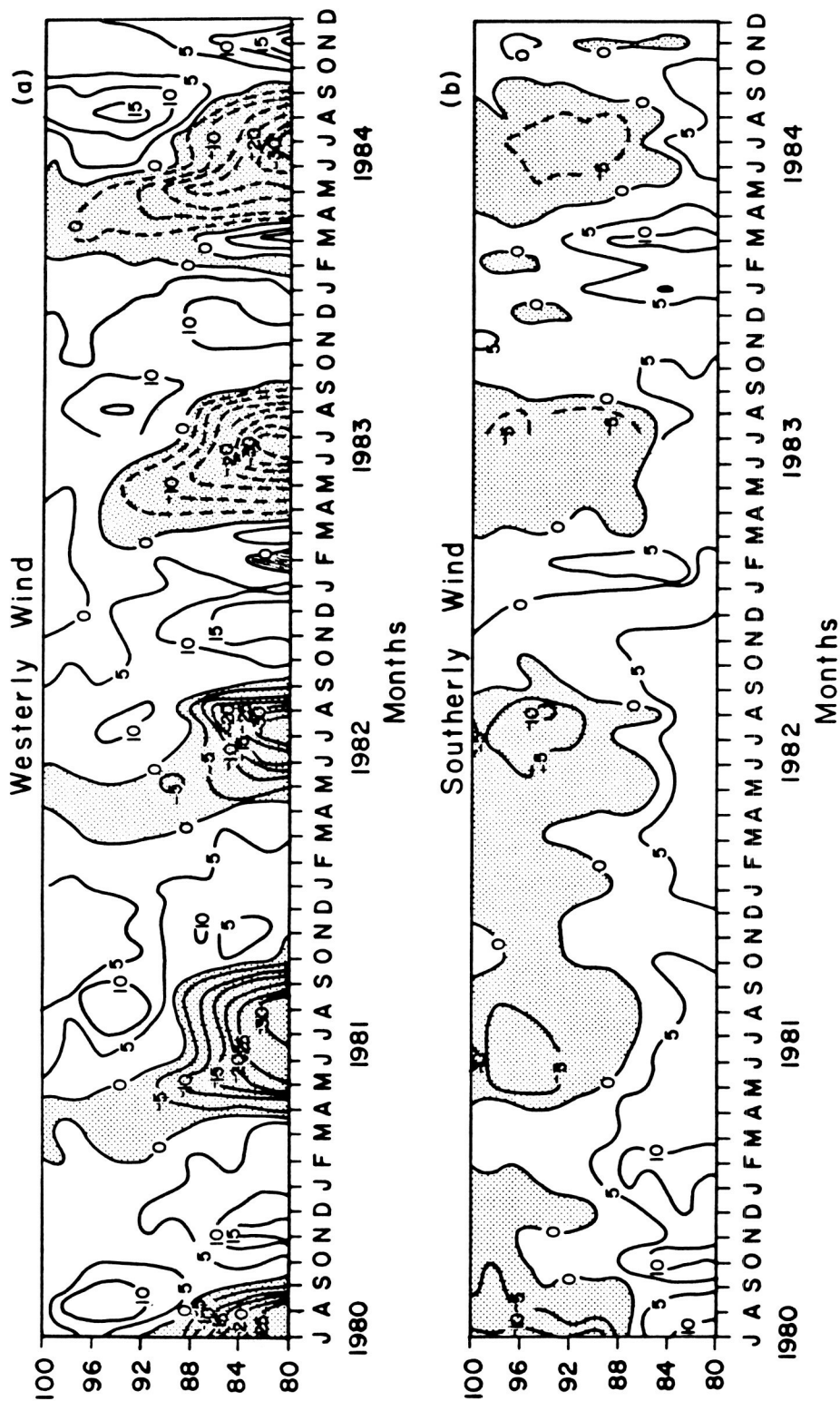


Fig. 11 Monthly mean wind climatologies at Poker Flat (from TETENBAUM and AVERY, 1986).

THE "CYCLONE" METEOR RADAR SYSTEM FOR ROUTINE WIND
MEASUREMENTS IN THE LOWER THERMOSPHERE

I. A. Lysenko, P. P. Mikhailiek, and B. I. Petrov

Institute of Experimental Meteorology (IEM)
Obninsk, USSR

A new meteor wind radar system called "Cyclone" has been devised at the Institute of Experimental Meteorology to extend and update the meteor radar network under the State Committee for Hydrometeorology and Control of the Natural Environment of the USSR. The system is designed for unattended operation.

The "Cyclone" meteor radar system obtains information from four directions simultaneously. Four transceiving aeriels switched by a computerized commutator serve to emit transmitter pulses and receive radio echoes. The commutator connects a series of transmitter pulses with each of the aeriels at a frequency of 100 Hz and breaks scanning to record individual echoes.

The transmitter pulse output is 10 kw, with a pulse duration of 200 μ s and a repetition frequency of 300 Hz. Thus, transmitter pulse energy is 2 J, i.e., the same as most meteor radar transmitters of moderate sensitivity (PORTNYAGIN and SHPRENGER, 1978). The "Cyclone" radar has the potential of recording 6-10 thousand wind velocity values a day.

To automate data processing a special digital device has been developed. The slant ranges are determined using an algorithm which first tests their authenticity and then, on the basis of a number of measurement results, calculates the mean range.

To determine the Doppler shifts the measurement algorithm proposed in PETERSON and NOWAK (1975) was adopted, which involves a displacement of the measured Doppler shift by a few tens of hertz. This algorithm makes it possible to eliminate selectivity with respect to slow velocity meteor drifts (see Fig. 1).

Fig. 2 is a block diagram of the "Cyclone" wind meteor radar system. In "transmitting" mode, the transmitter pulses are passed through one of four controlled gas-discharge arrestors (GDA) to the corresponding aerial while the input of the commuted HFA-receiver cascades is blocked by a segment of $\lambda/4$ line and diodes.

In the "receive" mode, the meteor echo is conveyed through the sensitive HFA receiver to the digital processor.

The "response" output signal is delivered to the input of the preprocessing unit (PPU) which matches the received signals by amplitude, duration and repetition frequency.

If a signal proves useful, a range gate is shaped in the PPU and conveyed to the digital range measurement unit (DRMU). This circuit in

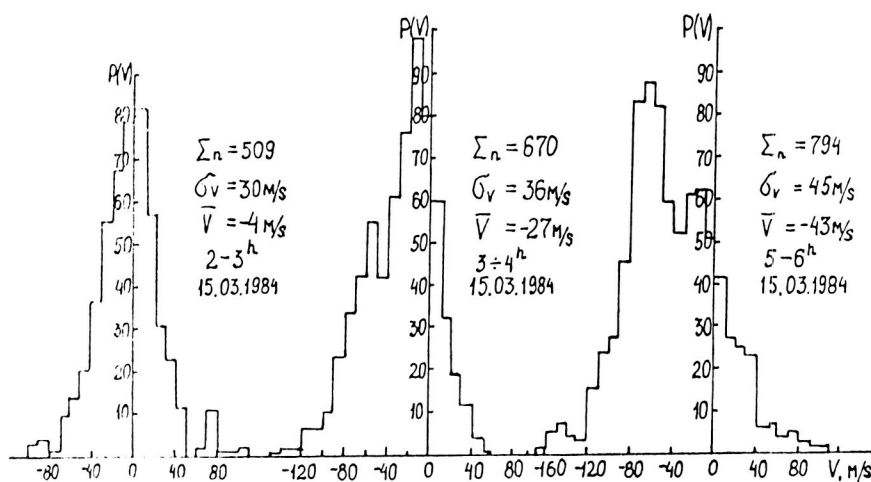


Fig. 1 Distribution of individual wind velocity values as revealed from "Cyclone" measurements of one-hour duration.

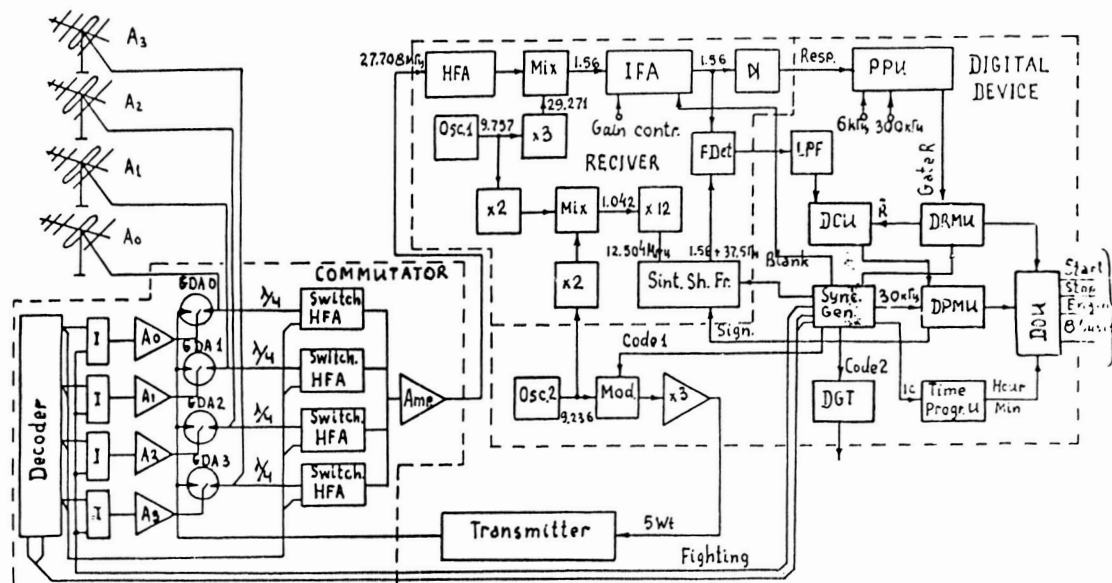


Fig. 2 Functional circuit of the "Cyclone" meteor radar system.

ORIGINAL PAGE IS
OF POOR QUALITY

turn shapes a mean range signal which is then used in the data conversion unit (DCU) as a gate.

The value of Doppler beat period is deduced from the DCU output signals.

The data output unit (DOU) records range, Doppler beat period and sounding direction values on the punched tape. In addition, the DOU conveys echo information averages to the microcomputer "Electronics-C5-12" which averages wind data obtained during ten minute measurement intervals.

The experimental measurements on the "Cyclone" system showed that the instrumental errors for range with a signal-to-noise ratio of 2 equal ± 3 km and $\pm(4-8)$ mps for wind velocities ranging from 0 to 150 mps.

The "Cyclone" experimental prototype has been operating in Khabarovsk practically non-stop since 1982. An example of results obtained in Khabarovsk is shown in Fig. 3.

It is pertinent to note the good agreement of diurnal variations in hourly mean values of wind velocities for zonal and meridional wind components as observed in opposite directions. Some discrepancy in the variations can be attributed to instrumental errors, but more particularly, to the spatial inhomogeneity of the wind field.

References

1. Wind measurements at 90-100 km altitudes by ground based techniques. Ed. by Portnyagin Yu. I., Shprenger K., 1978, Leningrad, Gidrometeoizdat, p. 348.
2. Peterson A., Nowak R. Stanford Meteor Radar System. In "Thermospheric Circulation", Ed. by W.L. Webb, 1975, Moscow, Mir Publishing House, pp. 238-249.

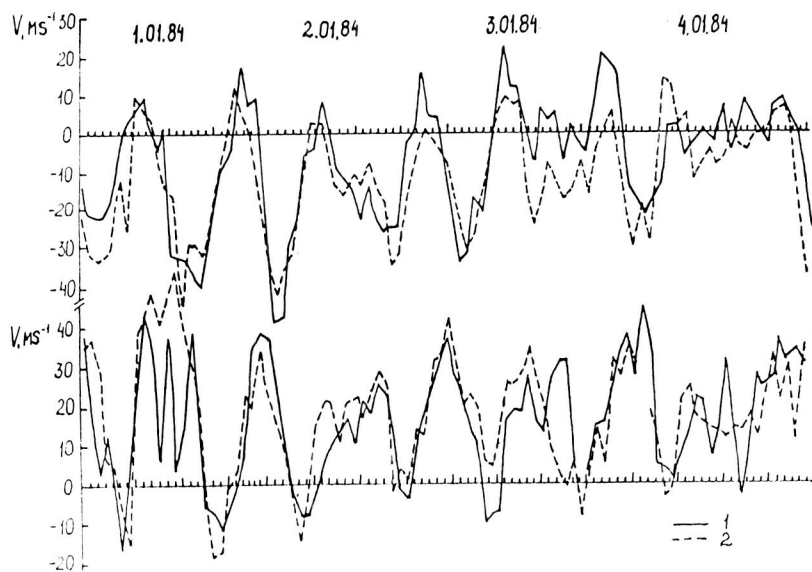


Fig. 3 Diurnal variations in zonal and meridional components of hourly mean wind velocity values as follow from observations in Khabarovsk conducted in four directions simultaneously. 1) N and E components, 2) W and S components.

THE NEWCASTLE METEOR RADAR

Colin Keay

Newcastle University
Newcastle NSW, 2308 Australia

At the time of the First GLOBMET Conference (August 1985) the Newcastle Meteor Radar system was being gradually brought into operation after a period of development extending over more than ten year. The geographical coordinates of the radar installation are $32^{\circ} 36' 42''$ S, $151^{\circ} 50' 50''$ E and its elevation is 130 m. The radar transmitter, receiver and common antenna are located at the field site on a hilltop 34 km from the University of Newcastle campus and a VHF data link is employed to convey the video data from the station to the University of Newcastle, New South Wales, where it is processes in real-time by a multiple microprocessor system which is the most innovative feature of the project.

The nominal parameters of the radar system are:

Frequency	25.2 MHz
Pulse repetition rate	100 Hz
Transmitted pulse width	66 microseconds
Peak pulse power	25 kW
Antenna gain (twin yagis)	14 db (over isotropic)
Antenna azimuth	78°

The antenna polarisation is horizontal. The receiver has a logarithmic IF amplifier. The link transmitter is frequency modulated and operates at 471.5 MHz.

A block diagram of the system is shown in Figure 1.

Most of the block diagram is self-explanatory, except for the multiple-microprocessor meteor signal analyser which is shown in more detail in a further block diagram, Figure 2.

The initial objective when the project was commenced was to develop an entirely digital analyser capable of recognizing meteor echo signals and recording as many of their parameters as possible. It was desired that the smallest possible meteor echoes should be registered while maintaining the false-alarm rate (the number of spurious echoes) close to zero. A meteor echo simulator was built (Graham, 1969) which generated artificial echoes having a wide range of characteristics in the presence of both Gaussian noise and Poissonian impulse noise. This permitted realistic tests of the digital meteor signal analyser during its development (KEAY and KENNEWELL, 1979). In particular, the essential role of the impulse suppressor stage was demonstrated. A rigorous theoretical treatment of the analyser was published later (KEAY, BUTLER and KENNEWELL, 1976) when theory and test results each showed that the analyser improved the detection of small meteors to an

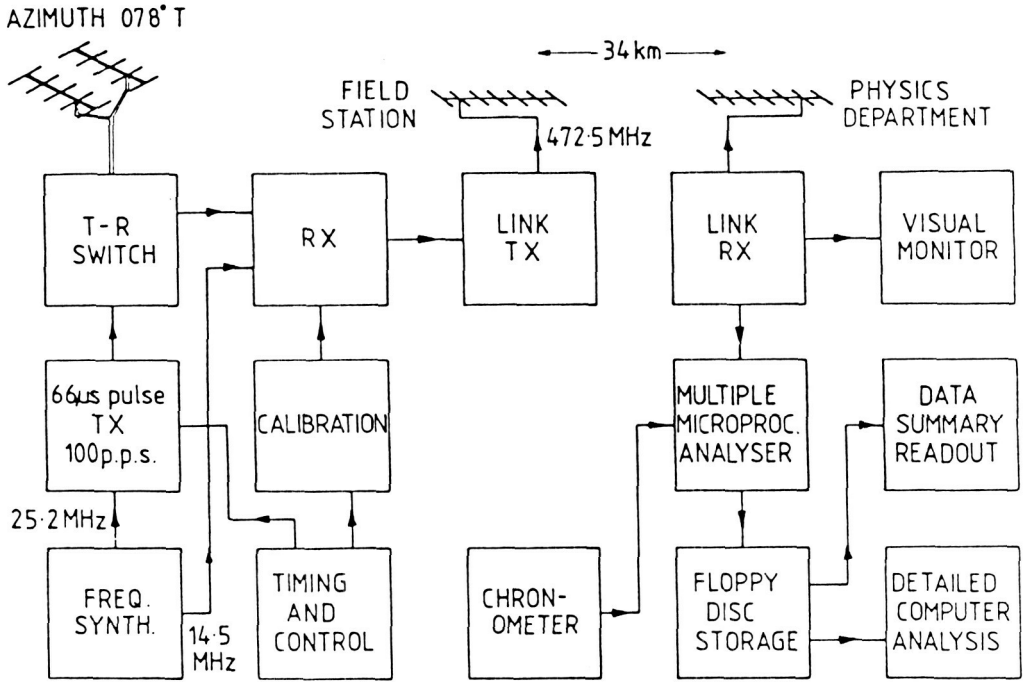


Fig. 1 Block diagram of the Newcastle Meteor Radar.

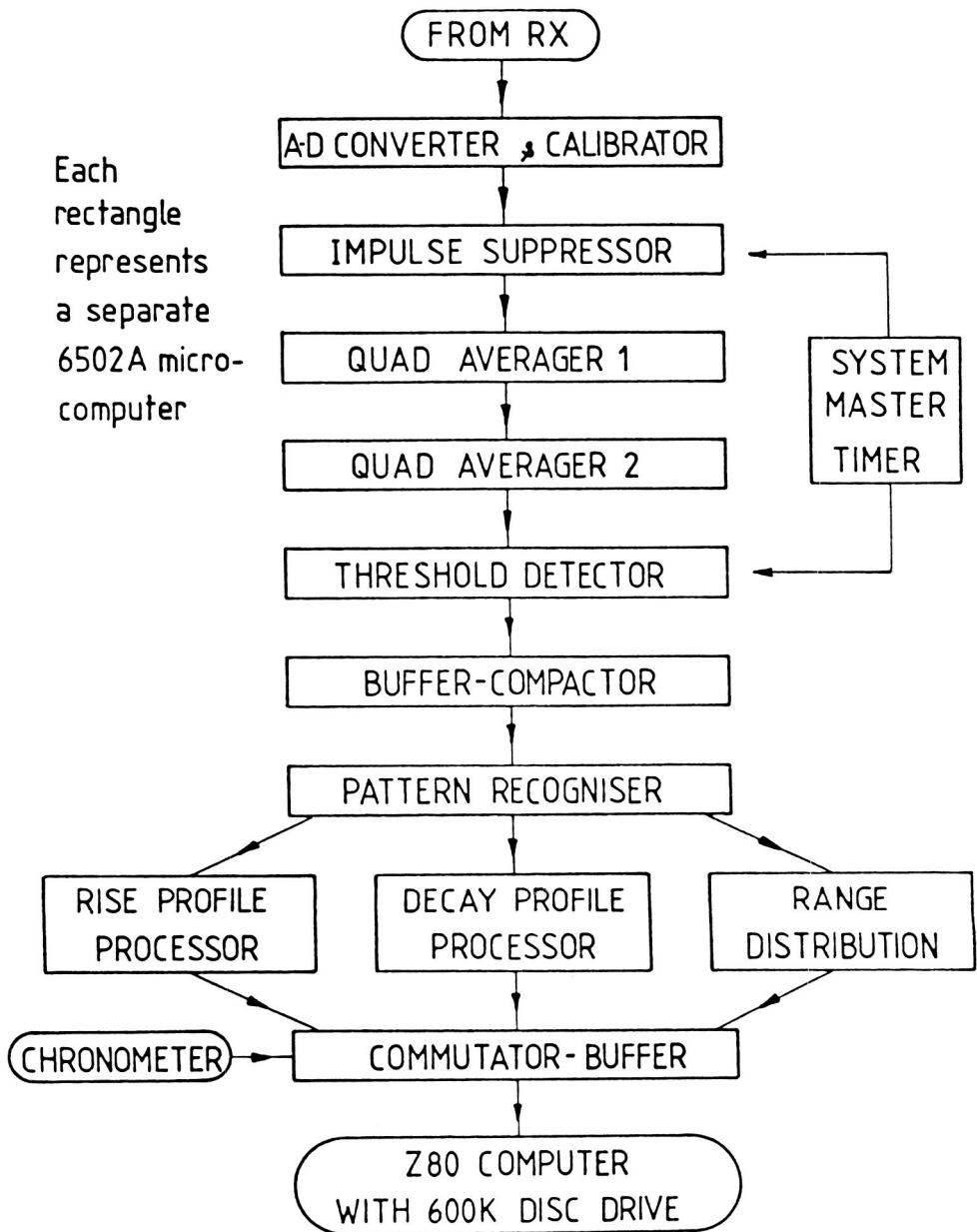


Fig. 2 Multiple microprocessor meteor signal analyser.

extent equivalent to a factor of four or five increase in transmitter power by comparison with a system without the analyser.

When the performance/cost ratio of microprocessors fell to the point where it became desirable to replace the hard-wired digital logic of the meteor signal analyser, a detailed comparison of all readily available microprocessor chips was undertaken (KEAY 1980). It was found that 16-bit types were no better than 8-bit types for the task. The most suitable microprocessor at the time proved to be the fast (2 MHz clock) version of the 6502 (the 6809 would now be a better choice) and it was chosen. Its powerful memory-oriented instruction set, including its fast zero-page instruction mode, enabled it to complete a useful processing loop within the 33 microseconds available in a system achieving 5 km range resolution. All programming is in machine code generated by a cross-assembler on a different microcomputer and loaded directly into type 2716 eeproms which control the 6502s.

The use of microprocessors made it possible to extend the analyser to include some echo parameter extraction in real-time before the data is written to disk, rather than perform all analysis of the raw meteor data later on a separate computer.

Details of the design of the microprocessor circuit board, memory map and interfacing have been published (ROGERS, KENNEWELL and KEAY, 1982).

The first microprocessor stage controls the analog-digital converter driven from the link receiver. It locks onto a negative-going pulse coincident with the transmitter pulse to synchronise the systems. Then it registers the level of the calibration pulse, which follows the synchronisation pulse, to set the reference level of the converter which then samples and digitises the analog signal every 33 microseconds for transfer to the subsequent analysis stages.

The impulse suppressor state is quite vital in preventing the averager stage(s) from generating false echoes from high amplitude noise spikes. The suppressor truncates all signals at any given range to no more than twice the amplitude of the preceding signal at that range. Thus the high energy Poisson distributed noise is reduced to a low energy pseudo-Gaussian component which is further reduced by the averager algorithm.

In the early stages of the development of the system, an exponentially weighted average algorithm was employed in order to reduce the memory storage requirements of the system. Upon changing to microprocessor techniques the availability of ample memory allowed the use of better averaging algorithms within the time constraints of the system. It was shown (ROGERS 1982) that two identical consecutive microprocessor stages, even averaging four equally weighted samples in

successive sweeps, produced an overall 1,2,3,4,3,2,1 weighting which was optimal for small meteors and yielded a noise variance reduction of 5.8. Much more complicated algorithms are required to gain further reduction in the noise variance.

The next stage is the threshold detector which not only rejects signals below a set level, but also rejects any signal which lasts for less than six successive sweeps. This further reduces the acceptance of false echoes by the system. This is very evident when local thunderstorms and other sources of noise intrude, but the system cannot cope with strong coherent interference from either back-scattered clutter or another transmitter.

Figure 3 shows the improvement in meteor echo detectability due to action of successive states of the signal analyser.

Following the threshold detector it is no longer necessary to process every range interval. Thereafter only the identified echoes are dealt with, allowing much more time for processing the individual echoes. The microprocessor stage referred to as the buffer-compactor acts as a buffer which stores only those echo amplitude values above the threshold level. Each group of values representing a single meteor is prefixed by the range value and is separated from the next by a single zero-byte delimiter instead of the many zeroes between successive echoes. In this way each scan is compressed in time to allow it to be passed on to the next stage as a compact packet. This removes the need for subsequent processing to strictly synchronised with the sweep rate. It is effectively a desynchronising stage.

The next stage carries the packet technique a step further by applying a pattern recognition approach to ensure that meteor echoes which drift in range, or fade and reappear, are associated with just a single meteor which is given an identification number. Only when a given echo has been absent for a period of time equal to its total echo duration is it deemed to be finished and passed on to the next stages, which may now operate in parallel.

At present the only two parallel stages are one which produces a cumulative echo count histogram as a function of range and another which derives the slope of decay of each echo. The histogram provides a check every six minutes on the range distribution of all echoes. This has value as a warning of the occurrence of false echoes and acts as a diagnostic of problems with the system. The decay-slope is, hopefully, the first of several which will examine various parameters of the meteor echoes. Figure 4 demonstrates how the information obtained from the meteor echoes will be treated to yield useful data on the meteor flux detected by the system.

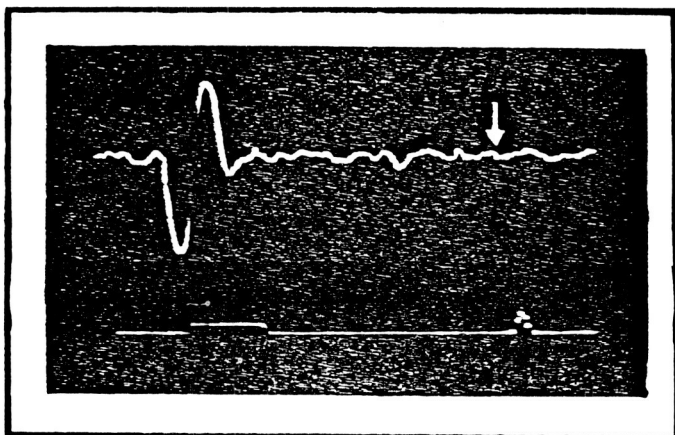


Fig. 3 The upper trace is the output signal from the link receiver, showing the negative transmitter synchronism pulse, the positive calibration pulse and noise with a meteor echo hidden within it. The lower trace is the processed output from the threshold detector, revealing a distance meteor echo. The sideways offset is due to the processing delay in the five microprocessor stages producing this result.

ORIGINAL PAGE IS
OF POOR QUALITY

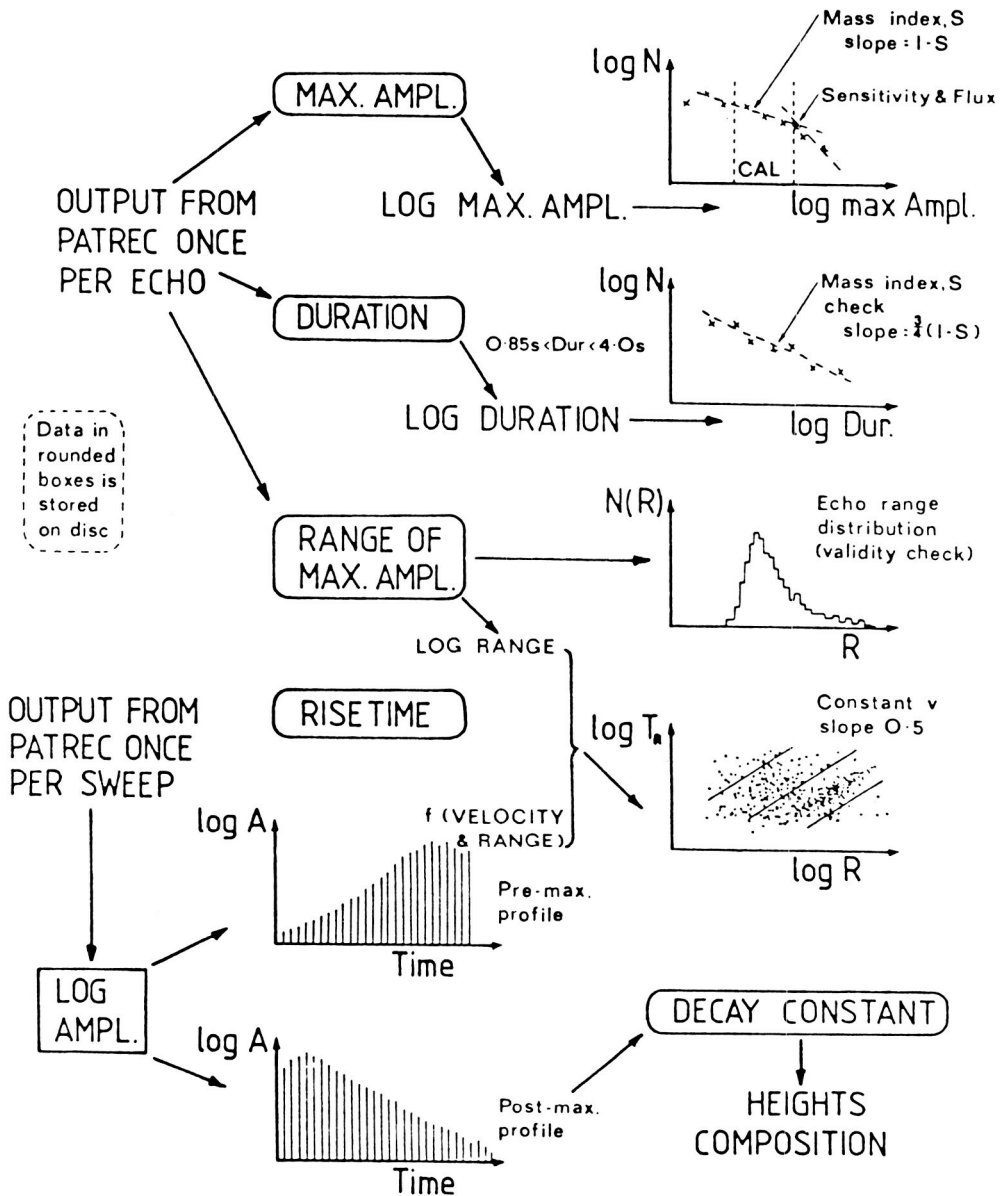


Fig. 4 Overview of the data reduction and analysis scheme.

Finally, the outputs from the parallel stages are brought together in an output stage which assembles the data for transfer out of the analyser to a Z80-based microcomputer which runs under the CP/M operating system and has a 1.2 megabyte floppy-disk drive for data storage.

Vital contributions to this project have been made by John Kennewell, Jim Butler and Lyndon Rogers. Others who have provided much needed assistance at various times include Jack Baggaley, Bob Evans, Ian Grahame, Tom Kaiser, Brian Mason, David Stevenson and Bruce Wood. Financial assistance from the Schmidt Bequest, the University of Newcastle and the Australian Research Grants Committee is acknowledged.

REFERENCES:

1. Graham, I.C., M.Sc. thesis, University of Newcastle, 1969.
2. Keay, C.S.L. and Kennewell, J.A., J. Phys. E: Scientific Instruments, 4, 376-381, 1971.
3. Keay, C.S.L., Butler, J.E. and Kennewell, J.A., J. Phys. E: Scientific Instruments, 9, 25-30, 1976.
4. Keay, C.S.L., Practical Computing, 3, 12, 72-73, 1980.
5. Rogers, L.J., Kennewell, J.A. and Keay, C.S.L., Australian Physicist, 19, 134-135, 1982.
6. Rogers, L.J., M.Sc. thesis, University of Newcastle, 1983.

N88-14557

NEW APPROACHES TO SOME METHODOLOGICAL
PROBLEMS OF METEOR SCIENCE

David D. Meisel

Department of Physics and Astronomy
State University College
Geneseo, New York

ABSTRACT: Several low-cost approaches to continuous radiosscatter monitoring of the incoming meteor flux are described. Preliminary experiments have been attempted using standard time-frequency stations WWVH and CHU (on frequencies near 15 MHz) during nighttime hours. Around-the-clock monitoring using the international standard aeronautical beacon frequency of 75 MHz has also been attempted. The techniques are simple and can be managed routinely by amateur astronomers with relatively little technical expertise. If a source of reliable long-term funding could be found, it is proposed that a volunteer network of amateur radiometeor observers be established to provide a valuable long-term baseline system to supplement professional studies.

Time-series analysis can now be performed using relatively inexpensive microcomputers. Several algorithmic approaches to the analysis of meteor rates will be discussed. Implementation of these on personal computers allow fairly sophisticated algorithms to be performed at relatively low cost including production of the power-spectrum of the daily and hourly rates even if there are missing data points or segments. Methods of obtaining optimal filter predictions of future meteor flux are also discussed.

For nearly three-fourths of a century, C.P. Olivier, the founder of the American Meteor Society, collected data on the hourly rates of meteors seen by single visual observers. This information formed the basis of four catalogs (Olivier, 1960, 1965, 1974a, 1974b) giving the average visual meteor rates seen for each hour of the night during the year. Three of the catalogs were for the northern hemisphere and one for the southern hemisphere. The northern hemisphere catalogs were average rates over the years 1901 through 1958, 1959 through 1963, and 1964 through 1972. With the introduction of radiosscatter detection methods, professional interest in such visual work (now done only routinely in the U.S. by amateur astronomers) waned considerably and in the decade following the publication of the last Olivier catalog, no serious attempt was made to update this compilation. Some recent developments now indicate that a radiometeor rate catalog based on amateur observations and linked statistically to visual and radar meteor rates is feasible and valuable.

First, it is becoming increasingly expensive for professional meteor observatories to maintain high-power radio transmissions on the continuous basis needed for a world-wide, routine patrol of meteor flux. Secondly, amateur radio operators and amateur astronomers around the world are presently acquiring receiving equipment with a sensitivity comparable to that in the hands of professional radio astronomers of one or two decades ago. Thirdly, these same amateurs are now in possession of one or more

microcomputing systems which are capable of tabulating, storing, and processing large amounts of meteor monitoring data continuously and unattended.

In an attempt at harnessing this large pool of unused talent, the American Meteor Society has carried out some preliminary experiments involving the use of low-power radio beacons or other readily available ambient signals to estimate the meteor flux. The immediate goal of this work is to use presently active, visual meteor observers to calibrate each radio system back to the set of visual hourly rate observations that were obtained in the years before routine radioscatteer observations were available.

The purpose of this paper is to review some of the amateur radio meteor work which has already been done by our group of observers and others and to sketch some of the methodology we hope to bring to bear on the problem of defining a radio equivalent of the visual rates. In the long-term, it is hoped that an index of visual/radio meteor activity (comparable in reliability to the familiar sunspot number/10 cm flux index of solar activity) can be developed.

Members of the American Meteor Society were among the first amateur astronomers to obtain scientifically useful VHF observations of radio meteors (HOUSTON, 1958). But domination of the field by professionals and interest in radioscatteer for defense communications soon led to a hiatus in its use for serious amateur work at least in North America. In 1983, as a part of the amateur observational activities of the International Halley Watch, an attempt was made by the AMS to revive interest in amateur observations, particularly by those in North America. Japanese amateur observers already had an active radio meteor group and were making observations of the Halley-related showers well before the critical 1984-88 period. It was hoped North American amateur astronomers could follow their lead. Some of the results reported here were obtained as a part of IHW activities, but the program to maintain a continuous radio meteor patrol is the responsibility of the AMS.

Amateur meteor observers in Japan and Europe have carried out a number of interesting passive radioscatteer experiments over the last decade. In Japan, the results of the Nippon Meteor Society and the FM Meteor Society have been especially noteworthy and sophisticated. Their work is based mainly on observations of domestic FM radio transmissions around 80 MHz and have been carried out daily for several years (FUKUDA, 1982; SHIMODA, 1982, 1983; SHIBATA, 1983a; SUZUKI, 1982, 1983). While these data are extremely valuable for flux determinations because they have been made daily for several years, they are not continuous over a full 24-hour period. Typical European amateur results with a similar degree of technical sophistication have been described by SCHIPPKE (1981). Results on frequencies of approximately 28, 50, 63, and 144 MHz are described in the most detail, but some observations in the HF bands were apparently also tried.

In North America, astronomically useful amateur radiometeor observations have lagged considerably behind those obtained in Europe and Japan. There are several reasons for this which should be mentioned. First, ambient radio transmissions in the 30-50 MHz range, until recently,

have been mainly of an intermittent nature. In the 50-89 MHz television bands, the transmissions are reasonably continuous, but strong local stations are often found on every available channel. In the commercial FM band (89-108 MHz) station crowding has become so chronic that a "clear" channel is almost never found. While meteors can certainly be detected on North American television and commercial FM transmissions, the transmitter powers are so high, the broadcast schedules so skewed (often avoiding the important early morning hours), and the stations so widely scattered that they really seem unsuitable for use as a meteor flux standard. The only results achieved in North America so far with a sophistication comparable to that available in Japan and Europe were obtained by PILON (1984) in Canada (Figs. 1, 2). Although outstanding from a technical point of view, unforeseen circumstances have resulted in termination of this volunteer program. Amateur radio operator M. Owen in Canton, New York has recently obtained additional FM observations and it is hoped this can help offset the loss of the Pilon program (Figs. 3, 4, 5).

In a paper circulated to members of the American Meteor Society, I proposed using available, low-power aeronautical beacons to serve as continuous monitoring devices for obtaining meteor flux information (MEISEL, 1977). In particular, the use of the standard 75 MHz frequency of the instrument landing system (ILS), was advocated. The first results using this frequency were obtained by BLACK (1983) in Florida and were described in several astronomical publications. When this system was later moved to an urban area (Atlanta, Georgia), however, it failed to perform properly because of overwhelming groundwave intensity.

Since the 75 MHz band is adjacent to the 73 MHz radio astronomy band, it is possible to modify published equipment designs (SWENSON and FRANKE, 1979) to use on this aeronautical channel. The feasibility of this has been demonstrated by G. Pokarney working with AMS Hawaii Group led by M. Morrow. Most of the major showers have now been sampled from this near-equatorial station using this modified equipment.

In January 1983, the Federal Communications Commission of the United States approved automatic beacon control for selected amateur radio bands including 28 MHz and 50 MHz. One AMS member, J. Hollar, pioneered transmissions in the 50 MHz band and several others are now planned. The main disadvantage of this approach is that transmitter facilities must be constructed and maintained.

The use of HF international broadcast frequencies for detecting meteors have been described (SETTEUCATI, 1960), but because these broadcasts are generally limited in length and have frequencies which are changed seasonally to maximize ionospheric reflection, they are not really suitable for serious meteor studies.

Because of the well-known frequency dependence of meteor trail reflectivities, the highest degree of sampling completeness of meteor flux will be obtained with the lowest frequencies. Thus some efforts to find suitable HF frequencies have been made. In 1975, during the last sunspot minimum, it was possible to utilize the Time Standard transmissions of station CHU, Ottawa, Canada for nighttime meteor scatter observations on 14.670 MHz during the major showers from Geneseo, New York. By late 1984,

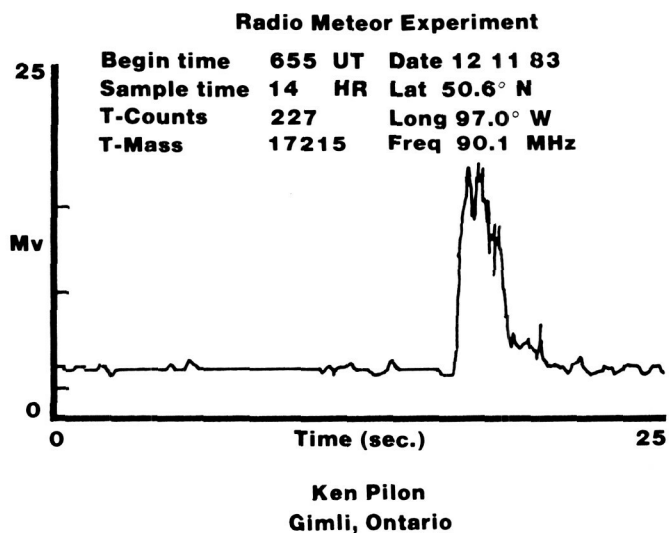


Fig. 1 Typical meteor echo measured as a forward scatter signal from a commercial FM radio station (from PILON, 1984).

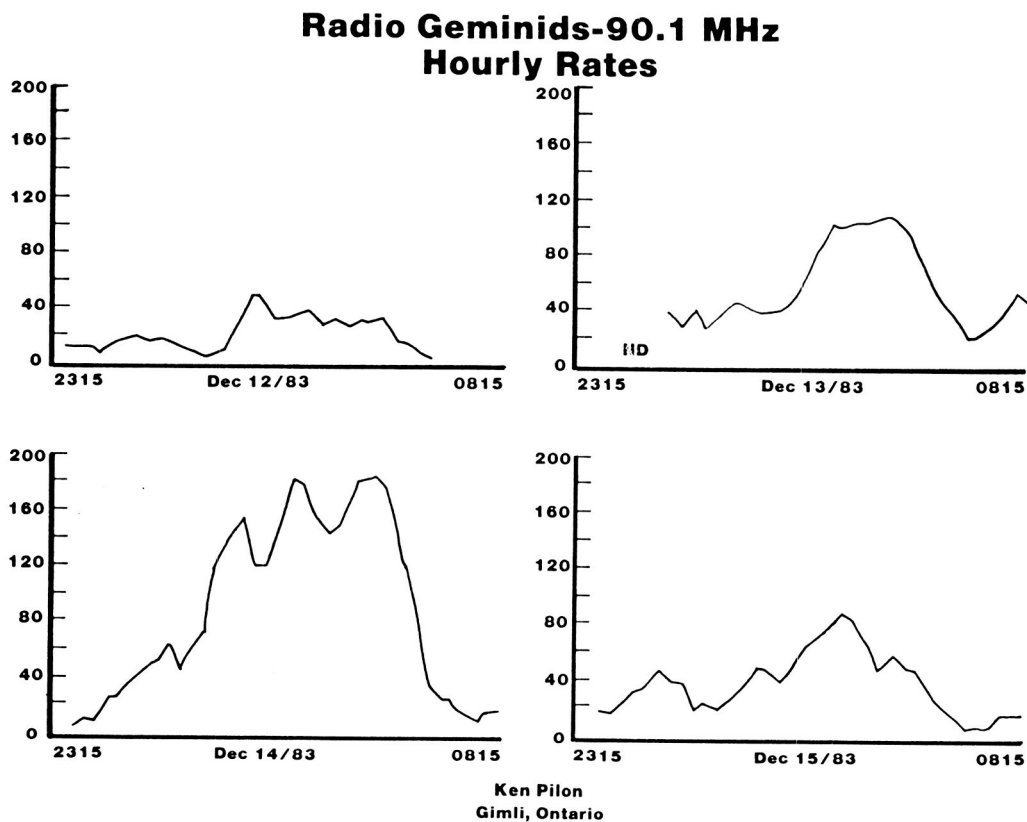


Fig. 2 Data rates measured as in Fig. 1 for the Geminids of December 12-15, 1983 (from PILON, 1984).

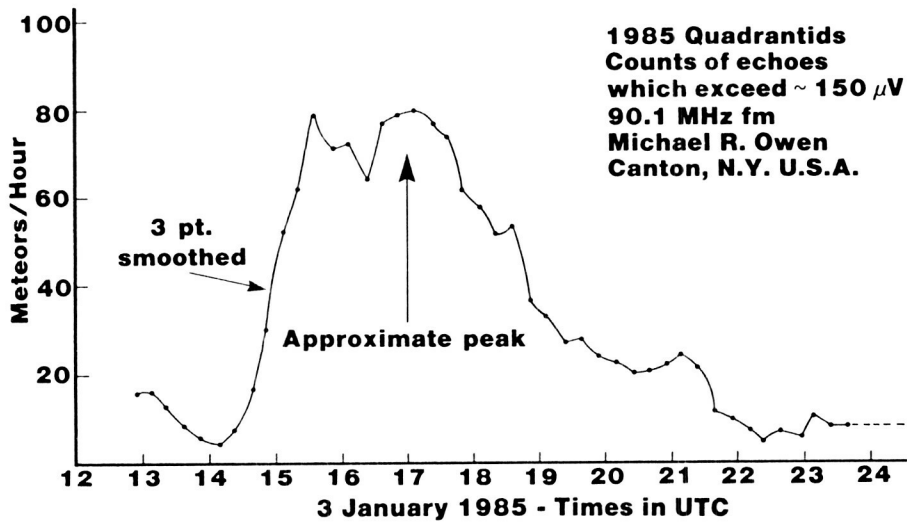


Fig. 3 Hourly counts during the Quadrantid shower, January 1985
M. Owen, private communication, 1985).

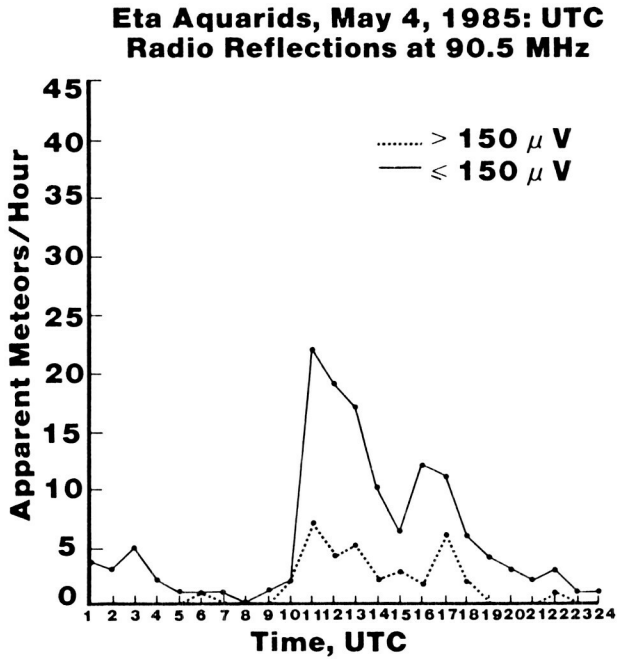


Fig. 4 As for Fig. 3, Eta Aquarids, May 4, 1985.

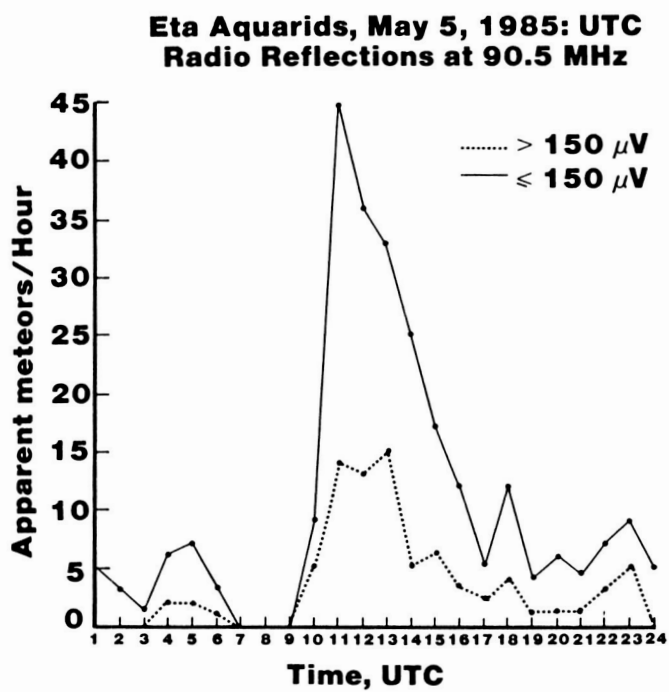


Fig. 5 As for Fig. 3, Eta Aquarids, May 5, 1985.

a low enough level of solar activity was achieved so that these were started once again (Figs. 6, 7). Similar results using WWVH on 15 MHz are being obtained by the AMS Hawaii Group (Fig. 8). All results so far indicate that at 15 MHz, the background flux is reasonably constant and the main effect of showers is to increase the number of longer-duration echos. This is in agreement with the findings of LINDBLAD (1980) who was studying the serial correlation of radio meteor echos.

A table of hourly meteor rates is really a time-series and so all of the powerful statistical techniques available from information theory for dealing with a time-series can be used to calibrate and analyze the data obtained. OLIVIER's first catalog of visual rates covers much too wide a range of years to be used without modification so as a part of the radio rate calibration, it is planned to go back to the original data and subdivide the information as much as possible (4 year blocks seem to be most reasonable since these represent two cycles of moonlight modulation of the results). The second and third catalogs were compiled for much shorter periods (5 years and 8 years) and therefore will not require quite so much work to repatriation. It is hoped that there will be enough extant material to at least go back to 1945 when radio rates began to be taken in a systematic way.

Time-series analysis of meteor data has rarely been undertaken, but it is a powerful technique that deserves to be used more. Among the few studies of meteors using time-series analysis are the papers by LINDBLAD (1980) and SHIBATA (1983b and 1983c). The LINDBLAD paper and the first SHIBATA paper deal with the problem of serial correlation of meteor rates. The second SHIBATA paper deals with prediction of meteor rates. I will return to the question of prediction presently. In all cases so far only equally-spaced data have been analyzed, but this is an unnecessary restriction.

It is well-known that time-series analysis can be approached most conveniently through the Fourier transform formalism (see SOLODOVNIKOV, 1960; RICE, 1954 or VAN DER ZIEL 1970 for example). The amount of literature dealing with standard time-series analysis is truly prodigious and no attempt will be made here to review much of it here. See the referenced works for a list of helpful texts and papers available in English.

There are several reasons why time-series analysis is not done more frequently. One is simply the large amount of computation required, but the wide availability of "micro" and personal computers will almost surely take care of this. Even if sufficient computational power is available, one of the most awkward problems to deal with is the question of what to do with samples taken at times and longitudes that are not equally spaced. A similar one is what to do with data with gaps due to interference or equipment problems. The data shown in the figures are good examples of such problems. In two papers, I have discussed several methods for handling some cases of particular astronomical interest (MEISEL, 1978, 1979). I will now emphasize and elaborate upon several approaches that are useful in analyzing meteor rate data.

Radioscatter-CHU 14.67 MHz 10 Min Cts. 08-10 UTC

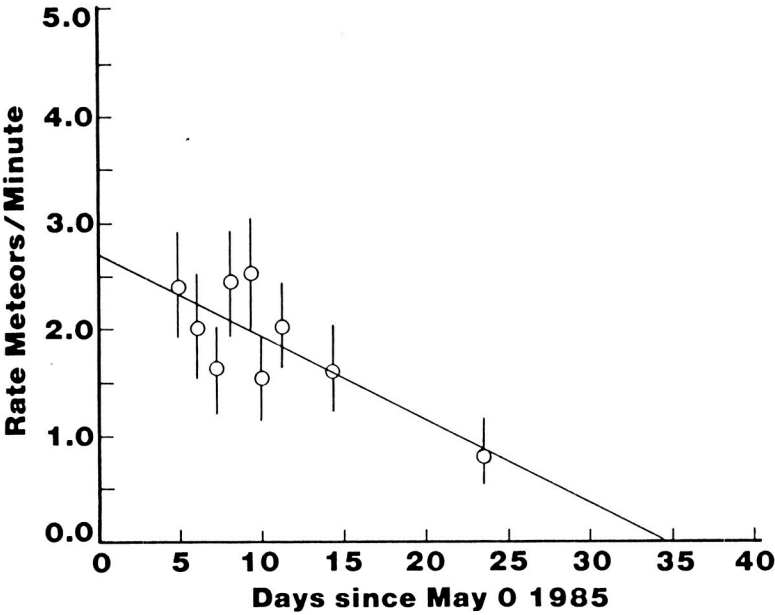


Fig. 6 Data rates measured in Geneseo, New York, using station CHU, Ottawa, Canada, on 14.670 MHz, May 1985.

Radioscatter-CHU 14.67 MHz 10 Min Cts. 00 < 01 UTC

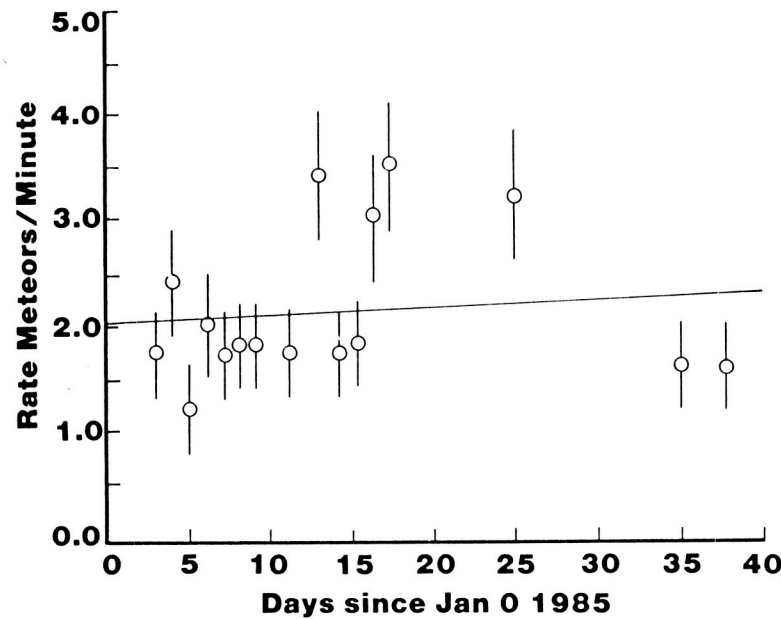


Fig. 7 As for Fig. 6, January 1985.

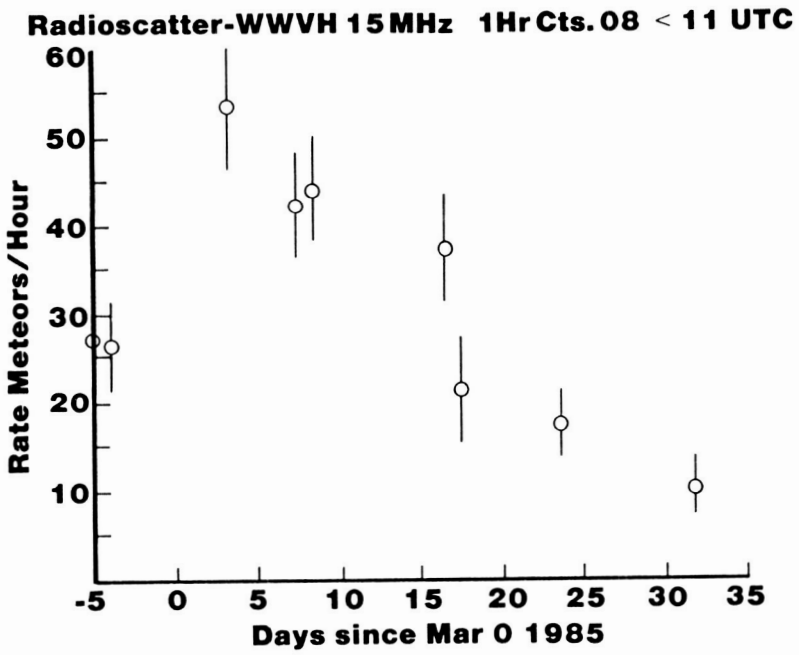


Fig. 8 As for Fig. 6, but using WWVH Honolulu, March 1985.

Interpolation of time-series data must be done with care since the usual polynomial methods can introduce distortions into the frequency domain. As discussed in my 1978 paper, the standard sinc ($\sin x/x$) interpolation series for band-limited functions is only appropriate when the "jitter" from the equal spacing case does not exceed 20 percent. Beyond that one must use special orthogonal polynomials constructed by the well-known Gram-Schmidt or analogous process to obtain a proper interpolation. Some possible approaches to the interpolation problem are given in my previous papers and will not be detailed here. Once the data are in equal-interval form, the Fourier series or transform can then be computed by standard techniques.

To obtain the serial correlation, one simply squares and adds the corresponding Fourier coefficients. These will be estimates of the power-spectrum frequency points which by the Wiener-Khinchine theorem are the cosine transforms of each lag product of the finite autocovariance.

The interpolation to equal intervals followed by a discrete Fourier transform computation is a two-step process that should be followed only if one really desires to have the original data available for other purposes such as a catalog of meteor rates.

If it is desired to skip the interpolation step explicitly, a computationally more convenient approach to the problem is to calculate the standard least-squares estimates of the coefficients of a finite Fourier series. The resulting covariance matrix will, of course, not be diagonal because of the unequal sampling intervals even though the functions used are orthogonal over the continuous interval. If the inverse of the covariance matrix is triangularized by a technique that leaves the row-column order unchanged (Cholesky method, for example) then the coefficient vector that results from multiplication of the "observation vector" by the inverse of the covariance matrix will be the estimates of the Fourier coefficients corresponding to the equivalent equal interval problem. The resulting coefficients may then be used to directly estimate the power spectrum of the data. (This process is equivalent to a time-domain Gram-Schmidt interpolation followed by a discrete Fourier transform.)

Should it be necessary to know either the equally-spaced original data or the serial correlation, it can always be generated from the orthogonalized Fourier coefficients.

In the Fourier formalism of random processes, prediction is simply an extension of interpolation. The theory of "optimal filtering" as applied to a time-series can be found in communications engineering literature under various names: for example, Kalman-Bucy filtering, Wiener-Kolmogorov filtering, state-space filtering, digital filtering, or simply signal processing. Analogous techniques of time-series analysis are used widely in econometric forecasting. A particularly coherent and lucid treatment of the subject from an engineering standpoint can be found in the text by ANDERSON and MOORE (1979). Although this treatment is meant for a technical audience, the notation is consistent with econometric use and is therefore recommended.

SHIBATA (1983c) has applied the "Group Method of Data Handling (GMDH)" to attempt a prediction of meteor rates, but the adopted algorithm is simply one variation of an optimal filter method. SHIBATA derives the covariance properties of a composite meteor time-series from radio observations (SHIBATA, 1983b) and uses this to minimize the prediction sum-of-squares. While there is nothing pedagogically wrong with SHIBATA's Method, it does not seem to be general enough to be widely useful.

For the past several years, I have been carrying out experiments on optimal filter forecasts of solar and geophysical indices using a personal computer. Since the same methodology is applicable to meteor rate data, we will experiment with predicting future meteor rates based on the compiled catalog of past values.

The most general time-series that can be assumed is a combination of an autoregressive process (AR) and a moving average (MA) process called simply an ARMA process. However, before one can apply the powerful techniques available, one must be sure to be dealing with data having a zero mean. This generally means that all secular trends must be removed before doing the time-series analysis. The preferred method of doing this is through specially constructed orthogonal polynomials which do not distort the power-spectrum properties of the data (ANDERSON, 1971; FULLER, 1976). In the time-series analysis of meteor flux, an initial problem is obtaining the correct orthogonal polynomials for detrending the time series (LINDBLAD, 1980). While the familiar "11-year cycle" permits this is the case of solar-geomagnetic forecasting, such a "secular" trend is not available in meteor work. However, since the time-series behavior of the sporadic meteor flux is quite different from the various shower fluxes, it will be possible to treat each shower separately using the sporadic results as the "secular" trend. Such a separation will only be possible if the data are available world-wide, on a nearly continuous basis.

For initial numerical experiments, an assumption of statistical stationarity is appropriate and prediction by means of standard Wiener filter theory is applicable. The discrete time formulation of Wiener filtering is called Levinson filtering (ANDERSON and MOORE, 1979). The scalar version of the Levinson filter has been used to attempt prediction of solar activity and geomagnetic parameters. A Levinson (or Wiener) filter is constructed from the past covariance (power-spectrum) structure of the signal. This represents the AR part of the covariance. The remaining part of the total covariance is assigned to a MA process. Thus the first order (linear) prediction equation for the detrended residuals becomes,

$$F(n) = K * \sum_j R_j * F(n-j) + (1-K) * \sum_j S_j * F(n-j)$$

where K is an adjustable parameter which is equal to the ratio of the moving average variance to the total variance, the R_j are the ratios of the j th covariance component to the variance (= the zeroth order covariance component), and the S_j are the autoregression coefficients defined by the Levinson filter. The appropriate K can be found by trial and error from

previous data, i.e., prediction of the last observed value using the remaining members of the series and choosing the K value that gives the best result. Details of the Levinson algorithm including a vector process version are given in ANDERSON and MOORE (1979) and will not be repeated here. The Levinson filter formulation requires equal intervals, but once the equal interval spectral components are estimated using the procedures outlined above, extension to a Levinson filter estimate is straight forward.

In many instances, it may be necessary to provide additional filtering (smoothing) to the prediction process. This is the domain of signal processing and is usually done again by trail and error. One particularly simple and useful technique is to use the LOGARITHM of the desired variable in the prediction equation. This is called exponential smoothing and its effect has well-known convergence properties (ANDERSON and MOORE, 1979). Other possible approaches abound in the signal processing literature and are beyond the scope of the present paper.

In conclusion it may be stated that amateur meteor observations made from several different locations around the world have now achieved a high enough level of technical sophistication to be useful for scientific purposes. These observers only need the support and guidance of the professional to be incorporated within the GLOBMET program. An outline for an initial effort involving standardization of amateur observations of meteor flux is the following:

- 1) Since ILS transmissions are available worldwide, we recommend that they serve as the nucleus of an amateur radio meteor network. On 75 MHz, the power available is quite low, but this is offset by the lack of interfering stations. At this frequency one obtains counts of mainly overdense trails so these should be easily statistically related to the standard visual hourly rates as compiled by OLIVIER and others. The frequency of 75 MHz is also high enough that ionospheric disturbance probabilities are very small. The 75 MHz transmissions are continuous and can be received during the daytime. Although VOR navigation beacons have the potential for enabling two-station triangulation of brighter meteors, the equipment required for doing this is apparently not readily available to amateur radio operators or amateur astronomers.

- 2) Although not numerous, there is a worldwide distribution of standard time/frequency stations that would permit nighttime monitoring of both underdense and overdense meteor echos at least during periods of low solar activity. The primary frequency for this would be 14-15 MHz. There are eight stations of this type which operate on 24 hour schedules. (Among these are: WWV, WWVH, CHU, JJY, RWM, RID, and RTA plus one due to start in Brazil. Station VNG operates continuously, but its top frequency is 12 MHz and it has not been established that useful meteor flux measurements could be made with it.) It is important to establish 75 MHz monitoring facilities within 30-300 km of these stations. Although these frequencies cannot be used continuously through the day or even through the years, the receiving equipment requirements are quite modest and readily available. It is possible that meteor scatter may be routinely observed using other sources of HF or VHF energy such as ionospheric sounders, but we have not explored this possibility.

3) The third standard frequency range for amateur monitoring could be in the 80-110 commercial FM band. While often not continuously available, this band does have the advantage of containing numerous high-power transmissions and readily available equipment. It will, however, not be an easy task to calibrate such radio observations with the rates obtained in other ways.

4) The choices for amateur meteor research using individually maintained beacon transmitters are 28 MHz and 50 MHz in North America and their equivalents elsewhere. These bracket the usual frequencies available for professional radiosscatter transmissions and have less rigorous instrumental requirements than the higher VHF bands.

5) Automated data collection and reduction in real-time at the receiving station will be encouraged with particular emphasis on microcomputer usage. In particular, it will be possible not only to count the meteors automatically (SHIBATA, 1983a), but it will be possible to record the signal decay of individual echoes (PHILON, 1984). However, as our recent work shows, useful rate information can be obtained by simple manual recording of the number and aural character of echoes.

6) For the purpose of intercalibration, it would be useful if professional meteor observatories themselves would start monitoring meteor flux on as many of the frequencies mentioned above as possible. Data recording does not have to be sophisticated. Much of the Japanese amateur data has been obtained with two identical receivers for each frequency (one on frequency, one slightly off frequency) feeding a comparator network with the AGC voltages, and recording the output by chart recorder. Because of the relatively low-power of the 15 MHz and 75 MHz transmissions, the data rates on these frequencies are usually quite nominal.

REFERENCES

1. Anderson B.D.O. and Moore J.B., 1979, Optimal Filtering, Prentice-Hall, Englewood Cliffs, N.J.
2. Anderson, T.W., 1971 The Statistical Analysis of Time-Series, John Wiley and Sons. New York, N.Y.
3. Black, W.H., 1983, "Observing Meteors by Radio", Sky and Telescope, July 1983, p. 61.
4. Fukuda, M. 1982, "FM Radio Observation Report No. 2", Radio Meteor Res. No. 9, pp. 78-101.
5. Fuller, W.A., 1976, Introduction to Statistical Time Series, John Wiley and Sons, New York, N.Y.
6. Houston, W.S., 1958, Mentioned in "The Amateur Scientist", Scientific American, July 1958, pp. 108-111.

7. Lindblad, B.A., 1980, "Serial Correlation of Meteor Radar Rates", in Solid Particles in the Solar System, I. Halliday and B.A. McIntosh eds. (I.A.U. Symposium No. 90), D. Reidel Pub. Dordrecht, Holland.
8. Meisel, D., 1977b, "Radiowave Scatter Detection of Meteors Using VHF Aeronautical Beacons", Am. Meteor Soc. Special Publication.
9. _____ 1977b, "The AMS Radio Scatter Program", Am. Meteor Soc. Special Publication.
10. _____ 1978, "Fourier Transforms of Data Sampled at Unequal Observational Intervals", Astron. Journal, Vol. 83, pp. 538-545.
11. _____ 1979, "Fourier Transforms of Data Sampled in Unequally Spaced Segments", Astron. Journal, Vol. 84, pp. 116-126.
12. Olivier, C. P. 1960, "Catalog of Hourly Meteor Rates", Smithsonian Contr. Astrophys., Vol. 4, pp. 1-14.
13. _____ 1965, "Second Catalog of Hourly Meteor Rates", Smithsonian Contr. Astrophys., Vol. 8, pp. 171-180.
14. _____ 1974a, "Daily Hourly Meteor Rate Catalog for Northern Hemisphere Observers", Am. Meteor Soc. Special Publication.
15. _____ 1974b, "Daily Hourly Meteor Rate Catalog for Southern Hemisphere Observers", Am. Meteor Soc. Special Publication.
16. Pilon, K. 1984, "Radio Meteor Astronomy with a Home Computer", METEOROS (British Meteor Soc.), Vol. 14, pp. 10-13.
17. Rice, S. O. 1954, "Mathematical Analysis of Random Noise" in Selected Papers on Noise and Stochastic Processes edited by N. Wax, Dover Publications, New York, N.Y.
18. Schippke, W. 1981, "Die Beobachtung Sporadischer Meteore und Meteorschauer Mittels Radiotechnischer Messeinrichtungen", Stern und Weltraum, Vol. 8, pp. 287-291.
19. Setteducati, A. F. 1960, "Listening to Meteors on Short Wave", Sky and Telescope, Apr. 1960, pp. 363-364.
20. Shibata, K. 1983a, "FM Radio Observation by Personal Computer", Radio Meteor Res. No. 10, pp. 2-19.
21. _____ 1983b, "Time History Analysis on the Meteors Appearance", Transaction of Nippon Meteor Soc. (1982), pp. 20-24.
22. _____ 1983c, "Forecasting the Number of Meteors Derived from Group Method of Data Handling using Predicted Sum Squares", Transaction of Nippon Meteor Soc. (1982), pp. 51-55.
23. Shimoda, C. 1982, "FM Radio Observation Report No. 1", Radio Meteor Res. No. 9, pp. 130-136.

24. _____ 1983, "The Annual Variation of FM Echos Derived From FM Radio Meteor Observations", Transaction of Nippon Meteor Soc. (1982) pp. 5-6.
25. Solodovnikov, V. V. 1960, Introduction to the Statistical Dynamics of Automatic Control Systems, Translated by J. Thomas and L. Zadeh, Dover Publications, New York, N.Y.
26. Suzuki, K. 1982, "Annual Variation of FM Radio Observation in Terms of Time Period and Echo Amplitude", Radio Meteor Res. No. 9, pp. 105-129.
27. _____ 1983, "Investigation of the Appearance Rate of Fireballs by Routine FM Radio Observation", Radio Meteor Res. No. 10, pp. 104-113.
28. van der Ziel, A. 1970, Noise: Sources, Characterization, Measurement, Prentice-Hall, Englewood Cliffs, N.J.

LIDAR INVESTIGATIONS OF M-ZONE

O. G. Ovezgeldiyev, K. Kurbanmuradov¹, M. F. Lagutin,
A. A. Zarudny, Yu. E. Meghel, A.A. Torba, V.E. Melnikov²

1. Physical Technology Institute, Ashkhabad, USSR
2. Institute of Radioelectronics, Kharkov, USSR

The creation of pulse dye lasers tuned to resonant line of meteor-produced admixtures of atmospheric constituents has made it possible to begin lidar investigations of the vertical distribution of mesospheric sodium concentration and its dynamics in the upper atmosphere. The Kharkov Institute of Radioelectronics began this method in 1973 by developing the resonance lidars which were subsequently used to measure sodium in the atmosphere over the Kharkov region. The initial experiments, the first of their kind in the world, were carried out in the Antarctic, in the region of energetic particle downpour above the Molodezhnaya (LAGUTIN et al., 1983) and Mirny (LAGUTIN et al., 1981) stations. In cooperation with the Tajik Physical Technology Institute, observations were started in the Ashkhabad region to study the altitude-longitudinal characteristics of the sodium layer (LAGUTIN et al., 1981). The seasonal and latitudinal winter anomaly of sodium was investigated taking into account both the photochemistry and the meteor source (LAGUTIN et al., 1983). The altitude distribution in the layer was analyzed. Using the photochemical balance equations for turbulent diffusion conditions, altitudinal variations of sodium atom formation from all ablating meteor sources (LAGUTIN et al., 1976) and acoustical/gravity wave parameters were estimated.

The observed morning increase of sodium concentration in the vertical column is probably caused by diurnal variations of sporadic meteors. To obtain a satisfactory agreement with experimental observations of the uppermost layer of sodium, the meteor source must either act in a narrow height interval (about 2 km for the height of 95 km) or turbulent diffusion and the sink for meteor matter in the mesosphere must be extremely high. The sink channel of mesosphere sodium is supposed to be transport by alkaline NaOH, NaO₂ and the water cluster aerosol down to the stratosphere.

The altitude stratification of the sodium layer of meteor origin must be closely connected with electrodynamic agents affecting sodium/water cluster ions which recharge very quickly through recombination with the basic ionospheric components of the D, E_s, and E layers.

The study of the dynamics of the sodium column concentration in the period of meteor streams activity confirms the suggestion of cosmic origin of these atoms. The short-lived increase of sodium concentration brought about by a meteor stream, however, exceeds by one order the level of the sporadic background. This contradicts the common estimate of meteor matter flux due to streams (LAGUTIN, 1977). These and other problems may be investigated by means of simultaneous probing of neutral and ionized components of the resonantly scattering admixtures of meteor origin. In this respect admixtures of mesospheric sodium, calcium, lithium and potassium are the only ones that can be investigated as far as ground-based laser probes are concerned. The lidar methods of distant resonance spectroscopy of basic atoms and ions of a meteor matter stream (such as Fe, Mg, Si, etc.) can be successfully realized only by satellite-based observations.

The monostatic lidar, used by the authors for studying mesospheric sodium, is equipped with a transceiver mounted at one point. The signal $S(z)$ returned from a height z of such a lidar is estimated from the following equation:

$$S(z) = \sigma_e(z) n(z) A \Delta z N_e T^2 \eta / z^2 \quad (1)$$

where $S(z)$ is the signal received from the height interval of $z - \Delta z/2$ to $z + \Delta z/2$. $\sigma_e(z)$ is the value of a resonance backscatter coefficient for the range Δz , $n(z)$ is the density value at a distance z , A is the surface area of the receiving telescope, N_e is the pulse energy, η is the overall efficiency of the receiver and, T is the loss of energy in the atmosphere.

In the case of a resonant scatter, the signals dispersed by alkaline metals of the mesosphere are so weak that a photon counting technique is needed to measure it.

The effective backscatter coefficient $\sigma_e(\lambda)$ depends on the laser emission spectrum:

$$\sigma_e(\lambda) = \int_0^\infty N_e(\lambda) \sigma(\lambda) d\lambda / \int_0^\infty N_e(\lambda) d\lambda \quad (2)$$

where both $N_e(\lambda)$ the laser energy, and $\sigma(\lambda)$ the alkaline atom backscatter coefficient, are functions of the wavelength λ .

The greatest difficulties in lidar upper atmosphere studies arise when the accuracy of concentration measurements require achieving a certain signal level.

On the assumption of the Poisson distribution of photons, the measurement precision will be $1/\sqrt{S}$ where S is the total number of photons detected from a given height interval Δz .

As measurements data is accumulated gradually after each probe, N_e represents a total number of photons transmitted for the period t . Thus, the mean power of a laser N_e/t constitutes an important parameter. On the other hand, N_e should be sufficient to meet the condition $S \gg N_n$, where N_n is the number of noise photons.

Fig. 1 presents a block-diagram of the lidar system functioning in Ashkhabad. The transmitter uses a flashlamp pump dye laser with the output energy of about 1 j and pulse duration of 4 μ s. Two Fabry-Perot etalons are used to filter it to 589.0 nm and maintain the 0.01 nm bandwidth.

As is seen from Fig. 1, the laser output beam is collimated by M_1 and M_2 to produce a final angular beamwidth of about 2 mR. A small fraction of the laser output is sampled by a partially reflecting mirror M_3 and is focused through a sodium vapour cell (3) maintained at 120°C. The light scattered by the sodium vapour (21) and measured by a photomultiplier (21) provides a means of keeping the laser energy within the D_2 line width. Changes in the laser output spectrum during observations occur due to changes in the quality of the dye, flashlamps, pumping, etc.

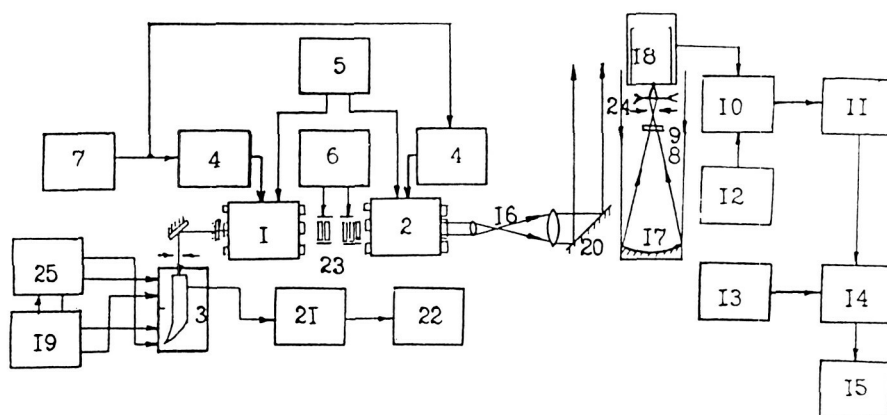


Fig. 1. Block-diagram lidar: 1-laser generator; 2-laser amplifier; 3-system wavelength control; 4-energy system (supply); 5-system pumping dye; 6-system F.P. thermostability resonators (23); 7-modulator and system trigger; 8-interference filter; 9-diaphragm; 10-preamplifier of PM I photoreceiver; 11-signal shaping circuitry; 12-V.H. supply PM I; 13-strobimpulse block; 14-multichannel recorder; 15-the monitoring documentation block; 16-collimator telescope; 17-zenith receiver telescope; 18-PM I; 19-the thermochamber resonance camera; 20-rotating mirror; 21-PM I of probing wave system; 22-probing wave indicator and output energy; 23-multiplex tuning Fabry-Perot (F.P.) interferometer; 24-focusing lens before PM I; 25-thermochamber resonance camera.

The receiver has a spherical mirror M_4 47 cm in diameter and 2,65 m focal length.

After passing through an adjustable diaphragm which determines the receiver angular beamwidth, the signals pass through a 2 nm bandwidth interference filter before being focused by (25) onto the PM-I photocathode (18).

The photon counts, usually accumulated for 200 laser shots, are transferred to a micro-computer which carries out its partial analysis and, in turn, transfers it to a display to be observed and recorded (Fig. 2). The data are also recorded on digital data cassettes and processed on an ES-computer.

References

1. Lagutin, M.F., 1974, Astron. Vestnik, Vol. 8, No. 8, pp. 145-153.
2. Lagutin, M.F., et al., 1970, Izvestiya Turkmenskoi Akademii Nauk, No. 4.
3. Lagutin, M.F., et al., 1983, The Soviet Antarctic Expedition Bulletin, No. 104, p. 81.
4. Lagutin, M.F., et al., 1981, Academy of Sciences Reports, Vol. 258, No. 2, pp. 334-335.
5. Lagutin, M.F., et al., Izvestiya Turkmenskoi Akademii Nauk, No. 1, pp. 32-40, 1981.
6. Lagutin, M.F., et al., 1983, Proceedings of the III All-Union symposium on upper atmosphere, pp. 68-75.
7. Lagutin, M.F., et al., Izvestiya Turkmenskoi Akademii Nauk, No. 6, pp. 61-61, 1976.
8. Lagutin, M.F., 1977 (abstr.), 8th International Laser Radar Conference, Philadelphia, p. 59.

ORIGINAL PAGE IS
OF POOR QUALITY

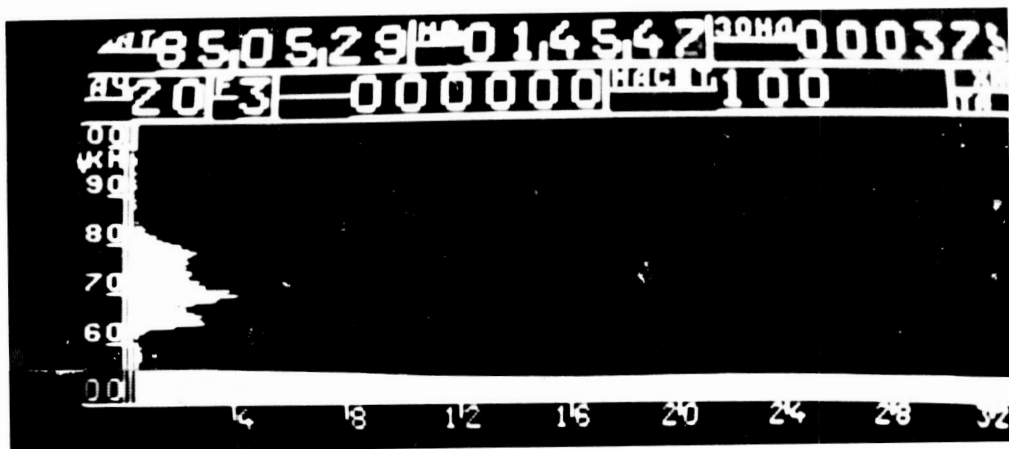


Fig. 2. A photograph from monitoring system TV.

OPTICAL ELECTRONICS FOR METEOR OBSERVATIONS

R. I. Shafiev, S. Mukhamednazarov, and I. A. Atamas

Institute of Physical Technology,
Ashkhabad, USSR

For several years, the Turkmen Academy of Sciences Institute of Physics and Technology has been carrying out spectral observations of meteors using an optical electronics facility. Interest has centered on faint meteors and their trails in the period of intensive meteor showers.

Over 800 meteors were registered during the observation period with spectrograms obtained for 170 of these. A total of 86 meteors were photographed from two sites and for 25 of these spectrograms of the meteors as well as their trails were obtained. The brightness of the photographed meteors ranged from (-3^m) to ($+9^m$). All meteors have undergone routine processing in order to determine atmospheric characteristics.

Sporadic meteors have great ranges of appearance as well as disappearance heights. This is explained by a great variety of entry velocities into the Earth's atmosphere and also by different composition and structure of meteor particles.

In the period from 1977 to 1981, 25 meteors of the Perseids were photographed from two sites and for 13 of them spectrograms were obtained. The brightest meteor had a visual stellar magnitude of -2^m and the faintest one $+6^m$. For the majority of meteors, the visual stellar magnitude was in the range ($+3^m$) to (5^m).

The radiant area of the Perseids in Fig. 1 is given on the basis of our observation results. Scatter in the early visual radiant (symbol = 0) is significant. It cannot be ruled out that some of them have nothing to do with the Perseids. When making allowances for diurnal motion of this distribution, the cross-section of the radiant area is about 4° diameter.

Fig. 2a shows the meteor mean velocity distribution for the Perseids. For most of the meteors, the velocities vary for 58 to 61 kms indicating an insignificant scatter of particle velocities within this stream.

The distribution of meteor beginning heights for our Perseids is shown in Fig. 2b. In comparison with ordinary photographic meteors, the heights in our case are somewhat high. This can be explained by the greater sensitivity of our equipment which allows better detection of the least visible upper part of a meteor trail. Most of the meteors in our sample had heights within the interval of 198-117 km. This confirms the previously indicated dispersion of particle velocities for this stream. The beginning heights of brighter members of this stream were observed as high as 120 km apparently due to excitation of the oxygen green line. This is clearly seen from a spectrogram of a meteor of the Perseids presented in Fig. 3. Since the mass of particles causing bright meteors is greater, they possess sufficient kinetic energy to cause the oxygen green line to glow at higher altitudes. Fainter meteors of the stream glow at lower

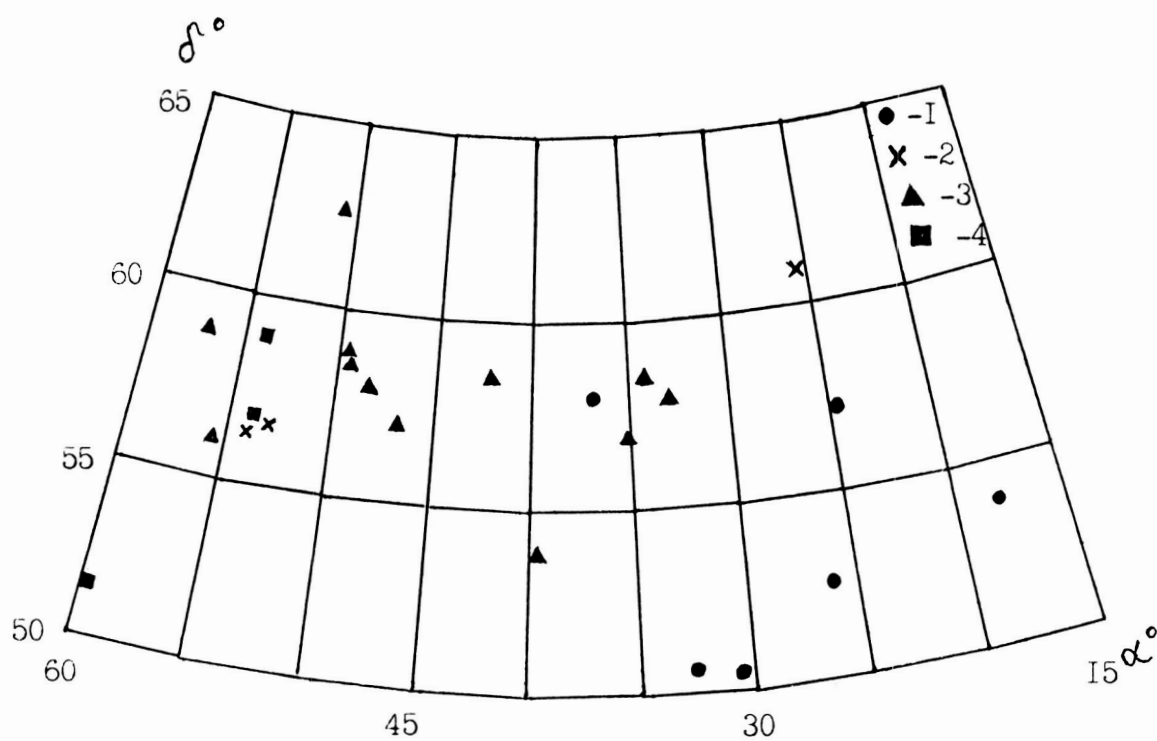


Fig. 1 Radiant area of Perseids. I - radiants obtained before August 9; 2 - August 10 and 11; 3 - August 12, 13, 14; 4 - after August 14.

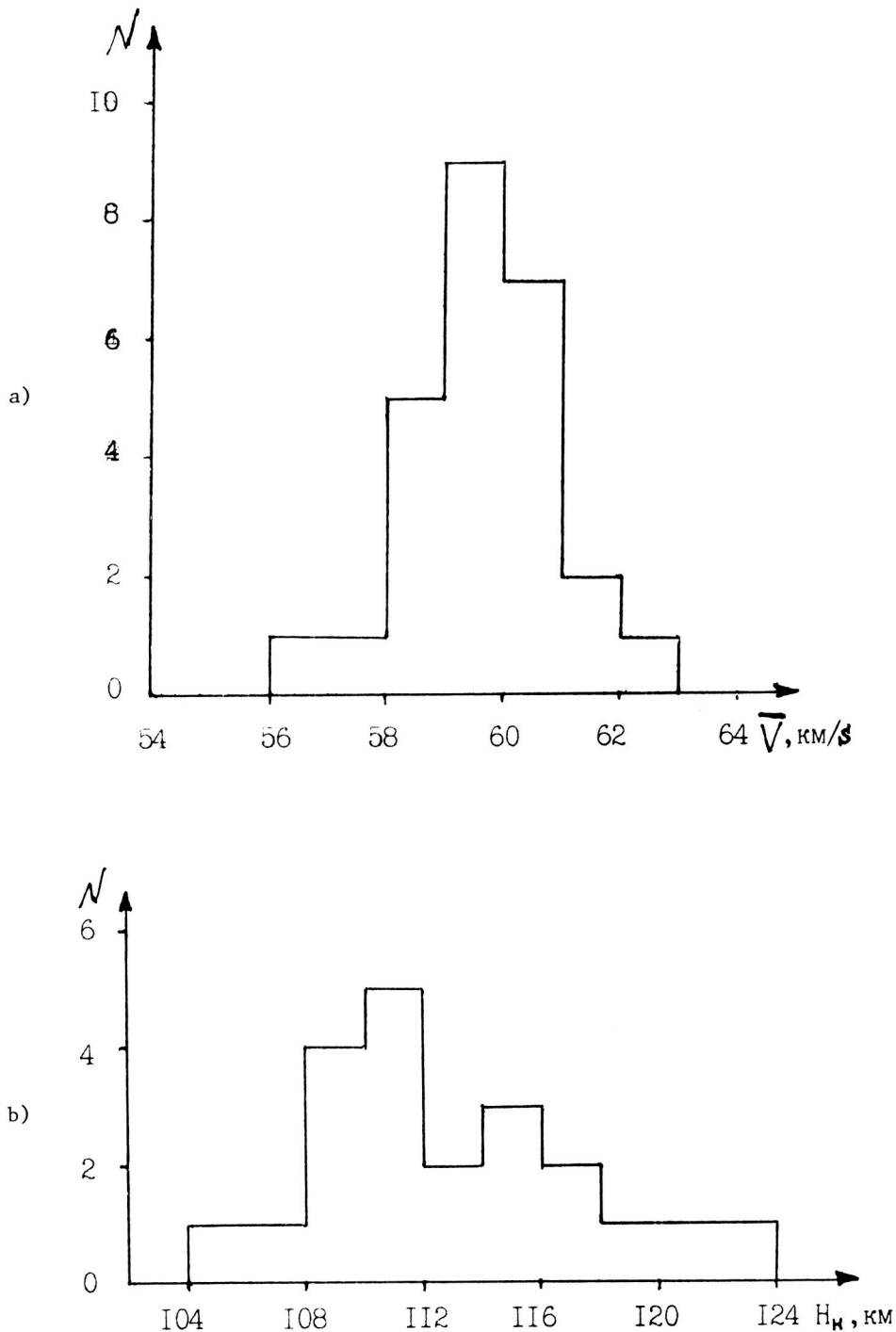


Fig. 2 Distributions of Perseid parameters. a) mean meteor velocity; b) meteor height; c) meteor disappearance height; d) pathlength.

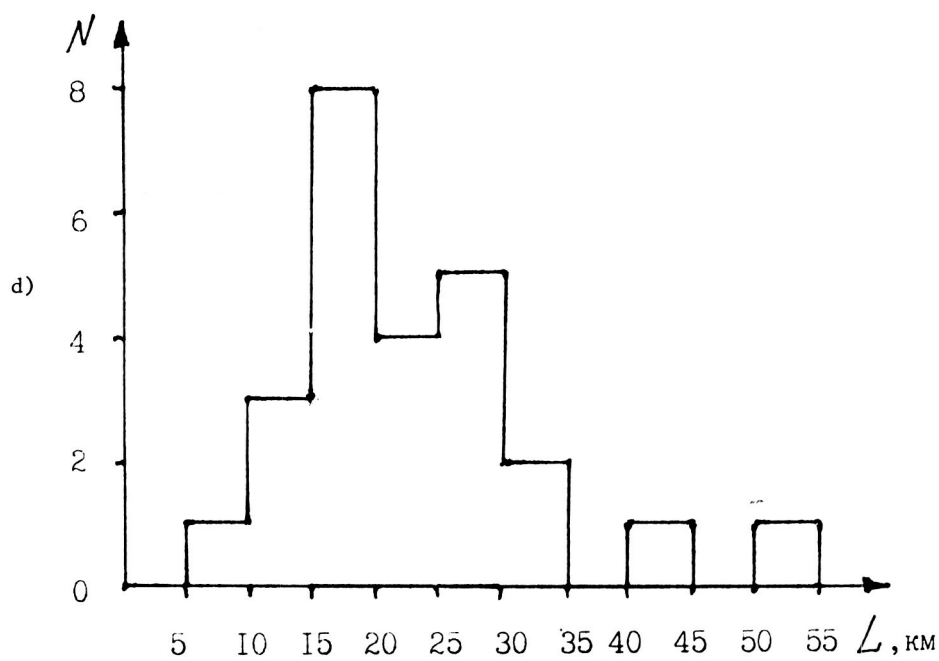
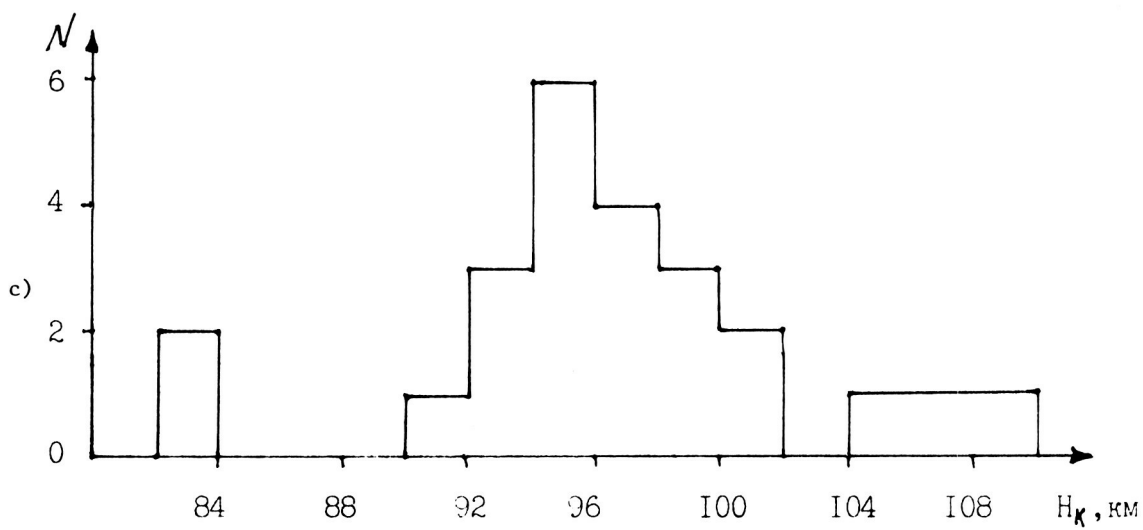


Fig. 2 Continued.

heights where concentration of oxygen atoms in the Earth's atmosphere is greater.

Fig. 2c gives the height distribution of meteor disappearance for our Perseids. The majority of our meteors had a height of disappearance in the interval from 92 to 100 km. This shows that particle mass dispersion of this stream is relatively small. Two bright meteors -2^m and -1^m of this sample disappeared with bursts at the height of 82-84 km.

Fig. 2d shows the path length distribution in the atmosphere for the Perseids. This shows the absence of small particles (i.e., preponderance of short trails) in the stream and confirms the previously indicated small dispersion of particle masses and indicates that most of the particles in our sample of the Perseids produce meteors in the $(+3^m)$ to $(+5^m)$ range.

The meteor spectra recorded by the optical electronics cameras usually differ from photographic spectra of bright meteors with intense lines and molecular bands of atmospheric components seen, especially in the red part.

The main emissions in the meteor spectra of the Perseids are the magnesium triplet, the oxygen green line, the sodium doublet and the oxygen red line (Fig. 3). The monochromatic curves of brightness are qualitatively similar and appear in the part of the trail, where there is little overlapping of the oxygen green line radiation. In composition, faint meteors of the Perseids do not appear to differ from bright ones.

Comparison of our results on faint meteors obtained by optical electronic devices and those obtained using other techniques shows that the former is more informative, especially when studying composition and interaction of meteor particles with the Earth's atmosphere.



ORIGINAL PAGE IS
OF POOR QUALITY

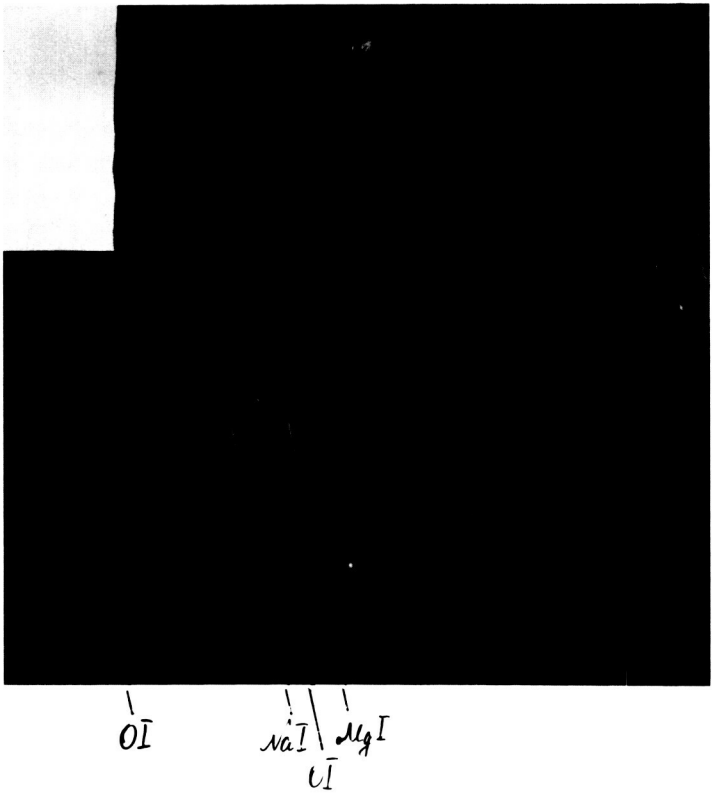


Fig. 3 Spectrogram of a +3m Perseid meteor obtained on August 16, 1979 by optical electronics camera. Bright emmissions on the spectrogram from left to right: oxygen red line, sodium doublet, oxygen green line and magnesium triplet.

HARD- AND SOFTWARE PROBLEMS OF SPACED METEOR OBSERVATIONS
BY OPTICAL ELECTRONICS

Shafiev R. I., Mukhamednazarov S., and Ataev A. Sh.

The Turkman Academy of Sciences Institute of Physical Technology
USSR

An optical electronic facility is being used for meteor observations at the Turkmen Academy of Sciences Institute of Physical Technology along with meteor radars and astronomical TV.

The main parts of the facility are cameras using UM-92 optical electronic image tubes. The three-cascade optical electronic image-tube with magnetic focusing has a 40-mm cathode and resolution in the center of up to 30 pairs of lines/mm. The photocathode is of a multislit S-20 type.

For meteor spectra observations, replica gratings of 200 and 300 lines/mm are used as the dispersive element. The set of available camera lenses give stellar fields with angular dimension from 30° to 10° and stellar magnitude limits of 7^m - 11^m . Depending on the combination of objective and replica used the spectrograms are recorded with inverse linear dispersions from 600 Å/mm to 250 Å/mm. In spectral observations, the limiting magnitude of the equipment for stars is 7^m - 9^m and depends on the type of the input objective and replica.

A two-paddle shutter with a 1:2 ratio of closed and open segments gives 48 breaks a second.

The image recorder reproduces an image from the output screen of the image-tube on a photographic film on a scale of 1:1. The exposure time is chosen to be short enough to maintain dot-like stellar images as the cameras are mounted on nonguiding supports. The end of the exposure on each 18 x 24 mm frame is marked with readings of an electronic watch.

The spectral sensitivity of the cameras depends on spectral sensitivity of image-tube photocathode as well as optical parameters of the objective and replica. Fig. 1 shows the curve of the spectral camera sensitivity plotted on the basis of spectra for stars of different spectral class.

Fig. 2 gives the averaged field errors for various sections of the image-tube screen as obtained from photometric images of stars with different brightness.

To determine a stellar meteor magnitude from characteristic curves, a correction (Δm) as a function of the meteor image displacement along the cathode is used (Fig.3).

Fig. 4 gives experimental data on the image brightness decay of the output screen.

To carry out spaced meteor observations using the optical electronics equipment, we used stations spaced at 20.2 km, 12.8 km and 5.7 km distance

*

C-6

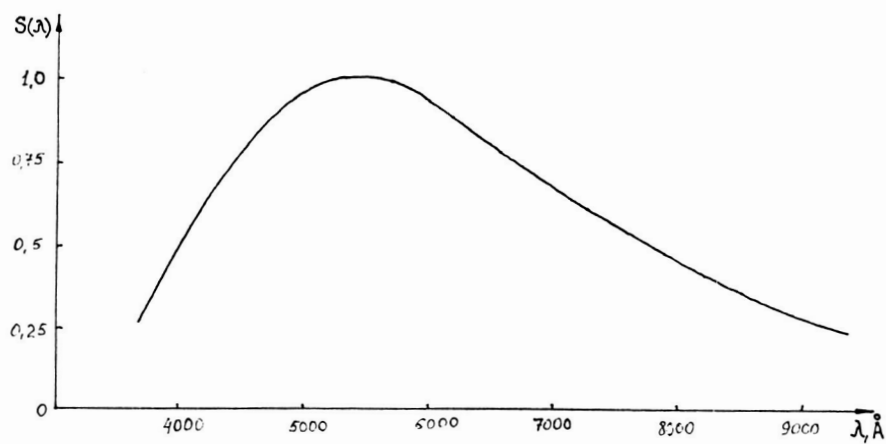


Fig. 1 Spectral sensitivity curve of the image-tube camera.

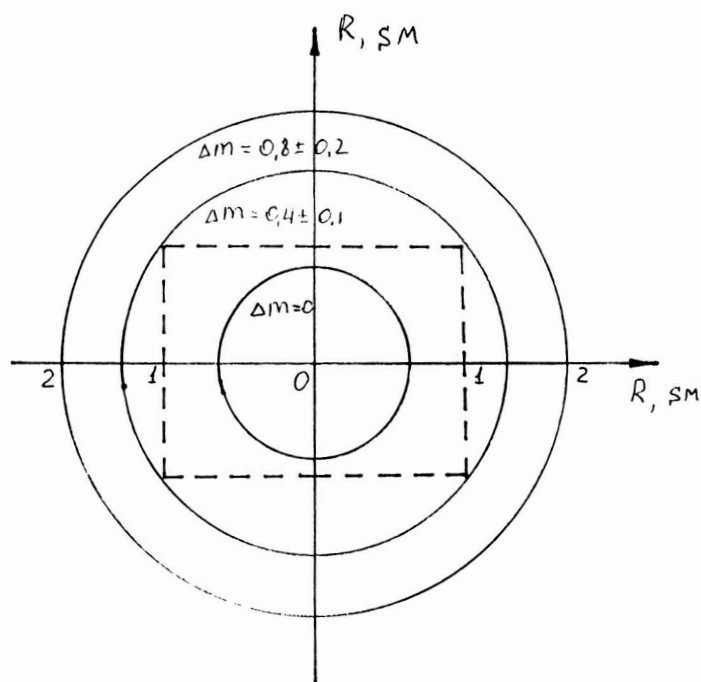


Fig. 2 Field error from the image-tube screen.

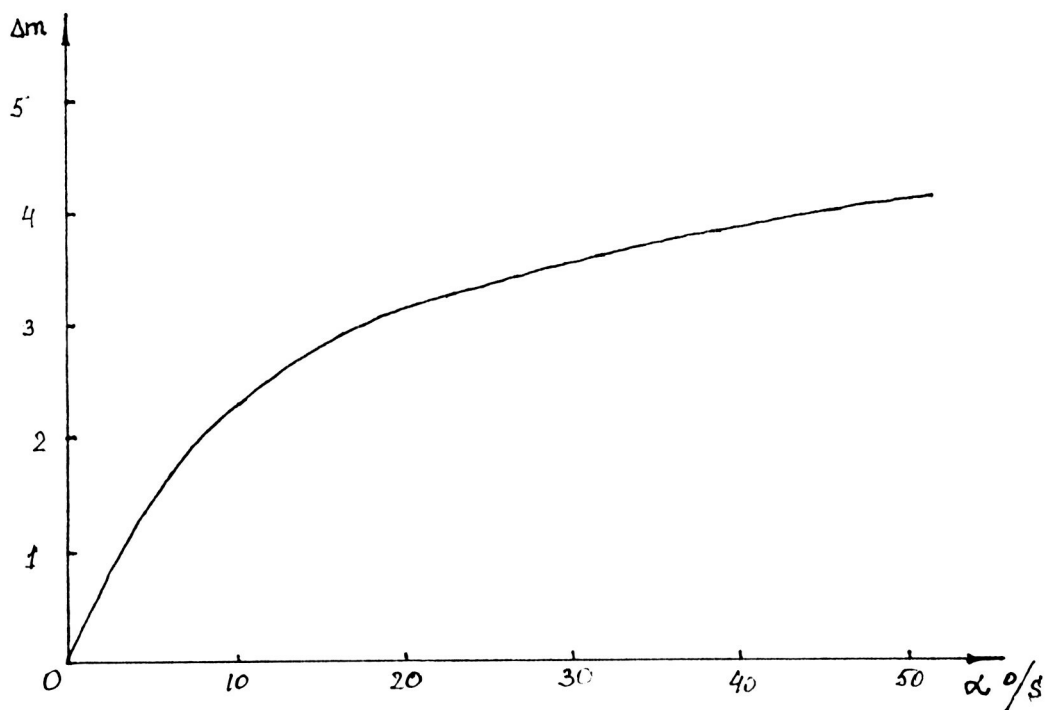


Fig. 3 Curve for determination of errors caused by meteor image displacement.

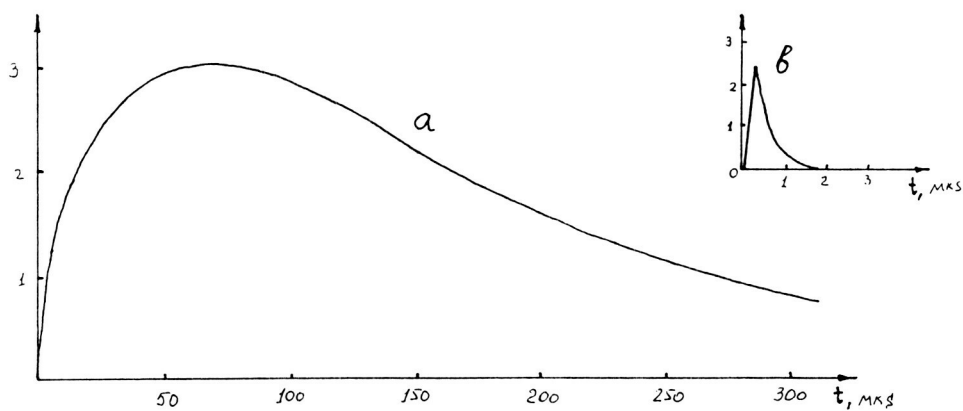


Fig. 4 Afterglow curve (a) observed on the image-tube output screen during photocathode lighting by light pulse of the form (b).

away from each other. Pairs of objectives for each base were selected so as to allow determination of characteristics of meteors from 0^m to $+9^m$ with about the same accuracy.

The center of the general viewing field was chosen along the line perpendicular to the base at 100 km.

The primary processing of basic meteor photographs involves:

1. identification and selection of standard stars;
2. measurement of standard stars and meteor points by measuring microscope;
3. photometric processing of negatives using a densitometer.

After identification of stars for each frame along the meteor path about 20 standard stars are chosen from both sides of the negative and some star closest to the geometrical center of the frame is chosen as the optical center of negative. Then the coordinates of the standard stars and optical center are taken from a catalogue.

Horizontal coordinates (X,Y) of standard stars, optical center and points on the meteor path are measured by a microscope. The frame is placed so that the direction of meteor movement coincides with that of one of the measuring microscope axes. Microscope setting of an investigated object is carried out three times and results for each measured point are averaged.

Photometric processing is carried out by an automatic densitometer MD-100. If there are images in the frames following the initial appearance, the meteor trail image is recorded, then the zero-order trail is also photometered in order to determine its decay. Then the meteor spectrum is photometered along the dispersion direction for individual lines and bands.

Mathematical processing of spaced optical electronic observations of meteors was carried out on the Electronica-100/25 computer using the RAFOS operational system with FORTRAN.

The program structure and arrangement of basic data are conditioned by peculiarities of the observation method along with the technical parameters of the optical electronics equipment. As star images on the negatives show as dots, the meteor coordinates are determined directly in the system of coordinates α , δ .

All the initial information obtained after measurement of the negatives as well as data on equipment, observation sites and reduce values are registered in separate files.

For the case when a meteor image is recorded in a sequence of subsequent frames additional data is recorded in a subsidiary file.

Distortion is taken into account by means of stars of known coordinates that are used as reference points. Approximation and

interpolation can both be used for meteor coordinate point calculations. Approximation may seem preferable at first sight. However, actual calculations showed that approximation with 8th order orthogonal polynomials in both variables describes the relationships with less accuracy than interpolation between the closest reference points. It was found out experimentally that interpolation over four nearest reference stars serves our purpose the best.

Processing of spaced-meteor observational data is performed in several stages. Firstly, the equatorial meteor coordinates are determined for each negative. Calculated coordinates of meteor points α_i , δ_i , are smoothed out and reduced to a large circle. Then the radiant, heights and meteor particle velocity are calculated. And finally, the meteoroid orbital elements are determined.

An error of faint meteors parameters observed by the optical electronic technique shows that this method is not inferior in accuracy to the photographic one applied to observations of bright meteors.

AUTHOR INDEX

Name	Page number(s)
Alimov, O.	261
Andreev, G. V.	305, 339
Andreev, V. V.	298
Ataev, A. Sh.	416
Atamas, I. A.	410
Avery, S. K.	361
Babadjanov, P. B.	2, 218, 294
Bekbasarov, R. B.	62, 186
Belkovich, O. I.	272, 298, 344
Bibarsov, R. Sh.	258, 294
Blokhin, A. V.	218
Ceplecha, Z.	280, 321
Cevolani, G.	121
Chebotarev, R. P.	62, 351
Djachenko, V. A.	180
Fakhrutdinova, A. N.	70, 138, 189
Ganin, V. A.	138
Gavrilov, N. M.	153, 167, 173
Getman, V. S.	294
Greisiger, K. M.	58, 66, 119
Hajduk, A.	329
Isamutdinov, Sh. O.	351
Jandieri, G. V.	207
Kalchenko, B. V.	112, 194
Kalov, E. D.	173
Karimov, K. A.	62, 143, 186
Kascheyev, B. L.	50
Kato, S.	45
Kazantsev, A. M.	356
Keay, C.	381
Kevanishvili, G. Sh.	207
Kikhvilashili, G. B.	200
Kolmakov, V. M.	294
Koshelkov, Yu. P.	76
Kostylev, K. K.	211
Kulikova, N. V.	336
Kurbanmuradov, K.	405
Kurschner, D.	58, 62, 66
Lebedinets, V. N.	218
Lagutin, M. F.	405
Lenin, V. I.	207
Liadze, Z. L.	200
Lysenko, I. A.	66, 180, 376
Makarov, N. A.	66
Makarov, V. A.	189
Maltsev, N. V.	222
Mathews, J. D.	228
Medvedev, A. S.	146
Meghel, Yu. E.	405

Meisel, D. D.	389
Melinkov, V. E.	405
Mikhailiek, P. P.	376
Mosashvili, N. V.	200
Mukhamednazarov, S.	222, 410, 416
Nabotov, Kh.	62
Nechitailenko, V. A.	22
Novikov, G. G.	218
Obrubov, Yu. V.	2
Oleinikov, A. N.	194
Ovezgeldyev, O. G.	11, 222, 405
Perevedentsev, I. P.	70
Petrov, B. I.	66, 376
Portnyagin, Yu. I.	31, 66, 180
Rajchl, J.	266
ReVelle, D. O.	204, 255
Riazanova, L. A.	62
Roper, R. G.	1
Rubtsov, L. N.	339
Ryabova, G. O.	344
Salimov, O. N.	316
Schminder, R.	58, 62, 66
Shafiev, R. I.	222, 410, 416
Sharadze, Z. S.	200
Sherbaum, L. M.	356
Sidorov, V. V.	138, 189
Simek, M.	288
Spurny, P.	321
Stepanov, A. M.	70
Suleimanov, N. I.	272
Svetashkova, N. V.	311
Takyrbashev, M. A.	186
Tarasenko, D. A.	101
Tarasova, I. I.	339
Tokhtashev, V. S.	211, 272
Torba, A. A.	405
Tsuda, T.	45
Volkov, N. G.	316
Yudin, V. A.	167
Zarudny, A. A.	405

CUMULATIVE LISTING FOR THE MAP HANDBOOK

Volume	Contents	Publication Date
1	National Plans, PMP-1 , PMP-2, PMP-3 Reports, Approved MAP Projects	June 1981
2	Symposium on Middle Atmosphere Dynamics and Transport	June 1981
3	PMP-5, MSG-1, MSG-2, MSG-3 Reports, Antarctic Middle Atmosphere Project (AMA), EXOS-C Scientific Observations, WMO Report No. 5., Updated Chapter 2 of MAP Planning Document, Condensed Minutes of MAPSC Meetings	November 1981
4	Proceedings of MAP Assembly, Edinburgh, August 1981 Condensed Minutes of MAPSC Meetings, Edinburgh, Proceedings of MAP Open Meeting, Hamburg, August 1981,	April 1982
5	A Catalogue of Dynamic Parameters Describing the Variability of the Middle Stratosphere during the Northern Winters	May 1982
6	MAP Directory	November 1982
7	Acronyms, Condensed Minutes of MAPSC Meetings, Ottawa, May 1982, MAP Projects, National Reports, Committee, PMP, MSG, and Workshop Reports, Announcements and Corrigendum	December 1982
8	MAP Project Reports: DYNAMICS, GLOBUS, and SSIM, MSG-7 Report, National Reports: Czechoslovakia, USA	July 1983
9	URSI/SCOSTEP Workshop on Technical Aspects of MST Radar, May 1983, Urbana	December 1983
10	International Symposium on Ground-Based Studies of the Middle Atmosphere, May 1983, Schwerin	May 1984
11	Condensed Minutes of MAPSC Meetings, Hamburg, 1983, Research Recommendations for Increased US Participation in the Middle Atmosphere Program, GRATMAP and MSG-7 Reports	June 1984
12	Coordinated Study of the Behavior of the Middle Atmosphere in Winter (PMP-1) Workshops	July 1984
13	Ground-Based Techniques	November 1984
14	URSI/SCOSTEP Workshop on Technical Aspects of MST Radar, May 1984, Urbana	December 1984
15	Balloon Techniques	June 1985
16	Atmospheric Structure and its Variation in the Region 20 to 120 km: Draft of a New Reference Middle Atmosphere	July 1985
17	Condensed Minutes of MAPSC Meeting, Condensed Minutes of MAP Assembly, MAP Project, MSG, and National Reports	August 1985
18	MAP Symposium, November 1984, Kyoto	December 1985
19	Rocket Techniques	March 1986
20	URSI/SCOSTEP Workshop on Technical and Scientific Aspects of MST Radar, October 1985, Aguadilla	June 1986
21	MAPSC Minutes, ATMAP Workshop, Atmospheric Tides Workshop, MAP/WINE Experimenters Meetings, National Reports: Co-ordinated Study of the Behavior of the Middle Atmosphere in Winter	July 1986
22	Middle Atmosphere Composition Revealed by Satellite Observations	September 1986
23	Condensed Minutes of MAPSC Meetings, Toulouse, June/July 1986	December 1986
24	MAP Directory	May 1987
25	First GLOBMET Symposium, Dushanbe, August 1985	August 1987

THE FIRST GLOBMET SYMPOSIUM

Session Topics

OPENING PLENARY.....	1
I. THE DYNAMICS OF ATMOSPHERIC PROCESSES IN THE METEOR ZONE	31
II. THE PHYSICS OF THE INTERACTION OF METEORS WITH THE EARTH'S ATMOSPHERE	207
III. METEOR FLUX AND STRUCTURE OF THE METEOR COMPLEX	272
IV. STRUCTURE AND EVOLUTION OF METEOR SHOWERS	321
V. METHODOLOGICAL PROBLEMS, TECHNIQUES AND FACILITIES FOR STUDYING METEORS AND THE MIDDLE ATMOSPHERE.	361